Environmental Microplastics

How the Surface properties of microplastic particles determine their particle-cell interactions

Kumulative Dissertation

Zur Erlangung des akademischen Grades einer Doktorin der Naturwissenschaften (Dr. rer. nat.) in der Bayreuther Graduiertenschule für Mathematik und Naturwissenschaften (BayNAT) der Universität Bayreuth

vorgelegt von

Anja Franziska Ruth Marie Ramsperger

aus Sigmaringen-Jungnau

Bayreuth, 2023

Die vorliegende Arbeit wurde in der Zeit von (11/2016) bis (4/2023) in Bayreuth am Lehrstuhl Tier-ökologie I (Prof. Dr. Christian Laforsch) und der Arbeitsgruppe Biologische Physik (Prof. Dr. Holger Kress) unter Betreuung von Herrn Prof. Dr. Christian Laforsch angefertigt.

Vollständiger Abdruck der von der Bayreuther Graduiertenschule für Mathematik und Naturwissenschaften (BayNAT) der Universität Bayreuth genehmigten Dissertation zur Erlangung des akademischen Grades einer Doktorin der Naturwissenschaften (Dr. rer. nat).

Form der Dissertation:	Kumulative Dissertation
Dissertation eingereicht am:	17.04.2023
Zulassung durch das Leistungsgremium:	17.05.2023
Wissenschaftliches Kolloquium:	18.12.2023

Amtierender Direktor:　　　　　　　　Prof. Dr. Jürgen Köhler

Prüfungsausschuss:

Prof. Dr. Christian Laforsch	(Gutachter)
JProf. Dr. Anke Nölscher	(Gutachterin)
Prof. Dr. Stefan Schuster	(Vorsitz)
Prof. Dr. Andreas Römpp	

(weiterer Gutachter:　　Prof. Dr. Thomas Braunbeck)

„Entschleierung der Wahrheit ist ohne Divergenz der Meinungen nicht denkbar.“

Alexander von Humboldt

„Ich ging hinaus zu einem Spaziergang und beschloss dann, bis zum Sonnenuntergang drau-ßen zu bleiben, denn ich stellte fest, dass Hinausgehen in Wirklichkeit Hineingehen war.“

John Muir

Die vorliegende Arbeit ist als Kumulative Dissertation in englischer Sprache verfasst.

Teile der Arbeit sind bereits in den folgenden Publikationen erschienen:

Nominally identical microplastic models differ greatly in their particle-cell interactions

Wieland, S*, **Ramsperger, A F R M***, Gross, W, Lehmann*, M, Witzmann, T, Caspari, A, Obst, M, Gekle, S, Auernhammer, G K, Fery, A, Laforsch, C, Kress, H (2024)

* shared first authorship

Nature Communications (15) 922

https://doi.org/10.1038/s41467-024-45281-4

Nano- and microplastics: a comprehensive review on their exposure routes, translocation, and fate in humans

Ramsperger A F R M, Bergamaschi E, Panizzolo M, Fenoglio I, Barbero F, Peters R, Undas A, Purker S, Giese B, Lalyer C R, Tamargo A, Moreno-Arribas V M, Grossart HP, Kühnel D, Dietrich J, Paulsen F, Afanou A K, Zienolddiny-Narui S, Eriksen Hammer S, Kringlen Ervik T, Graff P, Brinchmann B C, Nordby KC, Wallin H, Nassi M, Benetti F, Zanella M, Brehm J, Kress H, Löder M G J, Laforsch C (2023)

NanoImpact. (29) 100441

https://doi.org/10.1016/j.impact.2022.100441.

Repulsive Interactions of Eco-corona-Covered Microplastic Particles Quantitatively Follow Modeling of Polymer Brushes

Witzmann T, **Ramsperger A F R M**, Wieland S, Laforsch C, Kress H, Fery A, Auernhammer G K (2022)

Langmuir. (26) 38 (29):8748-8756.

https://doi.org/10.1021/acs.langmuir.1c03204.

From properties to toxicity: comparing microplastics to other airborne microparticles

Wieland, S, Balmes, A, Bender, J, Kitzinger, J, Meyer, F, **Ramsperger, A F R M**, Roeder, F, Tengelmann, C, Wimmer, B H, Laforsch, C, Kress, H (2022)

Journal of Hazardous Materials, 3(1), 128151

https://doi.org/10.1016/j.jhazmat.2021.128151

Supposedly identical microplastic particles substantially differ in their material properties influencing particle-cell interactions and cellular responses

Ramsperger, A F R M*, Jasinski, J*, Völkl, M*, Witzmann, T, Meinhart, M, Jérôme, V, Kretschmer, W P, Freitag, R, Senker, J, Fery, A, Kress, H, Scheibel, T, Laforsch, C (2022)

* shared first authorship

Journal of Hazardous Materials, 5(3), 425,127961

https://doi.org/10.1016/j.jhazmat.2021.127961

In situ Prokaryotic and Eukaryotic Communities on Microplastic Particles in a Small Headwater Stream in Germany

Weig, A; Löder, MGJ; **Ramsperger, A F R M**; Laforsch, C (2021)

Frontiers in Microbiology, 29(11)

https://doi.org/10.3389/fmicb.2021.660024

Environmental exposure enhances the internalisation of microplastic particles into cells

Ramsperger, A F R M; Bangalore Narayana, VK; Gross, Wolfgang; Mohanraj, John; Thelakkat, Mukkundan; Greiner, Andreas; Schmalz, Holger; Kress, Holger; Laforsch, C (2020)

Science Advances, 6(50)

https://doi.org/10.1126/sciadv.abd1211

Structural Diversity in Early-Stage Biofilm Formation on Microplastics Depends on Environmental Medium and Polymer Properties

Ramsperger, A F R M; Stellwag, A; Caspari, Anja; Fery, Andreas; Kress, Holger; Löder, MGJ; Laforsch, C (2021)

Water, 12(11), 3216

https://doi.org/10.3390/w12113216

Content

Abstract

The contamination of ecosystems with plastic particles is a global challenge that needs, due to its complexity, to be addressed by interdisciplinary research. Plastic particles were detected in every environmental compartment, where the particles eventually can interact with their surrounding. This interaction can be anything from the attachment of biomolecules and microorganisms on the surface of particles, over their uptake by organisms, up to the translocation of particles from exposed organs to other tissues, e.g. via cellular internalization. Interestingly, the interaction of an organism with plastic particles has been described to increase with decreasing particle sizes. Therefore, increased attention is paid to so-called microplastics, defined as particles < 5 mm. However, the pure definition of microplastics by their sizes is way too simplified to understand their potential adverse effects on the environment, organisms and human health. Microplastic is a hypernym of a plethora of different polymer types, each with specific and unique properties. However, the evaluation of the potential hazards deriving from microplastics currently relies on the controlled exposure of cells and organisms to model polystyrene microplastic particles. Although supposedly identical particles were used in different studies, the reported results varied tremendously. While some studies found toxic effects on cells and organisms, others reported that the model microplastic particles were non-toxic or not harmful to organisms. Since the bulk material of model microplastic particles used in effect studies is polystyrene (PS), the differences between the reported results are probably not polymer-based but must derive from other particle properties.

In my PhD thesis, I combine three interrelated topics that, in the end, all address one overall question: How do the surface properties of microplastic particles affect their interaction with cells and microorganisms? The three interrelated topics are (1) how the initial surface properties determine the particles' reactivity towards cells, (2) how the environmental exposure alters the surface properties of microplastic particles and whether this affects the particles' reactivity towards cells, and (3) whether the initial surface properties of microplastic particles of different polymer types determine their reactivity towards their interaction with microorganisms under laboratory and natural conditions.

(1) I investigated how the initial surface properties of model microplastic particles affect their interactions with cells and showed that supposedly identical microplastic particles substantially differ in their properties. Here, it crystalized that especially the zeta-potential may be one of the driving factors in how the model microplastic particles interact with cells and, subsequently, of cellular responses. However, not only the initial surface properties of model microplastic particles may determine their interactions with cells, but additional surface alterations may contribute to a potential health risk deriving from microplastic pollution.

(2) Under natural conditions, organisms and humans are mainly not exposed to pristine model microplastic particles but rather to particles that were previously exposed to the environments. Here, biomolecules can attach to the surface of microplastic particles, forming an eco-corona. Therefore, in the

second topic of my PhD project, I addressed this aspect by analyzing if the environmental exposure of microplastic particles alters the particles' surface and whether this affects their interactions with cells. I showed for the first time that the coating of micrometre-sized microplastic particles with an eco-corona alters the physicochemical and mechanical properties of the particles. Furthermore, I was the first to show that this coating with an eco-corona enhances the particle-cell interactions and subsequent internalization of the particles, indicating that the eco-corona is acting like a trojan-horse facilitating the internalization into cells.

(3) Based on the knowledge I have obtained from the first two topics of my PhD thesis, I wanted to shed light on whether the surface properties of different polymer types lead to a different formation and composition of a biofilm on larger microplastic particles. I found distinct biofilm formations and compositions on different polymer types under laboratory and natural conditions, due to the different properties of the different polymer types. Therefore, my previous findings that the surface properties determine the interactions between particles and cells is also true for the complex formation of a biofilm. Finally, I propose that the differences in the biofilm composition lead to defined variations in Raman bands, which can be used as a spectral variation library, enabling the detection of microplastic particles in environmental samples without the time and cost-consuming purification protocols.

The work presented in my PhD thesis clearly and unanimously emphasises the importance of the surface properties of microplastic particles for their interactions with biota. The key message of my thesis is that in future experiments, the microplastic particles used in effect studies must be thoroughly characterized. Furthermore, I highly recommend using environmentally exposed microplastic particles coated with an eco-corona since the use of pristine particles may lead to an underestimation of the risk deriving from plastic pollution since pristine particles interact significantly less with cells compared to environmentally exposed particles.

Zusammenfassung

Die Verschmutzung von Ökosystemen mit Plastikpartikeln ist eine globale Herausforderung, die aufgrund ihrer Komplexität durch interdisziplinäre Forschung angegangen werden muss. Kunststoffpartikel wurden in allen Umweltkompartiment nachgewiesen, wo die Partikel letztlich mit ihrer Umgebung interagieren können. Diese Interaktion kann von der Anhaftung von Biomolekülen und Mikroorganismen an der Oberfläche eines Partikels über die Aufnahme durch Organismen bis hin zu deren Übergang mittels zellulärer Internalisierung von exponierten Organen in andere Gewebe reichen. Interessanterweise nimmt die Interaktion eines Organismus mit Kunststoffpartikeln mit abnehmender Partikelgröße zu. Daher wird dem so genannten Mikroplastik, das als Plastikpartikel mit einer Größe von weniger als 5 mm definiert ist, erhöhte Aufmerksamkeit geschenkt. Die reine Definition von Mikroplastik anhand seiner Größe ist jedoch viel zu vereinfacht, um seine potenziell schädlichen Auswirkungen auf die Umwelt, Organismen und die menschliche Gesundheit zu verstehen. Mikroplastik ist ein Oberbegriff für eine Vielzahl verschiedener Polymertypen, die jeweils spezifische und einzigartige Eigenschaften aufweisen. Die Bewertung der potenziellen Gefahren von Mikroplastik beruht jedoch derzeit auf der kontrollierten Exposition von Zellen und Organismen gegenüber Modellpartikeln aus Polystyrol (PS). Obwohl in verschiedenen Studien vermeintlich identische Partikel verwendet wurden, variierten die Ergebnisse enorm. Während in einigen Studien toxische Wirkungen auf Zellen und Organismen festgestellt wurden, berichteten andere, dass die Modell-Mikroplastikpartikel nicht toxisch oder nicht schädlich für Organismen sind. Da das Hauptmaterial der in den Effektstudien verwendeten Modell-Mikroplastikpartikel PS ist, sind die Unterschiede zwischen den berichteten Ergebnissen wahrscheinlich nicht auf das reine Polymer zurückzuführen, sondern müssen durch andere Partikeleigenschaften bedingt sein.

In meiner Doktorarbeit kombiniere ich drei miteinander verbundene Themen, die letztendlich alle auf eine übergeordnete Frage abzielen: Wie beeinflussen die Oberflächeneigenschaften von Mikroplastikpartikeln ihre Interaktion mit Zellen und Mikroorganismen? Die drei miteinander verbundenen Themen sind (1) wie die ursprünglichen Oberflächeneigenschaften die Reaktivität der Partikel gegenüber Zellen bestimmen, (2) wie die Umweltexposition die Oberflächeneigenschaften von Mikroplastikpartikeln verändert und ob dies die Reaktivität der Partikel gegenüber Zellen beeinflusst, und (3) ob die ursprünglichen Oberflächeneigenschaften von Mikroplastikpartikeln verschiedener Polymertypen ihre Reaktivität in Bezug auf ihre Interaktion mit Mikroorganismen unter Labor- und natürlichen Bedingungen bestimmen.

(1) Ich untersuchte, wie sich die ursprünglichen Oberflächeneigenschaften von Modell-Mikroplastikpartikeln auf ihre Wechselwirkungen mit Zellen auswirken und konnte zeigen, dass sich vermeintlich identische Mikroplastikpartikel in ihren Eigenschaften erheblich unterscheiden. Dabei kristallisierte sich heraus, dass vor allem das Zeta-Potential einer der treibenden Faktoren für die Interaktion der Modell-Mikroplastikpartikel mit Zellen und damit auch für die zellulären Reaktionen sein kann. Doch

nicht nur die ursprünglichen Oberflächeneigenschaften von Modell-Mikroplastikpartikeln können ihre Wechselwirkungen mit Zellen bestimmen, sondern auch zusätzliche Oberflächenveränderungen können zu einem potenziellen Gesundheitsrisiko durch Mikroplastikverschmutzung beitragen.

(2) Unter natürlichen Bedingungen sind Organismen und Menschen meist nicht reinen ursprünglichen Modell-Mikroplastikpartikeln ausgesetzt, sondern eher Partikeln, die zuvor in der Umwelt exponiert waren. Hier können sich Biomoleküle an die Oberfläche von Mikroplastikpartikeln anlagern und eine so genannte Öko-Korona bilden. Im zweiten Teil meines Promotionsprojekts untersuchte ich daher, ob die Umweltexposition von Mikroplastikpartikeln die Oberfläche der Partikel verändert und ob dies ihre Wechselwirkungen mit Zellen beeinflusst. Ich konnte als Erste zeigen, dass die Beschichtung von Mikroplastikpartikeln mit einer Öko-Korona die physikochemischen und mechanischen Eigenschaften der Partikel verändert. Darüber hinaus konnte ich erstmals zeigen, dass die Beschichtung mit einer Öko-Korona die Wechselwirkungen zwischen Partikel und Zelle und die anschließende Internalisierung der Partikel begünstigt, was darauf hindeutet, dass die Öko-Korona wie ein trojanisches Pferd wirkt, das die Internalisierung in Zellen erleichtert.

(3) Ausgehend von den Erkenntnissen, die ich in den ersten beiden Themen meiner Doktorarbeit gewonnen habe, wollte ich herausfinden, ob die ursprünglichen Oberflächeneigenschaften verschiedener Polymertypen zu einer unterschiedlichen Bildung und Zusammensetzung eines Biofilms auf größeren Mikroplastikpartikeln führen können. Ich fand unterschiedliche Biofilmbildungen und -zusammensetzungen auf verschiedenen Polymertypen unter Labor- und natürlichen Bedingungen, was auf die unterschiedlichen Eigenschaften der verschiedenen Polymertypen zurückzuführen war. Daher gilt meine frühere Feststellung, dass die Oberflächeneigenschaften die Wechselwirkungen zwischen Partikeln und Zellen bestimmen, auch für die komplexe Bildung eines Biofilms. Basierend auf diesen Ergebnissen zeigten wir, dass die Unterschiede in der Zusammensetzung des Biofilms zu definierten Variationen in den Raman-Banden führen können, die als Bibliothek für spektrale Variationen verwendet werden können und den Nachweis von Mikroplastikpartikeln in Umweltproben ohne die zeit- und kostenintensiven Reinigungsprotokolle ermöglichen.

Die in meiner Dissertation vorgestellte Arbeit unterstreicht eindeutig und einstimmig die Bedeutung der Oberflächeneigenschaften von Mikroplastikpartikeln für ihre Wechselwirkungen mit Biota. Die Kernaussage meiner Arbeit ist, dass in zukünftigen Experimenten die Mikroplastikpartikel, die in Effektstudien verwendet werden, gründlich charakterisiert werden müssen. Darüber hinaus empfehle ich dringend, umweltexponierte Mikroplastikpartikel zu verwenden, die mit einer Öko-Korona beschichtet sind, da die Verwendung von reinen Partikeln zu einer Unterschätzung des Risikos ausgehend von der Plastikverschmutzung führen kann, da reine Partikel im Vergleich zu umweltbelasteten Partikeln deutlich weniger mit Zellen interagieren.

List of Abbreviations

CP-AFM	Colloidal probe atomic force microscopy
EPS	Extrapolymeric substances
IgG	Immunoglobulin G
LC-MS/MS	Liquid chromatography-mass spectrometry/mass spectrometry
MTT	3-(4,5-dimethylthiazol-2-yl)-2,5-diphenyltetrazolium bromide
NMR	Nuclear magnetic resonance spectroscopy
PA	Polyamide
PCA	Principle component analysis
PE	Polyethylene
PET	Polyethylene terephthalate
PP	Polypropylene
PS	Polystyrene
PVC	Polyvinyl chloride
ROS	Reactive oxygen species
SEM	Scanning electron microscopy

General Introduction

Never before have the beneficial properties of plastic been so evident as in the time of the SARS-CoV-2 pandemic. Personal protective equipment like medical face masks and FFP-2 masks are made of plastic materials and are deposited after usage. Therefore, plastic materials help prevent infections and help treat infected patients who need ventilation due to a severe disease course. Even the development and production of vaccines would not have been possible in such a manner without sterile single-use plastic materials. Nevertheless, although the need for sterile medical plastic products and personal protective equipment tremendously increased during the pandemic, the medical sector still plays a minor role in the overall demand for plastic materials. In 2020, the sector with the highest share of the 367 million tons of plastic produced worldwide was the packaging sector, with 40.5% (Plastics Europe, 2021). One advantage of plastic packaging materials is the reduction of transportation costs and the extension of the shelf life of food items (Chemical Sciences and Society Summit, 2020; Robertson, 2016; White & Lockyer, 2020). These examples are only a few of many to highlight the favourable properties of the polymers.

Plastic is a hypernym of a plethora of polymers, each having specific and unique properties for specific applications. Amongst the most often produced synthetic polymer types in 2020 are Polyethylene (in low and high density, PE), Polypropylene (PP), Polystyrene (extruded and solid, PS), Polyvinyl chloride (PVC), and Polyethylene terephthalate (PET) (PlasticsEurope, 2021). In general, plastics are lightweight, have high plasticity and durability with relatively low production costs, leading to an increased demand for plastic products (Barnes et al., 2009) and, therefore, mass production. As soon as a plastic product is no longer needed, it is often disposed of. Although the circular economy of plastic materials is gaining more and more attention (World Economic Forum, 2016), there is still a non-negligible share of plastic directly entering the environment. Besides the intentional release into the environment or the disposal of plastic waste into uncompacted pits and landfills, the improper treatment of wastewater (GESAMP, 2016) or tyre abrasion (Knight et al., 2020; Kole et al., 2017; Verschoor et al., 2016) are sources of plastic waste. Here, the properties of the plastic materials mainly define their fate in the environment. For instance, the high durability of plastic materials turns into an environmental problem since this property conversely leads to the accumulation of plastics in the environment.

Since the early 1970s, when one of the first studies on plastic waste in the marine environment was published (Carpenter & Smith, 1972), the monitoring of plastic pollution steadily increased, resulting in the fact that plastic is everywhere. Plastic was detected in all environmental compartments, from the marine (Andrady, 2011; Carpenter & Smith, 1972; Thompson et al., 2004) and limnetic (Dris et al., 2015; Imhof et al., 2013; Piehl et al., 2019) to the terrestrial compartment (Möller et al., 2020; Piehl et al., 2018) and even in the atmosphere (Dris et al., 2016; Gasperi et al., 2015, 2018; Kernchen et al., 2021; C. Liu et al., 2019; Stanton et al., 2019; Vianello et al., 2019). However, the occurrence of plastic pollution does not necessarily correlate with direct anthropogenic activities since plastics were found

in remote regions like islands (Imhof et al., 2017), the poles (Lacerda et al., 2019; Ross et al., 2021), and even in the deep sea (Woodall et al., 2014). Although the methods for monitoring plastic pollution are constantly developing and improving (Möller et al., 2020; O'Connor et al., 2019), we are still far from understanding the extent of the actual amount and concentrations of plastic materials occurring in nature.

Plastics in the environment are usually classified by size, shape, and polymer type. Larger plastic items are defined as macroplastics (> 20 mm) and followed by mesoplastic (20 – 5 mm) (Barnes et al., 2009). The study of Thompson et al. (2004) first described plastic particles of microscopic size, which was the starting point of focussing on the so-called microplastic particles. However, almost two decades later, there is still no official definition of the actual size range of microplastics. Arthur et al. (2009) defined a highly accepted and used upper size limit of 5 mm. Since then, many improvements in sampling and analysing smaller particles have been established, but there is still no definition for the actual lower size limit. It has mostly been set between 1 to 20 µm (Frias & Nash, 2019), which also depends on the scope of the study. In my PhD thesis, I will refer to the lower size limit of 1 µm for microplastic particles.

Next to size, microplastic particles found in the environment can be differentiated into primary and secondary microplastic particles. Primary microplastics are intentionally produced in small sizes, like raw pellets or particles added to cosmetics. Secondary microplastic results from the fragmentation of larger plastic items (Barnes et al., 2009; GESAMP, 2016) or tyre abrasion particles (Knight et al., 2020; Sommer et al., 2018). The mechanisms of fragmentation that have been described most frequently in the literature and are therefore of high evidential value are mechanical fragmentation, UV radiation, oxidation and hydrolysis (Barnes et al., 2009; Gerritse et al., 2020; Meides et al., 2021, 2022). Those processes lead to the leaching of additives and shortening of the polymer chains, eventually making them brittle and releasing particles in the micro-and nanometre size range (Gerritse et al., 2020). In this context, Meides et al. showed that the fragmentation of PS is a two-stage process, where photooxidation at the near-surface layer is the first step, followed by microcrack formation and particle rupturing, eventually releasing a multitude of even smaller particles (Meides et al., 2021). However, since the various polymer types with their unique initial properties may have different mechanisms of fragmentation, it is undeniable that microplastics occur as a highly heterogeneous group in the environment, making it challenging to draw generally valid conclusions. Here the properties of the microplastic particles, like their density and broad size range, determine their occurrence in natural habitats and consequently allow the interaction of different organisms with the particles.

Interaction of Organisms with Microplastic Particles

Among the more obvious and well-described direct effects of plastic pollution is the entanglement in lost fishing gear leading to injuries or immobility, and the ingestion of plastic items leading to a false feeling of satiation and starvation (Laist, 1997). Furthermore, with decreasing sizes, the potential risks

deriving from particulate matter increase (Anbumani & Kakkar, 2018; Jeong et al., 2016; Khadka et al., 2014), which makes microplastic particles available to a wide variety of organisms, ranging from uni-cellular organisms (Bulannga & Schmidt, 2022) to invertebrates (Brehm et al., 2022; Browne et al., 2008; Desforges et al., 2015; Devriese et al., 2015), up to vertebrates (Lu et al., 2016).

The main entry pathways for microplastics into the body are via inhalation and ingestion (Wright & Kelly, 2017). Upon uptake of microplastic particles, one potential risk is the translocation from the primarily exposed organs into surrounding tissues. The translocation of microplastic particles was already indicated more than a decade ago for marine mussels (Browne et al., 2008; von Moos et al., 2012). Since then, the evidence of microplastic particles translocation into tissues has increased since it has been shown in various species, ranging from invertebrate (Brehm et al., 2022; Browne et al., 2008; Messinetti et al., 2019; von Moos et al., 2012) up to vertebrate species (Zeytin et al., 2020), including mammals (Fournier et al., 2020; Hodges et al., 1995; Z. Liu et al., 2022). After administring PS model nanoplastic particles into the lung (Fournier et al., 2020) or gastrointestinal system (Liu et al., 2022) in mammals, the translocation was not only observed in other tissues (Liu et al., 2022) but even across the placental barrier and consequently are present in the foetal tissue which may impact the health of the offspring after birth (Fournier et al., 2020). The observation that plastic particles can translocate into tissues is not only true for laboratory experiments using model microplastic particles. For example, Barboza et al. (2020) showed microplastic particles in the dorsal muscel of three wild fish species. This finding is highly interesting since particles in the environment are substantially different to pristine model microplastic particles mainly used in laboratory experiments. To date, it is not understood how the microplastic particles used in laboratory studies or under natural conditions can overcome biological barriers leading to their translocation and fate within an organism. Besides the size of the particles, their initial surface properties and surface alterations due to environmental exposure may play a decisive role in particle uptake and tissue translocation. For instance, it has been shown that the environmental exposure alters the surface of a particle that consequently leads to enhanced ingestion by organisms (Hodgson et al., 2018; Vroom et al., 2017). The authors suggest that the enhanced ingestion is due to a higher palatability of the particles due to the coating with a biofilm (Hodgson et al., 2018; Vroom et al., 2017).

Formation and Composition of a Biofilm on Microplastic Particles

By definition, a biofilm is a community of microorganisms releasing extracellular polymeric substances (EPS) to attach to different surfaces. It can consist of either single-microbial species, e.g. infections, or multiple microbial species predominantly occurring in natural environments (O`Toole et al., 2000). A biofilm can develop in any environment that provides a moist surface (Sutherland, 2001), including plastics in the environment (Lobelle & Cunliffe, 2011; Oberbeckmann et al., 2015; Rummel et al., 2017). The surface properties of the substratum play a decisive role in microbial colonisation with enhanced colonisation for rough, hydrophobic and non-polar surfaces (Donlan, 2002). Most plastic materials

show hydrophobic surfaces (Leeden & Frens, 2002; Zettler et al., 2013), further facilitating biofilm formation. Biofilm development is mainly described as occurring in five successive steps (O`Toole et al., 2000; Renner & Weibel, 2011). First, microorganisms reversibly attach to surfaces via pili, flagella, or membrane proteins and further extrude EPS, which initiates the second step of biofilm formation. The EPS mainly consists of water, secreted proteins and polysaccharides, DNA and RNA, ions, and particulate matter like detritus from the surrounding environment (Sutherland, 2001). At this point, microorganisms have already irreversibly attached to the surfaces, proliferate, form smaller colonies, and release additional EPS within the third step. The ongoing proliferation leads to the formation of three-dimensional structures, described as the fourth step: the maturing of a substantial biofilm. Lastly, cells can detach from the biofilm again and colonise newly available surfaces (O`Toole et al., 2000; Renner & Weibel, 2011b). At the beginning of my PhD project little was known about the biofilm formation on microplastics particles, especially in freshwater environments. Particularly if the initial surface properties of different polymer types determine the formation and composition of a biofilm was not in the focus in microplastic research. But why is it important to investigate the biofilm formation on microplastic particles?

A biofilm's formation on a microplastic particles' surface tremendously changes its properties, leading to different environmental behaviour. For instance, it has been shown that marine biofilms on plastics can inhabit algae species associated with alga blooms or the presence of Vibrio, a human pathogenic bacteria (Kirstein et al., 2016a; Zettler et al., 2013). Furthermore, plastic particles are transported passively within the environment, which means that associated biofilms are transported between different environments leading to a potential increase in invasive species (Gregory, 2009). However, a plastic particle coated with a biofilm is not only transported between different environments but also within a single environment. A positive buoyant particle coated with a biofilm starts to sink in the water column due to a heavier weight (Semcesen & Wells, 2021), making the particle available to a range of aquatic organisms (Imhof et al., 2013). As already mentioned, the biofilm on the surface of a particle can lead to a higher likelihood of being ingested (Hodgson et al., 2018; Vroom et al., 2017), consequently increasing the bioavailability of microplastic particles.

Earlier in this thesis, I described the potential of a microplastic particle to translocate from a primarily exposed organ to other tissues and the circulatory system. However, translocation is only possible for particles in the lower micrometre size range and even smaller. Forming a biofilm on a single particle of such small size is impossible, as bacteria are in the same size range as the particles themselves and, therefore, unable to attach. However, the surfaces of particles in the micrometre size range are also altered due to environmental exposure. Here, the surface alterations can be anything from simple changes in functional groups (Mao et al., 2020) to the coating with very complex biological matrices, like eco-coronas (Galloway et al., 2017; Sutherland, 2001). At the beginning of my PhD project, it was discussed whether these surface alterations may affect the particles' reactivity towards cells. To understand how the alterations of the surface properties of a particulate matter may determine its reactivity

towards cells, some basic understanding of a corona-formation is essential, which will be summarized in the following.

Formation of an Eco-corona on small Microplastic Particles

Most of the findings on the formation of coronas on particle surfaces originate from nanomaterial sciences. Those studies mainly used biological media, like blood or serum from a single organism (Lundqvist et al., 2008, 2011; Tenzer et al., 2011, 2013) or well-defined culture media (Fadare et al., 2020; Nasser & Lynch, 2016). The obtained coronas on the nanoparticle surfaces consisted of up to 300 proteins and were consequently defined as protein coronas (Tenzer et al., 2013). Several material properties, like their size and bio-physicochemical surface properties, are essential for developing a corona. The surface of a particle has higher free energy than the bulk material itself, which means that biomolecules from the surrounding media will progressively and selectively adsorb to the surface of a particle (Lundqvist et al., 2008; Monopoli et al., 2012). With increasing nanoparticle size, the thickness of a corona was found to increase, probably due to the curvature of smaller particles that may cause a decrease in the binding of larger substances (Nasser et al., 2019). Functionalized nanoparticles show a size-dependency in the corona composition since only 50% of the proteins were shared between two different sizes (100 and 50nm). In contrast, plain particles, meaning no additional surface functionalization, of the same sizes shared 80% of the adsorbed proteins (Lundqvist et al., 2008). Tenzer et al. (2011) conclude that particle size rather quantitatively than qualitatively affects the protein corona since no mechanisms were described where size alone allows or completely abolishes the binding of specific proteins.

Within less than half a minute, the first proteins attach to a nanoparticle surface, and the amount of proteins increases with increasing incubation time (Tenzer et al., 2013). With time a so-called hard corona emerges, consisting of proteins with high binding affinities. On top of the hard corona, loosely bound proteins develop a soft corona which is in constant exchange with surrounding biomolecules (Lundqvist et al., 2008, 2011; Monopoli et al., 2012). Although the whole protein corona, the hard and the soft corona, is not a static but rather highly dynamic system, initial bound proteins stay as a fingerprint of the coronas' history even after the particle enters a different compartment (Lundqvist et al., 2011).

Once a particle is released into the environment, the surrounding media is much more complex than in experimental setups. It hosts different pro-and eukaryotes, conditioning the media with metabolites (Nasser et al., 2019). As a result, a particle released into this soup of organic matter faces a plethora of different biomolecules (Nasser et al., 2019), consequently coating the particle with a so-called conditioning film (Cooksey & Wigglesworth-Cooksey, 1995; Loeb & Neihof, 1975; Lorite et al., 2011; Rummel et al., 2017). The often unknown biomolecules occurring within the environmental media make identifying the constituents of the coating challenging. In literature, the term eco-corona was

established for the initial conditioning film on microplastic particles in the environment (Galloway et al., 2017; Nasser et al., 2019; Nasser & Lynch, 2016), to which I will refer to in the following. So far, the components of an eco-corona were described as proteins, humic and fulvic acids, amino acids, lipids, polysaccharides and carbohydrates (Galloway et al., 2017; Pulido-Reyes et al., 2017; Rummel et al., 2017).

These surface alterations may eventually change the particles' identity, altering the reactivity of the particles towards organisms, tissues, and cells (Albanese et al., 2014; Monopoli et al., 2012; Nasser & Lynch, 2016; Pulido-Reyes et al., 2017; Walkey et al., 2012) and are therefore essential to consider in ecotoxicological studies (Nasser et al., 2019). However, the question remains how the surface alterations due to the coating with an eco-corona may eventually alter the particles reactivity towards cells. Therefore, in the following I will describe the basic mechanisms how a particle can interact with cells and tissues.

Interactions of Microplastic Particles with Tissues and Cells

There are basically two pathways of how particulate matter can translocate across biological barriers, the para- and transcellular pathways. The paracellular pathway describes the transport in between cells, like through intercellular spaces and tight junctions (Carr et al., 2012). However, this pathway is restricted to molecules or small particulate matter in the nanometre size range (Carr et al., 2012; Fröhlich, 2012). The transcellular pathway is the direct interaction of a single cell with particulate matter and the subsequent cellular internalization. Here, cellular internalization can be subdivided into two steps: Within the first step, the surface of the particle interacts with the cell either by binding to cellular receptors (Aderem & Underhill, 1999) or by unspecific (e.g. electrostatic) interactions with the cell membrane (Forest et al., 2015). Upon adhesion to the cellular membrane, a particle can be internalised by various mechanisms. Among the different endocytosis mechanisms, phagocytosis and macropinocytosis are the ones which are relevant for micron-sized particles (Doherty & McMahon, 2009). Both phagocytosis and macropinocytosis are actin-dependent mechanisms (Aderem & Underhill, 1999; Canton, 2018). Phagocytosis is initiated by the interaction of ligands on the surface of a particle with specific receptors on the cellular membrane (Aderem & Underhill, 1999). A tight-fitting sleeve around a particle is formed through this direct interaction (Kerr & Teasdale, 2009). On the other hand, Macropinocytosis is not regulated directly through the interaction of a ligand associated with the particle surface and a membrane receptor but rather indirectly by the activation of receptor tyrosine kinases by different growth factors. This activation leads to a global increase in actin polymerisation at the cell surface and consequently forms membrane ruffles (Kerr & Teasdale, 2009). The process of macropinocytosis leads to a more fluid and loosely attached membrane surrounding the engulfed particle. The different mechanisms of endocytosis for micrometre-sized particles already highlights that the surface properties of a particle seems to be highly relevant for particle-cell interactions.

Interestingly, the cellular internalization and the intracellular transport of particulate matter have been studied since the 1960s using model microplastic particles, mainly PS and latex spheres (Korn & Weisman, 1967; Weisman & Korn, 1967). Since then, numerous commercial sources providing mono-disperse model particles have been established on the market. Here it has to be noted that the commercial availability of a huge size range of the PS model microplastic particles has led to frequent use in cytotoxicity and ecotoxicology studies investigating the potential effects of microplastic particles on the ecosystem, organismal and human health. Although the model microplastic particle may be suitable for understanding basic interaction mechanisms with particles and cells, they are not representative of microplastic particles in nature. Microplastic particles that occur in the environment, which consequently can be taken up by organisms allowing the particles to interact with cells, are unspecifically coated with an eco-corona. The coating with an eco-corona makes the environmentally exposed microplastic particles substantially different from the pristine surface properties of model microplastic particles. The biomolecules of an eco-corona, such as proteins, could possibly take over the function as a ligand, leading to a specific interaction with cell membrane receptors and thus initiating the internalization process. Nevertheless, due to the synthesis of the model microplastic particle, functional groups (e.g. carboxylic or amin groups) appear on their surfaces, allowing unspecific interactions with cellular membranes. Although the monodisperse particles available on the market supposedly have similar properties, the composition and distribution of the functional groups on the surface of model particles may be different due to the synthesis method, which consequently could lead to differences in their interactions with cells. Here it has to be noted that the reported results regarding the potential effects of microplastic particles using the beforementioned model particles were inconsistent. While some studies found toxic effects on cells and organisms, others reported that the model microplastic particles were non-toxic or not harmful to organisms.

At the beginning of my PhD thesis it has neither been investigated if the initial surface properties of model microplastic particles differ, nor if the environmental exposure of microplastic particles leads to the formation of an eco-corona. Furthermore, a systematic approach to evaluate the importance of the physicochemical properties of both pristine and environmentally exposed model microplastic particles for particle-cell interactions was missing.

Objectives of this thesis

My PhD thesis consists of three interrelated topics that, in the end, all address one overall question: How do the surface properties of microplastic particles affect their interaction with cells and microorganisms? I formulated several objectives to find answers to the very broad and open question. First, I investigated how the initial surface properties of model microplastic particles affect their interactions with cells and if these properties differ in supposedly identical particles. Second, I analyzed for the first time if the environmental exposure of microplastic particles alters the particles' surface and whether this affects their interactions with cells. Third, since the surface properties of the pristine particles already have a tremendous effect on how they interact with cells, I investigated if this finding exceeds to the biofilm formation and if we can take advantage of polymer-specific biofilm compositions for microplastic identification.

Hypothesis 1: The surface properties of model microplastic particles determine their interactions with cells

<u>1st objective</u>

Since microplastic particles can still be seen as a relatively new environmental stressor, little is known about their physico-chemical properties and how these may affect their potential toxicity. However, to not reinvent the wheel, it makes sense to take advantage of the extensive research conducted on other particulate matter. **Therefore, the 1st objective of my PhD project was to perform a comprehensive literature review on what is already known about the property-related effects of other particulate matter and how we potentially can transfer this knowledge to microplastic particles (Article 1).**

<u>2nd objective</u>

To date, microplastic particles used for effect studies have mainly been categorised by polymer type, shape, and size, while their physicochemical surface properties were hardly considered. Although supposedly the same model microplastic particles was used in effect studies, there have been contradictory statements, with some studies showing adverse effects and others showing none or very little. **Therefore, the 2nd objective of my thesis was to unravel if there are differences in the surface properties of supposedly the same model microplastic particles and whether this may lead to differences in the cellular responses (Article 2).**

<u>3rd objective</u>

From the first two objectives, I have learned that one of the main drivers a particle interacts with cells is the particles' zeta-potential. However, a systematic approach was missing for measuring the correlation of the zeta-potential and the particle adhesion to the cell membrane and subsequent internalization. **Therefore, the 3rd objective of my thesis was to systematically analyse how the zeta-potential of pristine, functionalized and environmentally exposed model microplastic particles affect their interactions with cells in (Article 3).**

Hypothesis 2: The environmental exposure alters the surface properties of microplastic particles and their interactions with cells

<u>4th objective</u>

The first three objectives of my PhD thesis mainly focused on pristine model microplastic particles and their interactions with cells. However, the microplastic particles in the environment do not have a pristine surface but are coated with an eco-corona. At the beginning of my PhD thesis, nothing was known about the surface alterations of micrometre-sized microplastic particles due to environmental exposure. **Therefore, the 4th objective of my thesis was to investigate the formation of an eco-corona on the surface of microplastic particles and if the eco-corona alters the particle-cell interactions and subsequent particle internalization (Article 4).**

<u>5th objective</u>

It is essential to analyze the physico-chemical properties of an environmentally exposed microplastic particle as precisely as possible to understand their interactions with cellular membranes. Next to the physico-chemical characteristics of an eco-corona, the mechanical properties may also be a detrimental factor for particle-cell interactions. **Therefore, the 5th objective of my PhD thesis was to understand the mechanical properties of environmentally exposed microplastic particles (Article 5).**

<u>6th objective</u>

I showed that the environmental exposure and, therefore, the coating with an eco-corona of a microplastic particle significantly affects their interactions with cells. However, which internalization mechanisms may be involved in the endocytosis process was not understood. **Therefore, the 6th objective, was to shed light on which basic cellular internalization mechanisms occur for microplastic particles coated with an eco-corona compared to their pristine counterparts (Article 6).**

<u>7th objective</u>

The main question from the public, stakeholders and policymakers is whether microplastics harm humans. However, since microplastic is a group of different particles with many different properties that consequently determine their potential effects, it is impossible to answer this question with sufficient scientific evidence. There is still some lack of knowledge regarding the exposure pathways of humans to microplastics, the potential translocation mechanisms of microplastics and their fate within human tissues. **Therefore, the 7th objective was to contribute closing this knowledge gap by reviewing the existing literature on the exposure pathways and setting a particular focus on the factors determining the tissue translocation of microplastics and whether this matches with found microplastic particles in the fate studies (Article 7).**

Hypothesis 3: The initial surface properties of polymers determine their interactions with microorganisms

<u>8th objective</u>

In the former objectives of my PhD thesis, I highlighted the importance of the surface properties of pristine and environmentally exposed microplastic particles for cellular internalization. However, besides the microplastic particles in the micrometre size range, larger particles of hundreds of micrometres up to millimetres interact with their surroundings in different environments. The extent to which the surface properties of microplastics play a role in their interaction with microorganisms has been little studied to date. **Therefore, the 8th objective was to understand how the initial surface properties of different polymer types determine the early-stage biofilm formation (Article 8).**

<u>9th objective</u>

To study the time-dependent biofilm formation on microplastic particles, laboratory conditions are favourable to understanding the underlying mechanisms. Since in Article 8, I was able to show a polymer and time-specific development of an early-stage biofilm, the question arises whether this is also true in natural environments. **The 9th objective was to understand if the direct exposure of different polymer types in a small freshwater stream leads to polymer-specific microbial biofilm compositions (Article 9).**

<u>10th objective</u>

To date, the isolation and subsequent identification of microplastic particles from environmental samples is time- and cost-intensive. The organic material must be removed from the environmental sample to allow the identification of the polymer types with particle-based analytical techniques, e.g. Raman spectroscopy. However, in the 8th and 9th objectives of my thesis, I was able to show that there are polymer-specific microbial biofilm development and compositions. **Therefore, the 10th objective was to develope a Raman library of spectral variances due to the polymer-specific coating with a biofilm, enabling the detection of a polymer coated with a biofilm without the time- and cost-intensive sample pre-processing (Article 10).**

Summary of the articles – Hypothesis I

Hypothesis 1: The surface properties of model microplastic particles determine their interactions with cells

<u>Objective 1:</u> Extensive literature review on what is already known about the property-related effects of other particulate matter and how we potentially can transfer this knowledge to microplastic particles

Article 1: From Properties to Toxicity: Comparing Microplastics to Other Airborne Microparticles

The term microplastics summarizes a plethora of different polymer types of different sizes, shapes and physicochemical surface properties. Understanding the potential polymer-related adverse effects would require many experiments combining all the different properties with different sizes and shapes. To date, such data is not available, making it difficult to assess the risk associated with microplastics. Since performing experiments of all possible combinations is not practical, we aimed to identify the most critical properties of particle toxicity. Therefore, I contributed to an interdisciplinary review article where we reviewed the literature on well-studied airborne particulate contaminants that are frequently associated with health risks and classified as hazardous materials, such as asbestos, soot, or wood dust. We identified essential parameters like particle size, shape, surface charge, eco- and bio-corona, and the particles' biopersistence being the main drivers for particle toxicity. By comparing the obtained information to existing knowledge on microplastics toxicity, we provide the basis for a mechanistic understanding of microplastics toxicity.

As a main result, we identified that the greatest adverse effects from microplastics potentially derive from very small (with a diameter smaller than 10 μm) particles and that surface alteration like ageing or the coating with an eco-corona can further accelerate their likeliness of toxicity. We furthermore outlined future directions for the research on microplastic toxicity. For instance, the microplastic particles used in an experimental setup should be characterized as well as possible. Here, the zeta-potential of a particle is a comparably ease-to-measure surface property and is highly recommended to be performed as a proxy of the particles' reactivity towards its surrounding, including cells. The use of well-defined microplastic particles in effect studies will eventually allow conclusions about the main driver of the particles' toxicity, similar to the other airborne particles described in the review article. Consequently, understanding the main drivers of toxicity will enable effective policymaking for finding solutions for the ongoing discussion on microplastic particle pollution and its' potential adverse effects on the environment, organisms and eventually human health.

Authors: Simon Wieland, Aylin Balmes, Julian Bender, Jonas Kitzinger, Felix Meyer, **Anja F. R. M. Ramsperger**, Franz Roeder, Caroline Tengelmann, Benedikt H. Wimmer, Christian Laforsch#, Holger Kress#

shared senior author

Own contribution: conceptualization, literature research, manuscript writing (section airborne micro-plastics 3.1-3.3), revision and finalization of the manuscript.

Author contributions as stated in the published version: H.K. initiated the article. All authors contributed to the conceptualization of the article. H.K., C.L., and S.W. supervised the writing process. S.W., C.T., and BH.W. wrote the introduction, C.T. wrote Section 2.1, F.M. Section 2.2, J.K. Section 2.3, J.B. Section 2.4, A.B. Sections 2.5 and 2.6, AFRM.R. and S.W. Section 3. S.W. wrote Section 4 with the help of F.R., and S.W. wrote the conclusions. All authors reviewed the manuscript and contributed to its finalization. J.B. designed the graphical abstract. S.W. designed Figs. 1 and 2 and performed the SEM preparation and imaging.

<u>Objective 2:</u> Unravelling differences in the surface properties of supposedly the same model micro-plastic particles and whether this may lead to differences in the cellular responses

Article 2: Supposedly Identical Microplastic Particles Substantially Differ in their Material Properties Influencing Particle-Cell Interactions and Cellular Responses

Rozman & Kalčíková (2022) stressed in their comprehensive review that the majority of studies used pristine PS microplastic particles with spherical shapes and sizes between 1-50 µm and only half of the microplastic effect studies took the effort to measure the particles' physicochemical properties. Regarding effect studies on a cellular level, this is even more pronounced. For example, Stock et al. (2021) just recently stressed that "(…) all existing studies dealing with microplastic uptake and toxicity exclusively used spherical, monodisperse model polystyrene particles.". Interestingly, although the numerous studies investigating the potential effects of microplastics used supposedly identical PS particles, the results show a large discrepancy, with some studies showing adverse effects and others showing none or very little. For instance, in toxicity studies of micro-and nanoplastics in mouse models, Stock et al. (2019) did not reveal histologically detectable lesions or significant signs of inflammatory responses after feeding mice with 1, 4 and 10 µm-sized PS microplastic particles. However, other studies also using PS model microplastic particles did observe severe effects on the gastrointestinal system, liver pathologies like inflammatory responses or lipid accumulation using similarly sized particles of 0.5, 5 and 50 µm (Deng et al., 2017; L. Lu et al., 2018; Luo et al., 2019). These inconsistencies further exceed to *in vitro* cell models. Some studies observed little or no cytotoxicity for PS particles (Hesler et al., 2019; Rudolph et al., 2021; Stock et al., 2019), whereas other studies showed significant cytotoxicity (Prietl et al., 2014; Wu et al., 2019).

I hypothesized that these discrepancies originate from the fact that nominally identical particles from different commercial sources substantially differ in their physico-chemical material properties and, consequently, their particle-cell interactions and cytotoxicity. We conducted an in-depth characterization of nominally identical plain PS particles of 3 µm in diameter from two different commercial sources. NMR-spectroscopy revealed significant differences in the particle's monomer content, and colloidal-probe atomic force microscopy (cp-AFM) depicted different surface charge densities leading to different zeta-potentials. The significantly different surface characteristics of the two particle types significantly alter the number of particle-cell-interactions and subsequent internalization by two murine macrophage cell lines. Additionally, cytotoxic effects are correlated to the particles´ properties since cells exposed to particles with a higher negative zeta-potential, and a higher monomer content decreased cell metabolism and proliferation.

My study was the first to show that nominally identical particles from different commercial sources tremendously differ in their properties, explaining the varying results in effect studies on microplastics. We highlight that an in-depth material characterization of microplastics is needed to obtain comparable

results in toxicology and therefore contributes significantly to assessing risks derived from microplastics. Furthermore, we emphasize that no general statements can be made about the effects of microplastics per se, not even for the same type of polymer in the same size class.

Authors: **Anja F. R. M. Ramsperger***, Julia Jasinski*, Matthias Völkl*, Thomas Witzmann, Marcel Meinhart, Valerie Jèrôme, Winfried P. Kretschmer, Ruth Freitag, Jürgen Senker, Andreas Fery, Holger Kress, Thomas Scheibel and Christian Laforsch

* shared first authorship

Own contribution: conceptualization and study design, experiments (particle-cell interactions and cellular internalization), data analysis and figures, interpretation and discussion of results, manuscript writing, revision and finalization.

Author contributions as stated in the published version: AFRM.R., J.J., M.V., V.J., R.F., J.S., A.F., H.K., T.S. and C.L. designed the experiment. AFRM.R., J.J., M.V., T.W., M.M., V.J., WP.K., R.F., J.S., A.F., H.K., T.S., and C.L. wrote the manuscript. All authors contributed to the interpretation and discussion of the results. J.J. conducted the ζ-potential measurements, DLS measurements and SEM analysis of the cells and particles. M.M. and WP.K. conducted the GPC, EDX and NMR experiments. T.W. conducted the CP-AFM measurements. AFRM.R. conducted the cellular internalisation experiments. M.V. conducted the MTT and cell proliferation experiments.

<u>Objective 3:</u> Systematic analysis of how the zeta-potential of pristine, functionalized and environmentally exposed model microplastic particles affects their interactions with cells

Article 3: Nominally identical microplastic models differ greatly in their particle-cell interactions

In literature, it has been described that the zeta-potential plays a decisive role in particle-cell interactions (Fröhlich, 2012; Jeon et al., 2018; Silva et al., 2014). When working on the 1st and 2nd objectives, it became evident that the zeta-potential is one of the main drivers for microplastic particle-cell interactions. However, the influence of the zeta-potential of nominally identical microplastic particles from commercial sources on the particle-cell interactions has not been systematically studied. Differences in the zeta-potential of nominally identical model microplastic particles may determine the experimental outcome. Understanding the underlying mechanisms of particle-cell interactions is an integral step in evaluating the potential toxicity of microplastics.

In article 3, a quantitative and highly multiplexed approach to investigate the role of the zeta-potential of nominally identical PS model microplastic particles from eight different manufacturers for particle-cell adhesion and internalization is described. Here, we developed a microfluidic microscopy platform that uses convolutional neural networks for digital image processing to measure the adhesion strength of the particles to cellular membranes. We demonstrated that the particle-cell adhesion strength and the absolute internalization probability increase by multiple orders of magnitude with the increasing zeta-potential. Furthermore, microplastic particles that eventually interact with cells and tissues under realistic scenarios are most probably not pristine model microplastic particles but are coated with biomolecules from the environment. Therefore, we included microplastic particles coated with an eco-corona in the analysis and also found a strong correlation between the particles' zeta-potential and their interactions with cells.

Our results highlight that each nominally identical microplastic particle from any commercial source substantially differed in its properties, leading to different particle-cell interactions. Thus, I can further substantiate that one possible reason for the contradictory results in effect studies is the physico-chemical properties of nominally identical particles from different manufacturers. Therefore, I highlight that it is of utmost importance to thoroughly characterise the microplastic particles used in effect studies, regardless of whether they are pristine or environmentally contaminated particles. Otherwise, statements about microplastic particles' cytotoxicity cannot be made sufficiently.

Authors: Simon Wieland *, **Anja F. R. M. Ramsperger***, Wolfgang Gross*, Moritz Lehman, Thomas Witzmann, Stephan Gekle, Günter Auernhammer, Andreas Fery, Christian Laforsch#, Holger Kress#

* shared first authorship   # shared senior author

Own contribution: conceptualization and study design, experiments (microplastic particle incubation, sample preparation for zeta-potential measurements, cell experiments regarding particle-cell interactions and internalization), data analysis, interpretation and discussion of results, manuscript writing, revision and finalization of the manuscript.

Author contributions as stated in the manuscript version: H.K., C.L., W.G., A.F.R.M.R. and S.W. initiated the research. H.K., C.L., A.F., G.K.A., W.G., A.F.R.M.R. and S.W. planned the research. W.G., M.L., S.G. and H.K. developed the microfluidic method. S.W., A.F.R.M.R., W.G., T.W., A.C., and M.O. performed the experiments. W.G., A.F.R.M.R., and S.W. wrote the draft of the manuscript. All authors revised and edited the manuscript.

Summary of the articles – Hypothesis II

Hypothesis 2: Environmental exposure alters the surface properties of microplastic particles and their interactions with cells

Objective 4: The formation of an eco-corona on the surface of microplastic particles and which role the eco-corona plays in particle-cell interactions and subsequent particle internalization

Article 4: Environmental exposure enhances the internalization of microplastic particles into cells

At the beginning of my PhD project, the interactions of microplastic particles with tissues and cells were only carried out with the described model microplastic particles. These model microplastic particles are often fluorescently labelled or functionalized. In objective 3, we highlighted that particles' functionalization and environmental exposure tremendously affect the particles' interactions with cells. Here, I want to focus on microplastic particles coated with an eco-corona since they differ substantially from model microplastic particles and resemble those occurring in nature.

To that date, we were not aware of any published methods to reliably get an eco-corona on the surfaces of micrometre-sized microplastic particles. Since the particles were that small (3μm), exposing them to nature was not feasible. For instance, incubating the particles in net cages would either mean that the particles would get lost, contaminating the environment, or the mesh or pore sizes would be too small to allow microorganisms or biomacromolecules to enter the space where the particles were located. Therefore, I decided to use glass vials to incubate the particles directly in the media and refreshed the incubation media three times a week to allow a healthy and diverse microorganismal community within the media. To investigate whether the coating of the particles with an eco-corona was successful, we performed a thorough analysis using SEM, micro-Raman spectroscopy and X-ray photoelectron spectroscopy. With all three techniques, we could show the presence of biomolecules on the surface of microplastic particles exposed to fresh- and salt water. However, we did not detect any signs of biomolecules on the surfaces of non-environmentally exposed pristine particles (negative control particles incubated in ultrapure water) without an eco-corona.

Fluorescence microscopy combined with fluorescently labelled microplastic particles was used to investigate particle-cell interactions. However, microplastic particles from the environment are usually not fluorescent, which consequently presents methodological difficulties for particle detection with standard fluorescence microscopy. Therefore, to be able to distinguish whether a particle has been internalized by a cell or only binds to the cell membrane, I chose the path of fluorescently labelling the filamentous actin of the cells. This approach enabled identifying environmentally exposed particles internalized by cells where the filamentous actin is surrounding the particle.

Finally, I analyzed whether microplastic particles coated with an eco-corona interact differently with cells than pristine microplastic particles. As this is a hitherto unexplored aspect and a sensitive topic, I worked with a high number of replicates. I incubated the microplastic particles either in fresh- or salt water to obtain an eco-corona on the surface of the particles. Furthermore, I used different control particles (particles incubated in ultrapure water or functionalized particles coated with antibodies) to understand the effect on microplastic particle-cell interactions and cellular internalization originating from the eco-corona.

I showed for the first time that microplastic particles coated with an eco-corona significantly more often interacted with and became internalized by cells than their pristine counterparts. My results indicate that environmentally exposed microplastic particles may pose more of a health risk to organisms that ingest these particles than pristine particles usually used in effect studies. The results of this study allow us to obtain a comprehensive picture of microplastic internalization by cells, which, in turn, will be indispensable for identifying how microplastic exposure might affect organisms in polluted environments.

Authors: **Anja F. R. M. Ramsperger**, Vinay K. Bangalore-Narayana, Wolfgang Gross, John Mohanraj, Mukkundan Thelakkat, Andreas Greiner, Holger Schmalz, Holger Kress[#] and Christian Laforsch[#]

[#] shared senior author

Own contribution: Conceptualization and study design, experiments (experiments on eco-corona formation, particle-cell interactions and cellular internalization, sample preparation for SEM, XPS, Raman), data analysis and figures, interpretation and discussion of results, manuscript writing, revision and finalization.

Author contributions as stated in the published version: AFRM.R., H.K., and C.L. designed the experiments, and AFRM.R., VK.BN., W.G., J.M., H.K. and C.L. wrote the manuscript. AFRM.R. conducted all cell experiments and prepared samples for SEM, micro-Raman spectroscopy, and XPS. VK.BN., A.G., and H.S. performed Raman measurements and data analysis. J.M. and M.T. performed XPS measurements and data analysis. W.G. wrote the cell detection algorithm.

<u>Objective 5:</u> Understanding the mechanical properties of environmentally exposed microplastic particles

Article 5: Repulsive Interactions of Eco-corona Covered Microplastic Particles Quantitatively Follow Modelling of Polymer Brushes

In the 3rd and 4th article of my PhD project, we learned that the surface of microplastic particles is chemically altered due to incubation in the environmental samples, also altering the particles' zeta-potential. However, besides the chemical alterations, changes in their physical properties could also affect the observed enhanced interactions with cells. For instance, the morphology of a particle and the particles' stiffness may contribute to the described phenomenon of the particles' higher reactivity. Hartmann et al. (2015) analyzed the stiffness-dependent internalization and subsequent transport of microparticles into cells. They showed that softer particles with a low stiffness are transported faster within cells than stiffer ones. Now, the question arises if the coating with an eco-corona may change the stiffness of a particle, potentially affecting the particles' internalization.

In article 5, we measured the repulsive forces with cp-AFM of the surface of microplastic particles coated with an eco-corona and compared the measured forces with their pristine counterparts. We measured single particle-particle interactions and found a pronounced increase of long-range repulsive interactions upon eco-corona formation. These repulsive interactions indicate that the formation of an eco-corona on microplastic particles introduces a soft film on the surface. This film changes the particles' mechanical behaviour, making the microplastic particles softer. We also have indications that the thicker the eco-corona gets, the softer the microplastic particle appears. Considering the observation of Hartman et al. (2015) that soft particles are internalized faster than hard particles, one may assume that this could also apply to particles with an eco-corona. In article 4, I found that particles incubated for longer periods in the environmental media show a higher number of particle-cell interactions and internalization than particles incubated for shorter periods. If we assume that the eco-corona becomes thicker and thus softer with increasing exposure time, the results described in article 5 would be a possible explanation for the increased cellular interactions.

Our study helps to further understand the complexity of an eco-corona and highlights that the chemical properties of the microplastic particles' surface and their physical properties can strongly influence their interactions with cells.

Authors: Thomas Witzmann, **Anja F. R. M. Ramsperger**, Simon Wieland, Christian Laforsch, Holger Kress, Andreas Fery, and Günter K. Auernhammer

Own contribution: experiments (incubation of microplastic particles), manuscript writing and revision.

Author contributions (not stated in the published version): T.W., A.F. and GK.A. designed the experiments, AFRM.R. and S.W. performed particle incubation, S.W. performed SEM sample preparation and imaging, T.W. performed cp-AFM measurements, T.W., A.F. and GK.A. performed data analysis and writing of the first draft manuscript, T.W., AFRM.R., S.W., H.K., C.L., A.F. and GK.A. wrote, revised and finalised the manuscript.

<u>Objective 6:</u> Which basic cellular internalization mechanisms occur for microplastic particles coated with an eco-corona compared to their pristine counterparts

Article 6: Cellular internalization pathways of environmentally exposed microplastic particles: Phagocytosis or Macropinocytosis?

In articles 3 and 4, we showed that in both environments, fresh- and salt water, an eco-corona develops on the surface of microplastic particles, altering their physico-chemical properties and, consequently, their interactions with cells. Interestingly, the origin of an eco-corona seems to play a minor role in the particles' reactivity towards cells since we did not find significant differences in their particle-cell interactions.

However, we found slightly different zeta-potentials in article 3, so I assumed that there should be differences in the composition of the eco-corona since fresh- and salt water are very different environments. Therefore, in article 6, we investigated the proteinaceous components of the eco-corona derived from fresh- and salt water using liquid-chromatography-mass-spectrometry/mass-spectrometry (LC-MS/MS). Interestingly, after correcting for background contamination, the proteinaceous composition of the eco-corona from fresh- or salt water was distinct. Therefore, I assumed there should be differences in how the particles interact with cellular membranes, although we did not see significant differences in our previous observations.

The surface of the plasma membrane is the outer leaflet of a cell communicating with its environment (Doherty & McMahon, 2009). Basically, cellular internalization can be subdivided into two steps once a cell encounters foreign particulate matter in the micrometre-size range. Within the first step, the surface of the particle interacts with the cell either by binding to cellular receptors (Aderem & Underhill, 1999) or by unspecific (e.g. electrostatic) interactions with the cell membrane (Forest et al., 2015). The biomolecules of an eco-corona, such as proteins, could possibly take over the function as a ligand and interact with membrane receptors, consequently leading to the adhesion of a particle to the cell membrane. However, the altered zeta-potential of the particles coated with an eco-corona may also determine their electrostatic interactions. Therefore, investigating the adhesion strength of microplastic particles coated with an eco-corona in detail is essential to estimate the underlying mechanisms for particle internalization.

To investigate the adhesion strength of microplastic particles coated with an eco-corona towards cells, we used the microfluidic microscopy platform described in article 3. With this approach, we can measure the forces needed to unbind a particle that attaches to cellular membranes, defining the particles' adhesion strength. Interestingly, there are no significant differences in the adhesion forces of particles to cells between fresh- and salt water derived eco-coronas, indicating that the origin of the eco-corona seems irrelevant to the particle binding strength to cells. This finding is consistent with the results from

article 5, showing that the enhancement of particle-cell interactions and internalization is independent of the origin of the eco-corona.

Although we did not investigate differences in the adhesion strength of eco-corona particles towards cells, the distinct proteinaceous composition of the different eco-coronas may still determine the internalization mechanisms for microplastic particles. To unravel the mechanisms relevant to internalizing microplastic particles coated with an eco-corona, we inhibited the most relevant internalization mechanisms, phagocytosis and macropinocytosis (Doherty & McMahon, 2009). First, we inhibited phagocytosis and macropinocytosis simultaneously (inhibitors: Cytochalasin D and Amiloride) by inhibiting actin polymerisation. Furthermore, we used Amantadine to inhibit receptor-mediated internalization, namely phagocytosis. Our results show that macropinocytosis is the main internalization mechanism for microplastic particles coated with an eco-corona derived from salt water, whereas for the other particle types both internalization mechanisms seem to be involved.

The results presented in article 6 are highly interesting since they show that the origin of an eco-corona does not influence the adhesion of a microplastic particle to a cellular membrane, whereas we present the first results, that the internalization mechanisms depend on the origin of the eco-corona. Based on our results, further investigations on the specific internalization mechanisms should be conducted to understand which properties of an eco-corona determine the enhanced microplastic particle-cell interactions and internalization.

Authors: **Anja F. R. M. Ramsperger***, Simon Wieland*, Magdalena V. Wilde*, Thomas Fröhlich, Christian Laforsch# & Holger Kress#

Status: manuscript will be submitted in 2023

Own contribution: Conceptualization and study design, experiments (experiments on eco-corona formation, cell experiments regarding internalization mechanisms, sample preparation for SEM), data analysis and figures, interpretation and discussion of results, manuscript writing, revision and finalization

Author contributions as stated in the manuscript: AFRMR, CL and HK initiated the research, all authors planned the research, AFRMR and SW performed the microplastic particle incubation experiments, AFRMR and SW prepared the SEM samples and SW imaged the SEM samples, AFRMR performed the cell experiments regarding particle-cell interactions, internalization and inhibition of internalization mechanisms, SW performed the particle adhesion experiments, LVW performed LC-MS/MS experiments and data evaluation, AFRMR, SW and LVW wrote the first draft of the manuscript. AFRMR, SW, LVW, TF, HK and CL reviewed and edited the manuscript

Objective 7: Closing knowledge gaps on the exposure pathways, the factors determining the tissue translocation and fate of microplastics in human tissues

Article 7: Nano- and microplastics: a comprehensive review on their exposure routes, translocation, and fate in humans

In the previous work of my PhD thesis, I showed that the surface properties of a microplastic particle determine their interactions with cells. Furthermore, the eco-corona acts as a game changer since the initial surface properties are additionally altered, enhancing the likelihood of particle-cell interactions and subsequent internalization. However, the overall question remains whether or not humans take up microplastic particles, if the particles interact with biological barriers, which may lead to their accumulation in human tissues, which consequently may induce adverse effects.

In article 7, I initiated an interdisciplinary literature review on the exposure pathways of humans to nano-and microplastics, describing the potential translocation mechanisms from primarily exposed organs to other tissues and evaluating the knowledge of the fate of microplastic particles in human tissues. We found the three main exposure pathways of how humans can come in contact with microplastics. The most important routes are via ingestion of a contaminated vector, inhaling microplastics with ambient air, or applying personal care products containing microplastics. To get a detailed overview of the potential exposure of humans to microplastics, we reviewed the current literature regarding microplastics in drinking water, beverages, and food for ingestion. We focused on the contamination levels of indoor environments and occupational sites for inhalation of microplastic particles. Furthermore, we summarized the current knowledge of microplastics in personal care products since those are directly applied to the skin or mucus membranes. We further summarized the current understanding of the translocation mechanism of particles from the primarily exposed organ (gastrointestinal tract, lung and skin) and critically reviewed the current literature regarding the fate of microplastics in human tissues.

The main finding of our review article is that there is a discrepancy between detected particle sizes described in human tissues and those that can theoretically be translocated. We then critically discuss that the limitations of the available analytical techniques and the lack or improper description of quality assurance and quality control are responsible for these discrepancies. Finally, we recommended that further development of reliable methods for the isolation, purification and analysis of small microplastics and nanoplastics is urgently needed to make accurate statements regarding the exposure and fate of nano-and microplastics within the human body.

Authors: **Anja F. R. M. Ramsperger**, Enrico Bergamaschi, Marco Panizzolo, Ivana Fenoglio, Francesco Babero, Ruud Peters, Anna Undas, Sebastian Purker, Bernd Giese, Carina R. Lalyer, Alba Tamargo, M. Victoria Moreno-Arribas, Hans-Peter Grossart, Dana Kühnel, Jana Dietrich, Friedrich

Paulsen, Anani K Afanou, Shan Zienolddiny-Narui, Stine Eriksen-Hammer, Torunn Kringlen-Ervik, Pål Graff, Bendik C. Brinchman, Karl-Christian Nordby, Hakan Wallin, Matteo Nassi, Federico Benetti, Michela Zanella, Julian Brehm, Holger Kress, Martin GJ Löder, Christian Laforsch

Own contribution: Conceptualization and study design, literature review (introduction, indoor air, personal care products, translocation, fate, reasons why reported studies should be interpreted critically), interpretation and discussion of results, manuscript writing (complete manuscript), revision and finalization

Author contributions as stated in the published version: All authors contributed to conceptualization, resources and funding acquisition. AFRM.R., H.K., J.B., MGJ.L., C.L., B.G., CR.L., S.P. and HP.G. wrote the introduction. AFRM.R., MGJ.L., C.L., HP.G. and D.K. wrote the chapter of NMP in drinking water. AFRM.R., H.K., J.B., MGJ.L., C.L., R.P., A.U., E.B., M.P., I.F., F.Ba., F.Be., M.Z., A.T. and V.M. wrote the chapter of NMP in food. AFRM.R., MGJ.L., C.L., J.D. and F.P. wrote the chapter of NMP in PCPs. AFRM.R., H.K., J.B., MGJ.L., C.L., F.Be., M.Z., M.N., H.W., AK.A., S.ZN., S.EH., T.KE., P.G., BC.B., KC.N., E.B., M.P., I.F. and F.Ba. wrote the chapter of NMP in indoor air and workplaces. AFRM.R., H.K., J.B., MGJ.L., C.L., F.P., H.W., AK.A., S.ZN., S.EH., T.KE., P.G., BC.B. and KC.N. wrote the chapter of NMP translocation. AFRM.R., H.K., J.B., MGJ.L., C.L. wrote the chapter of NMP fate in the human body, abstract and conclusion. AFRM.R., J.B., MGJ.L., C.L., D.K., B.G., CR.L. and S.P. wrote the Reasons why reported studies should be interpreted critically and risk assessment. AFRM.R., H.K., J.B., MGJ.L., C.L. wrote the first draft of the manuscript and all authors reviewed and edited the manuscript. J.B. and AFRM.R. designed the graphical abstract.

Summary of the articles – Hypothesis III

Hypothesis 3: The initial surface properties of polymers determine their interactions with microorganisms

Objective 8: Understanding how the initially different surface properties of different polymer types determine the early-stage formation of a biofilm

Article 8: Structural Diversity in Early-Stage Biofilm Formation on Microplastics Depends on Environmental Medium and Polymer Properties

In the first two topics of my PhD thesis, I demonstrated how important the surface properties of micrometre-sized microplastic particles are for particle-cell interactions. Within the environment, many more size classes of microplastic particles of different polymer types exist. Here, pro- and eukaryotic organisms may develop a biofilm on the surface of the microplastic particles. Most studies analyzed mature biofilms either by incubating the particles for several months or years (Artham et al., 2009; Hossain et al., 2019; Webb et al., 2009) or analysing microplastic particles isolated directly from the environment with unknown incubation times (Oberbeckmann et al., 2014; Zettler et al., 2013). At the beginning of my PhD, it has already been discussed that the surface properties, like the particles' surface morphology, surface charge (e.g. zeta-potential) or hydrophobicity, may determine the formation of a biofilm (Hossain et al., 2019; Rummel et al., 2017). However, a systematic approach was missing to correlate the initial surface properties with the development of a naturally grown biofilm.

I assumed that the polymers' initial surface properties might contribute the most to the early-stage biofilm. Therefore, I investigated the time-dependent development of an early-stage biofilm and correlated my findings with the particles' initial properties. We measured the initial zeta-potential of three different hydrophilic polymer types of different chemical compositions (PA-containing amid groups, PET-containing ester groups and PVC-containing chloride). For a consecutive time-series (0, 0.5, 1, 2, 5, 7, 11, and 14 days), we incubated the particles in two environmentally relevant media, fresh- and salt water. I analyzed the structural diversity on the surface of the particles by using SEM for each time point. Similar to what I found for the particle-cell interactions, the initial zeta-potential of the different polymer types determined the early-stage biofilm formation on the different polymer types. In freshwater environments, the microplastic particles made of PA with the highest initial zeta-potential showed the highest structural diversity, followed by PET with a lower zeta-potential and PVC having the lowest zeta-potential with the least structural diversity. Interestingly, PVC showed the highest structural diversity in the salt water treatment, followed by PA and PET. Although our results indicate that the early-stage biofilm formation depends on the incubation media and the particles' initial zeta-potential other properties may also contribute to the observed differences.

Furthermore, I descriptively discussed the microorganismal structures found on the surfaces of the particles. Interestingly, I observed microorganismal structures that were only present on PA and PET microplastic particles incubated in freshwater but absent on PVC. We assume that these microorganismal structures are attracted explicitly by the properties of PA and PET but are repelled by the properties of PVC. Overall, we show that less than half a day of incubation already leads to the initiation of an early-stage biofilm. Furthermore, the structural diversity increased during the incubation time on all polymer types in both environmentally relevant media, indicating a subsequent development of an early-stage biofilm. Interestingly, I found signs of extracellular polymeric substances (EPS) on the surface of PET and PVC in the salt water treatment after less than one week. The presence of EPS on a substrate indicates initiating the second step of biofilm formation, allowing microorganisms to proliferate and form colonies (Renner & Weibel, 2011).

The results described in article 8 once more highlight the importance of the initial surface properties of microplastic particles since it not only determines their interactions with cells but also their interactions with pro- and eukaryotic organisms within an environment.

Authors: **Anja F. R. M. Ramsperger**, Anja C. Stellwag, Anja Caspari, Andreas Fery, Tillmann Lueders, Holger Kress, Martin G. J. Löder, Christian Laforsch

Own contribution: Conceptualization and study design, experiments (sample preparation for SEM), interpretation and discussion of results, manuscript writing, revision and finalization

Author contributions as stated in the published version: AFRM.R., AC.S. and C.L. designed the experiments and AFRM.R., AC.S., A.C., A.F., T.L., MGJ.L., H.K. and C.L. wrote the manuscript. AFRM.R. and AC.S. conducted the experiments and prepared samples for SEM, AFRM.R., AC.S., C.L., MGJ.L., H.K. and T.L. evaluated the structural diversity A.C. conducted the ζ-potential measurements, A.C. and A.F. evaluated the ζ-potential data; All authors have read and agreed to the published version of the manuscript.

<u>Objective 9:</u> Understanding if the direct exposure of different polymer types in a small freshwater stream leads to polymer-specific microbial biofilm compositions

Article 9: In situ Prokaryotic and Eukaryotic Communities on Microplastic Particles in a Small Headwater Stream in Germany

Based on article 8, which results describe a fast and easy-to-measure technique to differentiate the early-stage biofilm formation on different polymer types under laboratory conditions, the question arises whether the distinct biofilm formation on different polymer types is also true in nature. The incubation of microplastic particles under laboratory conditions enables the detailed investigation of single factors influencing biofilm formation. However, this approach only shows half the truth since seasonal dynamics, which can significantly influence the formation and composition of a biofilm (Kaevska et al., 2016), are missing. Therefore, it is crucial to investigate the biofilm formation and composition grown under natural conditions directly in the environment. Several studies on the composition of a biofilm were performed on biofilms from marine aquatic environments (e.g., Oberbeckmann et al., 2015, 2016; Zettler et al., 2013), whereas data on freshwater biofilms is less abundant (Wright et al., 2021), especially in small headwater streams. Therefore, we directly exposed microplastic particles in a small headwater stream in Germany at two different time points within one year (spring and summer, four weeks of exposure, respectively). We chose four different polymer types (PE, PP, PS and PVC) to investigate if potential differences in the biofilm formation between polymers occur under natural conditions. We also used natural control particles made of quartz to elucidate polymer-specific effects. We used 16S and 18S amplicon sequencing and calculated the order of polymer type-specific pro-and eukaryotic community distances by Robust Aitchison principal component analysis (PCA). When we conducted these experiments, it was the first study focusing on prokaryotic and eukaryotic communities. It is essential to analyse both domains in biofilms, as a prokaryotic biofilm (consisting of bacteria and archaea) attracts eukaryotic predators such as protists and small metazoans. Analysing both makes it possible to depict the dynamics of a biofilm.

Our results show that different microplastic particle polymer types were colonized by different pro- and eukaryotic biofilm communities, irrespective of the season. PE particles always showed the highest number of detectable bacterial taxa. Significant differences to quartz samples were found for PE (in 16S data) and PP samples (in 18S data). The bacterial composition of the closely clustering PS and PVC samples in the PCA did not differ, while the reference samples were placed apart from these polymer types.

As described earlier in this thesis, it was shown that invertebrates more likely ingest microplastic particles coated with a biofilm compared to pristine particles (Hodges et al., 1995; Vroom et al., 2017). Therefore it is essential to closely investigate the composition of a biofilm since it has been described that pathogenic bacteria can be part of the biofilm community (Kirstein et al., 2016b; Oberbeckmann

et al., 2016; Zettler et al., 2013) and consequently enter an organism due to ingestion. In article 9, we did observe pathogenic bacteria, like *Enterobacter ludwigii*, in all samples and those exhibited a higher relative abundance in biofilm samples than in water samples.

The results of article 9 are consistent with my previous observations that the properties of a microplastic particle, determined by its' polymeric origin, lead to a distinct biofilm formation, also under natural conditions.

Authors: Alfons Weig, Martin G.J. Löder, **Anja F. R. M. Ramsperger**, Christian Laforsch

Status: Published in *Frontiers in Microbiology* (Impact Factor 2021: 6.064); https://doi.org/10.3389/fmicb.2021.660024

Own contribution: Contribution to the interpretation and discussion of results, manuscript writing, revision and contribution to finalization

Author contributions as stated in the published version: A.W. and C.L. created the project idea. A.W. conducted the experiment, processed the samples, analyzed that data, and wrote the manuscript. M.L., A.R., and C.L. revised the manuscript. All authors contributed to the article and approved the submitted version.

<u>Objective 10:</u> Develop a Raman library of spectral variances due to the polymer coating with a biofilm, which would enable the detection of a polymer coated with a biofilm without sample pre-processing

Article 10: Spatio-chemical analysis of the plastisphere using Raman spectroscopy

From the previous objectives in my PhD thesis, we learned that the composition of a biofilm can be distinct between different polymer types. To date, to identify the microplastic particles of different polymer types in an environmental sample it is essential to remove the organic material, e.g. the biofilm, from the plastic particles. This process of isolation and purification of an environmental sample to obtain the microplastic particles are costly, time-consuming, and often accompanied by the risk of contamination or loss of microplastic particles. To overcome the difficulties in isolation and purification, it would be helpful to establish a method allowing the spectroscopic analysis of microplastic particles coated with a biofilm without sample pre-processing.

Based on the polymer-specific biofilms that I described in article 8 and 9, we asked ourselves whether we could take advantage of these polymer-specific biofilms to identify microplastics using micro-Raman spectroscopy. Therefore, we incubated 11 different polymer types and an additional control particle made of glass for one month in a microcosm setup consisting of fresh- or salt water. We used SEM and micro-Raman spectroscopy to elucidate polymer-specific biofilm signatures. As a result, we found a heterogeneous distribution of molecular signatures that indicate the presence of EPS from biofilms, although not polymer-specific. However, the Raman signatures of the EPS were mostly present in parallel with the underlying surface signatures of the microplastic particles leading to spectral variances originating from the EPS. Therefore, we propose that the spectral variances of the microplastic particles coated with a biofilm can be used to infest a spectral variant library. This library will help to increase the efficiency associated with the spectroscopic identification of microplastic particles from an aqueous environment.

Authors: Vinay K. Bangalore-Narayana, **Anja F. R. M. Ramsperger**, Marvin Kiene, Julian Brehm, Martin G.J. Löder, Christian Laforsch

Status: Manuscript will be submitted 2023

Own contribution: SEM imaging and analysis, interpretation and discussion of results, manuscript writing, revision and finalization

Author contributions as stated in the manuscript: VKBN, ML and CL initiated the research, all authors planned the research, VKNB performed the incubation experiments, AFRMR, JB and VKBN prepared and imaged the SEM samples and performed image analysis, VKNB performed Raman sample preparation, data acquisition, analysis and interpretation of the data, MK developed the RaMPP R package, VKNB, AFRMR, JB and MK wrote the draft of the manuscript. All authors reviewed and edited the manuscript

Synopsis

The work presented in my PhD thesis clearly and unanimously emphasizes the importance of the surface properties of microplastic particles for their interactions with their surroundings. For instance, as soon as a microplastic particle enters the environment, its surface interacts with microorganisms, forming a biofilm or an eco-corona on the particles' surface, depending on the size of the particle. Here I showed that the polymer type and its specific surface properties determine the biofilm formation and composition on larger microplastic particles. However, a microplastic particles' surface properties are not solely determined by the polymer type. I showed that nominally the same model microplastic particles of the same polymer type tremendously differ in their properties, depending on the type and settings of the synthesis used by the commercial source. Here, the surface of the microplastic particles significantly differed, and I unravelled that especially the zeta-potential seems to be one of the main driving factors that a particle interacts with cells and tissues, consequently influencing the experimental outcome. Therefore, I want to highlight that a thorough characterization of the surface properties of microplastic particles is essential to allow concluding the mechanisms of toxicity.

However, under realistic scenarios, organisms and humans are not exposed to pristine microplastic particles. Still, they are mainly exposed to microplastic particles that previously interacted with environmental compartments and are coated with an eco-corona. I was the first to show the formation of an eco-corona on micrometre-sized microplastic particles, performing a thorough analysis to understand the physico-chemical and mechanical alterations of the surface properties and linked the surface properties to the particles' reactivity towards cells. Here, the eco-corona can be considered a turning point as it increases the adhesion strength of particles to cells, the number of particle-cell interactions and the number of internalized particles. The increased reactivity of the particles towards cells can consequently affect the experimental outcome in eco-toxicity studies.

Therefore, one question raised by media, stakeholders and policymakers whether we do have to be concerned about the potential health effects of deriving from plastic pollution cannot be answered at the moment since mainly pristine microplastic particles have been used. Nevertheless, my PhD project adds great value to be able to answer this question in the future. The key message of my thesis is that in future experiments, the microplastic particles used in effect studies must be thoroughly characterized. Furthermore, I highly recommend using environmentally exposed microplastic particles coated with an eco-corona since using pristine particles may lead to an underestimated risk deriving from plastic pollution since the particles interact significantly less with cells and tissues compared to environmentally exposed particles.

Outlook

One, if not the main question, whether microplastics can be harmful to an organism, was not aimed to be answered within the framework of my PhD thesis. However, since the interactions with and internalization of pristine microplastic particles and also particles coated with an eco-corona by cells seems to be mainly driven by the particles' physicochemical properties, these properties may eventually also trigger cytotoxic effects. For estimating the cytotoxicity of microplastic particles, different approaches are available, like measuring the metabolic activity by using an MTT- assay (MTT = 3-(4,5-dimethylthiazol-2-yl)-2,5diphenyltetrazolium bromide) or an increase in reactive oxygen species (ROS). Several studies show that only very high concentrations of microplastic particles can induce a decrease in metabolic activity (Rudolph et al., 2021; Stock et al., 2019, 2021) or an increase in ROS (Rudolph et al., 2021; Wang et al., 2021; Wu et al., 2019). Furthermore, Visalli et al. (2021) highlighted that ROS production was increased for short incubation of up to six hours when using high particle concentrations. In contrast, no increase in ROS can be detected after one-week exposure anymore (Visalli et al., 2021). This difference in ROS production indicates that cells *in vitro* are capable of homeostasis, but microplastic particles seem not devoid of consequences to human cell lines (Visalli et al., 2021).

To date, the available data is too limited to make reasonable statements about the cytotoxicity of microplastic particles (Brachner et al., 2020). This could be due to the fact that commonly used tests may not be sensitive enough to estimate the microplastic particle-induced cytotoxicity since they were originally designed to test soluble substances. Furthermore, the usual approaches to measuring cytotoxicity are based on the simultaneous examination of a pool of many cells. However, in my experimental setup performing single-cell analysis, I realised that not every cell interacts with a particle. If only a few individual cells interact with microplastic particles, potentially showing adverse effects, this effect may therefore be lost in the mass of simultaneously tested cells. To overcome this problem, single-cell analysis of particle-cell interactions would clearly show if a cell interacting with a particle shows signs of cytotoxicity or not. However, analysing individual cells using microscopic techniques is time-consuming and costly. But currently, it seems to be the only suitable technique to evaluate potential risks for cells interacting with microplastic particles.

During his visit to the *Chair of Biological Physics,* we discussed this issue with Prof. Dr. Gareth W. Griffiths from the *Department of Biosciences, University of Oslo, Norway.* He suggested that one possibility for single-cell effect studies could be imaging the activation of the nuclear factor 'kappa-light-chain-enhancer' of activated B-cells (NF$_k$B). The main function of NF$_k$B is the regulation of inflammation, mainly induced by ligand sensing at pattern-recognition receptors (PRRs). Cells of the innate immune system express PRRs to sense an extensive range of microbial components (pathogen-associated molecular patterns, PAMPs). These components may also be present in an eco-corona. In an inactive state, NF$_k$B is sequestered in the cytoplasm of a cell, and as soon as it becomes activated, it translocates into the nucleus

(for a review, see Liu et al., 2017). The translocation process of NF_kB can be imaged via the fluorescently labelling of NF_kB. Therefore I added the immuno-staining of the transcription factor NF_kB to my workflow for differentiating whether a particle has been internalized by a cell or whether a particle only adheres to the cell membrane (Ramsperger et al., 2020). With this approach, we can perform single-cell analysis and can even distinguish between potential effects derived by the adhesion to cellular membranes or the internalization of the particles by cells. Although with the highly acknowledged help of Wolfgang Groß from the *Chair of Biological Physics* developing MatLab-based automatic image analysis, single-cell analysis is still a very time-consuming approach. Therefore, I can only show preliminary results on the activation of NF_kB induced by PS microplastic particles coated with an eco-corona and the respective control treatments within this thesis.

As in our previous approaches, I incubated microplastic particles in either fresh- or salt water for the eco-corona coatings. As control treatments, I used the positive control of IgG and negative control of pristine particles without an eco-corona, as used in Ramsperger et al. (2020). Additionally, two more control treatments were conducted, control cells that were not exposed to any particulate matter and cells treated with lipopolysaccharides from *Escherichia coli*, known to induce the activation of NF_kB (Liu et al., 2017). I treated three different murine macrophage cell lines (C7, ImKC and J774A.1) with the corresponding treatments, fluorescently labelled the cells and after image acquisition, measured the three-dimensional mean intensity of NF_kB at the position of the nucleus of the cells. By explicitly analysing particle-cell interactions and comparing the fluorescence intensities to the respective control treatments, we can show that environmentally exposed microplastic particles induce the activation of NF_kB.

The activation strength seems to be depended on the cell line and treatment, indicating the specific role of macrophages from different body compartments. Interestingly, pristine microplastic particles without an eco-corona did not activate the NF$_k$B signaling pathway for any tested cell line (Figure 1).
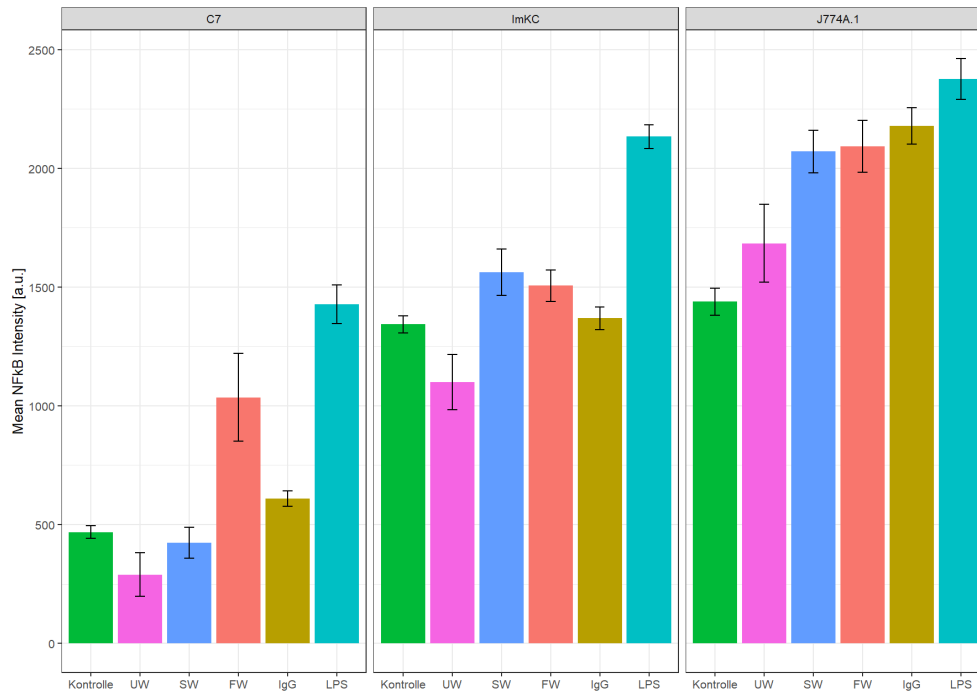

Figure 1: Fluorescent intensity of the transcription factor NF$_k$B at the location of the nucleus in three murine macrophage cell lines (C7, ImKC and J774A.1) after the treatment with microplastic particles coated with an eco-corona and control treatments. Control= untreated cells, UW= pristine microplastic particles, SW= microplastic particle coated with an eco-corona from saltwater, FW= microplastic particle coated with an eco-corona from freshwater, IgG= functionalized microplastic particles opsonized with the antibody IgG, LPS= lipopolysaccharides from gram-negative bacteria. In all cell lines, the LPS treatment induced the activation of the NF$_k$B translocation into the nucleus. For the C7 cell line, only microplastic particles coated with an eco-corona derived from FW activate the translocation of NF$_k$B into the nucleus. For the ImKC and J774A.1, both types of eco-corona coated microplastic particles induce the translocation of NF$_k$B into the nucleus. Statistical analysis pending. a.u. = arbitrary units.

This last but preliminary aspect of my PhD thesis shows that microplastic particles coated with an eco-corona are more frequently interacting with and become internalized by cells and ultimately cause stronger inflammatory responses than pristine particles. Liu et al. (2017) highlighted in their review article that "(…) deregulated inflammatory responses can cause excessive or long-lasting tissue damages, contributing to the development of acute or chronic inflammatory diseases.". Finally, I would like to encourage other research groups investigating the potential risk of plastic pollution to include environmentally exposed microplastic particles of different shapes in impact studies in order to draw realistic conclusions about the potential risk of microplastic particles for the environment, the organism and ultimately human health.

Published articles and manuscripts

Article 1

From properties to toxicity: comparing microplastics to other airborne microparticles

Review

# From properties to toxicity: Comparing microplastics to other airborne microparticles

Simon Wieland [a,b], Aylin Balmes [c], Julian Bender [d], Jonas Kitzinger [e], Felix Meyer [f], Anja FRM Ramsperger [a,b], Franz Roeder [g], Caroline Tengelmann [h,i], Benedikt H. Wimmer [j], Christian Laforsch [b,*], Holger Kress [a,*]

[a] Biological Physics, University of Bayreuth, Bayreuth, Germany
[b] Animal Ecology I and BayCEER, University of Bayreuth, Bayreuth, Germany
[c] Institute of Applied Physics, University of Tübingen, Tübingen, Germany
[d] Institute for Biochemistry and Biotechnology, Interdisciplinary Research Center HALOmem, Martin Luther University Halle-Wittenberg, Halle, Germany
[e] Department of Physics, Humboldt University of Berlin, Berlin, Germany
[f] Institute of Clinical Microbiology and Hygiene, University Hospital Regensburg, Regensburg, Germany
[g] Institute of Optics and Quantum Electronics, Friedrich Schiller University Jena, Jena, Germany
[h] Medical Faculty, University of Würzburg, Würzburg, Germany
[i] Department of Anesthesiology, Intensive Care Medicine and Pain Therapy, University Hospital of Würzburg, Würzburg, Germany
[j] Faculty of Science, University of Zurich, Zurich, Switzerland

HIGHLIGHTS

- Airborne microplastic (MP) is a potential hazard for human health.
- Size, shape, and surface charge are proposed as possible drivers for MP toxicity.
- Comparisons with other dusts allow identification of putative toxicity mechanisms.
- Mechanistic knowledge of airborne MP toxicity is crucial for hazard evaluation.

GRAPHICAL ABSTRACT
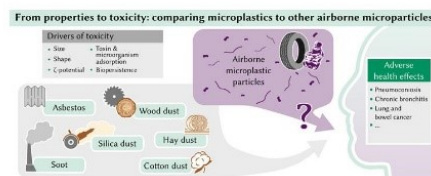
ARTICLE INFO

Editor: Dr. R. Teresa

ABSTRACT

Microplastic (MP) debris is considered as a potentially hazardous material. It is omnipresent in our environment, and evidence that MP is also abundant in the atmosphere is increasing. Consequently, the inhalation of these particles is a significant exposure route to humans. Concerns about potential effects of airborne MP on human health are rising. However, currently, there are not enough studies on the putative toxicity of airborne MP to adequately assess its impact on human health. Therefore, we examined potential drivers of airborne MP toxicity. Physicochemical properties like size, shape, ζ-potential, adsorbed molecules and pathogens, and the MP's biopersistence have been proposed as possible drivers of MP toxicity. Since their role in MP toxicity is largely unknown, we reviewed the literature on toxicologically well-studied non-plastic airborne microparticles (asbestos, silica, soot, wood, cotton, hay). We aimed to link the observed health effects and toxicology of these microparticles to the abovementioned properties. By comparing this information with studies on the effects of airborne MP, we analyzed possible mechanisms of airborne MP toxicity. Thus, we provide a basis for a

mechanistic understanding of airborne MP toxicity. This may enable the assessment of risks associated with airborne MP pollution, facilitating effective policymaking and product design.

1. Introduction

Since the 1950 s, plastics have become an essential part of our daily lives and have enabled many technical and medical innovations (Andrady and Neal, 2009; Thompson et al., 2009). The resulting global adoption of plastics and its often inappropriate disposal has been accompanied by a rapidly accumulating amount of waste in the environment, as most commodity plastics are very resistant against both physical and biological degradation (Geyer et al., 2017; Andrady, 2015). The disintegration of such improperly disposed plastic, processes like tire wear, and abrasion from synthetic textiles produce many microscopic plastic particles (microplastics, MP) (Brahney et al., 2021; Mbachu et al., 2020; Zhang et al., 2021). These particles formed by degradation or abrasion processes are classified as secondary MP. In contrast, primary MP is manufactured in a small size, often finding use in cosmetics, such as peelings or cleaning abrasives. It usually reaches the environment via the wastewater stream (Brahney et al., 2021; Syberg et al., 2015). The term MP usually refers to plastic particles smaller than 5 mm (Arthur et al., 2009). However, there is still no uniform definition of the lower size limit of MP. Most commonly, the lower size limit of MP is set between 0.1 and 100 μm (EFSA, 2016; Frias and Nash, 2019). In this review, we use the term MP to describe particles derived from synthetic polymers with sizes between 0.1 μm and 5 mm.

Reports about MP in the environment first focused on marine ecosystems (Thompson et al., 2004; Ng and Obbard, 2006; Imhof et al., 2017). Soon after these reports, MP pollution of other environmental compartments gained increasing attention: MP was also detected in freshwater and terrestrial ecosystems worldwide (Schell et al., 2020; Frei et al., 2019; Piehl et al., 2018; Imhof et al., 2018, 2013; Dris et al., 2015). Even in the most remote areas, MP pollution is detectable (Imhof et al., 2017; Gonzaandacute; lez-Pleiter et al., 2021; Teichert et al., 2021). Especially atmospheric transport of MP is an important driver of MP transfer around the globe (Zhang et al., 2019). As a consequence, attention to this airborne MP is continuously increasing (Brahney et al., 2021; Zhang et al., 2020).

Due to the omnipresence of MP, concerns about possible effects on environmental and human health are rising. It is well established that aquatic organisms interact with MP and consume it together with their food. For example, the ingestion of MP particles has been reported for various organisms, including zooplankton, bivalves, and vertebrates (Teichert et al., 2021; Desforges et al., 2015; Browne et al., 2008; Von Moos et al., 2012; Lu et al., 2016; Vinay Kumar et al., 2021). Upon ingestion, particles have been shown to translocate into the surrounding tissues and the circulatory system of the aquatic organisms (Browne et al., 2008; Von Moos et al., 2012; Lu et al., 2016). Therefore, the exposure of aquatic organisms to MP raised concerns about adverse effects of the particles on these organisms and aquatic ecosystems (Wright et al., 2013; Guzzetti et al., 2018). Also, potential human consumption of MP with contaminated food, e.g., seafood, gained increasing attention (Vinay Kumar et al., 2021; Smith et al., 2018; Cox et al., 2019). Consequently, more and more research focused on possible health issues associated with ingested MP (Carbery et al., 2018; De-la-Torre, 2020).

Likewise, due to the widespread presence of MP in the atmosphere, awareness of breathable MP pollution and potentially harmful effects on human health increased over the last years (Prata, 2018; Amato-Lourenço et al., 2020; Huang et al., 2020; Chen et al., 2020). Parameters like size, shape, surface charge, molecules and pathogens adsorbed to the MP particles, and the MP particles' bio-persistence may contribute to airborne MP toxicity (Prata, 2018; Wright and Kelly, 2017). Yet, the understanding of the role of these parameters concerning potentially adverse health effects of airborne MP is still limited; only very few

studies cover this issue. However, some non-plastic microparticles that are well-known drivers of diseases have already been studied in this respect. Therefore, to shed light on the potential effects of airborne MP on human health, it has been proposed to compare MP toxicity to other well-studied airborne particulate matter (Vethaak and Legler, 2021).

In general, human exposure to airborne microparticles depends on their size. For example, the inhalation of microparticles usually is determined by their aerodynamic equivalent diameter (AED, the diameter of a sphere with density 1 g cm^{-3} with the same settling velocity as the microparticle) rather than by their geometrical size (Chen and Fryrear, 2001; Reponen et al., 2001). Commonly, microparticles are categorized according to their AED into particles > 10 μm, particles < 10 μm (PM10), particles < 2.5 μm (PM2.5), and ultrafine particles < 0.1 μm (Kelly and Fussell, 2012). The large particles > 10 μm are assumed to collide with the upper airways upon respiration, whereas PM10 can enter the bronchioles, and PM2.5 and ultrafine particles may even penetrate the alveoli (Prata, 2018; Kelly and Fussell, 2012). Besides determining the exposure pathways, the size of microparticles can affect their toxicity. Because of their large surface-to-volume ratio, smaller particles are potentially more prone to interact with cells and tissues, leading to stronger responses at exposure sites (Schmid and Stoeger, 2016).

Also, the shape of a microparticle influences its toxicity by modifying interactions with cells and tissues. For example, microfibers interact with cells and tissues differently than microspheres, fragments, or films (Allegri et al., 2016). These altered interactions can lead to shape-specific toxicity of different microparticles.

Moreover, the surface charge of microparticles can affect their toxicity. A typical property to quantify the surface charge of microparticles is the particles' ζ-potential (Peltonen and Hirvonen, 2008). The ζ-potential can be a proxy for the electrostatic interactions of microparticles with cells and tissues, determining the adhesion of the microparticles (Silva et al., 2014). The adhesion strength of microparticles could potentially affect their bioavailability and consequently the toxicity of these particles.

Adsorption of molecules and microorganisms following the microparticles' environmental exposure can additionally modify their toxicity. In addition to biomolecules that may increase the bioavailability of the microparticles, the microparticles can also carry adsorbed toxins or pathogenic bacteria, which might enlarge their potential to impact human health (Prata, 2018; Ramsperger et al., 2020; Kirstein et al., 2016).

Lastly, all these potential modes of toxicity may be altered by the microparticles' bio-persistence. Therefore, bio-persistence has been discussed as an essential parameter for the microparticles' interactions with tissues because it potentially alters long-term exposure and associated chronic effects (Oberdorster et al., 1994).

Here, we aim to better comprehend the impact of the abovementioned parameters (size, shape, ζ-potential, adsorbed molecules and organisms, bio-persistence) on MP toxicity by comparing different well-studied non-plastic microparticles to MP. We reviewed the literature on six microparticle pollutants often associated with occupational diseases: Asbestos, silica dust, soot, wood dust, cotton dust, and hay dust. We set our focus on occupational safety and the pathogenesis of microparticle-associated diseases. By giving an overview of the diseases and the pathogenesis associated with each type of microparticle with respect to the abovementioned parameters, we aim to determine to what extent these parameters are the drivers of the microparticle's toxicity. We try to link our results to the existing knowledge on the properties of airborne MP particles, identifying possible mechanisms of their toxicity. Overall, this approach can contribute to understanding airborne MPs' potential

2

impact on human health and outline possible directions for future MP research.

2. Non-plastic airborne microparticles

2.1. Asbestos

Asbestos unites a group of naturally occurring hydrated silicates that form long and thin crystalline fibers (Pira et al., 2018; Solbes and Harper, 2018). Many beneficial characteristics of asbestos, like high flexibility, low thermal conductivity, and a very high mechanical and chemical resistance, led to a massive increase in its use throughout the 20th century for industrial purposes, such as brake linings, asbestos cement, asphalt concrete, and insulating material. Asbestos was also used in various products of everyday life, for example, artificial snow, shoes, and cigarette filters (Pira et al., 2018; Noonan, 2017). Even though asbestos has been prohibited in many countries, human exposure still occurs during repair and removal of older buildings (Kameda et al., 2014; Hagemeyer et al., 2006). Workplace concentrations of asbestos strongly depend on the materials, processing techniques, and engineering controls implemented to mitigate the asbestos release. During abatement of asbestos insulation, usually, concentrations between 0.02 and 0.2 fibers per cubic centimeter (f cm^3) have been reported, with maximum concentrations up to 100 f cm^3 (Williams et al., 2007). Next to occupational exposure, pollution of the ambient air, e. g. in areas with naturally occurring asbestos, increases the risk of asbestos-related diseases (Metintas et al., 2002). Also, some adverse health effects can already occur after contact with very low concentrations of asbestos (Hodgson and Darnton, 2000; Goodman et al., 1999). Therefore, it is common practice in most developed countries to avoid asbestos exposure as far as possible. For example, the US National Institute for Occupational Safety and Health (NIOSH) recommends that workers should not be exposed to more than one f cm^{-3} for 30 min. When working with asbestos, a self-contained breathing apparatus with a full facepiece is recommended by the NIOSH (Barsan, 2007).

It has been estimated that globally, about 100,000 people per year die from the consequences of asbestos exposure (Baumann et al., 2013). The main problems caused by asbestos inhalation are asbestosis, interstitial pulmonary fibrosis, pleural disorders and calcified plaques on the lung's outer lining, and several forms of cancer, especially malignant mesothelioma (Goodman et al., 1999; Sporn and Roggli, 2014; Alpert et al., 2020). Even though asbestosis is a nonmalignant disease, it can severely impact the patient's life quality. Eventually, it can lead to hypoxemia and increased lung pressure, potentially affecting the heart muscle in the long term (Sporn and Roggli, 2014).

Although diseases associated with the inhalation of asbestos are very well studied, the exact mechanisms leading to asbestos-related diseases are yet not fully understood (Huang et al., 2011). Accumulation of asbestos fibers is considered one of the main factors inducing a continuous inflammatory response, oxidative stress, and apoptosis (Solbes and Harper, 2018; Craighead and Mossman, 1982). Consequently, surrounding tissues are damaged. Furthermore, ROS (reactive oxygen species) and oxidative stress may also cause DNA damage, increasing the risk of malignant cell proliferation (Solbes and Harper, 2018). Next to inflammatory responses and oxidative stress, the direct influence of asbestos on signaling and transduction pathways is important. This leads to an alteration of various cellular processes governing gene expression, cellular growth and shape, and epithelial permeability (Solbes and Harper, 2018).

The properties of asbestos fibers (Fig. 1A, Table 1) play an essential role in their toxicity. For example, the size of asbestos fibers can vary substantially. In one instance, diameters in the range of 0.01 – 1.5 μm and lengths in the range of 0.01 – 64 μm have been reported (Stanton et al., 1981).

Their thin and elongated fiber shape (Fig. 1A) allows them to deeply penetrate the lung, while at the same time, phagocytosis is prohibited as

the fiber length exceeds the size of macrophages (Donaldson et al., 2010). Consequently, primarily long asbestos fibers (length > 5 μm) are the toxicologically most relevant fraction. Nevertheless, short asbestos fibers (length < 5 μm), making up the main part of airborne asbestos fibers, may also contribute to the overall toxicity of asbestos (Boulanger et al., 2014). When used, modified, or inhaled, the asbestos fibers may split up lengthwise and form even thinner fibers, increasing the associated risks (Boulanger et al., 2014; Roggli and Brody, 1984).

The ζ-potential of asbestos can cover a wide range between about − 60 mV and + 55 mV and depends on various parameters, including the mineral variety and the pH value of the medium during the measurement. Interestingly, the magnitude of the fibers' ζ-potential is positively correlated to their hemolytic activity (Light and Wei, 1977). Under conditions similar to the conditions in lung tissue, a negative ζ-potential of asbestos fibers was reported. This negative ζ-potential possibly leads to the formation of reactive oxygen species (ROS) and free radicals, likely increasing cytotoxicity and carcinogenicity of asbestos fibers (Pollastri et al., 2014).

When exposed to the environment, the structure of asbestos fibers may be altered by organic molecules (Holmes et al., 2012). It is not clear whether molecules and biofilms adsorbed during environmental exposure affect the toxicity of asbestos. However, this adsorption may be less relevant compared to other factors since asbestos exposure usually occurs in workplace environments, where the fibers are freshly released into the air.

Overall, the hazardous potential of asbestos fibers is increased by their high bio-persistence in the lung, leading to chronic effects (Donaldson et al., 2010). Although dissolution rates of asbestos depend on the exact mineral variety, the estimated lifetime of asbestos fibers in the lung range from several months to years (Jurinski and Rimstidt, 2001; Hume and Rimstidt, 1992; Oze and Solt, 2010).

2.2. Silica dust

The inhalation of silica (silicon dioxide) dust is a well-known cause of occupational diseases, predominantly silicosis. Silica forms minerals like quartz and is the major component of sand. Depending on its crystal structure, silica dust is classified as amorphous and crystalline silica dust, differing in their physicochemical properties. Crystalline silica dust is thought to be the primary driver of silicosis, although exposure to the amorphous form of silica has potential adverse effects, too (Silicosis Mortality, 2005; Merget et al., 2002). To what extent silica dust is associated with health effects may also depend on the dust's exact crystal structure (Wiessner et al., 1988). In various industrial workspaces, crystalline silica dust can occur at high concentrations. Especially workers in mining, road repair, construction, and brick working face the risk of exposure (Wagner, 1997). However, silica-related diseases are not just recorded in these industries but also among workers involved in processes like denim-jeans sandblasting or jewelry polishing, where the exposure to silica dust may lead to occupational diseases (Barnes et al., 2019). Furthermore, naturally occurring silica dust like Sahara dust is also associated with respiratory diseases and silicosis (Derbyshire, 2007).

Workplace concentrations of silica dust typically depend on the individual working processes. For example, silica dust concentrations of 0.26 mg m^{-3} were reported during wall grinding, whereas during concrete sawing, they were as high as 10.0 mg m^{-3} (Linch, 2002). The NIOSH recommended limit for exposed workers is 0.05 mg m^{-3} for up to ten hours a day. At higher concentrations, protective equipment is required (for D.C and Prevention, 1996). Nevertheless, even at the recommended limit, the risk of developing silicosis and death among lifetime exposed workers is significantly elevated (Mannetje et al., 2002).

Exposure to high concentrations of silica dust potentially leads to silicosis, a fibrotic lung disease. It is the most common type of pneumoconiosis (interstitial lung disease), which caused approximately 13,000 deaths worldwide in 2019 (Institute for Health Metrics and
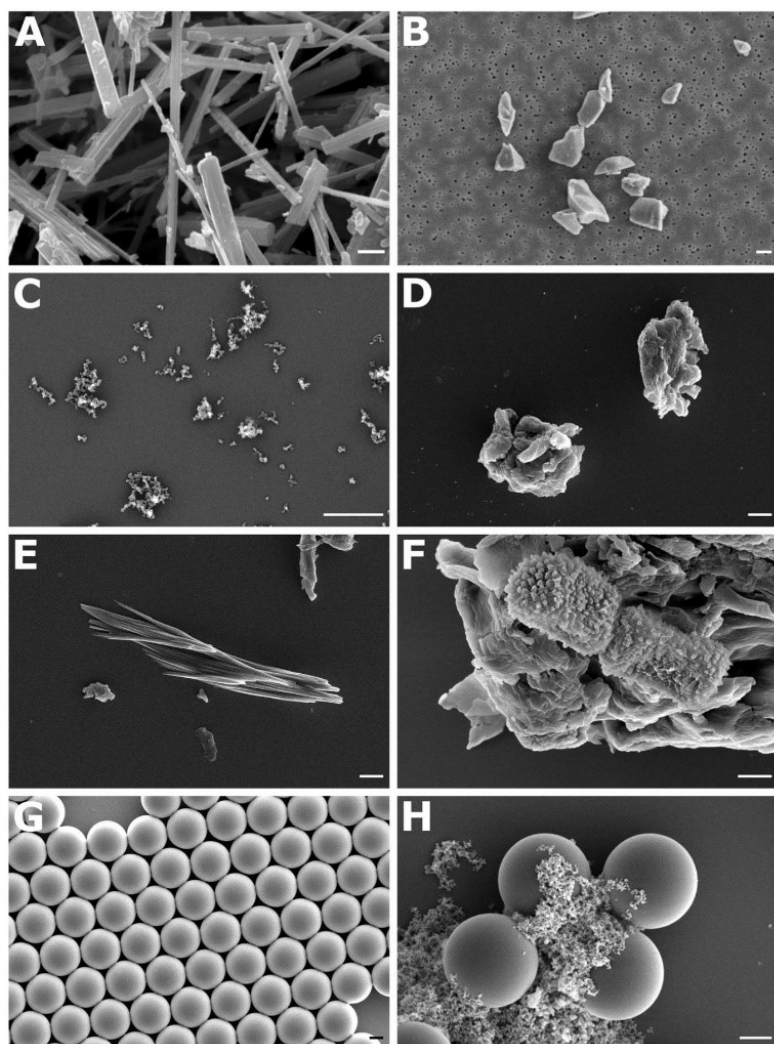
3

Fig. 1. Scanning electron micrographs of airborne microparticles. A) Amosite asbestos fibers, showing the typical thin and elongated shape. The SEM image was kindly distributed in the public domain by the U.S. Geological Survey (USGS) (Geological Survey, 2007) B) Crystalline silica dust particles, forming irregularly shaped, sharp-edged fragments. The SEM image was taken from S. Mischler et al.: 'Differential activation of RAW 264.7 macrophages by size-segregated crystalline silica' (Mischler et al., 2016) C) Soot particles from diesel exhaust forming grape-like, aciniform structures which are in the size range of several hundred nanometers to micrometers. D) Oak wood particles generated by manual filing (file with 46 cuts per cm) of wood, showing a very irregular surface. E) Cotton fragment formed during cryomilling of raw cotton fibers, showing an elongated shape, which is composed of thin fibers. F) Hay dust particle with adsorbed cells (possibly fungal spores). G) Pristine PS microbeads that are frequently used in MP research. These commercially available MP particles are very monodisperse and have a smooth surface. H) The same PS microbeads after 2 weeks incubation in salt water. Biomolecules adsorbed to their surface, forming an ecocorona. Scale bars: 1 μm. Sample preparation and imaging: Dust samples were manually transferred on a fragment of a silicon wafer, which was mounted on a specimen stub using a carbon adhesive pad. Prior to mounting, the plain and ecocorona-coated PS beads were fixed with Karnovsky's fixative (2% PFA and 2.5% glutaraldehyde in 1x PBS), dehydrated with an ethanol series (30%, 50%, 70%, 80%, 90% for 30 min each; 95% and 100% for 1 h each), and dried in hexamethyldisilazane (HMDS). All samples were coated with 4 nm platinum (Leica EM ACE600 sputter coater). The imaging was performed at 5 kV using an Everhart-Thornley detector (SEM: FEI Apreo VolumeScope, Thermo Fisher Scientific).

Evaluation IHME, 2020). Furthermore, exposure to silica dust is associated with chronic obstructive pulmonary disease (COPD), lung cancer, autoimmune diseases, and renal disease (Leung et al., 2012). There is also a higher prevalence of pulmonary tuberculosis (TeWaterNaude et al., 2006).

In the pathogenesis of silica-induced diseases, inflammatory responses and the stimulation of fibroblasts play an essential role (Barnes et al., 2019; Leung et al., 2012). Inhaled silica particles accumulate in the distal airways and are internalized by macrophages, which activate proinflammatory and pro-fibrotic pathways. The uptake by the macrophages leads to the death of the cell, after which silica particles are released and further intensify the inflammatory response. Subsequently, fibroblast growth is stimulated, leading to the formation of onion-like cellular structures around the sites of inflammation. These silicotic nodules have the potential to merge to sizes > 1 cm and form cavities. For example, *Mycobacterium tuberculosis*, the pathogen of tuberculosis, can persist in these cavities. Consequently, phagocytes are less in control of their growth, possibly explaining the higher prevalence of tuberculosis in silica-exposed workers (Barnes et al., 2019; Leung et al., 2012).

The observed adverse health effects of silica dust are related to the particles' properties (Fig. 1B, Table 1). The size of silica dust varies

among different sampling sites, working processes, and sampling methods used, making uniform statements about these parameters difficult. For example, in a granite quarry in Vermont, most aerosolized silica particles were inhalable with a size smaller than 10 μm. In the stone finishing areas of the quarry, more than half of the sampled particles were in the size range of 0.5 – 0.7 μm (Sirianni et al., 2008). Similarly, in three different mines in Alaska, Nevada, and South Africa, the average size of the silica particles ranged from 0.5 to 1.7 μm (Chubb and Cauda, 2017).

Dust particles generated during stonework generally have an irregular and fractured shape, which can be seen in crystalline silica dust from mine tailings (Andraos and Gulumian, 2020). This irregular, fractured shape with angular surfaces of dust particles was also observed in crystalline silica-rich ambient particular matter (Dong et al., 2015). Although earlier assumptions that this sharp-edged shape of crystalline silica dust is the primary driver of silicosis have been disproven (Winkler, 1975), mechanically fractured crystalline silica has stronger cytotoxic effects on human macrophages in vitro compared to more regularly-shaped grown crystalline silica (Leinardi et al., 2020).

The amorphous form of silica has a surface covered by hydroxyl groups, leading to hydrophilic properties (Vansant et al., 1995). The

4

Table 1

Overview of non-plastic microparticle properties and associated health effects. Here, information on shape, size, ζ-potential, and bio-persistence of different non-plastic microparticles is summarized, together with a short synopsis of the health risks. Abbreviations: COPD – chronic obstructive pulmonary disease; AED – aerodynamic equivalent diameter; PAH – polycyclic aromatic hydrocarbon, POP – persistent organic pollutant.

Particle type	Size	Shape	ζ-potential	Adsorbed molecules/ organisms	Bio-persistence	Health risks
Asbestos	Diameter 0.01 – 1.5 μm, length 0.01 – 64 μm (Stanton et al., 1981) Mostly long asbestos fibers > 5 μm toxicologically relevant (Boulanger et al., 2014)	Thin, elongated fibers (Stanton et al., 1981) Fibers longer 5 μm possibly main drivers of asbestos toxicity (Boulanger et al., 2014) In lung, fibers can split up lengthwise into thinner fibers (Boulanger et al., 2014; Roggli and Brody, 1984)	- 60 to + 55 mV, depending on the mineral variety (Light and Wei, 1977) Hemolytic activity correlated to ζ-potential (Light and Wei, 1977), formation of ROS associated with negative ζ-potential (Pollastri et al., 2014)	Environmental exposure alters surface of asbestos fibers (Holmes et al., 2012) However, effect on toxicity not known	Dissolution rates depend on the mineral variety, estimated lifetime of asbestos fibers in lung between several months to years leads to chronic toxicity (Jurinski and Rimstidt, 2001; Hume and Rimstidt, 1992; Oze and Solt, 2010)	Asbestosis, interstitial pulmonary fibrosis, calcified plaques and pleural disorders, cancer (especially mesothelioma) (Goodman et al., 1999; Sporn and Roggli, 2014; Alpert et al., 2020)
Silica dust	Airborne fragments usually in the breathable range < 10 μm, mostly between 0.5 and 2 μm (Sirianni et al., 2008; Chubb and Cauda, 2017)	Irregularly shaped fragments with sharp edges (Andraos and Gulumian, 2020; Dong et al., 2015), mechanically fractured crystalline silica more cytotoxic than regularly shaped grown crystalline silica (Leinardi et al., 2020)	-30 to – 10 mV under physiological pH conditions (Dong et al., 2015; Leinardi et al., 2020). Higher toxicity of freshly fractured quartz due to increased surface radicals (Vallyathan et al., 1995)	Adsorption of PAHs to biogenic amorphous silica (Rabovsky, 1995) However, contribution to overall silica toxicity unclear	Very low rates of dissolution under physiological conditions (Rimstidt and Barnes, 1980), theoretical lifetime of microparticles about 100 – 10000 years (Jurinski and Rimstidt, 2001) contributes to chronic toxicity	Silicosis (Wagner, 1997; Barnes et al., 2019; Derbyshire, 2007; Mannetje et al., 2002) COPD, lung cancer, autoimmune and renal disease (Leung et al., 2012) Increased risk for tuberculosis, due to formation of silicotic nodules (TeWaterNaude et al., 2006)
Soot	Size dependent on combustion process, mostly on the order of several hundreds of nanometers (Kleeman et al., 1999; Torvela et al., 2014), also larger structures up to 100 μm (Watson and Valberg, 2001) Particles grow in size after release due to aggregation and condensation of organic matter (Janssen et al., 2012; Patterson and Kraft, 2007). Size may affect toxicity (Frank et al., 2013), particles with a size of 70 – 110 nm potentially most toxic (Sarkar et al., 2014)	Depending on combustion process formation of grape-like aciniform structures, but also other shapes like xerogels and cenospheres (Watson and Valberg, 2001). Possibly formation of toxic radicals on particles with high curvature (Frank et al., 2013)	-50 to – 30 mV for diesel soot particles under physiological pH and salt conditions (Sarkar et al., 2014; Chen and Huang, 2017). Particles with ζ-potential of – 41 mV to – 37 mV especially bioreactive, causing inflammatory response (Sarkar et al., 2014)	Adsorption of organic compounds, especially PAHs, to soot particles during combustion process and after their release into the environment (Lee, 2010; Watson and Valberg, 2001; Eaves et al., 2017) Adsorbed PAHs play a major role in soot particle toxicity (Barfknecht, 1983; Kirrane et al., 2019)	Clearance from rat lungs decreases with exposure level, possibly leading to chronic effects; half-life of diesel soot particles between 80 and 250 days (Griffis et al., 1983; Wolff et al., 1987)	Occupational exposure: cancer of lung and esophagus (Pukkala et al., 2009), asthma, ischemic heart disease (Li et al., 2008; Hansen, 1983) Ambient exposure: increased risk for cardio-pulmonary diseases, possibly increase in cancer risk (Janssen et al., 2012; Lee, 2010; Stöber and Abel, 1996)
Wood dust	AED of wood dust collected at breathing height of workers between 10 μm and 100 μm (Harper et al., 2002) AED of wood dust directly sampled from sanding mostly < 10 μm, in the breathable range (Määttä et al., 2006; Ojima, 2016; Marková et al., 2018) AED of wood dust directly sampled from milling mostly > 125 μm (Očkajová et al., 2020)	Shape depends on wood type and processing techniques, usually irregularly shaped particles (Mazzoli and Favoni, 2012; Liu et al., 1985) Effect of shape on toxicity not yet studied	Intact spruce wood capillaries: − 10 to + 10 mV at pH 5.6 (Muff et al., 2018) Cellulose nanofibers from cedar wood: − 50 to − 30 mV at pH 6.8–7 (Uetani and Yano, 2012) Effect of ζ-potential on toxicity not known	Chemical treatments (e.g., chromate compounds) potential driver of wood dust toxicity (Klein et al., 2001). Also naturally occurring chemicals (terpenes, polyphenolic compounds) may affect wood dust toxicity (Naarala et al., 2003)	Lignin and cellulose only degradable by enzymes from specialized microorganisms (Slavin et al., 1981; Pérez et al., 2002; Eriksson et al., 1990), therefore likely no degradation of wood in the human lung, promoting chronic toxicity. Wood cellulose fibers persist in rat lungs after 1 year, higher bio-persistence compared to asbestos. Estimated half-life about 3 years (Muhle et al., 1997)	Classified as carcinogenic for humans, especially associated with cancer of nasal cavities and paranasal sinuses (Delzell, 1995). Also associated with lung cancer (Alonso-Sardón et al., 2015; Binazzi et al., 2015; Hancock et al., 2015). Evidence of association with other pulmonary diseases like cryptogenic fibrosing alveolitis and idiopathic pulmonary fibrosis (Hubbard et al., 1996; Gustafson et al., 2007)
Cotton dust	Classified according to size into trash (> 500 μm), dust (50 – 500 μm), micro dust (15 – 50 μm), and breathable dust (< 15 μm) (Dangi and Bhise, 2017). Mostly breathable fraction associated with health effects (Ellakkani et al., 1984)	Fragmented fibers, irregularly shaped particles (Goynes et al., 1986). Effects on toxicity not investigated	Not known	Adsorption of bacterial endotoxins and possibly also pesticides relevant for cotton toxicity (Wang et al., 2003; Rylander, 1987; Solbrig and Obendorf, 1985)	High biodurability of cellulose fibers relevant for chronic effects, degradation only by enzymes of specialized microorganisms (Eriksson et al., 1990). Degradation of cellulose fibers in vivo in mice and rats very slow (Muhle et al., 1997; Ilves et al.,	Asthma, bronchitis, byssinosis (Dangi and Bhise, 2017). Effects possibly also due to bacterial endotoxins and pesticides (Wang et al., 2003; Rylander, 1987; Solbrig and Obendorf, 1985)

5

Table 1 (*continued*)

Particle type	Size	Shape	ζ-potential	Adsorbed molecules/ organisms	Bio-persistence	Health risks
Hay dust	Ca. 95% of hay dust particles smaller than 5 µm, therefore breathable (Séguin et al., 2010; O'Connor et al., 2013)	Mostly spherical, but also irregularly shaped and rod-like particles (O'Connor et al., 2013) Effects of shape on toxicity not known	Not known	Dust contains significant amounts of bacterial and fungal spores, adsorbed endo- and mycotoxins (Séguin et al., 2010) These are likely the main causes of adverse health effects (Reboux et al., 2007; Cano Jiménez et al., 2016)	2018) Wood cellulose fibers half-life ~ 3 years in rat lungs, half life of cellulose fibers from recycled newspapers 72 days in rat lungs (Muhle et al., 1997) No significant degradation of cellulose in vitro in lung airway lining fluid and phagolysosomal fluid after up to 9 months (Stefaniak et al., 2014)	Farmer's lung disease (allergic alveolitis) (Gregory and Lacey, 1963; Siegel et al., 1991), likely caused by bacterial endotoxins and mycotoxins (Reboux et al., 2007; Cano-Jiménez et al., 2016)
Microplastics	Measured size distributions are likely influenced by sampling & detection limits (Zhang et al., 2020) Measured sizes for atmospheric MP fibers between 20 µm and 5 mm (Cai et al., 2017; Li et al., 2020; Szewc et al., 2021), predominantly 100–700 µm (Allen et al., 2019; Cai et al., 2017); fragments between 5 µm and 750 µm (Szewc et al., 2021); films between 10 µm and 1520 µm (Szewc et al., 2021). Studies with particularly low detection limits measured 70% of MP fallout particles < 63 µm (Klein and Fischer, 2019); at human respiratory height 80% of MP < 20 µm (Li et al., 2020)	Many reports of fibers (Liu et al., 2019; Abbasi et al., 2019; Cai et al., 2017; Dris et al., 2016; Szewc et al., 2021), but also fragments and films (Allen et al., 2019; Szewc et al., 2021). Higher prevalence of fibers indoors than outdoors (Liu et al., 2019; Dris et al., 2017). However, due to focus of MP research on spherical particles (Lim, 2021) role of shape in MP toxicity not known	Surface functionalization of plastics is a common method to adjust material properties (Johansson, 2017), furthermore functional surface groups induced by weathering and photodegradation of MP (Meides et al., 2021; Fechine et al., 2004; Fernando et al., 2007; Decker and Zahouily, 1999); therefore, ζ-potential of MP likely varies in a large range. Even supposedly identical model MP particles have substantially different ζ-potentials, affecting their interactions with cells (Ramsperger et al., 2021)	Adsorbed POPs and heavy metals (Rochman et al., 2014; Hirai et al., 2011; liang Liao and yan Yang, 2020) have a controversial role in MP toxicity (Koelmans et al., 2021); formation of ecocoronas and biofilms (Ramsperger et al., 2020; Galloway et al., 2017) enhances cellular internalization (Ramsperger et al., 2020); films possibly carry dangerous pathogens (Kirstein et al., 2016; Imran et al., 2019; Gkoutselis et al., 2021)	Extraordinarily high bio-persistence of conventional polymers (Andrady, 2015); therefore likely very high bio-persistence of MP particles in organisms. Biodegradation of biodegradable polymers usually by specialized microorganisms and conditions limited to industrial composting plants (Millican and Agarwal, 2021; Bagheri et al., 2017), therefore likely high bio-persistence in the lung. Due to bio-persistence accumulation of MP in the organism, leading to chronic exposure (Mohamed Nor et al., 2021)	Mainly diseases due to occupational exposure (Prata, 2018): Pneumoconiosis (Ng et al., 1991; Studnicka et al., 1995), interstitial lung disease (Cortez Pimentel et al., 1975; Kern et al., 1998; Eschenbacher et al., 1999), chronic bronchitis (Cortez Pimentel et al., 1975; Miller et al., 1975), cough and dyspnea (Valic and Zuskin, 1977; Zuskin et al., 1998; Lougheed et al., 1995; Kern et al., 2000), allergic and asthmatic reactions (Cortez Pimentel et al., 1975; Muittari and Veneskoski, 1978), lung cancer (Mastrangelo et al., 2002; Hours et al., 2007; Kern et al., 2011). Cancer in digestive system, large bowel, stomach, and esophagus (Mastrangelo et al., 2002; Vobecky et al., 1978; Gallagher et al., 2015)

ζ-potential of crystalline silica dust is pH-dependent. At physiological conditions, values of about − 30 – − 10 mV have been reported (Dong et al., 2015; Leinardi et al., 2020). Interestingly, freshly fractured crystalline silica is linked to a more intense inflammatory response, potentially due to increased surface radicals (Vallyathan et al., 1995).

There is evidence that biogenic amorphous silica (e. g. from the shells of diatoms) has the potential to adsorb toxic chemicals like polycyclic aromatic hydrocarbons (PAHs), acting as a vector for those chemicals into the body (Rabovsky, 1995). However, it is unclear in how far this contributes to the overall toxicity of silica dust, as the main part of silica-related health effects is caused by crystalline silica dust that is freshly generated during the processing of stone (Silicosis Mortality, 2005).

Due to the high bio-persistence of silica dust, chronic effects play a significant role in silica toxicity (Leung et al., 2012). Because of their low dissolution rates (Rimstidt and Barnes, 1980), crystalline silica particles are extraordinarily durable under physiological conditions. Under conditions similar to the lung, a lifetime of about 100 – 10,000 years has been estimated for crystalline silica microparticles (Jurinski and Rimstidt, 2001).

2.3. Soot

Soot is formed by the incomplete combustion of organic materials such as wood, coal, fossil fuels, and plastics (IARC, 2012). Its physical properties and chemical composition heavily depend on the type of burned material and the specific combustion conditions(Kleeman et al.,

1999). The dominant constituent is elemental carbon, accounting for about 60% of soot mass, followed by inorganic and organic matter, including PAHs (IARC, 2012).

For example, chimney sweeps are subjected occupationally to inhalable soot dust (Pukkala et al., 2009; Hogstedt et al., 2013). The median exposure level of Swedish chimney sweeps to inhalable soot dust was found to be 3.8 mg m^{-3} (Hogstedt et al., 2013). Other occupations with potentially increased soot exposure are industrial, maintenance, or service professions performed near fossil fuel combustion engines, such as truck drivers and miners (Donaldson et al., 2005).

Besides occupational exposure, contamination of the ambient air by environmental soot in particulate matter air pollution is also prevalent. Typical ambient exposure levels to soot particles < 10 µm close to a moderately frequented urban street lie in the range of 20–60 µg m^{-3} (Boogaard et al., 2010).

Chimney soot is classified as carcinogenic by the International Agency for Research on Cancer (IARC) (IARC, 2012). The discovery of high incidences of scrotal cancer in chimney sweeps during the 18th century was the first documented case of occupational cancer (Pott, 1775; Benmoussa et al., 2019). Although scrotal cancer due to soot exposure is nowadays mostly preventable, increased incidences of cancers of the lung and the esophagus, among other types of cancer, are still reported for chimney sweeps (Pukkala et al., 2009). Additional epidemiological evidence exists for their occupational risk of asthma and ischemic heart disease (Li et al., 2008; Hansen, 1983). Apart from occupational health risks, ambient exposure to airborne particulate matter, including soot, is also a well-known factor associated with

6

adverse health impacts. Soot-associated diseases include respiratory and cardiac diseases, which can increase mortality in exposed cohorts (Janssen et al., 2012; Lee, 2010). It is also discussed whether ambient exposure to soot particles is associated with an increase in cancer. For example, diesel exhaust is classified as carcinogenic by the IARC (IARC, 2014). However, whether ambient exposure to diesel exhaust particles (DEPs) is associated with diseases like lung cancer is still controversial (Stöber and Abel, 1996; Hesterberg et al., 2012). One difficulty in assessing the risk of ambient soot exposure is disentangling the specific health impacts of soot and other constituents of airborne particulate matter. Nevertheless, some evidence points towards the fraction of black carbon in the overall particulate matter mass being a robust indicator for adverse health effects (Janssen et al., 2011).

The toxicological pathways leading to the observed health effects of soot likely depend on the soot particle types. Usually, oxidative stress and inflammatory responses are involved (Donaldson et al., 2005). For example, upon exposure to DEPs, proinflammatory signaling pathways increase cytokine expression in vitro (Terada et al., 1999) and in human lungs in vivo (Salvi et al., 2000). Apart from inflammatory responses, ROS generated by soot particles has a mutagenic potential, possibly leading to cancer upon prolonged exposure (Watson and Valberg, 2001; Barfknecht, 1983).

The physicochemical properties of soot particles (Fig. 1C, Table 1) depend on the source material and the combustion conditions (Torvela et al., 2014). Size distributions of particles from wood smoke, for example, were found to peak at 0.1–0.2 µm in diameter. Particles from cigarette smoke displayed a distribution peak between 0.3 and 0.4 µm (Kleeman et al., 1999). Soot particles from highly efficient combustion processes, including modern diesel-fueled engines, have sizes in the order of tens of nanometers, which agglomerate to structures with a typical size of several hundred nanometers (Fig. 1C) (Watson and Valberg, 2001; Omidvarborna et al., 2015). During the combustion of heavy oil fuels, particles with an average size of 10–100 µm are formed. In domestic chimney soot, particles > 1 µm up to 1 mm are found (Watson and Valberg, 2001). After their release into the atmosphere, particle aggregation and the condensation of organic matter increases the soot particles' size (Janssen et al., 2012; Watson and Valberg, 2001; Patterson and Kraft, 2007). There is evidence that the soot particles' size affects their toxicity (Frank et al., 2013). In one study, the bioreactivity of soot in the size range of 70–110 nm was increased compared to smaller and larger particles, leading to an increased expression of cytokines (Sarkar et al., 2014).

The shapes of soot particles are similarly diverse. Particles formed from highly efficient combustion processes aggregate to form aciniform, grape-like structures (Fig. 1C) (Watson and Valberg, 2001; Omidvarborna et al., 2015). During the combustion of heavy fuel oils, cenospheres (hollow spheres) can be formed. In domestic chimney soot resulting from wood or coal burning, xerogels and irregular pieces of coke and char are prevalent. Xerogels are porous, carbonaceous fragments with an extraordinarily high surface area (Watson and Valberg, 2001). Potentially, the shape of soot particles can affect their toxicity. For example, by activating molecular oxygen on their surface, an increasing curvature might lead to a stronger reactivity of the soot particles (Frank et al., 2013).

The ζ-potential of DEPs lies mainly between − 50 to − 30 mV under physiological conditions (Sarkar et al., 2014; Chen and Huang, 2017). It was found that DEPs in the zeta-potential range between − 41 mV and − 37 mV showed bioreactivity in immune cells. This leads to an increase in cytokine expression and inflammatory responses (Sarkar et al., 2014).

An essential parameter in soot toxicity is adsorbed PAHs, such as benzo(a)pyrene (Barfknecht, 1983; Kirrane et al., 2019). These organic compounds condense on soot particles during the combustion process and after their release into the environment (Lee, 2010; Watson and Valberg, 2001; Eaves et al., 2017). Consequently, soot particles are a well-known exposure route to PAHs, known for their carcinogenicity (Lee, 2010). The fraction of PAHs and other organic compounds is

associated with the mutagenicity of soot particles (Medalia et al., 1983).

The bio-persistence of soot particles might contribute to their toxicity. From experiments with DEPs in lung cells of rats, the half-life time of persistence in the lung is known to lie between 80 and 250 days, while the clearance efficiency decreases with the exposure level (Griffis et al., 1983; Wolff et al., 1987).

2.4. Wood dust

The main components of wood particles are cellulose and lignin. Most commonly, wood dust is generated during the processing of wood. Typical exposition levels for woodworkers are (0.2 ± 2.6) mg m^{-3} for wood dust particles with a size < 4 µm, (0.3 ± 2.8) mg m^{-3} for particles in the size range 4 – 10 µm, and (1.5 ± 2.7) mg m^{-3} for dust in the size range 10 – 100 µm (Glindmeyer et al., 2008).

According to the IARC, wood dust is classified as carcinogenic to humans. In their report, the IARC concludes that hardwood is associated with the formation of adenocarcinoma of the nasal cavities and paranasal sinuses, whereas, at the time of the study, the correlation was less clear after exposure to softwood dust (Delzell, 1995). Since then, multiple meta-analyses have been published, strengthening the conclusion of the IARC of a strong association between lung cancer and wood dust (Alonso-Sardón et al., 2015; Binazzi et al., 2015; Hancock et al., 2015).

Another significant risk associated with wood dust are pulmonary diseases. For example, an increased risk for cryptogenic fibrosing alveolitis, a disease characterized by severe inflammation and fibrosis of the deep respiratory tract, was found in patients exposed to wood dust (Hubbard et al., 1996). Furthermore, idiopathic pulmonary fibrosis, which leads to the thickening of lung tissue, is significantly associated with exposure to both soft- and hardwood dust (Gustafson et al., 2007).

The pathogenesis of diseases associated with wood dust exposure includes inflammatory responses and the generation of ROS. For example, the carcinogenicity of particulate matter, including wood dust, is potentially linked to an immune response and the subsequent generation of ROS (Knaapen et al., 2004). Furthermore, although the exact mechanisms leading to idiopathic pulmonary fibrosis are still unclear, inflammation is likely involved (Gustafson et al., 2007). The role of ROS in wood dust toxicity was investigated in several in vitro studies, exposing mouse macrophages and human leukocytes to different hard- and softwood dust (Naarala et al., 2003; Klein et al., 2001).

Additionally, increased cyto- and chemokines expression was observed upon exposure to wood dust, indicating an inflammatory response (Long et al., 2004; Määttä et al., 2005, 2006). Interestingly, this was independent of the individual wood types, with similar inflammatory responses for soft- and hardwood dust (Määttä et al., 2006). An inflammatory response to wood dust was also observed in vivo in mice. In these studies, eosinophil cell counts were increased upon wood dust instillation, and lymphocytes and neutrophils migrated into the lung of the mice. Furthermore, the presence of these immune cells was associated with an increase in proinflammatory chemokines. Strikingly, no such effects were observed in the same experimental setup upon exposure to titanium dioxide particles of the same size, indicating that these immune system responses were wood-specific (Määttä et al., 2006).

Physical properties of wood dust (Fig. 1D, Table 1) likely depend on the wood type and processing technique. For example, when sampling directly at the milling of wood, the share of particles smaller than 125 µm is only between 1% and 15%, while larger particles make up most of the wood dust (Očkajová et al., 2020). However, the aerodynamic diameters of wood dust particles collected at breathing height at working places measure between 10 µm and 100 µm (Harper et al., 2002). Wood dust samples directly generated by sanding of hard and softwood shows a smaller aerodynamic diameter in the breathable range of < 10 µm (Määttä et al., 2006; Ojima, 2016; Marková et al., 2018), and particles of similar size were generated by manual filing (Fig. 1D).

Like the wood particles' size, also their shape depends on wood type and processing technique. Usually, the shape of wood dust particles is

7

complex and irregular, with a rough surface (Fig. 1D) (Mazzoli and Favoni, 2012; Liu et al., 1985). How the wood dust particles' shape affects their toxicity, has not been studied yet.

The ζ-potential of intact spruce wood capillaries was between − 10–+10 mV at pH 5.6 (Muff et al., 2018). Cellulose nanofibers produced from cedar wood powder at pH 6.8–7 showed a ζ-potential of − 50 - − 30 mV (Uetani and Yano, 2012). However, the effect of the ζ-potential on wood dust particle toxicity is not known.

The ROS production strongly depended on the individual wood types, possibly linked to different natural chemical compounds (e.g., terpenes in softwoods and polyphenolic compounds in hardwoods) (Naarala et al., 2003). However, chemicals used for wood treatment (e. g., chromate compounds) are also discussed as potential drivers of wood dust toxicity (Klein et al., 2001).

The very high bio-persistence of wood likely enhances wood dust toxicity in the lung. Biodegradation of lignin and cellulose requires enzymes found in specialized microorganisms (Slavin et al., 1981; Pérez et al., 2002; Eriksson et al., 1990). There is evidence that wood cellulose fibers persist in rat lungs even a year after exposure and that their estimated half-life is about three years (Muhle et al., 1997).

2.5. Cotton dust

A natural organic airborne pollutant is cotton dust, which is generated during the processing of cotton. It consists mainly of cotton fibers and contains bacteria, fungi, and other plant materials such as cotton stems and leaves (Ayer and Mackison, 1974). Cotton dust exposure in textile mills varies between different processes and mills; total dust concentrations in the range of about 0.1–10 mg m⁻³ were observed in a study investigating five textile mills and fourteen different processes (Hammad et al., 1981).

Increased exposure of cotton industry workers to cotton dust is associated with diseases such as asthma, bronchitis, byssinosis (a disease associated with breathing difficulties and chest tightness), and unspecific respiratory problems (Castranova et al., 1996; Dangi and Bhise, 2017). A 15-year follow-up observation showed that the cumulative incidence of byssinosis was 24% among cotton textile workers. In addition, chronic bronchitis and cough were more common and persistent than in the control group (Wang et al., 2003).

Several parameters (Fig. 1E, Table 1) affect the toxicity of cotton dust. The particles in cotton dust are grouped according to their size into 'trash' (> 500 μm), 'dust' (50–500 μm), 'micro dust' (15–50 μm) and 'breathable dust' (< 15 μm) (Dangi and Bhise, 2017). Usually, the breathable fraction of cotton dust is linked to adverse effects on animal and human health (Ellakkani et al., 1984).

Mill-collected cotton dust contains a significant fraction of fragmented fibers (Fig. 1E) and large pieces of plant material. The individual cotton dust particles are often irregularly shaped (Goynes et al., 1986).

To date, there have been no investigations of the ζ-potential of breathable cotton dust.

The diseases related to cotton dust exposure are likely not directly caused by the cotton particles but primarily by bacterial endotoxins or residual pesticides adsorbed to the cotton dust, possibly releasing mediators inducing inflammations (Wang et al., 2003; Rylander, 1987; Solbrig and Obendorf, 1985). Consistently, after exposing guinea pigs to breathable cotton dust, all treated animals showed a respiratory response, whereas no response was observed when the animals were exposed to pristine cellulose powder with the same particle size distribution (Ellakkani et al., 1984).

Cotton is likely very bio-persistent, possibly contributing to its chronic toxicity, because it contains a large amount of cellulose. As already mentioned in the section on wood dust, the degradation of cellulose requires enzymes that are only present in specialized microorganisms (Eriksson et al., 1990). In rat and mouse lungs in vivo, cellulose fibers were very persistent and had an estimated half-life of up to 3 years (Muhle et al., 1997; Ilves et al., 2018). Consistently, in lung

airway lining fluid and phagolysosomal fluid in vitro, there were no significant signs of degradation of cellulose after up to 9 months of exposure (Stefaniak et al., 2014).

2.6. Hay dust

Exposure to hay dust has been linked to occupational diseases of the lung. Apart from organic debris, pollen and toxins such as endotoxins and mycotoxins are significant contaminants in hay dust (Séguin et al., 2010). The exposure levels to hay dust vary broadly. For example, during the operation of a bedding chopper, the total dust level was found to be in the range of about 10–70 mg m⁻³ (Olenchock et al., 1990). Farmer's increased exposure to hay dust can lead to various respiratory symptoms; most prominently, the inhalation of dust from moldy hay can lead to the so-called farmer's lung disease (Gregory and Lacey, 1963; Siegel et al., 1991). Farmer's lung disease is the most common form of extrinsic allergic alveolitis; it is classified into an acute, subacute, and chronic stage (Reboux et al., 2007). Interestingly, also farm animals like dairy cows exposed to hay dust displayed asthma-like symptoms (Siegel et al., 1991).

The physicochemical properties of hay dust (Fig. 1F, Table 1) may contribute to its toxicity. For example, about 95% of hay dust particles are smaller than 5 μm, enabling them to enter the bronchioles upon inhalation (Séguin et al., 2010; O'Connor et al., 2013). Their shape is primarily spherical, although irregularly shaped and rod-like particles also occur in hay dust(O'Connor et al., 2013). It is not known whether their shape affects the hay dust particles' toxicity. To date, there have been no investigations of the ζ-potential of hay dust particles.

The most prominent parameter affecting hay dust toxicity are microorganisms, endotoxins, and mycotoxins associated with the hay dust (Séguin et al., 2010). Usually, these are the cause of the farmer's lung disease (Reboux et al., 2007; Cano-Jiménez et al., 2016). Since not the hay itself but inhaled microorganisms cause farmers' lung disease, studies focus on identifying relevant antigens present in the hay dust. The primary treatment of the disease is avoiding the antigens (Cano-Jiménez et al., 2016).

Moreover, like cotton, hay mainly consists of cellulose, likely making it very bio-persistent (Eriksson et al., 1990; Muhle et al., 1997; Ilves et al., 2018; Stefaniak et al., 2014).

2.7. Comparability of non-plastic microparticles and MP

In this section, we focused on different non-plastic microparticles of various materials that potentially determine their physicochemical properties. Some of these non-plastic microparticles are chemically more related to MP than others. For example, wood, cotton, and hay (Sections 2.4–2.6) consist mainly of cellulose, an organic polymer, and are therefore more similar to MP than asbestos or silica, which are inorganic crystals (Sections 2.1 and 2.2). MP, usually consisting of synthetic polymers, is a diverse group of contaminants with a wide range of physical and chemical properties (Rochman et al., 2019). However, although chemically very different, the physicochemical properties governing the different non-plastic and plastic microparticles' interactions with cells and tissues might still be comparable (Table 1). Similarities of particles in size, shape, ζ-potential, adsorbed molecules and microorganisms, and bio-persistence may explain similarities in their toxicity and the underlying toxicological mechanisms. Therefore, a comparison of the properties and toxicology of non-plastic particles with MP can improve the understanding of the role of physicochemical properties in MP toxicity.

3. Airborne MP

3.1. Occurrence of airborne MP pollution

Since the topic of MP pollution is relatively new and research mainly

8

focused first on aquatic and then terrestrial ecosystems, the number of literature on airborne MP is still very small (Enyoh et al., 2019). Nevertheless, first attempts to monitor airborne plastic pollution have been made.

There are different methodological approaches to identify MP in the atmosphere. For example, some studies investigated the MP concentration in dust samples either by directly collecting the dust (Liu et al., 2019; Abbasi et al., 2019; Yukioka et al., 2020) or by investigating the content of a vacuum cleaner bag (Dris et al., 2017). Furthermore, the atmospheric fallout has been measured by dry and wet sample collectors with different opening diameters (Allen et al., 2019; Cai et al., 2017; Dris et al., 2016), by collecting plant leaves with deposited particles on their surfaces (Liu et al., 2020), through direct filtering of the air (Dris et al., 2017; Li et al., 2020) or by using a human breathing thermal manikin (Vianello et al., 2019). However, the data's comparability is limited by the differences in sampling techniques and inconsistencies in data presentation, often quantifying particle fallout per area, particle count per volume, or particle mass per volume. Several earlier reviews focused on these issues (Mbachu et al., 2020; Amato-Lourenço et al., 2020; Huang et al., 2020; Enyoh et al., 2019; Can-Güven, 2021; Chen et al., 2020).

Airborne MP particles, including fibers, fragments, and films, have been found in various environments. Many reports focused on the occurrence of MP in urbanized areas. For example, Abbasi et al. monitored the MP pollution in street dust and the atmosphere (Abbasi et al., 2019). The dust samples mainly consisted of a heterogeneous mixture of MP shapes, whereas fibers were the predominant type of shape in atmospheric samples. This study is in concordance with numerous other studies, showing that the predominant type of MP in atmospheric samples are fibers (Liu et al., 2019; Cai et al., 2017; Dris et al., 2016; Szewc et al., 2021), with a higher amount found in indoor than in outdoor samples (Liu et al., 2019; Dris et al., 2017).

However, MP within the atmosphere is not restricted to urbanized areas. For example, Allen et al. sampled the atmospheric fallout in remote areas of the Pyrenean mountains and found MP fibers, films, and fragments in all samples (Allen et al., 2019). In contrast to other, more urbanized sampling locations, MP fragments ($< 50 \, \mu m$) were the predominant type. Sahara dust in these samples possibly indicates that MP fragments in the atmosphere can be transported similarly (Allen et al., 2019). Furthermore, airborne MP were also detected in the remote marine atmosphere of the Atlantic (Trainic et al., 2020) and the South China Sea as well as the East Indian Ocean (Wang et al., 2020) and were discussed to be able to travel hundreds to thousands of kilometers due to their irregular and elongated shapes (Trainic et al., 2020; Wang et al., 2020).

3.2. Properties of airborne MP

MP contamination of the atmosphere includes particles of all sizes (Table 1). Different studies report MP fibers ranging from smaller than 20 µm to 5 mm in length (Cai et al., 2017; Li et al., 2020; Szewc et al., 2021), with a predominant length of 100–700 µm (Allen et al., 2019; Cai et al., 2017). Detected MP fragments ranged from 5 µm to 750 µm (Szewc et al., 2021) and films from 10 µm to 1520 µm (Szewc et al., 2021). However, the reported size ranges are heavily influenced by sampling and detection limits, often making it challenging to quantify contamination of the atmosphere with microscopic particles (Zhang et al., 2020). To assess potential risks associated with airborne MP pollution, improved tools for the study of very small MP $< 10 \, \mu m$ will be required (Vethaak and Legler, 2021).

A study on atmospheric fallout of MP particles in Paris mentions a count of 118 fallout particles per square meter per day (p m^{-2} d^{-1}), ranging from 29 p m^{-2} d^{-1} to 280 p m^{-2} d^{-1} (Dris et al., 2015). Consistently, at different urban and suburban sites, fallouts of fibers of (110 ± 96) p m^{-2} d^{-1} and $53 \pm 38)$ p m^{-2} d^{-1} respectively were reported (Dris et al., 2016). Similarly, fallouts of 175–313 p m^{-2} d^{-1} occurred in an urban area in China (Cai et al., 2017). The corresponding MP fiber

concentrations at human respiratory height were reported to be between 0.3 and 20 particles per cubic meter (p m^{-3}) indoors and 0.1–0.5 p m^{-3} outdoors, the most abundant fraction of fibers being in the size class of 50–250 µm, which was the lowest size reported in this study (Dris et al., 2017). Furthermore, a study conducted in the catchment of the River Weser in Germany reported a mean concentration of 46 p m^{-3} of airborne MP only in the size range between 4 and 10 µm (Kernchen et al., 2021). All studies reported a large variability of observed particle numbers, possibly correlated with the amount of rainfall, time of year, and sampling site (Dris et al., 2017, 2016, 2015). Similarly, up to 4.18 p m^{-3} of suspended atmospheric MP particles were reported in Shanghai (Liu et al., 2019).

3.3. Inhalation and ingestion of airborne MP

Inhalation and ingestion are the main exposure routes of airborne MP to humans (Fig. 2A). Based on the results above, and assuming an average breathing volume of 6 l min^{-1}, it was estimated that humans might be exposed to 26–130 airborne MP of different sizes per day (Prata, 2018). A study using a human breathing thermal mannequin to simulate human exposure to indoor airborne MP contamination found even higher numbers since they measured 272 p d^{-1} of inhaled MP (Vianello et al., 2019). A critical shortcoming of these reports is their limited detection of MP smaller than 50–100 µm, likely leading to a gross underestimation of reported MP contamination. For example, in a study with a lower detection limit of 5–13 µm, about 70% of the detected MP fallout particles were smaller than 63 µm. Overall, a fallout of 136–512 p m^{2} d^{1} was reported (Klein and Fischer, 2019). More recently, a study with a lower detection limit of 0.8 µm reported a MP fiber concentration of about 5600 p m^{-3} at human respiratory height. More than 80% of all detected airborne particles were smaller than 20 µm (Li et al., 2020). Consequently, assuming an average breathing volume of 6 l min^{-1}, humans might be exposed to more than 48,000 MP p d^{-1} by inhalation. These findings reinforce the concerns about airborne MP contamination raised by earlier studies (Prata, 2018; Vianello et al., 2019). Furthermore, ingestion of airborne MP mainly occurs due to the fallout of atmospheric MP during meal preparation and consumption. Approximately, humans consume 40 – 190 p d^{-1} in this way (Catarino et al., 2018).

3.4. MP in the lung

Once inhaled, MP can infiltrate the lung depending on its aerodynamic diameter (Fig. 2B). Especially MP with an AED $< 10 \, \mu m$ has the potential to penetrate the lower respiratory tract (Prata, 2018; Martens and Jacobi, 1973; Foord et al., 1978; Williams et al., 2011; Lippmann et al., 1980). There is evidence that plastic fibers can penetrate the human deep lung (Pauly et al., 1998; Amato-Lourenço et al., 2021), and plastic fibers were present in the lower respiratory tract after inhalation by rats (Porter et al., 1999; Warheit et al., 2003). In addition, it has been shown that MP particles can penetrate the lungs' surface lining layer and are taken up by endothelial cells (Geiser et al., 2003, 2005; Deville et al., 2015; Goodman et al., 2021). Clearance (clearance from the respective organ, not necessarily the organism) of MP from the lung occurs via two main pathways: via the mucociliary escalator and via an internalization by pulmonary macrophages, the first enabling transport of inhaled MP into the gastrointestinal tract (Lippmann et al., 1980; Geiser et al., 2005).

3.5. MP in the gastrointestinal tract

Airborne MP may enter the gastrointestinal tract via inhalation and the mucociliary escalator (Fig. 2B) and by settling onto food during preparation and consumption (Catarino et al., 2018). Particles $> 50 \, \mu m$ are likely excreted from the gastrointestinal tract. Schwabl et al. (2019) reported 20 MP particles larger than 50 µm per 10 g in human stool samples (Schwabl et al., 2019). To which extent smaller MP are excreted from the gastrointestinal tract is not yet investigated. Other than
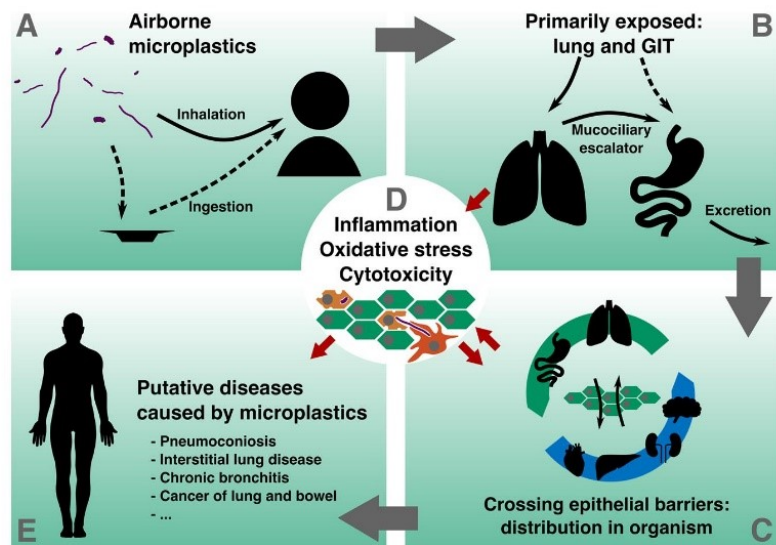
9

Fig. 2. Potential pathways of MP toxicity. A) Airborne MP can enter the human organism either by inhalation or ingestion, primarily exposing the lung and gastrointestinal tract (GIT) (Prata, 2018; Catarino et al., 2018). B) MP particles in the upper airways can be cleared via the mucociliary escalator, translocating these particles into the GIT, from which a share of the particles will be excreted (Lippmann et al., 1980; Schwabl et al., 2019). However, some of the MP particles are translocated deeper into the tissues of the lung and GIT(Geiser et al., 2005; Volkheimer, 1975; Carr et al., 2012; Sanders and Ashworth, 1961; Lefevre et al., 1989; Jani et al., 1989; Des Rieux et al., 2005). C) By crossing epithelial barriers, MP can also enter the lymphatic system and bloodstream (Volkheimer, 1975; Jani et al., 1989; Eyles et al., 2001). From there, MP particles can distribute in the whole organism, ultimately reaching different secondarily exposed organs (Volkheimer, 1975; Jani et al., 1989, 1990; Urban et al., 2000; Eyles et al., 2001; Deng et al., 2017; Wick et al., 2010; Ragusa et al., 2021). D) In exposed tissues, MP particles may cause inflammatory responses and oxidative stress, eventually leading to cytotoxicity (Geiser et al., 2005; Goodman et al., 2021; Mahadevan and Valiyaveettil, 2021). These effects reduce the epithelial barrier resistance, increase MP's mobility in the organism (Hamoir et al., 2003; Yacobi et al., 2008; Di Dong et al., 2020), and may potentially cause additional adverse effects on human health. E) Among others, diseases like pneumoconiosis (Ng et al., 1991; Studnicka et al., 1995), interstitial lung disease (Cortez Pimentel et al., 1975; Kern et al., 1998; Eschenbacher et al., 1999), chronic bronchitis (Cortez Pimentel et al., 1975; Miller et al., 1975), and cancer of the lung and bowel might be associated with MP (Mastrangelo et al., 2002; Hours et al., 2007; Kern et al., 2011; Vobecky et al., 1978; Gallagher et al., 2015). These diseases are prevalent in exposed workers of the flocking and VC/PVC industry (Prata, 2018).

excretion, important clearance mechanisms from the gastrointestinal tract are para- and transcellular internalization of MP into the surrounding tissues. It has been shown that MP can pass the epithelial layer between enterocytes in a paracellular manner (Volkheimer, 1975). For the transcellular translocation of microparticles, including MP, the uptake by M-cells into the Peyer's patches (lymphoid follicles in the small intestine) plays a significant role (Carr et al., 2012; Sanders and Ashworth, 1961; Lefevre et al., 1989; Jani et al., 1989; Des Rieux et al., 2005). Furthermore, it was shown that the translocation efficiency strongly depends on particles size (Carr et al., 2012; Jani et al., 1990). For example, the total uptake efficiency into rat gastrointestinal mucosa of polystyrene (PS) nanoparticles with a size of 50 nm and 100 nm was around 33% and 26%, respectively, much higher compared to 1 µm sized MP, of which only 4.5% were taken up (Jani et al., 1990). Nevertheless, studies report varying magnitudes of translocation efficiency, ranging from 0.04% to 4.5% for particles in the micrometer size range in rodent models (Carr et al., 2012; Jani et al., 1990).

3.6. Distribution of MP in the organism

MP that was displaced into tissues can become internalized by resident tissue macrophages (Geiser et al., 2005). Macrophages as professional phagocytes do not only internalize micrometer-sized bacteria (Underhill and Goodridge, 2012), but also microparticles with different surface properties (Ramsperger et al., 2020; Desjardins and Griffiths, 2003; Irmscher et al., 2013; Kress et al., 2007). Especially the uptake into Peyer's patches in the interstitium by M-cells enables interactions of MP with various immune cells and the subsequent transport to the lymphatic system (Jani et al., 1989). Also, paracellular transport allows MP to move from tissues into the lymphatic system (Volkheimer, 1975). Macrophages not only transport microparticles intracellularly (Keller et al., 2017), but they can also act as 'transporters' for MP inside the organism, distributing the MP through the lymphatic system to different organs (Walker and Bullough, 1973; Urban et al., 2000). Moreover, particles that have been displaced into the lymphatic system can enter the bloodstream (Eyles et al., 2001). There is also evidence for MP being

directly transferred from primarily exposed organs into the bloodstream (Volkheimer, 1975). Once in the blood, MP distributes in the whole organism and can be found in various secondarily exposed organs (Fig. 2C).

Many studies report evidence of MP migrating to various organs in humans and different model species, including mice, rats, and dogs. MP have been found in the liver (Volkheimer, 1975; Jani et al., 1990; Deng et al., 2017), spleen (Jani et al., 1990; Urban et al., 2000; Eyles et al., 2001), kidneys and urine (Volkheimer, 1975; Deng et al., 2017), bone marrow (Jani et al., 1990), brain and cerebrospinal fluid (Volkheimer, 1975), and the placenta (Wick et al., 2010; Ragusa et al., 2021). Interestingly, inflammatory responses at sites of MP exposure can reduce the integrity of epithelial barriers and activate macrophages. In this way, the mobility of MP in the body might be increased (Hamoir et al., 2003; Yacobi et al., 2008; Di Dong et al., 2020). Finally, the MP particles can irreversibly accumulate in tissues over the human lifetime (Mohamed Nor et al., 2021).

3.7. MP-associated diseases

There are some reports of MP-associated diseases (Fig. 2E, Table 1), most of which focus on people working in the textile, flocking, and VC/PVC (vinyl chloride/polyvinyl chloride) industries. In these industries, the concentration of airborne MP can reach extraordinarily high levels, up to 7–40 mg m^{-3} or 10^6 particles m^{-3} (Bahners et al., 1994; Burkhart et al., 1999). Due to these high levels of exposure to MP, it was possible to link occupational diseases to MP pollution. Many of the reported effects occurred in the lung and the gastrointestinal tract, the primarily exposed organs. A recent review discusses occupational diseases resulting from MP exposure (Prata, 2018). Briefly, there were reports about pneumoconiosis (Ng et al., 1991; Studnicka et al., 1995), interstitial lung disease (Cortez Pimentel et al., 1975; Kern et al., 1998; Eschenbacher et al., 1999), chronic bronchitis (Cortez Pimentel et al., 1975; Miller et al., 1975), and various other acute and chronic symptoms, including cough and dyspnea (Valic and Zuskin, 1977; Zuskin et al., 1998; Lougheed et al., 1995; Kern et al., 2000). Apart from that,

10

occupational exposure to MP has been correlated to allergic and asthmatic reactions (Cortez Pimentel et al., 1975; Muittari and Veneskoski, 1978). Additionally, studies reported a significantly increased risk of these workers for lung cancer (Mastrangelo et al., 2002; Hours et al., 2007; Kern et al., 2011).

Because of their high exposure to MP, workers in the textile and flocking industry are also subject to gastrointestinal tract diseases. Cases of cancer in the digestive system, large bowel, stomach, and esophagus that were assumed to be due to their high exposure were also reported (Mastrangelo et al., 2002; Vobecky et al., 1978; Gallagher et al., 2015). In addition, more recent in vivo studies on mice found decreased intestinal mucus and microbiome dysbiosis (a disruption of the gut microbiome) after exposure to MP (Lu et al., 2018; Jin et al., 2019).

There are also MP-associated diseases reported in secondary organs. Interactions of human red blood cells with PS MP led to blood cell aggregation and attachment to endothelial cells in vitro (Barshtein et al., 2016). In rats, injection of PS microspheres led to vascular occlusions, inflammation, and pulmonary embolism (Zagorski et al., 2003; Jones et al., 2003). *In vitro*, it was shown that exposure of sheep blood to MP induced hemolysis (Hwang et al., 2019). In lymph nodes of patients with total hip arthroplasty, granular histiocytosis caused by wear particles from the artificial joints, including MP, was observed (Hicks et al., 1996). In mice, inflammation of the liver and disturbed hepatic lipid metabolism were observed upon exposure to MP (Deng et al., 2017).

3.8. Toxicology of MP

Inflammation and oxidative stress contribute to the toxicity of MP (Fig. 2D). For example, in tissues, MP was observed to cause aggregations of macrophages, granulation tissue, and a foreign body response (Urban et al., 2000; Willert and Semlitsch, 1996; Doorn et al., 1996). Consequently, granulomas with a tendency towards necrosis are formed, leading to fibrosis and scarring of the tissue (Willert and Semlitsch, 1996). Inflammatory responses are regulated and enhanced by cytokine production. Upon exposure to PS particles, increased IL-6 and IL-8 production, inflammation, and oxidative bursts in multiple human and murine monocyte and macrophage cell lines were observed (Di Dong et al., 2020; Brown et al., 2001; Prietl et al., 2014).

Similarly, PE (polyethylene) MP also caused increased interleukin and TNFα production (Green et al., 1998; Nich and Goodman, 2014). Increased cytokine production can activate nearby macrophages, enhancing inflammatory responses in exposed tissues (Hicks et al., 1996; Nich and Goodman, 2014; Morawski et al., 1995; Devane et al., 1995). These inflammatory responses lead to the release of oxidizing species (Sternschuss et al., 2012). Furthermore, MP can carry oxidizing radicals on their surface due to weathering, inducing oxidative stress in cells (White and Turnbull, 1994; Gewert et al., 2015). Oxidative stress can also be enhanced by releasing adsorbed oxidizing chemicals, e.g., metals (Kelly and Fussell, 2012; Valavanidis et al., 2013).

Inflammatory responses and oxidative stress may induce cytotoxicity. For example, in hamster BHK-21 cells, PVC and PMMA (polymethyl methacrylate) MP with a size of $0.12\ \mu m$ and $0.14\ \mu m$, respectively, induced increased concentrations of ROS, leading to reduced cell viability (Mahadevan and Valiyaveettil, 2021). Similarly, reduced viability and striking morphological changes were observed in human lung A459 cells upon exposure to PS MP (Goodman et al., 2021). Moreover, genotoxic effects may result from MP exposure due to mechanic stress and leaching of monomers and additives, again leading to cytotoxicity and possibly cancer (Çobanoğlu et al., 2021).

Apart from that, MP may act as a vehicle for toxic chemicals to enter the organism. Studies showed that the leaching of monomers and additives from MP contribute to their toxicity (Porter et al., 1999; Mastrangelo et al., 2002; Xu et al., 2003). Furthermore, chemical compounds, including persistent organic pollutants and heavy metals, can adsorb to MP and can be released in the organism once ingested (Rochman et al., 2014; Hirai et al., 2011; liang Liao and yan Yang,

2020). These chemical pollutants may not only be cancerogenic (Chen et al., 2019), but also act as endocrine disruptors in organisms (Chen et al., 2019). Endocrine-disrupting chemicals can threaten fertility and reproductive health and affect the regulation of many vital functions (D'Angelo and Meccariello, 2021). For example, upon exposure to PS MP in mice, changes in serum neurotransmitters and increased acetylcholinesterase activity have been reported, potentially leading to neurotoxicity (Deng et al., 2017).

4. Potential drivers of MP toxicity

4.1. Size

A common way of classifying ambient microparticles is to group them according to their size (Kelly and Fussell, 2012). Due to their potential to enter the lower respiratory tract, especially particles with an AED < 10 μm are toxicologically relevant (Prata, 2018; Kelly and Fussell, 2012). This is the case for all microparticle types covered by this review article, including MP (Section 3). Furthermore, the transport of microparticles inside the organism takes place more readily for smaller micro- and nanoparticles (Kelly and Fussell, 2012). These fine and ultrafine particles increase the health risk due to their higher probability of passing epithelial barriers and because their reactivity with cells and tissues is increased (Kelly and Fussell, 2012; Geiser et al., 2005). In epidemiological studies about particulate pollution associated with road traffic (among others containing soot particles, Section 2.3), it was reported that fine PM2.5 and ultrafine particle pollution has stronger adverse health effects than larger particles (Schwartz et al., 1996; Dominici et al., 2006; Mirowsky et al., 2013). Although ultrafine particles substantially contribute to the toxicity of ambient particulate matter, it is not sufficiently well understood to what extent coarser particles are associated with adverse health effects (Kelly and Fussell, 2012). For MP particles, it has been shown in vivo in rats and in vitro in Mono Mac 6 cells that smaller particles at the lower size limit of MP and nanoparticles have stronger proinflammatory effects than larger particles (Brown et al., 2001). Their increased biological activity might be associated with the larger total surface area of smaller microparticles, leading to enhanced interactions between microparticles and cells (Kelly and Fussell, 2012; Schmid and Stoeger, 2016; Brown et al., 2001). Thus, the small PM10 and ultrafine MP particles are potentially important drivers of adverse effects on human health. Since their small size also enables them to enter the respiratory tract, we suggest for future studies quantifying airborne MP to focus on particles with an AED < 10 μm. This will be important to assess the risk for human health caused by airborne MP.

4.2. Shape

Interactions of microparticles with cells and tissues also depend on the microparticles' shape. Some pollutants, including asbestos and natural textile fibers like cotton (Sections 2.1 and 2.5), come in elongated fiber or rod shapes. Irregular shapes are prevalent in other airborne particles, like silica dust and soot particles (Sections 2.2 and 2.3). MP particles are found various shapes (Section 3): elongated fibers, for example, released by textile abrasion; irregularly shaped fragments, among others resulting from the natural degradation and fragmentation of larger plastic items; and well-defined spherical particles, often added as primary MP to cosmetic products. Various MP shapes were detected so far in the atmosphere, with fibers being the most common type. However, it has to be noted that this could be caused by the sampling and analytical methods used (Cai et al., 2017; Dris et al., 2016; Szewc et al., 2021).

Of all particle types, asbestos is a very prominent example of how fiber-shaped particles induce toxicity. The thin, long, inorganic fibers can enter the lung, where resident tissue macrophages try to clear them by phagocytosis. Due to the fiber length exceeding the typical

11

macrophages' size, the internalization process can often not be completed, which can cause chronic inflammation and cancer (Section 2.1) (Donaldson et al., 2010; Padmore et al., 2017). This 'frustrated phagocytosis' is a well-studied mechanism relevant to the toxicity of various fibers from chemically inert materials. For glass and titanium dioxide fibers, it was shown that frustrated phagocytosis leads to increased toxicity once a critical fiber length of 12–15 µm is exceeded (Padmore et al., 2017; Hamilton et al., 2009). There is evidence that fiber-shaped particles might have increased toxicity for titanium dioxide compared to spherical particles (Allegri et al., 2016). Possibly, next to the fibers' length, their bending stiffness might be determining their toxicity, affecting whether they can be crumpled and consequently phagocytosed (Lehmann et al., 2019). Since frustrated phagocytosis mostly depends on the particle geometry, this might be a highly relevant toxicological mechanism for all fiber-shaped microparticles, including MP fibers.

Workers in the textile and flocking industry exposed to high levels of MP fibers exhibit conditions that may be caused by fiber toxicity and frustrated phagocytosis, like pneumoconiosis and lung cancer (Section 3.7). However, to what extent frustrated phagocytosis is associated with these occupational diseases remains to be studied. Furthermore, to date, a large proportion of in vitro research on MP toxicity focuses on spherical PS particles, neglecting MP fiber pollution and other types of polymers (Lim, 2021). Therefore, to get a clearer view of the risks associated with MP fibers, we propose to increase the focus on MP fibers in future in vitro toxicity studies. Here, especially breathable MP fibers with a diameter up to 3 µm (AED < 10 µm) should be considered (Lippmann, 1990; Morgan, 1995). Furthermore, it will be crucial for risk assessment to identify the breathable portion of MP fiber pollution in indoor environments. Here, a high level of textile abrasion is expected, and a significant fraction of the world population spends most of their time indoors (Schweizer et al., 2007).

4.3. ζ-Potential

Another important physicochemical property for the assessment of MP toxicity may be the particles' ζ-potential. The ζ-potential of microparticles depends amongst others on their surface charge, resulting, for example, from functional surface groups. In the fabrication of plastic products, surface functionalization is a common method to adjust material properties (Johansson, 2017). Thus, MP particles most probably cover a broad range of ζ-potentials. It was recently shown that even supposedly identical model MP particles have substantially different ζ-potentials (Ramsperger et al., 2021). Also, once exposed to the environment, functional surface groups might be generated on MP particles due to photodegradation of the particles (Meides et al., 2021). For example, carboxylic groups can result from UV exposure of PET (polyethylene terephthalate), PE, PP (polypropylene), and acrylate polymers (Fechine et al., 2004; Fernando et al., 2007; Decker and Zahouily, 1999). Thus, weathering might alter the ζ-potential of MP particles by introducing negatively charged surface groups. It has been shown that the interaction of microparticles with cells changes with the particles' ζ-potential, indicating that hydrophobic interactions and electrostatic forces may play a crucial role in cell-particle interactions (Liu et al., 2013; Shao et al., 2015).

Furthermore, the cytotoxicity of polymeric, metal, and mineral nano- and microparticles has been linked to the particles' ζ-potential (Shao et al., 2015; Kaur and Tikoo, 2013; Motskin et al., 2009). For example, a study focusing on the interaction of *E. coli* and *D. magna* with differently coated silver particles showed that the strength of interaction and particle toxicity depends on the magnitude of the difference in ζ-potential between particle and organism (Silva et al., 2014). Similarly, for asbestos (Section 2.1), with increasing magnitude of the ζ-potential also the hemolytic activity increased (Light and Wei, 1977). In addition, more negatively charged asbestos fibers have been linked to increased ROS production (Pollastri et al., 2014). Due to electrostatic interactions,

similar results may be expected for the interaction of MP particles with mammalian cells. For example, Ramsperger et al. recently reported enhanced interactions between MP particles and cells for particles with a higher |ζ|, leading to an increased cytotoxicity (Ramsperger et al., 2021). Accordingly, the ζ-potential of MP particles might be an essential proxy for their toxicity. We think that it should therefore always be considered in future in vitro and in vivo effect studies with MP particles.

4.4. Adsorbed molecules and organisms

Additionally, microparticle toxicity might be altered by toxins, biomolecules, and pathogens adsorbed to the particles' surface. For example, soot particles (Section 2.3) adsorb organic matter and PAHs during the combustion process and after their release into the environment (Lee, 2010; Watson and Valberg, 2001; Eaves et al., 2017). PAHs are usually classified as hazardous due to their carcinogenicity (Lee, 2010). The inhalation of soot particles present in road dust is a well-known exposure route to PAHs (Kelly and Fussell, 2012; Lee, 2010). Like soot, MP particles can introduce humans to potentially toxic chemicals. This issue has been covered by several earlier reviews (Prata, 2018; Rochman et al., 2014; Prata et al., 2020; Campanale et al., 2020). For example, it is controversially discussed whether PAHs, persistent organic pollutants, and heavy metals may adsorb to MP in the environment, enabling them to enter the organism (Hirai et al., 2011; liang Liao and yan Yang, 2020; Koelmans et al., 2021).

Similarly, adsorbed biomolecules and pathogenic microorganisms can contribute to the toxicity of microparticles. For natural organic microparticles like hay dust, toxicity likely results from bacterial endotoxins and mycotoxins of microorganisms colonizing the hay particles (Section 2.6). Similar observations have been made for MP particles. Upon exposure to the environment, a biofilm or ecocorona may form on the particles' surface (Ramsperger et al., 2020; Ramsperger et al., 2020; Galloway et al., 2017). These films may carry potentially dangerous pathogens, including fungal pathogens and antibiotic-resistant bacteria (Kirstein et al., 2016; Imran et al., 2019; Gkoutselis et al., 2021).

Additionally, biomolecules found in the ecocorona of MP particles increase particle-cell interactions (Ramsperger et al., 2020) and potentially carry endotoxins and mycotoxins that cause an immune response leading to allergies. A similar effect leads to the farmer's lung disease upon exposure to hay dust (Section 2.6). Therefore, ecocorona and biofilm formation upon environmental exposure of MP should be considered when assessing the risk of airborne MP contamination. For future studies, we suggest including biodegradable polymers in this kind of research. MP particles made up from these materials might present an additional carbon source for the colonizing microorganisms, similar to natural organic particles like hay and cotton. Therefore, these particles might be preferable for microorganisms, possibly increasing the toxicity emerging from their environmental exposure.

4.5. Bio-persistence

All the modes of microparticle toxicity mentioned above also depend on the particles' residence time in exposed tissues. Therefore, the biopersistence of inhaled microparticles has been discussed as a critical parameter for their toxicity (Oberdorster et al., 1994). Microparticles that reside in the lung for several months or even many years, like asbestos or crystalline silica dust (Sections 2.1 and 2.2), are often associated with chronic inflammation, potentially leading to abnormal tissue growth (fibrosis) and cancer (Goodman et al., 1999; Wagner, 1997; Leung et al., 2012). Furthermore, non-degradable particles may accumulate inside the organism when exposed repeatedly, potentially leading to adverse health effects even at low environmental concentrations (Noonan, 2017; Metintas et al., 2002). In addition, certain types of microparticles which are often perceived as biodegradable, such as cellulose-based particles like cotton or wood dust (Sections 2.4 and 2.5), can be very bio-persistent inside mammalian organisms (Harper et al.,

12

2002; Eriksson et al., 1990). Although specialized fungi and microorganisms can enzymatically decompose these materials, they are not degradable in the lung due to a lack of the necessary enzymes (Eriksson et al., 1990; Stefaniak et al., 2014). Likewise, MP particles are likely very bio-persistent. Conventional carbon-based polymers are not biologically degradable and thus extraordinarily biodurable (Andrady, 2015), besides few exceptions like the enzymatic degradation of PET by the bacterium *Ideonella sakaiensis* (Tanasupawat et al., 2016).

Moreover, nominally biodegradable polymers like PLA (polylactic acid) or PBAT (polybutylene adipate terephthalate) are under environmental conditions often very bio-persistent: Effective degradation of these plastics is usually limited to industrial composting plants (Millican and Agarwal, 2021; Bagheri et al., 2017). Thus, these polymers, like conventional plastic, may not be decomposed in the lung and other exposed tissues. Because of their potential to accumulate in the organism (Mohamed Nor et al., 2021), we want to stress the importance of investigating the magnitude of breathable MP pollution in environments relevant to human exposure. We suggest for future studies to focus especially on indoor areas, where high levels of breathable MP pollution are expected.

4.6. Other possible drivers of toxicity

4.6.1. Surface roughness

Effects of microparticles on cells likely depend on their surface area (Kelly and Fussell, 2012; Schmid and Stoeger, 2016; Brown et al., 2001). However, with increasing surface roughness, the effective surface area of the microparticles also increases, potentially reinforcing interactions between microparticles and cells (Gatoo et al., 2014). For example, for chitosan microspheres, it was shown that cells adhere preferentially to rough particles (Zan et al., 2008). Stronger particle-cell interactions may potentially lead to enhanced particle toxicity (Silva et al., 2014). The different particle types we focused on in this review strongly vary in their surface roughness. Some particles, like PS microspheres readily employed for MP research (Section 3), usually have smooth surfaces, whereas other particle types like silica, soot, or wood particles (Sections 2.2–2.4) are more irregularly shaped and rough (Fig. 1). Since MP consists of various polymers with different properties, the surface roughness likely differs considerably between MP particles. However, to date, there is no well-established uniform quantification of the surface roughness of MP, making it difficult to assess its potential role in MP toxicity. We suggest for future research on MP toxicity that the surface roughness of model particles should be considered as one parameter that potentially impacts health effects. Since the surface area of micro- and nanoparticles has been discussed as the most effective dose metric for their toxicity (Schmid and Stoeger, 2016), it may be insightful to normalize effects to the effective surface area of MP particles, including surface roughness, which may be measured by gas adsorption to the particles using the Brunauer-Emmett-Teller theory (BET surface area) (Schmid and Stoeger, 2016; Ono-Ogasawara and Kohyama, 1999).

4.6.2. Chemical identity, monomers, and additives

Although some of the toxicological impacts of microparticles on human health can be attributed to universal physicochemical properties like size, shape, and ζ-potential, the chemical identity of microparticle pollution should not be neglected. Especially plastic is a highly diverse class of materials, consisting of numerous polymer types frequently used in various applications. It covers a broad spectrum of physical and chemical properties, often tuned by surface functionalization (Johansson, 2017). This complexity likely leads to a large diversity of MP particles containing a mixture of chemicals like unreacted monomers and additives, potentially contributing to their toxicity (Prata, 2018; Rochman et al., 2019; Prata et al., 2020). To date, most research on MP toxicity is based on PS microspheres (Lim, 2021; Jacob et al., 2020). This type of model MP alone might be insufficient to assess the risks associated with airborne MP contamination because different plastic types in the environment may lead to the formation of different MP particles that contain different monomers and additives. Thus, we think that future studies should take a more realistic suite of model MP particles from different polymers with different additives and surface functionalization into account. This can lead to a more complete understanding of the health risks associated with airborne MP pollution.

5. Conclusions and future perspectives

Identifying the potential drivers of MP toxicity is a crucial step towards better assessing the potential health risks caused by breathable MP pollution. Here, we focused on the potential role of the microparticles' size, shape, ζ-potential, adsorbed molecules and microorganisms, and bio-persistence in the toxicity of airborne MP. By reviewing the adverse effects on human health associated with six different, well-studied airborne non-plastic microparticle pollutants, we aimed to identify the role of these parameters in microparticle toxicity. We then compared our results to already existing knowledge about the putative toxicity of airborne MP, providing a basis for identifying possible ways in which the abovementioned parameters affect MP toxicity. The parameters we considered in this review article are likely relevant for assessing risks associated with airborne MP particles. To better understand their role, we suggest for future studies to consider the following points:

- Smaller MP particles may not only be more readily respired but may also interact stronger with cells and tissues due to their relatively larger surface area, making them toxicologically more relevant. Therefore, it will be essential to quantify the magnitude of breathable (AED $<$ 10 μm) MP pollution in outdoor and indoor environments.
- Their shape can affect how MP particles interact with cells. Especially fibers might have the potential to induce adverse effects by causing frustrated phagocytosis, leading to persisting inflammation. Thus, we propose that in vitro toxicity assays focus not exclusively on spherical microparticles but include particles of different shapes, especially fibers.
- The ζ-potential of MP particles is an easy-to-measure property that might proxy their interactions with cells and tissues and their surface reactivity. Thus, it should always be specified according to a consistent protocol in in vitro and in vivo toxicity studies to ensure comparability between studies.
- Environmental exposure of MP might significantly alter its toxicity due to the adsorption of toxic molecules, ecocoronas, and microorganisms. Therefore, to understand their potential role in MP toxicity, environmentally exposed MP should be included in effect studies.
- Since conventional and biodegradable MP is likely not degradable in the human organism, it can accumulate over the human lifetime, leading to chronic toxicity. Therefore, it will be crucial to assess the MP pollution in all areas that are relevant to human exposure.

However, other parameters than the abovementioned likely also affect the toxicity of airborne MP. For example, the surface roughness of MP might contribute to its toxicity by enlarging its effective surface area. Furthermore, the polymer type of an MP particle might determine its physicochemical properties and likely play a role in its toxicity. In addition, the leaching of potentially toxic monomers and additives can contribute to the toxicity of MP from different polymers.

Overall, understanding how microparticle properties influence adverse health effects may lead to a more fundamental understanding of MP toxicity and support risk assessments of MP pollution. However, since all these parameters likely play a combined role for MP toxicity, and due to the highly diverse nature of MP particles, a broad range of mechanistic knowledge will be required to enable effective policy-making regarding MP pollution.

13

S. Wieland et al.

Author contributions

H.K. initiated the article. All authors contributed to the conceptualization of the article. H.K., C.L., and S.W. supervised the writing process. S.W., C.T., and BH.W. wrote the introduction, C.T. wrote Section 2.1, F. M. Section 2.2, J.K. Section 2.3, J.B. Section 2.4, A.B. Sections 2.5 and 2.6, AFRM.R. and S.W. Section 3. S.W. wrote Section 4 with the help of F.R., and S.W. wrote the conclusions. All authors reviewed the manuscript and contributed to its finalization. J.B. designed the graphical abstract. S.W. designed Figs. 1 and 2 and performed the SEM preparation and imaging.

References

Abbasi, S., Keshavarzi, B., Moore, F., Turner, A., Kelly, F.J., Dominguez, A.O., Jaafarzadeh, N., 2019. Distribution and potential health impacts of microplastics and microrubbers in air and street dusts from Asaluyeh County, Iran. Environ. Pollut. 244, 153–164. https://doi.org/10.1016/j.envpol.2018.10.039.

Allegri, M., Bianchi, M.G., Chiu, M., Varet, J., Costa, A.L., Ortelli, S., Blosi, M., Bussolati, O., Poland, C.A., Bergamaschi, E., 2016. Shape-related toxicity of titanium dioxide nanofibres. PLoS One 11. https://doi.org/10.1371/journal.pone.0151365.

Allen, S., Allen, D., Phoenix, V.R., Galop, D., 2019. Atmospheric transport and deposition of microplastics in a remote mountain catchment. Nat. Geosci. 12 https://doi.org/10.1038/s41561-019-0335-5.

Alonso-Sardón, M., Chamorro, A.J., Hernández-García, I., Iglesias-De-sena, H., Martín-Rodero, H., Herrera, C., Marcos, M., Mirón-Canelo, J.A., 2015. Association between occupational exposure to wood dust and cancer: A systematic review and meta-analysis. PLoS One 10. https://doi.org/10.1371/journal.pone.0133024.

Alpert, N., van Gerwen, M., Taioli, E., 2020. Epidemiology of mesothelioma in the 21st century in Europe and the United States, 40 years after restricted/banned asbestos use. Transl. Lung Cancer Res 9. https://doi.org/10.21037/tlcr.2019.11.11.

Amato-Lourenço, L.F., dos Santos Galvão, L., de Weger, L.A., Hiemstra, P.S., Vijver, M.G., Mauad, T., 2020. An emerging class of air pollutants: Potential effects of microplastics to respiratory human health? Sci. Total Environ. 749, 141676 https://doi.org/10.1016/j.scitotenv.2020.141676.

Amato-Lourenço, L.F., Carvalho-Oliveira, R., Júnior, G.R., dos Santos Galvão, L., Ando, R.A., Mauad, T., 2021. Presence of airborne microplastics in human lung tissue. J. Hazard. Mater. 416 https://doi.org/10.1016/j.jhazmat.2021.126124.

Andrady, A.L., 2015. Persistence of plastic litter in the oceans. : Mar. Anthropog. Litter. https://doi.org/10.1007/978-3-319-16510-3_3.

Andrady, A.L., Neal, M.A., 2009. Applications and societal benefits of plastics. Philos. Trans. R. Soc. B Biol. Sci. 364 https://doi.org/10.1098/rstb.2008.0304.

Andraos, C., Gulumian, M., 2020. The toxicity of respirable South African mine tailings dust in relation to their physicochemical properties. Inhal. Toxicol. 32 https://doi.org/10.1080/08958378.2020.1836092.

Arthur, C., Baker, J., Bamford, H., 2009, Proceedings of the International Research Workshop on the Occurrence, Effects, and Fate of Microplastic Marine Debris, Group.

Ayer, H.E., Mackison, F.W., 1974. Occup. Expo. Cotton Dust. (https://stacks.cdc.gov/view/cdc/19341).

Bagheri, A.R., Laforsch, C., Greiner, A., Agarwal, S., 2017. Fate of So-Called Biodegradable Polymers in Seawater and Freshwater. Glob. Chall. 1 https://doi.org/10.1002/gch2.201700048.

Bahners, T., Ehrler, P., Hengstberger, M., 1994. Erste Untersuchungen zur Erfassung und Charakterisierung textiler Feinstäube. Melliand Text. 1, 24–30.

Barfknecht, T.R., 1983. Toxicology of soot. Prog. Energy Combust. Sci. 9 https://doi.org/10.1016/0360-1285(83)90002-3.

Barnes, H., Goh, N.S.L., Leong, T.L., Hoy, R., 2019. Silica-associated lung disease: An old-world exposure in modern industries. Respirology 24. https://doi.org/10.1111/resp.13695.

Barsan, M.E., 2007, NIOSH pocket guide to chemical hazards.

Barshtein, G., Livshits, L., Shvartsman, L.D., Shlomai, N.O., Yedgar, S., Arbell, D., 2016. Polystyrene Nanoparticles Activate Erythrocyte Aggregation and Adhesion to Endothelial Cells. Cell Biochem. Biophys. https://doi.org/10.1007/s12013-015-0705-6.

Baumann, F., Ambrosi, J.P., Carbone, M., 2013. Asbestos is not just asbestos: An unrecognised health hazard. Lancet Oncol. 14 https://doi.org/10.1016/S1470-2045(13)70257-2.

Benmoussa, N., Rebibo, J.D., Conan, P., Charlier, P., 2019. Chimney sweeps' cancer—early proof of environmentally driven tumourigenicity. Lancet Oncol. 20 https://doi.org/10.1016/S1470-2045(19)30106-8.

Binazzi, A., Ferrante, P., Marinaccio, A., 2015. Occupational exposure and sinonasal cancer: A systematic review and meta-analysis. BMC Cancer 15. https://doi.org/10.1186/s12885-015-1042-2.

Boogaard, H., Montagne, D.R., Brandenburg, A.P., Meliefste, K., Hoek, G., 2010. Comparison of short-term exposure to particle number, PM10 and soot concentrations on three (sub) urban locations. Sci. Total Environ. 408 https://doi.org/10.1016/j.scitotenv.2010.06.022.

Boulanger, G., Andujar, P., Pairon, J.C., Billon-Galland, M.A., Dion, C., Dumortier, P., Brochard, P., Sobaszek, A., Bartsch, P., Paris, C., Jaurand, M.C., 2014. Quantification of short and long asbestos fibers to assess asbestos exposure: A review of fiber size toxicity. Environ. Heal. A Glob. Access Sci. Source 13. https://doi.org/10.1186/1476-069X-13-59.

Brahney, J., Mahowald, N., Prank, M., Cornwell, G., Klimont, Z., Matsui, H., Prather, K. A., 2021. Constraining the atmospheric limb of the plastic cycle. Proc. Natl. Acad. Sci. U. S. A 118. https://doi.org/10.1073/pnas.2020719118.

Brown, D.M., Wilson, M.R., MacNee, W., Stone, V., Donaldson, K., 2001. Size-dependent proinflammatory effects of ultrafine polystyrene particles: A role for surface area and oxidative stress in the enhanced activity of ultrafines. Toxicol. Appl. Pharmacol. https://doi.org/10.1006/taap.2001.9240.

Browne, M.A., Dissanayake, A., Galloway, T.S., Lowe, D.M., Thompson, R.C., 2008. Ingested microscopic plastic translocates to the circulatory system of the mussel, Mytilus edulis (L.). Environ. Sci. Technol. 42 https://doi.org/10.1021/es800249a.

Burkhart, J., Piacitelli, C., Schwegler-Berry, D., Jones, W., 1999. Environmental study of nylon flocking process. J. Toxicol. Environ. Heal. - Part A 57. https://doi.org/10.1080/009841099157836.

Cai, L., Wang, J., Peng, J., Tan, Z., Zhan, Z., Tan, X., Chen, Q., 2017. Characteristic of microplastics in the atmospheric fallout from Dongguan city, China: preliminary research and first evidence. Environ. Sci. Pollut. Res. 24, 24928–24935. https://doi.org/10.1007/s11356-017-0116-x.

Campanale, C., Massarelli, C., Savino, I., Locaputo, V., Uricchio, V.F., 2020. A detailed review study on potential effects of microplastics and additives of concern on human health. Int. J. Environ. Res. Public Health 17. https://doi.org/10.3390/ijerph17041212.

Can-Güven, E., 2021. Microplastics as emerging atmospheric pollutants: a review and bibliometric analysis. Air Qual. Atmos. Heal 14, 203–215. https://doi.org/10.1007/s11869-020-00926-3.

Cano-Jiménez, E., Acuña, A., Botana, M.I., Hermida, T., González, M.G., Leiro, V., Martín, I., Paredes, S., Sanjuán, P., 2016. Revisión de la enfermedad del pulmón de granjero. Arch. Bronconeumol. 52 https://doi.org/10.1016/j.arbres.2015.12.001.

Carbery, M., O'Connor, W., Palanisami, T., 2018. Trophic transfer of microplastics and mixed contaminants in the marine food web and implications for human health. Environ. Int. 115 https://doi.org/10.1016/j.envint.2018.03.007.

14

Carr, K.E., Smyth, S.H., McCullough, M.T., Morris, J.F., Moyes, S.M., 2012. Morphological aspects of interactions between microparticles and mammalian cells: Intestinal uptake and onward movement. Prog. Histochem. Cytochem. https://doi.org/10.1016/j.proghi.2011.11.001.

Castranova, Vincent, Robinson A., Victor, Frazer G., David, 1996. Pulmonary Reactions to Organic Dust Exposures: Development of an Animal Model. Environmental Health Perspectives. https://doi.org/10.1289/ehp.96104s141.

Catarino, A.I., Macchia, V., Sanderson, W.G., Thompson, R.C., Henry, T.B., 2018. Low levels of microplastics (MP) in wild mussels indicate that MP ingestion by humans is minimal compared to exposure via household fibres fallout during a meal. Environ. Pollut. https://doi.org/10.1016/j.envpol.2018.02.069.

Chen, C., Huang, W., 2017. Aggregation Kinetics of Diesel Soot Nanoparticles in Wet Environments. Environ. Sci. Technol. 51 https://doi.org/10.1021/acs.est.6b04575.

Chen, G., Feng, Q., Wang, J., 2020. Mini-review of microplastics in the atmosphere and their risks to humans. Sci. Total Environ. 703 https://doi.org/10.1016/j.scitotenv.2019.135504.

Chen, G., Fu, Z., Yang, H., Wang, J., 2020. An overview of analytical methods for detecting microplastics in the atmosphere. TrAC - Trends Anal. Chem. 130, 115981 https://doi.org/10.1016/j.trac.2020.115981.

Chen, Q., Allgeier, A., Yin, D., Hollert, H., 2019. Leaching of endocrine disrupting chemicals from marine microplastics and mesoplastics under common life stress conditions. Environ. Int. https://doi.org/10.1016/j.envint.2019.104938.

Chen, Q., Zhang, H., Allgeier, A., Zhou, Q., Ouellet, J.D., Crawford, S.E., Luo, Y., Yang, Y., Shi, H., Hollert, H., 2019. Marine microplastics bound dioxin-like chemicals: Model explanation and risk assessment. J. Hazard. Mater. https://doi.org/10.1016/j.jhazmat.2018.10.032.

Chen, W., Fryrear, D.W., 2001. Aerodynamic and geometric diameters of airborne particles. J. Sediment. Res 71. https://doi.org/10.1306/2DC4094A–0E47–11D7-8643000102C1865D.

Chubb, L.G., Cauda, E.G., 2017. Characterizing particle size distributions of crystalline silica in gold mine dust. Aerosol Air Qual. Res 17. https://doi.org/10.4209/aaqr.2016.05.0179.

Çobanoğlu, H., Belivermiş, M., Sıkdokur, E., Kılıç, Ö., Çayır, A., 2021. Genotoxic and cytotoxic effects of polyethylene microplastics on human peripheral blood lymphocytes. Chemosphere 272, 129805. https://doi.org/10.1016/j.chemosphere.2021.129805.

Cortez Pimentel, J., Avila, R., Galvao Lourenco, A., 1975. Respiratory disease caused by synthetic fibres: a new occupational disease. Thorax. https://doi.org/10.1136/thx.30.2.204.

Cox, K.D., Covernton, G.A., Davies, H.L., Dower, J.F., Juanes, F., Dudas, S.E., 2019. Human Consumption of Microplastics. Environ. Sci. Technol. https://doi.org/10.1021/acs.est.9b01517.

Craighead, J.E., Mossman, B.T., 1982. The Pathogenesis of Asbestos-Associated Diseases. N. Engl. J. Med 306. https://doi.org/10.1056/nejm198206173062403.

D'Angelo, S., Meccariello, R., 2021. Microplastics: A Threat for Male Fertility. Int. J. Environ. Res. Public Health 18. https://doi.org/10.3390/ijerph18052392.

Dangi, B.M., Bhise, A.R., 2017. Cotton dust exposure: Analysis of pulmonary function and respiratory symptoms. Lung India 34. https://doi.org/10.4103/0970-2113.201319.

Decker, C., Zahouily, K., 1999. Photodegradation and photooxidation of thermoset and UV-cured acrylate polymers. Polym. Degrad. Stab. 64 https://doi.org/10.1016/S0141-3910(98)00205-5.

De-la-Torre, G.E., 2020. Microplastics: an emerging threat to food security and human health. J. Food Sci. Technol. 57 https://doi.org/10.1007/s13197-019-04138-1.

Delzell, E., 1995. Wood Dust Formaldehyde IARC Monogr. Eval. Carcinog. Risks Hum. Volume 62.

Deng, Y., Zhang, Y., Lemos, B., Ren, H., 2017. Tissue accumulation of microplastics in mice and biomarker responses suggest widespread health risks of exposure. Sci. Rep. https://doi.org/10.1038/srep46687.

Derbyshire, E., 2007. Natural Minerogenic Dust and Human Health. AMBIO A J. Hum. Environ. 36 https://doi.org/10.1579/0044-7447(2007)36[73:nmdahh]2.0.co;2.

Des Rieux, A., Ragnarsson, E.G.E., Gullberg, E., Préat, V., Schneider, Y.J., Artursson, P., 2005. Transport of nanoparticles across an in vitro model of the human intestinal follicle associated epithelium. Eur. J. Pharm. Sci. https://doi.org/10.1016/j.ejps.2005.04.015.

Desforges, J.P.W., Galbraith, M., Ross, P.S., 2015. Ingestion of Microplastics by Zooplankton in the Northeast Pacific Ocean. Arch. Environ. Contam. Toxicol. 69 https://doi.org/10.1007/s00244-015-0172-5.

Desjardins, M., Griffiths, G., 2003. Phagocytosis: Latex leads the way. Curr. Opin. Cell Biol. 15 https://doi.org/10.1016/S0955-0674(03)00083-8.

Devane, P.A., Bourne, R.B., Rorabeck, C.H., MacDonald, S., Robinson, E.J., 1995. Measurement of Polyethylene Wear in Metal-Backed Acetabular Cups. Clin. Orthop. Relat. Res. https://doi.org/10.1097/00003086-199510000-00034.

Deville, S., Penjweini, R., Smisdom, N., Notelaers, K., Nelissen, I., Hooyberghs, J., Ameloot, M., 2015. Intracellular dynamics and fate of polystyrene nanoparticles in A549 Lung epithelial cells monitored by image (cross-) correlation spectroscopy and single particle tracking. Biochim. Biophys. Acta - Mol. Cell Res. https://doi.org/10.1016/j.bbamcr.2015.07.004.

Di Dong, C., Chen, C.W., Chen, Y.C., Chen, H.H., Lee, J.S., Lin, C.H., 2020. Polystyrene microplastic particles: In vitro pulmonary toxicity assessment. J. Hazard. Mater. https://doi.org/10.1016/j.jhazmat.2019.121575.

Dominici, F., Peng, R.D., Bell, M.L., Pham, L., McDermott, A., Zeger, S.L., Samet, J.M., 2006. Fine Particulate Air Pollution and Hospital Admission for Cardiovascular and Respiratory Diseases. JAMA 295, 1127–1134. https://doi.org/10.1001/jama.295.10.1127.

Donaldson, K., Murphy, F.A., Duffin, R., Poland, C.A., 2010. Asbestos, carbon nanotubes and the pleural mesothelium: A review of the hypothesis regarding the role of long fibre retention in the parietal pleura, inflammation and mesothelioma. Part. Fibre Toxicol. 7 https://doi.org/10.1186/1743-8977-7-5.

Donaldson, K., Tran, L., Jimenez, L.A., Duffin, R., Newby, D.E., Mills, N., MacNee, W., Stone, V., 2005. Combustion-derived nanoparticles: A review of their toxicology following inhalation exposure. Part. Fibre Toxicol. 2 https://doi.org/10.1186/1743-8977-2-10.

Dong, F.Q., Chen, W., Dai, Q.W., Deng, Y.Q., He, P., He, X.C., Tang, J., Liu, L.Z., He, H., 2015. Characterization of mineralogy and surface zeta potential of atmospheric dust fall in northwest China. Mineral. Petrol. 109 https://doi.org/10.1007/s00710-014-0347-1.

Doorn, P.F., Campbell, P.A., Amstutz, H.C., 1996. Metal versus polyethylene wear particles in total hip replacements: A review. Clin. Orthop. Relat. Res. https://doi.org/10.1097/00003086-199608001-00018.

Dris, R., Gasperi, J., Saad, M., Mirande, C., Tassin, B., 2016. Synthetic fibers in atmospheric fallout: A source of microplastics in the environment? Mar. Pollut. Bull. https://doi.org/10.1016/j.marpolbul.2016.01.006.

Dris, R., Gasperi, J., Rocher, V., Saad, M., Renault, N., Tassin, B., 2015. Microplastic contamination in an urban area: A case study in Greater Paris. Environ. Chem. https://doi.org/10.1071/EN14167.

Dris, R., Imhof, H., Sanchez, W., Gasperi, J., Galgani, F., Tassin, B., Laforsch, C., 2015. Beyond the ocean: Contamination of freshwater ecosystems with (micro-)plastic particles. Environ. Chem. 12 https://doi.org/10.1071/EN14172.

Dris, R., Gasperi, J., Mirande, C., Mandin, C., Guerrouache, M., Langlois, V., Tassin, B., 2017. A first overview of textile fibers, including microplastics, in indoor and outdoor environments. Environ. Pollut. https://doi.org/10.1016/j.envpol.2016.12.013.

Eaves, N.A., Dworkin, S.B., Thomson, M.J., 2017. Assessing relative contributions of PAHs to soot mass by reversible heterogeneous nucleation and condensation. Proc. Combust. Inst. 36 https://doi.org/10.1016/j.proci.2016.06.051.

EFSA, 2016. Presence of microplastics and nanoplastics in food, with particular focus on seafood. EFSA J. 14 https://doi.org/10.2903/j.efsa.2016.4501.

Ellakkani, M.A., Alarie, Y.C., Weyel, D.A., Mazumdar, S., Karol, M.H., 1984. Pulmonary reactions to inhaled cotton dust: An animal model for byssinosis. Toxicol. Appl. Pharmacol. 74 https://doi.org/10.1016/0041-008X(84)90152-2.

Enyoh, C.E., Verla, A.W., Verla, E.N., Ibe, F.C., Amaobi, C.E., 2019. Airborne microplastics: a review study on method for analysis, occurrence, movement and risks. Environ. Monit. Assess. 191 https://doi.org/10.1007/s10661-019-7842-0.

Eriksson, K.-E.L., Blanchette, R.A., Ander, P., 1990. In: Eriksson, K.-E.L., Blanchette, R.A., Ander, P. (Eds.), Biodegradation of Cellulose BT - Microbial and Enzymatic Degradation of Wood and Wood Components. Springer Berlin Heidelberg, Berlin, Heidelberg, pp. 89–180. https://doi.org/10.1007/978-3-642-46687-8 2.

Eschenbacher, W.L., Kreiss, K., Lougheed, M.D., Pransky, G.S., Day, B., Castellan, R.M., 1999. Nylon flock-associated interstitial lung disease. Am. J. Respir. Crit. Care Med. https://doi.org/10.1164/ajrccm.159.6.9808002.

Eyles, J.E., Bramwell, V.W., Williamson, E.D., Alpar, H.O., 2001. Microsphere translocation and immunopotentiation in systemic tissues following intranasal administration. Vaccine. https://doi.org/10.1016/S0264-410X(01)00220-1.

Fechine, G.J.M., Rabello, M.S., Souto Maior, R.M., Catalani, L.H., 2004. Surface characterization of photodegraded poly(ethylene terephthalate). Eff. Ultrav. absorbers, Polym. (Guildf.) 45. https://doi.org/10.1016/j.polymer.2004.02.003.

Fernando, S.S., Christensen, P.A., Egerton, T.A., White, J.R., 2007. Carbon dioxide evolution and carbonyl group development during photodegradation of polyethylene and polypropylene. Polym. Degrad. Stab. 92 https://doi.org/10.1016/j.polymdegradstab.2007.01.032.

Foord, N., Black, A., Walsh, M., 1978. Regional deposition of 2.5-7.5 μm diameter inhaled particles in healthy male non-smokers. J. Aerosol Sci. https://doi.org/10.1016/0021-8502(78)90037-X.

for D.C., C., Prevention, 1996. Preventing Silicosis and Deaths in Construction Workers. Natl. Inst. Occup. Saf. Heal.

Frank, B., Schuster, M.E., Schlögl, R., Su, D.S., 2013. Emission of highly activated soot particulate - The other side of the coin with modern diesel engines. Angew. Chem. - Int. Ed. 52 https://doi.org/10.1002/anie.201206093.

Frei, S., Piehl, S., Gilfedder, B.S., Löder, M.G.J., Krutzke, J., Wilhelm, L., Laforsch, C., 2019. Occurence of microplastics in the hyporheic zone of rivers. Sci. Rep. 9 https://doi.org/10.1038/s41598-019-51741-5.

Frias, J.P.G.L., Nash, R., 2019. Microplastics: Finding a consensus on the definition. Mar. Pollut. Bull. 138 https://doi.org/10.1016/j.marpolbul.2018.11.022.

Gallagher, L.G., Li, W., Ray, R.M., Romano, M.E., Wernli, K.J., Gao, D.L., Thomas, D.B., Checkoway, H., 2015. Occupational exposures and risk of stomach and esophageal cancers: Update of a cohort of female textile workers in Shanghai, China. Am. J. Ind. Med. https://doi.org/10.1002/ajim.22412.

Galloway, T.S., Cole, M., Lewis, C., 2017. Interactions of microplastic debris throughout the marine ecosystem. Nat. Ecol. Evol. 1 https://doi.org/10.1038/s41559-017-0116.

Galloway, T.S., Cole, M., Lewis, C., 2017. Interactions of microplastic debris throughout the marine ecosystem. Nat. Ecol. Evol. 1, 1–8. https://doi.org/10.1038/s41559-017-0116.

Gatoo, M.A., Naseem, S., Arfat, M.Y., Mahmood Dar, A., Qasim, K., Zubair, S., 2014. Physicochemical properties of nanomaterials: Implication in associated toxic manifestations. Biomed. Res. Int 2014. https://doi.org/10.1155/2014/498420.

Geiser, M., Schürch, S., Gehr, P., 2003. Influence of surface chemistry and topography of particles on their immersion into the lung's surface-lining layer. J. Appl. Physiol. https://doi.org/10.1152/japplphysiol.00514.2002.

Geiser, M., Rothen-Rutishauser, B., Kapp, N., Schürch, S., Kreyling, W., Schulz, H., Semmler, M., Im Hof, V., Heyder, J., Gehr, P., 2005. Ultrafine particles cross cellular

15

membranes by nonphagocytic mechanisms in lungs and in cultured cells. Environ. Health Perspect. https://doi.org/10.1289/ehp.8006.

Gewert, B., Plassmann, M.M., Macleod, M., 2015. Pathways for degradation of plastic polymers floating in the marine environment. Environ. Sci. Process. Impacts. https://doi.org/10.1039/c5em00207a.

Geyer, R., Jambeck, J.R., Law, K.L., 2017. Production, use, and fate of all plastics ever made. Sci. Adv. 3 https://doi.org/10.1126/sciadv.1700782.

Gkoutselis, G., Rohrbach, S., Harjes, J., Obst, M., Brachmann, A., Horn, M.A., Rambold, G., 2021. Microplastics accumulate fungal pathogens in terrestrial ecosystems. Sci. Rep. 11, 13214. https://doi.org/10.1038/s41598-021-92405-7.

Glindmeyer, H.W., Rando, R.J., Lefante, J.J., Freyder, L., Brisolara, J.A., Jones, R.N., 2008. Longitudinal respiratory health study of the wood processing industry. Am. J. Ind. Med. 51 https://doi.org/10.1002/ajim.20594.

Gonzalez-Pleiter, M., Lacerot, G., Edo, C., Pablo Lozoya, J., Leganés, F., Fernández-Pina&tild;s, F., Rosal, R., Teixeira-De-Mello, F., 2021. A pilot study about microplastics and mesoplastics in an Antarctic glacier. Cryosphere 15. https://doi.org/10.5194/tc-15-2531-2021.

Goodman, K.E., Hare, J.T., Khamis, Z.I., Hua, T., Sang, Q.-X.A., 2021. Exposure of Human Lung Cells to Polystyrene Microplastics Significantly Retards Cell Proliferation and Triggers Morphological Changes. Chem. Res. Toxicol. https://doi.org/10.1021/acs.chemrestox.0c00486.

Goodman, M., Morgan, R.W., Ray, R., Malloy, C.D., Zhao, K., 1999. Cancer in asbestos-exposed occupational cohorts: A meta-analysis. Cancer Causes Control 10. https://doi.org/10.1023/A:1008980927434.

Goynes, W.R., Ingber, B.F., Palmgren, M.S., 1986. Microscopical comparison of cotton, corn, and soybean dusts. Environ. Health Perspect. VOL. 66 https://doi.org/10.1289/ehp.8666125.

Green, T.R., Fisher, J., Stone, M., Wroblewski, B.M., Ingham, E., 1998. Polyethylene particles of a "critical size" are necessary for the induction of cytokines by macrophages in vitro. Biomaterials. https://doi.org/10.1016/S0142-9612(98)00140-9.

Gregory, P.H., Lacey, M.E., 1963. Mycological examination of dust from mouldy hay associated with farmer's lung disease. J. Gen. Microbiol. 30 https://doi.org/10.1099/00221287-30-1-75.

Griffis, L.C., Wolff, R.K., Henderson, R.F., Griffith, W.C., Mokler, B.V., Mcclellan, R.O., 1983. Clearance of diesel soot particles from rat lung after a subchronic diesel exhaust exposure. Toxicol. Sci. 3 https://doi.org/10.1093/toxsci/3.2.99.

Gustafson, T., Dahlman-Höglund, A., Nilsson, K., Ström, K., Tornling, G., Torén, K., 2007. Occupational exposure and severe pulmonary fibrosis. Respir. Med. 101 https://doi.org/10.1016/j.rmed.2007.02.027.

Guzzetti, E., Sureda, A., Tejada, S., Faggio, C., 2018. Microplastic in marine organism: Environmental and toxicological effects. Environ. Toxicol. Pharmacol. 64 https://doi.org/10.1016/j.etap.2018.10.009.

Hagemeyer, O., Otten, H., Kraus, T., 2006. Asbestos consumption, asbestos exposure and asbestos-related occupational diseases in Germany. Int. Arch. Occup. Environ. Health 79. https://doi.org/10.1007/s00420-006-0091-x.

Hamilton, R.F., Wu, N., Porter, D., Buford, M., Wolfarth, M., Holian, A., 2009. Particle length-dependent titanium dioxide nanomaterials toxicity and bioactivity. Part. Fibre Toxicol. 6 https://doi.org/10.1186/1743-8977-6-35.

Hammad, Y.Y., Dharmarajan, V., Weill, H., 1981. Sampling of cotton dust for epidemiologic investigations. Chest 79. https://doi.org/10.1378/chest.79.4.108s.

Hamoir, J., Nemmar, A., Halloy, D., Wirth, D., Vincke, G., Vanderplasschen, A., Nemery, B., Gustin, P., 2003. Effect of polystyrene particles on lung microvascular permeability in isolated perfused rabbit lungs: Role of size and surface properties. Toxicol. Appl. Pharmacol. https://doi.org/10.1016/S0041-008X(03)00192-3.

Hancock, D.G., Langley, M.E., Chia, K.L., Woodman, R.J., Michael Shanahan, E., 2015. Wood dust exposure and lung cancer risk: A meta-Analysis. Occup. Environ. Med. 72 https://doi.org/10.1136/oemed-2014-102722.

Hansen, E.S., 1983. Mortality from cancer and ischemic heart disease in danish chimney sweeps: A five-year follow-up. Am. J. Epidemiol. 117 https://doi.org/10.1093/oxfordjournals.aje.a113526.

Harper, M., Muller, B.S., Bartolucci, A., 2002. Determining particle size distributions in the inhalable size range for wood dust collected by air samplers. J. Environ. Monit. 4 https://doi.org/10.1039/b202856p.

Hesterberg, T.W., Long, C.M., Bunn, W.B., Lapin, C.A., McClellan, R.O., Valberg, P.A., 2012. Health effects research and regulation of diesel exhaust: An historical overview focused on lung cancer risk. Inhal. Toxicol. 24 https://doi.org/10.3109/08958378.2012.691913.

Hicks, D.G., Judkins, A.R., Sickel, J.Z., Rosier, R.N., Puzas, J.E., O'Keefe, R.J., 1996. Granular histiocytosis of pelvic lymph nodes following total hip arthroplasty: The presence of wear debris, cytokine production, and immunologically activated macrophages. J. Bone Jt. Surg. - Ser. A. https://doi.org/10.2106/00004623-199604000-00002.

Hirai, H., Takada, H., Ogata, Y., Yamashita, R., Mizukawa, K., Saha, M., Kwan, C., Moore, C., Gray, H., Laursen, D., Zettler, E.R., Farrington, J.W., Reddy, C.M., Peacock, E.E., Ward, M.W., 2011. Organic micropollutants in marine plastics debris from the open ocean and remote and urban beaches. Mar. Pollut. Bull. https://doi.org/10.1016/j.marpolbul.2011.06.004.

Hodgson, J.T., Darnton, A., 2000. The quantitative risks of mesothelioma and lung cancer in relation to asbestos exposure. Ann. Occup. Hyg. 44 https://doi.org/10.1016/S0003-4878(00)00045-4.

Hogstedt, C., Jansson, C., Hugosson, M., Tinnerberg, H., Gustavsson, P., 2013. Cancer incidence in a cohort of Swedish chimney sweeps, 1958-2006. Am. J. Public Health 103. https://doi.org/10.2105/AJPH.2012.300860.

Holmes, E.P., Wilson, J., Schreier, H., Lavkulich, L.M., 2012. Processes affecting surface and chemical properties of chrysotile: Implications for reclamation of asbestos in the natural environment. Can. J. Soil Sci. 92 https://doi.org/10.4141/CJSS2010-014.

Hours, M., Févotte, J., Lafont, S., Bergeret, A., 2007. Cancer mortality in a synthetic spinning plant in Besançon, France. Occup. Environ. Med. https://doi.org/10.1136/oem.2006.028282.

Huang, S.X.L., Jaurand, M.C., Kamp, D.W., Whysner, J., Hei, T.K., 2011. Role of mutagenicity in asbestos fiber-induced carcinogenicity and other diseases. J. Toxicol. Environ. Heal. - Part B Crit. Rev. 14 https://doi.org/10.1080/10937404.2011.556051.

Huang, Y., Qing, X., Wang, W., Han, G., Wang, J., 2020. Mini-review on current studies of airborne microplastics: Analytical methods, occurrence, sources, fate and potential risk to human beings. TrAC - Trends Anal. Chem. 125, 115821 https://doi.org/10.1016/j.trac.2020.115821.

Hubbard, R., Lewis, S., Richards, K., Johnston, I., Britton, J., 1996. Occupational exposure to metal or wood dust and aetiology of cryptogenic fibrosing alveolitis. Lancet 347. https://doi.org/10.1016/S0140-6736(96)90465-1.

Hume, L.A., Rimstidt, J.D., 1992. The biodurability of chrysotile asbestos. Am. Mineral. 77.

Hwang, J., Choi, D., Han, S., Choi, J., Hong, J., 2019. An assessment of the toxicity of polypropylene microplastics in human derived cells. Sci. Total Environ. https://doi.org/10.1016/j.scitotenv.2019.05.071.

IARC, 2012. Chemical agents and related occupations - Volume 100 F: A review of human carcinogens. Int. Agency Res. Cancer Vol. 100F.

IARC, 2014. Diesel and Gasoline Engine Exhausts and Some Nitroarenes. IARC Monogr. Eval. Carcinog. Risk Chem. Hum. Vol. 46 (46).

Ilves, M., Vilske, S., Aimonen, K., Lindberg, H.K., Pesonen, S., Wedin, I., Nuopponen, M., Vanhala, E., Højgaard, C., Winther, J.R., Willemoës, M., Vogel, U., Wolff, H., Norppa, H., Savolainen, K., Alenius, H., 2018. Nanofibrillated cellulose causes acute pulmonary inflammation that subsides within a month. Nanotoxicology 12. https://doi.org/10.1080/17435390.2018.1472312.

Imhof, H.K., Ivleva, N.P., Schmid, J., Niessner, R., Laforsch, C., 2013. Contamination of beach sediments of a subalpine lake with microplastic particles. Curr. Biol. 23 https://doi.org/10.1016/j.cub.2013.09.001.

Imhof, H.K., Wiesheu, A.C., Anger, P.M., Niessner, R., Ivleva, N.P., Laforsch, C., 2018. Variation in plastic abundance at different lake beach zones - A case study. Sci. Total Environ. 613–614. https://doi.org/10.1016/j.scitotenv.2017.08.300.

Imhof, H.K., Sigl, R., Brauer, E., Feyl, S., Giesemann, P., Klink, S., Leupolz, K., Löder, M.G.J., Löschel, L.A., Missun, J., Muszynski, S., Ramsperger, A.F.R.M., Schrank, I., Speck, S., Steibl, S., Trotter, B., Winter, I., Laforsch, C., 2017. Spatial and temporal variation of macro-, meso- and microplastic abundance on a remote coral island of the Maldives, Indian Ocean. Mar. Pollut. Bull. 116 https://doi.org/10.1016/j.marpolbul.2017.01.010.

Imran, M., Das, K.R., Naik, M.M., 2019. Co-selection of multi-antibiotic resistance in bacterial pathogens in metal and microplastic contaminated environments: An emerging health threat. Chemosphere 215. https://doi.org/10.1016/j.chemosphere.2018.10.114.

Institute for Health Metrics and Evaluation (IHME), 2020, No Title. ⟨http://ghdx.healthdata.org/gbd-results-tool?params=gbd-api-2019-permalink/02f86ee23710bc377c27076075a07b8e⟩.

Irmscher, M., De Jong, A.M., Kress, H., Prins, M.W.J., 2013. A method for time-resolved measurements of the mechanics of phagocytic cups. J. R. Soc. Interface 10. https://doi.org/10.1098/rsif.2012.1048.

Jacob, H., Besson, M., Swarzenski, P.W., Lecchini, D., Metian, M., 2020. Effects of Virgin Micro- and Nanoplastics on Fish: Trends, Meta-Analysis, and Perspectives. Environ. Sci. Technol. 54 https://doi.org/10.1021/acs.est.9b05995.

Jani, P., Halbert, G.W., Langridge, J., Florence, A.T., 1989. The uptake and translocation of latex nanospheres and microspheres after oral administration to rats. J. Pharm. Pharm. https://doi.org/10.1111/j.2042-7158.1989.tb06377.x.

Jani, P., Halbert, G.W., Langridge, J., Florence, A.T., 1990. Nanoparticle Uptake by the Rat Gastrointestinal Mucosa: Quantitation and Particle Size Dependency. J. Pharm. Pharm. https://doi.org/10.1111/j.2042-7158.1990.tb07033.x.

Janssen, N.A., Gerlofs-Nijland, M.E., Lanki, T., Salonen, R.O., Cassee, F., Hoek, G., Fischer, P., Brunekreef, B., Krzyzanowski, M., 2012. Health Eff. Black Carbon, World Heal. …..

Janssen, N.A.H., Hoek, G., Simic-Lawson, M., Fischer, P., van Bree, L., Ten Brink, H., Keuken, M., Atkinson, R.W., Ross Anderson, H., Brunekreef, B., Cassee, F.R., 2011. Black carbon as an additional indicator of the adverse health effects of airborne particles compared with pm10 and pm2.5. Environ. Health Perspect. 119 https://doi.org/10.1289/ehp.1003369.

Jin, Y., Lu, L., Tu, W., Luo, T., Fu, Z., 2019. Impacts of polystyrene microplastic on the gut barrier, microbiota and metabolism of mice. Sci. Total Environ. https://doi.org/10.1016/j.scitotenv.2018.08.353.

Johansson, K.S., 2017. Surface Modification of Plastics. : Appl. Plast. Eng. Handb. Process. Mater. Appl. Second Ed. https://doi.org/10.1016/B978-0-323-39040-8.00020-1.

Jones, A.E., Watts, J.A., Debelak, J.P., Thornton, L.R., Younger, J.G., Kline, J.A., 2003. Inhibition of prostaglandin synthesis during polystyrene microsphere-induced pulmonary embolism in the rat. Am. J. Physiol. - Lung Cell. Mol. Physiol. https://doi.org/10.1152/ajplung.00283.2002.

Jurinski, J.B., Rimstidt, J.D., 2001. Biodurability of talc. Am. Mineral. 86 https://doi.org/10.2138/am-2001-0402.

Kameda, T., Takahashi, K., Kim, R., Jiang, Y., Movahed, M., Park, E.-K., Rantanen, J., 2014. Asbestos: use, bans and disease burden in Europe. Bull. World Health Organ 92. https://doi.org/10.2471/blt.13.132118.

16

Kaur, J., Tikoo, K., 2013. Evaluating cell specific cytotoxicity of differentially charged silver nanoparticles. Food Chem. Toxicol. 51 https://doi.org/10.1016/j.fct.2012.08.044.

Keller, S., Berghoff, K., Kress, H., 2017. Phagosomal transport depends strongly on phagosome size. Sci. Rep. https://doi.org/10.1038/s41598-017-17183-7.

Kelly, F.J., Fussell, J.C., 2012. Size, source and chemical composition as determinants of toxicity attributable to ambient particulate matter. Atmos. Environ. https://doi.org/10.1016/j.atmosenv.2012.06.039.

Kern, D.G., Kern, E., Crausman, R.S., Clapp, R.W., 2011. A retrospective cohort study of lung cancer incidence in nylon flock workers, 1998-2008. Int. J. Occup. Environ. Health. https://doi.org/10.1179/oeh.2011.17.4.345.

Kern, D.G., Crausman, R.S., Durand, K.T.H., Nayer, A., Kuhn, C., 1998. Flock worker's lung: Chronic interstitial lung disease in the nylon flocking industry. Ann. Intern. Med. https://doi.org/10.7326/0003-4819-129-4-199808150-00001.

Kern, D.G., Kuhn, C., Wesley Ely, E., Pransky, G.S., Mello, C.J., Fraire, A.E., Müller, J., 2000. Flock worker's lung: Broadening the spectrum of clinicopathology, narrowing the spectrum of suspected etiologies. Chest. https://doi.org/10.1378/chest.117.1.251.

Kernchen, S., Löder, M.G.J., Fischer, F., Fischer, D., Moses, S.R., Georgi, C., Nölscher, A. C., Held, A., Laforsch, C., 2021. Airborne microplastic concentrations and deposition across the Weser River catchment. Sci. Total Environ., 151812 https://doi.org/10.1016/j.scitotenv.2021.151812.

Kirrane, E.F., Luben, T.J., Benson, A., Owens, E.O., Sacks, J.D., Dutton, S.J., Madden, M., Nichols, J.L., 2019. A systematic review of cardiovascular responses associated with ambient black carbon and fine particulate matter. Environ. Int. 127 https://doi.org/10.1016/j.envint.2019.02.027.

Kirstein, I.V., Kirmizi, S., Wichels, A., Garin-Fernandez, A., Erler, R., Löder, M., Gerdts, G., 2016. Dangerous hitchhikers? Evidence for potentially pathogenic Vibrio spp. on microplastic particles. Mar. Environ. Res. 120 https://doi.org/10.1016/j.marenvres.2016.07.004.

Kleeman, M.J., Schauer, J.J., Cass, G.R., 1999. Size and composition distribution of fine particulate matter emitted from wood burning, meat charbroiling, and cigarettes. Environ. Sci. Technol. 33 https://doi.org/10.1021/es981277q.

Klein, M., Fischer, E.K., 2019. Microplastic abundance in atmospheric deposition within the Metropolitan area of Hamburg, Germany. Sci. Total Environ. 685 https://doi.org/10.1016/j.scitotenv.2019.05.405.

Klein, R.G., Schmezer, P., Amelung, F., Schroeder, H.G., Woeste, W., Wolf, J., 2001. Carcinogenicity assays of wood dust and wood additives in rats exposed by long-term inhalation. Int. Arch. Occup. Environ. Health 74. https://doi.org/10.1007/s004200000199.

Knaapen, A.M., Borm, P.J.A., Albrecht, C., Schins, R.P.F., 2004. Inhaled particles and lung cancer. Part A: Mechanisms. Int. J. Cancer 109. https://doi.org/10.1002/ijc.11708.

Koelmans, A.A., Diepens, N.J., Mohamed Nor, N.H., 2021. Weight of evidence for the microplastic vector effect in the context of chemical risk assessment. Plast. Environ. Pattern Process Springe Open.

Kress, H., Stelzer, E.H.K., Holzer, D., Buss, F., Griffiths, G., Rohrbach, A., 2007. Filopodia act as phagocytic tentacles and pull with discrete steps and a load-dependent velocity. Proc. Natl. Acad. Sci. U. S. A 104. https://doi.org/10.1073/pnas.0702449104.

Lee, B.-K., 2010. Sources, Distribution and Toxicity of Polyaromatic Hydrocarbons (PAHs) in Particulate Matter. : Air Pollut. https://doi.org/10.5772/10045.

Lefevre, M.E., Boccio, A.M., Joel, D.D., 1989. Intestinal uptake of fluorescent microspheres in young and aged mice. Proc. Soc. Exp. Biol. Med. https://doi.org/10.3181/00379727-190-42825.

Lehmann, S.G., Toybou, D., del Real, A.E.P., Arndt, D., Tagmount, A., Viau, M., Safi, M., Pacureanu, A., Cloetens, P., Bohic, S., Salomé, M., Castillo-Michel, H., Omaña-Sanz, B., Hofmann, A., Vulpe, C., Simonato, J.P., Celle, C., Charlet, L., Gilbert, B., 2019. Crumpling of silver nanowires by endolysosomes strongly reduces toxicity. Proc. Natl. Acad. Sci. U. S. A 116. https://doi.org/10.1073/pnas.1820941116.

Leinardi, R., Pavan, C., Yedavally, H., Tomatis, M., Salvati, A., Turci, F., 2020. Cytotoxicity of fractured quartz on THP-1 human macrophages: role of the membranolytic activity of quartz and phagolysosome destabilization. Arch. Toxicol. 94 https://doi.org/10.1007/s00204-020-02819-x.

Leung, C.C., Yu, I.T.S., Chen, W., 2012. Silicosis. Lancet 379, 2008–2018. https://doi.org/10.1016/S0140-6736(12)60235-9.

Li, X., Sundquist, J., Sundquist, K., 2008. Socioeconomic and occupational groups and risk of asthma in Sweden. Occup. Med. (Chic. Ill.) 58. https://doi.org/10.1093/occmed/kqn009.

Li, Y., Shao, L., Wang, W., Zhang, M., Feng, X., Li, W., Zhang, D., 2020. Airborne fiber particles: Types, size and concentration observed in Beijing. Sci. Total Environ. https://doi.org/10.1016/j.scitotenv.2019.135967.

liang Liao, Y., yan Yang, J., 2020. Microplastic serves as a potential vector for Cr in an in-vitro human digestive model. Sci. Total Environ. https://doi.org/10.1016/j.scitotenv.2019.134805.

Light, W.G., Wei, E.T., 1977. Surface charge and asbestos toxicity [18]. Nature 265. https://doi.org/10.1038/265537a0.

Lim, X.Z., 2021. Microplastics are everywhere - but are they harmful? Nature 593. https://doi.org/10.1038/d41586-021-01143-3.

Linch, K.D., 2002. Respirable concrete dust - Silicosis hazard in the construction industry. Appl. Occup. Environ. Hyg. 17 https://doi.org/10.1080/104732202753438298.

Lippmann, M., 1990. Effects of fiber characteristics on lung deposition, retention, and disease. : Environ. Health Perspect. https://doi.org/10.1289/ehp.9088311.

Lippmann, M., Yeates, D.B., Albert, R.E., 1980. Deposition, retention, and clearance of inhaled particles. Br. J. Ind. Med. https://doi.org/10.1136/oem.37.4.337.

Liu, C., Li, J., Zhang, Y., Wang, L., Deng, J., Gao, Y., Yu, L., Zhang, J., Sun, H., 2019. Widespread distribution of PET and PC microplastics in dust in urban China and their estimated human exposure. Environ. Int. 128, 116–124. https://doi.org/10.1016/j.envint.2019.04.024.

Liu, K., Wang, X., Song, Z., Wei, N., Li, D., 2020. Terrestrial plants as a potential temporary sink of atmospheric microplastics during transport. Sci. Total Environ. 742, 140523 https://doi.org/10.1016/j.scitotenv.2020.140523.

Liu, K., Wang, X., Fang, T., Xu, P., Zhu, L., Li, D., 2019. Source and potential risk assessment of suspended atmospheric microplastics in Shanghai. Sci. Total Environ. 675, 462–471. https://doi.org/10.1016/j.scitotenv.2019.04.110.

Liu, W.K., Wong, M.H., Tam, N.F.Y., Choy, A.C.K., 1985. Properties and toxicity of airborne wood dust in woodworking establishments. Toxicol. Lett. 26 https://doi.org/10.1016/0378-4274(85)90183-3.

Liu, Y., Yin, Y., Wang, L., Zhang, W., Chen, X., Yang, X., Xu, J., Ma, G., 2013. Surface hydrophobicity of microparticles modulates adjuvanticity. J. Mater. Chem. B. 1 https://doi.org/10.1039/c3tb20383b.

Long, H., Shi, T., Borm, P.J., Määttä, J., Husgafvel-Pursiainen, K., Savolainen, K., Krombach, F., 2004. ROS-mediated TNF-α and MIP-2 gene expression in alveolar macrophages exposed to pine dust. Part. Fibre Toxicol. 1 https://doi.org/10.1186/1743-8977-1-3.

Lougheed, M.D., Roos, J.O., Waddell, W.R., Munt, P.W., 1995. Desquamative interstitial pneumonitis and diffuse alveolar damage in textile workers: Potential role of mycotoxins. Chest. https://doi.org/10.1378/chest.108.5.1196.

Lu, L., Wan, Z., Luo, T., Fu, Z., Jin, Y., 2018. Polystyrene microplastics induce gut microbiota dysbiosis and hepatic lipid metabolism disorder in mice. Sci. Total Environ. https://doi.org/10.1016/j.scitotenv.2018.03.051.

Lu, Y., Zhang, Y., Deng, Y., Jiang, W., Zhao, Y., Geng, J., Ding, L., Ren, H., 2016. Uptake and Accumulation of Polystyrene Microplastics in Zebrafish (Danio rerio) and Toxic Effects in Liver. Environ. Sci. Technol. 50 https://doi.org/10.1021/acs.est.6b00183.

Määttä, J., Luukkonen, R., Husgafvel-Pursiainen, K., Alenius, H., Savolainen, K., 2006. Comparison of hardwood and softwood dust-induced expression of cytokines and chemokines in mouse macrophage RAW 264.7 cells. Toxicology 218. https://doi.org/10.1016/j.tox.2005.09.001.

Määttä, J., Majuri, M.L., Luukkonen, R., Lauerma, A., Husgafvel-Pursiainen, K., Alenius, H., Savolainen, K., 2005. Characterization of oak and birch dust-induced expression of cytokines and chemokines in mouse macrophage RAW 264.7 cells. Toxicology 215. https://doi.org/10.1016/j.tox.2005.06.021.

Määttä, J., Lehto, M., Leino, M., Tillander, S., Haapakoski, R., Majuri, M.L., Wolff, H., Rautio, S., Welling, I., Husgafvel-Pursiainen, K., Savolainen, K., Alenius, H., 2006. Mechanisms of particle-induced pulmonary inflammation in a mouse model: Exposure to wood dust. Toxicol. Sci. 93 https://doi.org/10.1093/toxsci/kfl026.

Mahadevan, G., Valiyaveettil, S., 2021. Understanding the interactions of poly(methyl methacrylate) and poly(vinyl chloride) nanoparticles with BHK-21 cell line. Sci. Rep. https://doi.org/10.1038/s41598-020-80708-0.

Mannetje, A. 'T., Steenland, K., Attfield, M., Boffetta, P., Checkoway, H., DeKlerk, N., Koskela, R.S., 2002. Exposure-response analysis and risk assessment for silica and silicosis mortality in a pooled analysis of six cohorts. Occup. Environ. Med 59. https://doi.org/10.1136/oem.59.11.723.

Marková, I., Ladomerský, J., Hroncová, E., Mračková, E., 2018. Thermal parameters of beech wood dust. BioResources 13. https://doi.org/10.15376/biores.13.2.3098-3109.

A. Martens, W. Jacobi, Die In-Vivo Bestimmung der Aerosolteilchen-deposition im Atemtrakt bei Mund-Bzw Nasenatmung [In vivo determination of aerosol particle deposition in the total respiratory tract], in: Aerosole Phys. Medizin Und Tech. Proc. Ann. Conf. Assoc. Aerosol Res., 1973: pp. 117–122.

Mastrangelo, G., Fedeli, U., Fadda, E., Milan, G., Lange, J.H., 2002. Epidemiologic evidence of cancer risk in textile industry workers: A review and update. Toxicol. Ind. Health. https://doi.org/10.1191/0748233702th139rr.

Mazzoli, A., Favoni, O., 2012. Particle size, size distribution and morphological evaluation of airborne dust particles of diverse woods by Scanning Electron Microscopy and image processing program. Powder Technol. 225 https://doi.org/10.1016/j.powtec.2012.03.033.

Mbachu, O., Jenkins, G., Pratt, C., Kaparaju, P., 2020. A New Contaminant Superhighway? A Review of Sources, Measurement Techniques and Fate of Atmospheric Microplastics. Water Air. Soil Pollut. 231 https://doi.org/10.1007/s11270-020-4459-4.

Medalia, A.I., Rivin, D., Sanders, D.R., 1983. A comparison of carbon black with soot. Sci. Total Environ. 31 https://doi.org/10.1016/0048-9697(83)90053-0.

Meides, N., Menzel, T., Poetzschner, B., Löder, M.G.J., Mansfeld, U., Strohriegl, P., Altstaedt, V., Senker, J., 2021. Reconstructing the Environmental Degradation of Polystyrene by Accelerated Weathering. Environ. Sci. Technol. 55 https://doi.org/10.1021/acs.est.0c07718.

Merget, R., Bauer, T., Küpper, H., Philippou, S., Bauer, H., Breitstadt, R., Bruening, T., 2002. Health hazards due to the inhalation of amorphous silica. Arch. Toxicol. 75 https://doi.org/10.1007/s002040100266.

Metintas, S., Metintas, M., Ucgun, I., Oner, U., 2002. Malignant mesothelioma due to environmental exposure to asbestos: Follow-up of a turkish cohort living in a rural area. Chest 122. https://doi.org/10.1378/chest.122.6.2224.

Miller, A., Teirstein, A.S., Chuang, M., Selikoff, I.J., Warshaw, R., 1975. Changes in pulmonary function in workers exposed to vinyl chloride and polyvinyl chloride. Ann. N. Y. Acad. Sci. https://doi.org/10.1111/j.1749-6632.1975.tb51079.x.

Millican, J.M., Agarwal, S., 2021. Plastic Pollution: A Material Problem? Macromolecules. https://doi.org/10.1021/acs.macromol.0c02814.

Mirowsky, J., Hickey, C., Horton, L., Blaustein, M., Galdanes, K., Peltier, R.E., Chillrud, S., Chen, L.C., Ross, J., Nadas, A., Lippmann, M., Gordon, T., 2013. The effect of particle size, location and season on the toxicity of urban and rural

17

particulate matter. Inhal. Toxicol. 25 https://doi.org/10.3109/08958378.2013.846443.

Mischler, S.E., Cauda, E.G., Di Giuseppe, M., McWilliams, L.J., Croix St., C., Sun, M., Franks, J., Ortiz, L.A., 2016. Differential activation of RAW 264.7 macrophages by size-segregated crystalline silica. J. Occup. Med. Toxicol. 11 https://doi.org/10.1186/s12995-016-0145-2.

Mohamed Nor, N.H., Kooi, M., Diepens, N.J., Koelmans, A.A., 2021. Lifetime Accumulation of Microplastic in Children and Adults. Environ. Sci. Technol. 55 https://doi.org/10.1021/acs.est.0c07384.

Morawski, D.R., Coutts, R.D., Handal, E.G., Luibel, F.J., Santore, R.F., Ricci, J.L., 1995. Polyethylene debris in lymph nodes after a total hip arthroplasty: A report of two cases. J. Bone Jt. Surg. - Ser. A. https://doi.org/10.2106/00004623-199505000-00014.

Morgan, A., 1995. Deposition of inhaled asbestos ani) man-made mineral fibres in the respiratory tract. Ann. Occup. Hyg. 39 https://doi.org/10.1093/annhyg/39.5.747.

Motskin, M., Wright, D.M., Muller, K., Kyle, N., Gard, T.G., Porter, A.E., Skepper, J.N., 2009. Hydroxyapatite nano and microparticles: Correlation of particle properties with cytotoxicity and biostability. Biomaterials 30. https://doi.org/10.1016/j.biomaterials.2009.02.044.

Muff, L.F., Luxbacher, T., Burgert, I., Michen, B., 2018. Investigating the time-dependent zeta potential of wood surfaces. J. Colloid Interface Sci. 518 https://doi.org/10.1016/j.jcis.2018.02.022.

Muhle, H., Ernst, H., Bellmann, B., 1997. Investigation of the Durability of Cellulose Fibres in Rat Lungs. Ann. Occup. Hyg. https://doi.org/10.1093/annhyg/41.inhaled_particles VIII.184.

Muittari, A., Veneskoski, T., 1978. Natural and synthetic fibers as causes of asthma and rhinitis. Ann. Allergy.

Naarala, J., Kasanen, J.P., Pasanen, P., Pasanen, A.L., Liimatainen, A., Pennanen, S., Liesivuori, J., 2003. The effects of wood dusts on the redox status and cell death in mouse macrophages (RAW 264.7) and human leukocytes in vitro. J. Toxicol. Environ. Heal. - Part A 66. https://doi.org/10.1080/15287390306406.

Ng, K.L., Obbard, J.P., 2006. Prevalence of microplastics in Singapore's coastal marine environment. Mar. Pollut. Bull. 52 https://doi.org/10.1016/j.marpolbul.2005.11.017.

Ng, T.P., Lee, H.S., Low, Y.M., Phoon, W.H., Ng, Y.L., 1991. Pulmonary effects of polyvinyl chloride dust exposure on compounding workers. Scand. J. Work. Environ. Heal. https://doi.org/10.5271/sjweh.1734.

Nich, C., Goodman, S.B., 2014. Role of macrophages in the biological reaction to wear debris from joint replacements. J. Long. Term. Eff. Med. Implants. https://doi.org/10.1615/jlongtermeffmedimplants.2014010562.

Noonan, C.W., 2017. Environmental asbestos exposure and risk of mesothelioma. Ann. Transl. Med. 5 https://doi.org/10.21037/atm.2017.03.74.

O'Connor, D.J., Healy, D.A., Sodeau, J.R., 2013. The on-line detection of biological particle emissions from selected agricultural materials using the WIBS-4 (Waveband Integrated Bioaerosol Sensor) technique. Atmos. Environ. 80 https://doi.org/10.1016/j.atmosenv.2013.07.051.

Oberdorster, G., Ferin, J., Lehnert, B.E., 1994. Correlation between particle size, in vivo particle persistence, and lung injury. : Environ. Health Perspect. https://doi.org/10.1289/ehp.102 1567252.

Očkajová, A., Kučerka, M., Kminiak, R., Krišťák, Ľ., Igaz, R., Réh, R., 2020. Occupational exposure to dust produced when milling thermally modified wood. Int. J. Environ. Res. Public Health 17. https://doi.org/10.3390/ijerph17051478.

Ojima, J., 2016. Generation rate and particle size distribution of wood dust by handheld sanding operation. J. Occup. Health 58. https://doi.org/10.1539/joh.16-0136-BR.

Olenchock, S.A., May, J.J., Pratt, D.S., Piacitelli, L.A., Parker, J.E., 1990. Presence of endotoxins in different agricultural environments. Am. J. Ind. Med. 18 https://doi.org/10.1002/ajim.4700180307.

Omidvarborna, H., Kumar, A., Kim, D.S., 2015. Recent studies on soot modeling for diesel combustion. Renew. Sustain. Energy Rev. 48 https://doi.org/10.1016/j.rser.2015.04.019.

Ono-Ogasawara, M., Kohyama, N., 1999. Evaluation of surface roughness of fibrous minerals by comparison of BET surface area and calculated one. Ann. Occup. Hyg. 43 https://doi.org/10.1016/S0003-4878(99)00069-1.

Oze, C., Solt, K., 2010. Biodurability of chrysotile and tremolite asbestos in simulated lung and gastric fluids. Am. Mineral. 95 https://doi.org/10.2138/am.2010.3265.

Padmore, T., Stark, C., Turkevich, L.A., Champion, J.A., 2017. Quantitative analysis of the role of fiber length on phagocytosis and inflammatory response by alveolar macrophages. Biochim. Biophys. Acta - Gen. Subj. 1861 https://doi.org/10.1016/j.bbagen.2016.09.031.

Patterson, R.I.A., Kraft, M., 2007. Models for the aggregate structure of soot particles. Combust. Flame. 151 https://doi.org/10.1016/j.combustflame.2007.04.012.

Pauly, J.L., Stegmeier, S.J., Allaart, H.A., Cheney, R.T., Zhang, P.J., Mayer, A.G., Streck, R.J., 1998. Inhaled cellulosic and plastic fibers found in human lung tissue. Cancer Epidemiol. Biomark. Prev.

Peltonen, L., Hirvonen, J., 2008. Physicochemical characterization of nano- and microparticles. Curr. Nanosci. 4 https://doi.org/10.2174/157341308783591780.

Pérez, J., Muñoz-Dorado, J., De La Rubia, T., Martínez, J., 2002. Biodegradation and biological treatments of cellulose, hemicellulose and lignin: An overview. Int. Microbiol. 5 https://doi.org/10.1007/s10123-002-0062-3.

Piehl, S., Leibner, A., Löder, M.G.J., Dris, R., Bogner, C., Laforsch, C., 2018. Identification and quantification of macro- and microplastics on an agricultural farmland. Sci. Rep. 8 https://doi.org/10.1038/s41598-018-36172-y.

Pira, E., Donato, F., Maida, L., Discalzi, G., 2018. Exposure to asbestos: Past, present and future. J. Thorac. Dis. 10 https://doi.org/10.21037/jtd.2017.10.126.

Pollastri, S., Gualtieri, A.F., Gualtieri, M.L., Hanuskova, M., Cavallo, A., Gaudino, G., 2014. The zeta potential of mineral fibres. J. Hazard. Mater. 276 https://doi.org/10.1016/j.jhazmat.2014.05.060.

Porter, D.W., Castranova, V., Robinson, V.A., Hubbs, A.F., Mercer, R.R., Scabilloni, J., Goldsmith, T., Schwegler-Berry, D., Battelli, L., Washko, R., Burkhart, J., Piacitelli, C., Whitmer, M., Jones, W., 1999. Acute inflammatory reaction in rats after intratracheal instillation of material collected from a nylon flocking plant. J. Toxicol. Environ. Heal. - Part A. https://doi.org/10.1080/009841099157845.

Pott, P., 1775. Chirurgical Observations Relative to the Cataract the Polypus of the Nose, the Cancer of the Scrotum, the Different Kinds of Ruptures, and the Mortification of the Toes and Feet, by Percivall Pott, F.R.S. printed by T.J. Carnegy,, London.

Prata, J.C., 2018. Airborne microplastics: Consequences to human health? Environ. Pollut. https://doi.org/10.1016/j.envpol.2017.11.043.

Prata, J.C., da Costa, J.P., Lopes, I., Duarte, A.C., Rocha-Santos, T., 2020. Environmental exposure to microplastics: An overview on possible human health effects. Sci. Total Environ. 702 https://doi.org/10.1016/j.scitotenv.2019.134455.

Prietl, B., Meindl, C., Roblegg, E., Pieber, T.R., Lanzer, G., Fröhlich, E., 2014. Nano-sized and micro-sized polystyrene particles affect phagocyte function. Cell Biol. Toxicol. https://doi.org/10.1007/s10565-013-9265-y.

Pukkala, E., Martinsen, J.I., Lynge, E., Gunnarsdottir, H.K., Sparn, P., Tryggvadottir, L., Weiderpass, E., Kjaerheim, K., 2009. Occupation and cancer follow-up of 15 million people in five Nordic countries. Acta Oncol. (Madr.) 48. https://doi.org/10.1080/02841860902913546.

Rabovsky, J., 1995. Biogenic amorphous silica. : Scand. J. Work. Environ. Heal.

Ragusa, A., Svelato, A., Santacroce, C., Catalano, P., Notarstefano, V., Carnevali, O., Papa, F., Rongioletti, M.C.A., Baiocco, F., Draghi, S., D'Amore, E., Rinaldo, D., Matta, M., Giorgini, E., 2021. Plasticenta: First evidence of microplastics in human placenta. Environ. Int. https://doi.org/10.1016/j.envint.2020.106274.

Ramsperger, A.F.R.M., Stellwag, A.C., Caspari, A., Fery, A., Lueders, T., Kress, H., Löder, M.G.J., Laforsch, C., 2020. Structural diversity in early-stage biofilm formation on microplastics depends on environmental medium and polymer properties. Water (Switz.) 12. https://doi.org/10.3390/w12113216.

Ramsperger, A.F.R.M., Narayana, V.K.B., Gross, W., Mohanraj, J., Thelakkat, M., Greiner, A., Schmalz, H., Kress, H., Laforsch, C., 2020. Environmental exposure enhances the internalization of microplastic particles into cells. Sci. Adv. https://doi.org/10.1126/sciadv.abd1211.

Ramsperger, A.F.R.M., Jasinski, J., Völkl, M., Witzmann, T., Meinhart, M., Jérôme, V., Kretschmer, W.P., Freitag, R., Senker, J., Fery, A., Kress, H., Scheibel, T., Laforsch, C., 2021. Supposedly identical microplastic particles substantially differ in their material properties influencing particle-cell interactions and cellular responses. J. Hazard. Mater., 127961 https://doi.org/10.1016/j.jhazmat.2021.127961.

Reboux, G., Piarroux, R., Roussel, S., Millon, L., Bardonnet, K., Dalphin, J.C., 2007. Assessment of four serological techniques in the immunological diagnosis of farmers' lung disease. J. Med. Microbiol 56. https://doi.org/10.1099/jmm.0.46953-0.

Reponen, T., Grinshpun, S.A., Conwell, K.L., Wiest, J., Anderson, M., 2001. Aerodynamic versus physical size of spores: Measurement and implication for respiratory deposition. Grana 40. https://doi.org/10.1080/00173130152625851.

Rimstidt, J.D., Barnes, H.L., 1980. The kinetics of silica-water reactions. Geochim. Cosmochim. Acta 44. https://doi.org/10.1016/0016-7037(80)90220 3.

Rochman, C.M., Hentschel, B.T., The, S.J., 2014. Long term sorption of metals is similar among plastic types: Implications for plastic debris in aquatic environments. PLoS One. https://doi.org/10.1371/journal.pone.0085433.

Rochman, C.M., Brookson, C., Bikker, J., Djuric, N., Earn, A., Bucci, K., Athey, S., Huntington, A., McIlwraith, H., Munno, K., De Frond, H., Kolomijeca, A., Erdle, L., Grbic, J., Bayoumi, M., Borrelle, S.B., Wu, T., Santoro, S., Werbowski, L.M., Zhu, X., Giles, R.K., Hamilton, B.M., Thaysen, C., Kaura, A., Klasios, N., Ead, L., Kim, J., Sherlock, C., Ho, A., Hung, C., 2019. Rethinking microplastics as a diverse contaminant suite. Environ. Toxicol. Chem. 38 https://doi.org/10.1002/etc.4371.

Roggli, V.L., Brody, A.R., 1984. Changes in numbers and dimensions of chrysotile asbestos fibers in lungs of rats following short-term exposure. Exp. Lung Res. 7 https://doi.org/10.3109/01902148409069674.

Rylander, R., 1987. The role of endotoxin for reactions after exposure to cotton dust. Am. J. Ind. Med. 12 https://doi.org/10.1002/ajim.4700120607.

Salvi, S.S., Nordenhall, C., Blomberg, A., Rudell, B., Pourazar, J., Kelly, F.J., Wilson, S., Sandström, T., Holgate, S.T., Frew, A.J., 2000. Acute exposure to diesel exhaust increases IL-8 and GRO-α production in healthy human airways. Am. J. Respir. Crit. Care Med. 161 https://doi.org/10.1164/ajrccm.161.2.9905052.

Sanders, E., Ashworth, C.T., 1961. A study of particulate intestinal absorption and hepatocellular uptake. Use of polystyrene latex particles. Exp. Cell Res. https://doi.org/10.1016/0014-4827(61)90092-1.

Sarkar, S., Zhang, L., Subramaniam, P., Lee, K.B., Garfunkel, E., Ohman Strickland, P.A., Mainelis, G., Lioy, P.J., Tetley, T.D., Chung, K.F., Zhang, J., Ryan, M., Porter, A., Schwander, S., 2014. Variability in bioreactivity linked to changes in size and zeta potential of diesel exhaust particles in human immune cells. PLoS One 9. https://doi.org/10.1371/journal.pone.0097304.

Schell, T., Rico, A., Vighi, M., 2020. Occurrence, Fate and Fluxes of Plastics and Microplastics in Terrestrial and Freshwater Ecosystems. Rev. Environ. Contam. Toxicol. https://doi.org/10.1007/398_2019_40.

Schmid, O., Stoeger, T., 2016. Surface area is the biologically most effective dose metric for acute nanoparticle toxicity in the lung. J. Aerosol Sci. 99 https://doi.org/10.1016/j.jaerosci.2015.12.006.

Schwabl, P., Koppel, S., Konigshofer, P., Bucsics, T., Trauner, M., Reiberger, T., Liebmann, B., 2019. Detection of various microplastics in human stool: A prospective case series. Ann. Intern. Med. https://doi.org/10.7326/M19-0618.

18

Schwartz, J., Dockery, D.W., Neas, L.M., 1996. Is Daily Mortality Associated Specifically with Fine Particles? J. Air Waste Manag. Assoc. 46 https://doi.org/10.1080/10473289.1996.10467528.

Schweizer, C., Edwards, R.D., Bayer-Oglesby, L., Gauderman, W.J., Ilacqua, V., Juhani Jantunen, M., Lai, H.K., Nieuwenhuijsen, M., Künzli, N., 2007. Indoor time-microenvironment-activity patterns in seven regions of Europe. J. Expo. Sci. Environ. Epidemiol. 17 https://doi.org/10.1038/sj.jes.7500490.

Séguin, V., Lemauviel Lavenant, S., Garon, D., Bouchart, V., Gallard, Y., Blanchet, B., Diquelou, S., Personeni, E., Gauduchon, P., Ourry, A., 2010. Effect of agricultural and environmental factors on the hay characteristics involved in equine respiratory disease. Agric. Ecosyst. Environ. 135 https://doi.org/10.1016/j.agee.2009.09.012.

Shao, X.R., Wei, X.Q., Song, X., Hao, L.Y., Cai, X.X., Zhang, Z.R., Peng, Q., Lin, Y.F., 2015. Independent effect of polymeric nanoparticle zeta potential/surface charge, on their cytotoxicity and affinity to cells. Cell Prolif. 48 https://doi.org/10.1111/cpr.12192.

Siegel, P.D., Olenchock, S.A., Sorenson, W.G., Lewis, D.M., Bledsoe, T.A., May, J.J., Pratt, D.S., 1991. Histamine and endotoxin contamination of hay and respirable hay dust. Scand. J. Work. Environ. Heal 17. https://doi.org/10.5271/sjweh.1702.

Silicosis Mortality, 2005, Prevention, and Control—United States, 1968–2002, JAMA. 293. ⟨https://doi.org/10.1001/jama.293.21.2585⟩.

Silva, T., Pokhrel, L.R., Dubey, B., Tolaymat, T.M., Maier, K.J., Liu, X., 2014. Particle size, surface charge and concentration dependent ecotoxicity of three organo-coated silver nanoparticles: Comparison between general linear model-predicted and observed toxicity. Sci. Total Environ. 468–469 https://doi.org/10.1016/j.scitotenv.2013.09.006.

Sirianni, G., Hosgood, H.D., Slade, M.D., Borak, J., 2008. Particle size distribution and particle size-related crystalline silica content in granite quarry dust. J. Occup. Environ. Hyg. 5 https://doi.org/10.1080/15459620801947259.

Slavin, J.L., Brauer, P.M., Marlett, J.A., 1981. Neutral detergent fiber, hemicellulose and cellulose digestibility in human subjects. J. Nutr. 111 https://doi.org/10.1093/jn/111.2.287.

Smith, M., Love, D.C., Rochman, C.M., Neff, R.A., 2018. Microplastics in Seafood and the Implications for Human Health. Curr. Environ. Heal. Rep. https://doi.org/10.1007/s40572-018-0206-z.

Solbes, E., Harper, R.W., 2018. Biological responses to asbestos inhalation and pathogenesis of asbestos-related benign and malignant disease. J. Investig. Med. 66 https://doi.org/10.1136/jim-2017-000628.

Solbrig, C.M., Obendorf, S.K., 1985. Distribution of Residual Pesticide Within Textile Structures as Determined by Electron Microscopy. Text. Res. J. 55 https://doi.org/10.1177/004051758505500904.

Sporn, T.A., Roggli, V.L., 2014. In: Oury, T.D., Sporn, T.A., Roggli, V.L. (Eds.), Asbestosis BT - Pathology of Asbestos-Associated Diseases. Springer Berlin Heidelberg, Berlin, Heidelberg, pp. 53–80. https://doi.org/10.1007/978-3-642-41193-9_4.

Stanton, M.F., Miller, E., May, M., Tegeris, A., Morgan, E., 1981. Relation of particle dimension to carcinogenicity in amphibole asbestoses and other fibrous minerals. J. Natl. Cancer Inst. 67 https://doi.org/10.1093/jnci/67.5.965.

Stefaniak, A.B., Seehra, M.S., Fix, N.R., Leonard, S.S., 2014. Lung biodurability and free radical production of cellulose nanomaterials. Inhal. Toxicol. 26 https://doi.org/10.3109/08958378.2014.948650.

Sternschuss, G., Ostergard, D.R., Patel, H., 2012. Post implantation alterations of polypropylene in the human. J. Urol. https://doi.org/10.1016/j.juro.2012.02.2559.

Stöber, W., Abel, U.R., 1996. Lung cancer due to diesel soot particles in ambient air? A critical appraisal of epidemiological studies addressing this question. Int. Arch. Occup. Environ. Health 68. https://doi.org/10.1007/bf00387825.

Studnicka, M.J., Menzinger, G., Drlicek, M., Maruna, H., Neumann, M.G., 1995. Pneumoconiosis and systemic sclerosis following 10 years of exposure to polyvinyl chloride dust. Thorax. https://doi.org/10.1136/thx.50.5.583.

Syberg, K., Khan, F.R., Selck, H., Palmqvist, A., Banta, G.T., Daley, J., Sano, L., Duhaime, M.B., 2015. Microplastics: Addressing ecological risk through lessons learned. Environ. Toxicol. Chem. 34 https://doi.org/10.1002/etc.2914.

Szewc, K., Graca, B., Dołęga, A., 2021. Atmospheric deposition of microplastics in the coastal zone: Characteristics and relationship with meteorological factors. Sci. Total Environ. 761, 143272 https://doi.org/10.1016/j.scitotenv.2020.143272.

Tanasupawat, S., Takehana, T., Yoshida, S., Hiraga, K., Oda, K., 2016. Ideonella sakaiensis sp. nov., isolated from a microbial consortium that degrades poly (ethylene terephthalate). Int. J. Syst. Evol. Microbiol 66. https://doi.org/10.1099/ijsem.0.001058.

Teichert, S., Löder, M.G.J., Pyko, I., Mordek, M., Schulbert, C., Wisshak, M., Laforsch, C., 2021. Microplastic contamination of the drilling bivalve Hiatella arctica in Arctic rhodolith beds. Sci. Rep. 11 https://doi.org/10.1038/s41598-021-93668-w.

Terada, N., Hamano, N., Maesako, K.I., Hiruma, K., Hohki, G., Suzuki, K., Ishikawa, K., Konno, A., 1999. Diesel exhaust particulates upregulate histamine receptor mRNA and increase histamine-induced IL-8 and GM-CSF production in nasal epithelial cells and endothelial cells. Clin. Exp. Allergy 29. https://doi.org/10.1046/j.1365-2222.1999.00406.x.

TeWaterNaude, J.M., Ehrlich, R.I., Churchyard, G.J., Pemba, L., Dekker, K., Vermeis, M., White, N.W., Thompson, M.L., Myers, J.E., 2006. Tuberculosis and silica exposure in South African gold miners. Occup. Environ. Med. 63 https://doi.org/10.1136/oem.2004.018614.

Thompson, R.C., Moore, C.J., Saal, F.S.V., Swan, S.H., 2009. Plastics, the environment and human health: Current consensus and future trends. Philos. Trans. R. Soc. B Biol. Sci. 364 https://doi.org/10.1098/rstb.2009.0053.

Thompson, R.C., Olson, Y., Mitchell, R.P., Davis, A., Rowland, S.J., John, A.W.G., McGonigle, D., Russell, A.E., 2004. Lost at Sea: Where Is All the Plastic? Science (80). https://doi.org/10.1126/science.1094559.

Torvela, T., Tissari, J., Sippula, O., Kaivosoja, T., Leskinen, J., Virén, A., Lähde, A., Jokiniemi, J., 2014. Effect of wood combustion conditions on the morphology of freshly emitted fine particles. Atmos. Environ. 87 https://doi.org/10.1016/j.atmosenv.2014.01.028.

Trainic, M., Flores, J.M., Pinkas, I., Pedrotti, M.L., Lombard, F., Bourdin, G., Gorsky, G., Boss, E., Rudich, Y., Vardi, A., Koren, I., 2020. Airborne microplastic particles detected in the remote marine atmosphere. Commun. Earth Environ. 1, 1–9. https://doi.org/10.1038/s43247-020-00061-y.

U.S. Geological Survey, 2007, UICC Asbestos Amosite Standard. ⟨https://www.usgs.gov/media/images/uicc-asbestos-amosite-standard⟩.

Uetani, K., Yano, H., 2012. Zeta potential time dependence reveals the swelling dynamics of wood cellulose nanofibrils. Langmuir 28. https://doi.org/10.1021/la203404g.

Underhill, D.M., Goodridge, H.S., 2012. Information processing during phagocytosis. Nat. Rev. Immunol. 12 https://doi.org/10.1038/nri3244.

Urban, R.M., Jacobs, J.J., Tomlinson, M.J., Gavrilovic, J., Black, J., Peoc'h, M., 2000. Dissemination of wear particles to the liver, spleen, and abdominal lymph nodes of patients with hip or knee replacement. J. Bone Jt. Surg. - Ser. A. https://doi.org/10.2106/00004623-200004000-00002.

Valavanidis, A., Vlachogianni, T., Fiotakis, K., Loridas, S., 2013. Pulmonary oxidative stress, inflammation and cancer: Respirable particulate matter, fibrous dusts and ozone as major causes of lung carcinogenesis through reactive oxygen species mechanisms. Int. J. Environ. Res. Public Health. https://doi.org/10.3390/ijerph10093886.

Valic, F., Zuskin, E., 1977. Respir.-Funct. Chang. Text. Work. Expo. Synth. Fibres.

Vallyathan, V., Castranova, V., Pack, D., Leonard, S., Shumaker, J., Hubbs, A.F., Shoemaker, D.A., Ramsey, D.M., Pretty, J.R., McLaurin, J.L., Khan, A., Teass, A., 1995. Freshly fractured quartz inhalation leads to enhanced lung injury and inflammation: Potential role of free radicals. Am. J. Respir. Crit. Care Med. 152 https://doi.org/10.1164/ajrccm.152.3.7663775.

Vansant, E.F., Van Der Voort, P., Vrancken, K.C., 1995. Charact. Chem. Modif. Silica Surf.

Vethaak, A.D., Legler, J., 2021. Microplastics and human health. Science (80). https://doi.org/10.1126/science.abe5041.

Vianello, A., Jensen, R.L., Liu, L., Vollertsen, J., 2019. Simulating human exposure to indoor airborne microplastics using a Breathing Thermal Manikin. Sci. Rep. https://doi.org/10.1038/s41598-019-45054-w.

Vinay Kumar, B.N., Löschel, L.A., Imhof, H.K., Löder, M.G.J., Laforsch, C., 2021. Analysis of microplastics of a broad size range in commercially important mussels by combining FTIR and Raman spectroscopy approaches. Environ. Pollut. 269 https://doi.org/10.1016/j.envpol.2020.116147.

Vobecky, J., Devroede, G., Lacaille, J., Watier, A., 1978. An occupational group with a high risk of large bowel cancer. Gastroenterology. https://doi.org/10.1016/0016-5085(78)90406-7.

Volkheimer, G., 1975. Hematogenous dissemination of ingested polyvinyl chloride particles. Ann. N. Y. Acad. Sci. https://doi.org/10.1111/j.1749-6632.1975.tb51092.x.

Von Moos, N., Burkhardt-Holm, P., Köhler, A., 2012. Uptake and effects of microplastics on cells and tissue of the blue mussel Mytilus edulis L. after an experimental exposure. Environ. Sci. Technol. 46 https://doi.org/10.1021/es302332w.

Wagner, R., 1997. Asbestosis and silicosis. Lancet 349, 1311–1315. https://doi.org/10.1016/S0140-6736(96)07336-9.

Walker, P.S., Bullough, P.G., 1973. The effects of friction and wear in artificial joints. Orthop. Clin. North Am. https://doi.org/10.1016/s0030-5898(20)30793-8.

Wang, X., Li, C., Liu, K., Zhu, L., Song, Z., Li, D., 2020. Atmospheric microplastic over the South China Sea and East Indian Ocean: abundance, distribution and source. J. Hazard. Mater. 389, 121846 https://doi.org/10.1016/j.jhazmat.2019.121846.

Wang, X.R., Eisen, E.A., Zhang, H.X., Sun, B.X., Dai, H.L., Pan, L.D., Wegman, D.H., Olenchock, S.A., Christiani, D.C., 2003. Respiratory symptoms and cotton dust exposure; results of a 15 year follow up observation. Occup. Environ. Med. 60 https://doi.org/10.1136/oem.60.12.935.

Warheit, D.B., Webb, T.R., Reed, K.L., Hansen, J.F., Kennedy, G.L., 2003. Four-week inhalation toxicity study in rats with nylon respirable fibers: Rapid lung clearance. Toxicology. https://doi.org/10.1016/S0300-483X(03)00304-4.

Watson, A.Y., Valberg, P.A., 2001. Carbon black and soot: Two different substances. Am. Ind. Hyg. Assoc. J. 62 https://doi.org/10.1080/15298660108984625.

White, J.R., Turnbull, A., 1994. Weathering of polymers: mechanisms of degradation and stabilization, testing strategies and modelling. J. Mater. Sci. https://doi.org/10.1007/BF00445969.

Wick, P., Malek, A., Manser, P., Meili, D., Maeder-Althaus, X., Diener, L., Diener, P.A., Zisch, A., Krug, H.F., Von Mandach, U., 2010. Barrier capacity of human placenta for nanosized materials. Environ. Health Perspect. https://doi.org/10.1289/ehp.0901200.

Wiessner, J.H., Henderson, J.D., Sohnle, P.G., Mandel, N.S., Mandel, G.S., 1988. The effect of crystal structure on mouse lung inflammation and fibrosis. Am. Rev. Respir. Dis. 138 https://doi.org/10.1164/ajrccm/138.2.445.

Willert, H.G., Semlitsch, M., 1996. Tissue reactions to plastic and metallic wear products of joint endoprostheses. Clin. Orthop. Relat. Res. https://doi.org/10.1097/00003086-199612000-00002.

Williams, P.R.D., Phelka, A.D., Paustenbach, D.J., 2007. A review of historical exposures to asbestos among skilled craftsmen (1940-2006). J. Toxicol. Environ. Heal. - Part B Crit. Rev. 10 https://doi.org/10.1080/10937400601034191.

Williams, R.O., Carvalho, T.C., Peters, J.I., 2011. Influence of particle size on regional lung deposition - What evidence is there? Int. J. Pharm. https://doi.org/10.1016/j.ijpharm.2010.12.040.

Winkler, E.M., 1975. Stone. Springer, Vienna. https://doi.org/10.1007/978-3-7091-3819-9.

19

Wolff, R.K., Henderson, R.F., Snipes, M.B., Griffith, W.C., Mauderly, J.L., Cuddihy, R.G., Mcclellan, R.O., 1987. Alterations in particle accumulation and clearance in lungs of rats chronically exposed to diesel exhaust. Toxicol. Sci. 9 https://doi.org/10.1093/toxsci/9.1.154.

Wright, S.L., Kelly, F.J., 2017. Plastic and Human Health: A Micro Issue? Environ. Sci. Technol. https://doi.org/10.1021/acs.est.7b00423.

Wright, S.L., Thompson, R.C., Galloway, T.S., 2013. The physical impacts of microplastics on marine organisms: a review. Environ. Pollut. 178 https://doi.org/10.1016/j.envpol.2013.02.031.

Xu, H., Dinsdale, D., Nemery, B., Hoet, P.H.M., 2003. Role of residual additives in the cytotoxicity and cytokine release caused by polyvinyl chloride particles in pulmonary cell cultures. Toxicol. Sci. https://doi.org/10.1093/toxsci/kfg003.

Yacobi, N.R., DeMaio, L., Xie, J., Hamm-Alvarez, S.F., Borok, Z., Kim, K.J., Crandall, E. D., 2008. Polystyrene nanoparticle trafficking across alveolar epithelium, Nanomedicine Nanotechnology. Biol. Med. https://doi.org/10.1016/j.nano.2008.02.002.

Yukioka, S., Tanaka, S., Nabetani, Y., Suzuki, Y., Ushijima, T., Fujii, S., Takada, H., Van Tran, Q., Singh, S., 2020. Occurrence and characteristics of microplastics in surface road dust in Kusatsu (Japan), Da Nang (Vietnam), and Kathmandu (Nepal). Environ. Pollut. 256, 113447 https://doi.org/10.1016/j.envpol.2019.113447.

Zagorski, J., Debelak, J., Gellar, M., Watts, J.A., Kline, J.A., 2003. Chemokines Accumulate in the Lungs of Rats with Severe Pulmonary Embolism Induced by Polystyrene Microspheres. J. Immunol. https://doi.org/10.4049/jimmunol.171.10.5529.

Zan, Q., Wang, C., Dong, L., Cheng, P., Tian, J., 2008. Effect of surface roughness of chitosan-based microspheres on cell adhesion. Appl. Surf. Sci. 255 https://doi.org/10.1016/j.apsusc.2008.06.074.

Zhang, Y., Gao, T., Kang, S., Sillanpää, M., 2019. Importance of atmospheric transport for microplastics deposited in remote areas. Environ. Pollut. 254 https://doi.org/10.1016/j.envpol.2019.07.121.

Zhang, Y., Kang, S., Allen, S., Allen, D., Gao, T., Sillanpää, M., 2020. Atmospheric microplastics: A review on current status and perspectives. Earth-Sci. Rev. 203 https://doi.org/10.1016/j.earscirev.2020.103118.

Zhang, Y.-Q., Lykaki, M., Alrajoula, M.T., Markiewicz, M., Kraas, C., Kolbe, S., Klinkhammer, K., Rabe, M., Klauer, R., Bendt, E., Stolte, S., 2021. Microplastics from textile origin – emission and reduction measures. Green. Chem. 23 https://doi.org/10.1039/d1gc01589c.

Zuskin, E., Mustajbegovic, J., Schachter, E.N., Kern, J., Budak, A., Godnic-Cvar, J., 1998. Respiratory findings in synthetic textile workers. Am. J. Ind. Med. https://doi.org/10.1002/(SICI)1097-0274(199803)33:3<263::AID-AJIM8>3.0.CO;2-X.

20

Article 2

Supposedly identical microplastic particles substantially differ in their material properties influencing particle-cell interactions and cellular responses

Research Paper

Supposedly identical microplastic particles substantially differ in their material properties influencing particle-cell interactions and cellular responses

A.F.R.M. Ramsperger [a,g,1], J. Jasinski [b,1], M. Völkl [c,1], T. Witzmann [d], M. Meinhart [e], V. Jérôme [c], W.P. Kretschmer [f], R. Freitag [c], J. Senker [e], A. Fery [d], H. Kress [g], T. Scheibel [b], C. Laforsch [a,*]

[a] Animal Ecology I and BayCEER, University of Bayreuth, Bayreuth, Germany
[b] Biomaterials, University of Bayreuth, Bayreuth, Germany
[c] Process Biotechnology, University of Bayreuth, Bayreuth, Germany
[d] Leibniz-Institute of Polymer Research e.V., Institute of Physical Chemistry and Polymer Physics & Physical Chemistry of Polymeric Materials, Technical University of Dresden, Dresden, Germany
[e] Inorganic Chemistry III and Northern Bavarian NMR Centre, University of Bayreuth, Bayreuth, Germany
[f] Inorganic Chemistry II and Sustainable Chemistry Centre, University of Bayreuth, Bayreuth, Germany
[g] Biological Physics, University of Bayreuth, Bayreuth, Germany

ARTICLE INFO

ABSTRACT

Microplastics and its putative adverse effects on environmental and human health increasingly gain scientific and public attention. Systematic studies on the effects of microplastics are currently hampered by using rather poorly characterised particles, leading to contradictory results for the same particle type. Here, surface properties and chemical composition of two commercially available nominally identical polystyrene microparticles, frequently used in effect studies, were characterised. We show distinct differences in monomer content, ζ-potentials and surface charge densities. Cells exposed to particles showing a lower ζ-potential and a higher monomer content displayed a higher number of particle-cell-interactions and consequently a decrease in cell metabolism and proliferation, especially at higher particle concentrations. Our study emphasises that no general statements can be made about the effects of microplastics, not even for the same polymer type in the same size class, unless the physicochemical properties are well characterised.

1. Introduction

Microplastics are found in marine (Eriksen et al., 2014; Imhof et al., 2017; Lacerda et al., 2019), limnetic (Imhof et al., 2013; Dris et al., 2015; Klein et al., 2015; Piehl et al., 2019), atmospheric (Dris et al., 2016; Gasperi et al., 2018; Evangeliou et al., 2020) and terrestrial environments including agricultural soils used for food production (Piehl et al., 2018; Rillig and Lehmann, 2020; Rillig, 2012). Due to their worldwide distribution and small sizes (< 5 mm, (Arthur et al., 2008; Frias and Nash, 2019)), they are considered to pose a risk to environmental and human health (Wright and Kelly, 2017; Prata et al., 2020; Campanale et al., 2020). The ingestion of microplastic particles together with food has been shown in a variety of organisms ranging from lower trophic levels up to human beings (Imhof et al., 2013; Wright and Kelly, 2017; Cole and Galloway, 2015; Laist, 1997; Barboza et al., 2020; Mohamed Nor et al., 2021; Schwabl et al., 2019). However, most plastic particles may pass the gastrointestinal system (Schwabl et al., 2019; Nelms et al., 2019), and putative effects, such as inflammation evoked by particles translocated into tissues, may depend on the material's properties. In this context, research on microplastics considered predominantly the size of the particles as a crucial factor responsible for observed effects (Triebskorn et al., 2019). Ingested, larger microplastic particles can induce gut blockage and cause physical tissue damage (Bjorndal et al., 1994; Wright et al., 2013), whereas microplastic particles in the lower micrometre size range can become internalised by cells (Ramsperger et al., 2020; Stock et al., 2019, Rudolph & Völkl et al.,

* Corresponding author.
E-mail address: christian.laforsch@uni-bayreuth.de (C. Laforsch).
[1] These authors contributed equally to this work.

2021), one pathway that has been described for tissue translocation (Wright and Kelly, 2017). For instance, in zebrafish exposed to 5 and 20 μm polystyrene particles, the 20 μm particles were found in the gastrointestinal tract and the gills, whereas 5 μm particles were also found in liver tissue (Lu et al., 2016; Deng et al., 2017). In mussels, it has been shown that 3.0 and 9.6 μm polystyrene particles were able to translocate from the gastrointestinal tract into the circulatory system with a significantly higher proportion for the smaller particles used in that study (Browne et al., 2008). Microplastics translocated into the circulatory system or tissues can cause inflammation (von Moos et al., 2012) or necrosis (Wright and Kelly, 2017; Triebskorn et al., 2019; Lu et al., 2016; Rahman et al., 2021; Rodriguez-Seijo et al., 2017). In contrast, some studies did not observe tissue translocation or any adverse effects when exposing organisms or their primary cells to microplastics (Elizalde-Velázquez et al., 2020, Riedl et al., 2021). The inconsistency in results may be explained by the fact that different polymer types were used. Given that these different types of microplastic particles differ in many properties, it is likely that they also elucidate different effects in ecotoxicological studies. However, the majority of studies used polystyrene (PS), mostly spherical, microparticles (Brachner et al., 2020; Jacob et al., 2020) as recently stressed by Stock et al. (2021): "all existing studies dealing with microplastic particle uptake and toxicity exclusively used spherical, monodisperse model polystyrene particles". Here, it may be assumed that the outcome of studies using PS microplastics of the same size and shape are comparable with each other.

However, such monodisperse, spherical PS microparticles are often functionalised, for example, with carboxylic or amino groups (Desjardins and Griffiths, 2003; Olivier et al., 2004), which alters their surface properties and renders them chemically activated. Furthermore, Ramsperger et al. (2020) recently showed that also non-functionalised PS microparticles' environmental exposure leads to a surface functionalisation with biomolecules. This so-called eco-corona enhanced the particle's interaction with cells and subsequently their internalisation. In addition, even in commercially available microparticles without intended surface functionalisation, the polymerisation method, often surfactant-free emulsion polymerisation or dispersion polymerisation (Ober et al., 1985; Telford et al., 2013), may alter the surface properties of the synthesised microparticles. Since microplastic particles have a high surface-to-volume ratio, these surface properties can be expected to exert an influence on their effects. In the end, functionalisation, whether intended or inherent, may influence the interaction of such particles with the cellular membranes, potentially even the activation of possible cellular internalisation mechanisms (Lunov et al., 2011; Patiño et al., 2015). Hence, the outcome of studies using microplastics of the same type, size and shape may also not be comparable with each other.

However, to date, microplastic particles used for effect and cellular internalisation studies have mainly been categorised by polymer type, shape, and size (Wright et al., 2013; Stock et al., 2021), while their physicochemical surface properties were hardly considered. A fact highlighted in the comprehensive review of Yong et al. (2020), stating that results from different studies were contradictory, even if the "same type" of microplastic particles were used. For instance, Stock et al. (2019) observed no or only little cytotoxicity for polystyrene particles in the micrometre size range, whereas Dong et al. (2020) did show cytotoxic effects for polystyrene particles in the same size range (Stock et al., 2019; Yong et al., 2020; Di Dong et al., 2020).

We hypothesise that this discrepancy originates from the fact that the supposedly identical microparticles used in the various studies did nevertheless differ concerning some important yet unacknowledged properties. In order to investigate this hypothesis, we used supposedly identical 3 μm plain polystyrene (PS) microplastic particles, both provided with no surface functionalisation, from two different manufacturers (Polysciences and Micromod, referred to as P-MPP and M-MPP, respectively). According to the suppliers, both particle types (P-MPP and M-MPP) used were similar in size, chemistry, and surface conditions

("slight anionic charge due to residues of sulphate ester groups"). To test if both particle types can be regarded as identical, we characterised the particles' surface morphology, ζ-potential, surface charge distribution and further analysed both PS particle types' chemical composition. We correlated the observed surface properties of the microparticles with their interaction and internalisation with two murine macrophage cell lines. To estimate putative cellular responses evoked by different surface properties, we measured cell viability and proliferation after treating the cells with both microplastic particle types.

2. Materials and methods

2.1. Materials

Chemicals were obtained from Merck, Carl Roth, Sigma Aldrich or Biozym, cell culture materials from Greiner bio-one (Greiner Bio-One International GmbH, Frickenhausen, Germany), if not otherwise indicated. Plain polystyrene beads in aqueous solution with a nominal diameter of 3 μm were purchased from Polysciences (Polysciences Inc., Warrington, PA, USA, Cat. # 17134-15, 25 mg/mL, $1.7 * 10^9$ particles/mL) and Micromod (Micromod Partikeltechnologie GmbH, Rostock, Germany, Cat. # 01-00-303, 50 mg/mL, $3.4 * 10^9$ particles/mL). Both commercial sources state the polydispersity with a coefficient of variation to be < 5%, indicating no relevant size differences between the particle types. Furthermore, the customer services of the two commercial sources declared that both particle types are prepared by emulsion polymerisation using a radical initiator. Polysciences further declared to add 0.05% sodium azide to prevent bacterial growth, whereas the particles from Micromod are solely suspended in water (information obtained by both providers after request). We calculated the concentration of sodium azide used in our experiments to estimate potential interference in the cellular response experiments. Sodium azide has a molecular weight of 65 g/mol resulting in a concentration of 7.7 mM of sodium azide in the stock solution of P-MPP. Since the particles were further diluted (max. dilution: 1:17,000 (particle concentration: 1.5 μg/mL) and min. dilution: 1:17 (particle concentration: 1500 μg/mL)) the concentration of sodium azide in the experiments is further diluted to a range between 0.45 μM and 0.45 mM. The highest sodium azide concentration in our experiments (MTT assay with 1500 μg/mL) corresponds to a final concentration of 0.45 mM sodium azide. Weyermann et al. (2005) described that in MTT assays, a hypertonic concentration of 300 mM sodium azide is required to trigger a cytotoxic reaction. Microplastic particles obtained from Polysciences and Micromod are further abbreviated as P-MPP and M-MPP, respectively.

2.1.1. Cell lines and culture conditions

The murine ImKC cell line was obtained from Merck (SCC119) and cultured in RPMI 1640 medium, the J774A.1 cells (DSMZ GmbH, ACC170) were cultured in Dulbecco's Modified Eagle's Medium (DMEM, Lonza Group Ltd, Basel, Switzerland). To obtain cell culture growth media, DMEM and RPMI were supplemented with 10% (v/v) FCS (Sigma Aldrich, St. Louis, USA), 4 mM L-Glutamine (Gibco, Fisher Scientific, Schwerte, Germany), and 100 U/mL penicillin/streptomycin (Lonza Group Ltd, Basel, Switzerland). Both cell lines were passaged three times a week with a starting cell density of 100,000 cells/mL for cell maintenance. The cells were collected non-enzymatically by incubation (5 min incubation time for J774A.1, 10 min incubation for ImKC) in pre-warmed (37 °C) citric saline buffer (135 mM potassium chloride, 15 mM sodium citrate) or by scraping.

2.2. Methods

2.2.1. ζ-potential and dynamic lights scattering (DLS) measurements

The ζ-potential was measured before (stock solution, from manufacturer), after washing the particles with Milli-Q water, and after incubating the particles in two cell culture media (DMEM or RPMI). All

2

ζ-potential measurements were performed in 1 mM KCl to ensure equimolar salt concentrations and conductivity. For each treatment, 4 μL of a 25 mg/mL particle solution was diluted in 1 mL of the appropriate medium (described below) to a final concentration of 0.1 mg/mL. For the stock solution samples, the particles were diluted in freshly prepared 1 mM KCl and immediately measured. No further preparation of the particles originating from the stock solution was performed. For washed samples, loosely bound surfactants had to be removed. Therefore, the particles were washed with Mili-Q water. The washing procedure consisted of a washing step followed by centrifugation at 17,000g for 20 min at room temperature. The washing procedure was repeated three times. After the third wash, the pellet was then resuspended in freshly prepared 1 mM KCl and immediately measured. Compared to the stock solution and washed samples, a more realistic situation at cell culture conditions was tested. The particles were incubated in cell culture growth medium (DMEM or RPMI) overnight at 37 °C. Since the ionic strength of the cell culture medium is too high for the ζ-potential measurement, a medium change to 1 mM KCl using centrifugation was necessary. One centrifugation step at 17,000 g for 20 min at room temperature was performed to avoid removing a possible protein corona from the particle surface. The pellet was resuspended in freshly prepared 1 mM KCl and immediately measured.

The ζ-potential measurements were performed using Omega cuvettes (Mat.No.: 155765, Anton Paar Germany GmbH, Ostfildern-Scharnhausen, Germany) and a LiteSizer 500 (Anton Paar Germany GmbH, Ostfildern-Scharnhausen, Germany). Three measurements with at least 100 runs each were performed at 21 °C with an adjusted voltage of 200 V, and the ζ-potential was calculated using the Helmholtz-Smoluchowski equation (Drechsler et al., 2020; Smoluchowski, 1916). For the stock solution particles, the ζ-potentials were additionally measured at different pH values using a pH titration. The pH value was adjusted automatically by the Methrom dosing system (Metrohm GmbH & Co.KG, Filderstadt, Germany) with 0.1 M HCl or 0.1 M KOH in pH steps of ± 0.5. P-MPP and M-MPP were measured within a pH range from 2.5 to 10.5 and 2.5 to 11, respectively. Starting at pH 6, HCl was added to measure at the acidic pH range (pH 6–2.5), or KOH was added to measure the ζ-potential at the basic pH range (pH 6–11). For both pH ranges, separate samples of particles originating from the stock solution were used. The pH 6 in the 1 mM KCl is stable for at least 1 h, and since the measurement at one specific pH were performed within 5 min, we can be sure that the pH values are correct during the measurements. During this time, no precipitation of surfactants was observed.

For DLS measurements, 2 μL of the corresponding particle solution was diluted in 1 mL 1 mM KCl, resulting in a final particle concentration of 0.05 mg/mL. The measurements with at least 10 runs each were performed at 21 °C using the backscatter (angle 175°) using a LiteSizer 500 (Anton Paar Germany GmbH, Ostfildern-Scharnhausen, Germany).

2.2.2. Colloidal probe atomic force microscopy (CP-AFM)

Prior to the AFM measurements, tipless cantilevers (CSC38, Mikro-Masch, Sofia, Bulgaria) were calibrated via thermal noise (Hutter and Bechhoefer, 1993) and had a spring constant between 0.03 and 0.4 N/m. Cantilevers were cleaned in Milli-Q water, ethanol, Milli-Q water, and acetone and treated with air-plasma for 10 min (SmartPlasma, plasma technology GmbH, Herrenberg-Gülstein, Germany). Silica colloidal particles (nominal diameter of 4.8 μm, microParticles GmbH, Berlin, Germany) were attached to the cantilevers with 2-components epoxide glue (UHU Plus Endfest, UHU GmbH & Co. KG, Bühl/Baden, Germany). Glass slides were cleaned with acetone, isopropanol, ethanol, ethanol/Milli-Q water (50:50) and Milli-Q water for 10 min each in an ultrasonic bath at room temperature. After drying with nitrogen, the substrates were treated in air-plasma for 10 min. One-half of the substrate was covered with 1 g/L polyethyleneimine for an hour before rinsing with Milli-Q water and drying with argon. Microplastic particles were washed 3 times with Milli-Q water, and droplets of the suspension were placed onto the polyethyleneimine-covered side of the substrates

until the water evaporated. Thereafter, the substrate with particles was mounted into a liquid cell and rinsed three times with 0.1 mM NaCl to remove not immobilised microplastic particles.

CP-AFM measurements were performed in a 0.1 mM NaCl-solution and at slightly acidic pH due to dissolved CO_2 using an MFP-3D Bio (Asylum Research Inc., Santa Barbara, USA) mounted on an inverted optical microscope (Axio Observer Z1, Zeiss, Oberkochen, Germany). After a first optical alignment, force maps for P-MPP (500 nm^2, 10 × 10 pts) and M-MPP (300 nm^2, 6 × 7 pts) were conducted to determine the apex of each particle. This allows a precision of nearly 50 nm in the XY direction. 15–20 particles were evaluated, and each particle was measured three times with feedback of the lateral deflection. The precision was sufficient, as there were no significant differences in lateral deflection between measurements with centred spheres and spheres with an offset of up to 100 nm. After the alignment of the colloidal probe and microplastic particle, the measurements were executed with a tip velocity of 1 μm/s and a scan rate of 0.5 Hz.

2.2.3. Gel permeation chromatography (GPC)

Gel permeation chromatography (GPC) was carried out on an Agilent (Polymer Laboratories Ltd., Church Stretton, UK) PL-GPC 220 high-temperature chromatographic unit equipped with DP and RI detectors and three linear mixed beds with guard columns (Olexis). GPC analysis was performed at 150 °C using 1,2,4-trichlorobenzene as the mobile phase. Both particle types were centrifuged and subsequently dried. Afterwards, the particles were dissolved (0.1 wt%) in the mobile phase in an external oven (150 °C) and the solutions were chromatographed without filtration. The molecular weights of the samples were referenced to polystyrene standards (Mw = 518–2,500,000 g/mol, K = 12.100 and Alpha = 0.707).

2.2.4. Nuclear magnetic resonance (NMR)

Both particle types were centrifuged and subsequently dried. For NMR, both particle types were dissolved in $CDCl_3$. ^1H and ^{13}C liquid-state NMR spectra were acquired on an Avance III HD spectrometer (Bruker, Massachusetts, USA) operating at a B_0 field of 16.4 T. The spectrometer is equipped with a helium-cooled TCI-CryoProbe. The ^1H NMR spectra (ν_0 (^1H) = 700.2 MHz) were obtained with a single pulse (SP) excitation with a pulse length of 3.0 μs corresponding to 30° tip angle and a recycle delay of 1 s to allow for quantitative analysis of the spectral intensities. The ^{13}C NMR spectra (ν_0 (^{13}C) = 176.0 MHz) were acquired with an SP sequence, a 6 μs pulse length corresponding to a 45° tip angle and a recycle delay of 3 s. During ^{13}C acquisition, proton broadband decoupling was applied using a waltz-16 sequence with ν_{nut} = 3.6 kHz. Both, the ^{13}C and ^1H NMR spectra are referenced to tetra-methylsilane (TMS).

2.2.5. Energy-dispersive X-ray spectroscopy (EDX)

Both particle types were dried after recovery by centrifugation and applied on graphite. EDX spectroscopy was carried out using a Zeiss Ultraplus (Carl Zeiss AG, Oberkochen, Germany) equipped with a 30 mm^2 Thermo Scientific UltraDry EDS Detector using a beam voltage of 20 kV.

2.2.6. Scanning electron microscopy (SEM)

100,000 cells per slide were seeded on Ø 13 mm Nunc™ Therma-nox™ slides (Thermo Fisher Scientific, Waltham, MA, USA) and incubated for 24 h under cell culture conditions in cell culture growth medium. 5 μL of a 180 μg/mL particle solution in cell culture growth medium was added to the cells (≙ 20 particles per cell). After 24 h incubation, the cells were directly fixed using Karnovsky's reagent (4% (v/v) formaldehyde, 5% (v/v) glutaraldehyde, with a final concentration of 32 mM PBS, pH 7.4) for 1 h at room temperature and afterwards dehydrated using an ethanol series 50%, 70%, 80% for 30 min, 90% and absolute ethanol for 1 h. The overnight air-dried samples were sputter-coated with platin and depicted using SEM (FEI Apreo Volumescope,

3

Thermo Fisher Scientific, magnification 8000, 2 kV, Everhart-Thornley detector). A 1 mg/mL aqueous particle suspension was dried overnight on a silicon wafer for the particle characterisation. The samples were sputter-coated with platin and imaged using SEM (FEI Apreo Volumescope, Thermo Fisher Scientific, magnification 20,000 and 150,000, 1.5 kV, T2 detector).

2.2.7. Confocal microscopy

The cells were prepared as described in Ramsperger et al. (2020). In brief, for each particle type and cell line three coverslips (Ø 18 mm) with 5×10^4 cells per mL were cultivated for 24 h at cell culture conditions in 12 well plates before incubation with the microplastic particles. For the experimental procedure, the microplastic particle stock solutions were diluted in Dulbecco's phosphate buffer saline (DPBS, Merck) to obtain the same number of particles (P-MPP 1:50; M-MPP: 1:100; microplastic particles: DPBS, concentration: 500 µg/mL). 100 µL of each microplastic particle dilution was directly added to pre-cultured cells in cell culture growth media resulting in a final microplastic particle concentration of 5 µg/mL, corresponding to 340,000 particles per mL or seven particles per cell. After 1 h incubation on ice to allow particle sedimentation, the well plates were incubated at 37 °C and 5% CO$_2$ for 2 h to activate the cellular metabolism and allow the internalisation of the particles. The coverslips were washed three times with DPBS to remove unattached particles. Cells were fixed with 4% PFA and fluorescently labelled with Alexa Fluor™ Phalloidin 488 (Invitrogen, Carlsbad, USA) as described in Ramsperger et al. (2020).

To determine the total number of particle-cell-interactions (PCI), which is defined as a particle in close proximity to a cell, five randomly chosen regions of interest (ROI) (0.29 mm^2 each) were selected and imaged by using a DMI 6000 microscope (LEICA, Wetzlar, Germany, HCX PL APO 63 ×/1.30 oil objective) including a spinning disc unit (CSU X1, YOKOGAWA, Musashino, Japan) with an EMCCD camera (Evolve 512, PHOTOMETRICS, Tucson, Arizona, including an additional 1.2 × magnification lens). Procedures were adapted from Ramsperger et al. (2020). A differential interference contrast (DIC) microscopy image was acquired from each ROI to quantify the PCI and confocal stacks of fluorescently labelled cells were acquired using a 488 nm laser (50 mW, Sapphire 488, COHERENT, Santa Clara, California) at a spinning disc speed of 5000 rpm to excite fluorescence. Axial stacks of the cells were acquired with a vertical distance of 0.2 µm. As the ImKC cells are smaller than the J774A.1 cells, the confocal stacks were used to calculate the area covered by cells within an ROI using the algorithm described in.

To quantify the number of microplastic particles internalised by the cells, we screened each sample for 100 PCI, to distinguish between particles attached to cell membranes or internalised as described in Ramsperger et al. (2020). The coverslips were screened in the DIC-channel until 100 particle-cell-interactions were detected, or until the whole coverslip was screened entirely (e.g., in the case of ImKC cells treated with M-MPP, where less than 100 particle-cell-interactions were detected).

For better comparability between P-MPP and M-MPP treatments and different cell lines, a standardisation was performed to the same area covered by cells on a coverslip (17.7 mm^2, which corresponds to 7% coverage of a coverslip resulting in a mean of 20,000 cells per coverslip). This has been performed as the two cell lines showed different areas covered with cells due to the different sizes of the cells (mean individual cell size J774A.1: 810 ± 190 µm^2 and ImKC: 350 ± 20 µm^2, calculated from ROI images of the fluorescent channel). The number of PCI were extrapolated to a whole coverslip. As the areas on the coverslips covered by cells differ between replicates and cell lines each coverslip was standardised (Mean cell area ± SE: J774A 0.1 P-MPP: 18.4 ± 0.25 mm^2, M-MPP: 32.6 ± 1.5 mm^2; ImKC P-MPP: 3.6 ± 0.03 mm^2, M-MPP: 6.4 ± 0.26 mm^2).

2.2.8. Metabolic activity assay (MTT)

J774A.1 and ImKC cells were detached with citrate buffer as described above and 10,000 cells in 100 µL were seeded per well in a 96-well plate and cultured at cell culture conditions for 24 h. Afterwards, freshly prepared particle dilutions (1.5, 15, 37.5, 75, 112.5, 150, 750–1500 µg/mL in the corresponding cell culture growth medium, concentrations are correlating to used concentrations in the literature (Stock et al., 2019; Harvilchuck and Carlson, 2006) were added for another 24 h. Additionally, two control treatments were performed. Cells that were not exposed to microplastic particles are defined as non-treated cells representing 100% metabolic activity ('negative control'), and cells treated with 0.3% Triton X-100 are defined as cells representing 0% metabolic activity ('positive control'). During experimental setting of the assay we analysed (under cell-free conditions) the influence of the microplastic particles on the absorbance measurement. We showed that even the highest amount of microplastic particles used does not interfere with the absorption measurement. After 24 h incubation, the cells were washed with DPBS and 50 µL freshly prepared MTT reagent (1 mg/mL 3-(4,5-dimethyl-2-thiazolyl)-2,5-Diphenyl-2H-tetrazolium bromide (MTT) in serum-free Modified Eagle Medium without phenol red) was added to each well. After 2 h incubation, the MTT reagent was removed, and 100 µL isopropanol were added per well. After 5 min rotating at 600 rpm, the absorbance at 570 nm (reference wavelength 650 nm) was measured using a TECAN GENios Pro plate reader (Tecan Austria GmbH, Gröding). Each cell line – MPP type and concentration was run in triplicate (except for ImKC, where 6 biological replicates were used for 0–150 µg/mL microplastic particle concentrations), and each experiment was run in 6 technical replicates.

2.2.9. Proliferation assay

100,000 cells were seeded in 1 mL growth medium per well in a 12-well plate and left to settle for 3 h at cell culture conditions. Afterwards, the cells were treated with 37.5, 150 and 1500 µg/mL of either particle suspension (≙ 25, 100, 1000 particles per cell). The cells were collected after 0, 24, 48 and 72 h with citric saline buffer as described above and resuspended in 1 mL cell growth medium. Cell number was evaluated using the automated fluorescence cell counter Luna II (Logos Biosystems, Gyeonggi-do, Korea). A 2 µL sample of the cell suspension was mixed with 18 µL Staining-Mix (Acridine Orange and Propidium iodide, proprietary concentrations, Logos Biosystems) and loaded into the chamber of a PhotonSlide (Logos Biosystems). Cells incubated without particles at otherwise identical conditions were used as reference.

2.3. Statistical analysis

Statistical analysis was conducted either using Origin software 2019b (Origin, Northampton, MA, USA) or R studio software (Version 1.2.5019, R Core Team 2020). All data were tested for normal distribution (Shapiro-Wilk test) and homogeneity of variances (Levene test). To investigate differences between the particle types in the ζ-potential-measurements a one-way ANOVA with a Tukey post hoc test was used. For PCI and internalisation experiments and MTT, a Kruskal-Wallis test with a Games Howell post hoc test (p-adjust method for multiple nesting: Bonferroni Holm) was conducted to check for differences between treatments. For the MTT assay, outliers of $> 15\%$ of the overall mean were excluded from the statistical analysis. For the proliferation experiments, a one-way ANOVA with a Tukey post hoc test was used.

3. Results

3.1. Surface structures and size distributions of P-MPP and M-MPP

Scanning electron microscopy (SEM) analysis revealed that the morphological surface structures of the P-MPP and the M-MPP differed (Fig. 1A). Apart from that, both particle types showed a highly monodisperse size distribution in the SEM images, which we further
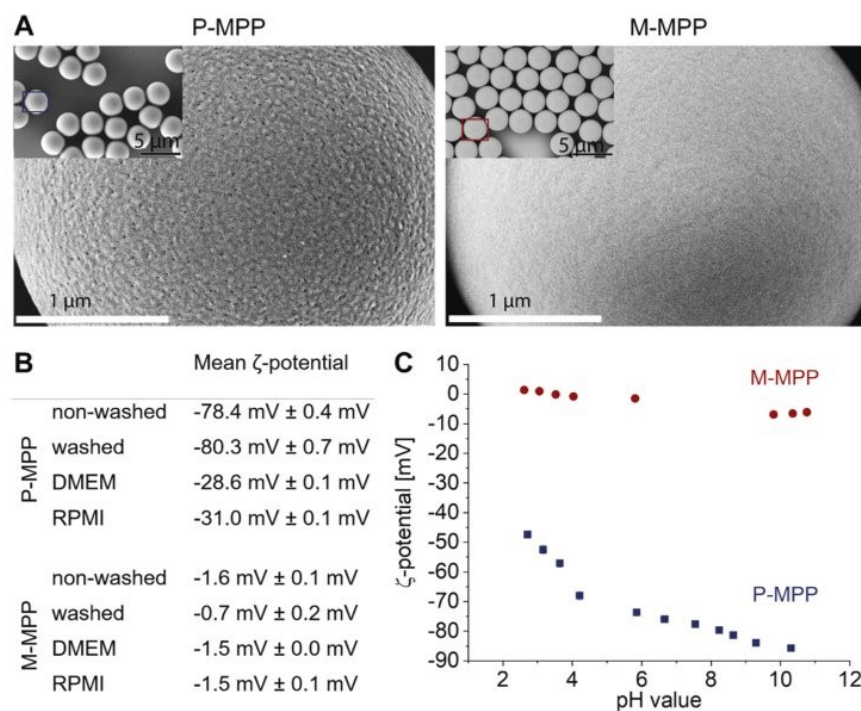
4

Fig. 1. (A) SEM images show differences in surface morphology of both particle types. (B and C) ζ-potential measurements of P-MPP (blue) and M-MPP (red) particles. The ζ-potential measurements were performed in 1 mM KCl at pH 6 (B) and selected pH values during a pH titration (C). (B) Both particles were measured in stock solution and after incubation in MilliQ water as well as after incubation in two cell culture media (DMEM and RPMI) supplemented with 10% (v/v) FCS. (C) For the titration, stock particles were used. Data points represent mean ± SD, n = 3. The surface charge of P-MPP was significantly more negative than that of M-MPP, regardless of the pH of the medium used. (For interpretation of the references to color in this figure legend, the reader is referred to the web version of this article.)

confirmed by using dynamic light scattering (DLS). Here, the diameter of P-MPP was 3.1 ± 0.4 μm and that of M-MPP 3.0 ± 0.5 μm, showing that P-MPP and M-MPP did not differ significantly in size.

3.2. Differences in particles' ζ-potentials

We measured the ζ-potentials at pH 6 of both particle types after the incubation in three different media (Milli Q-water and two cell culture media DMEM and RPMI) (Fig. 1B). The initial ζ-potentials of both particle types were slightly altered by incubation in Milli Q-water from −78.4 ± 0.4 mV (initial) to −80.3 ± 0.7 mV for P-MPP (p < 0.01) and from −1.6 ± 0.1 mV (initial) to −0.7 ± 0.2 mV for M-MPP (p < 0.05). The incubation of P-MPP in both cell culture media supplemented with 10% v/v FCS showed a significant change in ζ-potential from −78.4 ± 0.4 mV (initial) to −28.6 ± 0.1 mV in DMEM and −31.0 ± 0.1 mV in RPMI (p < 0.01). For M-MPP no significant changes in ζ-potential were observed after incubation in both cell culture media (from −1.6 ± 0.1 mV to −1.5 ± 0.0 mV in DMEM and from −1.6 ± 0.1 mV to −1.5 ± 0.1 mV in RPMI) (Fig. 1B). This shows that a considerable difference in the ζ-potentials of both particle types remains under cell culture conditions. To investigate the effect of pH on the ζ-potentials, a pH titration was performed. Here, the ζ-potential of the P-MPP taken from the stock solution of the supplier decreased from −47 mV at pH 2.5 to −85 mV at pH 10.5, whereas the ζ-potential of the M-MPP changed from +1.5 mV at pH 2.5 to −6.9 mV at pH 11 (Fig. 1C). Overall, the surface charge of P-MPP was significantly more negative than that of M-MPP, regardless of the pH of the medium used.

3.3. Particles' chemical composition and surface charge distribution

For a better understanding of where the differences of the ζ-potential of both particle types may originate from, we measured the particles' chemical compositions and average PS chain lengths by using liquid-state nuclear magnetic resonance (NMR), energy dispersive X-ray (EDX) spectroscopy, and gel permeation chromatography (GPC) (Fig. 2

and Table 1). The NMR spectroscopic analysis showed that both particle types display a similar and small number of carboxylic groups on their surfaces. For P-MPP, we found no characteristic NMR signals for co-monomers and surfactants. However, P-MPP exhibits a content of 3‰ of negatively charged chain-terminating sulphate (-SO$_4^-$) units with a number-averaged molecular weight (M$_n$) of 38,100 g/mol and a poly-dispersity of 5.0, indicating a higher molecular weight distribution compared to M-MPP. The negative ζ-potential of P-MPP indicates that the sulphate groups are preferentially exposed on the particles` surfaces. EDX analysis confirmed the presence of sulphur on the P-MPP surface, which was absent on the M-MPP. We further analysed surface charge distribution by colloidal probe atomic force microscopy (CP-AFM). We deduced the effective Debye length from this method, which describes the range of the electrostatic repulsive forces for like-charged surfaces. We found a constant effective Debye length of about 24 nm in multiple P-MPP given by the curves' slope (Fig. 3A and B) as well as on one and the same particle (Fig. S1B). This indicates a homogeneously distributed negative surface charge of P-MPP.

The significantly smaller ζ-potentials for M-MPP suggest that fewer charged groups are assembled on the particle surfaces compared to P-MPP. Chemical composition analysis of M-MPP revealed a content of 1% charge-neutral chain-terminating benzoic acid ester units which confirms the measured low ζ-potential. The smaller number-averaged molecular weight (M$_n$) of 9500 g/mol corresponds to shorter polymer chains with a polydispersity of 2.3, resulting in more end groups. One might assume that considering the higher molecular weight distribution of P-MPP compared to M-MPP, the density of two beads should be different. However, the difference in density is defined by the difference in defects (functional groups), in the present case, essentially end groups resulting from the initiator. Despite the difference in the molecular weight distribution of P-MPP and M-MPP, the number of end groups is too small to cause significant differences in density. More importantly, the radical polymerisation mechanism in styrene droplets leads to a preferred accumulation of defects on the surface of the resulting particles, but to a lesser extent, in the bulk material. Thus, we focused on the

5
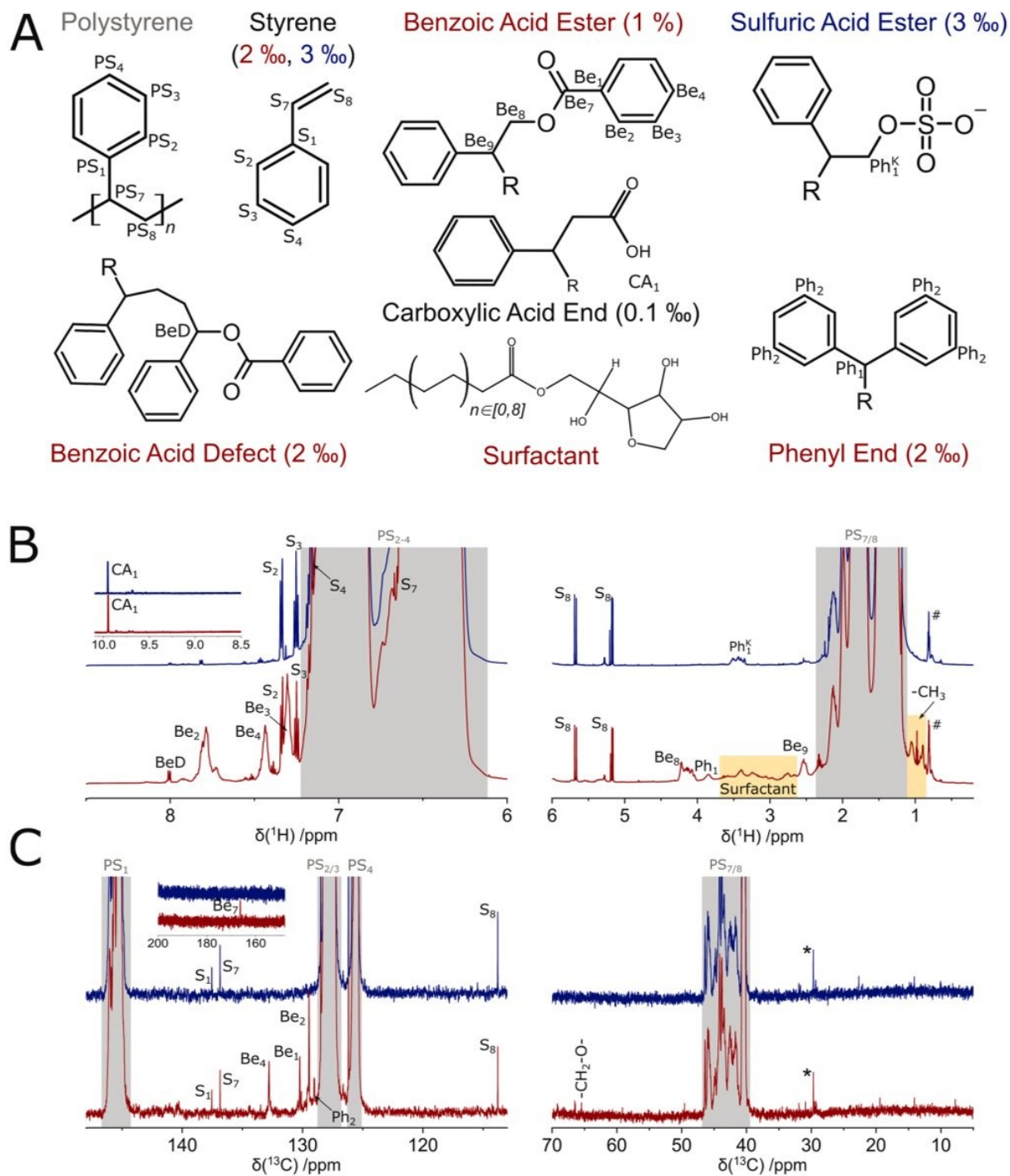
Fig. 2. Analysis by ^{1}H and ^{13}C liquid-state NMR of the 3 μm-sized P-MPP and M-MPP. (A) Chemical composition with estimated proportions and labelling of the characteristic units. The chemical structure of the surfactant is exemplarily expressing observed ester and sugar groups. (B) ^{1}H NMR spectra and (C) ^{13}C NMR spectra including assignment of characteristic resonances. Spectra, proportions and characteristic chemical units are given in a colour code (black refers to both particle types, blue refers to P-MPP, red represents M-MPP). Resonances within the grey regions are assigned to the repeating unit of PS and the other region represents the surfactant.

6

Table 1

Results of the GPC Measurement. M_n = number average molecular weight, M_w = weight average molecular weight, Polydispersity = molecular weight distribution. Each sample was measured twice and averaged.

	M_n (g/mol)	M_w (g/mol)	Polydispersity
P-MPP	38,072	190,385	5.04
M-MPP	9462	22,145	2.34

physicochemical properties of the particles' surfaces. Small characteristic resonances for ether and sugar groups containing surfactants were observed for M-MPP. They might provide sufficient charges to match the observed low ζ-potentials and prevent self-aggregation of the particles. The force curves for M-MPP gained by AFM differed strongly between measurements on different particles (Fig. 3C). Moreover, only weak attractive van-der-Waals forces were observed compared to P-MPP, and the effective Debye length of the electrostatic repulsive forces differed between 9 nm and 22 nm. These varying effective Debye lengths suggest that the surface charge is heterogeneously distributed on the M-MPP's surfaces, which was subsequently verified by measuring four different spots on the same M-MPP (Fig. S1A). For two spots, electrostatic repulsive forces and attractive van-der-Waals forces were found, whereas the other two spots showed only slightly repulsive electrostatic forces. Therefore, M-MPP showed not only surface charge heterogeneities between single particles but on the very same particle.

Next to differences in surface charge, P-MPP and M-MPP also differ in their residual monomer content as shown by the ^{1}H- and ^{13}C NMR spectra. In P-MPP, 3‰ of residual styrene monomers were dissolved within the PS particles, whereas in M-MPP 2‰ were found (Fig. 2B and C).

3.4. Particle-cell interactions and subsequent internalisation

Our results show, that although both particle types are sold as plain polystyrene microplastic particles of similar size and surface characteristics, distinct differences exist, in particular, regarding the surface properties and monomer content. Both properties may alter the interaction with cells which we investigated by using two murine macrophage cell lines (J774A.1 and ImKC). In this context, SEM analysis revealed a qualitative difference on the type of particle-cell-interactions (PCI). A PCI consists of particles being solely attached to cellular membranes (Fig. 4, indicated by white arrows) or particles being covered by cellular membranes and, therefore, internalised (Fig. 4, indicated by orange arrows). For both analysed cell lines, the SEM images depicted that P-MPP were more often internalised than M-MPP.

Subsequently, this qualitative observation was confirmed by spinning disc confocal microscopy (Fig. 5). In cell line J774A.1, the observed PCI were 150 times more frequent for P-MPP than for M-MPP, and P-MPP were significantly internalised 80 times as often. Similarly, the ImKC cells, significantly more often interacted (factor of 260) with P-MPP than with M-MPP, and P-MPP were by a factor of 360 more often internalised than M-MPP (all differences for both cell lines were highly significant $p \leq 0.001$) (Fig. 6; factors rounded to the nearest integer).

3.5. Cellular responses MTT results

To test if differences in PCI and internalisation are affecting the cells, we measured the metabolic activity (Fig. 7) and proliferation (Fig. 8) of both macrophage cell lines upon exposure to both particle types. ImKC cells showed a significant increase in metabolic activity after treatment with 15 and 37.5 µg/mL P-MPP ($p < 0.05$) and a significant decrease for 1500 µg/mL P-MPP compared to the negative control ($p < 0.05$). For the J774A.1 cell line, we did observe a trend towards a lower metabolic activity with a rising P-MPP concentration, but the differences compared to non-treated (100% metabolic activity, negative control) were not statistically significant. The M-MPP did not significantly affect the metabolic activity from either cell line at particle concentrations tested.

Furthermore, we analysed possible effects on cell proliferation upon exposure to a low, medium, and high concentration (37.5 µg/mL, 150 µg/mL, 1500 µg/mL) for both particle types. In the case of cells incubated with P-MPP cell counts showed a dependence on the particle concentration for both cell lines. For the ImKC cell line, 150 µg/mL yielded a significant lower cell count after 72 h compared to the control ($p < 0.05$) and a slight increase at 37.5 µg/mL. J774A.1 was not affected by the latter concentrations. The highest concentration of P-MPP significantly inhibited the proliferation for both cell lines ($p < 0.001$). Growth rates and cell counts for M-MPP did not show significant differences ($p > 0.05$) for both cell types (Fig. 8) at any used concentration.

4. Discussion

Overall, our findings show that chemical composition and surface
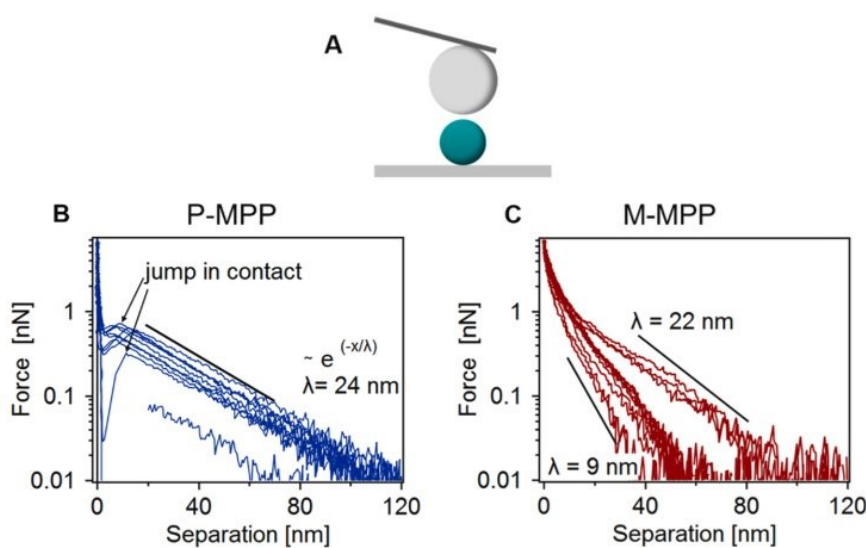
Fig. 3. Scheme of a CP-AFM measurement (A) of P-MPP (B) and M-MPP (C). (A) CP-AFM measurements were performed with a silica colloidal probe (grey, 4.8 µm) attached to a cantilever on polystyrene beads (green, 3 µm, P-MPP and M-MPP) and obtained in an aqueous solution of 0.1 mM NaCl (calculated Debye length $\lambda = 30$ nm) and pH 5–6. Semi-logarithmic force-separation curves of more than ten particles are plotted and the straight solid lines indicate exponential Debye fits. Force curves in (B) show a constant effective Debye length of 24 nm indicating a homogeneously distributed surface charge for P-MPP. In contrast, the effective Debye length differs (9–22 nm) for each of the particles seen in (C) suggesting a heterogeneously distributed surface charge for M-MPP. The M-MPP also show an additional slowly increasing force below 10 nm separation. This indicates a steric repulsive force. Whereas the curves of P-MPP show a jump in contact at the same separation induced by attractive van-der-Waals forces. (For interpretation of the references to color in this figure legend, the reader is referred to the web version of this article.)

Fig. 4. Qualitative study on particle-cell-interaction (PCI) and internalised microplastic particles via SEM of J774A.1 and ImKC macrophages incubated with the two different microplastic particle types. The cells were incubated with 20 particles per cell for 24 h. The P-MPP are more often covered by cellular membranes and therefore internalised (orange arrows) by both cell lines compared to the M-MPP, bei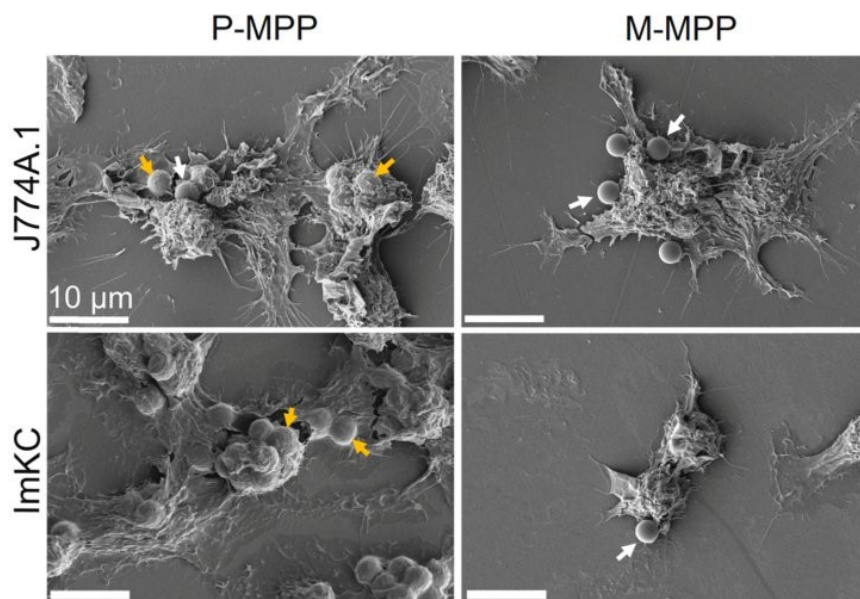ng solely attached to membranes of both cell lines (white arrows). Scale bar: 10 μm. (For interpretation of the references to color in this figure legend, the reader is referred to the web version of this article.)

characteristics of nominally identical microplastic particles from different suppliers significantly differ and suggest that these differences influence PCI and cellular responses on two murine macrophage cell lines.

The differences in the surface properties of P-MPP and M-MPP particles most likely originate from the differences in the synthesis conditions. Our results indicate that different radical initiators were used, affecting surface morphology, surface charge, and chemical composition. The pronounced difference in the ζ-potentials of P-MPP and M-MPP was surprising since the supplier described both particle types as bearing a slightly negative surface charge due to the presence of sulphate ester groups. However, whereas in the case of P-MPP, we did observe anionic sulphate groups on the surface, most likely originating from the chosen initiator (Moad et al., 1982; Van Berkel et al., 2003), we did not find such evidence for M-MPP. In M-MPP, the heterogeneously distributed slightly negative ζ-potential on the surface is most likely caused by a small portion of carboxyl groups probably formed by oxidation reactions during the polymerisation process (Beachell and Smiley, 1967; Yousif and Haddad, 2013; Arráez et al., 2019). The NMR spectroscopic data indicate that a similar process was presumably active in the synthesis of P-MPP, but the contribution to the P-MPP surface net charge and charge distribution is negligible compared to the anionic groups from the used initiator. Moreover, whereas the highly charged P-MPP show a homogeneously distributed surface charge, the much lower surface charge of M-MPP is widely and heterogeneously distributed over the surface. Since they cannot rely on electrostatic repulsion for colloidal stabilisation, M-MPP seem to be stabilised by charge-neutral surfactants. In contrast, in P-MPP the absence of characteristic NMR signals for co-monomers and surfactants indicates that the interaction with sister particles and, therefore, also cell membranes is predominantly electrostatic. Given the high surface-to-volume ratio of microplastic particles, not only the overall charge but also the charge distribution may affect how cellular membranes and particles interact, since our findings show that the homogeneously charged P-MPP show significantly higher PCI compared to the heterogeneously and significantly less charged M-MPP.

Fröhlich (2012) describe in their comprehensive review that, amongst other properties, the surface morphology of a particle can play a role in how the particles interact with cells. Our SEM analysis depicts that the surface structure was slightly more pronounced in P-MPP compared to M-MPP, which might affect PCI and the propensity for internalisation. For human epithelial cells, a correlation of the surface roughness with the likelihood of internalisation has been shown, with a rougher surface of a nanoparticle leading to a higher internalisation compared to smooth particles (Niu et al., 2015). This is consistent with our results, where P-MPP become internalised more often than the smoother M-MPP. In contrast, other studies showed a decreased cellular internalisation of rougher compared to smoother nanoparticles (Piloni et al., 2019; Kim et al., 2021), indicating that the surface roughness is not the dominant factor triggering PCI and internalisation. This has already been highlighted by Schrade et al. (2012), suggesting that surface charge is more important for internalisation than surface morphology. For instance, Musyanovych et al. (2011), e.g. showed that PS nanoparticles with an anionic surfactant with a ζ-potential of -60 mV (in KCl, -28 mV in cell culture medium with 10% FCS) were internalised by HeLa cells more often than nanoparticles stabilised with a non-ionic surfactant and having a ζ-potential of -5 mV (in KCl, -12 mV in cell culture medium with 10% FCS). This is in concordance with our findings that both murine macrophage cell lines showed a higher number of PCI and internalised particles for the more negatively charged P-MPP compared to M-MPP. This may be explained by the main biological function of macrophages, which is the internalisation of negatively charged bacteria via phagocytosis (Fröhlich, 2012). Gebicki and James (1962) described the ζ-potential of bacteria with -22 mV at pH 7.0, which is in the range of the P-MPPs ζ-potential in cell culture media. Besides, with 3 μm in diameter the PS particles used in our experiments are within the size range of bacteria (Levin and Angert, 2015).

Another aspect of potential relevance for PCI and internalisation is the formation of a corona on the surface of the particles altering their initial surface properties (Lundqvist et al., 2008; Tenzer et al., 2013; Monopoli et al., 2012). The changes in ζ-potential recorded after incubating the particles in cell culture media are highly indicative of the formation of a protein corona (Partikel et al., 2019). It has already been shown that the protein corona formation is influenced by the surface properties like modification with chemical groups or surface charge (Lundqvist et al., 2008; Tenzer et al., 2013; Shannahan et al., 2013; Cao et al., 2019; Saavedra et al., 2019). Our results show that the initially higher negative ζ-potential of P-MPP seems to be more altered by the incubation in cell culture media than that of M-MPP, although the
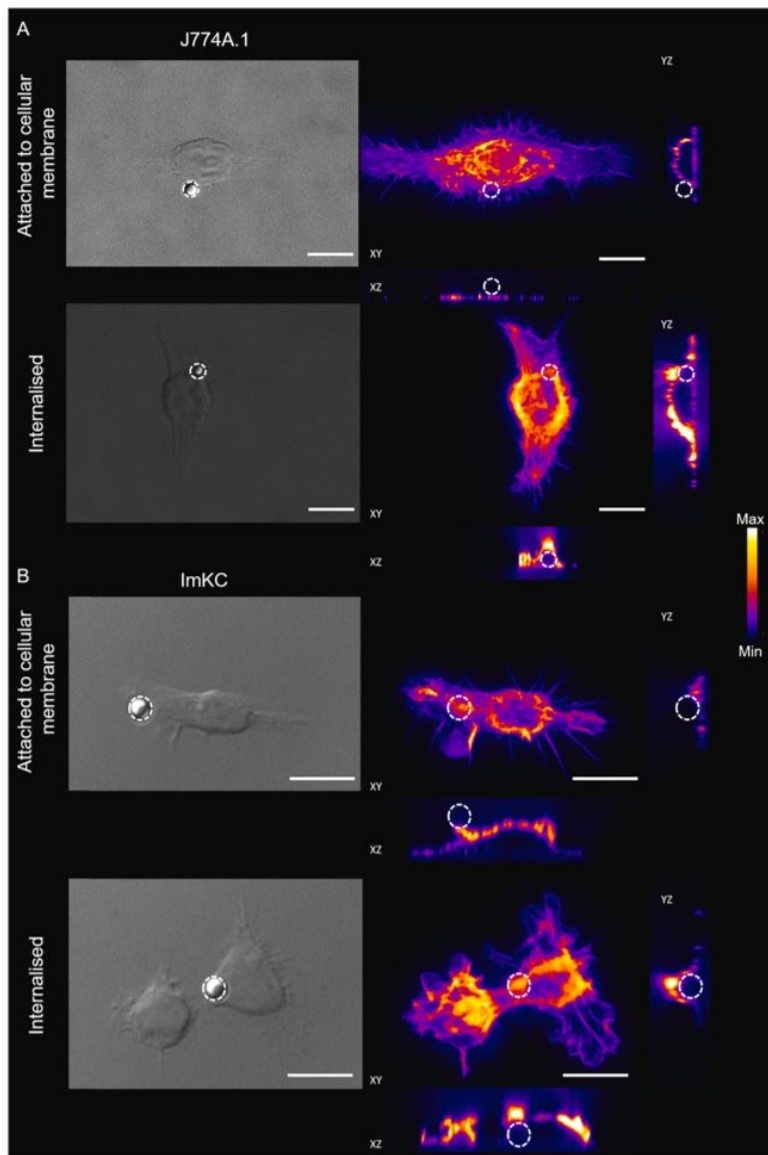
Fig. 5. Representative images for the differentiation of microplastic particles attached to cellular membranes and internalised particles. Differential interference contrast (DIC) microscopy images (left column) of M-MPP-cell interactions with cells from the J774A.1 (A) cell line and cells from the ImKC cell line (B). Fluorescence images were acquired by spinning disc confocal microscopy (right side) of the same cells from DIC images with fluorescently labelled filamentous actin (false colour maximum intensity projection, arbitrary units). XY-, YZ- and XZ-projections of three-dimensional confocal stacks allow the differentiation of microplastic particles attached to cell membranes from internalised microplastic particles. Circles indicate microplastic particle positions. Only those particles being completely covered by the filamentous actin were considered to be internalised (A and B lower panel), whereas the other particles were only attached to cellular membranes. Scale bars: 10 μm.

difference in ζ-potential between the particles remain after the incubation. This indicates the formation of a more pronounced protein corona on P-MPP, which may additionally explain the distinctly higher numbers of PCI and internalised particles. However, most of the findings of protein corona formation were reported for nanoparticles (Lundqvist et al., 2008; Tenzer et al., 2013; Monopoli et al., 2012; Shannahan et al., 2013). It has to be noted that care must be taken when comparing nano- and microparticles, as the particles reactivity is much higher for smaller particles (Buzea et al., 2007) and the internalisation mechanisms by macrophages may be different depending on the particle size (Koval et al., 1998). Nevertheless, it has been shown that the internalisation of 3 μm PS particles coated with biomolecules forming an eco-corona into cells is enhanced compared to uncoated microplastic particles (Ramsperger et al., 2020), indicating that the coating of a particle is an important factor for PCI and internalisation.

Distinct differences between P-MPP and M-MPP in ζ-potential, surface charge distribution and residual monomer content may also explain the observed differences in cell metabolism and cell proliferation.

No cellular responses were observed for M-MPP in any of the experiments. In contrast, P-MPP induced a significant reduced metabolic response in both cell lines in the highest used concentration (1500 μg/mL). The lower metabolic activity is reflected by an inhibited cell proliferation in both cell lines, indicating that the properties of the used PS particles interfere with the viability of the cells. Further, the ImKC cells showed an increase in metabolic activity for the lowest concentrations (15 μg/mL and 37.5 μg/mL) only when exposed to P-MPP. This is characteristic for a hormesis effect, showing an increase in metabolic activity at low concentrations of a contaminant with a continuous drop at higher concentrations (Calabrese and Why, 2008; Gopi and Rattan, 2019). The higher sensitivity observed by the ImKC compared to the J774A.1 cells may arise from the fact that the cell lines originate from different body compartments. The J774A.1 cell line was derived from a murine reticulum cell carcinoma (Ralph and Nakoinz, 1975), whereas the ImKC cell line was established from murine resident liver Kupffer
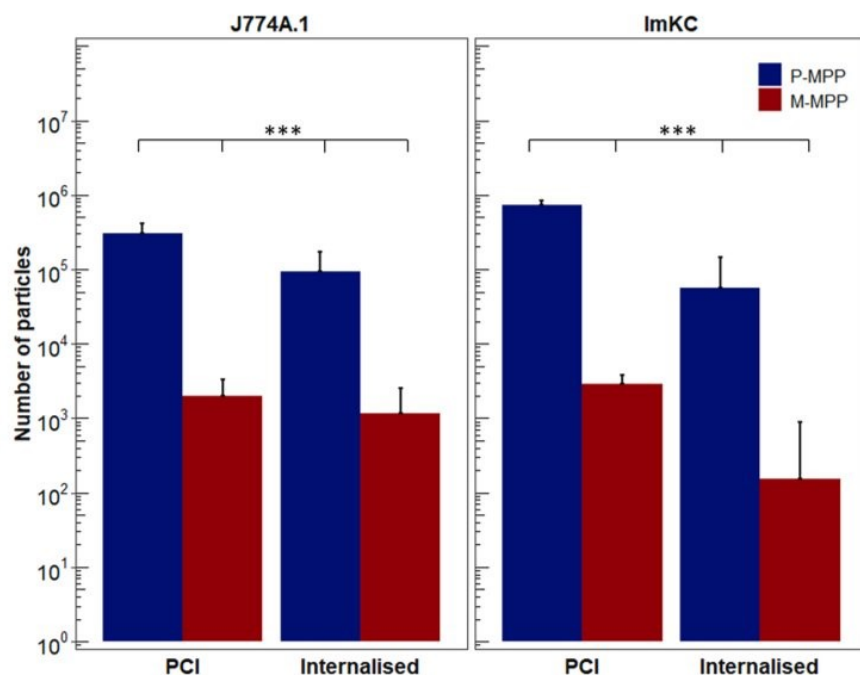
9

Fig. 6. Comparison of P-MPP and M-MPP with two macrophage cell lines concerning their particle-cell interactions and number of internalised particles. The cells were incubated with 5 µg/mL microplastic particles for 2 h. The numbers of particle-cell interactions and internalised microplastic particles were standardised to coverslips with 20,000 cells for better comparison, as the relative cell area on a coverslip for both cell lines differed. Data points represent mean + SD, n = 300 images (P-MPP & M-MPP J774A.1, P-MPP ImKC), n = 41 images (M-MPP, ImKC), significance level: *** = p ≤ 0.001.
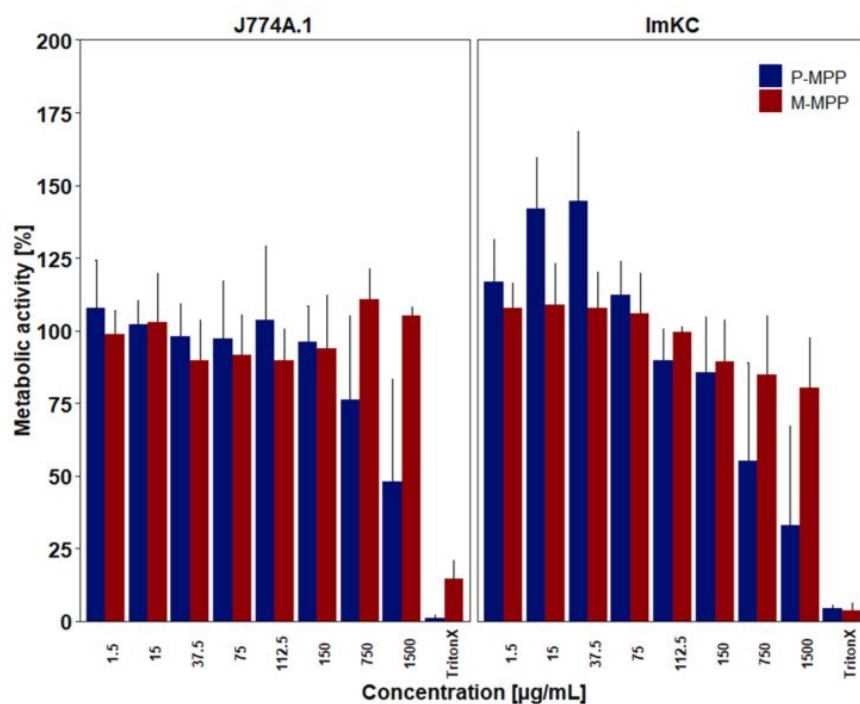
Fig. 7. MTT cell metabolism measurements with both cell lines after 24 h incubation with the respective particles. Results are shown as mean + SD. Data are given as the percentage of the particular experiment to the viability of the negative control (cells without particles). While there is no cytotoxicity for concentrations below 150 µg/mL, cytotoxicity at higher concentrations was dependent on particle type as well as on the cell line. Triton X-100 was used as a cell toxic positive control. Data points represent mean + SD, independent experimental replicates: n = 3–9.

cells (Wang et al., 2014). Kupffer cells were described to be more sensitive to stress factors than some other macrophage cell lines (Tanifum et al., 2018), whereas J774A.1 cells have generally been described as less sensitive to particle exposure. For instance, J774A.1 cells exposed to similar concentrations of 2 µm carboxylated-PS particles (Mutzke et al., 2015) or sulphate-functionalised 4 µm PS particles (Stock et al., 2019)

did not show cytotoxicity.

The observed cellular responses of the P-MPP compared to the M-MPP may originate from the higher amount of residual styrene monomers in P-MPP. It has been shown that styrene monomers induce particularly hepatotoxic effects (Harvilchuck and Carlson, 2006; Withey, 1976), which could explain the stronger cellular response of

10

Fig. 8. Cell proliferation of J774A.1 and ImKC cell lines in a time and concentration-dependent manner for P-MPP and M-MPP. Each experiment was performed in 12–well tissue culture plates. M-MPP did not significantly influence cell proliferation independent of the concentration. Cells incubated with P-MPP showed almost no proliferation at 1500 µg/mL and a significantly lower cell count for ImKC at 150 µg/mL after 72 h. Data represent mean ± SD, n = 3 and were slightly offset.

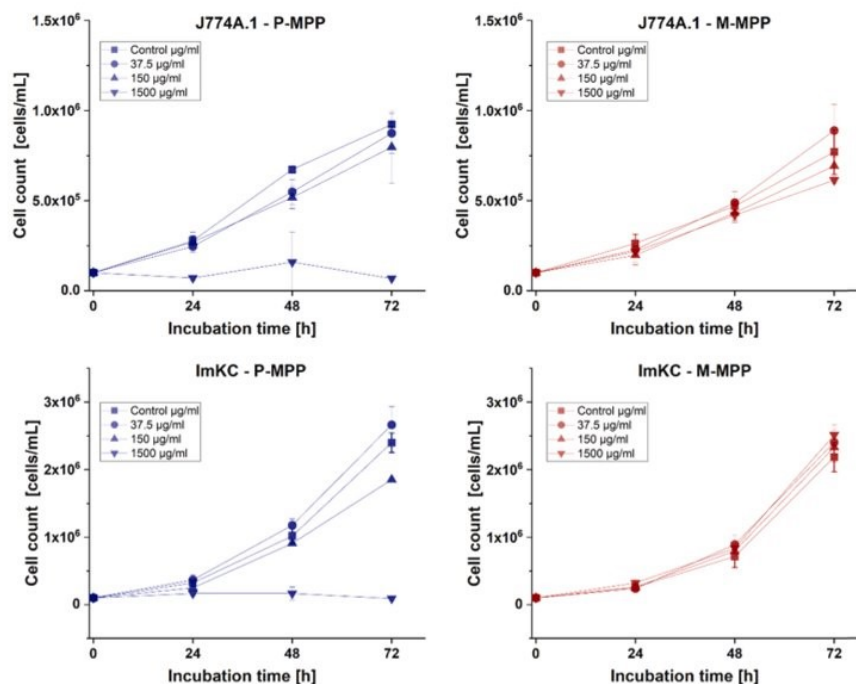ImKC cells. Upon cellular internalisation, these monomers might leach into the cytoplasm. Leaching of residual monomers is a known problem in biomedical applications e.g., dental braces (Kloukos et al., 2013). Furthermore, the higher number of internalised P-MPP could induce cell damage, leading to reduced cell proliferation. Recently, Goodman et al. (2021) showed a reduced proliferation ability for a human lung epithelial cell line after the exposure to 1 and 10 µm PS particles. An increase in particle internalisation has been shown to induce oxidative stress (Schirinzi et al., 2017; Hwang et al., 2019), which is known to damage DNA (Townley et al., 2012) and leads to bioenergetic failure (Fang and Maldonado, 2018) and, therefore, might lower the proliferation rate as well. In addition, the internalisation of particles occurs most probably by an energy-dependent mechanism like phagocytosis (Hirsch, 1965). The higher internalisation rate of P-MPP might therefore result in less energy available for cell proliferation compared to M-MPP, which are internalised less frequently. Hence, various particle properties may act synergistically in causing adverse effects. Surface charge and morphology enhance particle internalisation, and residual monomers and increased numbers of internalised particles may affect the viability of the cells. However, since these effects occurred only at higher concentrations, the relevance for exposure to animals and humans is still debatable. Nevertheless, microplastic particles occurring in nature may exhibit a huge variety of chemical and physical properties, which may alter particle cell interaction even at lower concentrations. Further, microplastic contamination in nature is expected to distinctly rise in the future (Lebreton and Andrady, 2019), enhancing the number of ingested or inhaled microplastic particles and might lead to chronic exposure to particles having properties that potentially cause adverse effects.

5. Conclusion

Overall, our results show that nominally "identical" plain polystyrene microparticles from different manufacturers differ highly in their chemical composition and surface properties resulting in

pronounced differences in PCI and the proportion of internalised particles by murine macrophages. Particles showing a more negative ζ-potential and a higher residual monomer content induced a significant metabolic response in a sensitive cell line and altered cell proliferation, especially at higher particle concentrations. Our study paves the way to explain the discrepancy in the results of previously published effect studies while highlighting the need for well-characterised microplastic particles in hazard assessment studies as particles from different manufacturers lead to non-comparable results. It further emphasises that no general conclusions can be drawn concerning the toxicity of microplastics per se, even for the same type of polymer in the same size range having the same shape. Hence, only a detailed characterisation of microplastics' chemical composition and surface properties allows for comparability between toxicological studies and enables unravelling those properties that may render specific types of microplastics hazardous.

Funding

CRediT authorship contribution statement

A.F.R.M. Ramsperger: Conceptualization, Methodology, Investigation, Writing – original draft, Writing – review & editing, Formal analysis, Visualization, Project administration, Validation. **J. Jasinski:** Conceptualization, Methodology, Investigation, Writing – original draft, Writing – review & editing, Formal analysis, Visualization, Project administration, Validation. **M. Völkl:** Conceptualization, Methodology,

Investigation, Writing – original draft, Writing – review & editing, Formal analysis, Visualization, Project administration, Validation. **T. Witzmann:** Conceptualization, Methodology, Investigation, Writing – original draft, Writing – review & editing, Formal analysis, Visualization, Validation. **M. Meinhart:** Conceptualization, Methodology, Investigation, Writing – original draft, Writing – review & editing, Formal analysis, Visualization, Validation. **V. Jerome:** Conceptualization, Methodology, Writing – original draft, Writing – review & editing, Formal analysis, Validation, Supervision. **W. Kretschmer:** Methodology, Investigation, Formal analysis, Validation, Supervision. **R. Freitag:** Conceptualization, Methodology, Writing – original draft, Writing – review & editing, Formal analysis, Validation, Resources, Supervision, Project administration, Funding acquisition. **J. Senker:** Conceptualization, Methodology, Writing – original draft, Writing – review & editing, Formal analysis, Validation, Resources, Supervision, Project administration, Funding acquisition. **A. Fery:** Conceptualization, Methodology, Writing – original draft, Writing – review & editing, Formal analysis, Validation, Resources, Supervision, Project administration, Funding acquisition. **H. Kress:** Conceptualization, Methodology, Writing – original draft, Writing – review & editing, Formal analysis, Validation, Resources, Supervision, Project administration, Funding acquisition. **T. Scheibel:** Conceptualization, Methodology, Writing – original draft, Writing – review & editing, Formal analysis, Validation, Resources, Supervision, Project administration, Funding acquisition. **C. Laforsch:** Conceptualization, Methodology, Writing – original draft, Writing – review & editing, Formal analysis, Validation, Resources, Supervision, Project administration, Funding acquisition.

Declaration of Competing Interest

The authors declare that they have no known competing financial interests or personal relationships that could have appeared to influence the work reported in this paper.

Data availability

All data are available in the main text or the supplementary materials.

Acknowledgements

Author contributions

AFRM.R., J.J., M.V., V.J., R.F., J.S., A.F., H.K., T.S. and C.L. designed the experiment. AFRM.R., J.J., M.V., T.W., M.M., V.J., WP.K., R.F., J.S., A.F., H.K., T.S., and C.L. wrote the manuscript. All authors contributed to the interpretation and discussion of the results. J.J. conducted the ζ-potential measurements, DLS measurements and SEM analysis of the cells and particles. M.M. and WP.K. conducted the GPC, EDX and NMR experiments. T.W. conducted the CP-AFM measurements. AFRM.R. conducted the cellular internalisation experiments. M.V. conducted the MTT and cell proliferation experiments.

Appendix A. Supplementary material

Supplementary data associated with this article can be found in the online version at doi:10.1016/j.jhazmat.2021.127961.

References

Arráez, F.J., Arnal, M.L., Müller, A.J., 2019. Thermal degradation of high-impact polystyrene with pro-oxidant additives. Polym. Bull. 76, 1489–1515. https://doi.org/10.1007/s00289-018-2453-4.

Arthur, C., Baker, J., Bamford, H., 2008. In: Proceedings of the International Research Workshop on the Occurrence, Effects, and Fate of Microplastic Marine Debris, 9–11 September 2008. NOAA Technical Memorandum NOS-OR&R-30. ⟨https://repository.library.noaa.gov/view/noaa/2509⟩.

Barboza, L.G.A., Lopes, C., Oliveira, P., Bessa, F., Otero, V., Henriques, B., Raimundo, J., Caetano, M., Vale, C., Guilhermino, L., 2020. Microplastics in wild fish from North East Atlantic Ocean and its potential for causing neurotoxic effects, lipid oxidative damage, and human health risks associated with ingestion exposure. Sci. Total Environ. 717, 134625 https://doi.org/10.1016/j.scitotenv.2019.134625.

Beachell, H.C., Smiley, L.H., 1967. Oxidative degradation of polystyrene. J. Polym. Sci. Part A-1 Polym. Chem. 5, 1635–1643. https://doi.org/10.1002/pol.1967.150050713.

Bjorndal, K.A., Bolten, A.B., Lagueux, C.J., 1994. Ingestion of marine debris by juvenile sea turtles in coastal Florida habitats. Mar. Pollut. Bull. 28, 154–158. https://doi.org/10.1016/0025-326X(94)90391-3.

Brachner, A., Fragouli, D., Duarte, I.F., Farias, P.M.A., Dembski, S., Ghosh, M., Barisic, I., Zdzieblo, D., Vanoirbeek, J., Schwabl, P., Neuhaus, W., 2020. Assessment of human health risks posed by nano-and microplastics is currently not feasible. Int. J. Environ. Res. Public Health 17, 1–10. https://doi.org/10.3390/ijerph17238832.

Browne, M.A., Dissanayake, A., Galloway, T.S., Lowe, D.M., Thompson, R.C., 2008. Ingested microscopic plastic translocates to the circulatory system of the mussel, Mytilus edulis (L.). Environ. Sci. Technol. 42, 5026–5031. https://doi.org/10.1021/es800249a.

Buzea, C., Pacheco, I.I., Robbie, K., 2007. Nanomaterials and nanoparticles: Sources and toxicity. Biointerphases 2, MR17–MR71. https://doi.org/10.1116/1.2815690.

Calabrese, E.J., 2008. Hormesis. Why it is importantto toxicology and toxicologists. Edited by Foxit Reader. Toxicol. Chem. 27, 1451–1474.

Campanale, C., Massarelli, C., Savino, I., Locaputo, V., Uricchio, V.F., 2020. A detailed review study on potential effects of microplastics and additives of concern on human health. Int. J. Environ. Res. Public Health 17. https://doi.org/10.3390/ijerph17041212.

Cao, X., Han, Y., Li, F., Li, Z., McClements, D.J., He, L., Decker, E.A., Xing, B., Xiao, H., 2019. Impact of protein-nanoparticle interactions on gastrointestinal fate of ingested nanoparticles: not just simple protein corona effects. NanoImpact 13, 37–43. https://doi.org/10.1016/j.impact.2018.12.002.

Cole, M., Galloway, T.S., 2015. Ingestion of nanoplastics and microplastics by pacific oyster larvae. Environ. Sci. Technol. 49, 14625–14632. https://doi.org/10.1021/acs.est.5b04099.

Deng, Y., Zhang, Y., Lemos, B., Ren, H., 2017. Tissue accumulation of microplastics in mice and biomarker responses suggest widespread health risks of exposure. Sci. Rep. 7, 1–10. https://doi.org/10.1038/srep46687.

Desjardins, M., Griffiths, G., 2003. Phagocytosis: latex leads the way. Curr. Opin. Cell Biol. 15, 498–503. https://doi.org/10.1016/S0955-0674(03)00083-8.

Di Dong, C., Chen, C.W., Chen, Y.C., Chen, H.H., Lee, J.S., Lin, C.H., 2020. Polystyrene microplastic particles: in vitro pulmonary toxicity assessment. J. Hazard. Mater. 385, 121575 https://doi.org/10.1016/j.jhazmat.2019.121575.

Drechsler, A., Caspari, A., Synytska, A., 2020. Influence of roughness and capillary size on the zeta potential values obtained by streaming potential measurements. Surf. Interface Anal. 52, 991–995. https://doi.org/10.1002/sia.6792.

Dris, R., Gasperi, J., Rocher, V., Saad, M., Renault, N., Tassin, B., 2015. Microplastic in urban sources and receiving water within an urban area: a case study in Greater Paris. Environ. Chem. 12, 592–599. https://doi.org/10.1071/EN14167.

Dris, R., Gasperi, J., Saad, M., Mirande, C., Tassin, B., 2016. Synthetic fibers in atmospheric fallout: a source of microplastics in the environment? Mar. Pollut. Bull. 4–7. https://doi.org/10.1016/j.marpolbul.2016.01.006.

Elizalde-Velázquez, A., Carcano, A.M., Crago, J., Green, M.J., Shah, S.A., Cañas-Carrell, J.E., 2020. Translocation, trophic transfer, accumulation and depuration of polystyrene microplastics in Daphnia magna and Pimephales promelas. Environ. Pollut. 259, 113937 https://doi.org/10.1016/j.envpol.2020.113937.

Eriksen, M., Lebreton, L.C.M., Carson, H.S., Thiel, M., Moore, C.J., Borerro, J.C., Galgani, F., Ryan, P.G., Reisser, J., 2014. Plastic pollution in the world's oceans: more than 5 trillion plastic pieces weighing over 250,000 tons afloat at sea. PLoS One 9, 1–15. https://doi.org/10.1371/journal.pone.0111913.

Evangeliou, N., Grythe, H., Klimont, Z., Heyes, C., Eckhardt, S., Lopez-Aparicio, S., Stohl, A., 2020. Atmospheric transport is a major pathway of microplastics to remote regions. Nat. Commun. 11 https://doi.org/10.1038/s41467-020-17201-9.

Fang, D., Maldonado, E.N., 2018. VDAC regulation: a mitochondrial target to stop. Cell Proliferation, first ed. Elsevier Inc. https://doi.org/10.1016/bs.acr.2018.02.002.

Frias, J.P.G.L., Nash, R., 2019. Microplastics: finding a consensus on the definition. Mar. Pollut. Bull. 138, 145–147. https://doi.org/10.1016/j.marpolbul.2018.11.022.

Fröhlich, E., 2012. The role of surface charge in cellular uptake and cytotoxicity of medical nanoparticles. Int. J. Nanomed. 7, 5577–5591. https://doi.org/10.2147/IJN.S36111.

Gasperi, J., Wright, S.L., Dris, R., Collard, F., Mandin, C., Guerrouache, M., Langlois, V., Kelly, F.J., Tassin, B., 2018. Microplastics in air: are we breathing it in? Curr. Opin. Environ. Sci. Health 1, 1–5. https://doi.org/10.1016/j.coesh.2017.10.002.

Gebicki, J.M., James, A.M., 1962. The Electrokinetic Properties of the Spheroplasts of Aerobacter Arogenes, pp. 158–167.

Goodman, K.E., Hare, J.T., Khamis, Z.I., Hua, T., Sang, Q.X.A., 2021. Exposure of human lung cells to polystyrene microplastics significantly retards cell proliferation and

triggers morphological changes. Chem. Res. Toxicol. https://doi.org/10.1021/acs.chemrestox.0c00486.

Gopi, I.K., Rattan, S.I.S., 2019. Biphasic dose–response and hormetic effects of stress hormone hydrocortisone on telomerase-immortalized human bone marrow stem cells in vitro. Dose-Response 17, 1–9. https://doi.org/10.1177/1559325819889819.

Harvilchuck, J.A., Carlson, G.P., 2006. Comparison of styrene and its metabolites styrene oxide and 4-vinylphenol on cytotoxicity and glutathione depletion in Clara cells of mice and rats. Toxicology 227, 165–172. https://doi.org/10.1016/j.tox.2006.08.001.

Hirsch, J.G., 1965. Phagocytosis. Annu. Rev. Microbiol. 339–350. https://doi.org/10.1038/179290c0.

Hutter, J.L., Bechhoefer, J., 1993. Calibration of atomic-force microscope tips. Rev. Sci. Instrum. 64, 1868–1873. https://doi.org/10.1063/1.1143970.

Hwang, J., Choi, D., Han, S., Choi, J., Hong, J., 2019. An assessment of the toxicity of polypropylene microplastics in human derived cells. Sci. Total Environ. 684, 657–669. https://doi.org/10.1016/j.scitotenv.2019.05.071.

Imhof, H.K., Ivleva, N.P., Schmid, J., Niessner, R., Laforsch, C., 2013. Contamination of beach sediments of a subalpine lake with microplastic particles. Curr. Biol. 23, R867–R868. https://doi.org/10.1016/j.cub.2013.09.001.

Imhof, H.K., Sigl, R., Brauer, E., Feyl, S., Giesemann, P., Klink, S., Leupolz, K., Löder, M.G.J., Löschel, L.A., Missun, J., Muszynski, S., Ramsperger, A.F.R.M., Schrank, I., Speck, S., Steibl, S., Trotter, B., Winter, I., Laforsch, C., 2017. Spatial and temporal variation of macro-, meso- and microplastic abundance on a remote coral island of the Maldives, Indian Ocean. Mar. Pollut. Bull. 116, 340–347. https://doi.org/10.1016/j.marpolbul.2017.01.010.

Jacob, H., Besson, M., Swarzenski, P.W., Lecchini, D., Metian, M., 2020. Effects of virgin micro- and nanoplastics on fish: trends, meta-analysis, and perspectives. Environ. Sci. Technol. 54, 4733–4745. https://doi.org/10.1021/acs.est.9b05995.

Kim, H.J., Kim, S.H., Kim, H.M., Kim, Y.S., Oh, J.M., 2021. Surface roughness effect on the cellular uptake of layered double hydroxide nanoparticles. Appl. Clay Sci. 202, 105992 https://doi.org/10.1016/j.clay.2021.105992.

Klein, S., Worch, E., Knepper, T.P., 2015. Occurrence and spatial distribution of microplastics in river shore sediments of the rhine-main area in Germany. Environ. Sci. Technol. 49, 6070–6076. https://doi.org/10.1021/acs.est.5b00492.

Kloukos, D., Pandis, N., Eliades, T., 2013. Bisphenol-A and residual monomer leaching from orthodontic adhesive resins and polycarbonate brackets: a systematic review. Am. J. Orthod. Dentofac. Orthop. 143, S104–S112. https://doi.org/10.1016/j.ajodo.2012.11.015 e2.

Koval, M., Preiter, K., Adles, C., Stahl, P.D., Steinberg, T.H., 1998. Size of IgG-opsonized particles determines macrophage response during internalization. Exp. Cell Res. 242, 265–273. https://doi.org/10.1006/excr.1998.4110.

Lacerda, A.L.d.F., dos, L., Rodrigues, S., van Sebille, E., Rodrigues, F.L., Ribeiro, L., Secchi, E.R., Kessler, F., Proietti, M.C., 2019. Plastics in sea surface waters around the Antarctic Peninsula. Sci. Rep. 9, 1–12. https://doi.org/10.1038/s41598-019-40311-4.

Laist, D., 1997. Impacts of marine debris: entanglement of marine life in marine debris including a comprehensive list of species with entanglement and ingestion records. In: Coe, J.M., Rogers, D.B. (Eds.), Marine Debris & Plastics: Environmental Concerns, Sources, Impacts and Solutions. Springer-Verlag, New York, pp. 99–139. https://doi.org/10.1007/978-1-4613-8486-1_10.

Lebreton, L., Andrady, A., 2019. Future scenarios of global plastic waste generation and disposal. Palgrave Commun. 5, 1–11. https://doi.org/10.1057/s41599-018-0212-7.

Levin, P.A., Angert, E.R., 2015. Small but mighty: cell size and bacteria. Cold Spring Harb. Perspect. Biol. 7, 1–11. https://doi.org/10.1101/cshperspect.a019216.

Lu, Y., Zhang, Y., Deng, Y., Jiang, W., Zhao, Y., Geng, J., Ding, L., Ren, H., 2016. Uptake and accumulation of polystyrene microplastics in zebrafish (Danio rerio) and toxic effects in liver. Environ. Sci. Technol. 50, 4054–4060. https://doi.org/10.1021/acs.est.6b00183.

Lundqvist, M., Stigler, J., Elia, G., Lynch, I., Cedervall, T., Dawson, K.A., 2008. Nanoparticle size and surface properties determine the protein corona with possible implications for biological impacts. Proc. Natl. Acad. Sci. USA 105. https://doi.org/10.1073/pnas.0805135105, 14265–70.

Lunov, O., Syrovets, T., Loos, C., Beil, J., Delacher, M., Tron, K., Nienhaus, G.U., Musyanovych, A., Mailänder, V., Landfester, K., Simmet, T., 2011. Differential uptake of functionalized polystyrene nanoparticles by human endothelial cells and a monocytic cell line. ACS Nano 5, 1657–1669. https://doi.org/10.1021/nn2000756.

Moad, G., Solomon, D.H., Johns, S.R., Willing, R.I., 1982. Structure of benzoyl peroxide initiated polystyrene: determination of the initiator-derived functionality by ^{13}C NMR. Macromolecules 15, 1188–1191. https://doi.org/10.1021/ma00232a045.

Mohamed Nor, N.H., Koelmans, A., Kooi, M., Diepens, N., 2021. Lifetime accumulation of microplastic in children and adults. Environ. Sci. Technol. 55, 5084–5096. https://doi.org/10.1021/acs.est.0c07384.

Monopoli, M.P., Åberg, C., Salvati, A., Dawson, K.A., 2012. Biomolecular coronas provide the biological identity of nanosized materials. Nat. Nanotechnol. 7, 779–786. https://doi.org/10.1038/nnano.2012.207.

von Moos, N., Burkhardt-Holm, P., Koehler, A., 2012. Uptake and effects of microplastics on cells and tissue of the blue mussel Mytilus edulis L. after an experimental exposure. Environ. Sci. Technol. 46, 327–335. https://doi.org/10.1021/es302332w.

Musyanovych, A., Dausend, J., Dass, M., Walther, P., Mailänder, V., Landfester, K., 2011. Criteria impacting the cellular uptake of nanoparticles: a study emphasizing polymer type and surfactant effects. Acta Biomater. 7, 4160–4168. https://doi.org/10.1016/j.actbio.2011.07.033.

Mutzke, E., Chomyshyn, E., Nguyen, K.C., Blahoianu, M., Tayabali, A.F., 2015. Phagocytosis-coupled flow cytometry for detection and size discrimination of anionic polystyrene particles. Anal. Biochem. 483, 40–46. https://doi.org/10.1016/j.ab.2015.04.034.

Nelms, S.E., Parry, H.E., Bennett, K.A., Galloway, T.S., Godley, B.J., Santillo, D., Lindeque, P.K., 2019. What goes in, must come out: combining scat-based molecular diet analysis and quantification of ingested microplastics in a marine top predator. Methods Ecol. Evol. 10, 1712–1722. https://doi.org/10.1111/2041-210X.13271.

Niu, Y., Yu, M., Meka, A., Liu, Y., Zhang, J., Yang, Y., Yu, C., 2015. Understanding the contribution of surface roughness and hydrophobic modification of silica nanoparticles to enhanced therapeutic protein delivery. J. Mater. Chem. B 4, 212–219. https://doi.org/10.1039/c5tb01911g.

Ober, C.K., Lok, K.P., Hair, M.L., 1985. Monodispersed, micron-sized polystyrene particles by dispersion polymerization. J. Polym. Sci. Polym. Lett. Ed. 23, 103–108. https://doi.org/10.1002/pol.1985.130230209.

Olivier, V., Rivière, C., Hindié, M., Duval, J.-L., Bomila-Koradjim, G., Nagel, M.-D., 2004. Uptake of polystyrene beads bearing functional groups by macrophages and fibroblasts. Colloids Surf. B Biointerfaces 33, 23–31. https://doi.org/10.1016/j.colsurfb.2003.08.008.

Partikel, K., Korte, R., Mulac, D., Humpf, H.U., Langer, K., 2019. Serum type and concentration both affect the protein-corona composition of PLGA nanoparticles. Beilstein J. Nanotechnol. 10, 1002–1015. https://doi.org/10.3762/BJNANO.10.101.

Patiño, T., Soriano, J., Barrios, L., Ibáñez, E., Nogués, C., 2015. Surface modification of microparticles causes differential uptake responses in normal and tumoral human breast epithelial cells. Sci. Rep. 5, 11371. https://doi.org/10.1038/srep11371.

Piehl, S., Leibner, A., Löder, M.G.J., Dris, R., Bogner, C., Laforsch, C., 2018. Identification and quantification of macro- and microplastics on an agricultural farmland. Sci. Rep. 8, 1–9. https://doi.org/10.1038/s41598-018-36172-y.

Piehl, S., Mitterwallner, V., Atwood, E.C., Bochow, M., Laforsch, C., 2019. Abundance and distribution of large microplastics (1–5 mm) within beach sediments at the Po River Delta, northeast Italy. Mar. Pollut. Bull. 149, 110515 https://doi.org/10.1016/j.marpolbul.2019.110515.

Piloni, A., Wong, C.K., Chen, F., Lord, M., Walther, A., Stenzel, M.H., 2019. Surface roughness influences the protein corona formation of glycosylated nanoparticles and alter their cellular uptake. Nanoscale 11, 23259–23267. https://doi.org/10.1039/c9nr06835j.

Prata, J.C., da Costa, J.P., Lopes, I., Duarte, A.C., Rocha-Santos, T., 2020. Environmental exposure to microplastics: an overview on possible human health effects. Sci. Total Environ. 702, 134455 https://doi.org/10.1016/j.scitotenv.2019.134455.

Rahman, A., Sarkar, A., Yadav, O.P., Achari, G., Slobodnik, J., 2021. Potential human health risks due to environmental exposure to nano- and microplastics and knowledge gaps: a scoping review. Sci. Total Environ. 757, 143872 https://doi.org/10.1016/j.scitotenv.2020.143872.

Ralph, P., Nakoinz, I., 1975. Phagocytosis and cytolysis by a macrophage tumour and its cloned cell line MACROPHAGES. Nature 257, 393–394.

Ramsperger, A.F.R.M., Narayana, V.K.B., Gross, W., Mohanraj, J., Thelakkat, M., Greiner, A., Schmalz, H., Kress, H., Laforsch, C., 2020. Environmental exposure enhances the internalization of microplastic particles into cells. Sci. Adv. 6, 1–10. https://doi.org/10.1126/sciadv.abd1211.

Rillig, M.C., 2012. Microplastic in terrestrial ecosystems and the soil? Environ. Sci. Technol. 46, 6453–6454 https://doi.org/dx.doi.org/10.1021/es302011r.

Rillig, M.C., Lehmann, A., 2020. Microplastic in terrestrial ecosystems. Science 368. https://doi.org/10.1126/science.abb5979 (80-.).

Rodriguez-Seijo, A., Lourenço, J., Rocha-Santos, T.A.P., da Costa, J., Duarte, A.C., Vala, H., Pereira, R., 2017. Histopathological and molecular effects of microplastics in Eisenia andrei Bouché. Environ. Pollut. 220, 495–503. https://doi.org/10.1016/j.envpol.2016.09.092.

Rudolph, J., Völkl, M., Jérôme, V., Scheibel, T., Freitag, R., 2021. Noxic effects of polystyrene microparticles on murine macrophages and epithelial cells. Sci. Rep. 11 (1), 15702 https://doi.org/10.1038/s41598-021-95073.

Riedl, S.A.B., Völkl, M., Holzinger, A., 2021. In vitro cultivation of primary intestinal cells from Eisenia fetida as basis for ecotoxicological studies. Ecotoxicology. https://doi.org/10.1007/s10646-021. https://doi.org/10.1007/s10646-021.

Saavedra, J., Stoll, S., Slaveykova, V.I., 2019. Influence of nanoplastic surface charge on eco-corona formation, aggregation and toxicity to freshwater zooplankton. Environ. Pollut. 252, 715–722. https://doi.org/10.1016/j.envpol.2019.05.135.

Schirinzi, G.F., Pérez-Pomeda, I., Sanchís, J., Rossini, C., Farré, M., Barceló, D., 2017. Cytotoxic effects of commonly used nanomaterials and microplastics on cerebral and epithelial human cells. Environ. Res. 159, 579–587. https://doi.org/10.1016/j.envres.2017.08.043.

Schrade, A., Mailänder, V., Ritz, S., Landfester, K., Ziener, U., 2012. Surface roughness and charge influence the uptake of nanoparticles: fluorescently labeled pickering-type versus surfactant-stabilized nanoparticles. Macromol. Biosci. 12, 1459–1471. https://doi.org/10.1002/mabi.201200166.

Schwabl, P., Koppel, S., Konigshofer, P., Bucsics, T., Trauner, M., Reiberger, T., Liebmann, B., 2019. Detection of various microplastics in human stool: a prospective case series. Ann. Intern. Med. 171, 453–457. https://doi.org/10.7326/M19-0618.

Shannahan, J.H., Lai, X., Ke, P.C., Podila, R., Brown, J.M., Witzmann, F.A., 2013. Silver nanoparticle protein corona composition in cell culture media. PLoS One 8, e74001. https://doi.org/10.1371/journal.pone.0074001.

Smoluchowski, M.V., 1916. Drei vortage uber diffusin, brwonsche bewegung und koagulation von kolloidteilchen. Z. Phys. 17, 557–585.

Stock, V., Böhmert, L., Lisicki, E., Block, R., Cara-Carmona, J., Pack, L.K., Selb, R., Lichtenstein, D., Voss, L., Henderson, C.J., Zabinsky, E., Sieg, H., Braeuning, A., Lampen, A., 2019. Uptake and effects of orally ingested polystyrene microplastic particles in vitro and in vivo. Arch. Toxicol. 93, 1817–1833. https://doi.org/10.1007/s00204-019-02478-7.

Stock, V., Laurisch, C., Franke, J., Dönmez, M.H., Voss, L., Böhmert, L., Braeuning, A., Sieg, H., 2021. Uptake and cellular effects of PE, PP, PET and PVC microplastic particles. Toxicol. Vitr. 70, 105021 https://doi.org/10.1016/j.tiv.2020.105021.

13

Tanifum, E.A., Devkota, L., Ngwa, C., Badachhape, A.A., Ghaghada, K.B., Romero, J., Pautler, R.G., Annapragada, A.V., 2018. A hyperfluorinated hydrophilic molecule for aqueous 19 F MRI contrast media. Contrast Media Mol. Imaging (2018). https://doi.org/10.1155/2018/1693513.

Telford, A.M., Pham, B.T.T., Neto, C., Hawkett, B.S., 2013. Micron-sized polystyrene particles by surfactant-free emulsion polymerization in air: synthesis and mechanism. J. Polym. Sci. Part A Polym. Chem. 51, 3997–4002. https://doi.org/10.1002/pola.26841.

Tenzer, S., Docter, D., Kuharev, J., Musyanovych, A., Fetz, V., Hecht, R., Schlenk, F., Fischer, D., Kiouptsi, K., Reinhardt, C., Landfester, K., Schild, H., Maskos, M., Knauer, S.K., Stauber, R.H., 2013. Rapid formation of plasma protein corona critically affects nanoparticle pathophysiology. Nat. Nanotechnol. 8 https://doi.org/10.1038/nnano.2013.181, 772–81.

Townley, H.E., Rapa, E., Wakefield, G., Dobson, P.J., 2012. Nanoparticle augmented radiation treatment decreases cancer cell proliferation. Nanomed. Nanotechnol. Biol. Med. 8, 526–536. https://doi.org/10.1016/j.nano.2011.08.003.

Triebskorn, R., Braunbeck, T., Grummt, T., Hanslik, L., Huppertsberg, S., Jekel, M., Knepper, T.P., Krais, S., Müller, Y.K., Pittroff, M., Ruhl, A.S., Schmieg, H., Schür, C., Strobel, C., Wagner, M., Zumbülte, N., Köhler, H.R., 2019. Relevance of nano- and microplastics for freshwater ecosystems: a critical review. TrAC Trends Anal. Chem. 110, 375–392. https://doi.org/10.1016/j.trac.2018.11.023.

Van Berkel, K.Y., Russell, G.T., Gilbert, R.G., 2003. Entry in emulsion polymerization: effects of initiator and particle surface charge. Macromolecules 36, 3921–3931. https://doi.org/10.1021/ma025695y.

Wang, Z.Y., Burlak, C., Klaunig, J.E., Kamendulis, L.M., 2014. Development of a cytokine-producing immortalized murine Kupffer cell line. Cytokine 70, 165–172. https://doi.org/10.1016/j.cyto.2014.07.251.

Weyermann, J., Lochmann, D., Zimmer, A., 2005. A practical note on the use of cytotoxicity assays. Int. J. Pharm. 288, 369–376. https://doi.org/10.1016/j.ijpharm.2004.09.018.

Withey, J.R., 1976. Quantitative analysis of styrene monomer in polystyrene and foods including some preliminary studies of the uptake and pharmacodynamics of the monomer in rats. Environ. Health Perspect. 17, 125–133. https://doi.org/10.1289/ehp.7617125.

Wright, S.L., Kelly, F.J., 2017. Plastic and human health: a micro issue? Environ. Sci. Technol. 51, 6634–6647. https://doi.org/10.1021/acs.est.7b00423.

Wright, S.L., Thompson, R.C., Galloway, T.S., 2013. The physical impacts of microplastics on marine organisms: a review. Environ. Pollut. 178, 483–492. https://doi.org/10.1016/j.envpol.2013.02.031.

Yong, C.Q.Y., Valiyaveetill, S., Tang, B.L., 2020. Toxicity of microplastics and nanoplastics in Mammalian systems. Int. J. Environ. Res. Public Health 17. https://doi.org/10.3390/ijerph17051509.

Yousif, E., Haddad, R., 2013. Photodegradation and photostabilization of polymers, especially polystyrene: review. SpringerPlus 2, 1–32. https://doi.org/10.1186/2193-1801-2-398.

Supplementary Materials

Figs. S1

Supplementary Information
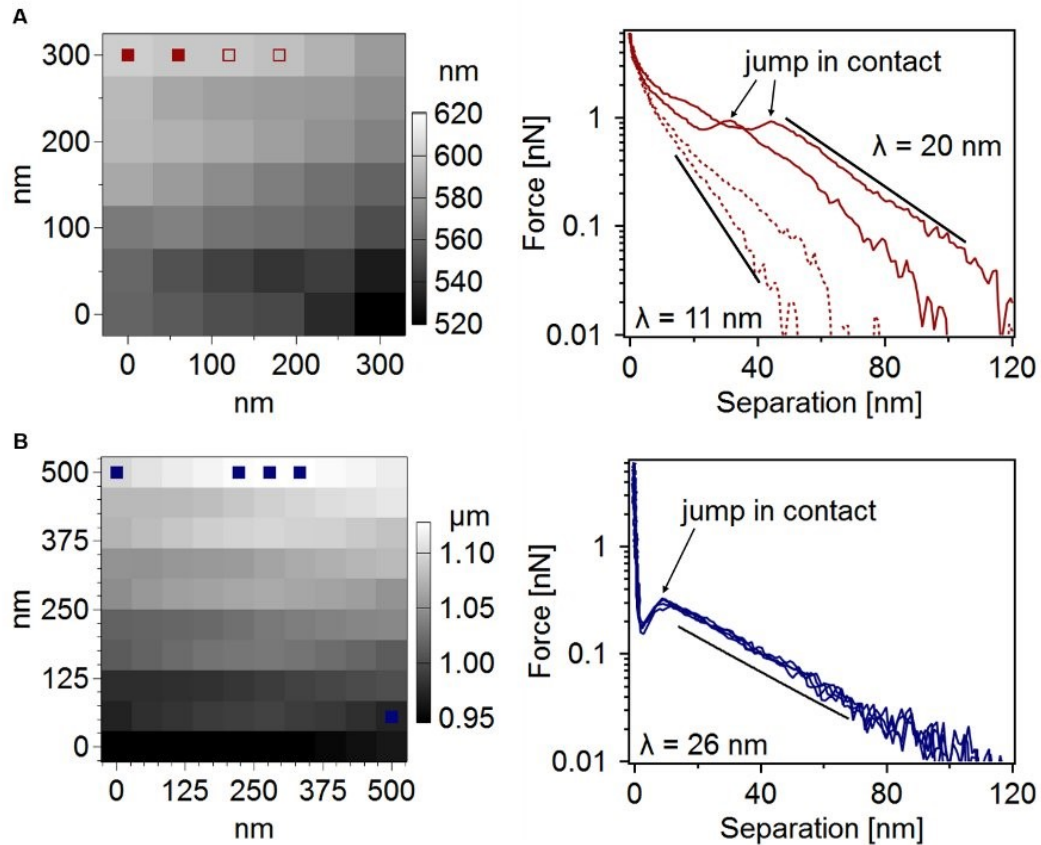
Fig. S1. *Force map (left) of a M-MPP, and the corresponding semi-logarithmic force-separation curves (right) (B) and of a P-MPP (C). Obtained in an aqueous solution of 0.1 mM NaCl (λ = 30 nm) in a slightly acidic pH 5 -6 through dissolved CO_2, which also reduces the calculated Debye length. The straight solid lines resemble the exponential Debye fit. Force Maps show the relative height in XY-direction close to the apex of a particle. Colored pixels show the measurement locations of the force curves displayed right. The brighter the pixel the closer is the measurement location to the apex. Varying attractive van-der-Waals and repulsive electrostatic forces (measured Debye length 11 nm – 20 nm) with measurement location are visible for M-MPP in A. For 2 spots (solid squares & curves) we found van-der-Waals and stronger electrostatic forces than for the other 2 spots (open squares & dashed curves) In contrast, P-MPP show constant attractive van-der-Waals and repulsive electrostatic forces (measured Debye length 26 nm) for every measurement location. The jump into contact is also always visible.*

Article 3

Nominally identical microplastic models differ greatly in their particle-cell interactions

nature communications

Nominally identical microplastic models differ greatly in their particle-cell interactions

Check for updates
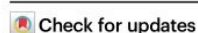
Simon Wieland [1,2,7], Anja F. R. M. Ramsperger[1,2,7], Wolfgang Gross[1,7], Moritz Lehmann [3], Thomas Witzmann [4], Anja Caspari[4], Martin Obst[5], Stephan Gekle [3], Günter K. Auernhammer [4], Andreas Fery [4,6], Christian Laforsch [2,8] & Holger Kress [1,8]

Due to the abundance of microplastics in the environment, research about its possible adverse effects is increasing exponentially. Most studies investigating the effect of microplastics on cells still rely on commercially available polystyrene microspheres. However, the choice of these model microplastic particles can affect the outcome of the studies, as even nominally identical model microplastics may interact differently with cells due to different surface properties such as the surface charge. Here, we show that nominally identical polystyrene microspheres from eight different manufacturers significantly differ in their ζ-potential, which is the electrical potential of a particle in a medium at its slipping plane. The ζ-potential of the polystyrene particles is additionally altered after environmental exposure. We developed a microfluidic microscopy platform to demonstrate that the ζ-potential determines particle-cell adhesion strength. Furthermore, we find that due to this effect, the ζ-potential also strongly determines the internalization of the microplastic particles into cells. Therefore, the ζ-potential can act as a proxy of microplastic-cell interactions and may govern adverse effects reported in various organisms exposed to microplastics.

The first observation of microscopically small plastic particles in the ocean was made by Carpenter et al. in 1972[1], and 50 years later, plastic particles were detected in all environmental compartments[2]. In 2004, Thompson et al. coined the term microplastics, defined as particles smaller than 5 mm[3,4]. The abundance of microplastics in the environment is associated with potential risks for environmental and human health[5,6]. Organisms are predominantly exposed to microplastics via inhalation or ingestion. The latter has already been described for a

variety of organisms ranging from protozoans[7] to even vertebrates[8,9]. Upon ingestion or inhalation, microplastic particles can translocate from the gastrointestinal tract or the respiratory organs into the circulatory system[6,10] and surrounding tissues, leading to adverse effects such as inflammatory responses[9,11]. Here, the cellular internalization of microplastic particles is a potential pathway for the translocation into tissues[12]. The cellular internalization of microplastic particles was reported for pristine particles[13,14] as well as environmentally exposed

[1]Biological Physics, University of Bayreuth, Bayreuth, Germany. [2]Animal Ecology I and BayCEER, University of Bayreuth, Bayreuth, Germany. [3]Biofluid Simulation and Modeling – Theoretical Physics VI, University of Bayreuth, Bayreuth, Germany. [4]Leibniz Institut für Polymerforschung Dresden e. V., Institute of Physical Chemistry and Polymer Physics, Dresden, Germany. [5]Experimental Biogeochemistry, BayCEER, University of Bayreuth, Bayreuth, Germany. [6]Physical Chemistry of Polymeric Materials, Technische Universität Dresden, Dresden, Germany. [7]These authors contributed equally: Simon Wieland, Anja F. R. M. Ramsperger, Wolfgang Gross. [8]These authors jointly supervised this work: Christian Laforsch, Holger Kress. e-mail: christian.laforsch@uni-bayreuth.de; holger.kress@uni-bayreuth.de

particles coated with an eco-corona[15]. Among other cell types, a focus was set on macrophages, since in many organ systems, such as the lungs, macrophages are among the first cells to encounter inhaled or ingested microplastic particles[6,16]. Furthermore, due to the mobility of these cells they can act as transporters for microplastic particles that translocate them into tissues and lead to their distribution in the organism[6].

To date, the predominantly used polymer in microplastics research is polystyrene[17,18] and the vast majority of studies was conducted with monodisperse, spherical polystyrene particles[19–22]. For studies that use the same polymer type, shape, and size range, one should expect that the results are comparable and consistent with each other. However, studies on potential negative effects of microplastics on organisms show a large variety of sometimes seemingly contradictory results. For instance, negative effects, such as a reduction in metabolism and gamete production, inhalation toxicity, inflammation, and oxidative stress were found in oysters[23], rats[24], and mice[25]. In contrast, no such negative effects were found in other studies in barnacle larvae[26] and mice[13]. On the cellular level, similar discrepancies have been observed. For example, studies using spherical polystyrene particles in the micrometer size range showed that microplastic particles were readily internalized by the cells, inducing an increase in reactive oxygen species and cytotoxic effects[14,27]. In contrast, another study using similar particles observed that only a minor fraction of microplastic particles were internalized by cells, causing no or only little cytotoxicity[13].

Current microplastics research is based on particles produced by a large number of manufacturers[14,27–31]. Although these particles are all sold as polystyrene microspheres, particles from different commercial sources can significantly differ in their physico-chemical properties. Ramsperger et al. showed that two types of polystyrene particles without a dedicated surface functionalization differed in their monomer content, ζ-potential, and surface charge densities, leading to differences in metabolic activity and cell proliferation[32].

Especially the ζ-potential, which is the electrical potential at the shear plane of a particle in a suspension[33], has been discussed to influence the particle-cell interactions and the internalization[6,32,34]. For nanoparticles, it is a well-established fact that cellular interactions (including internalization) and cytotoxicity depend on the particle's surface charge and the ζ-potential[35–38]. While neutral nanoparticles only minimally interact with cells[35,36], positively charged nanoparticles interact strongly with both phagocytic and non-phagocytic cells[36,37], whereas negatively charged nanoparticles interact more frequently with phagocytic cells[35]. Additionally, the mechanism of internalization seems to depend on the polarity and density of the nanoparticles' surface charge[35,36]. However, not only the physicochemical properties of the nanoparticles, but also the cell type seems to affect the internalization of nanoparticles into cells[35,36].

Although the role of surface charge and ζ-potential for cellular interactions and internalization is well-known for nanoparticles, research findings for microparticles are less unanimous. On the one hand, studies with microparticles are not conclusive about the role of their surface charge and ζ-potential for their cellular interactions and internalization. Since cells generally possess a net negative ζ-potential[39], it is expected that microparticles with a net positive ζ-potential interact with cells more frequently and become internalized more often[40]. This has indeed been observed for polylactic acid (PLA), polylactide-co-glycolic acid (PLGA), and polyethylene oxide/polylactic acid block copolymer (PELA) microparticles, where less negatively charged microparticles adhere stronger to cells and become internalized more often[41,42]. In contrast, other studies showed that both negatively and positively charged microparticles are phagocytosed efficiently[43], and an increase in negative surface charge can lead to an increase in internalization efficiency[43,44].

On the other hand, results from nanoparticles cannot simply be transferred to microparticles:[45–47] For example, due to their different surface-to-volume ratio, nanoparticles and microparticles interact differently with cells and tissues[47,48]. Furthermore, the mechanisms of cellular internalization strongly differ between nanoparticles and microparticles. Nanoparticles can be internalized by cells via a number of different endocytic pathways, including clathrin-mediated endocytosis, caveolin-mediated endocytosis, macropinocytosis, and passive transport into cells[35,47]. However, due to their size, internalization of microparticles is limited to the actin-dependent processes of phagocytosis and macropinocytosis[47,49,50].

The effect of the ζ-potential of microplastic particles on their interactions with cells and organisms is even less clear. Of 216 studies about possible effects of microplastics for aquatic or mammalian models currently listed in the ToMEx database, only 17% provided the ζ-potential of the microplastic particles[51]. Furthermore, despite the indications for a role of the ζ-potential for cellular interactions and the seemingly contradictory results in microplastic cytotoxicity studies, the role of the ζ-potential has not yet been systematically investigated for otherwise identical microplastic particles. Furthermore, it was shown that environmental exposure, leading to the formation of an eco-corona on the particles, alters particle-cell interactions[15]. However, it is not clear whether these changes in particle-cell interactions are caused by changes in the ζ-potential.

To shed light on the role of the ζ-potential as one driver for microplastic-cell interactions, we investigated nominally identical polystyrene particle types from eight different manufacturers (detailed information and subsequent abbreviations see Table 1). Next to the pristine microplastic particles we additionally incubated spherical PS-particles from MM in salt and freshwater to investigate the influence of the environmental exposure on the ζ-potential. We measured the particles' ζ-potential with a zetasizer for each particle type and developed a single-cell single-particle multiplexed microfluidic platform with an artificial intelligence-based data analysis to quantify the particle-cell adhesion strength. Furthermore, we measured the proportion of internalized microplastic particles for each particle type by confocal microscopy. In this way, we aim to quantify how the ζ-potential of nominally identical microplastic particles, which may be additionally altered by exposure to environmental media, affects their binding kinetics, adhesion strength, and cellular internalization probability.

Results

The ζ-potential of nominally identical microplastics differ

Although nominally identical, the microplastic particles from the different manufacturers were different in scanning electron micrographs. There were differences in their equivalent diameter, eccentricity, and surface roughness (Fig. 1, Supplementary Note 1, Supplementary Table 1). Furthermore, the ζ-potential of the particles from different manufacturers varied from −93.1 mV (ST) to −4.7 mV (MM) (Table 1). ST (−93.1 mV) and PY (−83.8 mV) had similar strongly negative ζ-potentials whereas TJ (−45.5 mV) had a medium ζ-potential. All other pristine particles had ζ-potentials closer to zero: TS, MG, PX, KI, MM (−13.7 mV, −12.6 mV, −7.5 mV, −5.3 mV, and −4.7 mV, respectively).

Incubation of the microplastic particles in cell culture media led to a decrease in the magnitude of their ζ-potential. However, the ζ-potential after incubation of the microplastic particles in cell culture media was strongly correlated to their initial ζ-potential (Pearsons's $R = 0.8$, $P = 0.004$): particle types that were strongly negative initially were still strongly negative after incubation, and particle types that had an initial ζ-potential close to zero were still almost neutral after incubation in cell culture media (Supplementary Table 1, Supplementary Fig. 1). All particle types showed a high colloidal stability in the cell experiments, no significant aggregation of particles occurred (Supplementary Fig. 2)

Table 1 | Specifications of all polystyrene microparticles

Sample	Manufacturer	Product name	Product no.	Modification	Nominal diameter (µm)	Measured diameter (µm)	ζ (mV)
PY	Polysciences, Inc.	Polybead® Microspheres	17134-15	None	3.00	3.08 ± 0.2	−83.8 ± 0.3
MM	Micromod GmbH	micromer®	01-00-303	None	3	2.94 ± 0.02	−4.7 ± 0.3
MG	Microparticles GmbH	PS-Forschungspartikel	None	None	3.03	2.97 ± 0.11	−12.6 ± 0.3
KI	Kisker Biotech GmbH & Co.KG	Polystyrene microparticles	PPS-3.0	None	3	2.96 ± 0.03	−5.3 ± 0.5
ST	Spherotech, Inc.	none	PP-30-10	None	3.43	3.47 ± 0.26	−93.1 ± 1.1
TS	ThermoFisher Scientific, Inc.	Latex Microspheres	5300 A	None	2.8	2.84 ± 0.03	−13.7 ± 0.2
TJ	Tianjin BaseLine Chromatographic Technology	Unibead PS-Microspheres	6-1-0300	None	3.0	3.36 ± 0.07	−45.5 ± 0.7
PX	Phosphorex, Inc.	Polyspherex	11	None	3.246	3.13 ± 0.33	−7.5 ± 0.4
MM-SW2	Micromod GmbH	micromer®	01-00-303	Salt water incubation, 2 weeks	3	2.97 ± 0.17	−10.0 ± 0.7
MM-SW4	Micromod GmbH	micromer®	01-00-303	Salt water incubation, 4 weeks	3	3.03 ± 0.14	−7.2 ± 1.3
MM-FW2	Micromod GmbH	micromer®	01-00-303	Freshwater incubation, 2 weeks	3	2.88 ± 0.28	−9.2 ± 0.5
MM-FW4	Micromod GmbH	micromer®	01-00-303	Freshwater incubation, 4 weeks	3	2.96 ± 0.04	−16.0 ± 2.3

Measured diameters were determined by scanning electron microscopy (see Supplementary Note 1, Supplementary Table 1). Values of measured diameter and ζ-potential represent mean ± standard deviation. For the measured diameter, $n = 10$ particles were analyzed per sample. The ζ-potential measurements were replicated $n = 3$ times.
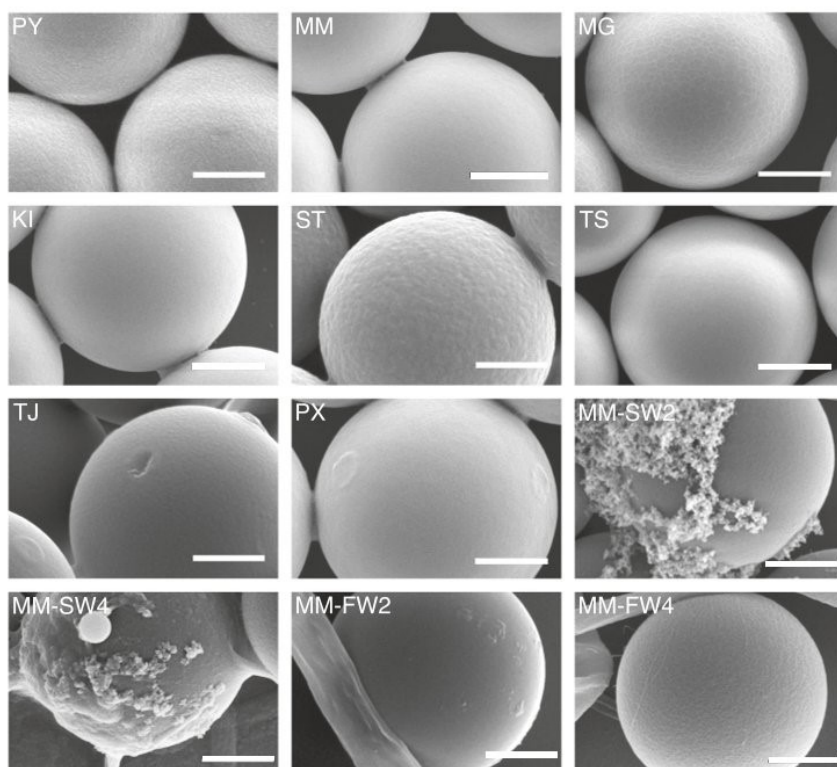
Fig. 1 | Scanning electron microscopy micrographs of the polystyrene particles. An overview of the abbreviations and specifications is given in Table 1. The surface morphologies of the different types of particles varied strongly. TJ had the roughest surface (see Supplementary Table 1), where TJ showed elevations and indentations and PX elevations. MG seemed to be covered by a net-like structure. All other particles are highly spherical with smooth surfaces. Those particles exposed to salt water particles (MM-SW2 and MM–SW4) have larger elevations, probably originating from salts whereas particles exposed to freshwater (MM-FW2 and MM–FW4) show rather smooth surfaces with little elevations. Scale bars: 1 µm.

Eco-coronas affect the ζ-potential of microplastic particles

The exposure of MM microplastic particles to environmental salt and freshwater for 2 and 4 weeks lead to the formation of an eco-corona. In the environmental media, several microorganisms were present, including cyanobacteria, green algae of the genus *Lagerheimia*, and diatoms (Supplementary Fig. 3). Scanning electron microscopy showed that some of the microplastic particles were visibly coated with an eco-corona, probably originating from biomolecules released by the microorganisms (Fig. 1). Accordingly, the equivalent diameters of the particles slightly increased for MM-SW2, MM-SW4, and MM-FW4. Their respective standard deviations substantially increased for all particle types, indicating that they became less monodisperse (Table 1). Furthermore, the eccentricity and surface roughness increased for all environmentally exposed particles compared to the pristine MM particles (Supplementary Table 1).

In a previous study with identically prepared MM particles, we showed that this eco-corona forms heterogeneous polymer structures on the particles' surface with properties of anchored high molecular weight polymer coatings[52]. Furthermore, we previously identified amino acids, nucleic acids, and lipids on MM particles incubated in freshwater using Raman spectroscopy[15]. To further analyze the eco-corona in this study, we performed synchrotron-based scanning transmission X-ray microscopy (STXM, Supplementary Fig. 4, Supplementary Table 2). We observed small amounts of protein-associated C-O and sugar-associated C-OH groups on the MM particles. After incubation in freshwater, these signals significantly increased, indicating the formation of an eco-corona. However, we could not observe an increase in the amount of proteins and sugars on MM particles exposed to salt water. A potential explanation could be that parts of the eco-corona were washed off due to the change in ionic strength in the seawater-incubated sample during the rinsing procedure that was required to avoid salt precipitation during drying of the samples. As the surface sensitivity of STXM as a transmission technique is limited, we additionally used X-ray photoelectron spectroscopy (XPS, Supplementary Table 3). The XPS spectra showed that exposure of MM to salt and freshwater altered the microplastic particles' surface. We detected nitrogen on the surfaces of the environmentally exposed particles, which was absent in the pristine MM particles, possibly indicating the presence of biomolecules or other natural organic matter. Small changes in silicon and oxygen signals could not be reliably separated from potential influences of the substrate (thermally oxidized silicon wafer). On the surface of the microplastic from salt water we additionally identified traces of sodium, magnesium, sulfur, and chlorine compared to the pristine particles.

The particles exposed to environmental media had a more negative ζ-potential compared to the pristine MM particles. Like the pristine microplastic particles, the environmentally exposed microplastic particles slightly changed the magnitude of their ζ-potential after incubation in cell culture media (Supplementary Table 1, Supplementary Fig. 1).

Particle-cell adhesion depends on the ζ-potential

We developed a microfluidic platform and used a convolutional neural network to quantify the influence of the ζ-potential on the particle-cell binding kinetics and the adhesion strength to cells. Particles were diluted to a concentration of approximately 10^7 particles per mL in imaging medium and carefully flushed into the microfluidic channels containing the cells. In a first step, we used the microfluidic platform to analyze the diffusive motion of individual particles during the sedimentation onto the cells. By classifying binding and unbinding events from and to cells using a convolutional neural network (Fig. 2a), we quantified the average binding kinetics of each particle type with their respective on-rates k_{on} and their off-rate k_{off} (Fig. 2b). A high k_{on} and a low k_{off} corresponds to fast binding and slow unbinding respectively and therefore to a strong adhesion. Some particles bound and never detached until the end of the

experiment. We classified the corresponding binding events to be irreversible. In a second step, we exerted a tunable hydrodynamic shear force on the particles and quantified the number of remaining particles after 30 s. Using a lattice Boltzmann method, we related the flow rate in the microchannels to the hydrodynamic shear force on the particles. With this method, we therefore quantified four parameters (on-rate, off-rate, percentage of irreversible binding events and percentage of bound particles under shear force) which enable us to assess the strength of particle-cell interactions. Since different endocytic pathways such as phagocytosis depend on particle-cell binding and adhesion this binding strength is expected to be a relevant parameter for the absolute internalization probability.

The binding kinetics of different particle types varied significantly (Supplementary Table 4, Supplementary Data 1) by multiple orders of magnitude. Between particles and cells, k_{on} varied between $(8.1 \pm 0.8) \times 10^{-4}\,\mathrm{s}^{-1}$ (MM) and $2.5 \times 10^{-2}\,\mathrm{s}^{-1}$ (ST) (Fig. 2c, Kruskal–Wallis test: two-sided $P = 1.75 \times 10^{-14}$) while k_{off} varied between $(1.5 \pm 0.1) \times 10^{-4}\,\mathrm{s}^{-1}$ (PY) and $2.5 \times 10^{-2}\,\mathrm{s}^{-1}$ (MM) (Fig. 2d, Kruskal–Wallis test: two-sided $P = 3.00 \times 10^{-10}$). Between particles and coverslips, we measured rates of a similar magnitude (Supplementary Fig. 5). This means that particles which strongly bound to cells also bound strongly to coverslips. However, particle-coverslip adhesion was in general slightly weaker than particle-cell adhesion. This was reflected by a generally lower k_{on} to coverslips and a higher k_{off} from coverslips (Supplementary Fig. 5). The fraction of irreversible binding events to cells varied between (32 ± 11) % (MM) and (98.6 ± 0.3) % (PY, Fig. 2e, Kruskal–Wallis test: two-sided $P = 6.71 \times 10^{-11}$) and in a similar range for coverslips (Supplementary Fig. 5).

Previously, we showed that exposure to environmental media alters the cellular interactions and internalization of microplastic particles[15]. Therefore, we wanted to investigate whether environmental exposure affects their binding kinetics and adhesion strength to cells. We found that MM particles coated with an eco-corona, regardless of the eco-corona origin (salt or freshwater), adhered stronger to cells and coverslips than MM particles without an eco-corona. While unmodified MM particles rarely bound to cells and coverslips, particles with an eco-corona commonly bound to cells and coverslips. For example, k_{on} to cells increased about an order of magnitude from $(8.1 \pm 0.8) \times 10^{-4}\,\mathrm{s}^{-1}$ to $(8.0 \pm 0.9) \times 10^{-3}\,\mathrm{s}^{-1}$ after two weeks in salt water and to $(8.1 \pm 1.0) \times 10^{-3}\,\mathrm{s}^{-1}$ after two weeks in freshwater. k_{off} decreased from $(2.5 \pm 0.2) \times 10^{-2}\,\mathrm{s}^{-1}$ to $(1.4 \pm 0.1) \times 10^{-2}\,\mathrm{s}^{-1}$ after two weeks in salt water and to $(1.1 \pm 0.1) \times 10^{-2}\,\mathrm{s}^{-1}$ after two weeks in freshwater (Fig. 2). The fraction of irreversible binding events changed from (32 ± 11) % (MM) to (44 ± 6) % and (46 ± 3) % after two- and four-weeks exposure to salt water, and (81 ± 3) % and (32 ± 5) % after two and four weeks exposure to freshwater. We observed a similar increase of k_{on}, decrease of k_{off}, and an increase of the fraction of irreversible binding events for the interaction of eco-corona-coated MM with the coverslips (Supplementary Fig. 5).

The particle-cell as well as the particle-coverslip binding was strongly correlated to the ζ-potential (Fig. 2c–e, Supplementary Fig. 5). With increasing negative ζ-potential k_{on} increased (Pearson's $R = 0.9$, two-sided $P = 4 \times 10^{-5}$), k_{off} decreased (Pearson's $R = -0.9$, two-sided $P = 0.0003$), and the fraction of irreversible binding events increased (Pearson's $R = 0.8$, two-sided $P = 0.0007$). Overall, the analysis of the microplastic particle binding kinetics indicates that particles with a more negative ζ-potential interact stronger with cells than more neutral microplastic particles.

Since different interaction processes such as phagocytosis depend on the adhesion between microplastic particles and cells, we also quantified the adhesive strength under a well-defined shear force. Therefore, we exerted a constant hydrodynamic drag force of (50 ± 5) pN (Eq. (7)) for 30 s on the particles after the sedimentation phase (Fig. 3a) and determined the fraction of remaining particles, which were not ruptured off (Fig. 3b, c). The measured adhesion strengths varied
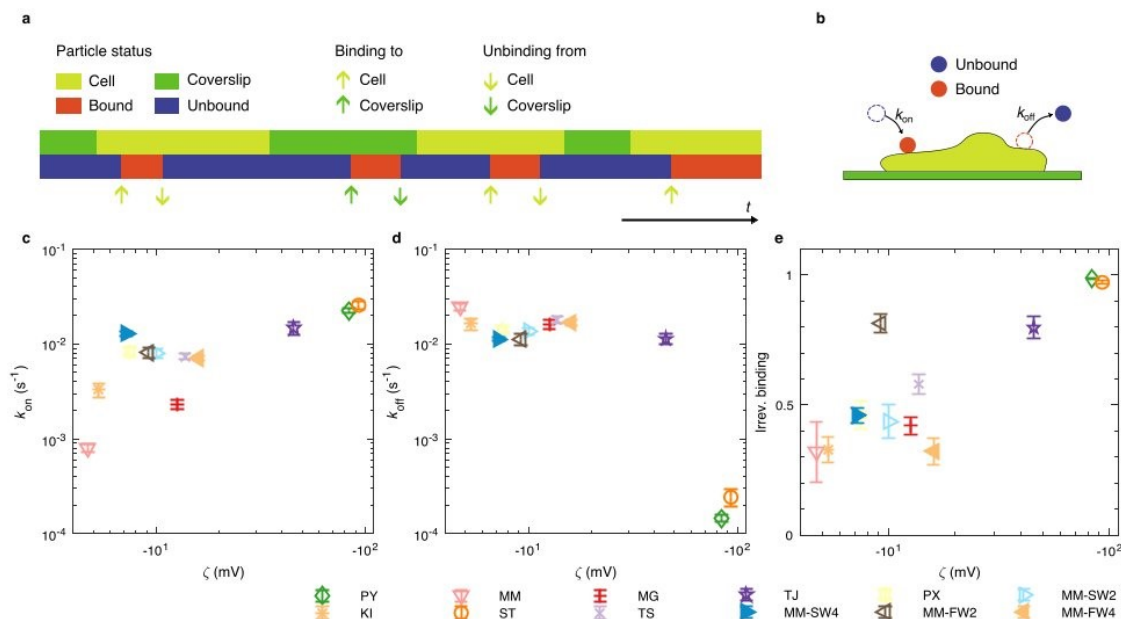
Fig. 2 | Particle binding and unbinding kinetics. a Schematic representation of the status of a single particle as a function of time. The light green and green bars indicate whether the particle is close to a cell (light green) or close to the coverslip (green) and the blue and red bars indicate whether the particle is bound (to either cell or coverslip, red) or unbound (blue) at a given time point. In this example, there are three binding events to a cell (light green up arrows) and two unbinding events from a cell (light green down arrows) as well as one binding event to the coverslip (green up arrow) and one unbinding event from the coverslip (green down arrow). The binding kinetics is characterized by the respective binding and unbinding rates k_{on} and k_{off} (**b**). **c** Binding rates k_{on} to cells significantly differed between samples (Kruskal-Wallis test, two-sided $P = 1.75 \times 10^{-14}$). **d** Unbinding rates k_{off} from cells significantly differed between samples (Kruskal–Wallis test, two-sided $P = 3.00 \times 10^{-10}$). **e** Fraction of irreversible binding events to cells significantly

differed between samples (Kruskal–Wallis test, two-sided $P = 6.71 \times 10^{-11}$). In general, k_{on} was higher for particles with a more negative ζ-potential (Pearson's $R = 0.9$), two-sided $P = 4 \times 10^{-5}$, (**c**). k_{off} was lower for particles with a more negative ζ-potential (Pearson's $R = -0.9$), two-sided $P = 0.0003$, (**d**). The fraction of irreversible binding events also strongly depended on the particle type. Particle-cell and particle-coverslip binding events with PY and ST particles were almost always irreversible, while 25–75% of the bonds did rupture spontaneously for MM, MG, KI, TS, MM-SW2, MM-SW4, and MM-FW4 particles. We found that the fraction of irreversible binding events is higher for particles with a more negative ζ-potential (Pearson's $R = 0.8$), two-sided $P = 0.0007$, (**e**). In all panels, error bars represent standard error of mean of $n = 9$ measurements (for each measurement, on average 550 particles were analyzed). For particle abbreviations and characteristics see Table 1. Source data are provided as a Source Data file.

significantly (Supplementary Table 4, Supplementary Data 1) between particles of different suppliers. For the adhesion to cells, we observed a remaining fraction between (3 ± 1) % (MM), indicating that most of these particles were readily flushed away, and (102 ± 1) % (PY), showing that these particles were not ruptured off the cells (Fig. 3d, Kruskal–Wallis test: two-sided $P = 2.05 \times 10^{-9}$). The results for the adhesion to coverslips was similar. However generally, the adhesion strength was slightly lower in this case (Supplementary Fig. 6). Particles that strongly adhered to cells also strongly adhered to coverslips and vice versa.

The fraction of remaining particles increased for microplastic particles coated with an eco-corona (MM-SW2, MM-SW4, MM-FW2, and MM-FW4), compared to the respective particles without an eco-corona (MM). For example, the fraction of particles remaining on cells increased from (3 ± 1) % to (24 ± 6) % after two weeks in salt water and to (18 ± 3) % after two weeks in freshwater. After four weeks in salt water, the fraction of remaining particles increased to (28 ± 2) %, and after four weeks in freshwater, the fraction of remaining particles increased to (20 ± 1) %. We observed a similar increase of the fraction remaining particles on coverslips after exposure to salt and fresh water for two and four weeks (Supplementary Figure 6).

The particle-cell and particle-coverslip adhesion was strongly correlated to the microplastic particles' ζ-potential (Fig. 3d, Supplementary Fig. 6). With increasingly negative ζ-potential, the fraction of remaining particles on cells strongly increased (Pearson's $R = 0.95$, two-sided $P = 1.4 \times 10^{-6}$). Overall, the analysis of the number of particles remaining bound to cells even under a hydrodynamic shear force

indicate that the adhesive forces between microplastic particles and cells increase with a more negative ζ-potential, while more neutral particles barely adhered to the cells.

Absolute internalization probability depends on ζ-potential

To investigate whether adhesion is a key determinant for particle internalization, we studied whether particles which adhered stronger to cells had a higher internalization probability. To this end, microplastic particles were added to the cells, which were then incubated 1 h on ice, so that the particles could sediment. Once the particles sedimented, the cells were incubated for 2 h at 37 °C so that they could internalize the microplastic particles. They were then fixed and analyzed using confocal fluorescence microscopy to quantify the number of internalized particles. The conditional internalization probability (Fig. 4a) denotes the probability that a particle is internalized by a cell if it is already attached to the cell. The highest conditional internalization probability was found for MG (77 ± 2) % particles, whereas TS particles had the lowest conditional internalization probability (13 ± 2) %, (Fig. 4a). Particles from the other manufacturers ranged between (27 ± 1) % (PY) and (55 ± 3) % (TJ). Although the microfluidics experiments showed a correlation between the ζ-potential and the adhesion of the particles to cells and coverslips, the conditional internalization probability did not correlate with the ζ-potential (Pearson's $R = -0.2$, $P = 0.6$). However, the probability that a microplastic particle is internalized by a cell depends on both, the probability to adhere to a cell (i.e., the adhesion strength) and the subsequent probability to get
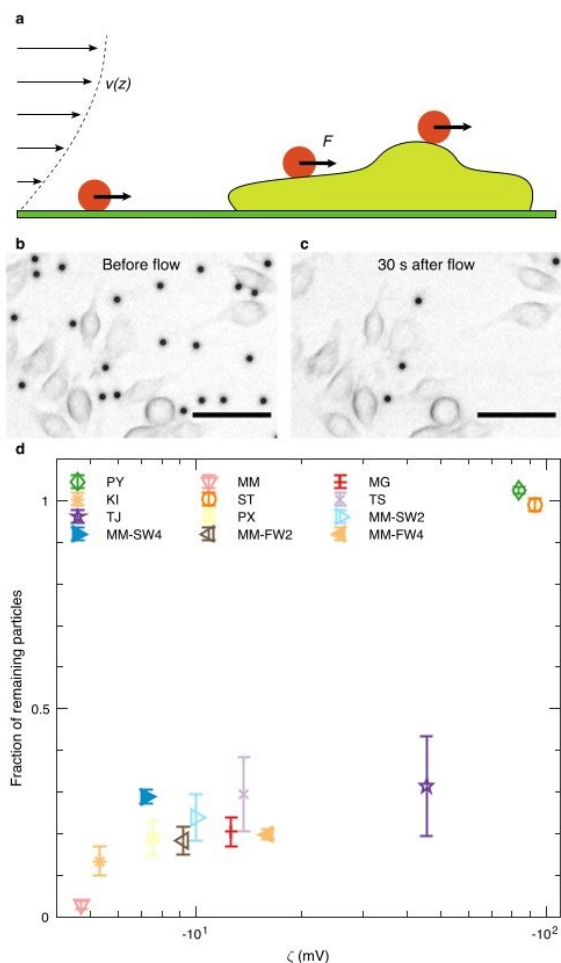
Fig. 3 | Adhesion of microplastic particles to cells under shear force. a After the particles sedimented and bound (red) to the cells (light green) and the coverslip (green) for 10 min in the microfluidic chamber, we turned on a Poiseuille flow with a profile $v(z)$ given by Eq. (15) in our channels, imposing a hydrodynamic force of $F = (50 \pm 5)$ pN (Eq. (7)) on the particles. **b, c** Right before the flow, all particles sedimented and attached to cells or coverslips. We determined the fraction remaining particles after 30 s of flushing. Scale bars: 50 μm. **d** Fraction of particles remaining on cells. The observed fraction of particles remaining on cells significantly differed between samples (Kruskal–Wallis test, two-sided $P = 2.05 \times 10^{-9}$). The adhesion strength of microplastic particles was strongly correlated with their ζ-potential (Pearson's $R = 0.95$, two-sided $P = 1.4 \times 10^{-6}$). While neutral particles barely adhered to cells, the adhesive forces between microplastic particles and cells increased with a more negative ζ-potential. In all panels, error bars represent standard error of mean of $n = 9$ measurements (for each measurement, on average 550 particles were analyzed). Source data are provided as a Source Data file.

Fig. 4 | Conditional and absolute internalization probability of microplastic particles into cells. a The conditional internalization probability displayed as a function of the ζ-potential of the particles indicates no correlation between the two parameters (Pearson's $R = -0.2$, two-sided $P = 0.6$), whereas the absolute internalization probability (**b**) does (Pearson's $R = 0.9$, two-sided $P = 5.4 \times 10^{-5}$). The internalization probability of particles coated with an eco-corona (MM-SW2, MM-SW4, MM-FW2 and MM-FW4) was calculated from the data published by Ramsperger et al.[15]. In (**a**), error bars represent standard error of mean of $n = 3$ replicates (for each replicate, 100 particle-cell interactions were analyzed). The error bars in (**b**) were propagated from the uncertainties in (**a**) and Fig. 3d. Source data are provided as a Source Data file.

internalized if it is bound. Therefore, we determined the absolute internalization probability by multiplying the conditional internalization probability with the fraction of remaining particles (Fig. 4b). The absolute internalization probability varied by almost two orders of magnitude and ranged from (1.1 ± 0.4) % (MM) to (40 ± 2) % (ST). Furthermore, it correlated with the ζ-potential (Pearson's $R = 0.9$, $P = 5.4 \times 10^{-5}$). The MM particles coated with an eco-corona showed a higher absolute internalization probability (MM-SW2: (11 ± 3) %, MM-SW4: (16 ± 2) %, MM-FW2: (8 ± 2) % and MM-FW4: (11 ± 1) %) than the unmodified MM particles without an eco-corona (1.1 ± 0.4) %, which

correlated with the more negative ζ-potential of the environmentally exposed particles (Table 1).

Microplastics internalized via actin-dependent pathways

To verify our results about the internalization of the particles, we performed additional experiments where we investigated the internalization process using live cell imaging. Due to their size, we

expected that the microplastic particles were internalized either by phagocytosis or macropinocytosis. Both internalization mechanisms require remodeling of the actin cytoskeleton, and once the particles are internalized, they undergo a similar maturation process where they interact with lysosomes and become acidified[53–55]. To test this hypothesis, we monitored the actin cytoskeleton during particle internalization by cells that were stably transfected with a LifeAct-GFP construct. Furthermore, we treated the cells with LysoTracker dye, to monitor the subsequent maturation process (Supplementary Fig. 7). We found that all particle types undergo a similar form of internalization and maturation (Supplementary Fig. 8): First, there was a substantial peak in the LifeAct signal around the microplastic particles, indicating that filamentous actin was polymerized. Eventually, the LifeAct signal around the particles decayed, indicating depolymerization of the actin filaments and successful internalization of the microplastic particle. Subsequently, the LysoTracker signal gradually increased over time, showing that internalized microplastic particles underwent a maturation process during which they interacted with lysosomes and were acidified. We found that 100% of the particles that were acidified during the measurement time showed a LifeAct peak before the acidification process started, independent of the microplastic particle type (Supplementary Fig. 9). Overall, these results show that all particle types were internalized via phagocytosis or macropinocytosis.

Discussion

We showed in a systematic approach that the ζ-potential of nominally identical model microplastic particles differed by up to more than one order of magnitude, leading to significant differences in their particle-cell interactions. These differences were likely related to the manufacturing process of the particles, since different methods of polymerization can lead to different functional groups on the surface of the particles, originating from different surfactants, initiators, or catalyzers used[32,56–58]. These differences in microparticle properties are likely not only relevant for particles from different manufacturers, but also for different batches of the same particle type from the same manufacturer. Therefore, it is important to always thoroughly characterize the model microplastic particles that are used.

In previous studies, it has been established that the ζ-potential affects the interactions of nano- and microparticles with cells[6,32,35–37]. However, especially for microparticles, the results were not unanimous. For example, with increasingly negative ζ-potential, both increasing[43,44] and decreasing[41,42] interactions of microparticles and cells have been reported. We provide deeper insight here, since we systematically analyzed the cellular interactions of twelve different microparticle types spanning a wide range of ζ-potentials from −4.7 mV to −93.1 mV., We individually assessed the role of the ζ-potential for the microparticle binding kinetics, adhesion strength, conditional internalization probability, and absolute internalization probability.

Using our multiplexed single-cell single-particle microfluidic platform, we quantified the binding kinetics during the sedimentation of the particles, and the particles remaining attached upon exertion of 50 pN hydrodynamic force. Our results indicate that polystyrene microplastic particles of the same size and shape with a more negative ζ-potential bound faster, unbound slower, and adhered stronger to the cells. Overall, these measurements agree with previous studies on the adhesive forces of different particle types. Using magnetic tweezers Chen et al.[59] reported adhesion forces of about 15 pN between the particles and coverslips for polystyrene microplastic particles coated with extracellular polymeric substances (EPS). Using much larger 10 µm sized particles, Liu et al.[42] quantified adhesive forces by atomic force microscopy (AFM) between PLA, PLGA, and PELA microparticles and cells. These measurements yielded adhesion forces of 1.63 nN (PLGA), 1.85 nN (PELA), and 2.38 nN (PLA). These forces were higher

than in our study, likely because a much larger particle size that was used in that study (11 times larger surface area than our particles) and due to the measurement method applied. With our approach, the microplastic particles sedimented freely onto cells and coverslips, whereas in AFM measurements, they were pushed with a force of several nN onto the cells, potentially leading to a larger contact area and therefore stronger interactions between particles and the cell membrane[60]. Furthermore, the forces were oriented differently in both experiments. Whereas with the AFM the forces were exerted perpendicular to the cell surface, they were oriented parallel to the surface in our approach.

In general, electrostatic interactions quantified by the ζ-potential or the specific binding of ligands to membrane receptors can mediate particle-cell binding and adhesion[61]. In our experiments, we observed similar particle-cell and particle-coverslip adhesion strengths. The fact that the particles' binding strength both to cells and coverslips was strongly correlated with their ζ-potential indicates that local electrostatic interactions between the charged groups on microplastic particles and the cell membrane (presumably supported by multivalent ions from the medium[43]) are highly important for their binding strength.

This might be also true for the coating with biomolecules from salt and freshwater forming an eco-corona on the surface of a microplastic particle. We showed in previous works that environmental exposure substantially alters the surface of microplastic particles and leads to the formation of an eco-corona[15,52]. In this study, we additionally performed SEM imaging, STXM, and XPS to further quantify the eco-corona structure and constituents. The constituents creating an eco-corona on the surface of a microplastic particle were previously described as proteins, humic and fulvic acids, amino acids, lipids, polysaccharides, and carbohydrates[15,62–64]. Consistently, the STXM measurements showed an increase in proteins and sugars on the surface of freshwater-exposed microplastic particles, and the XPS measurements indicated the presence of organic nitrogen on salt and freshwater-exposed microplastic particles. Molecules like humic and fulvic acids have multiple carboxylic groups, carrying negative charges[65–67]. As these make up the largest fraction of natural organic matter[68], they potentially caused the more negative ζ-potential of the environmentally exposed microplastic particles in our study. Therefore, different charged sites and different densities of the charged sites on the surface of the particles lead to different electrostatic forces between particles and cellular membranes and between particles and coverslips.

This is in concordance with earlier works that already indicate that the adhesion of a particle to cellular membranes is mainly driven by the surface charge of a particle[43,69,70]. However, the cellular membrane overall has a negative surface charge, which led to the widely accepted assumption that the binding of positively charged particles to cellular membranes is more likely than the binding of negatively charged particles[69,71,72]. Nevertheless, there already was evidence that also negatively charged particles can bind to cellular membranes[43,71,72]. The binding of negatively charged particles to on average negatively charged cell membranes is potentially supported by a heterogeneous surface charge of cells. Perry et al.[39] demonstrated that the surface of human adipocytes is locally positively charged, with µm-sized patches with charge densities of up to 50 mC m^{-2}, among areas with an average negative charge density of −15 mC m^{-2}. Furthermore, in the presence of multivalent positive ions, overcharging of the negative surfaces can occur[73,74]. Overcharging describes the process, when a multivalent positive ion is attracted by a monovalent negative surface group. This leads to a local overcompensation of the negative surface charge. This mechanism is also involved in the Schulze-Hardy rule that describes the limits of colloidal stability in solutions of multivalent ions[75–77]. Therefore, particles with a more negative ζ-potential may interact stronger with the cells. However, some microplastic particle types,

which had similar ζ-potentials, differed slightly in their binding kinetics and adhesion. These differences may reflect ligand-receptor interactions, for example due to binding of the polystyrene or surfactants to scavenger receptors[78].

Furthermore, in the environment, microplastics are exposed to numerous natural factors such as UV irradiation[79] and eco-corona formation[15,80] which can change its ζ-potential and therefore its interactions with cells. Consistently, we observed that the eco-corona-coated microplastic particles had a more negative ζ-potential compared to the uncoated particles, and therefore also a higher binding strength. Additionally, the higher mobility of the charged groups in the eco-corona may facilitate an optimal arrangement of the charged groups on the incubated particle and the coverslip or cells. The higher portion of optimally aligned charged groups can therefore increase the adhesion force and subsequent internalization.

We showed that the microplastic particles were internalized either by phagocytosis or macropinocytosis. For phagocytosis, the adhesion of microplastic particles to cells is a prerequisite for their internalization. In the case of macropinocytosis, both particles that adhered to the cell membrane and freely diffusing particles can be internalized. However, the probability of macropinocytosis is higher for particles adhered to the cell surface since their residence time in the direct vicinity of the cell is increased compared to freely diffusing particles. Therefore, the internalization of microplastic particles can be regarded as a two-stage process[38]. First, the microplastic particles adhere to the cell membrane. Second, the attached particles are internalized. Here, we demonstrated that microplastic particle-cell adhesion is strongly determined by the ζ-potential of the particles. However, the conditional internalization probability of the different microplastic particles did not correlate with the ζ-potential. This may indicate that for the process of internalization, unspecific electrostatic forces play a minor role, whereas the biological identity of a particle plays a larger role for the internalization.

Depending on the particles' surface groups, macrophages can internalize for example polystyrene, silicon, and metal microparticles via scavenger receptor-mediated phagocytosis[78,81,82]. Unlike phagocytosis, which is tightly controlled by these receptor-ligand interactions, macropinocytosis is a more stochastic process. Nevertheless, it is not completely receptor-independent, as some receptors like EGFR can enhance the formation of membrane ruffles, which lead to increased rates of macropinocytosis[83,84]. Therefore, different chemical surface groups of the microplastic particles in our study might affect their interactions with different macrophage receptors, leading to varying conditional internalization probabilities. However, since adhesion facilitates particle internalization, the absolute internalization probability was strongly correlated with the ζ-potential.

Furthermore, biomolecules present in the eco-corona of microplastic particles may enhance internalization. Such biomolecules have been reported to trigger endocytic pathways such as scavenger-receptor mediated phagocytosis, increasing the overall conditional internalization probability[15,85,86]. Consistently, we observed an increased conditional internalization probability for the eco-corona particles (MM-FW2, MM-FW4, MM-SW2, and MM-SW4) compared to pristine particles (MM) without an eco-corona. Additionally, internalization of environmentally exposed microplastic particles is enhanced due to the increased particle-cell binding affinity.

Because of this two-step internalization process, particle-cell adhesion is a very important part for particle internalization. It has been reported that adhesion and internalization are prerequisites for cytotoxicity[32]. Thus, at similar concentrations, particles with a more negative ζ-potential can potentially be more toxic than particles with a ζ-potential close to 0, since interactions with cells are more likely[32]. To ensure that ecotoxicological studies on microplastics are comparable with each other, it will be of utmost importance to thoroughly characterize the model microplastic particles that are used, because even

nominally identical particles can strongly differ in their ζ-potential. We want to emphasize that this is also relevant for experiments using the same particle type from the same manufacturer, as batch-to-batch variations may occur. This will be equally relevant for effect studies using other polymer types, as these can similarly differ in their ζ-potential[80]. Furthermore, the ζ-potential of microplastic particles can additionally be modified by the adsorbed biomolecules forming an eco-corona. Therefore, the environmental exposure in complex ecosystems likely affects the hazard potential of the microplastic particles, making further studies in this direction necessary.

With our study we highlight that nominally identical particles from various manufacturers differ in their ζ-potential and in their interactions with cells. We identified the ζ-potential as one of the major drivers for particle-cell adhesion and consequently the absolute internalization probability. We also demonstrated that environmental exposure of microplastic particles alters their ζ-potential and thus their internalization probability as well. With our microfluidic approach, we enable an efficient quantification of the binding kinetics and adhesion strength of single particles attached to single cells in a highly multi-plexed manner. Due to the importance of the ζ-potential for the absolute internalization probability, the choice of model microplastics may drastically impact the results of microplastic effect studies, since cellular interactions and internalization of microplastic particles are one prerequisite for their toxicity[32,87]. As the ζ-potential of microplastic particles additionally changes with the formation of an eco-corona, the environmental exposure in complex ecosystems likely affects the hazard potential of microplastic particles.

Methods
Microplastic particles
Polystyrene particles were purchased from the following different manufacturers: Polysciences, Inc. (Warrington, PA), Micromod Partikeltechnologie GmbH (Rostock, Germany), Microparticles GmbH (Berlin, Germany), Kisker Biotech GmbH & Co.KG (Steinfurt, Germany), Spherotech Inc. (Lake Forest, IL), ThermoFisher Scientific Inc. (Waltham, MA), Tianjin BaseLine Chromatographic Technology (Tianjin, China) and Phosphorex, Inc. (Hopkinton, MA) (see Table 1). Particles obtained from Tianjin BaseLine Chromatographic Technology were provided as a powder, whereas all other particles were provided in an aqueous solution. The particles from Tianjin BaseLine Chromtech were dispersed in ultrapure water.

Environmental exposure
Microplastic particles from Micromod Partikeltechnologie GmbH (MM, see Table 1) were exposed to environmental media as described by Ramsperger et al.[15] 100 μL of the particle stock solution was dispersed in 900 μL environmental media (salt water from a sea water aquarium and freshwater from an outside freshwater pond) in a 1.5 mL autosampler vial. To prevent sedimentation of the particles, the vials were placed on a sample roller. To keep the microbial communities in the respective media intact, the salt water and freshwater was replaced 3× per week. For that, samples were centrifuged for 20 min at 2000× g, 900 μL of the supernatant was discarded and replaced with 900 μL of fresh environmental media. Microplastic particles were incubated for 2 and 4 weeks, respectively.

Microplastic particle characterization
Scanning electron microscopy. To investigate the surface structures of microplastic particles, samples were analyzed using a scanning electron microscope (SEM, FEI Apreo Volumescope, Thermo Fisher Scientific, 5 kV, working distance 10 mm, Everhart-Thornley detector for qualitative images; 3 kV, WD 5 mm, T1 in-lens detector for quantitative analysis). First, each stock solution of the microplastic particles was diluted in ultrapure water (1:100), and 100 μL of this dilution was pipetted onto a silicon wafer placed on carbon conductive tabs (Ø

12 mm Plano GmbH, Wetzlar, Germany) fixed to aluminum stubs (Ø 12 mm, Plano GmbH, Wetzlar, Germany). To preserve the eco-corona, the environmentally exposed beads were fixed using Karnovsky's fixative (2% PFA (reagent grade, Sigma Aldrich, Merck KgA, Germany) and 2.5% glutaraldehyde (for electron microscopy, Carl Roth GmbH, Germany) in 1× PBS) prior to dehydration in an ethanol series (30%, 50%, 70%, 80%, 90% for 30 min each, 95% and absolute ethanol for 1 h each, Ethanol purity >99.9%, VWR International S.A.S., France) and dried in hexamethyldisilazane (HMDS, purity > 98%, Carl Roth GmbH, Germany)[88]. The stubs were then transferred into a desiccator and stored until the images were acquired. Samples were subsequently coated with a 4 nm-thick platinum layer (208HR sputter coater, Cressington, Watford, UK) and analyzed using the SEM.

SEM micrographs (pixel size: 2.08 nm) were analyzed quantitatively using a custom-coded SEMParticleAnalyzer MATLAB program. The micrographs were filtered using a median filter with a radius of 3 pixels. To automatically detect the microplastic particles in the micrographs, the gradient of the images was calculated. This gradient image was binarized by choosing a suitable threshold, usually around 30–35% of the maximal pixel value. Then, binary components were dilated by 5 pixels, and remaining holes were filled. The resulting binary components were eroded by 5 pixels. Components smaller than 5×10^5 pixels (equivalent diameter of 1 μm) and components touching the border of the image were discarded.

To analyze the particle properties, the equivalent diameter, major axis length, minor axis length, and the perimeter of the particles were evaluated using the regionprops() function of MATLAB. We analyzed the equivalent diameter, the eccentricity, and the roughness of the particles. We defined the eccentricity as the quotient of the major and minor axis length. An eccentricity value of 1 would correspond to perfectly spherical particles, larger values indicate aspherically shaped particles. The roughness was defined as the particles' perimeter divided by the perimeter of a circle with the same equivalent diameter. Roughness values of 1 indicate perfectly smooth surfaces, larger values indicate an increased surface roughness. Due to the median filtering and dilation/erosion during image segmentation, only surface irregularities on length scales larger than 10 nm were detected.

ζ-Potential. ζ-potential was measured with a Zetasizer Nano ZS (Malvern Panalytical, Worcestershire, UK) at 24 °C after an equilibration time of 120 s. The ζ-potential was obtained by 3 single measurements with 50 runs each lasting 1 s. Particles were dispersed in 1 mM KCl. The pH in the samples ranged from 5.5 to 6.1, and the conductivity from 0.18 mS cm^{-1} to 0.22 mS cm^{-1}. To measure the influence of an incubation of the particles in cell culture media, the particles were incubated for 2 h in 9 mL cell culture media at a concentration of 1.5×10^6 particles mL^{-1}. After the incubations, particles were centrifuged for 20 min at 2000× g, washed 1× in 1 mM KCl, and resuspended in 1 mL 1 mM KCl. Then, their ζ-potential was measured as described above. The pH in the incubated samples ranged from 5.4 to 6.7, and the conductivity from 0.16 mS cm^{-1} to 0.21 mS cm^{-1}.

Synchrotron-based scanning transmission X-ray microscopy. Samples for STXM analysis were gently rinsed in DI water to avoid salt precipitation during drying. Samples were wet deposited from aqueous suspensions onto formvar coated 300 mesh Cu TEM grids, blotted and dried immediately. Samples were analyzed at beamline 10ID-1 at the Canadian Light Source. Image stacks across the C1s absorption edge were recorded between 275 and 340 eV with 0.1 eV steps in the energy region of interest. Images were aligned and converted from transmission to linear absorbance scale (optical density (OD)) using aXis2000[89]. The surface regions were selected in the STXM images based on the average optical density (OD) range of 0.1–0.9 across the C1s absorption edge, which is equivalent to a cumulative

thickness of up to 100 nm, arranged tangentially around the PS particles. The equivalent thickness was calculated using the atomic scattering factors[90], the formula C_8H_8 and an assumed density of 1.09 g cm^{-3} of the polystyrene. All 3 spectra were decomposed into a sum of individual gaussian peaks plus the ionization edge modelled as an arctan function. A minimum of 7 analytical peaks was required and used for fitting the respective spectra: 284.0 eV (quinone C = O), 285.0 and 285.4 eV (aromatic C = C), 287.4 eV (aliphatic C-C), 288.2 eV (protein C-O), 288.9 eV (carboxylic C-O), 289.5 (polysaccharide C-O). Peak energies and widths were optimized and fixed at the same values for all 3 spectra, whereas the respective peak areas were fitted using the peak fitting algorithm of Athena[91].

X-ray photoelectron spectroscopy. All XPS studies were carried out by means of an Axis Ultra photoelectron spectrometer (Kratos Analytical, Manchester, UK). The spectrometer was equipped with a monochromatic Al K-alpha (1486.6 eV) X-ray source of 300 W at 15 kV. The kinetic energy of photoelectrons was determined with hemispheric analyzer set to pass energy of 160 eV for wide-scan spectra and 20 eV for high-resolution spectra. During all measurements, electrostatic charging of the sample was avoided by means of a low-energy electron source working in combination with a magnetic immersion lens. Later, all recorded peaks were shifted by the same value that was necessary to set the component peak of the sp^3-hybridized carbon atoms to 285.00 eV. The polystyrene particles were deposited as a particle film from their aqueous suspension on a thermally oxidized silicon wafer. Quantitative elemental compositions were determined from peak areas using experimentally determined sensitivity factors and the spectrometer transmission function. The spectrum background was subtracted according to Shirley[92]. The high-resolution spectra were deconvolved by means of the Kratos spectra deconvolution software. Free parameters of component peaks were their binding energy (BE), height, full width at half maximum and the Gaussian-Lorentzian ratio.

Cell lines and cell culture conditions. Murine macrophage J774A.1 cells (DSMZ, Braunschweig, Germany) and a stable J774A.1 cell line transfected with a LifeAct-GFP construct[93] were cultured under standard culture conditions (37 °C, 5% CO$_2$, humidified) in Dulbecco's Modified Eagle's Medium (DMEM, Thermo Fisher Scientific Inc., Waltham, MA), supplemented with 10% (v/v) FCS (Thermo Fisher Scientific Inc., Waltham, MA) and 1% penicillin/streptomycin (Thermo Fisher Scientific Inc., Waltham, MA)[15,94]. To maintain suitable cell concentrations, cells were passaged three times per week and cultured in T-25 culture flasks (CORNING, New York, USA).

Microfluidics. Custom-built flow chambers were used to quantify the adhesion strength between microplastic particles and cells. Flow chambers were built from a plastics top part (sticky-Slide I Luer, nominal channel height 0.1 mm, nominal width 5 mm, nominal length 48 mm, ibidi GmbH, Gräfelfing, Germany), which was glued to a glass coverslip (24 mm × 60 mm, #1, Menzel Gläser, Thermo Fisher Scientific Inc., Waltham, MA) with a thin film of epoxy resin one day before the experiments.

Prior to the microfluidic experiments, the cells from culture stocks were scraped off the culture flasks into the culture medium, centrifuged (150× g, 2 min, 20 °C) and re-suspended with 600 μL of cell culture medium. Into each flow chamber, 200 μL of cell suspension was added and transferred back into the incubator at 37 °C and 5% CO$_2$ for 1 h until the cells adhered to the bottom coverslip of the flow chamber.

Live cell imaging was performed with a frame rate of 1 Hz on an inverted, motorized microscope (Nikon Eclipse Ti, Nikon, Tokyo, Japan) with a 10× objective (CFI Plan Fluor DL 10×, Nikon, NA = 0.3), which was equipped with a CCD camera (pco.pixelfly usb, PCO AG,

Kehlheim, Germany). The microscope body was enclosed in a custom-built incubation chamber which keeps the body of the microscope and the sample at a temperature of 37 °C. A high precision linear stage (L511.20DG10, Physik Instrumente, Karlsruhe, Germany) was used to drive the piston of a syringe ($r_{\text{piston}} = 6.135\,\text{mm}$) with a controlled motor velocity v_m to control the flow in the chamber. The syringe was connected to the flow chamber with a tubing system, in which check valves (RVMINI-32, Piper Filter GmbH, Zwischenahn, Germany) were used similarly to the way diodes are used to build a bridge rectifier in an electrical circuit to ensure the flow direction inside the chamber stays the same after the motor reverses its direction. The motor and the camera were controlled with a custom-written MATLAB program (MATLAB 2019b, The MathWorks Inc, Natick, MA), which was used to set the motor velocity according to the channel geometry and the desired force of 50 pN exerted on the particles during the experiments. Thus, even though the geometry of different channels differed slightly, we were able to exert reproducible forces on particles in different channels.

All microfluidic experiments were performed in imaging medium (Minimum Essential Medium), (Thermo Fisher Scientific Inc.) supplemented with 5% HEPES (Thermo Fisher Scientific Inc.) as a pH buffer and 1% penicillin-streptomycin. The medium was pre-warmed to 37 °C overnight to free it from dissolved gas and avoid bubble formation during the experiments. The microparticles were added to the microfluidic system and were briefly dispersed in the microfluidic system right before the first experiment started. Furthermore, we repeated the experiments 40 min and 80 min after the particles were added to the microfluidic system. Each time series for each particle type was replicated three times, yielding 9 experiments per particle type. For each experiment, on average 550 particles were analyzed.

Derivation of the hydrodynamic drag force on the microparticles

Poiseuille flow in a rectangular channel. The laminar flow in a rectangular channel with length L, width w and height h (Supplementary Fig. 10) has the velocity profile[95,96]

$$v_x(y,z) = \frac{4h^2 \Delta p}{\pi^3 \eta L} \sum_{n,\text{odd}}^{\infty} \frac{1}{n^3} \left[1 - \frac{\cosh\left(n\pi \frac{y}{h}\right)}{\cosh\left(n\pi \frac{w}{2h}\right)} \right] \sin\left(n\pi \frac{z}{h}\right), \quad (1)$$

whereby $-\frac{w}{2} \leq y \leq \frac{w}{2}$ and $0 \leq z \leq h$ are the coordinates in the channel cross section. ρ is the density of the fluid and η is the dynamic viscosity of the fluid. Δp is the pressure drop along the x-direction, which is defined by the volume flow rate Q[96]:

$$\Delta p = \frac{12\eta L Q}{wh^3} \left[1 - \sum_{n,\text{odd}}^{\infty} \frac{192h}{n^5 \pi^5 w} \tanh\left(n\pi \frac{w}{2h}\right) \right]^{-1} \quad (2)$$

Estimation of the expected force on the particle. If a spherical particle is located in the center of the chamber ($y = 0$), it experiences a drag force due to the laminar fluid flow. This drag force is first estimated with Stokes drag using the flow velocity at the sphere center. To approximate this velocity, the channel is assumed to have infinite width $w \gg h$, meaning the Poiseuille flow is approximated to be only two-dimensional (2D):

$$v_x(z) = \frac{\Delta p w}{2\eta L} \left(\left(\frac{h}{2}\right)^2 - \left(z - \frac{h}{2}\right)^2 \right). \quad (3)$$

The pressure gradient Δp for a given volume flow rate Q is then:

$$\Delta p = \frac{12\eta L Q}{wh^3} \quad (4)$$

In this model system, we place the spherical particle directly at the bottom wall of the channel and neglect the effect of the cell on the flow. To approximate the viscous drag force on the sphere, we evaluate the velocity at the center of the sphere at $z = r$, i.e. one sphere radius away from the bottom wall at $z = 0$, resulting in

$$v_x(z = r) = \frac{\Delta p w}{2\eta L} \left(\left(\frac{h}{2}\right)^2 - \left(r - \frac{h}{2}\right)^2 \right) = 6Q\frac{r(h-r)}{wh^3} \quad (5)$$

which is inserted in the Stokes drag force on a sphere ($F = 6\pi\eta r v$):

$$F \approx 36\,\pi\eta Q \frac{r^2(h-r)}{wh^3} \quad (6)$$

This approximation represents a lower estimate of the hydrodynamic force on the particle in our experiments. Firstly, the channels used in this work had a slightly parabolic height profile $h = h(y)$, which leads to an increased flow velocity in the center of the channel compared to a rectangular channel geometry. Secondly, the presence of the channel wall modifies the force estimate from Eq. (6) which strictly holds in an infinite medium only. As the force on the particle is directly proportional to the flow velocity in the vicinity of the particle, we account for both effects by two correction factors C_1 and C_2, which will be derived in the following sections.

$$F \approx 36 C_1 C_2\,\pi\eta Q \frac{r^2(h-r)}{wh^3} \quad (7)$$

Equation (7) was used to calculate the required motor velocity v_m to achieve a force of 50 pN using the relation

$$v_m = \frac{Q}{\pi r_{\text{piston}}^2} \quad (8)$$

Influence of the parabolic height profile: Derivation of C_1. At a given pressure drop Δp, the flow rate Q in a long, rectangular channel is given by Bruus[96]:

$$Q(h,w,L) = \frac{h^3 w \Delta p}{12\eta L} \left[1 - \sum_{n,\text{odd}}^{\infty} \frac{192 h}{n^5 \pi^5 w} \tanh\left(n\pi \frac{w}{2h}\right) \right]. \quad (9)$$

The channels that we used were not perfectly rectangular but had a slightly curved shape at the top along the y axis, which could be approximated with a parabola. In this case, the channel height is given by:

$$h(y) = h_0 + \alpha y + \beta y^2. \quad (10)$$

Typically, the channels were 150 to 200 μm high in the middle and about 10 to 20 μm thinner near the side walls. To attribute for this, we calculated the corrected pressure drop in the channel in the following manner. When the boundary effects of the side walls of the channel are negligible, i.e. $h/w \to 0$ Eq. (9) can be simplified to:

$$Q \approx \frac{h^3 w \Delta p}{12\eta L}. \quad (11)$$

The total flow rate through a channel with a parabolic height profile can be approximated as the sum of flow rates through infinitesimally thin rectangular channels with varying height, considering only the boundary effects at the bottom and at the top of the infinitesimally thin channels with width dy:

$$Q \approx \int_{y=-w/2}^{w/2} dQ = \int_{y=-w/2}^{w/2} \frac{h(y)^3 \Delta p_{\text{par}}}{12\eta L}\, dy. \quad (12)$$

Comparing Eqs. (11, 12), we can identify the effective channel height of the curved channel as:

$$h_{\text{eff}} = \left(\frac{1}{w} \int_{y=-w/2}^{w/2} h(y)^3 \, dy \right)^{1/3}$$

$$= \left[h_0^3 + \frac{1}{4} h_0^2 \beta w^2 + \frac{1}{4} h_0 \alpha^2 w^2 + \frac{3}{80} h_0 \beta^2 w^4 + \frac{3}{80} \alpha^2 \beta w^4 + \frac{1}{448} \beta^3 w^6 \right]^{1/3}.$$

$$(13)$$

Taking the full channel profile into account, we model the pressure drop in the curved channel at a given flow rate by:

$$\Delta p_{\text{par}}(h_{\text{eff}}) \approx \frac{12 \eta L Q}{h_{\text{eff}}^3 w} \left[1 - \sum_{n,\text{odd}}^{\infty} \frac{192 h_{\text{eff}}}{n^5 \pi^5 w} \tanh\left(n\pi \frac{w}{2 h_{\text{eff}}} \right) \right]^{-1}, \quad (14)$$

and consequently, the velocity profile in a parabolic channel is approximated in analogy to Eq. (1):

$$v_{x,\text{par}}(y,z) \approx \frac{4 h(y)^2 \Delta p_{\text{par}}(h_{\text{eff}})}{\pi^3 \eta L} \sum_{n,\text{odd}}^{\infty} \frac{1}{n^3} \left[1 - \frac{\cosh\left(n\pi \frac{y}{h(y)} \right)}{\cosh\left(n\pi \frac{w}{2h(y)} \right)} \right] \sin\left(n\pi \frac{z}{h(y)} \right),$$

$$(15)$$

This approximation corrects for the pressure change due to the parabolic height profile and ensures that the velocity at the boundary of the channel is 0. Thus, the velocity correction factor C_1 can be approximated by:

$$v_{x,\text{par}}(y,z) \approx \frac{\Delta p_{\text{par}}(h_{\text{eff}})}{\Delta p(h_0)} v_x(y,z). \quad (16)$$

Since Δp_{par} was always larger than Δp in our experiments, at the given flow rate Q in the experiment, the velocity in the center $v_x(0,z)$ was always larger than it would have been if the channel had been rectangular with a height h_0. Since the force on the particle is proportional to the velocity in the channel, C_1 can be identified to be:

$$C_1 \approx \frac{\Delta p_{\text{par}}(h_{\text{eff}})}{\Delta p(h_0)}. \quad (17)$$

Assuming that $h_{\text{eff}} \ll w$, C_1 simplifies to:

$$C_1 \approx \frac{h_0^3}{h_{\text{eff}}^3}. \quad (18)$$

The chambers used during the experiments had a typical height in the range between 150 and 175 μm. Typically, h_0 was on the order of 165 μm, h_{eff} was about 155 μm and consequently, C_1 was about 1.2, indicating that the force increased by about 20%. Thus, the height profile was measured for every channel before the experiment by focusing on the top and on the bottom layer of the channels with a 40× water immersion objective and by noting the z positions of the (motorized) objective. We validated the resulting velocity profile experimentally and tested whether the velocity inside the channel scales linearly with the flow rate (Supplementary Note 2, Supplementary Figs. 11, 12).

Influence of the particle on the flow profile: Derivation of C_2 via lattice Boltzmann method simulations. The correction factor C_2 for the force on the particle (see Eq. (7)) was determined by lattice Boltzmann method (LBM) simulations with the software FluidX3D[97]. To reduce floating-point errors and improve the overall accuracy, units were converted from SI-units to simulation units and back. To distinguish these two-unit systems, we introduced the superscripts "SI" and "sim".

A spherical microplastic particle with radius $r^{\text{SI}} = 1.5\,\mu$m was adhered to the bottom center of a rectangular microchannel with the dimensions (19.0,1.0,0.1) mm. The flow rate was $0.1\,\mu$L s$^{-1} \le Q^{\text{SI}} \le 50.0\,\mu$L s^{-1}. For the fluid, we assumed the density and viscosity of water at $T^{\text{SI}} = 37\,^\circ$C. In SI-units the given parameters were: Particle radius $r^{\text{SI}} = 1.5 \times 10^{-6}$ m; channel dimensions $L^{\text{SI}} = 19.0 \times 10^{-3}$ m, $w^{\text{SI}} = 1.0 \times 10^{-3}$ m, $h^{\text{SI}} = 0.1 \times 10^{-3}$ m; volume flow rate $Q^{\text{SI}} = [0.1, 50.0] \times 10^{-9}$ m^3 s^{-1}; fluid density $\rho^{\text{SI}} = 993.36$ kg m^{-3}; fluid dynamic viscosity $\mu^{\text{SI}} = 0.6922 \times 10^{-3}$ kg m^{-1} s^{-1}; fluid kinematic shear viscosity $\nu^{\text{SI}} = \frac{\mu^{\text{SI}}}{\rho^{\text{SI}}} = 6.968 \times 10^{-7}$ m^2 s^{-1}. The force on the particle was then computed as the sum of the forces on all lattice points making up the particle[97] and the simulation was run until the force value converges.

The simulations were conducted with the FluidX3D software[97–99] on an AMD Radeon VII graphics processing units (GPUs) with 16 GB memory. With these memory limitations in mind, we simulated only the neighborhood of the particle and at the edge of the simulation domain. We set the velocity via moving bounce-back boundaries[97]. The simulation box dimensions were

$$L_{\text{box}} = w_{\text{box}} = k\,r \quad (19)$$

$$h_{\text{box}} = \left(\frac{k}{2} + 1 \right) r \quad (20)$$

with $k = 16$ being chosen as large as GPU memory allows. At $z = 0$ there was a non-moving boundary representing the bottom channel wall. The other simulation box boundaries did not coincide with the channel boundaries. The particle was placed at

$$\mathbf{x}_0 = \left(\frac{L_{\text{box}}}{2}, \frac{w_{\text{box}}}{2}, r + 1 \right)^T \quad (21)$$

Setting the velocity at the simulation box boundaries (other than at $z = 0$ to $\mathbf{v}_x(y,z)$ (Eq. (15))) would enforce straight streamlines at the boundaries, thereby artificially constricting the flow and increasing the force on the particle (case A). However, we also could not set the boundary velocity to the analytic velocity for a laminar flow around a sphere with the z-dependent Poiseuille flow velocity $\mathbf{v}_x(y = 0, z)$, as this would not constrict the flow even infinitely far away from the particle, so the force would be too small (case B).

In the rectangular channel, the channel walls enforce straight streamlines. To minimize the difference of the force between the cases A and B, which confine the possible force corridor, the boundaries must be as far away as possible, but the particle still must be resolved sufficiently, so we chose $r^{\text{sim}} = 16$ as a compromise for all simulations. The true force is somewhere in between the forces given by case A and case B and an interpolation of the velocities of both variants will give the best results (case C). We determined the interpolation factor as the volume fraction of the simulated volume to the total volume of the microchannel. The interpolation factors used in case C for the velocity boundaries at $r^{\text{sim}} = 16$ were $\eta(v_A) = 11.39\%$ and $\eta(v_B) = 1 - \eta(v_A) = 88.61\%$.

We ran simulations for a volume flow rate of $Q^{\text{SI}} \in \{0.1, 1.0, 2.0, 3.0, 4.0, 5.0, 7.0, 10.0, 15.0, 20.0, \ldots, 50.0\}\,\mu$L s^{-1} for the boundary definitions (A), (B) and (C). During each set of simulations, we kept the velocity v^{sim} in simulation units constant while varying the kinematic shear viscosity ν^{sim} in simulation units to prevent too small v^{sim} and large variations in ν^{sim} that would decrease the simulation accuracy. By setting $\nu^{\text{sim}} = 1$ for the midway flow rate $Q^{\text{SI}} = 25\,\mu$L s^{-1}, we determined the corresponding velocity

$$v_x^{\text{sim}} = \frac{\nu^{\text{sim}} r^{\text{SI}}}{\nu^{\text{SI}} r^{\text{sim}}} v_x^{\text{SI}} \left(y^{\text{SI}} = 0, z^{\text{SI}} = \frac{h^{\text{SI}}}{2}, w^{\text{SI}}, h^{\text{SI}}, Q^{\text{SI}} \right) \quad (22)$$

in simulation units at the channel center for all simulations in one row. This velocity was numerically evaluated to be $v_x^{\text{sim}}(y = 0, z = \frac{h^{\text{sim}}}{2}) =$

0.053846 and the fluid velocity in simulation units at the center of the particle was numerically evaluated to be $v_x^{\text{sim}}(y=0, z=r^{\text{sim}}) = 0.003182$ for all Q^{SI}. When during the simulation row Q was varied, the kinematic shear viscosity in simulation units varied between $\nu_x^{\text{sim}} \in [0.5, 250.0]$ for $Q^{\text{SI}} \in [0.1, 50.0]\,\mu\text{L s}^{-1}$, while Q^{sim} remained constant. Our Radeon VII GPUs allowed for $k = 36$ at $r^{\text{sim}} = 16$ or a box size of (576, 576, 304).

The force increases linearly with the flow rate in agreement with the prediction of Eq. (7) (Supplementary Fig. 13). We fitted $F(Q)$ with Eq. (7) with $C_1 = 1$, to get the correction factor C_2:

$$C_2 = 1.618 \pm 0.002 \tag{23}$$

Analysis of the microfluidics experiments

To quantify the transition kinetics between the bound and unbound state during the sedimentation phase, the particles were detected in every frame with a custom-written MATLAB algorithm. The detection algorithm was based on cross correlation, comparing the frames in the video with a reference image of a particle. Local maxima in the correlation image were detected with a custom-written peak finding routine. To achieve subpixel resolution, a 2-dimensional Gaussian function was fitted to every peak. Then, the particles were tracked with uTrack 2.3[100-102]. The derivative of the position vector was calculated to determine the instantaneous velocity of the particles, which was subsequently filtered with a symmetric median filter of ±15 s (which amounts to 31 subsequent frames) to reduce positioning noise. Particles were defined to be bound when the median filtered velocity was below $0.25\,\mu\text{m s}^{-1}$ and unbound when it exceeded this threshold. This threshold is well suited to separate both regimes as it minimizes the number of motion state changes both for highly adhesive and non-adhesive particles (see Supplementary Fig. 14). For further analysis, the trajectories were filtered with the following conditions to exclude tracking errors:

- Only particle trajectories which started during the sedimentation phase were used to exclude particles which happened to bind before the sedimentation phase.

- Only trajectories of particles which were unbound in the first frame were used. This excluded tracking errors in cases where a particle is lost and retracked, but already bound, which would lead to an underestimation of the fraction of irreversible binding events.

- Furthermore, only trajectories which did not end earlier than 5 s before the start of the rupture phase were used for evaluation. As by experiment design, particles never vanish during the sedimentation phase, this excludes further tracking errors when a particle was lost by the tracker during the sedimentation phase.

- To remove particle clusters, particles which were closer than $4.5\,\mu\text{m}$ to another particle for more than 30 s were excluded from the data analysis.

Examples of trajectories and the classification of their respective binding state are given in Supplementary Fig. 15.

To determine whether a particle is close to a cell or close to a coverslip, we used the convolutional neural net GoogLeNet[103] pretrained with the ImageNet database[104]. We adapted the network to our needs using transfer learning[105] by replacing the 'loss3-classifier'-layer with a custom fully-connected-layer with an output size of 2, representing whether or not the particle is close to a cell. As input images, we cropped subimages of $52 \times 52\,\mu\text{m}^2$ around every particle, showing the particle in the center along with its nearest environment. The subimages were scaled to match the input size of GoogLeNet. In total, 1560 manually classified subimages of particles close to cells and 1560 manually classified subimages of particles close to the coverslip were

used for training (Supplementary Fig. 16) and about 400 images of each of the two categories were used as validation data. Both data sets were augmented by random reflection, rotation, scale, slight shear of up to 15°, and slight translation of up to $1.5\,\mu\text{m}$ to regularize the training process[106]. Adaptive moment estimation[107] was used to train the network. Particles manually classified to be close to a cell were classified identically in 96.6% of the cases by the network. Particles manually classified to be close to the coverslip were classified identically in 96.3% of the cases by the network. Most of the discrepancies were edge cases, which were also difficult to discriminate by eye.

To quantify the binding kinetics of the particles, the scheme illustrated in Fig. 2 a was used. Whenever a particle switches from the unbound to the bound state, a binding event was registered. In the opposite case, an unbinding event was registered. We define the on rate $k_{\text{on,cell}}$, with which particles bind to the cells as the total number of binding events near a cell $N_{\text{binding,cell}}$ divided by the total time the particles are unbound $T_{\text{unbound,cell}}$ while near a cell:

$$k_{\text{on,cell}} = \frac{N_{\text{binding,cell}}}{T_{\text{unbound,cell}}}. \tag{24}$$

Analogously, the off rate $k_{\text{off,cell}}$ is defined by the number of unbinding events $N_{\text{unbinding,cell}}$ divided by the total time $T_{\text{bound,cell}}$, the particles are bound to a cell:

$$k_{\text{off,cell}} = \frac{N_{\text{unbinding,cell}}}{T_{\text{bound,cell}}}. \tag{25}$$

The on rate $k_{\text{on,coverslip}}$ and the off rate $k_{\text{off,coverslips}}$, which describe the binding kinetics between the particles and the coverslips are defined analogously. We observed that some particles never unbound. To quantify this behavior, binding events which started at least 200 s before and lasted until the end of the sedimentation phase were classified to be irreversible.

Measuring the binding kinetics of microplastic particles

In each experiment, we used a low flow speed of $9\,\mu\text{L s}^{-1}$ to flush microplastic particles into microfluidic flow chambers and allowed the particles to sediment for 10 min without a flow. During this phase, we observed the binding and unbinding events between the particles and the cells as well as between the particles and the coverslips. Depending on the particle type, we observed different transition kinetics between the bound and the unbound state. We characterized the particles' binding kinetics by their respective binding and unbinding rates during the first 10 min after flushing (see Fig. 2c, d). k_{on} and k_{off} to and from cells and coverslips were determined and the results of the trajectories of all 9 independent experiments were averaged. Each experiment typically contained a few hundred independent trajectories.

To investigate whether components of the image medium adhered to the particles and thereby changed the adhesion between particles and cells or whether sticky particles got stuck in the tubing of the microfluidic device, we performed the same experiments 0, 40, and 80 min after the addition of the particles. We did not detect a time dependency of the results in most cases. Only in rare cases, a tendency to slightly weaker adhesion with time was found, which was reflected by a slightly increasing k_{on} and a slightly decreasing k_{off} with time (Supplementary Fig. 17). For this reason, we decided to pool the data of the experiments that were done 0, 40, and 80 min after the addition of the particles.

Measuring the Adhesion strength of microplastic particles

To evaluate the adhesion strength between particles and cells as well as between particles and coverslips, we applied a constant hydrodynamic drag force of 50 pN to the particles after the sedimentation phase. To

remove any moving particles before the analysis of these experiments, a rolling median filter in time with a window size of 3 s was applied to the image sequence. The remaining static particles were then detected and classified as described above. We defined the fraction of particles that is still attached after 30 s of applied hydrodynamic force as the fraction of remaining particles.

Similar to the binding and unbinding rates, we found no significant differences in the relative attachment of particles to cells and to coverslips 0, 40, and 80 min after the addition of the particles, indicating that the incubation time is negligible in almost all cases (Supplementary Fig. 18). Therefore, we decided to pool for each particle type the data of the relative attachment of the three time points. After each measurement, the channels were disconnected from the microfluidic system and cleaned with trypsin, deionized water and 70% ethanol for 10 min each, removing cells and particles left in the channel. After each time series, the medium in the tubing of the microfluidic system was discarded, and the tubing was cleaned with deionized water and 70% ethanol to remove remaining particles in the system. The channels were reused three times with the same type of microplastic particles.

Internalization experiment
The experiments were carried out as described in Ramsperger et al.[15]. In brief, prior to the experiments, the cells were scraped off the culture flask bottoms into the culture media, centrifuged ($200\times$ g, 2 min, 20 °C) and re-suspended with 5 mL of cell culture medium in a Falcon tube (CORNING, Corning, New York, USA). Then, the cells were counted using a haemocytometer (Neubauer improved, Brand, Wertheim, Germany), seeded on microscope coverslips (diameter: 18 mm, #1, MENZEL GLAESER, Braunschweig, Germany) in 12-well plates (CellStar, GREINER BIO-ONE, Frickenhausen, Germany) in 1 mL of cell culture medium and allowed to adhere to the coverslips under standard culture conditions (37 °C, 5% CO_2, humidified) overnight. On each coverslip, 50,000 cells per mL were seeded to obtain a mean number of about 40,000 cells per coverslip (not all cells adhered to and remained on the coverslips during the preparation of the samples).

The following procedure was implemented to obtain samples for the quantification of microplastic particles interacting with cells (particle-cell-interaction), the measurement of the area covered by cells on the coverslips and for investigating the number of internalized microplastic particles from the particle-cell interactions. The 12-well plates containing the prepared cells were placed on ice for 1 h to reduce cellular activity. Due to different particle concentrations of the particle stock solutions, we diluted the stock solutions with PBS to obtain 150,000 beads per coverslip for each particle type. Three coverslips for each particle type were prepared, yielding a total of 33 coverslips. The particles were added to each coverslip and the experiment proceeded[15]. First, we quantified the number of particle-cell interactions and the area covered with cells on each coverslip within five regions of interest (ROIs) (0.29 mm²) using a DMI 6000 microscope (LEICA, Wetzlar, Germany, HCX PL APO 63× oil immersion objective, NA = 1.30) including a spinning disc unit (CSU-X1, YOKO-GAWA, Musashino, Japan) with an EMCCD camera (Evolve 512, PHO-TOMETRICS, Tucson, Arizona, including an additional 1.2× magnification lens). A differential interference contrast (DIC) microscopy image was acquired to quantify the particle-cell interactions within the ROIs using the Fiji ImageJ (version 1.53c) cell counter software. Additionally, spinning disk confocal stacks of fluorescently labelled cells were acquired using a 488 nm laser (50 mW, Sapphire 488, COHERENT, Santa Clara, California) at a spinning disc speed of 5000 rpm to excite fluorescence. Axial stacks of the cells were acquired with a vertical distance of 0.2 μm, which is sufficient to oversample the image given the axial resolution of the microscope[108].

To calculate the area covered by cells, both the DIC and fluorescence images were used[15]. First, a local contrast filter was applied to the DIC images to approximate the cell mask M_{DIC} at any given position (i,j):

$$M_{DIC}(i,j) = \begin{cases} 1, \text{ if } \Delta I_{DIC} > T_{DIC} \\ 0, \text{ if } \Delta I_{DIC} \leq T_{DIC} \end{cases} \quad (26)$$

The local intensity difference ΔI_{DIC} was evaluated within a circular region with a radius of 3 pixels. The threshold T_{DIC} was chosen manually to optimize the cell detection. Next, the fluorescence images were evaluated to obtain the cell mask M_F. The maximum projection of each stack was calculated, and a manually chosen threshold T_F was applied:

$$M_F(i,j) = \begin{cases} 1, \text{ if } I(i,j) > T_F \\ 0, \text{ if } I(i,j) \leq T_F \end{cases} \quad (27)$$

To obtain the final cell masks, both individual masks were multiplied:

$$M(i,j) = M_{DIC}(i,j)M_F(i,j) \quad (28)$$

Finally, small holes up to a size of 40 μm² were filled, and the masks were smoothed using a Gaussian filter with a radius of 3 pixels. Objects smaller than 80 μm² were excluded to reduce background noise. Finally, the area covered by cells within a ROI was extrapolated to the whole coverslip (245.5 μm²).

To quantify the number of particle-cell interactions, slight variations of the area covered by the cells and the number of microplastic particles was considered by standardizing each coverslip[15]. First, the measured number of particle-cell interactions were extrapolated to a whole coverslip, PCI_{CS}. Then, the number of cells on a standard coverslip $N_{cells,standardCS}$ was calculated by dividing the mean over all treatments of the area covered by cells on a coverslip by the area of an average single cell. The number of microplastic particles on a standard coverslip $N_{particles,standardCS}$ was the mean over all treatments of the number of particles added to the coverslips. Then, the number of particle-cell interactions on a coverslip was calculated:

$$PCI_{stand} = PCI_{CS} \left(\frac{N_{cells,standardCS}}{\frac{A_{CS}}{A_{singleCell,CS}}} \right) \left(\frac{N_{particles,standardCS}}{N_{particles,CS}} \right) \quad (29)$$

With the measured number of particle-cell interactions on a single coverslip PCI_{CS}, the measured cell area on the coverslip A_{CS}, the average area of a single cell on the coverslip $A_{singleCell,CS}$, and the number of particles added to the coverslip $N_{particles,CS}$.

After quantification of the particle-cell interactions, we measured the conditional internalization probability. From the same samples used to quantify particle-cell interactions and areas covered with cells on coverslips, we visually screened each sample for single particle-cell interactions to distinguish between particles that were only attached to cells and particles that were internalized by cells. The above mentioned DMI 6000 microscope with a higher magnification (100× oil immersion objective, NA = 1.40) was used here. Beginning from a randomly defined starting point, the coverslips were screened in the DIC-channel until 100 particle-cell interactions were detected. Once a particle-cell-interaction was found, a DIC-image was taken, and axial confocal stacks of fluorescently labelled cells were acquired (vertical distance of the axial stacks: 0.2 μm). To evaluate internalization of the microplastic particles, each confocal stack of cells with fluorescently labelled actin filaments was analyzed with Fiji ImageJ (version: 1.53c) orthogonal views. The microplastic particles used in the experiments were non-fluorescent and therefore not directly visible in the confocal stacks. The DIC images were used to mark the particle positions (using the ROI manager in Fiji ImageJ). These positions were then transferred

to the confocal stacks, in which internalized particles were visible as spherical black regions within the actin network. Only microplastic particles that were fully surrounded by actin filaments were considered to be internalized. Microplastic particles that were only partly surrounded were considered to be attached to the cells. Finally, the internalization probability was calculated as the ratio of internalized particles to the number of particle-cell interactions. For the calculation of the internalization probability for particles coated with an eco-corona, namely salt and freshwater particles incubated for two and four weeks the data published by Ramsperger et al.[15] were used.

Internalization mechanisms

To test our hypothesis that the microplastic particles were internalized via an actin-dependent mechanism such as phagocytosis or macropinocytosis, we performed experiments with live cells, monitoring the actin dynamics during particle internalization and the subsequent acidification of the particles. Two days before an experiment, 5×10^4 J774A.1 cells stably transfected with a LifeAct-GFP construct were seeded on 18 mm glass coverslips (MENZEL GLAESER, Braunschweig, Germany) in a 12-well plate (CellStar, GREINER BIO-ONE, Frickenhausen, Germany) containing 1 mL of cell culture medium. 30 min before an experiment, the medium was exchanged with cell culture medium containing $0.1 \,\mu\text{L mL}^{-1}$ (final concentration of 100 nM) of LysoTracker Red DND99 (Thermo Fisher Scientific Inc, Waltham, MA). Right before the experiment, the coverslips were mounted on a custom aluminum sample holder. The cells were covered with 84 μL of imaging medium containing $3 \,\mu\text{L mL}^{-1}$ of the corresponding bead stock solution, and the sample was covered with another 18 mm coverslip. The sample was immediately mounted on the fluorescence microscope and live cell imaging started.

Imaging was performed with a frame rate of 0.32 Hz on an inverted, motorized microscope (Nikon Eclipse Ti-E, Nikon, Tokyo, Japan) with a 40× water immersion objective (CFI Apo LWD 40× WI λS, Nikon, NA = 1.15), which was equipped with a EMCCD camera (Andor Luca R, Oxford Instruments, Belfast, United Kingdom). The microscope body was enclosed in a custom-built incubation chamber which keeps the body of the microscope and the sample at a temperature of 37 °C. The imaging modes were either brightfield illumination or widefield epi-fluorescence microscopy (Nikon Intensilight). For each frame, we imaged 3 channels: Brightfield (exposure time 100 ms), GFP-L (LifeAct channel, exc. 460–500 nm, em. >510 nm; exposure time 700 ms), and Texas Red (LysoTracker channel, exc. 540–580 nm, em. 600–660 nm; exposure time 500 ms). Imaging was continued for 45 min, leading to a total of 864 acquired images.

For the evaluation of individual internalization and maturation events, particles were tracked in the brightfield channel using a custom tracking algorithm based on radial symmetry[109]. Only particles that stayed in the focal plane of the objective were considered for evaluation. LifeAct and LysoTracker intensities were evaluated using MATLAB. Based on the particle trajectories from the brightfield channel, the images in the LifeAct and LysoTracker channels were cropped to a ROI of 60×60 pixels around the particle. The radius of each individual microplastic particle was determined, to account for the dispersity in size of some particle types. The particle radius r in pixels (px) was chosen in a way that maximized the signal-to-background ratio of both fluorescence channels. Then, the average LifeAct and LysoTracker intensities were evaluated for each frame in a ring-shaped ROI in the interval $[r - 3 \text{ px}, r + 2 \text{ px}]$, around the particle surface. This intensity was normalized to the average intensity of a ring-shaped ROI further apart from the particles surface, in the interval $[r + 9 \text{ px}, r + 12 \text{ px}]$. This normalization of the LifeAct and LysoTracker intensities corrected for artifacts like photobleaching. Furthermore, it enabled the evaluation of very localized actin dynamics and acidification around the microplastic particles' surface since global changes of fluorescence intensity did not contribute.

Statistical analysis

Statistical analysis was conducted using R studio software (version 4.0.2, 2020-06-22) with the packages: "car", "carData", "rstatix", "multcompView". To test for significant differences between the particle types, and whether there was a significant time dependence, the data for the relative attachment were tested for normal distribution (Shapiro–Wilk test) and homogeneity of variances (Levene test). If the Shapiro–Wilk test or the Levene test were significant, a two-sided Kruskal–Wallis test with a Games Howell post hoc test was conducted to check for differences between microplastic particle types. Otherwise, a one-way ANOVA with a Tukey post hoc test was performed. Correlation coefficients (Pearson's R) were calculated using MATLAB. A detailed summary of all statistical tests is provided in Supplementary Data 1.

Reporting summary

Further information on research design is available in the Nature Portfolio Reporting Summary linked to this article.

Data availability

The data that support the findings of this study are available via Zenodo[110] and from the corresponding authors upon request. Source data are provided with this paper.

Code availability

All code used in the analysis is available via Zenodo[110] and from the corresponding authors upon request.

References

1. Carpenter, E. J., Anderson, S. J., Harvey, G. R., Miklas, H. P. & Peck, B. B. Polystyrene spherules in coastal waters. *Science* **178**, 749–750 (1972).
2. Schell, T., Rico, A. & Vighi, M. Occurrence, fate and fluxes of plastics and microplastics in terrestrial and freshwater ecosystems. *Rev. Environ. Contam. Toxicol.* **250**, 1–43 (2020).
3. Arthur, C., Baker, J. & Bamford, H. Proceedings of the international research workshop on the occurrence, effects, and fate of microplastic marine debris. *NOAA Tech. Memo. NOS-OR&R 30* (2009).
4. Thompson, R. C. et al. Lost at sea: where is all the plastic? *Science* **304**, 838–838 (2004).
5. Laist, D. W. Impacts of marine debris: entanglement of marine life in marine debris including a comprehensive list of species with entanglement and ingestion records. in *Marine Debris - Sources, Impacts and Solutions*. (eds. Coe, J. M. & Rogers, D. B.) 99–139 (Springer, New York, 1997).
6. Wieland, S. et al. From properties to toxicity: Comparing microplastics to other airborne microparticles. *J. Hazard. Mater.* **428**, 128151 (2022).
7. Fulfer, V. M. & Menden-Deuer, S. Heterotrophic dinoflagellate growth and grazing rates reduced by microplastic ingestion. *Front. Mar. Sci.* **8**, 716349 (2021).
8. Harper, P. C. & Fowler, J. A. Plastic pellets in New Zealand storm-killed prions (Pachyptila spp.) 1958–1977. *Notornis* **34**, 65–70 (1987).
9. Lu, Y. et al. Uptake and accumulation of polystyrene microplastics in Zebrafish (Danio rerio) and toxic effects in liver. *Environ. Sci. Technol.* **50**, 4054–4060 (2016).
10. Browne, M. A., Dissanayake, A., Galloway, T. S., Lowe, D. M. & Thompson, R. C. Ingested microscopic plastic translocates to the circulatory system of the mussel, Mytilus edulis (L.). *Environ. Sci. Technol.* **42**, 5026–5031 (2008).
11. von Moos, N., Burkhardt-Holm, P. & Köhler, A. Uptake and effects of microplastics on cells and tissue of the Blue Mussel Mytilus edulis L. after an experimental exposure. *Environ. Sci. Technol.* **46**, 11327–11335 (2012).

12. Wright, S. L. & Kelly, F. J. Plastic and human health: a micro issue? *Environ. Sci. Technol.* **51**, 6634–6647 (2017).
13. Stock, V. et al. Uptake and effects of orally ingested polystyrene microplastic particles in vitro and in vivo. *Arch. Toxicol.* **93**, 1817–1833 (2019).
14. Rudolph, J., Völkl, M., Jérôme, V., Scheibel, T. & Freitag, R. Noxic effects of polystyrene microparticles on murine macrophages and epithelial cells. *Sci. Rep.* **11**, 15702 (2021).
15. Ramsperger, A. F. R. M. et al. Environmental exposure enhances the internalization of microplastic particles into cells. *Sci. Adv.* **6**, eabd1211 (2020).
16. Prata, J. C. Airborne microplastics: consequences to human health? *Environ. Pollut.* **234**, 115–126 (2018).
17. Jacob, H., Besson, M., Swarzenski, P. W., Lecchini, D. & Metian, M. Effects of virgin micro- and nanoplastics on fish: trends, meta-analysis, and perspectives. *Environ. Sci. Technol.* **54**, 4733–4745 (2020).
18. Brachner, A. et al. Assessment of human health risks posed by nano-and microplastics is currently not feasible. *Int. J. Environ. Res. Public Health* **17**, 1–10 (2020).
19. Patiño, T., Soriano, J., Barrios, L., Ibáñez, E. & Nogués, C. Surface modification of microparticles causes differential uptake responses in normal and tumoral human breast epithelial cells. *Sci. Rep.* **5**, 11371 (2015).
20. Lunov, O. et al. Differential uptake of functionalized polystyrene nanoparticles by human macrophages and a monocytic cell line. *ACS Nano* **5**, 1657–1669 (2011).
21. Olivier, V. et al. Uptake of polystyrene beads bearing functional groups by macrophages and fibroblasts. *Colloids Surf., B* **33**, 23–31 (2004).
22. Heinrich, P., Hanslik, L., Kämmer, N. & Braunbeck, T. The tox is in the detail: technical fundamentals for designing, performing, and interpreting experiments on toxicity of microplastics and associated substances. *Environ. Sci. Pollut. Res.* **27**, 22292–22318 (2020).
23. Gardon, T., Reisser, C., Soyez, C., Quillien, V. & Le Moullac, G. Microplastics affect energy balance and gametogenesis in the pearl oyster pinctada margaritifera. *Environ. Sci. Technol.* **52**, 5277–5286 (2018).
24. Lim, D. et al. Inhalation toxicity of polystyrene micro(nano)plastics using modified OECD TG 412. *Chemosphere* **262**, 128330 (2021).
25. Wei, Y. et al. Polystyrene microplastics disrupt the blood-testis barrier integrity through ROS-Mediated imbalance of mTORC1 and mTORC2. *Environ. Pollut.* **289**, 117904 (2021).
26. Yu, S.-P. & Chan, B. K. K. Effects of polystyrene microplastics on larval development, settlement, and metamorphosis of the inter-tidal barnacle Amphibalanus amphitrite. *Ecotoxicol. Environ. Saf.* **194**, 110362 (2020).
27. Pan, L. et al. Polystyrene microplastics-triggered mitophagy and oxidative burst via activation of PERK pathway. *Sci. Total Environ.* **781**, 146753 (2021).
28. Merkley, S. D. et al. Polystyrene microplastics induce an immu-nometabolic active state in macrophages. *Cell Biol. Toxicol.* **38**, 31–41 (2022).
29. Shimizu, Y. et al. Influence of 50-nm polystyrene particles in inducing cytotoxicity in mice co-injected with carbon tetra-chloride, cisplatin, or paraquat. *Pharmazie* **67**, 712–714 (2012).
30. Kwon, W. et al. Microglial phagocytosis of polystyrene micro-plastics results in immune alteration and apoptosis in vitro and in vivo. *Sci. Total Environ.* **807**, 150817 (2022).
31. Lu, C., Kania, P. W. & Buchmann, K. Particle effects on fish gills: an immunogenetic approach for rainbow trout and zebrafish. *Aquaculture* **484**, 98–104 (2018).
32. Ramsperger, A. F. R. M. et al. Supposedly identical microplastic particles substantially differ in their material properties
33. influencing particle-cell interactions and cellular responses. *J. Hazard. Mater.* **425**, 127961 (2022).
33. Delgado, A. V., González-Caballero, F., Hunter, R. J., Koopal, L. K. & Lyklema, J. Measurement and interpretation of electrokinetic phenomena (IUPAC technical report). *Pure Appl. Chem.* **77**, 1753–1805 (2005).
34. Jeon, S. et al. Surface charge-dependent cellular uptake of poly-styrene nanoparticles. *Nanomaterials* **8**, 1028 (2018).
35. Fröhlich, E. The role of surface charge in cellular uptake and cytotoxicity of medical nanoparticles. *Int. J. Nanomed.* **7**, 5577 (2012).
36. Verma, A. & Stellacci, F. Effect of surface properties on nanoparticle–cell interactions. *Small* **6**, 12–21 (2010).
37. Foged, C., Brodin, B., Frokjaer, S. & Sundblad, A. Particle size and surface charge affect particle uptake by human dendritic cells in an in vitro model. *Int. J. Pharm.* **298**, 315–322 (2005).
38. Lesniak, A. et al. Nanoparticle adhesion to the cell membrane and its effect on nanoparticle uptake efficiency. *J. Am. Chem. Soc.* **135**, 1438–1444 (2013).
39. Perry, D. et al. Surface charge visualization at viable living cells. *J. Am. Chem. Soc.* **138**, 3152–3160 (2016).
40. Kutscher, H. L. et al. Enhanced passive pulmonary targeting and retention of PEGylated rigid microparticles in rats. *Int. J. Pharm.* **402**, 64–71 (2010).
41. Prior, S. et al. In vitro phagocytosis and monocyte-macrophage activation with poly(lactide) and poly(lactide-co-glycolide) microspheres. *Eur. J. Pharm. Sci.* **15**, 197–207 (2002).
42. Liu, Y. et al. Surface hydrophobicity of microparticles modulates adjuvanticity. *J. Mater. Chem. B* **1**, 3888 (2013).
43. Tabata, Y. & Ikada, Y. Effect of the size and surface charge of polymer microspheres on their phagocytosis by macrophage. *Biomaterials* **9**, 356–362 (1988).
44. Roser, M., Fischer, D. & Kissel, T. Surface-modified biodegradable albumin nano- and microspheres. II: effect of surface charges on in vitro phagocytosis and biodistribution in rats. *Eur. J. Pharm. Biopharm.* **46**, 255–263 (1998).
45. Gigault, J. et al. Nanoplastics are neither microplastics nor engi-neered nanoparticles. *Nat. Nanotechnol.* **16**, 501–507 (2021).
46. Mitrano, D. M., Wick, P. & Nowack, B. Placing nanoplastics in the context of global plastic pollution. *Nat. Nanotechnol.* **16**, 491–500 (2021).
47. Kohane, D. S. Microparticles and nanoparticles for drug delivery. *Biotechnol. Bioeng.* **96**, 203–209 (2007).
48. Otto, D. P., Otto, A. & de Villiers, M. M. Differences in physico-chemical properties to consider in the design, evaluation and choice between microparticles and nanoparticles for drug deliv-ery. *Expert Opin. Drug Deliv.* **12**, 763–777 (2015).
49. Freeman, S. A. & Grinstein, S. Phagocytosis: receptors, signal integration, and the cytoskeleton. *Immunol. Rev.* **262**, 193–215 (2014).
50. Wolf, A. J. & Underhill, D. M. Phagocytosis. In *Macrophages: Biol-ogy and Role in the Pathology of Diseases* (pp. 91–109. Springer, New York, 2014).
51. Thornton Hampton, L. M. et al. A living tool for the continued exploration of microplastic toxicity. *Microplast. Nanoplast.* **2**, 13 (2022).
52. Witzmann, T. et al. Repulsive interactions of eco-corona-covered microplastic particles quantitatively follow modeling of polymer brushes. *Langmuir* **38**, 8748–8756 (2022).
53. Vieira, O. V., Botelho, R. J. & Grinstein, S. Phagosome maturation: aging gracefully. *Biochem. J.* **366**, 689–704 (2002).
54. Lim, J. P. & Gleeson, P. A. Macropinocytosis: an endocytic pathway for internalising large gulps. *Immunol. Cell Biol.* **89**, 836–843 (2011).

55. Wang, F. et al. The biomolecular corona is retained during nanoparticle uptake and protects the cells from the damage induced by cationic nanoparticles until degraded in the lysosomes. *Nanomed. Nanotechnol. Biol. Med.* **9**, 1159–1168 (2013).

56. Ober, C. K., Lok, K. P. & Hair, M. L. Monodispersed, micron-sized polystyrene particles by dispersion polymerization. *J. Polym. Sci. Polym. Lett. Ed.* **23**, 103–108 (1985).

57. Telford, A. M., Pham, B. T. T., Neto, C. & Hawkett, B. S. Micron-sized polystyrene particles by surfactant-free emulsion polymerization in air: Synthesis and mechanism. *J. Polym. Sci. Part A Polym. Chem.* **51**, 3997–4002 (2013).

58. Kawaguchi, H. Functional polymer microspheres. *Prog. Polym. Sci.* **25**, 1171–1210 (2000).

59. Chen, C.-S. et al. Stickiness of extracellular polymeric substances on different surfaces via magnetic tweezers. *Sci. Total Environ.* **757**, 143766 (2021).

60. Berghoff, K., Gross, W., Eisentraut, M. & Kress, H. Using blinking optical tweezers to study cell rheology during initial cell-particle contact. *Biophys. J.* **120**, 3527–3537 (2021).

61. Forest, V. & Pourchez, J. Preferential binding of positive nanoparticles on cell membranes is due to electrostatic interactions: A too simplistic explanation that does not take into account the nanoparticle protein corona. *Mater. Sci. Eng. C* **70**, 889–896 (2017).

62. Pulido-Reyes, G., Leganes, F., Fernández-Piñas, F. & Rosal, R. Bio-nano interface and environment: a critical review. *Environ. Toxicol. Chem.* **36**, 3181–3193 (2017).

63. Rummel, C. D., Jahnke, A., Gorokhova, E., Kühnel, D. & Schmitt-Jansen, M. Impacts of Biofilm Formation on the Fate and Potential Effects of Microplastic in the Aquatic Environment. *Environ. Sci. Technol. Lett.* **4**, 258–267 (2017).

64. Galloway, T. S., Cole, M. & Lewis, C. Interactions of microplastic debris throughout the marine ecosystem. *Nat. Ecol. Evol.* **1**, 0116 (2017).

65. Kretzschmar, R., Sticher, H. & Hesterberg, D. Effects of adsorbed humic acid on surface charge and flocculation of kaolinite. *Soil Sci. Soc. Am. J.* **61**, 101–108 (1997).

66. Jayalath, S., Larsen, S. C. & Grassian, V. H. Surface adsorption of Nordic aquatic fulvic acid on amine-functionalized and non-functionalized mesoporous silica nanoparticles. *Environ. Sci. Nano* **5**, 2162–2171 (2018).

67. Ritchie, J. D. & Perdue, E. M. Proton-binding study of standard and reference fulvic acids, humic acids, and natural organic matter. *Geochim. Cosmochim. Acta* **67**, 85–96 (2003).

68. Sillanpää, M. General Introduction. in *Natural Organic Matter in Water* (ed. Sillanpää, M. B. T.-N. O. M. in W.) 1–15 (Elsevier, 2015).

69. Honary, S. & Zahir, F. Effect of zeta potential on the properties of nano-drug delivery systems - a review (Part 1). *Trop. J. Pharm. Res.* **12**, 255–264 (2013).

70. Silva, T. et al. Particle size, surface charge and concentration dependent ecotoxicity of three organo-coated silver nanoparticles: Comparison between general linear model-predicted and observed toxicity. *Sci. Total Environ.* **468–469**, 968–976 (2014).

71. Forest, V., Cottier, M. & Pourchez, J. Electrostatic interactions favor the binding of positive nanoparticles on cells: a reductive theory. *Nano Today* **10**, 677–680 (2015).

72. Ma, N. et al. Influence of nanoparticle shape, size, and surface functionalization on cellular uptake. *J. Nanosci. Nanotechnol.* **13**, 6485–6498 (2013).

73. Szilagyi, I., Sadeghpour, A. & Borkovec, M. Destabilization of colloidal suspensions by multivalent ions and polyelectrolytes: from screening to overcharging. *Langmuir* **28**, 6211–6215 (2012).

74. Metcalfe, I. M. & Healy, T. W. Charge-regulation modelling of the Schulze–Hardy rule and related coagulation effects. *Faraday Discuss. Chem. Soc.* **90**, 335–344 (1990).

75. Schulze, H. Schwefelarsen in wässriger Lösung. *J. für. Prakt. Chem.* **25**, 431–452 (1882).

76. Hardy, W. B. A preliminary investigation of the conditions which determine the stability of irreversible hydrosols. *Proc. R. Soc. Lond.* **66**, 110–125 (1900).

77. Trefalt, G., Szilágyi, I. & Borkovec, M. Schulze-Hardy rule revisited. *Colloid Polym. Sci.* **298**, 961–967 (2020).

78. Kanno, S., Furuyama, A. & Hirano, S. A murine scavenger receptor MARCO recognizes polystyrene nanoparticles. *Toxicol. Sci.* **97**, 398–406 (2007).

79. Meides, N. et al. Reconstructing the environmental degradation of polystyrene by accelerated weathering. *Environ. Sci. Technol.* **55**, 7930–7938 (2021).

80. Ramsperger, A. F. R. M. et al. Structural diversity in early-stage biofilm formation on microplastics depends on environmental medium and polymer properties. *Water* **12**, 3216 (2020).

81. França, A. et al. Macrophage scavenger receptor A mediates the uptake of gold colloids by macrophages in vitro. *Nanomedicine* **6**, 1175–1188 (2011).

82. Orr, G. A. et al. Cellular recognition and trafficking of amorphous silica nanoparticles by macrophage scavenger receptor A. *Nanotoxicology* **5**, 296–311 (2011).

83. Kerr, M. C. & Teasdale, R. D. Defining Macropinocytosis. *Traffic* **10**, 364–371 (2009).

84. Swanson, J. A. & Watts, C. Macropinocytosis. *Trends Cell Biol.* **5**, 424–428 (1995).

85. Platt, N. & Gordon, S. Is the class A macrophage scavenger receptor (SR-A) multifunctional? — The mouse's tale. *J. Clin. Invest.* **108**, 649–654 (2001).

86. Underhill, D. M. & Goodridge, H. S. Information processing during phagocytosis. *Nat. Rev. Immunol.* **12**, 492–502 (2012).

87. Tong, Z. et al. Microfluidic cell microarray platform for high throughput analysis of particle–cell interactions. *Anal. Chem.* **90**, 4338–4347 (2018).

88. Laforsch, C. & Tollrian, R. A new preparation technique of daphnids for Scanning Electron Microscopy using hexamethyldisilazane. *Fundam. Appl. Limnol.* **149**, 587–596 (2000).

89. Hitchcock, A. P. Analysis of X-ray images and spectra (aXis2000): a toolkit for the analysis of X-ray spectromicroscopy data. *J. Electron Spectros. Relat. Phenom.* **266**, 147360 (2023).

90. Henke, B. L., Gullikson, E. M. & Davis, J. C. X-Ray interactions: photoabsorption, scattering, transmission, and reflection at E = 50–30,000 eV, Z = 1–92. *Data Nucl. Data Tables* **54**, 181–342 (1993).

91. Ravel, B. & Newville, M. ATHENA, ARTEMIS, HEPHAESTUS: data analysis for X-ray absorption spectroscopy using IFEFFIT. *J. Synchrotron Radiat.* **12**, 537–541 (2005).

92. Shirley, D. A. High-Resolution X-Ray photoemission spectrum of the valence bands of gold. *Phys. Rev. B* **5**, 4709–4714 (1972).

93. Kashekodi, A. B., Meinert, T., Michiels, R. & Rohrbach, A. Miniature scanning light-sheet illumination implemented in a conventional microscope. *Biomed. Opt. Express* **9**, 4263 (2018).

94. Keller, S., Berghoff, K. & Kress, H. Phagosomal transport depends strongly on phagosome size. *Sci. Rep.* **7**, 17068 (2017).

95. Mortensen, N. A., Okkels, F. & Bruus, H. Reexamination of Hagen-Poiseuille flow: shape dependence of the hydraulic resistance in microchannels. *Phys. Rev. E* **71**, 057301 (2005).

96. Bruus, H. *Theoretical Microfluidics*. (Oxford University Press, Oxford, 2008).

97. Lehmann, M. High Performance Free Surface LBM on GPUs. *Master's Thesis* https://doi.org/10.15495/EPub_UBT_00005400 (2021).

98. Laermanns, H. et al. Tracing the horizontal transport of microplastics on rough surfaces. *Microplast. Nanoplast.* **1**, 11 (2021).

114

99. Lehmann, M., Oehlschlägel, L. M., Häusl, F. P., Held, A. & Gekle, S. Ejection of marine microplastics by raindrops: a computational and experimental study. *Microplast. Nanoplast.* **1**, 18 (2021).

100. Jaqaman, K. et al. Robust single-particle tracking in live-cell time-lapse sequences. *Nat. Methods* **5**, 695–702 (2008).

101. Applegate, K. T. et al. PlusTipTracker: quantitative image analysis software for the measurement of microtubule dynamics. *J. Struct. Biol.* **176**, 168–184 (2011).

102. Ng, M. R., Besser, A., Danuser, G. & Brugge, J. S. Substrate stiffness regulates cadherin-dependent collective migration through myosin-II contractility. *J. Cell Biol.* **199**, 545–563 (2012).

103. Szegedy, C. et al. Going deeper with convolutions. *2015 IEEE Conf. Comput. Vis. Pattern Recognit.* (2015).

104. Russakovsky, O. et al. ImageNet large scale visual recognition challenge. *Int. J. Comput. Vis.* **115**, 211–252 (2015).

105. Ravishankar, H. et al. Understanding the Mechanisms of Deep Transfer Learning for Medical Images. In: Carneiro, G. et al. Deep Learning and Data Labeling for Medical Applications. DLMIA LABELS 2016 Lect. Notes Comp. Sci., Springer, Cham. **10008**, 188–196, https://doi.org/10.1007/978-3-319-46976-8_20 (2016).

106. Shorten, C. & Khoshgoftaar, T. M. A survey on image data augmentation for deep learning. *J. Big Data* **6**, 60 (2019).

107. Kingma, D. P. & Ba, J. Adam: A Method for Stochastic Optimization. *3rd Int. Conf. Learn. Represent. ICLR 2015 - Conf. Track Proc.* https://arxiv.org/abs/1412.6980v9 (2014).

108. Jonkman, J. E. N., Swoger, J., Kress, H., Rohrbach, A. & Stelzer, E. H. K. Resolution in optical microscopy. *Methods Enzymol.* **360**, 416–446 (2003).

109. Eisentraut, M., Sabri, A. & Kress, H. The spatial resolution limit of phagocytosis. *Biophys. J.* **122**, 868–879 (2023).

110. Wieland, S. et al. Data and code for 'Nominally identical microplastic models differ greatly in their particle-cell interactions'. *Zenodo* https://doi.org/10.5281/zenodo.10514299 (2024).

Author contributions
H.K., C.L., W.G., A.F.R.M.R. and S.W. initiated the research. H.K., C.L., A.F., G.K.A., W.G., A.F.R.M.R. and S.W. planned the research. W.G., M.L., S.G. and H.K. developed the microfluidic method. S.W., A.F.R.M.R., W.G., T.W., A.C., and M.O. performed the experiments. W.G., A.F.R.M.R., and S.W. wrote the draft of the manuscript. All authors revised and edited the manuscript.

Competing interests
The authors declare no competing interests.

Additional information
Supplementary information The online version contains Supplementary Material available at https://doi.org/10.1038/s41467-024-45281-4.

Correspondence and requests for materials should be addressed to Christian Laforsch or Holger Kress.

Peer review information *Nature Communications* thanks the anonymous, reviewers for their contribution to the peer review of this work. A peer review file is available.

Reprints and permissions information is available at http://www.nature.com/reprints

Publisher's note Springer Nature remains neutral with regard to jurisdictional claims in published maps and institutional affiliations.

115

Supplementary information for

Nominally identical microplastic models differ greatly in their particle-cell interactions

Simon Wieland[†,1,2], Anja FRM Ramsperger[†,1,2], Wolfgang Gross[†,1], Moritz Lehmann[3], Thomas Witzmann[4], Anja Caspari[4], Martin Obst[5], Stephan Gekle[3], Günter K Auernhammer[4], Andreas Fery[4,6], Christian Laforsch[*,2], Holger Kress[*,1]

[1] Biological Physics, University of Bayreuth, Bayreuth, Germany
[2] Animal Ecology I and BayCEER, University of Bayreuth, Bayreuth, Germany
[3] Biofluid Simulation and Modeling – Theoretical Physics VI, University of Bayreuth, Bayreuth, Germany
[4] Leibniz Institut für Polymerforschung Dresden e. V., Institute of Physical Chemistry and Polymer Physics, Dresden, Germany
[5] Experimental Biogeochemistry, BayCEER, University of Bayreuth, Bayreuth, Germany
[6] Physical Chemistry of Polymeric Materials, Technische Universität Dresden, Dresden, Germany
[†] These authors contributed equally to this work.
[*] These authors jointly supervised this work. Corresponding authors: christian.laforsch@uni-bayreuth.de, holger.kress@uni-bayreuth.de

This PDF file includes:

      Supplementary Notes 1 and 2
      Supplementary Figures 1 to 18
      Supplementary Tables 1 to 4
      Supplementary References

1

Supplementary Notes

Supplementary Note 1: Particle SEM micrographs

The size and shape of the microplastic particles were investigated by using scanning electron microscopy (SEM). Most microplastic particle types deviated by less than 3% from the nominal diameter specified by the manufacturers. However, TJ, and PX deviated by 12% and 4% (Table 1). Furthermore, we found that the surface morphologies of the pristine microplastic particles show clear differences between the particle types (Figure 1, Supplementary Table 1). ST and TJ particles had the most irregular surfaces compared to all other particles. We observed indentations on the surfaces of the TJ particles and elevations on the PX and TJ particles. The other particles displayed in Figure 1 (MM-C, MM, MG, KI and TS) were highly spherical with smooth surfaces, although MG seemed to be covered by a net-like structure. The environmentally exposed particles (MM-SW2 and MM-SW4, MM-FW2, and MM-FW4) were coated heterogeneously by biomolecules and organic debris (eco-corona) as shown previously[1] and further analyzed by STXM and XPS measurements (Supplementary Figure 4, Supplementary Tables 2 and 3). The average diameter of MM-SW2, MM-SW4, and MM-FW4 increased slightly by a few nanometers, indicating a thin layer of biomolecules[1]. Furthermore, the standard deviation of the mean diameter of all environmentally exposed microplastic particles substantially increased, indicating that they became less monodisperse. Accordingly, also their eccentricity and surface roughness increased.

Supplementary Note 2: Validation of the flow profile

To validate that the derived velocity profile $v_{x,par}(y, z)$ given by equation (15) matches the flow field, which is established in the channels, we measured the velocity profile inside the channel with a high-speed camera and particle tracking. A small number of carboxylated polystyrene MPs with a diameter of 1 μm (micromer, micromod Partikeltechnologie GmbH, Rostock, Germany) was dispersed in MilliQ water at a concentration of approximately 2×10^5 μL^{-1}. The solution was pumped through the channel at flow rates between 0.2 μL s^{-1} and 2 μL s^{-1}, which was controlled by setting the motor velocity according to equation (8). The resulting flow field $v_{x,par}(y, z)$ (equation (15)) was measured on an inverted, motorized microscope (Nikon Eclipse Ti, Nikon, Tokyo, Japan) with a 40x water immersion objective with a high numerical aperture to minimize the focal depth (CFI Apo LWD 40× WI λS, Nikon, NA = 1.15). Brightfield images of the flow at various y and z positions were captured with a high-speed camera (IDT Nx4-S2, Integrated Design Tools, Pasadena, California) at frame rates of up to 2000 Hz.

To detect the particles automatically, the images were filtered with a spatial band pass filter in order to reduce noise and to remove any signals on length scales larger than the particles. Secondly, the images were filtered with a moving median filter in time to single out all stationary objects, e.g. sensor dust. These filtered images were then subtracted from the images. The moving particles were then detected with a custom-written peak-finding routine and tracked with a particle tracking algorithm[2]. The code was implemented in MATLAB 2019b. For every position inside the channel, the velocity of typically 50-100 particles was averaged. Slight deviations from the mean value could be attributed to particles located in slightly lower or higher z positions than the main focal plane, which were still sharp enough to be tracked. The measured flow profile $v_x(y, z)$ was in agreement with the theoretical prediction (Supplementary Figure 11).

As we used different flow rates during the rupture experiments, we also tested whether the velocity inside the channel scales linearly with the flow rate as expected from equations (14) and (15). The

2

high-speed camera was fast enough to capture particles with velocities of up to 3.5 mm s^{-1} at a flow rate of 2 µL s^{-1} with sufficiently short frame time intervals for the particle tracking algorithm. Up to 2 µL s^{-1}, we found perfectly linear scaling, demonstrating that the pressure even at relatively low flow rates is high enough to properly close the check valves in the tubing system (see Supplementary Figure 12). During the calibration experiments and during the cell experiments, we observed straight particle trajectories far away from the cells, indicating laminar flow in the channels.

Since the measured velocity profile $v_x(y,z)$, both in shape and magnitude, was in excellent agreement with the theoretical prediction (see Supplementary Figures 11 and 12), we concluded that equation (17) can be used to correct for the parabolic height profile.

3
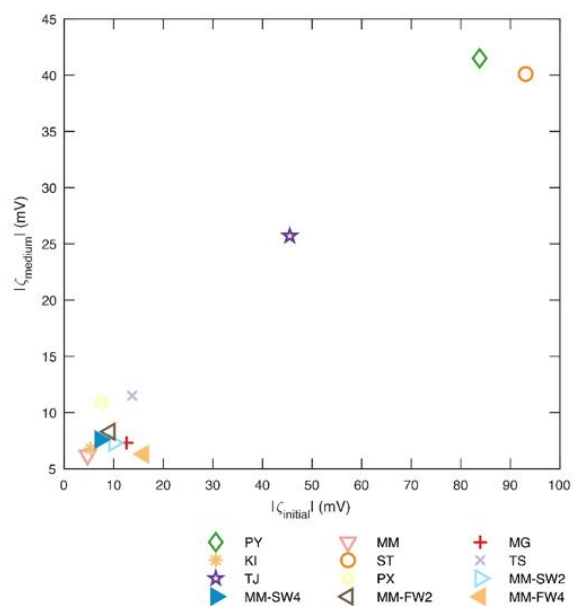
Supplementary Figure 1: ζ-potential before and after incubation in cell culture media.
The ζ-potential of microplastic particles after an incubation of 2 h in cell culture media ζ_{medium} was strongly correlated to their initial ζ-potential $\zeta_{initial}$ (Pearsons's $R = 0.8$, $P = 0.004$). Detailed values of the ζ-potential are given in Supplementary Table 1. Source data are provided as a Source Data file.

4
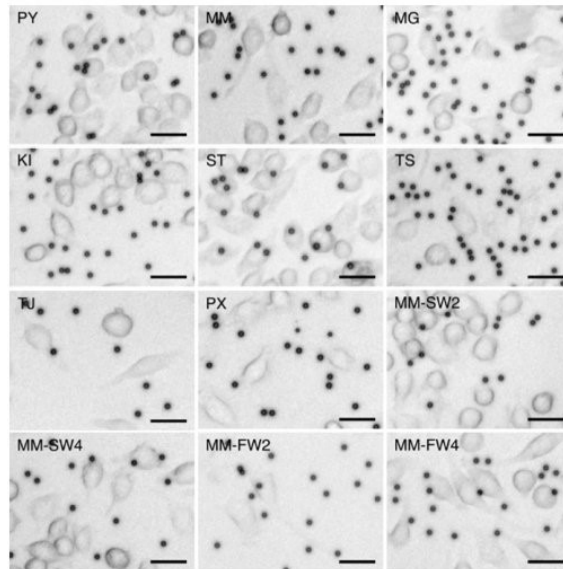
Supplementary Figure 2: Colloidal stability of microplastic particles.
All particle types showed a high colloidal stability during cell experiments, no significant aggregation of beads occurred. Here, example images of particles and cells during the microfluidic experiments are shown. These images were acquired after the sedimentation phase, before the flow was turned on to flush the particles off the cells. Scale bar: 25 µm.

5
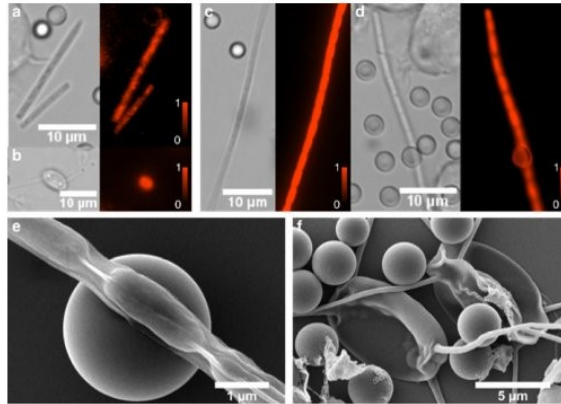
Supplementary Figure 3: Organisms in environmental media.
Various microorganisms were present in the environmental media. (**a**) and (**b**) show examples of freshwater organisms in brightfield and fluorescence microscopy (Texas Red channel, exc. 542-582 nm, em. 604-644 nm; color scales represent fluorescence in arbitrary units). (**c**) and (**d**) show examples of saltwater organisms in brightfield and fluorescence microscopy. (**e**) and (**f**) show scanning electron micrographs of freshwater organisms. (**a**) possibly shows a diatom. (**b**) and (**f**) possibly show green algae of the genus *Lagerheimia*. (**c**), (**d**), and (**e**) possibly show examples of cyanobacteria. The autofluorescence of the microorganisms in the Texas Red channel might be caused by chlorophyll.

6
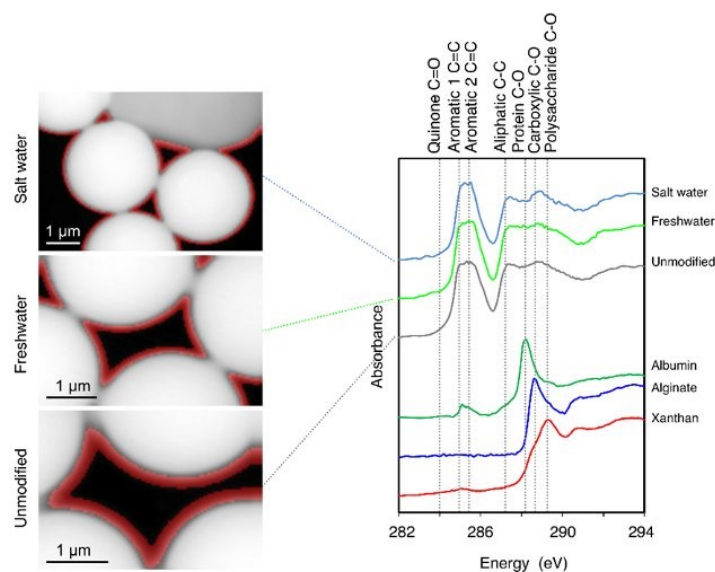
Supplementary Figure 4: STXM analysis of the eco-corona.

C1s NEXAFS spectra extracted from Scanning Transmission X-ray Microscopy (STXM) datasets from regions directly at the surface of PS beads that were previously incubated in seawater, freshwater and deionized water respectively. The surface regions, highlighted in red, were selected in the STXM images based on the average optical density (OD) range of 0.1-0.9 across the C1s absorption edge, which is equivalent to a cumulative thickness of up to 100 nm, arranged tangentially around the PS beads. These regions are marked in red in the respective STXM images. The equivalent thickness was calculated using the atomic scattering factors[3], the formula C_8H_8 and an assumed density of 1.09 g cm^{-3} of the polystyrene. All 3 spectra were decomposed into a sum of individual gaussian peaks plus the ionization edge modelled as an arctan function. A minimum of 7 analytical peaks was required and used for fitting the respective spectra: 284.0 eV (quinone C=O), 285.0 and 285.4 eV (aromatic C=C), 287.4 eV (aliphatic C-C), 288.2 eV (protein C-O), 288.9 eV (carboxylic C-O), 289.5 (polysaccharide C-O). Peak energies and widths were optimized and fixed at the same values for all 3 spectra, whereas the respective peak areas were fitted (Supplementary Table 2) using the peak fitting algorithm of Athena[4]. For illustrating the peak energies that are subtle only in the spectra of the thin regions of the eco-corona around the PS bead, 3 reference materials are presented as well, for protein (albumin), acidic polysaccharides (alginate) and neutral polysaccharides (xanthan)[5]. The dashed grey lines indicate the respective peak energies of the gaussians used for fitting. The data lines of the spectra were offset for clarity.

7
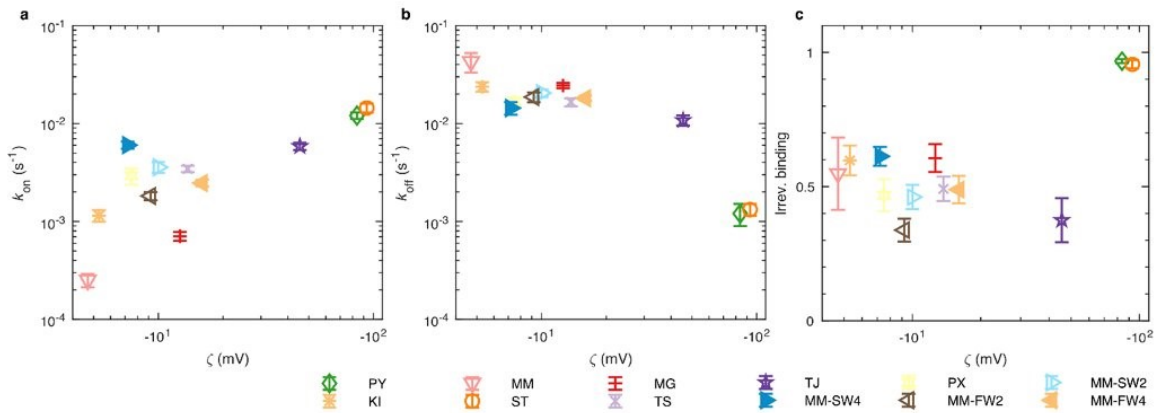
Supplementary Figure 5: Binding kinetics of microplastic particles to coverslips.
Binding kinetics to coverslips significantly differed between samples (k_{on}: Kruskal-Wallis test, two-sided $P = 8.69 \times 10^{-16}$; k_{off}: Kruskal-Wallis test, two-sided $P = 5.77 \times 10^{-10}$; Irreversible binding: Kruskal-Wallis test, two-sided $P = 2.83 \times 10^{-6}$). We measured rates of a similar magnitude as for the binding of microplastic particles to cells. This means that particles which strongly bound to cells also bound strongly to coverslips. However, particle-coverslip adhesion was in general slightly weaker than particle-cell adhesion (compare Figure 2). This was reflected by a generally lower k_{on} (**a**) to coverslips, a higher k_{off} (**b**) from coverslips, and a generally lower fraction of irreversible binding events (**c**). Like for the binding to cells, the binding kinetics were strongly correlated to the particles' ζ-potential. With increasing negative ζ-potential k_{on} increased (Pearson's $R = 0.9$, two-sided $P = 9.4 \times 10^{-6}$), k_{off} decreased (Pearson's $R = -0.8$, two-sided $P = 0.003$), and the fraction of irreversible binding events increased (Pearson's $R = 0.8$, two-sided $P = 0.003$). In all panels, error bars represent standard error of mean of $n = 9$ measurements (for each measurement, on average 550 particles were analyzed). Source data are provided as a Source Data file.

8
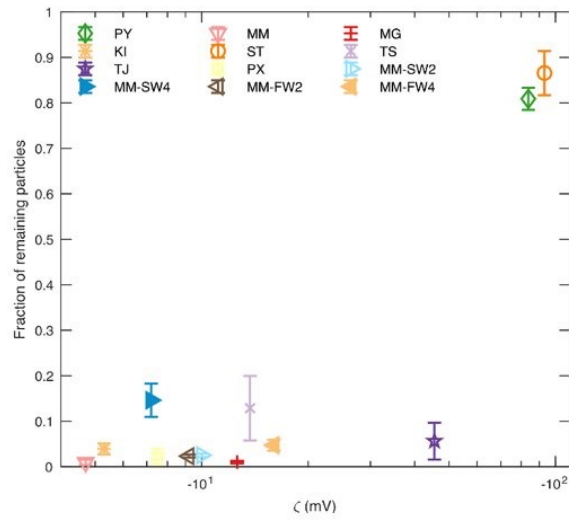
Supplementary Figure 6: Adhesion strength of microplastic particles to coverslips.
Adhesion of particles to coverslips significantly differed between samples (Kruskal-Wallis test: two-sided $P = 1.24 \times 10^{-10}$). Particles that strongly adhered to cells also strongly adhered to coverslips and vice versa. Generally, the fraction of microplastic particles remaining on coverslips after flushing with a hydrodynamic force of 50 pN for 30 s was slightly lower compared to the fraction of particles remaining on cells (compare Figure 3). The fraction of particles remaining on coverslips was correlated to the particles' ζ-potential. With increasing negative ζ-potential, the fraction of remaining particles strongly increased (Pearson's $R = 0.9$, two-sided $P = 9.4 \times 10^{-6}$). Error bars represent standard error of mean of $n = 9$ measurements (for each measurement, on average 550 particles were analyzed). Source data are provided as a Source Data file.

9
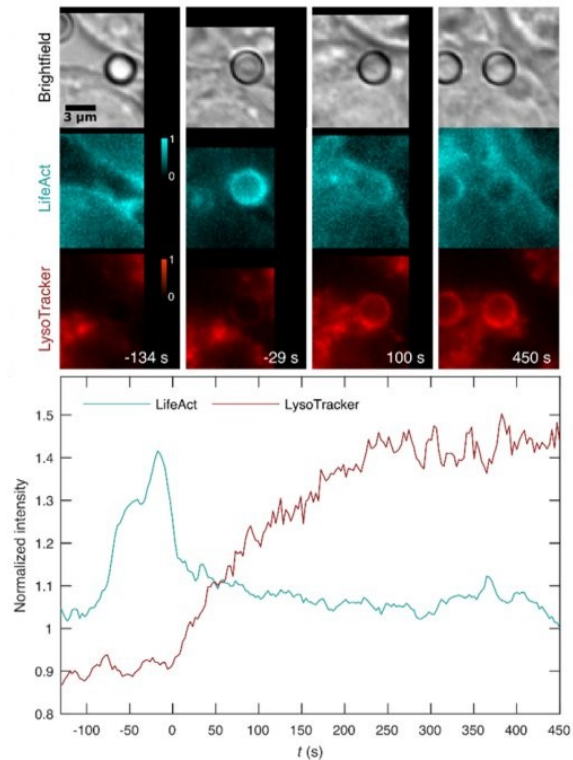
Supplementary Figure 7: Internalization and maturation of microplastic particles.
To test, if the microplastic particles were internalized by phagocytosis or macropinocytosis, we monitored the actin cytoskeleton during particle internalization by cells that were stably transfected with a LifeAct-GFP construct. Since this construct binds to filamentous actin, it is enriched at sites of actin polymerization. Furthermore, we treated the cells with LysoTracker dye, which is enriched in acidic organelles like lysosomes. In this example, the internalization and subsequent maturation of a TS particle is shown. Color scales in the fluorescence images represent fluorescence in arbitrary units. First, the particle interacted with the surface of a cell ($t = -134$ s). Then we observed a significant peak in the LifeAct intensity around the particle, indicating polymerization of actin filaments ($t = -29$ s). After the LifeAct signal decayed ($t = 0$ s), the LysoTracker intensity increased gradually ($t = 100$ s) until it reached a plateau at the end of the measurement ($t = 450$ s), showing interactions with lysosomes and the acidification of the internalized particle. Source data are provided as a Source Data file.

10
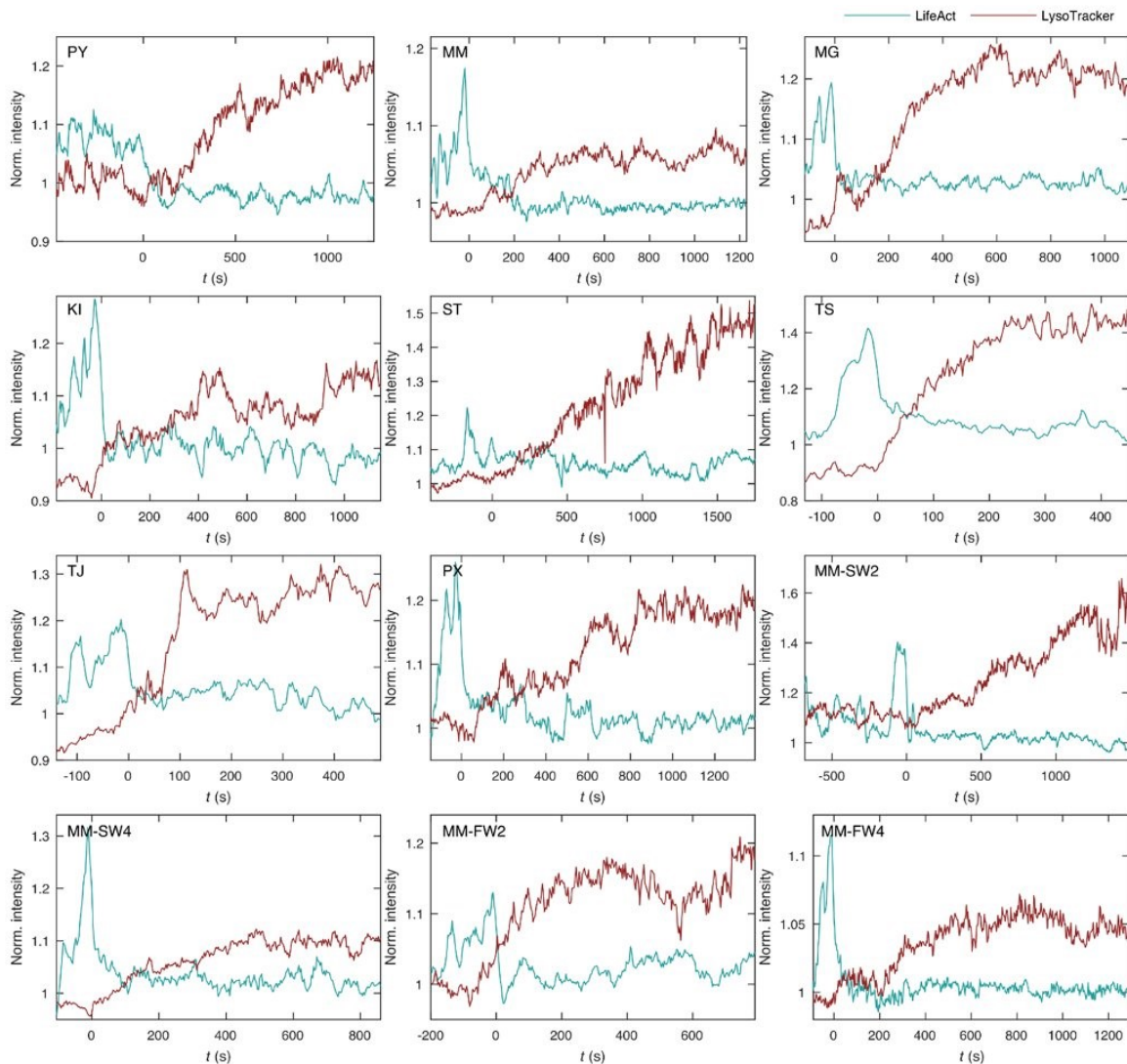
Supplementary Figure 8: Internalization and maturation of all particle types.
All particle types underwent a similar form of internalization and maturation: After the particles interacted with the cells, there was a substantial increase in the LifeAct signal at the site of the particles, indicating that filamentous actin was polymerized. This shows that particles were internalized by an actin-dependent pathway, such as phagocytosis or macropinocytosis. After the LifeAct signal around the particle decayed, indicating depolymerization of the actin filaments, the LysoTracker signal gradually increased over time. This shows that internalized particles interacted with lysosomes and became acidic, undergoing a maturation process that is typical for phagosomes or macropinosomes. Source data are provided as a Source Data file.

11
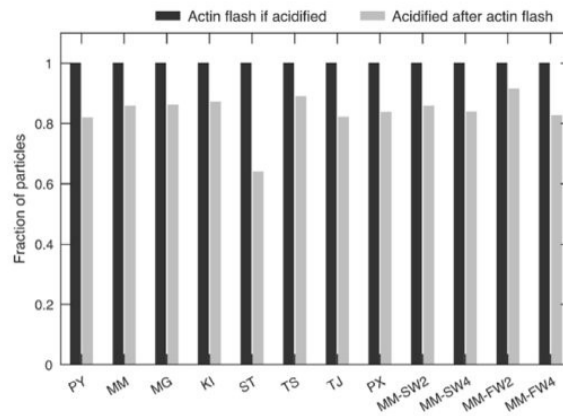
Supplementary Figure 9: Internalization mechanisms of microplastic particles.
All particles that were acidified over the course of a measurement showed an actin peak before the acidification process started, indicating internalization via an actin-dependent pathway (dark bars). This was observed for all particle types. Moreover, most of the particles which at some point during the measurement time showed a LifeAct peak were acidified later (light bars). In cases where particles showed no acidification after a LifeAct peak, the actin-dependent internalization process might not have been completed or the maturation process might not yet have started before the end of a measurement. Overall, these results indicate that the microplastic particles were always internalized via the actin-dependent processes of phagocytosis or macropinocytosis. Number n of evaluated uptake processes: PY: 33, MM: 35, MG: 36, KI: 31, ST: 72, TS: 36, TJ: 39, PX: 49, MM-SW2: 35, MM-SW4: 37, MM-FW2: 35, MM-FW4: 23. Source data are provided as a Source Data file.

12
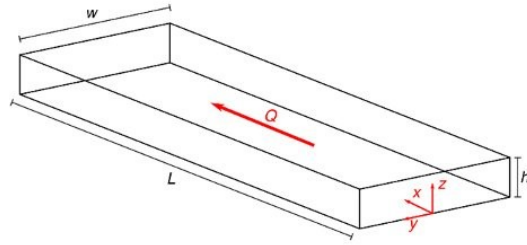
Supplementary Figure 10: Flow geometry in a rectangular channel
Visualization of the channel parameters used to derive the Poiseuille flow profile.

13
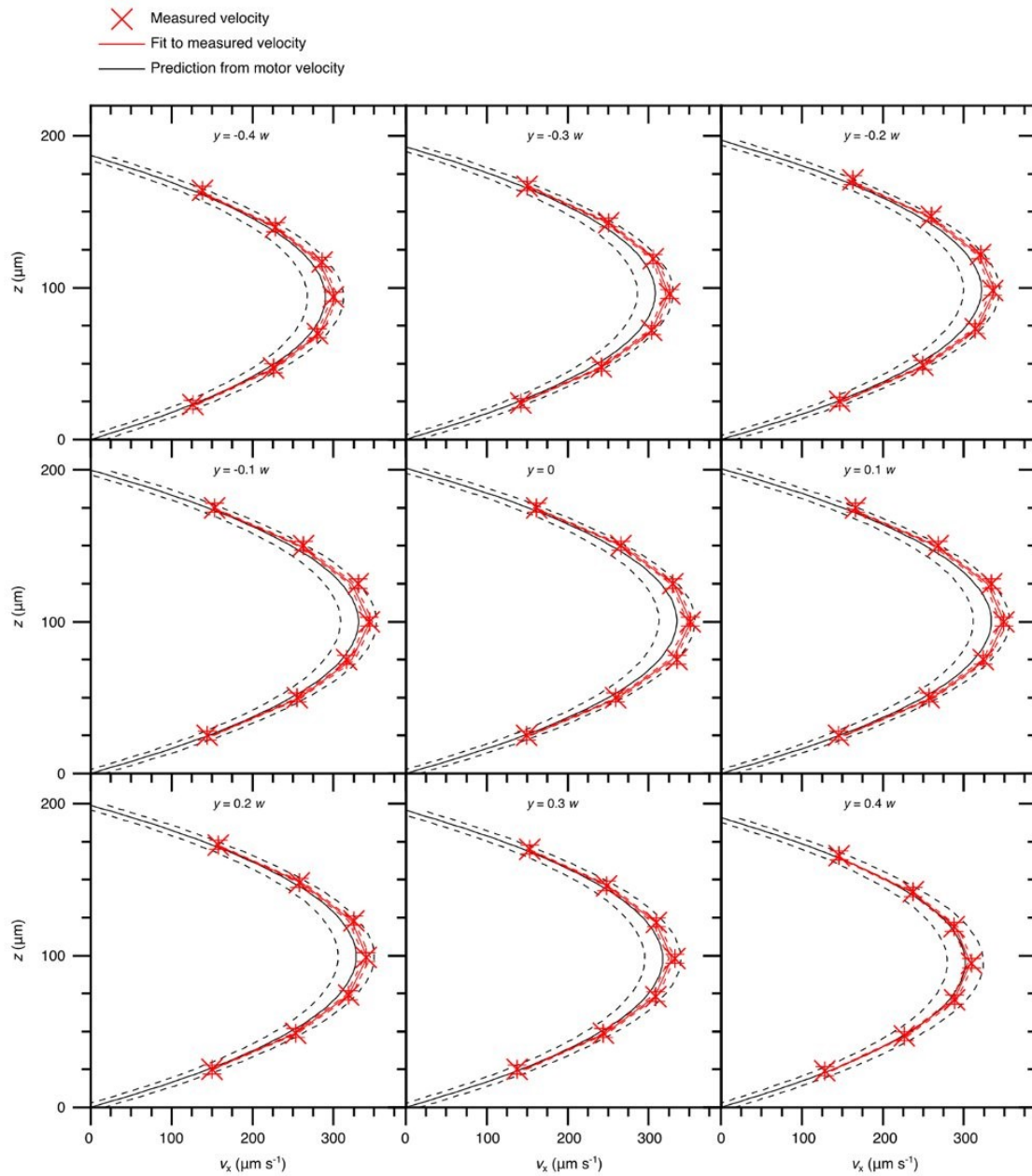
Supplementary Figure 11: Velocity field $v_x(y,z)$ inside a flow channel
Velocity field $v_x(y,z)$ inside a flow channel measured by tracking tracer particles at a flow rate of 0.2 μL s^{-1}. The data points represent mean velocities of typically 50-100 particles. Error bars represent the standard deviation of all measured velocities. Note that the channel was approximately 15 μm higher in the center at $y = 0$ than near the side walls at $y = \pm 0.4\, w$. The

14

velocity field given by equation (15) was fitted to the measured data with the flow rate in the center as the only free parameter. The measured velocity field matched the velocity field $v_{(x,par)}$ calculated from the motor velocity and the channel geometry within the margin of error. The measured flow field inside the channel matched the flow field predicted from equations (8), (14), and (15) within the margin of error, which was calculated by gaussian error propagation. Notably, this was also the case near the side walls of the channel, where the channel was approximately 15 μm thinner. Source data are provided as a Source Data file.

15
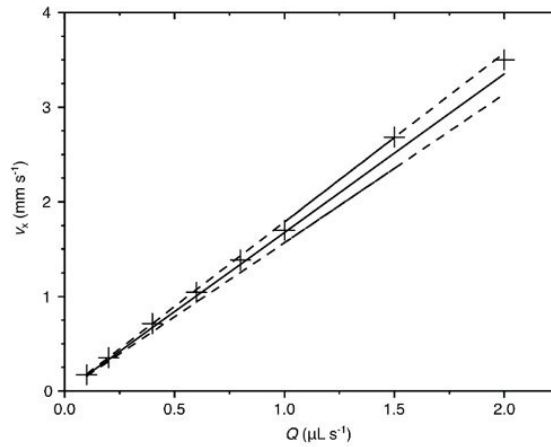
Supplementary Figure 12: Velocity $v_x(0, h/2)$ as a function of the flow rate Q
Velocity $v_x(0, h/2)$ in the middle of the channel as a function of the flow rate Q. The solid line and the dashed lines show the expected flow velocity at the set motor velocity v_m in the middle of the cannel calculated from equations (8), (14), and (15). The error was calculated using Gaussian error propagation. Source data are provided as a Source Data file.

16
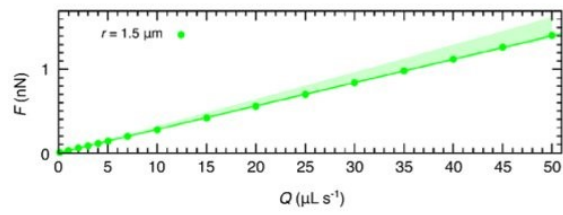
Supplementary Figure 13: The force $F(Q)$ as a function of the flow rate Q.
The filled dots represent the interpolated simulations (case C). The lightly colored range is the corridor between case A and case B. We performed a linear fit (equation (7) with $C_1 = 1$), illustrated as a continuous line.

17
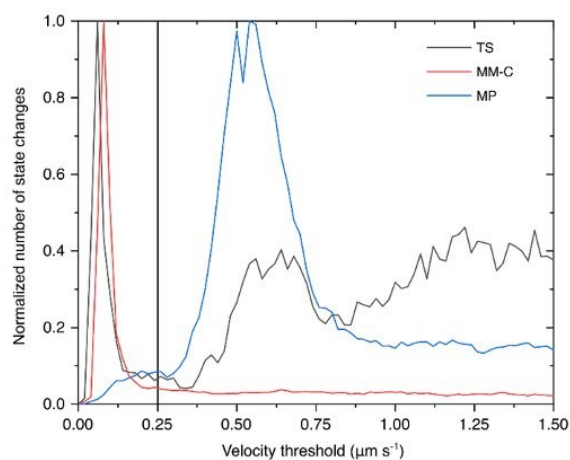
Supplementary Figure 14: Estimation of the threshold velocity.
Number of particle state changes between bound and unbound state as a function of the velocity threshold for exemplary particle types (TS, MM-C and MG). Non-adhesive particles such as MG diffuse in the sample and have velocities which were typically higher than 0.25 μm s^{-1} while the observed velocity of sticky particles such as MM-C was determined by noise and below 0.25 μm s^{-1}. TS particles of which some were bound, and some were unbound showed the same two different regimes in their velocity distribution. Both regimes could be separated by a threshold at 0.25 μm s^{-1}. Source data are provided as a Source Data file.

18
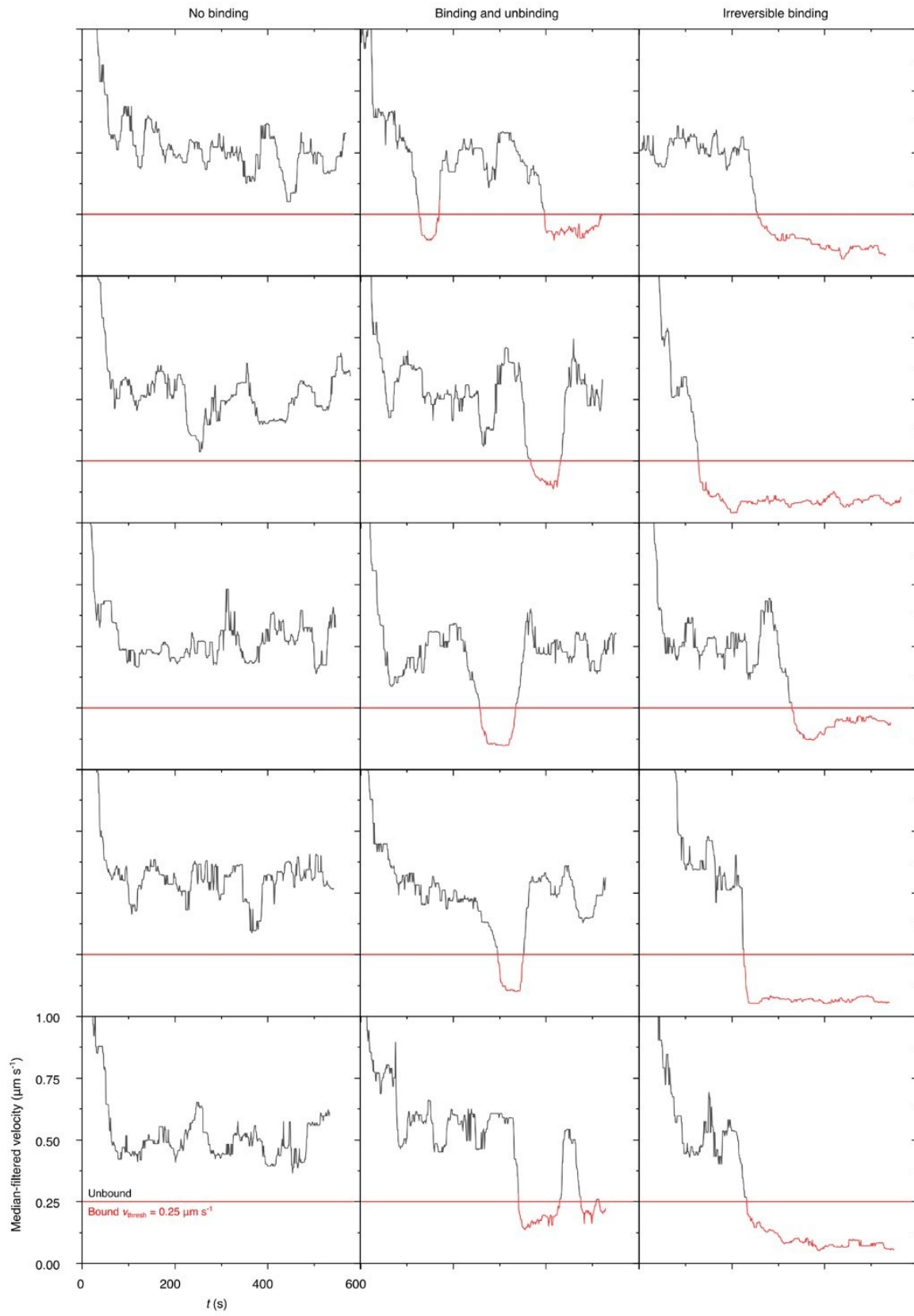
Supplementary Figure 15: Examples of particle trajectories and their binding states.
Median filtered particle velocities and their respective binding states. The velocity was filtered with a median filter with a length of 31 s to remove noise. The binding state was determined via thresholding (Supplementary Figure 14) and is color coded in the panels (red: bound ($v < v_{\text{thresh}}$); black: unbound ($v > v_{\text{thresh}}$)). The state changes of the particles differed drastically. Some particles never bound (left column), others bound and unbound shortly after the binding event (center column) and some bound and did not detach until the end of the experiment (right column). Source data are provided as a Source Data file.

20
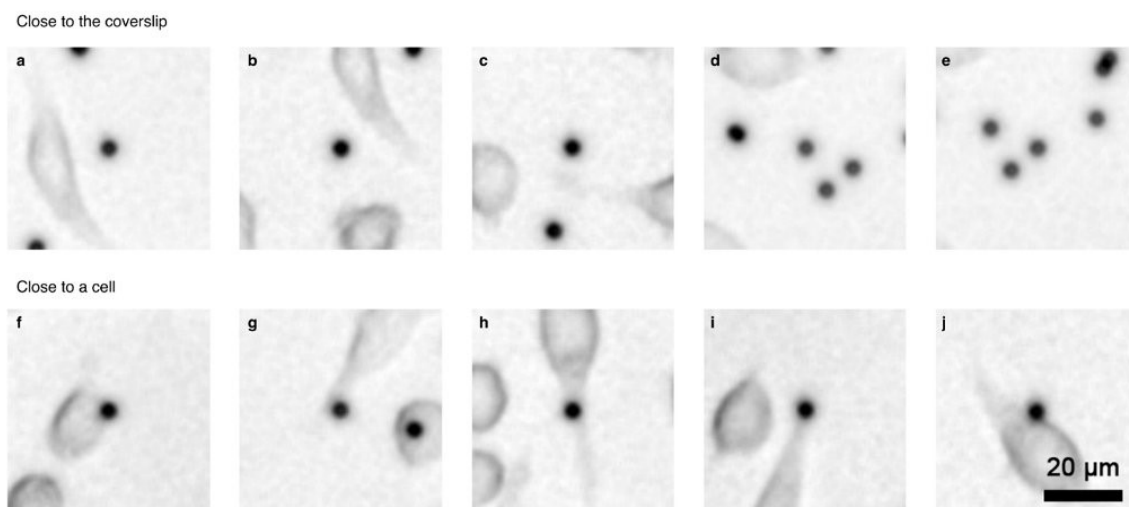
Supplementary Figure 16: Example images used for training the convolutional neural net. The network was trained to classify whether the particle in the center of the image was close to the coverslip (**a-e**) or close to a cell (**f-j**).

21
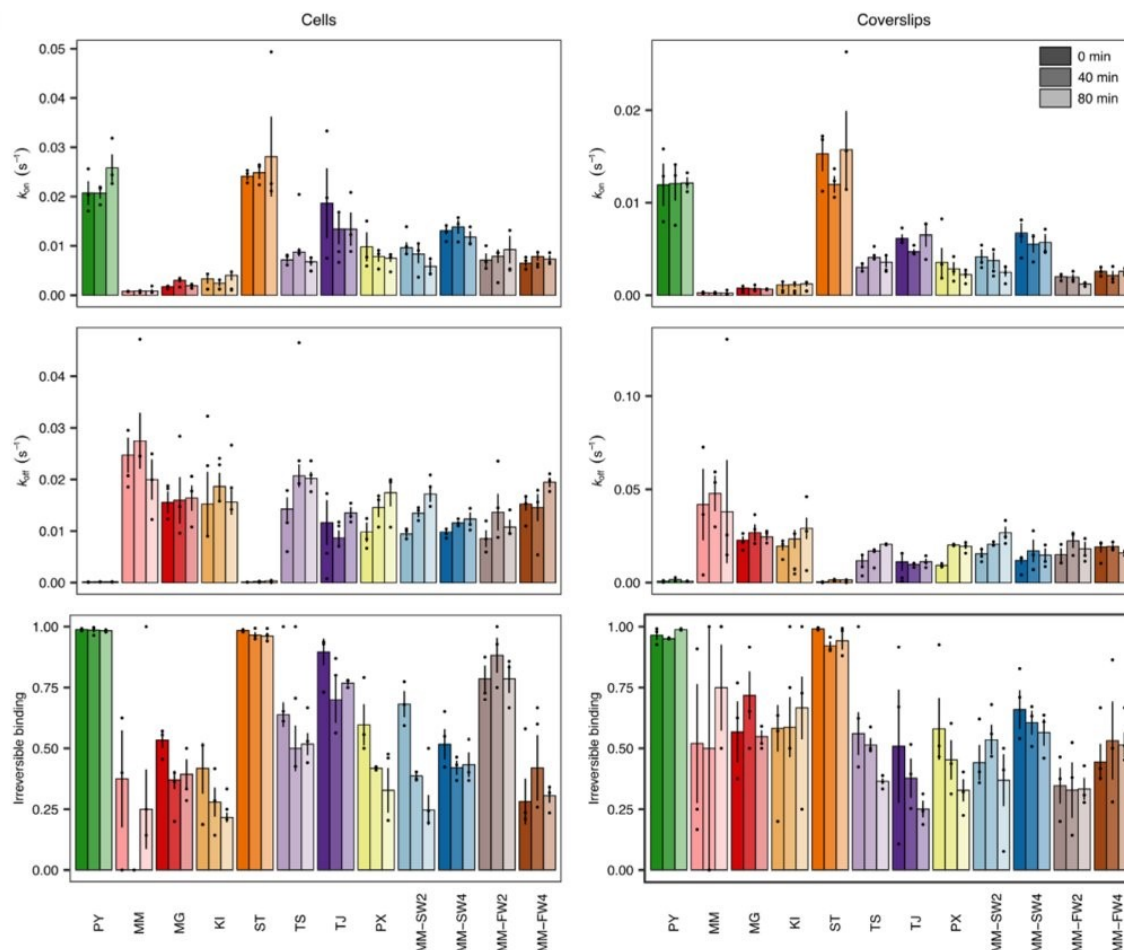
Supplementary Figure 17: Time dependence of binding kinetics.
We performed measurements after $t = 0$ min (dark colors), 40 min (medium colors), and 80 min (light colors) after the particles were added to the microfluidic system to investigate possible interactions of the particles with the image medium. k_{on}, k_{off}, and the fraction of irreversible binding events did not depend on t in most cases. Only the fraction of irreversible binding events to cells decreased slightly with time for PX and MM-SW2 particles. Error bars represent standard error of mean of $n = 3$ individual measurements (indicated as black dots, for each measurement, on average 550 particles were analyzed). Source data are provided as a Source Data file.

22
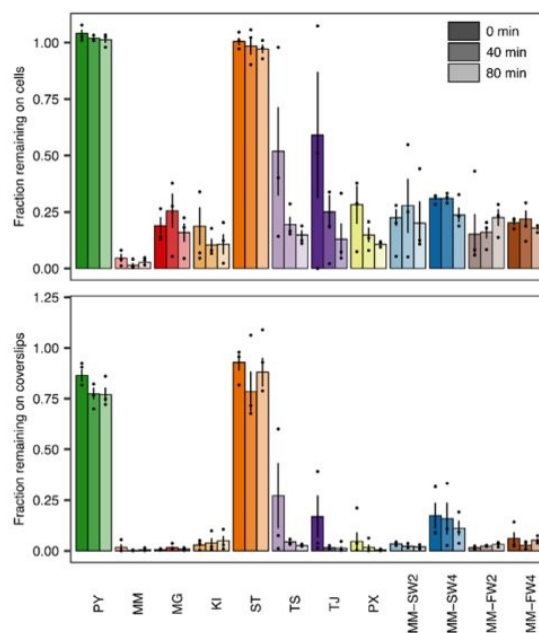
Supplementary Figure 18: Time dependence of adhesion strength.
We performed measurements after $t = 0$ min (dark colors), 40 min (medium colors), and 80 min (light colors) after the particles were added to the microfluidic system to investigate possible interactions of the particles with the image medium. Although some microplastic particles showed a decrease of the average number of remaining particles over time (e.g., TS, TJ), this was not statistically significant. This may indicate that factors other than protein corona formation dominate the variance of the measured adhesive strength. Error bars represent standard error of mean of $n = 3$ individual measurements (indicated as black dots, for each measurement, on average 550 particles were analyzed). Source data are provided as a Source Data file.

23

Particle type	Nominal density (g cm^{-3})	Equivalent diameter (μm)	Eccentricity	Roughness	$\zeta_{initial}$ (mV)	ζ_{medium} (mV)
PY	n.a.	3.08 ± 0.20	1.003 ± 0.001	1.04 ± 0.01	-83.8 ± 0.3	-41.5 ± 0.5
MM	1.03	2.94 ± 0.02	1.005 ± 0.001	1.04 ± 0.01	-4.7 ± 0.3	-6.2 ± 1.0
MG	1.05	2.97 ± 0.11	1.01 ± 0.03	1.05 ± 0.02	-12.6 ± 0.3	-7.3 ± 0.2
KI	n.a.	2.96 ± 0.03	1.005 ± 0.001	1.05 ± 0.01	-5.3 ± 0.5	-6.8 ± 0.4
ST	1.05	3.47 ± 0.26	1.005 ± 0.002	1.06 ± 0.04	-93.1 ± 1.1	-40.1 ± 1.0
TS	1.05	2.84 ± 0.03	1.005 ± 0.004	1.05 ± 0.02	-13.7 ± 0.2	-11.5 ± 0.4
TJ	n.a.	3.36 ± 0.07	1.008 ± 0.004	1.07 ± 0.02	-45.5 ± 0.7	-25.7 ± 6.3
PX	1.06	3.13 ± 0.33	1.02 ± 0.03	1.037 ± 0.004	-7.5 ± 0.4	-10.9 ± 0.5
MM-SW2	-	2.97 ± 0.17	1.04 ± 0.08	1.18 ± 0.15	-10.0 ± 0.7	-7.3 ± 0.4
MM-SW4	-	3.03 ± 0.14	1.02 ± 0.01	1.07 ± 0.04	-7.2 ± 1.3	-7.6 ± 1.3
MM-FW2	-	2.88 ± 0.28	1.005 ± 0.006	1.07 ± 0.04	-9.2 ± 0.5	-8.3 ± 0.5
MM-FW4	-	2.96 ± 0.04	1.01 ± 0.01	1.08 ± 0.07	-16.0 ± 2.3	-6.3 ± 0.7

Supplementary Table 1: Physicochemical particle properties.
The nominal density of the particles was obtained from the respective data sheets. The equivalent diameter, eccentricity, and roughness of the particles were quantified using SEM images. Eccentricity values of 1 correspond to perfect spheres, larger values indicate a more aspherical shape of the particles. Roughness values of 1 correspond to perfectly smooth spheres, larger values indicate more irregular surfaces. Only surface irregularities on length scales larger than 10 nm were detected. For each sample, n = 10 individual particles were analyzed. The ζ-potential of microplastic particles was measured before and after incubation in cell culture medium using a zetasizer. The values of the ζ-potential of microplastic particles after an incubation in cell culture media for 2 h ζ_{medium} are correlated to their initial ζ-potential $\zeta_{initial}$ (Supplementary Figure 2). The ζ-potential measurements were replicated n = 3 times. Errors represent standard deviation. Source data are provided as a Source Data file.

24

Absorption peak	MM	MM-SW2	MM-FW2
Quinone C=O	0.14	0.05	0.07
1) Aromatic C=C	0.08	0.10	0.08
2) Aromatic C=C	1.17	1.14	1.13
Aliphatic C-C	0.25	0.22	0.25
Protein C-O	0.10	0.07	0.14
Carboxylic COOH	0.18	0.21	0.18
Sugar C-OH	0.07	0.07	0.10

Supplementary Table 2: STXM data.
Fitted peak areas (arbitrary units) from the synchrotron-based scanning transmission X-ray microscopy (STXM). In the absorption spectra we observed signatures from aromatic C=C bonds of polystyrene. The aromatic C=C bonds at two different energies represent the two different types of C-atoms in the aromatic ring of the polymer. Their signatures did not significantly change upon exposure to salt or freshwater. Furthermore, we observed small amounts of quinone C=O bonds that decreased upon exposure to salt or freshwater. The aliphatic C-C bonds were likely part of the bulk polymer and did not change upon exposure to environmental media. Carboxylic groups (COOH) were present on the particles' surface, likely because of oxidation processes. The amount of COOH weakly increased for MM particles exposed to salt water but did not change for freshwater-exposed particles. We observed small amounts of protein-associated C-O bonds and sugar-associated C-OH groups on the MM particles. The amount of these groups significantly increased for MM particles exposed to freshwater, indicating the formation of an eco-corona. However, we could not observe a similar build-up of proteins and sugars on MM particles exposed to salt water. A potential explanation could be that parts of the eco-corona were washed off due to the change in ionic strength in the seawater-incubated sample during the rinsing procedure that was required to avoid salt precipitation during drying of the samples.

Due to the OD range of 0.1-0.9 that was required to obtain a decent spectral quality for peak fitting (which was equivalent to a cumulative thickness of 100 nm tangentially around the particles), the 3 spectra represent a mixture of the polymer itself and a potential eco-corona that is dominated by the polymer. Therefore, we additionally performed X-ray photoelectron spectroscopy, which is more suitable for the analysis of thin surface layers because of its much higher surface sensitivity. (Supplementary Table 3). Source data are provided as a Source Data file.

25

Element ratio	MM	MM-SW2	MM-FW2
[N]:[C]	-	0.4%	0.3%
[O]:[C]	31.4%	27.6%	30.9%
[Si]:[C]	0.1%	0.7%	0.9%
[Na]:[C]	-	0.2%	-
[Mg]:[C]	-	1.6%	-
[S]:[C]	-	0.2%	-
[Cl]:[C]	-	1.8%	-

Supplementary Table 3: XPS data.
Element concentration ratios were calculated from the energy dispersive XPS spectra. Depending on the element, the detection limit was approximately 0.1%, signals below the detection limit were indicated with "-". We observed that the surface of environmentally exposed microplastic particles was significantly altered compared to the pristine particles. We observed small amounts of organic nitrogen on MM particles that were incubated in salt and freshwater, which was not present on the pristine MM particles. This could potentially indicate the presence of biomolecules or other natural organic matter, like humid acids, on the microplastics' surface. Furthermore, there was a substantial increase in the amount of silicon on the environmentally exposed particles, which might be caused by the presence of silicic acid. Silicic acid plays a role in the metabolism of algae like diatoms, but also of other plants and animals. However, since the substrate for the XPS measurements was made from thermally oxidized silicon, this finding should be interpreted with caution. Additionally, we observed a significant decrease of the amount of organically bonded oxygen on the particles surface from the high-resolution C1s spectra. This might be related to the production of the MM particles, where possibly non-ionic surfactants, e.g. oligoethoxides, were applied to control the particle growth, which might have been washed out in the environmental media. Furthermore, for the MM particles incubated in salt water, we observed the presence of salts: We could identify significant amounts of sodium, magnesium, sulfur, and chlorine. Source data are provided as a Source Data file.

26

Particle	PY	MM	MG	KI	ST	TS	TJ	PX	MM-FW2	MM-FW4	MM-SW2	MM-SW4
$k_{(on,cells)}$	A	B	C	BC	A	DE	ADE	DE	DE	D	E	E
$k_{(on,coverslips)}$	A	ABC	B	ABC	A	BC	BC	BC	BC	B	C	BC
$k_{(off,cells)}$	A	B	B	B	A	B	B	B	B	B	B	B
$k_{(off,coverslips)}$	A	ABC	CD	ABCD	A	BCD	D	BCD	BC	BD	BCD	BC
Irreversible binding events to cells	A	ABCDE	BC	B	AD	CDE	E	BC	BC	BC	DE	BC
Irreversible binding events to coverslips	A	ABC	B	ABC	A	BC	BC	BC	BC	B	C	BC
Relative attachment to cells	A	B	BCD	BD	A	BCD	BCD	BCD	BCD	D	BCD	C
Relative attachment to coverslips	A	B	BCD	BC	A	BCD	BCD	BCD	BCD	C	BCD	D

Supplementary Table 4: Summary of the statistical analysis.
Statistical testing of the relative attachment between particles and cells as well as between particles and coverslips. Particles of different manufacturers attach significantly different to cells as well as coverslips. The data was tested for a normal distribution using a Shapiro-Wilk test and for a homogeneity of the variances with a Levene test. Differences between particles were identified with a Kruskal-Wallis test together with a Games-Howell post-hoc test. Different letters denote groups of particle types between which significant differences with a two-sided $P < 0.05$ were detected. For example, k_{on} to cells of PY was statistically different to MM, MG, KI, TS, PX, MM-FW2, MM-FW4, MM-SW2, and MM-SW4, but no statistically significant differences existed between PY and ST and TJ. A detailed summary of all statistics is presented in Supplementary Data 1.

27

Supplementary References

1. Ramsperger, A. F. R. M. *et al.* Environmental exposure enhances the internalization of microplastic particles into cells. *Sci. Adv.* **6**, eabd1211 (2020).
2. Crocker, J. C. & Grier, D. G. Methods of digital video microscopy for colloidal studies. *J. Colloid Interface Sci.* **179**, 298–310 (1996).
3. Henke, B. L., Gullikson, E. M. & Davis, J. C. X-Ray Interactions: Photoabsorption, Scattering, Transmission, and Reflection at E = 50-30,000 eV, Z = 1-92. *At. Data Nucl. Data Tables* **54**, 181–342 (1993).
4. Ravel, B. & Newville, M. ATHENA , ARTEMIS , HEPHAESTUS : data analysis for X-ray absorption spectroscopy using IFEFFIT. *J. Synchrotron Radiat.* **12**, 537–541 (2005).
5. Dynes, J. J. *et al.* Quantitative mapping of chlorhexidine in natural river biofilms. *Sci. Total Environ.* **369**, 369–383 (2006).

28

Article 4

Environmental exposure enhances the internalization of microplastic particles into cells

SCIENCE ADVANCES | RESEARCH ARTICLE

ENVIRONMENTAL STUDIES

Environmental exposure enhances the internalization of microplastic particles into cells

A. F. R. M. Ramsperger[1,2], V. K. B. Narayana[1], W. Gross[2], J. Mohanraj[3], M. Thelakkat[3], A. Greiner[4], H. Schmalz[4], H. Kress[2]*[†], C. Laforsch[1]*[†]

Microplastic particles ubiquitously found in the environment are ingested by a huge variety of organisms. Subsequently, microplastic particles can translocate from the gastrointestinal tract into the tissues likely by cellular internalization. The reason for cellular internalization is unknown, since this has only been shown for specifically surface-functionalized particles. We show that environmentally exposed microplastic particles were internalized significantly more often than pristine microplastic particles into macrophages. We identified biomolecules forming an eco-corona on the surface of microplastic particles, suggesting that environmental exposure promotes the cellular internalization of microplastics. Our findings further indicate that cellular internalization is a key route by which microplastic particles translocate into tissues, where they may cause toxicological effects that have implications for the environment and human health.

INTRODUCTION

Microplastic particles are ubiquitous in marine and freshwater ecosystems (1, 2). Once microplastic particles are introduced into these environments, microorganisms and biomolecules attach to their surfaces, forming an eco-corona that can enhance their ingestion by organisms (3). The ingestion of microplastic particles has been shown in a huge variety of organisms (4) ranging from zooplankton (5, 6), to bivalves (7, 8), up to vertebrates (9). From the gastrointestinal tract, which represents the main entry point for ingested foreign particulate matter, microplastic particles can translocate into the circulatory system (7) and the tissues, where their effects include inflammatory responses (8) and necrosis (9). The translocation of microplastic particles into tissues has been suggested to occur via cellular internalization (7, 8). The gastrointestinal system comprises a plethora of different cell types (10), including macrophages. This cell type occurs in all body compartments including the digestive system. Macrophages additionally occupy a central position within the innate immune response to foreign particulate matter and are specialized on the internalization of foreign material (11). Hence, they may play a decisive role for cellular internalization of microplastic particles.

An established approach to investigating the cellular internalization of particles by macrophages is the use of specifically surface-functionalized particles, like carboxylated and, therefore, negatively charged particles (12, 13) or opsonized particles coated with antibodies such as immunoglobulin G (IgG) (14) to induce receptor-mediated phagocytosis (12, 15). Smaller-sized particles are more likely internalized by cells than larger microparticles (16, 17). This may be because of the fact that smaller particles, especially in the nano size range (18), can passively cross cellular membranes, whereas for larger particles, mechanisms of active endocytosis play a crucial role (19). The abovementioned functionalized and pristine

particles, predominantly used in toxicological studies, do not resemble microplastic particles found in nature, since plastic in the environment is of different shape and size and is additionally coated with an eco-corona (3). However, in research on the effects of larger microplastic particles, a recent comprehensive review (19) highlighted that "factors other than size have so far hardly been considered when studying tissue translocation." Recently, Nasser et al. (20) proposed in their comprehensive review that the inclusion of biological matter, like eco-corona coatings, should become a prerequisite for ecotoxicity testing (20). Already seconds after exposure, plastic surfaces are covered by biomolecules (21) forming an initial corona. Over time, biomolecules with higher binding affinities substitute biomolecules with lower binding affinities forming the so called "hard corona," and biomolecules can adhere to already strongly attached biomolecules forming the "soft corona" (22). This process leads to the formation of a substantial coating that mainly consists of biomolecules, like carbohydrates, lipids, and proteins (3, 23), which raises the intriguing possibility that this eco-corona could promote microplastic particle internalization by host cells. Given that specific protein coatings other than, e.g., IgG can also increase particle internalization into cells (24, 25), we hypothesized that microplastic particles exposed to aquatic environments adsorb biomolecules, forming an eco-corona that enhances the particles' attachment to and internalization into cells compared with pristine microplastic particles.

RESULTS

To test our hypothesis, we investigated the internalization of fresh water– and salt water–exposed spherical microplastic particles with a diameter of 3 μm, a size class reported to occur in the environment (26) and of appropriate size of active endocytosis (27). As a cell system, we used the established murine macrophage cell line J774A.1 with a mean single cell area of 495 ± 22 μm^2 (all numbers shown are the means ± standard error of the mean, unless otherwise stated). We incubated the microplastic particles (nonfluorescent plain polystyrene without any functionalization such as opsonization or carboxylation) in fresh water from an artificial pond or salt water from a marine aquarium (both of which were inhabited by diverse

[1]Animal Ecology I and BayCEER, University of Bayreuth, Bayreuth, Germany. [2]Biological Physics, University of Bayreuth, Bayreuth, Germany. [3]Macromolecular Chemistry I, Applied Functional Polymers and Bavarian Polymer Institute, University of Bayreuth, Bayreuth, Germany. [4]Macromolecular Chemistry II and Bavarian Polymer Institute, University of Bayreuth, Bayreuth, Germany.
*Corresponding author. Email: holger.kress@uni-bayreuth.de (H.K.); christian.laforsch@uni-bayreuth.de (C.L.)
†Joint senior authors.

animal, plant, and microbial communities; fig. S1). Microplastic particles incubated in ultrapure water (pristine particles) under sterile conditions with no biomolecules present were used as negative controls, and IgG-opsonized microplastic particles, known to induce receptor-mediated phagocytosis (14), were used as positive controls. Although some biomolecules are adsorbed by surfaces within seconds (21), we incubated the microplastic particles for 2 and 4 weeks to allow the formation of a substantial eco-corona, resembling conditions a microplastic particle is exposed to in nature. For the internalization experiments, $23,000 \pm 1000$ cells were cultured on glass coverslips, and $29,000 \pm 700$ microplastic particles were added and allowed to sediment onto the cells for 1 hour on ice. Afterward, the cells and the sedimented particles were incubated for 2 hours. After this incubation, unattached particles were washed off using buffer, and the cells were preserved with paraformaldehyde (PFA). Filamentous actin, as being part of the cytoskeleton and intimately involved in the process of the internalization of particulate matter in the used size (15), was fluorescently labeled to distinguish between internalized and attached microplastic particles: Only those microplastic particles that were fully surrounded by fluorescently labeled actin were considered to have been internalized (Fig. 1 and fig. S2). With our experimental approach, we can show that nonfluorescent microplastic particles exposed to the environment are fully surrounded by cellular material and are therefore

unambiguously internalized by the cells. To verify that these particles were indeed the used incubated polystyrene microplastic particles and not contaminants (e.g., dust of a similar size and shape), single Raman spectra were acquired from 10 randomly chosen particles from each treatment and incubation time. All particles were confirmed to be the used polystyrene particles (fig. S3).

Our results show that microplastic particles exposed to fresh water or salt water for either incubation time (2 or 4 weeks) attached to and became internalized by cells approximately 10 times more often than pristine microplastic particles. The nonparametric Kruskal-Wallis test was used to investigate differences between all tested treatments: $P < 0.001$ for 2 ($_{2w}$) and 4 ($_{4w}$) weeks of incubation. A Games-Howell post hoc test was conducted for pairwise analysis (e.g., FW versus SW). Particle-cell interactions (PCI): FW_{2w} versus UW_{2w} $P < 0.01$, $FW4_w$ versus UW_{4w} $P < 0.001$, SW_{2w} versus UW_{2w} $P < 0.05$, SW_{4w} versus UW_{4w} $P \leq 0.001$; internalized: FW_{2w} versus UW_{2w} $P < 0.01$, $FW4_w$ versus UW_{4w} $P < 0.01$, SW_{2w} versus UW_{2w} $P < 0.01$, SW_{4w} versus UW_{4w} $P \leq 0.001$ (Fig. 2). IgG-opsonized microplastic particles attached to and were internalized by cells more often than microplastic particles exposed to fresh water and salt water by a factor of approximately 10, and more often than pristine microplastic particles by a factor of approximately 100 (PCI and internalized: $IgG_{2w\&4w}$ versus $FW/SW/UW_{2\&4w}$ $P \leq 0.001$). Furthermore, between 2 and 4 weeks of incubation, we detected significant increases in the numbers of attached microplastic particles exposed to salt water and internalized microplastic particles exposed to fresh water or salt water (for pairwise comparisons of the incubation times within one treatment, a nonparametric Mann-Whitney U test was performed: PCI: SW_{2w} versus SW_{4w} $P < 0.01$; internalized: SW_{2w} versus SW_{4w} $P < 0.01$, FW_{2w} versus FW_{4w} $P < 0.05$; Fig. 2). We did not observe a statistically significant difference between microplastic particles incubated in fresh water and salt water for either incubation time (summary statistical analysis, see table S2).

The increased number of attachments and internalizations observed for the pretreated particles is likely because of the presence of an eco-corona. To determine whether an eco-corona was present, we first investigated the surface morphology of microplastic particles using scanning electron microscopy (SEM). The microplastic particles exposed to fresh water showed heterogeneously distributed irregular surface modifications (Fig. 3A), indicating the adhesion of molecules (28), which might be components of an eco-corona. Those exposed to salt water seemed to be homogeneously covered with structures resembling salt crystals (Fig. 3B), which were likely derived from air drying and which impeded the detection of an eco-corona. In contrast, the pristine microplastic particles had plain surfaces without any visible modifications (Fig. 3C), and IgG-opsonized microplastic particles showed rough but homogeneous surfaces (Fig. 3D), as is characteristic of particles that are opsonized with proteins (28). This finding is supported by the fact that the diameters of these structures were in the same size range (20 to 40 nm) as individual IgG antibodies (29).

Then, to determine whether the surface modifications detected by SEM might represent biomolecules in an eco-corona, we investigated the chemical signatures of these coatings using micro-Raman spectroscopy. We found that the surfaces of particles exposed to fresh water harbored Raman bands, indicating the presence of biomolecules such as carbohydrates (C—O—C band), amino acids (C—N—S band), nucleic acids (PO_4 band), lipids (C—H, C—H_2
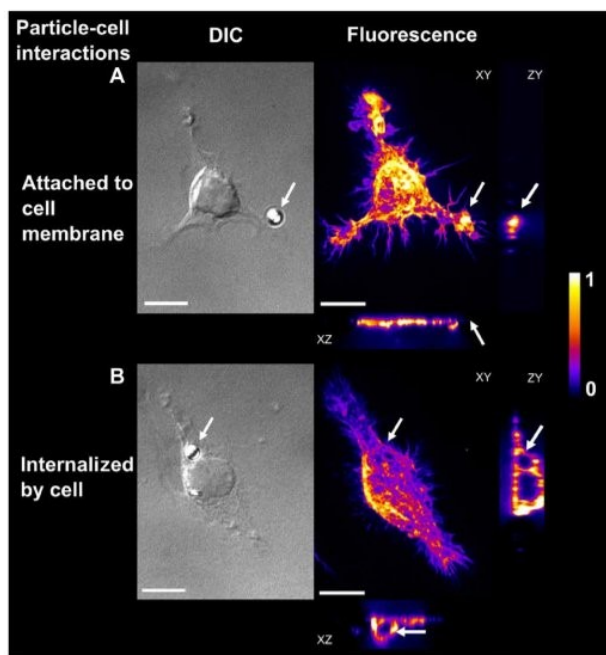
Fig. 1. Images of particle-cell interactions of microplastic particles exposed to fresh water for 2 weeks. DIC: Differential interference contrast microscopy images of particle-cell interactions. Fluorescence: Spinning disc confocal images of the cells with fluorescently labeled filamentous actin (false color image, maximum intensity projection showing arbitrary units). XY, YZ, and XZ projections of three-dimensional confocal images allow the differentiation of microplastic particles (**A**) attached to cell membranes or (**B**) internalized microplastic particles. Arrows indicate microplastic particle position. Scale bars, 10 μm.
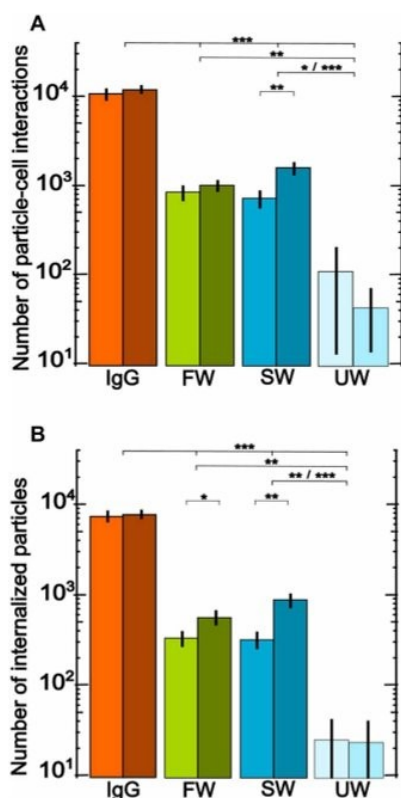
Fig. 2. Combined results of particle-cell interactions and internalized microplastic particles. (**A**) Numbers of particle-cell interactions and (**B**) numbers of internalized microplastic particles following 2 (light color) or 4 (dark color) weeks of incubation (all numbers indicate the means ± SE, table S1; IgG, positive control; FW, particles exposed to fresh water; SW, particles exposed to salt water; UW, negative control, pristine particles from ultrapure water). The numbers of particle-cell interactions and internalized microplastic particles were standardized to coverslips with 23,000 cells to which 29,000 particles were added. Because the data span almost three orders of magnitude, the ordinate is scaled logarithmically. The IgG treatment differs highly significant from all other treatments for either incubation time. Fresh water and salt water differ significantly from ultrapure water (except where specified otherwise, a Kruskal-Wallis test followed by a Games-Howell post hoc test was conducted to investigate significant differences between treatments, ***$P \leq 0.001$, **$P \leq 0.01$, *$P = 0.05$). The salt water treatment shows a significant increase in the numbers of particle-cell interactions and internalized microplastic particles over the incubation time, and fresh water shows a significant increase in the number of internalized microplastic particles during the incubation time (Mann-Whitney U test: **$P \leq 0.01$, *$P = 0.05$).

band), and proteins (C—H and C=O band) (30), which are known constituents of an eco-corona (Fig. 4) (3, 23). In contrast, we did not detect Raman bands specific for biomolecules on the pristine microplastic particles. We were not able to detect any chemical signatures specific to biomolecules on the surfaces of microplastic particles exposed to salt water, most likely because of the incrustation with salt crystals that was observed by SEM and bright-field imaging (fig. S4). The very prominent SO_4^{2-} salt Raman band may have masked other bands specific for biomolecules (fig. S5).

Therefore, we further analyzed the elemental composition of surface coatings of microplastic particles incubated in ultrapure,

fresh water, and salt water using x-ray photoelectron spectroscopy (XPS, Fig. 5). Microplastic particles incubated in fresh water and salt water displayed a distinct feature corresponding to nitrogen, which was absent on microplastic particles incubated in ultrapure water (fig. S7). In addition, salt water–incubated microplastic particles showed carbon from either —O=C—O— or —O=C—N— groups (fig. S8) (31). The origin of this signal is more likely from —O=C—N— groups as the presence of nitrogen was unequivocally confirmed on microplastic particles incubated in salt water (Fig. 5B). This is further supported by the nitrogen peak position (400.1 eV) found on both salt water– and fresh water–incubated microplastic particles, which is characteristic of amino acids (31). The presence of a variety of functional groups on microplastic particles incubated in fresh water and salt water was further supported by their broad S 2p and O 1s core spectra (fig. S9). Hence, XPS analysis strongly indicate the presence of biomolecules not only on the surface of fresh water–incubated but also even on the surface of salt water–incubated microplastic particles. Furthermore, the fact that particles incubated in salt water attached to and were internalized by cells as often as particles incubated in fresh water indicates that the two types of particles have similar biomolecular coatings.

DISCUSSION

Overall, our findings suggest that the coating of the particles with biomolecules enhances the cellular internalization of microplastic particles, indicating that the presence of an eco-corona is an important factor inducing the cellular internalization of microplastics.

It has been shown that some proteins act as opsonins that enhance the internalization of particles into cells, since surface proteins play an important role in nanoparticle-cell interactions (32, 33). For instance, Walkey et al. (25) showed that the internalization of gold nanoparticles by the same murine macrophage cell line as that used in our study is positively correlated with the concentration of proteins adsorbed onto the particle surface. Our results show that the role of surface coatings extends to microplastic particles in the lower micrometer range exposed to fresh water and salt water. Once biomolecules adsorb onto microplastic particle surfaces, they may function as a chemical stimulus for the attachment and internalization of those particles into cells, similar to mechanisms known for specifically functionalized particles. The internalization of foreign materials by macrophages is triggered by membrane receptors such as Fc or scavenger receptors (34). While, for example, Fcγ receptors are highly specific for binding the Fc region of IgG antibodies (15), scavenger receptors are known for their broad range of ligand binding (34). Therefore, the internalization of microplastic particles coated with an eco-corona may occur via scavenger receptor–induced phagocytosis. Consistently, we found that pristine microplastic particles with no eco-corona were very rarely internalized compared with microplastic particles incubated in fresh water and salt water. Although pristine microplastic particles do not have an eco-corona, a coincidental internalization of these particles could be because of membrane ruffling and macropinocytosis, as both processes occur in macrophages (35, 36). Membrane ruffling is intimately linked to the formation of macropinosomes, which can be up to 5 μm in size (32), and therefore, pristine microplastic particles with no chemical stimulus on their surfaces could be nonspecifically internalized together with fluid because of this process.
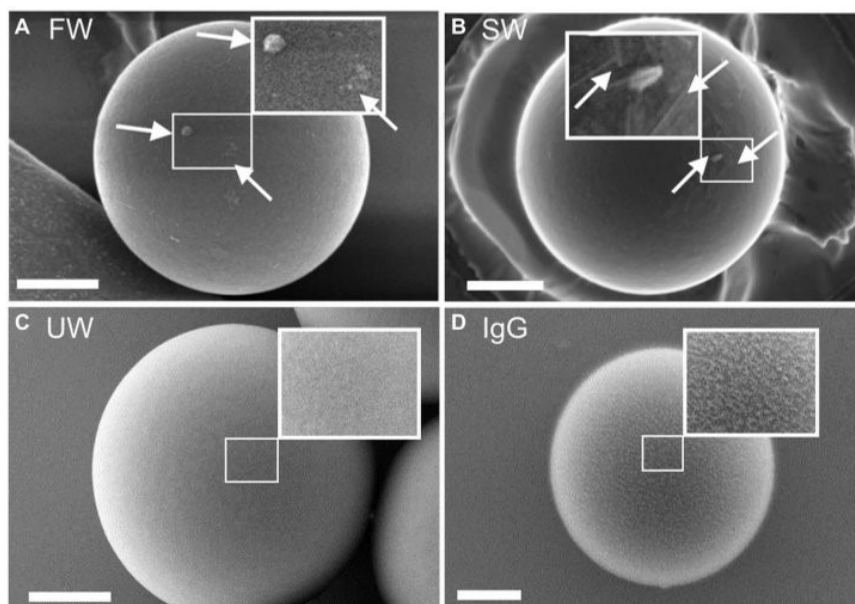
Fig. 3. Representative SEM images of microplastic particles after 4 weeks of incubation, with enlarged views of the surface. (**A**) FW: Microplastic particles incubated in fresh water, with an enlarged view of the irregular surface modifications (arrows). (**B**) SW: Microplastic particles incubated in salt water, with an enlarged view of the irregular surface modifications with small salt crystals (arrows). (**C**) UW: Microplastic particles incubated in ultrapure water showing a plain surface. (**D**) IgG: Microplastic particles opsonized with IgG with an enlarged view of its homogeneously rough surface. Scale bars, 1 μm; SEM settings: 2 to 3 kV, InLens/SE2 detector.
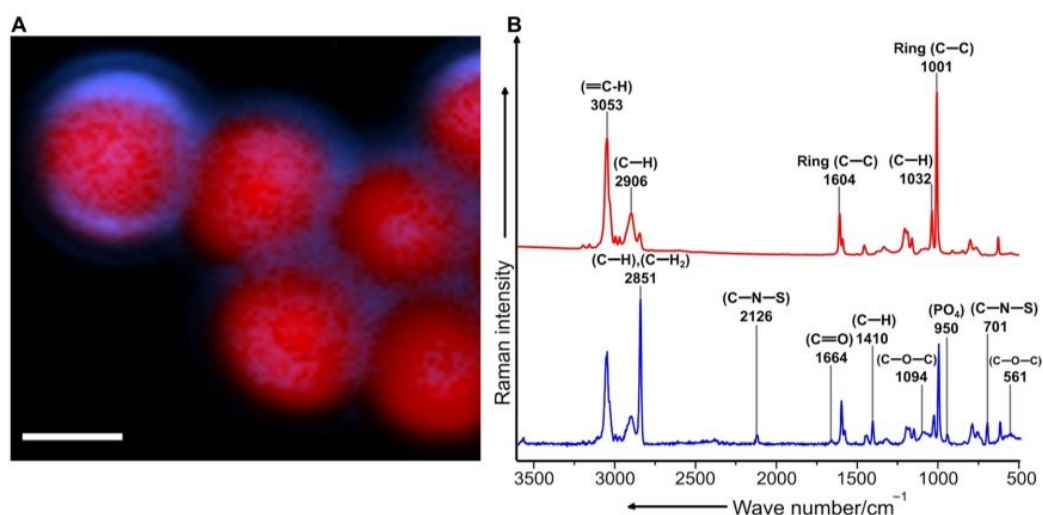
Fig. 4. Raman spectroscopic analysis of the coating of microplastic particles incubated with fresh water. (**A**) False color Raman image of the microplastic particles (red) and the biomolecules forming a putative eco-corona (blue) on their surfaces, generated from the spectral mapping data. Scale bar, 2 μm. (**B**) The spectrum in red represents Raman signatures corresponding to the microplastic particles, and the spectrum in blue corresponds to signatures representative of the eco-corona. The Raman vibrational modes associated with biomolecules are mainly the C-S stretching mode (701 cm^{-1}), the PO$_4$ stretching mode (950 cm^{-1}), the C—H bending mode (1410 cm^{-1}), the C=O stretching mode (1664 cm^{-1}), the C—H and C—H$_2$ stretching mode (2851 cm^{-1}), and the Raman band at 2126 cm^{-1} (C—N—S), together with the stretching mode at 701 cm^{-1}, which could be indicative of the presence of thiocyanate molecules. Spectral signatures such as the =C—H stretching mode (3053 cm^{-1}), the C—H bending mode (2906 cm^{-1}), the C—C bending mode (1604 cm^{-1}), the C—H bending mode (1032 cm^{-1}), and the C—C ring stretching mode (1001 cm^{-1}) correspond to the PS microplastic particles.
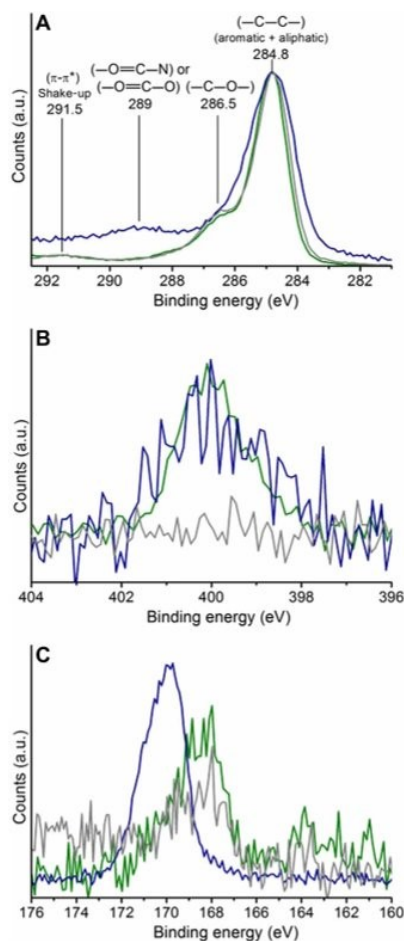
Fig. 5. Core-level spectra of microplastic particles incubated in ultrapure water (gray), fresh water (green), and salt water (blue). (**A**) C 1s region showing the characteristic PS signals at 284.8 and 291.5 eV corresponding to carbon from (—C—C— aliphatic and aromatic) and π-π* shake-up processes, respectively (44). In addition, all the samples display a signal at 286.5 eV, attributable to the carbon bound to oxygen as in alcohol or ether functional groups. Microplastic particles from salt water additionally show a signal at 289 eV, possibly from the carbon in —O═C—N or —O═C—O functional groups. (**B**) N 1s region from all the samples, confirming the presence of nitrogen on the surface of microplastic particles incubated in fresh water and salt water with the maximum at 400.1 eV. (**C**) S 2p region showing prominent signals at 168.5 and 169.8 eV on the surface of microplastic particles from ultrapure water and fresh water, and salt water, respectively, corresponding to sulfate functional group.

We show that an eco-corona formed under environmental conditions facilitates cellular internalization of microplastics in a size range frequently found in nature (26). Hence, it may not be pristine plastic particles per se but rather microplastics exposed to the environment that pose a health risk. It enhances the probability of cellular internalization and therefore may pose more of a health risk to organisms that ingest these particles along with their food. The coating with an eco-corona may then lead to a "Trojan horse" effect that particles normally not interacting with membrane receptors

become internalized (37). Thus, the generally prevailing assumption that plastic itself behaves as an "inert" material from a toxicological point of view (23, 38) is not valid for microplastic particles when exposed to fresh water and salt water. This is in concordance with the suggestion of Galloway et al. (3) that environmental coating plays an important role in the interaction of microplastics with cells and tissues and therefore in determining their ecological impact.

We anticipate our results to be a starting point for investigations on the cellular mechanisms of microplastic internalization from fresh water and salt water and even terrestrial environments. This will allow us to obtain a comprehensive picture of microplastic internalization by cells, which, in turn, will be indispensable for identifying how microplastic exposure might affect organisms in polluted environments.

MATERIALS AND METHODS
Experimental design
Cell line and cell culture conditions
Murine macrophage J774A.1 cells (DSMZ, Braunschweig, Germany) were cultured as described previously by Keller et al. (39). To maintain suitable cell concentrations, cells were passaged three times per week to an appropriate number and cultured in T-75 culture flasks (Corning, New York, USA). Before the experiments, the cells were scraped off of the culture flask surfaces into the culture media, centrifuged (200g, 2 min, 20°C), and resuspended with 5 ml of cell culture medium in a Falcon tube (Corning, Corning, New York, USA). Then, the cells were counted using a hemocytometer (Neubauer improved, Brand, Wertheim, Germany), seeded on microscope coverslips (diameter, 18 mm; #1, MENZEL GLÄSER, Braunschweig, Germany) in 12-well plates (CellStar, Greiner Bio-One, Frickenhausen, Germany) in 1 ml of cell culture medium, and allowed to adhere onto the coverslips under standard culture conditions (37°C, 5% CO_2, humidified) overnight. On each coverslip, 40,000 cells per milliliter were seeded to obtain a mean number of 23,000 cells per coverslip (not all cells adhered to and remained on the coverslips during the experimental procedure).
Microplastic particles and pretreatment conditions
Plain nonfluorescent white polystyrene beads (microplastic particles) with a diameter of 3 μm (Micromod, Rostock, Germany, white particles, micromer plain, Prod. Nr. 01-00-303) were incubated in fresh water or salt water for the environmental samples, or in ultrapure water (Veolia Purelab flex, Veolia, Celle, Germany) to serve as the "pristine microplastic particle" negative control. Freshwater samples were obtained from an artificial outdoor pond, whereas saltwater samples were collected from a marine aquarium facility with a defined salinity of 35 ‰ (fig. S1). Twenty microliters of microplastic particle stock solution (50 mg ml⁻¹) was added to 980 μl of the corresponding water sample (fresh, salt, and ultrapure water) in a glass vial (autosampler vials, 1.2 ml; neoLab, Heidelberg, Germany). The ultrapure water (Veolia Purelab flex, Veolia, Celle, Germany) was filtered (Whatman Puradisc syringe filter, 0.2 μm: GE Healthcare, Freiburg, Germany) under sterile conditions to exclude microbial activity. For each treatment (fresh, salt, and ultrapure water), 10 replicates (glass vials) were prepared. To ensure vital microbial communities within the environmental samples during the incubation process, the corresponding water samples were changed three times per week. Each glass vial was centrifuged (2000g, 20 min,

room temperature), and 900 μl of supernatant was replaced by the same amount of new corresponding water samples. To prevent aggregation of the microplastic particles by sedimentation, all samples were placed on a shaker (100 rpm at room temperature) for the whole incubation time. Although we did not add additional surfactant to avoid aggregation of the microplastic particles, only occasionally aggregates were found in all samples. Microplastic particles from fresh, salt, and ultrapure water were collected for the cell experiments after 2 weeks of incubation, while the remaining particles were further incubated under the same conditions for an additional 2 weeks within the same vials.

For the positive control, IgG antibodies (native IgG primary antibodies from mouse serum; Merck Millipore, Darmstadt, Germany) were passively adsorbed onto carboxylated microplastic particles (Micromod, Rostock, Germany, white particles, micromer COOH, Prod. Nr. 01-02-303) according to the protocol described by Keller *et al.* (*39*). Opsonization was verified by antibody-antibody labeling with goat anti-mouse IgG cross-adsorbed fluorescent secondary antibody (Dy-Light 488, Thermo Fisher Scientific). The IgG-opsonized microplastic particle stock solution was stored at 4°C for later use as a positive control for assessing internalization.

Quantifying numbers of pretreated, positive, and negative control microplastic particles

The numbers of microplastic particles within each treatment were quantified, because due to the media exchange of microplastic particles incubated in fresh, salt, and ultrapure water, an unknown number of particles were lost. The quantification of the numbers of microplastic particles from fresh, salt, and ultrapure water was conducted in subsamples for both incubation times (2 and 4 weeks). The number of microplastic particles within the IgG treatment was only counted once because those particles were obtained from an unmodified stock solution (no media exchange was performed, and therefore, a loss of IgG particles can be ruled out). To quantify the numbers of microplastic particles for each treatment and incubation time, 100 μl of microplastic particle dilutions [fresh, salt, and ultrapure water:phosphate-buffered saline (PBS) 1:100; IgG stock solution:PBS 1:1000] was added to two sample wells per treatment within a 12-well plate, and the particles were allowed to sediment. For imaging, the 12-well plates were placed onto an inverted microscope (Nikon Eclipse Ti, NIKON, Tokyo, Japan, 20×/0.45 objective), and spatial image series were acquired with an electron-multiplying charge-coupled device (EMCCD) camera (Luca-R, Andor, Belfast, Northern Ireland). For each sample well, three regions of interest (ROIs) (4.23 mm² each) were imaged, and the numbers of microplastic particles were counted using the Fiji ImageJ cell counter software (*40*). We tested the distribution of particles within one sample well by microscopy. Heterogeneities of the particle numbers did occur, but we compensated for this by standardizing to 29,000 particles for each treatment for a whole coverslip (245.50 mm²).

Cell experiment

The following experimental procedure was implemented to obtain samples for the quantification of microplastic particles interacting with cells (PCI), the measurement of the area covered by cells on the coverslips, and for investigating the number of internalized microplastic particles from the PCI.

After 2 or 4 weeks of exposure to fresh, salt, and ultrapure water, microplastic particles were added to cells, which were prepared on coverslips in 12-well plates the day before the experiments, as described above. Microplastic particles pretreated with fresh, salt,

or ultrapure water and IgG-opsonized microplastic particles were diluted in cell culture medium (fresh, salt, and ultrapure water 1:100; IgG stock solution 1:1000). The 12-well plates containing the prepared cells were placed on ice for 1 hour to reduce cellular activity. From each treatment of the pretreated microplastic particles and the IgG-opsonized particles, 100 μl of each microplastic particle dilution was added to a coverslip. Ten coverslips for each treatment and exposure time were prepared, yielding a total of 80 coverslips. After 1 hour of microplastic particle sedimentation, the well plates were incubated at 37°C (Kelvitron kl BK6160, Heraeus, Hanau, Germany) for 2 hours to activate cells. Then, the coverslips were washed three times with PBS to remove unattached microplastic particles. Cells were fixed using a PBS-PFA solution containing 4% PFA (Sigma Aldrich, St. Louis, Missouri) for 15 min on ice. Then, the coverslips were washed again three times with PBS, and 50 μl of labeling solution was added and allowed to sit for 25 min to label filamentous actin. The labeling solution consisted of Alexa Fluor Phalloidin 488 (Invitrogen, Carlsbad, USA) and dilution buffer, consisting of 98.7% PBS, including 0.3% Triton and 1% bovine serum albumin (AppliChem, Darmstadt, Germany), to a final concentration of 1:25. The coverslips were again washed three times with PBS and transferred to 1 ml of ultrapure water. Last, the coverslips were mounted on glass slides (Servoprax, Wesel, Germany) with Fluoromount-G (SouthernBiotech, Birmingham, Alabama) mounting media and allowed to dry overnight. The next day, the coverslips were fixed to the glass slides with nail polish (fig. S2).

Quantification of PCI and area covered with cells on coverslips

To determine the total number of PCI on each coverslip, five randomly chosen ROIs (0.29 mm²) were selected and imaged by using a DMI 6000 microscope (Leica, Wetzlar, Germany, HCX PL APO 63×/1.30 oil objective) including a spinning disc unit (CSU-X1, Yokogawa, Musashino, Japan) with an EMCCD camera (Evolve 512, Photometrics, Tucson, Arizona, including an additional ×1.2 magnification lens). A differential interference contrast (DIC) microscopy image was acquired to quantify the PCI within the ROIs using the Fiji ImageJ cell counter software. In addition, confocal stacks of fluorescently labeled cells were acquired using a 488-nm laser (50 mW, Sapphire 488, Coherent, Santa Clara, California) at a spinning disc speed of 5000 rpm to excite fluorescence. Axial stacks of the cells were acquired with a vertical distance of 0.2 μm, which is sufficient to oversample the image given the axial resolution of the microscope (*41*).

The confocal stacks were used to calculate the area covered by cells within an ROI. The area covered by cells was detected using both the DIC and the fluorescence channel simultaneously to obtain robust results. As described previously (*42*), a local contrast filter was applied to the DIC images to obtain a rough approximation of the cell mask M_{DIC}. The local contrast filter highlights areas in which the difference ΔI between the local intensity maximum and minimum is larger than a given threshold T_{DIC}

$$M_{DIC,i,j} = \begin{cases} 1 \text{ if } \Delta I_{DIC,circle} > T_{DIC} \\ 0 \text{ if } \Delta I_{DIC,circle} \leq T_{DIC} \end{cases}$$

A circular filter with a radius of 3 px was chosen. To obtain a mask M_F of the area covered by cells in the fluorescence channel, the axial stacks of 25 images I_F (index k) were projected to the intensity maximum, and a simple threshold T_F was applied to the resulting image

$$M_{F,i,j} = \begin{cases} 1 \text{ if } \max(\{I_{F,k}\})_{i,j} > T_F \\ 0 \text{ if } \max(\{I_{F,k}\})_{i,j} \leq T_F \end{cases}$$

The masks were multiplied to obtain a mask M that highlights areas in which cells were detected in both channels

$$M_{i,j} = M_{DIC,i,j} * M_{F,i,j}$$

In the resulting mask, small holes were filled up to a size of 40 μm^2, which corresponds to 8% of the average cell size. Next, the mask was smoothed by a Gaussian filter approximation (43) with an SD of 3 px = 0.6 μm to reduce pixel noise at the cell boundary. Objects in the background with an area of less than 80 μm^2 were excluded, which appear in M mainly because of noise in the background (42). In this step, care was taken not to exclude any cells (fig. S6). Areas covered by cells within an ROI were extrapolated to a whole coverslip (245.50 mm^2). The whole algorithm was implemented in MATLAB 2017b (MathWorks Inc.).

Investigation of internalized microplastic particles
From the same samples used to quantify PCI and areas covered with cells on coverslips, we visually screened each sample for single PCI to distinguish between particles that were only attached to cell membranes or were internalized. All samples were scored blind to exclude personal bias. The same DMI 6000 microscope including a spinning disc unit with a higher magnification (100×/1.40 oil objective) was used. Beginning from a randomly defined starting point, the coverslips were screened in the DIC channel until 100 to 110 PCI were detected or until the whole coverslip was completely screened. Once a PCI was found, a DIC image was taken, and axial stacks of fluorescently labeled cells were acquired (vertical distance of the axial stacks, 0.2 μm). To evaluate internalization of the microplastic particles, each confocal stack of cells with labeled actin filaments was analyzed with Fiji ImageJ (version: 2.0.0-rc-54/1.51 h 2016-09-08) orthogonal views. The microplastic particles used in the experiments were not fluorescent and therefore were not directly visible in the confocal stacks. DIC images were used to mark the particle positions (using the ROI manager in Fiji ImageJ). These positions were then transferred to the confocal stacks, in which internalized particles were visible as spherical black regions within the actin network. Only microplastic particles that were fully surrounded by actin filaments were considered to be internalized. Microplastic particles that were only partly surrounded were considered to be attached to cell membranes.

Combination and standardization of the results
The number of PCI (ROI-PCI experiment, 0.29 mm^2) and the number of microplastic particles added (ROI–quantifying numbers of pretreated, positive, and negative control microplastic particles, 4.23 mm^2) were extrapolated to a whole coverslip (245.50 mm^2). As the areas on the coverslips covered by cells differ slightly between replicates and time points and as the microplastic particle concentrations differed between treatments (because of the loss during media exchange), each coverslip was standardized. A standard coverslip contains $CellNumber_{standCS}$ = 23,000 cells and $ParticleNumber_{standCS}$ = 29,000 microplastic particles, which represent the rounded mean values (rounded to the nearest thousand) of the numbers of cells and particles over all treatments and time points. The cell number $CellNumber_{standCS}$ was determined by calculating the mean area covered by cells on a coverslip (11.33 mm^2) divided by the average size of a single cell

(495 μm^2), which led to 23,000 cells on a standard coverslip. The number of microplastic particles $ParticleNumber_{standCS}$ was the mean number of microplastic particles added to the coverslips. The standardization was performed with the following equation to obtain comparability between the treatments and incubation times despite slightly varying cell and particle numbers

$$PCI_{stand} = PCI_{CS} * \left(\frac{CellNumber_{standCS}}{\frac{CellArea_{CS}}{SingleCellArea_{CS}}} \right) * \left(\frac{ParticleNumber_{standCS}}{ParticleNumber_{CS}} \right)$$

All PCI determined for a single coverslip (PCI_{CS}) were multiplied with the $CellNumber_{standCS}$ divided by the ratio of the exact area of cells on the coverslip $CellArea_{CS}$ and the area of a single cell ($SingleCellArea_{CS}$) on this specific coverslip and furthermore multiplied with the $ParticleNumber_{standCS}$ divided by the actual number of microplastic particles counted on this specific coverslip ($ParticleNumber_{CS}$).

Scanning electron microscopy
To visualize the surface structures of microplastic particles, samples were analyzed using a scanning electron microscope (LEO1530 Zeiss, Oberkochen, Germany; magnification, ×500 to ×50,000, 2 to 3 kV; InLens/SE2 detector). First, each sample of the pretreated and IgG-opsonized microplastic particles was diluted in ultrapure water (1:100), and 10 µl of this dilution was pipetted onto a silicon wafer placed on carbon conductive tabs (Ø 12 mm Plano GmbH, Wetzlar, Germany) fixed to aluminum stubs (Ø 12 mm, Plano GmbH, Wetzlar, Germany). The stubs were then transferred into a desiccator and stored until the images were acquired. Samples were subsequently coated with a 2-nm-thick platinum layer (208HR sputter coater, Cressington, Watford, UK) and analyzed using the scanning electron microscope.

Micro-Raman spectroscopy
All Raman spectroscopic measurements were performed using a micro-Raman spectrometer (WITec Alpha 300 RA+, Ulm, Germany) equipped with a UHTS 300 spectrometer and a back-illuminated Andor Newton 970 EMCCD camera. A frequency-doubled Nd-YAG laser with a wavelength of 532 nm was used as the excitation source. The exciting laser radiation was coupled to a Zeiss microscope through a wavelength-specific single-mode optical fiber. The laser beam was focused onto the sample by means of a 50× long working distance [numerical aperture (NA) = 0.7, lateral resolution ca. 500 nm] and 100× (NA = 0.9, lateral resolution ca. 300 nm) Zeiss objective. The focal length of the spectrometer is 800 mm, and it is equipped with a diffraction grating having a groove density of 600 lines per millimeter to give a spectral resolution of ~3 to 4 cm^{-1}. The laser power used was approximately 5 to 15 mW at the fiber for all measurements. Raman scattered light was detected by a Peltier-cooled complementary metal oxide semiconductor–based CCD with a sensor size of 1600 × 200 px. The instrument was operated by the integrated Witec Control Five software (version 5). All spectra were acquired in the 3600 to 500 cm^{-1} spectral range. The acquired data were preprocessed using Witec Project Five software (version 5) that allowed compensating for cosmic radiation and other background signals. A true component analysis was also performed using the Witec Project Five software to visualize the spatial distribution of different components within the Raman image (for example, the cell, polystyrene microplastic particles, and mounting media).

SCIENCE ADVANCES | RESEARCH ARTICLE

Single spectrum acquisition mode with a 50× long working distance objective ($NA = 0.7$) was used to confirm that the chosen particles from detected PCI showed spectral signatures specific to polystyrene, which showed that the particles were the used microplastic particles and not contaminants of a similar shape and size. For each treatment and incubation time, 10 PCI were investigated per sample. The integration times ranged between 10 and 15 s for single spectrum acquisitions. Second, the chemical components on the surface of the microplastic particles after exposure to fresh water and salt water were investigated. Raman imaging mode was used for these investigations. Therefore, 2×20 μl of microplastic particle samples from fresh, salt, and ultrapure water after 4 weeks of incubation and the corresponding water were pipetted onto two marked positions on a glass slide (SERVOPRAX, Wesel, Germany), transferred into a desiccator, and allowed to dry. Raman images were acquired from these samples with the following parameters: 100× objective ($NA = 0.9$), scan area of 15×15 μm, step size of 100 nm, and integration time of 0.5 s/pixel.

X-ray photoelectron spectroscopy
For sample preparation, 2×20 μl of microplastic particle solutions from fresh, salt, and ultrapure water after 4 weeks of incubation and the corresponding water were pipetted onto a glass slide (Servoprax, Wesel, Germany). Samples were transferred into a desiccator, and by using a water jet vacuum pump, a slight vacuum was produced and samples were allowed to dry. XPS spectra were measured with the PHI 5000 VersaProbe III system fitted with an Al Kα excitation source ($h\nu = 1486.6$ eV) and a dual neutralizer (electron gun and Ar^+) at 10^{-10} mbar pressure. An x-ray source diameter of 100 μm was used to locally excite the samples; the corresponding photoemission with 45° take-off angle was collected at the multichannel analyzer. The survey and the detailed spectra were measured with pass energies of 224 and 69 or 112 eV, respectively. The SD on the reported energy values is ±0.1 eV. The reproducibility of the observed results was confirmed by performing at least three measurements at different places of the samples. The spectra were analyzed with a Multipak software pack, provided by the manufacturer. All emission signals were referenced to adventitious C 1s peak at 284.8 eV. For quantitative analysis of the spectra, Shirley background correction was used. For deconvolution of C 1s and S 2p spectra of salt water– and fresh water–incubated samples, respectively, a combination of Gaussian and Lorentzian functions was used without fixing any constrain on the peak position or FWHM; however, in S 2p spectrum, the multiplet splitting parameters for 2p orbitals were assigned prior to fit the bands. For comparative purposes, the C 1s, N 1s, and S 2p spectra shown in the main text were normalized.

Statistical analysis
Statistical analysis was conducted using R studio software (Version 1.0.143). The data for PCI, as well as for internalized microplastic particles, were tested for normal distribution (Shapiro-Wilk test) and homogeneity of variances (Levene test). A Kruskal-Wallis test with a Games-Howell post hoc test (P-adjust method for multiple nesting: Bonferroni Holm) was conducted to check for differences between treatments. To check for differences within one treatment regarding the incubation time, a Mann-Whitney U test was performed.

SUPPLEMENTARY MATERIALS
Supplementary material for this article is available at http://advances.sciencemag.org/cgi/content/full/6/50/eabd1211/DC1

REFERENCES AND NOTES

1. K. A. Connors, S. D. Dyer, S. E. Belanger, Advancing the quality of environmental microplastic research. *Environ. Toxicol. Chem.* **36**, 1697–1703 (2017).
2. J. L. Conkle, C. D. Báez Del Valle, J. W. Turner, Are we underestimating microplastic contamination in aquatic environments? *Environ. Manag.* **61**, 1–8 (2018).
3. T. S. Galloway, M. Cole, C. Lewis, Interactions of microplastic debris throughout the marine ecosystem. *Nat. Ecol. Evol.* **1**, 0116 (2017).
4. D. Laist, Impacts of marine debris: Entanglement of marine life in marine debris including a comprehensive list of species with entanglement and ingestion records, in *Marine Debris - Sources, Impacts Solution*, J. M. Coe, D. B. Rogers, Eds. (Springer-Verlag, New York, 1997), pp. 99–139.
5. J.-P. W. Desforges, M. Galbraith, P. S. Ross, Ingestion of microplastics by zooplankton in the Northeast Pacific ocean. *Arch. Environ. Contam. Toxicol.* **69**, 320–330 (2015).
6. L. I. Devriese, M. D. van der Meulen, T. Maes, K. Bekaert, I. Paul-Pont, L. Frère, J. Robbens, A. D. Vethaak, Microplastic contamination in brown shrimp (*Crangon crangon*, Linnaeus 1758) from coastal waters of the Southern North Sea and Channel area. *Mar. Pollut. Bull.* **98**, 179–187 (2015).
7. M. A. Browne, A. Dissanayake, T. S. Galloway, D. M. Lowe, R. C. Thompson, Ingested microscopic plastic translocates to the circulatory system of the mussel, *Mytilus edulis* (L). *Environ. Sci. Technol.* **42**, 5026–5031 (2008).
8. N. von Moos, P. Burkhardt-Holm, A. Köehler, Uptake and effects of microplastics on cells and tissue of the blue mussel *Mytilus edulis* L. after an experimental exposure. *Environ. Sci. Technol.* **46**, 327–335 (2012).
9. Y. Lu, Y. Zhang, Y. Deng, W. Jiang, Y. Zhao, J. Geng, L. Ding, H. Ren, Uptake and accumulation of polystyrene microplastics in zebrafish (Danio rerio) and toxic effects in liver. *Environ. Sci. Technol.* **50**, 4054–4060 (2016).
10. F. Delie, Evaluation of nano- and microparticle uptake by the gastrointestinal tract. *Adv. Drug Deliv. Rev.* **34**, 221–233 (1998).
11. J. R. Grainger, J. E. Konkel, T. Zangerle-Murray, T. N. Shaw, Macrophages in gastrointestinal homeostasis and inflammation. *Pflugers Arch.* **469**, 527–539 (2017).
12. V. Olivier, C. Rivière, M. Hindié, J.-L. Duval, G. Bomila-Koradjim, M.-D. Nagel, Uptake of polystyrene beads bearing functional groups by macrophages and fibroblasts. *Colloids Surf. B Biointerfaces* **33**, 23–31 (2004).
13. V. Stock, L. Böhmert, E. Lisicki, R. Block, J. Cara-Carmona, L. K. Pack, R. Selb, D. Lichtenstein, L. Voss, C. J. Henderson, E. Zabinsky, H. Sieg, A. Braeuning, A. Lampen, Uptake and effects of orally ingested polystyrene microplastic particles in vitro and in vivo. *Arch. Toxicol.* **93**, 1817–1833 (2019).
14. F. Nimmerjahn, J. V. Ravetch, Fcγ receptors as regulators of immune responses. *Nat. Rev. Immunol.* **8**, 34–47 (2008).
15. A. Aderem, D. M. Underhill, Mechanisms of phagocytosis in macrophages. *Annu. Rev. Immunol.* **17**, 593–623 (1999).
16. M. P. Desai, V. Labhasetwar, E. Walter, R. J. Levy, G. L. Amidon, The mechanism of uptake of biodegradable microparticles in Caco-2 cells is size dependent. *Pharm. Res.* **14**, 1568–1573 (1997).
17. C. Q. Y. Yong, S. Valiyaveetill, B. L. Tang, Toxicity of microplastics and nanoplastics in mammalian systems. *Int. J. Environ. Res. Public Health* **17**, 1509 (2020).
18. M. Mahmoudi, K. Azadmanesh, M. A. Shokrgozar, W. S. Journeay, S. Laurent, Effect of nanoparticles on the cell life cycle. *Chem. Rev.* **111**, 3407–3432 (2011).
19. R. Triebskorn, T. Braunbeck, T. Grummt, L. Hanslik, S. Huppertsberg, M. Jekel, T. P. Knepper, S. Krais, Y. K. Müller, M. Pittroff, A. S. Ruhl, H. Schmieg, C. Schür, C. Strobel, M. Wagner, N. Zumbülte, H.-R. Köhler, Relevance of nano- and microplastics for freshwater ecosystems: A critical review. *TrAC Trends Anal. Chem.* **110**, 375–392 (2019).
20. F. Nasser, J. Constantinou, I. Lynch, Nanomaterials in the Environment Acquire an "Eco-Corona" Impacting their Toxicity to Daphnia Magna—a Call for Updating Toxicity Testing Policies. *Proteomics* **20**, 1800412 (2020).
21. G. Loeb, R. Neihof, Marine conditioning films. *Adv. Chem.* **145**, 319–335 (1975).
22. M. P. Monopoli, C. Åberg, A. Salvati, K. A. Dawson, Biomolecular coronas provide the biological identity of nanosized materials. *Nat. Nanotechnol.* **7**, 779–786 (2012).
23. C. D. Rummel, A. Jahnke, E. Gorokhova, D. Kühnel, M. Schmitt-Jansen, Impacts of biofilm formation on the fate and potential effects of microplastic in the aquatic environment. *Environ. Sci. Technol. Lett.* **4**, 258–267 (2017).
24. M. W. Smith, N. W. Thomast, P. G. Jenkinst, N. G. A. Miller, D. Cremaschit, C. Portat, Selective transport of microparticles across Peyer's patch follicle-associated M cells from mice and rats. *Exp. Physiol.* **80**, 735–743 (1995).
25. C. D. Walkey, J. B. Olsen, H. Guo, A. Emili, W. C. W. Chan, Nanoparticle size and surface chemistry determine serum protein adsorption and macrophage uptake. *J. Am. Chem. Soc.* **134**, 2139–2147 (2012).
26. K. L. Ng, J. P. Obbard, Prevalence of microplastics in Singapore's coastal marine environment. *Mar. Pollut. Bull.* **52**, 761–767 (2006).
27. Y. Tabata, Y. Ikada, Effect of the size and surface charge of polymer microspheres on their phagocytosis by macrophage. *Biomaterials* **9**, 356–362 (1988).

SCIENCE ADVANCES | RESEARCH ARTICLE

28. T. Zhou, K. Zhang, T. Kamra, L. Bülow, L. Ye, Preparation of protein imprinted polymer beads by Pickering emulsion polymerization. *J. Mater. Chem. B* **3**, 1254–1260 (2015).

29. Y. Chen, J. Cai, Q. Xu, Z. W. Chen, Atomic force bio-analytics of polymerization and aggregation of phycoerythrin-conjugated immunoglobulin G molecules. *Mol. Immunol.* **41**, 1247–1252 (2004).

30. Z. Movasaghi, S. Rehman, I. U. Rehman, Raman spectroscopy of biological tissues. *Appl. Spectrosc. Rev.* **42**, 493–541 (2007).

31. J. S. Stevens, A. C. de Luca, M. Pelendritis, G. Terenghi, S. Downes, S. L. M. Schroeder, Quantitative analysis of complex amino acids and RGD peptides by x-ray photoelectron spectroscopy (XPS). *Surf. Interface Anal.* **45**, 1238–1246 (2013).

32. C. C. Norbury, Drinking a lot is good for dendritic cells. *Immunology* **117**, 443–451 (2006).

33. M. Markiewicz, J. Kumirska, I. Lynch, M. Matzke, J. Köser, S. Bemowsky, D. Docter, R. H. Stauber, D. Westmeier, S. Stolte, Changing environments and biomolecule coronas: Consequences and challenges for the design of environmentally acceptable engineered nanoparticles. *Green Chem.* **20**, 4133–4168 (2018).

34. B. O. Fabriek, C. D. Dijkstra, T. K. van den Berg, The macrophage scavenger receptor CD163. *Immunobiology* **210**, 153–160 (2005).

35. J. A. Champion, A. Walker, S. Mitragotri, Role of particle size in phagocytosis of polymeric microspheres. *Pharm. Res.* **25**, 1815–1821 (2008).

36. M. C. Kerr, R. D. Teasdale, Defining macropinocytosis. *Traffic* **10**, 364–371 (2009).

37. F. Wang, L. Yu, M. P. Monopoli, P. Sandin, E. Mahon, A. Salvati, K. A. Dawson, The biomolecular corona is retained during nanoparticle uptake and protects the cells from the damage induced by cationic nanoparticles until degraded in the lysosomes. *Nanomed. Nanotechnol. Biol. Med.* **9**, 1159–1168 (2013).

38. D. Lithner, J. Damberg, G. Dave, Å. Larsson, Leachates from plastic consumer products – Screening for toxicity with *Daphnia magna*. *Chemosphere* **74**, 1195–1200 (2009).

39. S. Keller, K. Berghoff, H. Kress, Phagosomal transport depends strongly on phagosome size. *Sci. Rep.* **7**, 17068 (2017).

40. J. Schindelin, I. Arganda-Carreras, E. Frise, V. Kaynig, M. Longair, T. Pietzsch, S. Preibisch, C. Rueden, S. Saalfeld, B. Schmid, J.-Y. Tinevez, D. J. White, V. Hartenstein, K. Eliceiri, P. Tomancak, A. Cardona, Fiji: An open-source platform for biological-image analysis. *Nat. Methods* **9**, 676–682 (2012).

41. J. E. N. Jonkman, J. Swoger, H. Kress, A. Rohrbach, E. H. K. Stelzer, Resolution in optical microscopy. *Methods Enzymol.* **360**, 416–446 (2003).

42. K. Berghoff, S. Keller, W. Gross, L. Gebhardt, H. Kress, Application of optical tweezers for biochemical and thermal cell stimulation. *Light Robot. Struct. Mediated Nanobiophoton.* **2017**, 385–410 (2017).

43. P. Kovesi, Fast almost-Gaussian filtering, in *Proceedings of the 2010 Digital Image Computing Techniques and Applications (DICTA 2010)* (IEEE, Sydney, Australia, 2010), pp. 121–125.

44. C. Girardeaux, J.-J. Pireaux, Analysis of polystyrene (PS) by XPS. *Surf. Sci. Spectra.* **4**, 130–133 (1996).

155

Science Advances

MAAAS

Supplementary Materials for

Environmental exposure enhances the internalization of microplastic particles into cells

A. F. R. M. Ramsperger, V. K. B. Narayana, W. Gross, J. Mohanraj, M. Thelakkat, A. Greiner, H. Schmalz, H. Kress*, C. Laforsch*

*Corresponding author. Email: holger.kress@uni-bayreuth.de (H.K.); christian.laforsch@uni-bayreuth.de (C.L.)

This PDF file includes:

Figs. S1 to S9
Tables S1 and S2

Supplementary Figures and Tables
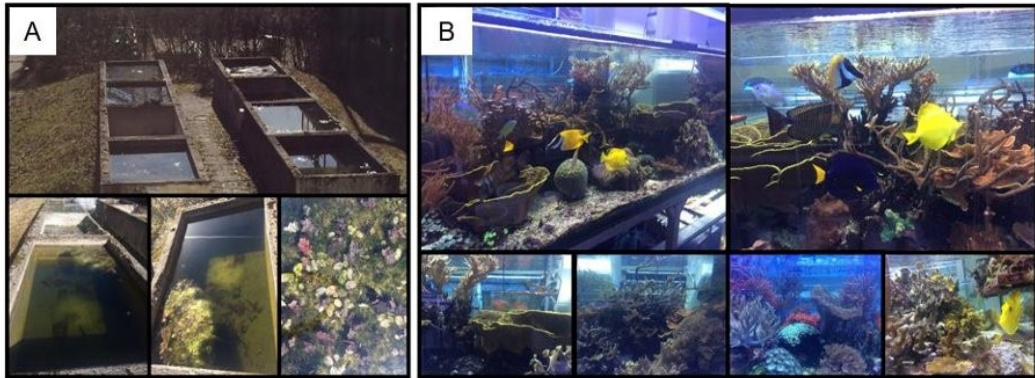
Fig. S1. Images of the sampling sites for the incubation waters. A) Freshwater was obtained from an artificial pond and B) saltwater was obtained from a marine aquaria facility, both inhabiting a rich floral and faunal population. Photo Credit: Anja F.R.M. Ramsperger, University of Bayreuth.
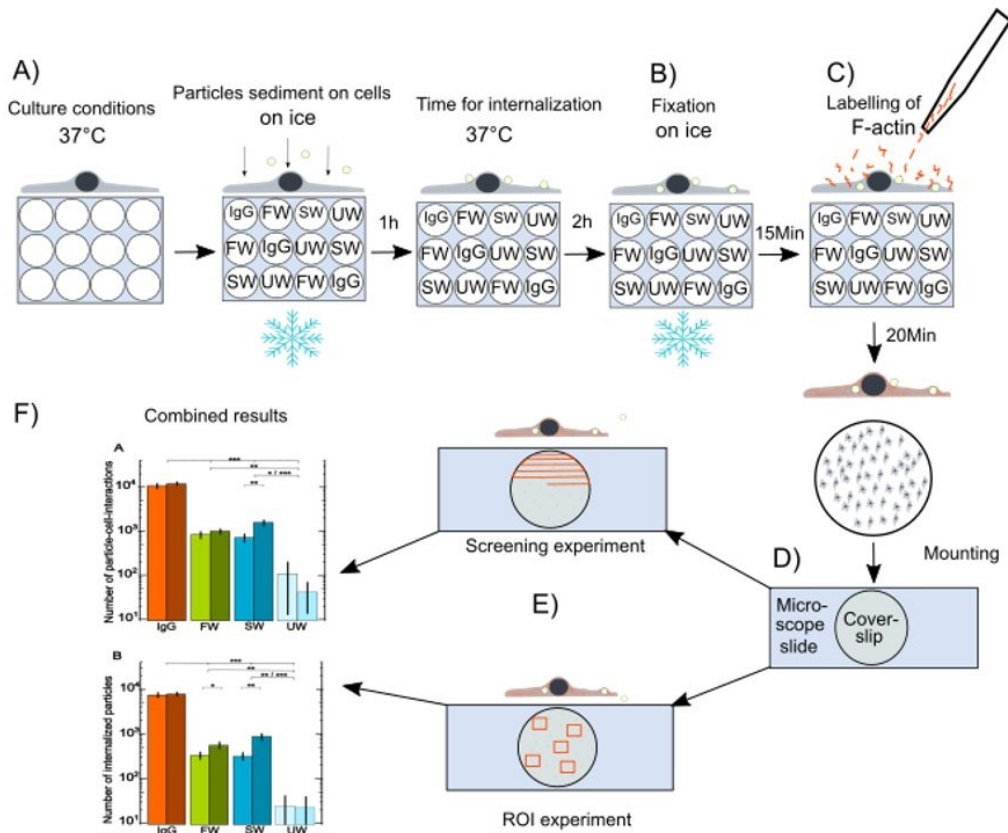
Fig. S2. Scheme of experimental procedure for the cell experiments. A) Cells were cultured under standard culture conditions and then transferred on ice to pause cellular activity. Corresponding treatments were randomly added to coverslips within a well plate and microplastic particles sedimented onto coverslips for one hour. Afterwards, the well plates were transferred to 37 °C culture condition to allow internalization of microplastic particles for all cells at the same time. B) After two hours of internalization time, coverslips were washed with PBS buffer to remove unattached microplastic particles and cells were fixed with 4 % paraformaldehyde for 15 minutes on ice to stop cellular activity for all cells simultaneously. C) Coverslips were again washed and filamentous actin was fluorescently labelled within 20 minutes at room temperature. D) Finally, coverslips were mounted on glass objective holders and stored at 4 °C until microscopic analysis. E) From each coverslip region of interest (ROI) experiments were conducted to evaluate the number of particle–cell-interactions and to calculate the area covered with cells on a whole coverslip using maximum intensity projected images of confocal stacks. On the same coverslip, single cells were observed to evaluate the number of internalized microplastic particles using single differential interference contrast images and confocal stacks of fluorescently labelled cells (screening experiment). F) Results were combined to compare treatments.
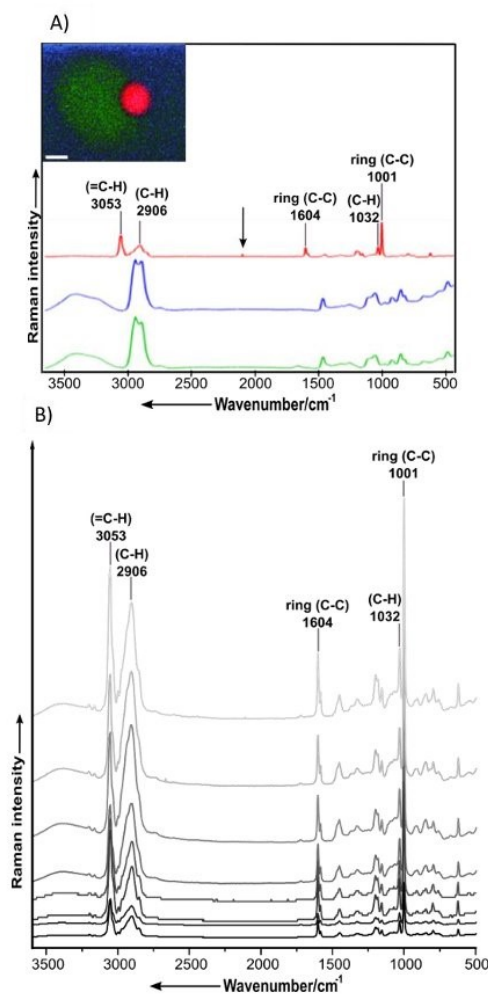
Fig. S3. Raman spectral analysis of a particle and a cell to investigate whether the particle is one of the utilized polystyrene microplastic particles. A) False color Raman image of a cell-particle-interaction (in this case, the particle was exposed to freshwater, scale bar: 2 μm). Colors from Raman image match colors in corresponding spectra. The red spectrum shows peaks specific for polystyrene, the blue spectrum shows peaks corresponding to the mounting media and the green spectrum shows peaks corresponding to cells. Arrow in the red spectrum highlights specific peak for thiocyanate, which is a possible component of the eco-corona on microplastic particles exposed to freshwater as the same peak was found in the eco-corona analysis (Fig. 4 main text). B) Each spectrum represents a mean spectrum acquired from ten particles measured from each of the eight treatments (IgG, freshwater, saltwater and ultrapure water two and four weeks, respectively). All spectra have been vector normalized and offset for the ease of representation and show Raman signatures specific to polystyrene.
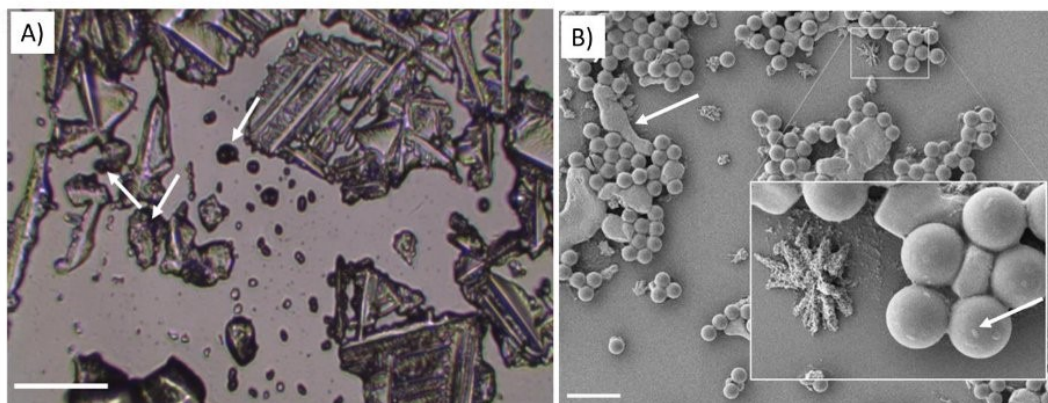
Fig. S4. Bright field image and SEM-image of microplastic particles exposed to saltwater. (A) Bright field image with arrows highlighting the position of microplastic particles which are embedded within salt crystals; scale bar: 100 μm. (B) SEM image with magnified area shows that microplastic particles are embedded in larger salt crystals (arrow) and show circular layers on microplastic particles in magnified view (arrow); scale bar: 10 μm.
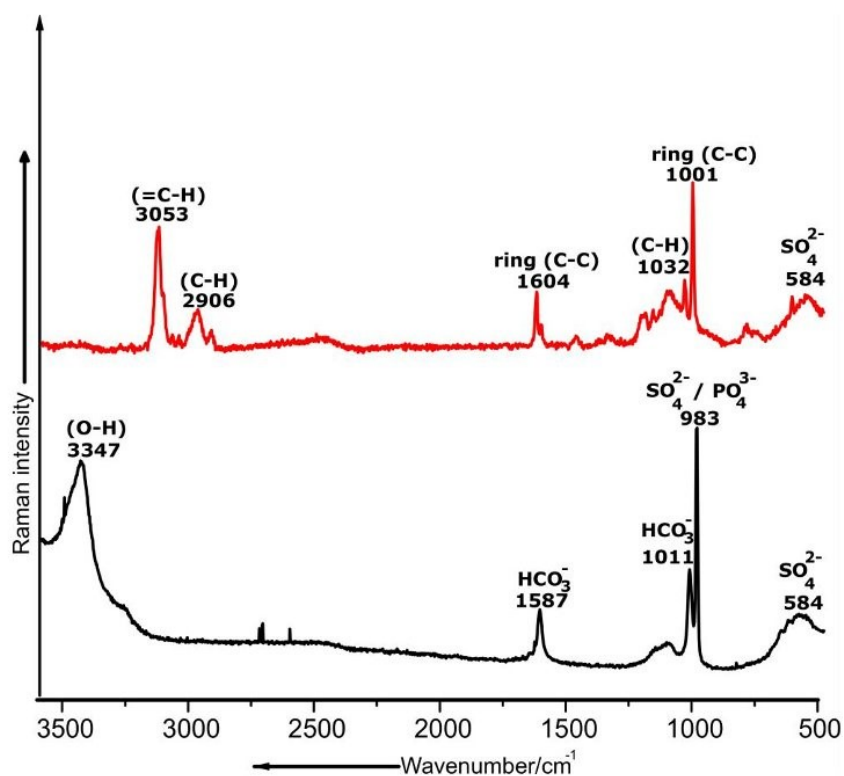
Fig. S5. Raman spectrum of microplastic particles exposed to saltwater (red) and spectrum of the saltwater itself (black). Spectral signatures such as =C-H stretching mode (3053 cm^{-1}), the C-H bending mode (2906 cm^{-1}), the ring C-C skeletal stretching mode (1604 cm^{-1}), the C-H bending mode (1032 cm^{-1}) and C-C ring stretching mode (1001 cm^{-1}) correspond to the polystyrene microplastic particle from saltwater in the red spectrum. Likewise, signatures corresponding to the salts such as sulphates, bicarbonate and phosphates are observed in the black spectrum. A comparison of the two spectra indicates that the Raman signatures of PS microplastic particles incubated in saltwater are likely to have contribution from the sulphates, bicarbonate and phosphates-based salts whose Raman bands appear to coincide with the bands of the PS microplastic particle.
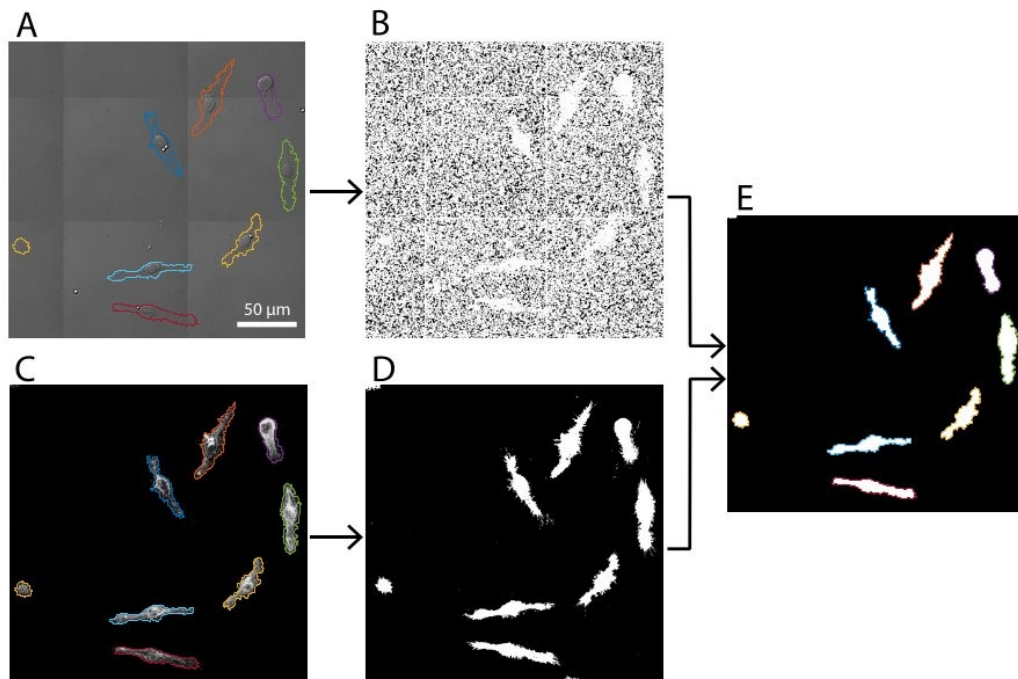
Fig. S6. Illustration of the cell detection algorithm used in the ROI- experiments. A local contrast filter was applied to DIC images (A) to achieve a rough mask of the regions covered by the macrophages (B). To refine the mask, we applied a threshold to the fluorescence images (C) to get a mask depicting the locations of the cells in the fluorescence channel. Both masks were combined by an 'AND'-operation, small, remaining objects were removed and the resulting mask was filtered by a gaussian filter with a size of 3 px to achieve a smooth and robust final cell mask (E). The outlines shown in (A) and (C) are identical to the outlines of the final mask (E). The algorithm was implemented in Matlab 2017b (The MathWorks, Inc.).
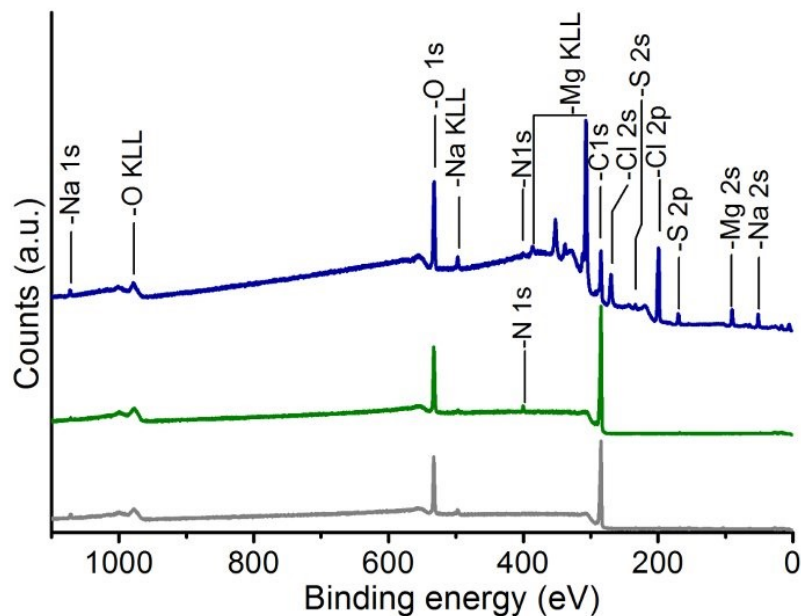
Fig. S7. XPS survey spectra of microplastic particles incubated in different water samples. The survey spectra of dried ultrapure water (gray), fresh- (green) and saltwater (blue) samples showing prominent signals correspond to carbon (C 1s, 284.8 eV), oxygen (O 1s and O KLL, ca. 532. 5 eV and 979.1 eV, respectively), nitrogen (N 1s, 400.1 eV), sodium (Na 1s and 2s, ca. 1072 and 51.5 eV, respectively), magnesium (Mg 2s and Mg KLL, 90.1 eV and ca. 307-385 eV), chlorine (Cl 2p and 2s, 199.1 eV and 270.1 eV) and sulphur (S 2p, 169.7 eV) elements.
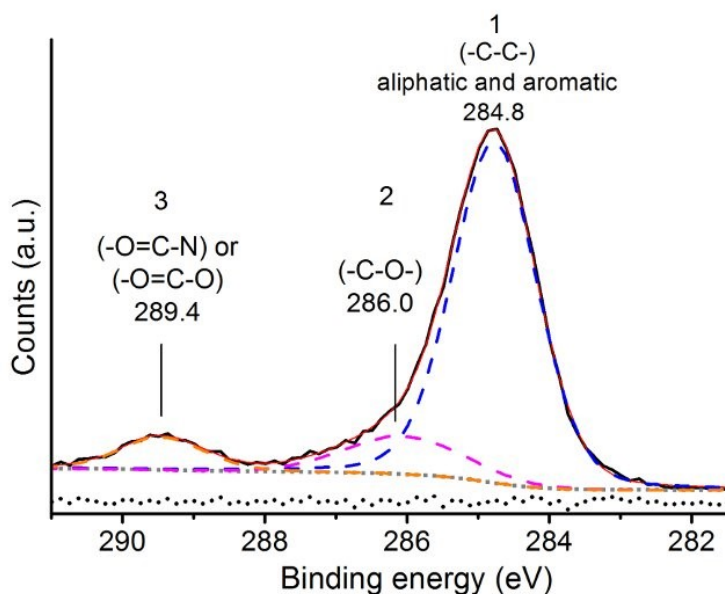
Fig. S8. The deconvolved C 1s core level spectrum of microplastic particles incubated in saltwater. Color code: original spectrum (black); composite spectrum (red); fitted band 1 (blue dashed line) with the peak maximum at 284.8 eV, corresponding to the carbon from $-C_{aliphatic\ and\ aromatic}$ units; fitted band 2 (magenta dashed line) with the peak maximum at 286.0 eV corresponds to the carbon from a -C-O- group; fitted band 3 (magenta dashed line) with the peak maximum at 289.4 eV (orange dotted line) attributed to the carbon from either -O=C-N- or -O=C-O- groups; background (gray dashed line) and fit residual (black dotted line).
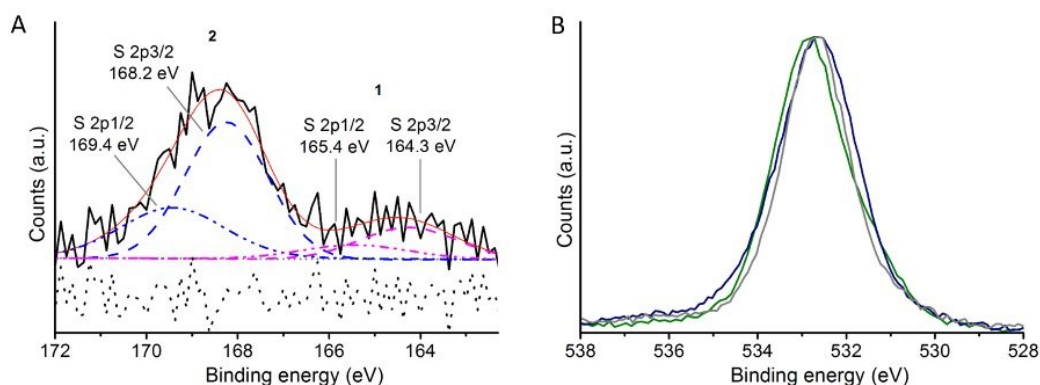
Fig. S9. The deconvolved S 2p and O 1s core level spectra of microplastic particles incubated in freshwater. (A) The deconvolved S 2p spectrum of microplastic particles incubated in freshwater. Color code: original spectrum (black); composite spectrum (red); band 1 – multiplet splitting of the S 2p band centered at 164.5 eV to S 2p3/2 (164.3 eV) and S 2p1/2 (165.4 eV), corresponding to the sulphur from thiophenic, thiols and thioether functional groups; band 2 - multiplet splitting of the S 2p band centered at 168.5 eV to S 2p3/2 (168.2 eV) and S 2p1/2 (169.4 eV), originating from the sulphate groups (*42*). (B) O 1s core level spectra of microplastic particles incubated in ultrapure water (gray), fresh- (green) and saltwater (blue) centered at ca. 532.5 eV with the full-width-half-maximum (FWHM) of 1.74 eV, 2.04 eV and 2.1 eV, respectively. In line with the indication for the presence of –C-O-, -O=C-N- and sulphate functional groups on microplastic particles incubated in fresh- and saltwater, their O1s core level peaks FWHM (ca. 2.0 eV) is slightly higher than that of the microplastic particles incubated in ultrapure water (1.74 eV). In addition, the O/C atomic ratio calculated from the area under the corresponding O 1s and C 1s peaks increases from microplastic particles incubated in ultrapure water (0.17) to freshwater (0.18) and saltwater(0.75), which corroborates the highly functionalized surfaces of microplastic particles incubated in fresh- and saltwater.

Table S1. Summary of the mean numbers of particle-cell-interactions ("PCI") and the numbers of microplastic particles internalized by cells ("Internalized") for all treatments and incubation times and the corresponding standard errors of mean ("s.e."). Significant differences (Kruskal-Wallis rank sum test) are highlighted in grey. IgG = IgG-opsonized, FW = freshwater-, SW = saltwater-, UW= ultrapure water-exposed microplastic particles, respectively.

Category	Incubation time [weeks]	N per treatment	Treatment	Mean	± se	Kruskal- Wallis rank sum test		
						Chi-squared	Df	p
PCI	2	10	IgG	10,504.36	1,494.40	30.606	3	$1.029e^{-06}$
			FW	829.14	155.23			
			SW	710.57	155.49			
			UW	106.66	93.89			
PCI	4	10	IgG	11,872.38	1,261.52	34.429	3	$1.608e^{-07}$
			FW	992.45	134.47			
			SW	1,555.79	244.01			
			UW	41.36	27.90			
Internalized	2	10	IgG	7,457.40	1,046.95	32.128	3	$4.919e^{-07}$
			FW	329.60	63.48			
			SW	319.68	65.19			
			UW	24.77	17.25			
Internalized	4	10	IgG	7,803.31	849.56	34.043	3	$1.94e^{-07}$
			FW	566.13	101.30			
			SW	876.88	150.36			
			UW	20.19	20.19			

Table S2: Summary statistical analysis for differences between treatments and incubation time. Subsequent to the non-parametric Kruskal Wallis test to investigate differences between all tested treatments a Games-Howell-post hoc test was conducted. The Games-Howell post hoc test analyzes each treatment and incubation time combination (e.g. IgG 2 weeks vs. FW 2 weeks, IgG 2 weeks vs. SW 2 weeks, etc.) to compare the differences in the particle-cell-interactions (PCI) and number of internalized particles. For pairwise comparisons of the incubation times within one treatment a non-parametric Mann-Whitney U test was performed. Grey color highlights statistically significant values. IgG= IgG-opsonized, FW = freshwater, SW = saltwater, UW= ultrapure water.

Category	Incubation time [weeks]	Groups tested		Mean difference	s.e.	t	df	p	Upper limit	Lower limit	Mann-Whitney U			
											Groups tested [weeks]		W	P
PCI	2	IgG	FW	-9,575.21	1,062.39	6.44	9.19	0.001	-5,004.93	-14,345.50	IgG 2	IgG 4	41	0.528
			SW	-9,793.79	1,062,33	6.52	9.19	0.000	-5,123.56	-14,464.02				
			UW	-10,397.69	1,058,78	6.94	9.07	0.000	-5,730.70	-15,064.69				
		FW	SW	-118.58	154,86	0.54	18.00	0.948	500.404	-737.56	FW 2	FW 4	40	0.481
			UW	-722.48	128,28	3.98	14.807	0.006	-198.81	-1,246.15				
		SW	UW	-603.90	127,83	3.34	14.850	0.021	-92.24	-1,125.57				
PCI	4	IgG	FW	-10,879.93	897.08	8.58	9.2	0.000	-6,937.19	-14,822.66	SW 2	SW 4	15	0.007
			SW	-10,316.59	908.56	8.03	9.67	0.000	-6,361.40	-14,271.78				
			UW	-11,831.02	892.25	9.38	9.01	0.000	-7,892.62	-15,769.41				
		FW	SW	563.34	197.01	2.02	14.01	0.226	1,373.10	-246.43	UW 2	UW 4	50	1
			UW	-951.09	97.11	6.93	9.77	0.000	-529.16	-1,373.02				
		SW	UW	-1,514.43	173.67	6.17	9.24	0.001	-751.66	-2,277.20				
Internalized	2	IgG	FW	-7,127.91	741.66	6.80	9.07	0.000	-3,858.27	-10,397.32	IgG 2	IgG 4	40	0.481
			SW	-7,137.71	741.74	6.80	9.07	0.000	-3,868.12	-10,407.30				
			UW	-7,432.63	740.41	7.10	9.01	0.000	-4,164.18	-10,701.08				
		FW	SW	-9.92	64.34	0.11	17.99	1.000	247.25	-267.10	FW 2	FW 4	23	0.043
			UW	-304.84	46.51	4.63	10.32	0.004	-104.74	-504.95				
		SW	UW	-294.92	47.68	4.37	10.26	0.006	-89.54	-500.30				
Internalized	4	IgG	FW	-7,237.17	604.99	8.48	9.26	0.000	-4,581.14	-9,893.20	SW 2	SW 4	12	0.003
			SW	-6,926.42	610.07	8.03	9.56	0.000	-4,264.96	-9,587.89				
			UW	-7,783.11	600.90	9.16	9.01	0.000	-5,130.81	-10,435.42				
		FW	SW	310.75	128.20	1.71	15.77	0.349	830.26	-208.76	UW 2	UW 4	54	0.670
			UW	-545.94	73.04	5.29	9.71	0.002	-228.25	-863.63				
		SW	UW	-856.69	107.27	5.65	9.33	0.001	-386.41	-1,326.96				

Article 5

**Repulsive Interactions of Eco-corona Covered Microplastic Particles
Quantitatively Follow Modelling of Polymer Brushes**

LANGMUIR

Article

Repulsive Interactions of Eco-corona-Covered Microplastic Particles Quantitatively Follow Modeling of Polymer Brushes

Thomas Witzmann, Anja F. R. M. Ramsperger, Simon Wieland, Christian Laforsch, Holger Kress, Andreas Fery,* and Günter K. Auernhammer*

Read Online

ACCESS | Metrics & More | Article Recommendations | Supporting Information

ABSTRACT: The environmental fate and toxicity of microplastic particles are dominated by their surface properties. In the environment, an adsorbed layer of biomolecules and natural organic matter forms the so-called eco-corona. A quantitative description of how this eco-corona changes the particles' colloidal interactions is still missing. Here, we demonstrate with colloidal probe-atomic force microscopy that eco-corona formation on microplastic particles introduces a compressible film on the surface, which changes the mechanical behavior. We measure single particle−particle interactions and find a pronounced increase of long-range repulsive interactions upon eco-corona formation. These force-separation characteristics follow the Alexander−de Gennes (AdG) polymer brush model under certain conditions. We further compare the obtained fitting parameters to known systems like polyelectrolyte multilayers and propose these as model systems for the eco-corona. Our results show that concepts of fundamental polymer physics, like the AdG model, also help in understanding more complex systems like biomolecules adsorbed to surfaces, i.e., the eco-corona.
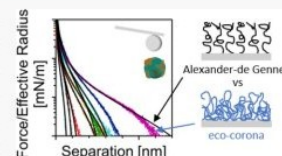
1. INTRODUCTION

Plastic litter is an environmental concern as it is ubiquitous in water, air, and on land.[1−5] Exposed to environmental conditions like changing temperature, mechanical stress, or UV radiation, it degrades into smaller particles.[6,7] Next to these particles, abrasion from any plastic product and particles generated in the size range below 5 mm are termed as microplastics.[8] Its ubiquitous abundance and small size pose a risk to organisms and the human health due to particle ingestion and inhalation.[9,10] In the last decade, toxicity tests on various organisms and cells with different polymer types, sizes, and shapes were performed.[11−13] Most of the studies focused thereby on spherical model particles, which are either pristine (plain) or functionalized. Although it is necessary to start investigations with well-defined particles, results of such studies do not represent the properties of real environmental microplastics.[14]

As the particles disintegrate and shrink in size, their surface area to volume ratio increases. Therefore, the surface is dominating the interaction with its surrounding making it essential to consider its properties. In addition to the increased surface area, the underlying mechanisms that cause disintegration do also change the surface properties.[7,15] However, not only disintegration leads to surface modification. In the moment microplastic particles enter the environment, they are exposed to a mix of different biomolecules (proteins and polysaccharides) and natural organic matter (NOM) like humic acids. These molecules adsorb to the particle surface forming an eco-corona.[16] The adsorption of these molecules alters eventually the microplastics surface morphology, charge, chemistry, and potentially mechanics.[17−20]

Several aspects are affected when the surface changes its properties.[21−27] Singh et al.[28] investigated the aggregation behavior of polystyrene (PS) nanoparticles. They demonstrated in the presence of different salt concentrations and humic acids that these particles are stabilized due to steric forces upon adsorption of these molecules. In accordance to these results, Wu et al.[29] also found humic acids to stabilize PS nanoplastics in solution preventing aggregation.

Another aspect affected by eco-corona formation is particle−cell interaction. Ramsperger et al.[30] showed that the induced change of the surface properties leads to an increase of particle−cell attachment and uptake. The eco-corona and its effects on the cell interactions might therefore also change toxicity of microplastic particles. Whether surface charge, mechanics, morphology, chemistry, or the contribution of several factors plays the dominant role for changes in particle−cell interactions is yet unknown. The role of mechanical properties of particles in cellular uptake has received attention recently.[31] Hartmann et al.[32] investigated with the help of colloidal probe-atomic force microscopy (CP-AFM) the stiffness-dependent uptake of microparticles into cells. They could show that softer particles are transported faster to lysosomes than stiffer ones. Due to the adsorption of hydrated molecules eco-corona covered particles are expected to be

8748

softer at the surface than plain particles. Therefore, stiffness-dependent uptake is expected to be important for eco-corona-covered microplastics as well. Examining the mechanical properties before and after the eco-corona formation is crucial. It clarifies the impact of environmental exposure onto the particle mechanical properties and opens the way to study how cellular uptake is affected.

Using CP-AFM, it was shown for pristine microplastic particles that transport in porous media is determined by ionic strength and flow velocity.[33] Furthermore, aggregation behavior is dependent on pH, ion type and valency, surface chemistry, and charge.[34−38] This is not only true for microplastic particles but colloids in general.[37,39] Focusing on microplastic particles and to be more precise, their physicochemical properties is important as pristine particles can show different interaction behavior although they are identical in shape, size, and polymer type.[40] This makes it necessary to address interactions to certain properties instead of their polymer type. As mentioned above, microplastic particles that are exposed to the environment adsorb molecules. The amount adsorbed to the surface is dependent on chemistry and charge of the particle and molecules, respectively.[41−43] In addition, the concentration of adsorbing biomolecules is influencing the surface coverage and therefore affecting the interaction forces as it has been shown for polyelectrolytes.[44−48] Moreover, Block et al. quantified repulsive interaction forces occurring after polyelectrolyte adsorption with Alexander−de Gennes (AdG) polymer brush theory.[49−52]

Direct force measurements on microplastic particles covered by an eco-corona have not been performed, let alone measurements that compare particles prior and after eco-corona formation. However, colloidal probe measurements in the presence of humic acid[53] or extracellular polymeric substances[54] on polymer membranes showed a change in adhesion forces compared to the plain membrane.

We carried out a systematic study on microplastic particles covered with an eco-corona. Investigating the interaction of microplastic particles with surrounding macromolecules is of high importance. It was shown recently that eco-coronas obtained from salt or fresh water environments lead to different surface properties.[17,30] Since the marine environment is assumed as one major sink of plastic pollution, we incubated polystyrene microplastic particles in water of a marine experimental setup.[55] In this study, single particle−particle interaction forces were measured with CP-AFM from 10 pN to several 10 nN with a vertical resolution of 20 pm and a lateral resolution of 50 nm. This means that attractive or repulsive forces occurring between the colloidal probe and microplastic particles can be detected. Interaction forces are measurable during approach and retraction of the probe from the sample particle. To measure only mechanical repulsive interactions with CP-AFM but in a realistic environment, we focused on physiological salt concentrations. With this, we reveal the changes induced by the eco-corona formation and describe quantitatively the repulsive interactions using established models for polymer (brush) surface layers. This work helps to understand and describe the physical structure of the eco-corona. It therefore gives a quantitative measure to improve and implement well-controlled model systems for environmental microplastic particles.

2. METHODS AND MATERIALS

2.1. Microplastic Particles and Pre-treatment Conditions. The particles were incubated as described in Ramsperger et al.[30] In brief, 3 μm sized, spherical, non-functionalized polystyrene microplastic particles (Micromod, Rostock, Germany, white particles, micromer plain, Prod. Nr. 01-00-303) were incubated in saltwater to allow the formation of an eco-corona. Therefore, 20 μL of the polystyrene stock solution was given into a glass vial and 980 μL of salt water was added. The salt water was taken from a highly biodiverse coral reef aquarium with a salinity of 3.5% (Figure S1). These conditions are comparable to that of oceans since the aquarium is usually used to keep fishes. The water is not prone to seasonal changes and is therefore a good marine model environment. Consecutively, the salt water was exchanged with new media three times per week via centrifugation (2000g, 20 min at room temperature). This procedure was repeated for two weeks, and it has been shown by Ramsperger et al. that biomolecules adsorb to the particle surface.[30] Finally, the microplastic particles were investigated with scanning electron microscopy (SEM) and CP-AFM.

2.2. Colloidal Probe-Atomic Force Microscopy (CP-AFM). Direct force measurements were conducted with a MFP-3D Bio (Asylum Research Inc., Santa Barbara, USA) mounted on an inverted optical microscope (Axio Observer Z1, Zeiss, Oberkochen, Germany). Before the measurements, tipless cantilevers (CSC37, MikroMasch, Sofia, Bulgaria) were calibrated according to the thermal noise method.[56,57] Cantilevers had a spring constant of 0.24 and 0.28 N/m. To prepare colloidal probes, cantilevers were rinsed in Milli-Q water, ethanol, Milli-Q water, and acetone and treated with air-plasma for 10 min (SmartPlasma, plasma technology GmbH, Herrenberg-Gülstein, Germany) before silica colloidal particles (nominal diameter of 1.76 μm, microParticles GmbH, Berlin, Germany) were attached to the cantilevers with 2-component epoxy glue (UHU Plus Endfest, UHU GmbH & Co. KG, Bühl/Baden, Germany). We preferred silica over the microplastic as the probe so that one surface is very well-defined, smooth, and homogeneous. These asymmetric measurements allow us to account for single microplastic particle contributions to the interaction force instead of the mean value of two interacting microplastic particles. This makes silica a good probe for initial experiments on an unknown and complex system like the eco-corona.

Microplastic particles were allowed to sediment onto glass slides in fluid cells for 60 min. Prior to sedimentation, glass slides were cleaned in an ultrasonic bath. During this, they were exposed to acetone, iso-propanol, ethanol, ethanol:water, and water for 10 min each. In between, the glasses were flushed with ultrapure water (Milli-Q Advantage A10). Eco-corona particles stick on the substrate without prior modification of the substrate. For pristine microplastic particles, the adhesion of the particles is not strong enough to ensure reliable measurements. For this reason, a nanoscopic coating with bound polydimethylsiloxane (PDMS) was applied to the glass to increase the adhesion of the pristine particles on the substrate using the following procedure. A precleaned glass slide was covered with 100 μL of 5 cSt PDMS (Gelest Inc., Morrisville, USA) on a heating plate at 200 °C for 3 min. Afterward, it was cleaned in an ultrasonic bath with acetone and ethanol for 10 min each to remove residual PDMS. This surface modification is an adapted version of Eifert et al.[58−60] After sedimentation of the microplastic particles, the liquid cell of the AFM was rinsed three times with 150 mM aqueous KCl solution. Subsequently, CP-AFM measurements were performed with a tip velocity of 300−400 nm/s at a scan rate of 0.5 Hz in 150 mM aqueous KCl solution of pH 6−7. Deflection sensitivity was determined by conducting measurements on the hard undeformable glass slide and line fitting the slope in the constant compliance region. Zero separation is consecutively defined as the regime where the mean value of the slope is the same value as the predetermined deflection sensitivity in the constant compliance regime. Three force curves for each individual particle per sample were taken with no significant change in the interaction profile and evaluated.

With CP-AFM, it is possible to measure interaction forces from about 10 pN to several Newtons with a vertical resolution of 20 pm

and lateral resolution of 50 nm. CP-AFM works as follows (see Figure 1): with the help of a colloidal probe, in this case a silica sphere, glued
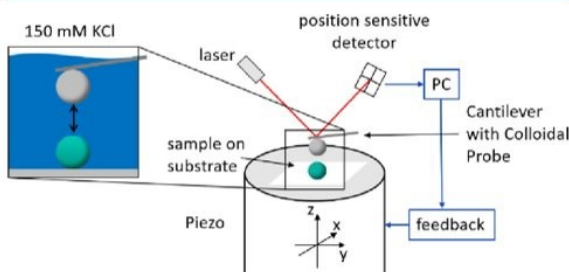

Figure 1. Schematic setup of a colloidal probe-atomic force microscope. The interaction of a silica colloidal probe and a microplastic particle leads to deflection of the cantilever and is position-sensitive detected by a laser. Attractive and repulsive contact and non-contact forces are detectable.

to a cantilever, interaction forces are measured. Any attractive or repulsive force between the colloidal probe and the sample deflects the cantilever. The cantilever deflection is measured through a laser beam focused on the back of the cantilever and reflected on a quadrant photodiode for a sensitive position detection of the incident laser light.

In force vs separation curves, positive force values indicate a repulsive force between the colloidal probe and the sample and negative force values correspond to an attraction. Zero separation is defined at the incompressible contact of two hard materials, often called the constant compliance regime. Forces are detected when the colloidal probe is approaching the sample (approach curves) or when the colloidal probe is retracted from the sample (retraction curve). Approach curves give information about non-contact interaction like van der Waals, electrostatic forces, and forces due to mechanical deformation or steric repulsion. The retraction curves describe additionally the adhesion between the colloidal probe and sample.

2.3. Estimating the Irrelevance of Electrostatic Interactions. Salt water, which was used to incubate the eco-corona particles, has a salinity of 35 ‰. This translates to a hypothetic KCl ion concentration of 469 mM. Compared to the measurement solution of 150 mM KCl, it is more than three times higher. We note, however, that the scaling and mechanisms of Alexander−de Gennes theory are independent for salt concentrations higher than 150 mM. At this level, electrostatic interactions can be safely neglected according to Debye−Hückel theory.[61]

Around a charged surface, the resulting electric field forms in an electrolyte solution an electric double layer. The first layer is made up of adsorbed ions oppositely charged to the surface. The second layer consists of free ions diffusing in the vicinity of the charged surface, the

diffuse layer. The ion concentration in the diffuse layer decreases exponentially away from the charged surface. The decay length of this decrease is dependent on the ionic strength of the solution and is described by the Debye length (eq 1).

$$\lambda_D = \sqrt{\frac{\varepsilon_r \varepsilon_0 k_B T}{2 N_A e^2 I}} \tag{1}$$

Here, λ_D is the Debye length and describes the theoretical electrostatic interaction range between CP and microplastic particle in nanometer. The parameter ε_r and ε_0 are the relative and vacuum permittivity, respectively. $k_B T$ is the thermal energy at lab temperature (293 K), N_A is the Avogadro constant, e is the elementary charge, and I is the ionic strength in mol/L. The higher the ionic strength, the lower the potential between the charged surface and the electrolyte solution in equilibrium. Thus, the concentration gradient is smaller and the diffuse layer shrinks in size. This translates into a smaller Debye length. According to eq 1, the electrostatic interaction range of the 150 mM KCl measurement solution is 0.8 nm. In the case of two like charged surfaces, the Debye length is the theoretical length at which electrostatic repulsive interactions can occur. However, Debye−Hückel theory is neglecting the finite ion size and the hydration shell, which reduces the true Debye length even further.[61] Therefore, at an ion concentration of 150 mM, every electrostatic interaction is screened and can be safely neglected at the length scales we consider in this work.

2.4. Scanning Electron Microscopy (SEM). For both particle types, pristine and particles coated with an eco-corona, 100 μL of a 50 mg/mL suspension was pipetted onto a glass coverslip (Ø 12 mm, Menzel slides, Thermo Scientific). Both particle types were subjected to an identical preparation procedure. The particles were fixed using Karnovsky's fixative (2% PFA and 2.5% glutaraldehyde in 1 × PBS) prior to dehydration in an ethanol series (30%, 50%, 70%, 80%, and 90% for 30 min each, 95% and absolute ethanol for 1 h each). Then, the samples were dried in hexamethyldisilazane (HMDS, Carl Roth GmbH). The dry samples were placed on carbon conductive tabs (Ø 12 mm, Plano GmbH, Wetzlar, Germany) fixed to aluminum stubs (Ø 12 mm, Plano GmbH, Wetzlar, Germany). Subsequently, the samples were coated with a 4 nm-thick platinum layer (208HR sputter coater, Cressington, Watford, UK). They were analyzed with a scanning electron microscope (FEI Apreo VolumeScope) at 5 kV using an Everhart−Thornley detector.

3. RESULTS

3.1. Scanning Electron Microscopy (SEM). The SEM images in Figure 2 show a clear difference between the pristine particles (Figure 2A) and particles that were incubated in salt water (Figure 2B). The pristine particles are monodisperse with a homogeneous and smooth surface. The incubation of these particles in salt water for 2 weeks leads to the formation of an eco-corona. This eco-corona is heterogeneously
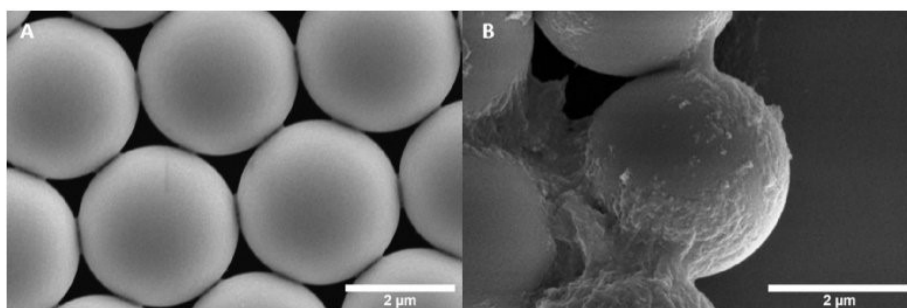

Figure 2. Comparison of the surface morphology of pristine polystyrene microplastic particles (A) and the same type of particles bearing an eco-corona after incubation in salt water (B). Microplastic particles have a diameter of 3 μm.

distributed over the surface of the particles. While some particles are heavily covered, others only show slight coverage.

3.2. Direct Force Measurements with the Colloidal Probe AFM. Direct force measurements were conducted in an asymmetric fashion, meaning between silica, the colloidal probe, and the microplastic particles. The experiment was performed in a 150 mM aqueous KCl solution. Therefore, contributions of electrostatic forces can be neglected as explained in detail in Section 2.3 and only steric forces are present.

The CP-AFM approach curves on pristine and incubated particles differ substantially, as shown in Figure 3 (pristine
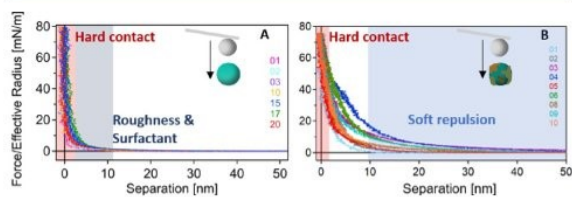

Figure 3. Normalized force vs separation curves between the silica probe and pristine polystyrene particles (A) and between the silica probe and particles covered with an eco-corona (B) at 150 mM KCl. Approach curves show soft mechanical repulsion of the eco-corona in (B). For pristine particles in (A), no additional interaction forces were measured other than the one of the hard contact and roughness (RMS = 1.27 nm). Colored numbers indicate the order in which particles were measured.

microplastic particles (panel (A)) and eco-corona covered particles (panel (B))). Force curves in panel (A) show typical mechanical interaction of two hard materials, in this case, the pristine polystyrene particle and the silica colloidal probe. The repulsive force increases suddenly at low separation. After deforming the pristine particles' asperities (RMS roughness = 1.27 nm) and residues of surfactant from particle synthesis, which has been shown elsewhere,[40,62] force curves reach the constant compliance regime, i.e., no further deformation is done. RMS roughness was obtained by AFM imaging in air. Three particles were measured in an area of 1 μm^2. The mean value of these measurements is presented. In contrast, the data for eco-corona covered particles in graph Figure 3B looks very different. Even at separations above 50 nm, there is already a small repulsive force detectable (Figure 4). This repulsion increases slowly during the further approach and will be discussed in detail later on. Such a behavior is typical for compressing a soft material and is therefore called soft repulsion. In our case, the compression of the eco-corona is
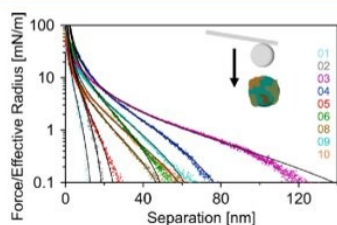
Figure 4. Normalized force vs separation curves between silica probe and various eco-corona particles at 150 mM KCl. Black lines correspond to an asymmetric Alexander–de Gennes fit at 293 K. Colored numbers indicate the order in which particles were measured.

visible by the soft repulsion regime. In Figure 3B, only below 10 nm separation the repulsive force increases more rapidly and eventually ends in the constant compliance regime of the hard contact at 0 nm. In this process, the eco-corona gets more and more compressed and finally the hard material of the underlying polystyrene is dominating the interaction. No time-dependent trends in the interaction behavior, like a restructuring of the eco-corona, were observed over the experimental duration of 5 h.

In comparison with Figure 3A, the force curves in Figure 3B show more variations between the different particles. The range and magnitude of the soft repulsion are different for different particles. This can be explained by the general heterogeneous appearance of the eco-corona-covered particles, also shown in the SEM images in Figure 2. However, the force curves can give clear information whether a particle is covered with an eco-corona.

We find no systematic trend of the repulsive interactions dominating the approach data for repeated measurements on the same particles. This indicates elastic behavior of the eco-corona. However, we find a decreasing attractive force (Figure S3) during the approach of consecutive measured particles in the beginning of the experiment. This agrees with the data acquired on the retraction of the cantilever, which shows an adhesion signature (Figure S4), which decreases with the measurement on consecutive particles. This can be explained by transfer of the eco-corona material to the probe particle, which alters the particle–particle adhesion (see Figure S5), but has only a negligible influence on the nanomechanical properties of the particle–particle contact.

3.3. Repulsive Interactions of Eco-corona Particles: Quantitative Description. The eco-corona is probably a highly swollen biomolecular material that is physisorbed to the particle surface. In polymer physical terms, this reflects more a pseudo-brush with polymer chains randomly adsorbed to a hard surface, as described by Guiselin and co-workers.[63,64] In a similar system, Block and Helm observed that polyelectrolytes adsorbed from solutions with high ionic strength can be described by Alexander–de Gennes polymer brush theory.[49−52] The equivalence of the description of the pseudo brush by Guiselin and the AdG model was actually shown earlier for a certain range of separation.[63] Polymer brushes and pseudo-brushes share the anchoring of the polymer chains to a surface. In the case of the eco-corona, the molecular structure is probably not brush-like but rather unordered with some chemical or physical cross-links in the material. We discuss this in more detail later on. The AdG model has the advantage of giving an analytical expression for the expected force–separation curves. Thus, we compare the measured force curves for the eco-corona to the prediction of the AdG model in Figure 4.

The model by Alexander and de Gennes deals with polymer brushes of different swelling and relies on scaling laws.[65,66] It only uses apparent quantities like the distance between two grafting points and the overall thickness of the brush. The interaction force is dependent on the separation between the CP surface and the hard surface of the microplastic particle. The brush thickness and grafting distance were obtained by the fit. For other polymer brush models like the polymer brush mean-field theory of Millner, Witten, and Cates[67] or the polymer adsorption layer model by Guiselin,[63,64] molecular weight or monomer size is necessary to describe interactions.

The eco-corona however is not made up of a single biomolecule with easily characterizable properties. Instead, it is a variety of different proteins, polysaccharides, lipids, and humic acids with no clear molecular structure.[19,30,68] A model that does not need information in the molecular details of the biomolecules in the eco-corona is therefore needed. AdG fulfills this requirement.

To a first approximation, the colloidal probe is supposed to have a bare surface, see below for a discussion of this approximation. Consequently, the data was fitted with the asymmetric AdG model proposed by O'Shea[69] for an interaction of a polymer brush with a plain surface. Four assumptions are made to describe the interaction in AdG theory. (i) Brushes are end-grafted. This means that each polymer chain is attached to the surface with only one point of the chain, i.e., no loops or more complex structures play a role. (ii) Brushes do not interpenetrate, which can be neglected for the asymmetric case because there is only one brush. (iii) The density profile of polymer chains within the brush is uniform and is zero outside. This assumption translates in a monodisperse distribution of molar masses of the polymers in the brush. (iv) No electrostatic forces are present. Only steric forces due to the fluctuations of the polymer are relevant. Assumption (ii) is valid at the beginning of the measurements and (iv) for the whole experiment. Due to the unknown molecular structure of the eco-corona, we do not expect that assumptions (i) and (iii) are fulfilled. However, these assumptions might be effectively fulfilled,[63,64] i.e., deviations from these assumptions may or may not influence the interaction of the probe with the eco-corona.

The asymmetric AdG model considers two mechanisms to describe the interaction of a polymer brush with an inert surface. (i) Polymer chains stretch to avoid overlapping and form brushes. (ii) Stretched polymers are an entropic spring and store elastic energy. In equilibrium, both mechanisms balance each other. When a second surface is approaching and compressing the brush, the polymer concentration increases and an osmotic repulsion arises. Contrary to that, entropic elastic energy is released by chain relaxation. With the help of the Derjaguin relation,[70] the interaction force of the two spheres was normalized to two planar surfaces (for D < L)..

$$\frac{F_{\text{asym}}(D)}{R^*} = \frac{4\pi\,k_BTL}{35\,s^3}\left[7\left(\frac{D}{L}\right)^{-5/4} + 5\left(\frac{D}{L}\right)^{7/4} - 12\right] \quad (2)$$

Here, R^* is the reduced radius and describes the contact radius between CP and the microplastic particle. The parameter s is the (apparent) average grafting distance from one anchor point of a polymer chain to the next, k_BT is the thermal energy at lab temperature (293 K), L is the (apparent) brush thickness, and D is the separation between the two surfaces. We denote the grafting distance and brush thickness as apparent parameters because assumptions (i) and (iii) of the AdG model, mentioned above, are not fulfilled. D is the separation given by the AFM, whereby 0 nm separation is defined as the hard, incompressible contact of the two surfaces. L is the separation at the onset of the repulsive force. The only parameters to be fitted are s and L. We fitted all curves seen in Figure 4 in the normalized force range of 0.1−4 mN/m. The results are given in Figure 5. The apparent brush thickness L is varying from 15 to 204 nm. These values do not reflect the true thickness of the eco-corona but give an idea about the dimensions. This will be discussed later on in more detail. The apparent grafting
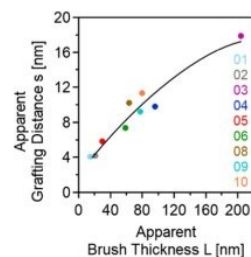
Figure 5. Obtained apparent parameters after applying the AdG fit to force−separation curves. Increasing apparent grafting distance of the eco-corona with apparent brush thickness. Thin films are more compressed while thick ones are likely more hydrated. Fit scales with $s \sim L^{0.57}$.

distance s is within the range of 4 to 18 nm. A mean grafting distance of $s = 8.9$ nm was calculated, which corresponds to a grafting density of $1/s^2 = 0.023$ nm^{-2}.

4. DISCUSSION

As depicted in Figure 5, the apparent grafting distance and the apparent brush thickness are not independent from each other but strongly correlate with each other. Especially, the apparent brush thickness is much higher than the apparent grafting distance. Along the lines of the AdG model, this implies that the assumed brush configuration is actually reflected in the fitted parameters ($s \ll L$). Moreover, there seems to be a small parameter corridor for possible apparent grafting distances in dependence on the apparent brush thickness.

The overall image from these fits in Figure 4 is that the AdG model is able to describe the repulsive interaction of an eco-corona. Moreover, it is capable of characterizing eco-coronas obtained from other environments like fresh water (Figure S6) too. This observation requires however a further discussion of the assumptions used in the AdG model. Here, we partially adapt the arguments by Aubouy et al. to the adsorbed eco-corona.[63] Above, we identified two of the assumptions as not obviously fulfilled: (i) Brushes are end-grafted. This criterion is obviously not met. The physisorption of the water-soluble biomolecules induces the attachment to the surface with more than one point of the molecule chain. Others might only have (chemical or physical) cross-links to physisorbed chains. Hence, the conformation of the eco-corona is different to that of a polymer brush. Interestingly, physisorbed block-copolymers[71] show grafting distances and brush thicknesses in the same range as our eco-corona with the thinnest layers. Polyelectrolyte multilayers of poly(styrene sulfonate) (PSS) and poly(diallyldimethylammonium chloride) (PDADMAC) were investigated by Mohamad et al.[72] They obtained a mean grafting distance of 43.2 nm and high brush thicknesses of more than 100 nm at low ionic strengths. These examples illustrate that the AdG model in fact can reproduce force−separation curves for non-brush systems that are indeed in a similar range to our values for the eco-corona. (ii) Brushes do not interpenetrate. This assumption could be generally neglected for the asymmetrical AdG model as there is only one surface bearing an eco-corona that can act like a polymer brush. In our case however, the asymmetrical model is the better approximation, although we have shown in Figure S5 that biomolecules of the eco-corona attach to the CP during the experiment. If the transferred material would have a similar thickness as the eco-corona, the symmetric system should be

more appropriate as the two opposing surfaces are covered. The fits, however, result in a better agreement of the interaction profile with the asymmetric model. From this, we conclude that the amount of eco-corona transferred to the CP is not enough to affect the repulsive interaction. (iii) Uniform density profile of the polymer chains within the brush. The eco-corona is a natural and hence very heterogeneous system as already discussed. It is likely made up of different biomolecules with different moieties, molecular weights, and conformations. Therefore, it is unlikely that the density profile of the eco-corona is uniform and all biomolecule chains protrude equally long into the solution. We attribute the differences between the model and the measured data in Figure 4 at low forces and high separation distances to a decreased biomolecule concentration in this part of the eco-corona. This non-constant biomolecule concentration can cause differences between the actual thickness of the eco-corona and the fitted apparent brush thickness. (iv) No electrostatic forces are present. The measurements were performed at 150 mM, and the electrostatic interactions are therefore screened. Hence, only steric repulsion was observed.

In our study, apparent grafting distances s increased with the apparent brush thickness L of the eco-corona by $s \sim L^{0.57}$ (Figure 5). Thus, the intermolecular distance between biomolecules increases at high brush thickness. In the following, we derive simple scaling arguments that support such a dependency. As already mentioned, biomolecules are not end grafted to the surface but physisorbed with several segments of the chain. They adsorb either directly to the surface or bind more loosely to other biomolecules and form a complex layer. With this increasing amount of loosely attached molecules, the eco-corona becomes more compressible. This is in agreement with the proposed model of the "hard" and "soft" protein corona" by Monopoli et al.[73] The term "hard corona" corresponds to the adsorption of biomolecules with high surface affinity. These are supposed to bind strongly onto the surface, which would result in a more rigid less compressible shell. The soft corona is forming due to attachment of biomolecules onto the pre-formed hard corona. They are more loosely bound, which increases their apparent grafting distance and build therefore a more compressible second shell around the microplastic particles. Our data suggest a gradual transition between the hard and soft corona.

For a polymer brush in a good solvent, Auroy et al.[74] determined the relation of

$$Ls^{2/3} \sim M \tag{3}$$

with L brush thickness, s grafting distance, and M molecular weight. For brushes that are synthesized in a grafting-to approach, Michalek et al.[75] experimentally obtained a more accurate relation compared to the standard estimation of grafting distance, which we simplify to

$$s^2 \sim M \tag{4}$$

By inserting eq 3 into eq 4 and simplifying, we obtain

$$s \sim L^{3/4} \tag{5}$$

This relationship shows that for polymer brushes synthesized by grafting-to, s increases with L with an exponent of 0.75, in this simple model. For our data, we obtain a relation of $s \sim L^{0.57}$, which follows roughly our simple argument. Additionally, our experimental scaling $s \sim L^{0.57}$ is surprisingly close to the scaling observed by Block et al. for adsorbed polystyrene

sulfonate layers ($s \sim L^{0.52}$).[51] That the scaling in eq 5 is not more accurate is no surprise as this model also assumes the molecules to be end-grafted instead of attached with more than one point of the chain. In addition, Michalek et al. mentioned that this scaling exponent will be slightly different for different polymers and is more providing a range than an exact exponent. However, assuming a grafting-to scaling shows a similar relation between s and L and is hence a better approach to describe the eco-corona scaling.

The AdG theory seems to be more capable than what it was made for. Its scaling laws not only describe end-grafted polymer brushes but also physisorbed polyelectrolyte (multi)-layers[49−52,72,76] as well as adsorbed polymers.[71] Polymer melts have been also described by this model.[77] Scaling arguments on pseudo brushes actually support this observation.[63] Furthermore, we have shown that AdG theory is applicable for even more complex systems like the eco-corona consisting of well more than two different physisorbed biomolecules. The model is very precise at intermediate separation. Deviations at low and high separation are probably due to the assumption of end-grafted and monodisperse polymers, respectively.

5. CONCLUSIONS

Here, we demonstrated with CP-AFM measurements that the formation of the eco-corona on microplastic particles introduces a compressible film, which changes the mechanical behavior on the surface. This heterogeneous film is different for individual particles. The eco-corona formation around particles leads to the onset of long-range repulsive surface interactions. We have shown that the Alexander−de Gennes model can describe the separation dependency of these interactions. This theory was originally developed to describe the interaction of polymer brushes. However, the AdG model has already been successfully applied to adsorbed polymer layers.[49−52,71] With this study, we extend the range of possible applications to more complex systems. The eco-corona's essential physics of the long-range interactions can be captured by an effective brush description. Using an apparent brush thickness and apparent grafting distance, we have shown that these model parameters scale with each other. Interestingly, the effective brush parameters of the eco-corona are in a similar range as found for adsorbed polyelectrolyte (multi)-layers and polymers.[49,72,78] This suggests that polyelectrolyte multilayer-coated microplastics can serve as model systems for studying its interaction with cells. Polyelectrolyte multilayers are applicable to different geometries and sizes.[79,80] They can be tuned in their mechanics and surface charge enabling to account effects to certain properties.

Furthermore, we have shown that with increasing eco-corona thickness, the surface becomes more compressible. The higher amount of loosely attached biomolecules leads to an increased intermolecular distance. The compressibility is expected to influence the particle−cell interactions and, as Hartmann et al. demonstrated, cellular uptake.[32] The stiffness-dependent uptake of microparticles potentially explains the increased internalization of eco-corona particles found by Ramsperger et al. too.[30] However, it is not clear whether other surface properties contribute to this effect as well. These results make it even more important to shift the focus on realistic microplastic samples covered by an eco-corona. It also highlights the importance of characterizing the surface properties of microplastic particles as they influence cellular

interactions, which may in turn be responsible for adverse effects on environmental and human health.

The knowledge about polymer brush swelling behavior and interaction with surfaces enables predictions about the transport, bioavailability, and aggregation behavior of eco-corona-covered microplastic particles. Polymer brush interactions could be therefore used in a coarse-grained description for the eco-corona and other complex systems. An effective brush will facilitate modeling its impact with a much lower computational cost than explicitly modeling polymer adsorption layers, opening the door toward larger system simulations.

■ ASSOCIATED CONTENT

ⓈⒾ Supporting Information

The Supporting Information is available free of charge at https://pubs.acs.org/doi/10.1021/acs.langmuir.1c03204.

> Marine aquarium facility and artificial freshwater pond where water was taken to incubate particles (Figures S1 and S2); normalized approach curves of eco-corona particles (Figure S3); normalized retraction curves (Figure S4); SEM images prior and after CP-AFM measurements on eco-corona particles (Figure S5); normalized force-separation curves of eco-corona particles obtained from freshwater environment with their corresponding AdG fit (Figure S6) (PDF)

■ AUTHOR INFORMATION

Corresponding Authors

Andreas Fery — *Leibniz Institute of Polymer Research Dresden e.V., Institute of Physical Chemistry and Polymer Physics, 01069 Dresden, Germany; Physical Chemistry of Polymeric Materials, Technische Universität Dresden, 01069 Dresden, Germany;* ⓞ orcid.org/0000-0001-6692-3762; Email: fery@ipfdd.de

Günter K. Auernhammer — *Leibniz Institute of Polymer Research Dresden e.V., Institute of Physical Chemistry and Polymer Physics, 01069 Dresden, Germany;* ⓞ orcid.org/0000-0003-1515-0143; Email: auernhammer@ipfdd.de

Authors

Thomas Witzmann — *Leibniz Institute of Polymer Research Dresden e.V., Institute of Physical Chemistry and Polymer Physics, 01069 Dresden, Germany;* ⓞ orcid.org/0000-0001-6698-926X

Anja F. R. M. Ramsperger — *Animal Ecology I and BayCEER and Biological Physics, University of Bayreuth, 95447 Bayreuth, Germany*

Simon Wieland — *Animal Ecology I and BayCEER and Biological Physics, University of Bayreuth, 95447 Bayreuth, Germany;* ⓞ orcid.org/0000-0001-5439-1594

Christian Laforsch — *Animal Ecology I and BayCEER, University of Bayreuth, 95447 Bayreuth, Germany*

Holger Kress — *Biological Physics, University of Bayreuth, 95447 Bayreuth, Germany*

Complete contact information is available at:
https://pubs.acs.org/10.1021/acs.langmuir.1c03204

Notes

The authors declare no competing financial interest.

■ REFERENCES

(1) Barnes, D. K. A.; Galgani, F.; Thompson, R. C.; Barlaz, M. Accumulation and fragmentation of plastic debris in global environments. *Philos. Trans. R. Soc. London, Ser. B* **2009**, *364*, 1985−1998.

(2) Cole, M.; Lindeque, P.; Halsband, C.; Galloway, T. S. Microplastics as contaminants in the marine environment: A review. *Mar. Pollut. Bull.* **2011**, *62*, 2588−2597.

(3) de Souza Machado, A. A.; Kloas, W.; Zarfl, C.; Hempel, S.; Rillig, M. C. Microplastics as an emerging threat to terrestrial ecosystems. *Global Change Biol.* **2018**, *24*, 1405−1416.

(4) Imhof, H. K.; Ivleva, N. P.; Schmid, J.; Niessner, R.; Laforsch, C. Contamination of beach sediments of a subalpine lake with microplastic particles. *Curr. Biol.* **2013**, *23*, R867−R868.

(5) Gasperi, J.; Wright, S. L.; Dris, R.; Collard, F.; Mandin, C.; Guerrouache, M.; Langlois, V.; Kelly, F. J.; Tassin, B. Microplastics in air: are we breathing it in? *Curr. Opin. Environ. Sci. Health* **2018**, *1*, 1−5.

(6) Andrady, A. L. The plastic in microplastics: A review. *Mar. Pollut. Bull.* **2017**, *119*, 12−22.

(7) Meides, N.; Menzel, T.; Poetzschner, B.; Löder, M. G. J.; Mansfeld, U.; Strohriegl, P.; Altstaedt, V.; Senker, J. Reconstructing the Environmental Degradation of Polystyrene by Accelerated Weathering. *Environ. Sci. Technol.* **2021**, *55*, 7930−7938.

(8) Frias, J. P. G. L.; Nash, R. Microplastics: finding a consensus on the definition. *Mar. Pollut. Bull.* **2019**, *138*, 145−147.

(9) Prata, J. C.; da Costa, J. P.; Lopes, I.; Duarte, A. C.; Rocha-Santos, T. Environmental exposure to microplastics: An overview on possible human health effects. *Sci. Total Environ.* **2020**, *702*, No. 134455.

(10) Rillig, M. C.; Lehmann, A.; de Souza Machado, A. A.; Yang, G. Microplastic effects on plants. *New Phytol.* **2019**, *223*, 1066−1070.

(11) Wright, S. L.; Thompson, R. C.; Galloway, T. S. The physical impacts of microplastics on marine organisms: a review. *Environ. Pollut.* **2013**, *178*, 483−492.

(12) Stock, V.; Laurisch, C.; Franke, J.; Dönmez, M. H.; Voss, L.; Böhmert, L.; Braeuning, A.; Sieg, H. Uptake and cellular effects of PE, PP, PET and PVC microplastic particles. *Toxicol. In Vitro* **2021**, *70*, No. 105021.

(13) Rudolph, J.; Völkl, M.; Jérôme, V.; Scheibel, T.; Freitag, R. Noxic effects of polystyrene microparticles on murine macrophages and epithelial cells. *Sci. Rep.* **2021**, *11*, 15702.

(14) Rubin, A. E.; Sarkar, A. K.; Zucker, I. Questioning the suitability of available microplastics models for risk assessment − A critical review. *Sci. Total Environ.* **2021**, *788*, No. 147670.

(15) Luo, H.; Zhao, Y.; Li, Y.; Xiang, Y.; He, D.; Pan, X. Aging of microplastics affects their surface properties, thermal decomposition, additives leaching and interactions in simulated fluids. *Sci. Total Environ.* **2020**, *714*, No. 136862.

(16) Lynch, I.; Dawson, K. A.; Lead, J. R.; Valsami-Jones, E. Chapter 4 - Macromolecular Coronas and Their Importance in Nanotoxicology and Nanoecotoxicology. In *Frontiers of Nanoscience*; Lead, J. R.; Valsami-Jones, E., Eds.; Elsevier, 2014; Vol. 7, pp. 127−156, DOI: 10.1016/B978-0-08-099408-6.00004-9.

(17) Ramsperger, A. F. R. M.; Stellwag, A. C.; Caspari, A.; Fery, A.; Lueders, T.; Kress, H.; Löder, M. G. J.; Laforsch, C. Structural Diversity in Early-Stage Biofilm Formation on Microplastics Depends on Environmental Medium and Polymer Properties. *Water* 2020, 12, 3216.

(18) Saavedra, J.; Stoll, S.; Slaveykova, V. I. Influence of nanoplastic surface charge on eco-corona formation, aggregation and toxicity to freshwater zooplankton. *Environ. Pollut.* 2019, 252, 715−722.

(19) Rummel, C. D.; Lechtenfeld, O. J.; Kallies, R.; Benke, A.; Herzsprung, P.; Rynek, R.; Wagner, S.; Potthoff, A.; Jahnke, A.; Schmitt-Jansen, M. Conditioning Film and Early Biofilm Succession on Plastic Surfaces. *Environ. Sci. Technol.* 2021, 55, 11006−11018.

(20) Bhagwat, G.; O'Connor, W.; Grainge, I.; Palanisami, T. Understanding the Fundamental Basis for Biofilm Formation on Plastic Surfaces: Role of Conditioning Films. *Front. Microbiol.* 2021, 12, 1615.

(21) Trefalt, G.; Cao, T.; Sugimoto, T.; Borkovec, M. Hetero-aggregation between Charged and Neutral Particles. *Langmuir* 2020, 36, 5303−5311.

(22) Oney, D. M.; Nason, J. A. Natural organic matter surface coverage as a predictor of heteroaggregation between nanoparticles and colloids. *Environ. Sci.: Nano* 2021, 8, 687−697.

(23) Li, X.; He, E.; Xia, B.; Liu, Y.; Zhang, P.; Cao, X.; Zhao, L.; Xu, X.; Qiu, H. Protein corona-induced aggregation of differently sized nanoplastics: impacts of protein type and concentration. *Environ. Sci.: Nano* 2021, 8, 1560−1570.

(24) Li, X.; He, E.; Jiang, K.; Peijnenburg, W. J. G. M.; Qiu, H. The crucial role of a protein corona in determining the aggregation kinetics and colloidal stability of polystyrene nanoplastics. *Water Res.* 2021, 190, No. 116742.

(25) Junaid, M.; Wang, J. Interaction of nanoplastics with extracellular polymeric substances (EPS) in the aquatic environment: A special reference to eco-corona formation and associated impacts. *Water Res.* 2021, 201, No. 117319.

(26) Bhagwat, G.; Tran, T. K. A.; Lamb, D.; Senathirajah, K.; Grainge, I.; O'Connor, W.; Juhasz, A.; Palanisami, T. Biofilms Enhance the Adsorption of Toxic Contaminants on Plastic Micro-fibers under Environmentally Relevant Conditions. *Environ. Sci. Technol.* 2021, 55, 8877−8887.

(27) Mao, R.; Lang, M.; Yu, X.; Wu, R.; Yang, X.; Guo, X. Aging mechanism of microplastics with UV irradiation and its effects on the adsorption of heavy metals. *J. Hazard. Mater.* 2020, 393, No. 122515.

(28) Singh, N.; Tiwari, E.; Khandelwal, N.; Darbha, G. K. Understanding the stability of nanoplastics in aqueous environments: effect of ionic strength, temperature, dissolved organic matter, clay, and heavy metals. *Environ. Sci.: Nano* 2019, 6, 2968−2976.

(29) Wu, J.; Jiang, R.; Lin, W.; Ouyang, G. Effect of salinity and humic acid on the aggregation and toxicity of polystyrene nanoplastics with different functional groups and charges. *Environ. Pollut.* 2019, 245, 836−843.

(30) Ramsperger, A. F. R. M.; Narayana, V. K. B.; Gross, W.; Mohanraj, J.; Thelakkat, M.; Greiner, A.; Schmalz, H.; Kress, H.; Laforsch, C. Environmental exposure enhances the internalization of microplastic particles into cells. *Sci. Adv.* 2020, 6 (), DOI: 10.1126/sciadv.abd1211.

(31) Yao, C.; Akakuru, O. U.; Stanciu, S. G.; Hampp, N.; Jin, Y.; Zheng, J.; Chen, G.; Yang, F.; Wu, A. Effect of elasticity on the phagocytosis of micro/nanoparticles. *J. Mater. Chem. B* 2020, 8, 2381−2392.

(32) Hartmann, R.; Weidenbach, M.; Neubauer, M.; Fery, A.; Parak, W. J. Stiffness-dependent in vitro uptake and lysosomal acidification of colloidal particles. *Angew. Chem., Int. Ed.* 2015, 54, 1365−1368.

(33) Zhao, W.; Zhao, P.; Tian, Y.; Shen, C.; Li, Z.; Peng, P.; Jin, C. Investigation for Synergies of Ionic Strength and Flow Velocity on Colloidal-Sized Microplastic Transport and Deposition in Porous Media Using the Colloidal-AFM Probe. *Langmuir* 2020, 36, 6292−6303.

(34) Montes Ruiz-Cabello, F. J.; Oncsik, T.; Rodríguez-Valverde, M. A.; Maroni, P.; Cabrerizo-Vilchez, M. Specific Ion Effects and pH

Dependence on the Interaction Forces between Polystyrene Particles. *Langmuir* 2016, 32, 11918−11927.

(35) Trefalt, G.; Szilágyi, I.; Borkovec, M. Schulze-Hardy rule revisited. *Colloid Polym. Sci.* 2020, 298, 961−967.

(36) Ruiz-Cabello, F. J. M.; Moazzami-Gudarzi, M.; Elzbieciak-Wodka, M.; Maroni, P. Forces between different latex particles in aqueous electrolyte solutions measured with the colloidal probe technique. *Microsc. Res. Tech.* 2017, 80, 144−152.

(37) Trefalt, G.; Behrens, S. H.; Borkovec, M. Charge Regulation in the Electrical Double Layer: Ion Adsorption and Surface Interactions. *Langmuir* 2016, 32, 380−400.

(38) Montes Ruiz-Cabello, F. J.; Trefalt, G.; Oncsik, T.; Szilagyi, I.; Maroni, P.; Borkovec, M. Interaction Forces and Aggregation Rates of Colloidal Latex Particles in the Presence of Monovalent Counterions. *J. Phys. Chem. B* 2015, 119, 8184−8193.

(39) Patiño, J. E.; Kuhl, T. L.; Morales, V. L. Direct Measurements of the Forces between Silver and Mica in Humic Substance-Rich Solutions. *Environ. Sci. Technol.* 2020, 54, 15076−15085.

(40) Ramsperger, A. F. R. M.; Jasinski, J.; Völkl, M.; Witzmann, T.; Meinhart, M.; Jérôme, V.; Kretschmer, W. P.; Freitag, R.; Senker, J.; Fery, A.; Kress, H.; Scheibel, T.; Laforsch, C. Supposedly identical microplastic particles substantially differ in their material properties influencing particle-cell interactions and cellular responses. *J. Hazard. Mater.* 2022, 425, No. 127961.

(41) Maroni, P.; Montes Ruiz-Cabello, F. J.; Cardoso, C.; Tiraferri, A. Adsorbed Mass of Polymers on Self-Assembled Monolayers: Effect of Surface Chemistry and Polymer Charge. *Langmuir* 2015, 31, 6045−6054.

(42) Sakata, S.; Inoue, Y.; Ishihara, K. Quantitative Evaluation of Interaction Force between Functional Groups in Protein and Polymer Brush Surfaces. *Langmuir* 2014, 30, 2745−2751.

(43) Adamczyk, Z.; Nattich-Rak, M. Formation of Myoglobin Corona at Polymer Microparticles. *Colloids Interfaces* 2021, 5, 27.

(44) Borkovec, M.; Szilagyi, I.; Popa, I.; Finessi, M.; Sinha, P.; Maroni, P.; Papastavrou, G. Investigating forces between charged particles in the presence of oppositely charged polyelectrolytes with the multi-particle colloidal probe technique. *Adv. Colloid Interface Sci.* 2012, 179-182, 85−98.

(45) Finessi, M.; Sinha, P.; Szilágyi, I.; Popa, I.; Maroni, P.; Borkovec, M. Charge reversal of sulfate latex particles by adsorbed linear poly(ethylene imine) probed by multiparticle colloidal probe technique. *J. Phys. Chem. B* 2011, 115, 9098−9105.

(46) Popa, I.; Gillies, G.; Papastavrou, G.; Borkovec, M. Attractive and Repulsive Electrostatic Forces between Positively Charged Latex Particles in the Presence of Anionic Linear Polyelectrolytes. *J. Phys. Chem. B* 2010, 114, 3170−3177.

(47) Popa, I.; Gillies, G.; Papastavrou, G.; Borkovec, M. Attractive Electrostatic Forces between Identical Colloidal Particles Induced by Adsorbed Polyelectrolytes. *J. Phys. Chem. B* 2009, 113, 8458−8461.

(48) Borkovec, M.; Papastavrou, G. Interactions between solid surfaces with adsorbed polyelectrolytes of opposite charge. *Curr. Opin. Colloid Interface Sci.* 2008, 13, 429−437.

(49) Block, S.; Helm, C. A. Measurement of long-ranged steric forces between polyelectrolyte layers physisorbed from 1M NaCl. *Phys. Rev. E* 2007, 76, No. 030801.

(50) Block, S.; Helm, C. A. Conformation of Poly(styrene sulfonate) Layers Physisorbed from High Salt Solution Studied by Force Measurements on Two Different Length Scales. *J. Phys. Chem. B* 2008, 112, 9318−9327.

(51) Block, S.; Helm, C. A. Single Polyelectrolyte Layers Adsorbed at High Salt Conditions: Polyelectrolyte Brush Domains Coexisting with Flatly Adsorbed Chains. *Macromolecules* 2009, 42, 6733−6740.

(52) Block, S.; Helm, C. A. Equilibrium and Nonequilibrium Features in the Morphology and Structure of Physisorbed Polyelectrolyte Layers. *J. Phys. Chem. B* 2011, 115, 7301−7313.

(53) Johnson, D.; Galiano, F.; Deowan, S. A.; Hoinkis, J.; Figoli, A.; Hilal, N. Adhesion forces between humic acid functionalized colloidal probes and polymer membranes to assess fouling potential. *J. Membr. Sci.* 2015, 484, 35−46.

178

(54) Yu, Z.; Chu, H.; Zhang, W.; Gao, K.; Yang, L.; Zhang, Y.; Zhou, X. Multi-dimensional in-depth dissection the algae-related membrane fouling in heterotrophic microalgae harvesting: Deposition dynamics, algae cake formation, and interaction force analysis. *J. Membr. Sci.* **2021**, *635*, No. 119501.

(55) Woodall, L. C.; Sanchez-Vidal, A.; Canals, M.; Paterson, G. L. J.; Coppock, R.; Sleight, V.; Calafat, A.; Rogers, A. D.; Narayanaswamy, B. E.; Thompson, R. C. The deep sea is a major sink for microplastic debris. *R. Soc. Open Sci.* **2014**, *1*, No. 140317.

(56) Hutter, J. L.; Bechhoefer, J. Calibration of atomic-force microscope tips. *Rev. Sci. Instrum.* **1993**, *64*, 1868−1873.

(57) Butt, H.-J.; Jaschke, M. Calculation of thermal noise in atomic force microscopy. *Nanotechnology* **1995**, *6*, 1−7.

(58) Eifert, A.; Paulssen, D.; Varanakkottu, S. N.; Baier, T.; Hardt, S. Simple Fabrication of Robust Water-Repellent Surfaces with Low Contact-Angle Hysteresis Based on Impregnation. *Adv. Mater. Interfaces* **2014**, *1*, 1300138.

(59) Krumpfer, J. W.; McCarthy, T. J. Rediscovering Silicones: "Unreactive" Silicones React with Inorganic Surfaces. *Langmuir* **2011**, *27*, 11514−11519.

(60) Teisala, H.; Baumli, P.; Weber, S. A. L.; Vollmer, D.; Butt, H.-J. Grafting Silicone at Room Temperature—a Transparent, Scratch-resistant Nonstick Molecular Coating. *Langmuir* **2020**, *36*, 4416−4431.

(61) Debye, P.; Hückel, E. The Theory of Electrolytes. I. Freezing Point Depression and Related Phenomenon. *Phys. Z.* **1923**, *24*, 185−206.

(62) Zou, Y.; Jayasuriya, S.; Manke, C. W.; Mao, G. Influence of Nanoscale Surface Roughness on Colloidal Force Measurements. *Langmuir* **2015**, *31*, 10341−10350.

(63) Aubouy, M.; Guiselin, O.; Raphaël, E. Scaling Description of Polymer Interfaces: Flat Layers. *Macromolecules* **1996**, *29*, 7261−7268.

(64) Guiselin, O. Irreversible Adsorption of a Concentrated Polymer-Solution. *Europhys. Lett.* **1992**, *17*, 225−230.

(65) Alexander, S. Adsorption of chain molecules with a polar head a scaling description. *J. Phys.* **1977**, *38*, 983−987.

(66) de Gennes, P. G. Conformations of Polymers Attached to an Interface. *Macromolecules* **1980**, *13*, 1069−1075.

(67) Milner, S. T.; Witten, T. A.; Cates, M. E. Theory of the Grafted Polymer Brush. *Macromolecules* **1988**, *21*, 2610−2619.

(68) Pulido-Reyes, G.; Leganes, F.; Fernández-Piñas, F.; Rosal, R. Bio-nano interface and environment: A critical review. *Environ. Toxicol. Chem.* **2017**, *36*, 3181−3193.

(69) O'Shea, S. J.; Welland, M. E.; Rayment, T. An atomic force microscope study of grafted polymers on mica. *Langmuir* **1993**, *9*, 1826−1835.

(70) Derjaguin, B. Analysis of friction and adhesion IV The theory of the adhesion of small particles. *Kolloid-Z.* **1934**, *69*, 155−164.

(71) McLean, S. C.; Lioe, H.; Meagher, L.; Craig, V. S. J.; Gee, M. L. Atomic Force Microscopy Study of the Interaction between Adsorbed Poly(ethylene oxide) Layers: Effects of Surface Modification and Approach Velocity. *Langmuir* **2005**, *21*, 2199−2208.

(72) Mohamad, H. S.; Neuber, S.; Helm, C. A. Surface Forces of Asymmetrically Grown Polyelectrolyte Multilayers: Searching for the Charges. *Langmuir* **2019**, *35*, 15491−15499.

(73) Monopoli, M. P.; Åberg, C.; Salvati, A.; Dawson, K. A. Biomolecular coronas provide the biological identity of nanosized materials. *Nat. Nanotechnol.* **2012**, *7*, 779−786.

(74) Auroy, P.; Auvray, L.; Léger, L. Characterization of the brush regime for grafted polymer layers at the solid-liquid interface. *Phys. Rev. Lett.* **1991**, *66*, 719−722.

(75) Michalek, L.; Mundsinger, K.; Barner-Kowollik, C.; Barner, L. The long and the short of polymer grafting. *Polym. Chem.* **2019**, *10*, 54−59.

(76) Nugroho, R. W. N.; Pettersson, T.; Odelius, K.; Höglund, A.; Albertsson, A.-C. Force Interactions of Nonagglomerating Polylactide Particles Obtained through Covalent Surface Grafting with Hydrophilic Polymers. *Langmuir* **2013**, *29*, 8873−8881.

(77) Butt, H.-J.; Wang, J.; Stark, R.; Kappl, M.; Wolf, B. A.; Eckelt, J.; Knopf, A. Forces Between Solid Surfaces Across Polymer Melts as Revealed by Atomic Force Microscopy. *Soft Mater.* **2007**, *5*, 49−60.

(78) Claesson, P. M.; Poptoshev, E.; Blomberg, E.; Dedinaite, A. Polyelectrolyte-mediated surface interactions. *Adv. Colloid Interface Sci.* **2005**, *114-115*, 173−187.

(79) Decher, G.; Hong, J. D.; Schmitt, J. Buildup of Ultrathin Multilayer Films by a Self-Assembly Process: III. Consecutively Alternating Adsorption of Anionic and Cationic Polyelectrolytes on Charged Surfaces. *Thin Solid Films* **1992**, *210-211*, 831−835.

(80) Caruso, F.; Caruso, R. A.; Möhwald, H. Nanoengineering of inorganic and hybrid hollow spheres by colloidal templating. *Science* **1998**, *282*, 1111−1114.

179

Repulsive interactions of eco-corona covered microplastic particles quantitatively follow modelling of polymer brushes

Thomas Witzmann[1], Anja F. R. M. Ramsperger[2, 3], Simon Wieland[2, 3], Christian Laforsch[2],

Holger Kress[3], Andreas Fery*[1, 4], and Günter K. Auernhammer*[1]

[1] *Leibniz-Institute of Polymer Research Dresden e.V., Institute of Physical Chemistry and Polymer Physics, Hohe Str. 6, 01069 Dresden, Germany*

[2] *Animal Ecology I and BayCEER, University of Bayreuth, 95447 Bayreuth, Germany*

[3] *Biological Physics, University of Bayreuth, 95447 Bayreuth, Germany*

[4]*Physical Chemistry of Polymeric Materials, Technische Universität Dresden, Hohe Str. 6, 01069 Dresden, Germany*

Corresponding authors: *fery@ipfdd.de, auernhammer@ipfdd.de*

Supporting Information

1.1. Description of marine aquarium facility

The water samples were taken directly from the aquarium facility nearby the filtering system. Here biofilms within the filter systems are present, ensuring the occurrence of microorganisms. Within the marine aquarium facility different fish, coral, snail, Crustacea, and Echinodermata species as well as variety of plant and unicellular eu- and prokaryotic organisms are present. We term this as highly biodiverse. The facility is running for over 15 years and fish as well as invertebrates were either exchanged with other research facilities or purchased. Hence, the exact number of species is not known, however, it resembles a heathy coral reef (Figure S 1) and therefore hosts a highly diverse community. The combination of the different species releases a variety of biomolecules through their metabolism, which subsequently are available within the water sample. The attachment of biomolecules on the microplastic particle surface after two weeks of incubation has been shown recently (*Ramsperger et al. 2020, Science Advances, 10.1126/sciadv.abd1211*). However, the water conditions are semi-stable since depending on the nutrition of the different species the released biomolecules can vary over time, similar to seasonal changes in natural environments. Therefore, we changed the incubation media three times a week during the incubation process, to allow a variety of biomolecules being present within the incubation media. The aim was to simulate the exposure of very small microplastic particle in a marine coral reef environment.

Figure S 1 Images of the highly biodiverse marine aquarium facility for the incubation waters

Figure S 2 Image of the artificial freshwater pond. This water was used to incubate microplastic particles in Figure S 6

1.2. Attractive forces of pristine and eco-corona particles
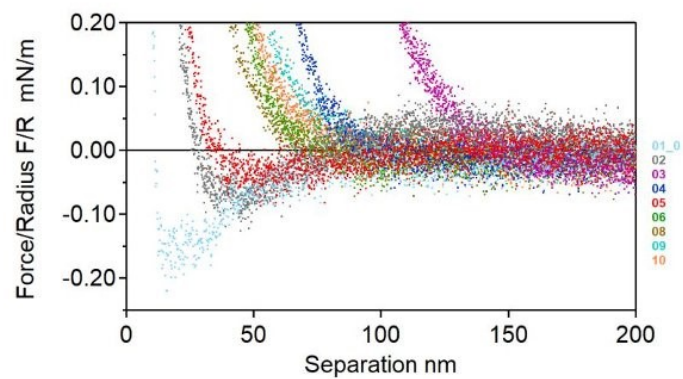
Figure S 3 Normalized approach curves of eco-corona particles reveal long range attractive forces for several particles at 150 mM KCl. Coloured numbers indicate in which order particles where measured. The attractive force was only visible for three particles which were performed in the first half of the experiment

S2

Figure S 4 displays retraction curves of plain A and eco-corona covered microplastic particles B. Both plain and eco-corona particles show a dependency of the adhesion with the number of particles measured. The adhesion between CP and microplastic particles decreases in each case with the number of measurements performed during the experiment. The consecutive measuring seems to modify the surface of the CP by transferring molecules from the sample surface which results in less attractive force during retraction. For plain particles in A presumably surfactant molecules, stabilizing the particles in dispersion, are transferred. As long as the surface of the probe is not completely coated attractive forces are abundant but vanish at complete coverage. The same holds true for eco-corona particles. But instead of surfactant decreasing the adhesion biomolecules from the eco-corona now adsorb to the surface of the CP. However, the tendency of the reduced adhesion is not as strict as it is for the plain particles. This may be explained by the heterogeneity of the eco-corona seen in Figure 2B which leads to different interactions with the CP depending on how the particles are covered with biomolecules. In any case the transfer of surfactant does not lead to pronounced repulsive forces as it does for the eco-corona shown in the approach curves in Figure 3. Thus, the number of transferred molecules is marginal and alters attractive but not repulsive interaction.
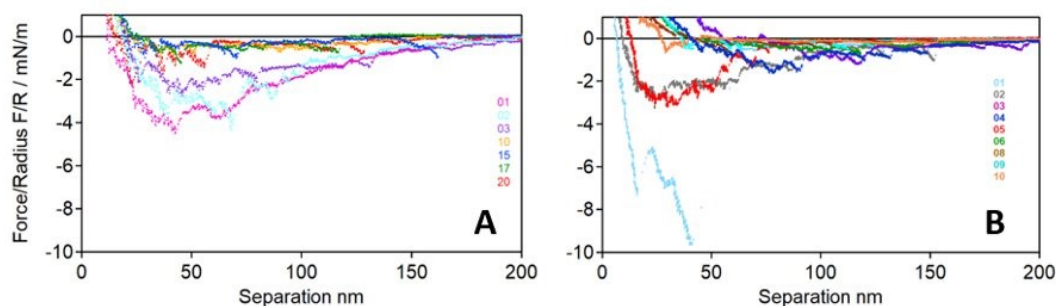
Figure S 4 Normalized retraction curves of pristine particles A and eco-corona particles B at 150 mM KCl. Eco-corona covered particles in B show decreasing adhesive forces with every particle measured. Pristine particles in A show also a dependency of the number of measurements. Coloured numbers indicate in which order particles where measured.

A good example of increasing coverage of the CP is the first measured eco-corona covered particle light blue curve in Figure 3B. This approach force curve looks similar to the approach force curves of the pristine particles. However, when looking at the retraction curve of this very particle, Figure S 4B light blue curve, it seems to have a characteristic adhesive interaction which is distinctive to any other curve. Sudden jumps in this force curve to less negative values are probably due to pull-off events which are accounted to the rupture of polymer chains from the particle surface or within the eco-corona. These polymers attach to the colloidal probe and eventually cover it. During the experiment the colloidal probe converts from a clean surface with adhesion Figure S 5A over a partially covered with less adhesion to a fully eco-corona coated surface with barely any adhesion Figure S 5B. The schematic conversion is also visible in Figure S 5C.

S3
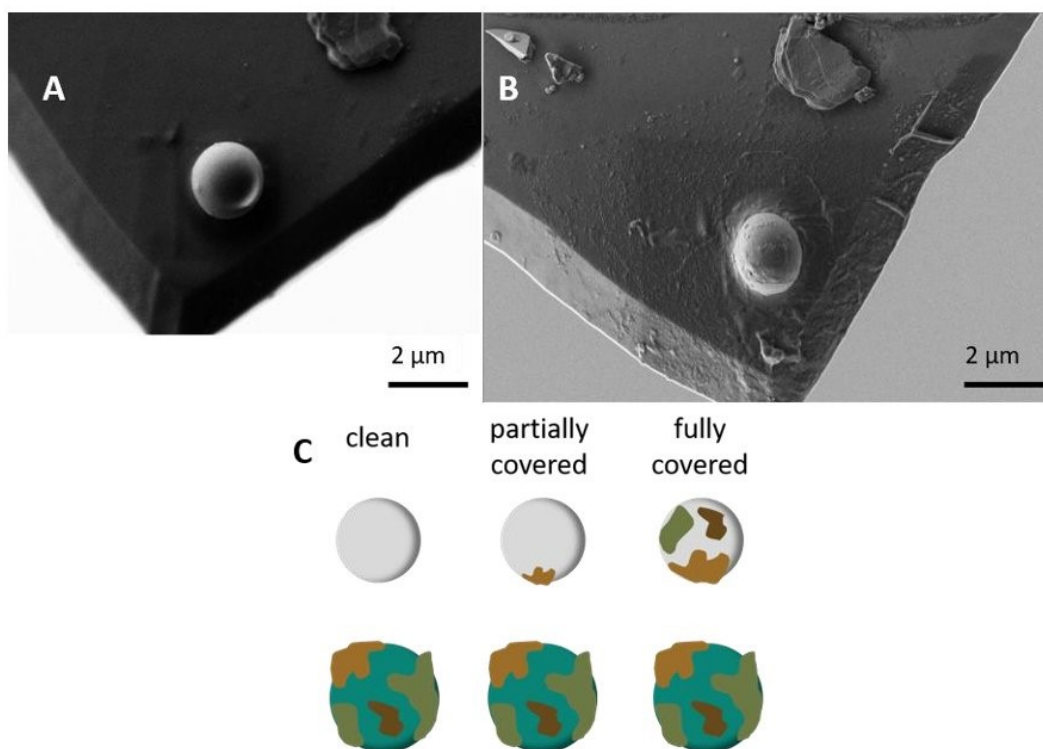
Figure S 5 Colloidal probe before A and after the measurement of eco-corona particles B. Scheme of the conversion from clean to fully covered colloidal probe after measurement of eco-corona particles in C. Colloidal Probe has a diameter of 1.76 µm.

1.3. Repulsive interactions of freshwater eco-corona particles
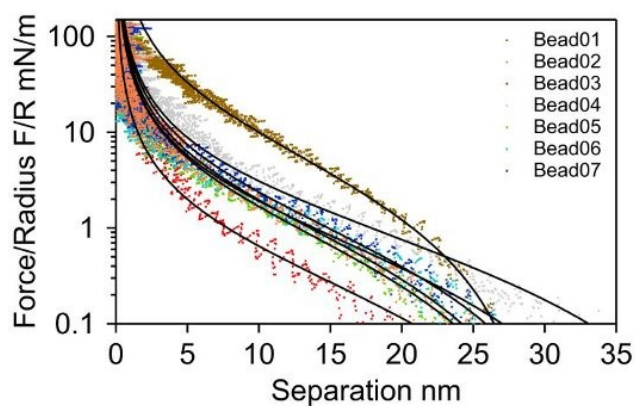
Figure S 6 Exemplary normalized force vs separation curves between silica probe and various eco-corona particles at 150 mM KCl. These eco-corona covered microplastic particles were obtained from incubation in freshwater. Salt and freshwater incubated particles show he same scaling and mechanisms. Black lines correspond to asymmetric Alexander-de Gennes fit at 293 K fitted in the range of 0.1 – 4 mN/m. Numbers indicate in which order particles were measured.

The experimental data from Figure S 6 was obtained from particle-particle measurements on freshwater incubated particles. These microplastic particles are covered by an eco-corona and were prepared and investigated in the same way as the particles incubated in salt water from the marine aquarium. The freshwater used to incubate these particles was taken from an artificial pond (Figure S 2). Although the eco-corona is formed from biomolecules of a different media AdG theory is still able to quantitatively describe the interactions.

S4

Article 6

Cellular internalization pathways of environmentally exposed microplastic particles: Phagocytosis or Macropinocytosis?

1   Manuscript

2   **Title**

3   Cellular internalization pathways of environmentally exposed microplastic particles: Phagocytosis or
4   Macropinocytosis?

5   **Authors:**

6   Anja FRM Ramsperger[1,2#], Simon Wieland[1,2#], Magdalena V Wilde[3#], Thomas Fröhlich[3], Holger Kress[2*] &
7   Christian Laforsch[1*]

8   **Affiliation:**

9   [1] Animal Ecology I and BayCEER, University of Bayreuth, Bayreuth, Germany

10   [2] Biological Physics, University of Bayreuth, Bayreuth, Germany

11   [3] Gene Center Munich, Laboratory for Functional Genome Analysis (LAFUGA), L.M.U., Munich, Germany

12   [#] shared first authorship

13   [*] shared senior authors

14

15 **Abstract**

16 The contamination of the environment with microplastic particles is increasingly gaining scientific and

17 public attention due to their potential adverse effects on the environment, organisms and human health.

18 One potential risk from microplastic pollution is their uptake by various organisms, including humans, and

19 the subsequent particle translocation into tissues. The translocation of microplastic particles has been

20 suggested to occur via cellular internalization either para- or transcellulary. The transcellular pathway is more

21 likely to occur for particles in the micro-metre size range via macropinocytosis or phagocytosis.

22 Macropinocytosis is rather non-specific internalization mechanism, whereas phagocytosis is a precise

23 mechanism via ligand-receptor interaction. Since plastic is described as an inert material, a low particle-cell

24 interaction and internalization may occur, probably mainly driven by electrostatic forces. However,

25 microplastic particles that occur in the environment are coated with different biomolecules forming an eco-

26 corona on the particles' surface, which could consequently lead to a specific interaction of the constituents

27 of the eco-corona with membrane receptors. To date, it was not investigated how strong microplastic

28 particles with and without an eco-corona bind to cellular membranes and which underlying mechanisms are

29 responsible for cellular internalization. Therefore, using a microfluidic microscopy platform, we investigated

30 the adhesion strength of 3μm polystyrene microplastic particles to cellular membranes. We used microplastic

31 particles coated with an eco-corona derived from fresh- (FW) and salt water (SW) and compared those to

32 pristine microplastic particles (UW). Furthermore, we used functionalized microplastic particles with the

33 antibody immunoglobulin G (IgG) as an internal standard for high particle adhesion strengths and specific

34 phagocytosis internalization mechanism. We characterized the internalization mechanisms of the different

35 microplastic particles (IgG, FW, SW, UW) by inhibiting both phagocytosis and macropinocytosis (inhibitor:

36 Cytochalasin D and Amiloride) or phagocytosis (inhibitor: Amantadine). Additionally, we analyzed the

37 proteinaceous composition of two different eco-coronas (FW and SW) by liquid chromatography-mass

38 spectrometry/ mass spectrometry (LC-MS/MS) to unravel which proteinaceous components of the eco-

39 corona may contribute to the adhesion to cellular membranes and internalization mechanisms. We show

40 that the coating with an eco-corona significantly enhances the adhesion of the microplastic particles to

41 cellular membranes compared to pristine microplastic particles, irrespective of the origin of the eco-corona.

42 However, for the internalization mechanisms, we show that microplastic particles coated with an SW eco-

43 corona are mainly internalized via macropinocytosis, whereas the other particle types become internalized

44 via a combination of both the specific phagocytosis and non-specific macropinocytosis. Interestingly the

45 LC-MS/MS measurements revealed that the proteinaceous composition of the eco-coronas from FW and

46 SW are distinct, which could be one explanation for the different internalization mechanisms. Our results

47 help better understand how microplastic particles from the environment interact with cells and how the

48 particles may become internalized, leading to potentially adverse effects.

49

50 **Keywords:** Microplastic, eco-corona, microfluidics, cellular internalization, particle-cell-interactions, LC-

51 MS/MS

Introduction

Microplastic particles, synthetic polymeric particles smaller than 5mm (Arthur, Baker and Bamford, 2009), are ubiquitously found in all environmental compartments (Shahul Hamid *et al.*, 2018; MacLeod *et al.*, 2021). The overall abundance of microplastic particles comes along with the potential risk of particle uptake by organisms, including humans. To date, numerous studies describe the uptake of microplastic particles from various organisms, like zooplankton (Dris *et al.*, 2015; Imhof *et al.*, 2017), mussels (Browne *et al.*, 2008; Brehm *et al.*, 2022; Ritschar *et al.*, 2022) up to vertebrates (Puskic, Lavers and Bond, 2020). One risk that has been intensively discussed is the translocation of microplastic particles from the primarily exposed organs, like the gastrointestinal or respiratory tract, into other tissues (Wright and Kelly, 2017; Ramsperger *et al.*, 2023). In addition, an increasing number of studies show the presence of microplastic particles in tissue samples of different organisms, including humans (Dong *et al.*, 2023; Ramsperger *et al.*, 2023). However, to date, how microplastic particles can translocate through biological barriers is not understood.

The translocation of particulate matter through biological barriers was suggested via cellular internalization and subsequent particle transportation (Wright and Kelly, 2017; Ramsperger *et al.*, 2023). The plasma membrane is a cell's outer boundary, and the communication interface with its environment (Doherty and McMahon, 2009). Once a cell encounters foreign particulate matter in the micrometre-size range, a potential internalization can be subdivided into two steps. Within the first step, the surface of the particle interacts with the cell either by binding to cellular receptors (Aderem and Underhill, 1999; Rohrbach *et al.*, 2020) or by unspecific (e.g. electrostatic) interactions with the cell membrane (Forest, Cottier and Pourchez, 2015). Subsequently, the particle can be internalized by various mechanisms. Among these mechanisms for endocytosis, phagocytosis and macropinocytosis are the ones which are relevant for micron-sized particles since the other mechanisms are restricted to particles in the lower nanometre size range (Doherty and McMahon, 2009). Both phagocytosis and macropinocytosis are actin-dependent processes (Aderem and Underhill, 1999; Canton, 2018). Filamentous actin is part of the cytoskeleton and regulates cell shape changes during cell migration, proliferation and endocytic processes (Greenberg, Burridge and Silverstein, 1990; Schmidt and Hall, 1998; Stricker, Falzone and Gardel, 2010). Phagocytosis is initiated by the interaction of ligands on the surface of a particle with specific receptors on the cellular membrane (Aderem and Underhill, 1999). Through this direct interaction of a ligand with, for example, the Fc receptors, a tight-fitting sleeve around a particle is formed (Irmscher *et al.*, 2013), differentiating it from the more loosely attached membrane of a macropinosome (Kerr and Teasdale, 2009). Macropinocytosis can either be performed constitutively for nutrient acquisition in cells of the innate immune system (Swanson *et al.*, 1995; Canton, 2018) or can be induced via different growth factors. The process of macropinocytosis is defined as a global increase in actin polymerization at the cell surface and consequently forming membrane ruffles (Kerr and Teasdale, 2009). If a particle interacts with a cell membrane via electrostatic forces, it could therefore be internalized accidentally via the unspecific process of macropinocytosis.

In literature, there is rising evidence that microplastic particles can interact with cells and subsequently become internalized (e.g. Stock *et al.*, 2019, 2021; Ramsperger *et al.*, 2020, 2021). However, to date, whether

89 the internalization process occurs via phagocytosis or macropinocytosis is not understood. In a previous

90 study, we showed that pristine microplastic particles, described as inert materials, only occasionally interact

91 with cells of the innate immune system and become internalized (Ramsperger *et al.*, 2020), suggesting the

92 process of macropinocytosis. However, microplastic particles occurring in the environment we are exposed

93 to are not pristine but coated with biomolecules from their surrounding environment, forming an eco-

94 corona. An eco-corona can consist of biomolecules like amino acids, lipids or proteins (Galloway, Cole and

95 Lewis, 2017, Ramsperger et al., 2020), which coating changes their physico-chemical properties, making the

96 particles softer compared to pristine particles (Witzmann *et al.*, 2022). Furthermore, the coating with an eco-

97 corona leads to an enhanced number of particle-cell interactions and internalization, indicating that the

98 mechanisms of particle adhesion and subsequent internalization are different from pristine particles without

99 an eco-corona (Ramsperger *et al.*, 2020). However, to date, it was not investigated how pristine and

100 microplastic particles coated with an eco-corona interact with cellular membranes and whether there are

101 differences in the mechanism of internalization due to the biomolecules present in an eco-corona.

102 Therefore, using a microfluidic microscopy platform, we investigated the binding strength of microplastic

103 particles with and without eco-corona to cellular membranes. In order to assess which mechanisms are

104 responsible for the internalization of eco-corona-coated microplastic particles, we inhibited the most likely

105 occurring internalization mechanisms, namely phagocytosis and macropinocytosis and compared the

106 cellular internalization efficiency to untreated cells. Furthermore, we analyzed the components of the eco-

107 corona with liquid chromatography-mass spectrometry/mass spectrometry (LC-MS/MS) to understand

108 better the mechanisms of particle binding to cellular membranes and subsequent cellular internalization.

109 With our study, we aim to understand which components of an eco-corona may induce the binding of a

110 particle to cellular membranes, how strong this binding occurs and if an eco-corona influence the

111 internalization mechanism.

112

Materials & Methods

113

Cell line and cell culture conditions

114

115 Murine macrophage J774A.1 cells (DSMZ, Braunschweig, Germany) were cultured as described previously

116 (Ramsperger *et al.*, 2020; Berghoff *et al.*, 2021; Ramsperger *et al.*, 2021). In brief, cells were cultured in

117 Dulbecco's Modified Eagle's Medium (DMEM, Lonza Group Ltd, Basel, Switzerland), supplemented with

118 10 % v/v FCS (Sigma Aldrich, St. Louis, USA) and 100 U/mL penicillin/streptomycin (Lonza Group Ltd,

119 Basel, Switzerland) in T-25 culture flasks (CORNING, New York, USA) under standard cell culture

120 conditions (37 °C, 5 % CO2, humidified) and passaged three times per week. Before the experiments, the

121 cells were scraped off, centrifuged (200×g, 2 minutes) and resuspended with 5 mL cell culture media.

122

123

124   *Microplastic particles and pre-treatment conditions*

125   Plain, non-fluorescent, white monodisperse polystyrene spheres (microplastic particles) with a diameter of

126   3 µm (MICROMOD, Rostock, Germany, white particles, micromer® plain, Prod.-Nr.: 01-00-303) were

127   exposed to the corresponding environmental media as described in Ramsperger et al. (2020). In brief, the

128   microplastic particles were incubated for two weeks in fresh- or salt water or in ultrapure water (Veolia pure

129   lab flex, Veolia, Celle, Germany, and Milli-Q, MERCK MILLIPORE, Darmstadt, Germany). The

130   incubation in ultrapure water was carried out to provide pristine microplastic particles. 100 µL of

131   microplastic particle stock solution (50 mg mL^{-1}) was added to 900 µL of the corresponding water sample

132   (fresh-, salt or ultrapure water) in a glass vial (autosampler vials, 1.2 mL, neoLab, Heidelberg, Germany). To

133   ensure vital microbial communities, the corresponding fresh- or salt water samples were changed three times

134   per week by centrifugation (2000×g, 20 minutes, room temperature), and 900 µL of supernatant was

135   replaced by the same amount of new corresponding water samples. The same procedure was performed for

136   the ultrapure water treatment. Before adding the ultrapure water, it was filtered (Whatman Puradisc syringe

137   filter, 0.2 µm, GE Healthcare, Freiburg, Germany) under sterile conditions. To prevent aggregation of the

138   microplastic particles by sedimentation, all samples were placed on a shaker (100 rpm at room temperature).

139   Although we did not add surfactant to avoid aggregation of the microplastic particles, only occasionally

140   aggregates were found in all samples. For the positive control, IgG antibodies (native immunoglobulin G

141   primary antibodies from mouse serum; MERCK MILLIPORE, Darmstadt, Germany) were passively

142   adsorbed onto carboxylated microplastic particles (MICROMOD, Rostock, Germany, white particles,

143   micromer® COOH, Prod.-Nr.: 01-02-303) according to the protocol described by Keller et al.(2017).

144   Opsonization was verified by antibody-antibody labelling with goat anti-Mouse IgG cross-adsorbed

145   fluorescent secondary antibody (Dy-Light 488, THERMO SCIENTIFIC). Before adding the particles to

146   the cells, the concentration of all microplastic particle samples was determined using a haemocytometer

147   (Neubauer improved, Brand, Wertheim, Germany) to ensure comparable particle concentrations.

148   *Scanning electron microscopy*

149   As described above, cells were prepared on coverslips in 12-well plates the day before experiments. The

150   cells were counted using a haemocytometer (Neubauer improved, Brand, Wertheim, Germany), 100,000

151   cells per mL were seeded on microscope coverslips (diameter: 18 mm, #1, MENZEL GLAESER,

152   Braunschweig, Germany) in 12-well plates (CellStar, GREINER BIO-ONE, Frickenhausen, Germany) in

153   1 mL of cell culture medium and allowed to adhere onto the coverslips under standard cell culture conditions

154   (37 °C, 5 % CO2, humidified) overnight. On the following day, 10^6 microplastic particles (10 particles per

155   cell) of the corresponding treatment (fresh- or salt water) were added and left to settle for one hour in ice.

156   Afterwards, the cells were transferred to cell culture conditions for two hours to allow internalization.

157   Subsequently, the cells were fixed using Karnovsky's reagent (12 % v/v paraformaldehyde, 8 % v/v

158   glutaraldehyde in 0.1 M buffer) for 1 h at room temperature. Cells were washed three times with ultrapure

159   water and afterwards dehydrated using an ethanol series 30 % (3x 15min at 4°C), 50 % (3x 15min at 4°C),

160   70 % (3x 15min at -20°C) for 90 min (3x 15min at -20°C), absolute ethanol (3x 20min at -20°C) and

161   Hexamethyldisilazane (2x 10Min at room temperature) and let dry overnight in a desiccator. The air-dried

162   samples were sputtered with 2nm platinum and microscopy was performed using SEM (FEI Apreo

163   Volumescope, Thermo Fisher Scientific, magnification 5000-6500, 5 kV, Everhart-Thornley detector;

164   Figure 1&2).

165

166   *Microfluidic microscopy platform – Relative attachment of the particles to cellular membranes*

167   Custom-built perfusion chambers were used to quantify the adhesion strength between microplastic

168   particles and cells. A high precision linear stage (L511.20DG10, Physik Instrumente, Karlsruhe, Germany)

169   was used to drive the piston of a syringe (R = 6.135 mm) with a controlled motor velocity v_m. to control

170   the flow rate in the system, which is given as

$$Q = \pi R^2 v_m.$$

171   Flow chambers were built from a plastics top part (sticky-Slide I Luer, nominal channel height 0.1 mm,

172   nominal width 5 mm, nominal length 48 mm, ibidi GmbH, Gräfelfing, Germany), which was coupled to a

173   glass coverslip (24 mm x 60 mm, #1, Menzel Gläser, Thermo Fisher Scientific Inc., Waltham, MA) with a

174   thin film of epoxy resin one day before the experiments. The chambers used during the experiments had a

175   typical height in the range between 150 and 200μm. Thus, for every channel, the height profile was measured

176   independently before the. The perfusion chamber was connected to the syringe via a tubing system, in which

177   check valves (RVMINI-32, Piper Filter GmbH, Zwischenahn, Germany) were used to ensure the flow

178   direction stays the same after the motor reverses its direction. We assembled an extra tubing system for each

179   type of microplastic particle to avoid cross-contamination between the treatments. Into each flow chamber,

180   200μL of cell suspension was added and allowed to settle and attach to the bottom of the coverslip of the

181   flow chamber under standard culture conditions for 1h. All microfluidic experiments were performed in

182   imaging medium (Minimum Essential Medium, (Thermo Fisher Scientific Inc.) supplemented with 5 %

183   HEPES (Thermo Fisher Scientific Inc.) as a pH buffer and 1 % penicillin-streptomycin. The medium was

184   pre-warmed at 37 °C overnight to free it from dissolved gas and avoid bubble formation during the

185   experiments. The microparticles were added to the microfluidic system and were briefly dispersed in the

186   microfluidic system right before the first experiment.

187   Live cell imaging was performed on an inverted, motorized microscope (Nikon Eclipse Ti, Nikon, Tokyo,

188   Japan) with a 10x objective (CFI Plan Fluor DL 10x, Nikon, NA = 0.3), which was equipped with a CCD

189   camera (pco.pixelfly USB, PCO AG, Kehlheim, Germany). The microscope body was enclosed in a custom-

190   built incubation chamber, which kept the body of the microscope and the sample at a temperature of 37°C.

191   The stage motor and the camera were controlled with a custom-written MATLAB program (MATLAB

192   2019b, The MathWorks Inc, Natick, MA), which set the motor velocity according to the channel geometry

193   and the desired force exerted on the particles during the experiments.

194   Next, the channel with the cells was connected to the microfluidic system. With a low flow rate of 9 μL s⁻¹,

195   microplastic particles were flushed into the channel. Subsequently, the flow was turned off for 10 min to

196   allow the particles to sediment and attach to the cells. After the sedimentation phase, the flow was turned

197   on with a high flow rate, which induced a 50 pN hydrodynamic drag force on the particles attached to cells

198   and the coverslip. This rupture phase was continued for 30 s. During the measurement (sedimentation phase

199   and rupture phase), images were acquired with a frame rate of 1 fps and an exposure time of 10 ms.

200

201   *Confocal experiments – Inhibition of internalization mechanisms*

202   The cells were prepared as reported in Ramsperger et al. (2020), with slight modifications described in the

203   following: 50,000 cells per mL were seeded on microscope coverslips in 12-well plates in 1 mL of cell culture

204   medium. The cells were allowed to adhere onto the coverslips under standard cell culture conditions

205   overnight. To analyze the internalization mechanisms for microplastic particle cellular internalization the

206   cells were prepared the same way, with the cell culture medium replaced by cell culture medium containing

207   the respective inhibitor (Cytochalasin D, Amiloride or Amantadine). The concentrations of the inhibitors

208   were chosen as described in the literature (Garcia Gil and Sanchez Crespo, 1983; Koivusalo *et al.*, 2010;

209   Gould, Min and Day, 2011). Cytochalasin D was used to inhibit actin-dependent endocytosis in general

210   (2 μM, diluted in DMEM), Amiloride was described to inhibit macropinocytosis by preventing the process

211   of membrane ruffling (130 μM, diluted in DMEM) and Amantadine was used to inhibit receptor-mediated

212   endocytosis (100 μM, diluted in DMEM). However, Amiloride was described to not specifically inhibit

213   membrane ruffling, but the polymerization of actin filaments (Lagana *et al.*, 2000) and must therefore be

214   seen as an equivalent inhibitor to Cytochalasin D.

215   The cells treated with the corresponding inhibitor and the control cells without inhibitor were incubated for

216   30 min under cell culture conditions. Then, 150,000 microplastic particles pre-treated with fresh-, salt- or

217   ultrapure water or IgG-opsonized microplastic particles were added. The cells were placed on ice for one

218   hour to reduce cellular activity during the particle sedimentation. Three coverslips for each microplastic

219   particle treatment and inhibitor/control treatment combination were prepared, yielding a total of 48

220   coverslips. After one hour of microplastic particle sedimentation, the well plates were incubated under cell

221   culture conditions for two hours to allow cellular internalization of the particles. Then, the cells were fixed

222   with 4 % PFA (SIGMA-ALDRICH, St. Louis, Missouri) for 20 min on ice and subsequently labelled with

223   Alexa Fluor Phalloidin 488 (Invitrogen, Carlsbad, USA) and dilution buffer, consisting of 98.7 % PBS,

224   including 0.3 % Triton and 1 % bovine serum albumin (BSA, APPLICHEM, Darmstadt, Germany) to a

225   final concentration of 1: 25 for 25 min.

226

227   *Quantification of particle-cell-interactions*

228   The procedure was adapted from Ramsperger et al. (2020). To determine the total number of particle-cell-

229   interactions on each coverslip, five randomly chosen region of interest (ROIs, 0.10 mm^2) were selected and

230   imaged by using a DMI 6000 microscope (LEICA, Wetzlar, Germany, HCX PL APO 63 ×/1.30 oil

231   objective) including a spinning disc unit (CSU-X1, YOKOGAWA, Musashino, Japan) with an EMCCD

232   camera (Evolve 512, PHOTOMETRICS, Tucson, Arizona, including an additional 1.2× magnification

233   lens). A differential interference contrast (DIC) microscopy image was acquired to quantify the particle-cell-

234   interactions within the ROIs using the Fiji ImageJ cell counter software. Additionally, confocal stacks of

235   fluorescently labelled cells were acquired using a 488 nm laser (50 mW, Sapphire 488, COHERENT, Santa

236   Clara, California) at a spinning disc speed of 5000 rpm to excite fluorescence. Axial stacks of the cells were

237   acquired with a vertical distance of 0.2 μm, which is sufficient to oversample the image given the axial

238   resolution of the microscope (Jonkman *et al.*, 2003). The confocal stacks were used to calculate the area

239   covered by cells within an ROI. The area covered by cells was detected using both the DIC and the

240   fluorescence channel simultaneously to obtain robust results.

241   *Quantification of internalized microplastic particles*

242   From the same samples used to quantify the number of particle-cell-interactions and the areas covered with

243   cells on coverslips, we visually screened each sample for single particle-cell-interactions to distinguish

244   between particles that were only attached to cells and particles that were completely internalized. The same

245   DMI 6000 microscope, including a spinning disc unit with a higher magnification (100×/1.40 oil objective),

246   was used. Beginning from a randomly defined starting point, the coverslips were screened in the DIC-

247   channel until 100 to 110 particle-cell-interactions were detected, or the whole coverslip was screened

248   entirely. Once a particle-cell-interaction was found, a DIC-image was taken, and axial stacks of fluorescently

249   labelled cells were acquired (vertical distance of the axial stacks: 0.2 μm). To evaluate the internalization of

250   the microplastic particles, each confocal stack of cells with labelled actin filaments was analyzed with Fiji

251   ImageJ (version: 2.0.0-rc-54/1.51h 2016-09-08) orthogonal views. The microplastic particles used in the

252   experiments were not fluorescent and were not directly visible in the confocal stacks. DIC images were used

253   to mark the particle positions (using the ROI manager in Fiji ImageJ). These positions were then transferred

254   to the confocal stacks, in which internalized particles were visible as spherical black regions within the actin

255   network. Only microplastic particles that were entirely surrounded by actin filaments were considered to be

256   internalized. Microplastic particles that were only partly surrounded were considered to be attached to cell

257   membranes (Figure 1).

258
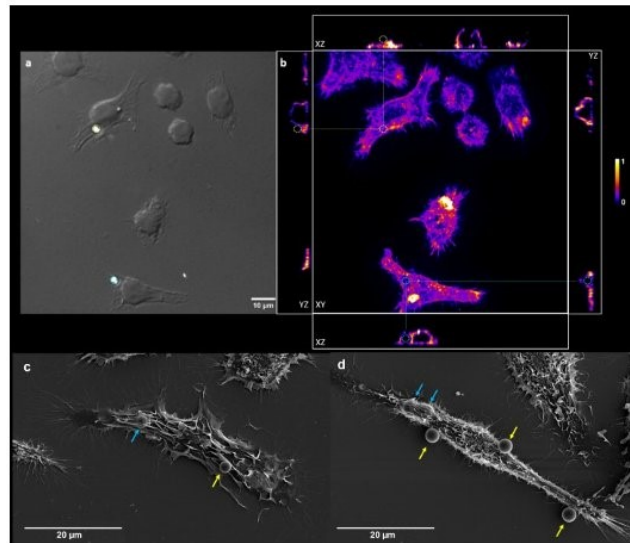
Figure 1: Illustration of the differentiation in particle-cell-interactions (PCIs) and attached or internalized microplastic particles. (a) Example of J77A.1 murine macrophage cells without internalization inhibitor and microplastic particles incubated in SW. The DIC images were used to localize microplastic particles within the DIC images (a) and within the confocal z-stacks (b). The filamentous actin was fluorescently labelled and orthogonal views (XZ and YZ) allowed the differentiation between microplastic particles that are attached (yellow circle) to the cells and microplastic particles that are internalized (blue circle) microplastic particles. Internalized particles are completely surrounded by filamentous actin. (c,d) Scanning electron microscopy images of J774A.1 murine macrophages incubated with 3μm sized microplastic particles coated with an ecocorona from FW (c) and SW (d). Yellow arrows indicate particles that are only attached to cells and blue arrows indicate internalized microplastic particles; scale bar: 20μm.

Combination and standardization of the results

The number of particle-cell-interactions was extrapolated to a whole coverslip (245.50 mm²). As the areas on the coverslips covered by cells differ slightly between replicates and treatment-inhibitor-combinations each coverslip was standardized as described in Ramsperger et al. (2020).

Statistical Analysis

Statistical analysis was conducted using R studio software (Version 1.0.143). The data for the relative attachment, particle-cell-interactions, and internalized microplastic particles were tested for normal distribution (Shapiro-Wilk test) and homogeneity of variances (Levene test). For the relative attachment, the assumptions for an ANOVA with a Tukey post-hoc test were met, whereas for the particle-cell-interactions and number of internalized particles, a Kruskal-Wallis test with a Games Howell post hoc test (p-adjust method for multiple nesting: Bonferroni Holm) was conducted.

285   *Eco-corona analysis – Proteome and LC-MS/MS*

286   For proteome analysis, 500μl of incubated microplastic particles were centrifuged for 15 min (4°C, 500 rcf).

287   Supernatant was removed and 50 μl of 2 x Laemmli buffer (0.25 M Tris-HCL; pH 6.8, 40 % (v/v) Glycerol,

288   8 % (v/v) SDS, 0.4 % (v/v) 1 % bromphenol blue) were added to the particles, vortexed shortly, incubated

289   at 95°C (5 min) and centrifuged for 5 min (20,000 rcf). Samples were then transferred onto a NuPAGE 4-

290   12% Bis-Tris Gel (Invitrogen, USA). Gels were run for 4 min at 200 V. Gels were stained overnight using

291   Roti Blue staining solution (Roth, Germany). Protein-containing areas were excised, destained and washed

292   with 50mM NH_4HCO_3. Supernatant was discarded, samples were reduced with 45 mM DTE (30 min, 55°C)

293   and subsequently alkylated with 100 mM iodoacetamide in the dark at room temperature. Gel pieces were

294   washed and a sequential in-gel digestion was performed. First with Lys-C (4 h, 37 °C, Lysyl Endopeptidase,

295   Mass Spectrometry Grade (FUJIFILM Wako Pure Chemical Corporation, USA)) followed by trypsin (17 h,

296   37 °C, 200 ng trypsin (sequencing grade modified trypsin, Promega, Germany)). Supernatants were

297   collected, and peptides were extracted using 70% acetonitrile (ACN). Collected supernatants were pooled

298   and dried using a vacuum centrifuge (Vacuum concentrator, Bachofer, Germany).

299   Samples were dissolved in 15 μl solvent A (0.1% formic acid), loaded on a trap column (PEP-Map100 C18,

300   75μm x 2cm, 3 μm particles (Thermo Fisher Scientific, U.S.A)) and separated on a reversed-phase column

301   (PepMap RSLC C18, 75 μm × 50 cm, 2 μm particles, Thermo Scientific, U.S.A) at a flow rate of 250 nl/min

302   with a 30-min gradient of 3-25% solvent B followed by 5-min increase to 40%. Solvent B consisted of 0.1 %

303   formic acid in ACN. After separation, the column was washed with 85% solvent B for 10-min. MS/MS

304   analysis was performed with a Q Exactive HF-X mass spectrometer (Thermo Scientific, U.S.A). The data-

305   dependent acquisition method consisted of cycles of one MS scan with a mass range of m/z 300-1600 at a

306   resolution of 60000, followed by a maximum of 15 MS/MS scans at a resolution of 15000.

307   Spectra were searched with MASCOT V2.6.2 (Matrix Science Limited, UK) (Perkins et al., 1999). The

308   MS/MS data was searched against two different databases. In one case we used a bacteria subset of the

309   NCBIprot database (updated: Nov 2020), in the other a compiled algae database downloaded from NCBI

310   (March 2022). In both cases an additional common contaminant database (from MaxQuant) was used.

311   Identified proteins were filtered for and FDR < 1% and a minimum number of 2 peptides. An emPAI

312   quantification (Ishihama et al., 2005) was done in Scaffold (version Scaffold_4.10.0, Proteome Software

313   Inc., Portland, USA) and only proteins with a protein identification rate higher than 95% were further

314   analyzed. The mass spectrometry proteomics data have been deposited to the ProteomeXchange

315   Consortium (http://proteomecentral.proteomexchange.org) via the PRIDE partner repository (Perez-

316   Riverol et al., 2019).

317   For protein quantity estimations, all peaks in the total ion chromatogram (TIC) were integrated and areas

318   calculated using the Excalibur Qual Browser (Thermo Fisher Scientific, U.S.A). Total areas were corrected

319   by subtracting the peak areas of a blank run without sample. The ratios between protein amounts from the

320   IgG preparation and the samples were calculated.

321 **Results**

322 <u>Particle-cell adhesion strength, particle-cell-interactions and particle internalization</u>

323 To understand the first interaction of microplastic particles with cellular membranes we treated the cells for
324 10 min with the particles and used a microfluidic device to define the adhesion of the particles to cells.
325 Furthermore, we investigated the number of particle-cell interactions and subsequent internalization within
326 two hour incubation.

327 Our results show that microplastic particles that were incubated in either FW or SW were coated with an
328 eco-corona (Figure 2) leading to a significantly increased cell adhesion, particle-cell interaction and number
329 of internalized particles by cells ($p < 0.001$).
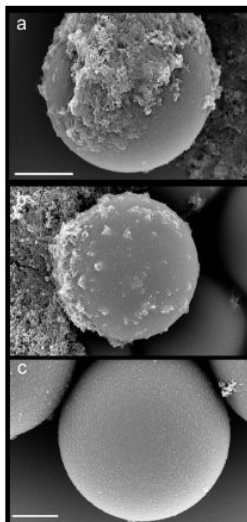
330

331 **Figure 2: Scanning electron microscopy images of 3 μm sized microplastic particles with different**
332 **treatments.** Microplastic particles coated with an eco-corona due to FW (a) or SW incubation (b) and
333 particles without an eco-corona due to incubation in UW (c). Both particles coated with an eco-corona show
334 deposits on the initially smooth surface; scale bar: 1μm.

335 The cell adhesion, particle-cell interaction and number of internalized functionalized particles coated with
336 immunoglobulin G (IgG) was significantly higher compared to the eco-corona coated particles and their
337 pristine counterparts ($p < 0.001$; Figure 3 & 4). Although there was a slightly higher adhesion of microplastic
338 particles coated with an eco-corona from FW (rel. attachment: 0.41 ±0.05) compared to SW (rel. attachment:
339 0.36 ±0.03), there was no significant difference ($p > 0.05$) between the adhesion of particles coated with the
340 different eco-coronas after 10 min treatment.

341
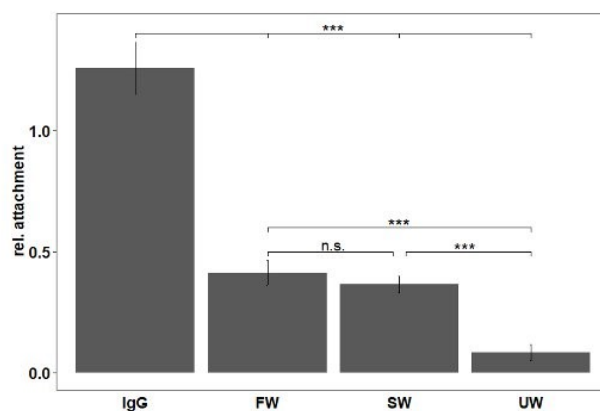
Figure 3: Adhesion of microplastic particles to cells. Shown is the percentage of particles (rel. attachment) that remain attached to untreated cells after experiencing a microfluidic shear force of 50 pN for 30 s. IgG = microplastic particles opsonized with immunoglobulin G (positive control), FW = microplastic particles incubated for two weeks in freshwater, SW = microplastic particles incubated for two weeks in saltwater and UW = microplastic particles incubated for two weeks in ultrapure water (*** = p ≤ 0.001;numbers indicate means ± se).

However, the number of particle-cell interactions and internalized microplastic particles differed significantly between FW and SW (p < 0.001). Our results give first insights that the initial adhesion between a cell and a particle (within less than 10min) is probably mainly driven by the particles physical properties such as coatings and roughness, whereas the particle-cell interaction and the subsequent internalization is driven by the biological identity of the particles' surface.

354
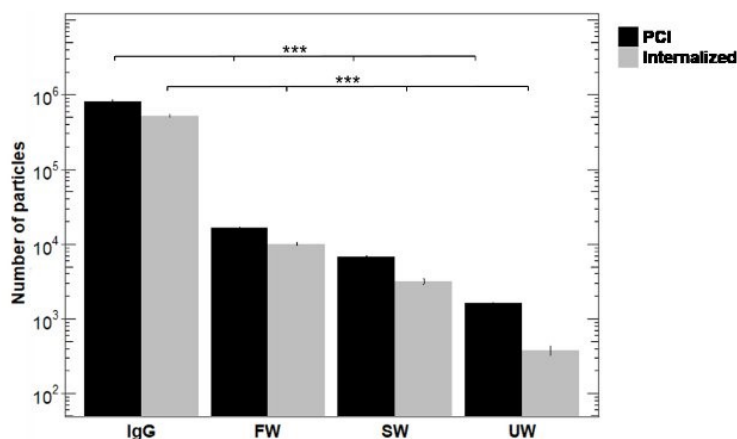
Figure 4: Number of particle-cell-interactions (PCI) and number of internalized microplastic particles for untreated cells (cells without internalization inhibitors)internalization. IgG = microplastic particles opsonized with immunoglobulin G (positive control), FW = microplastic particles incubated for two weeks in freshwater, SW = microplastic particles incubated for two weeks in saltwater and UW = microplastic particles incubated for two weeks in ultrapure water (no ecocorona, negative control). Since the data spans more than three orders of magnitude, the ordinate is scaled logarithmically. Each microplastic particle type differs highly significant in PCIs and number of internalized particles from the other particle types (*** = p ≤ 0.001, numbers indicate means ± se).

364   Internalization mechanisms

365   To better understand how particles coated with an eco-corona become internalized by cells, we inhibited

366   the most common internalization mechanisms involved for the used size class of particles. We inhibited all

367   actin-dependent endocytosis mechanisms using Cytochalasin D and Amiloride and receptor-mediated

368   internalization mechanisms by using Amantadine. Cytochalasin D, as well as Amiloride, significantly

369   ($p < 0.001$) inhibited the internalization for all particle types compared to their corresponding control

370   (Figure 5). The treatment with Amantadine to inhibit receptor-mediated endocytosis was not sufficient to

371   inhibit the internalization of particles coated with an eco-corona from SW, but significantly (IgG/FW:

372    $p < 0.001$; UW: $p < 0.01$) inhibited the internalization of all other particle types compared to the

373   corresponding controls.
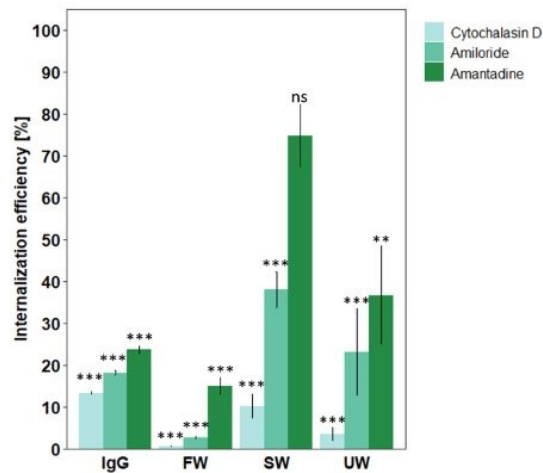
374

375   **Figure 5: Internalization efficiency after drug treatment compared to control (100% = control).** For
376   each particle type a corresponding control without inhibiting the internalization mechanisms was conducted.
377   IgG = microplastic particles opsonized with immunoglobulin G (positive control), FW = microplastic
378   particles incubated for two weeks in freshwater, SW = microplastic particles incubated for two weeks in
379   saltwater and UW = microplastic particles incubated for two weeks in ultrapure water (no ecocorona,
380   negative control). Cytochalasin D and Amiloride significantly inhibited the internalization for all
381   microplastic particle types compared to their corresponding controls (*** = $p \leq 0.001$). Amantadine
382   significantly inhibited the internalization of IgG, FW (*** = $p \leq 0.001$) and UW (** = $p \leq 0.01$) but not for
383   microplastic particles incubated in saltwater (ns= $p > 0.05$, all numbers indicate means ± se).

384

385   Eco-corona analysis

386   Since we found differences in the internalization mechanisms of particles coated with eco-coronas of

387   different origins, we further characterized the eco-corona with scanning electron microscopy (SEM) and

388   LC-MS/MS. The SEM images clearly show that particles coated with an eco-corona have deposits on their

389   surface compared to the very smooth surface of the particles without an eco-corona (Fig. 2). Since SEM

390   does not allow in-depth characterization of the composition of an eco-corona, we used LC-MS/MS to

391   unravel potentially different protein compositions within the eco-coronas. Overall, the protein content in

392   both FW and SW derived eco-coronas, were comparably low to the particles opsonized with a homogenous

393   coating of IgG, which was on average 2.8 times higher. However, the composition of proteins in FW or SW

394   eco-coronas was distinct from each other. After excluding the overall contamination found on the particles

395   without an eco-corona, none of the proteins found in an FW derived eco-corona were present in an SW

396   eco-corona and *vice versa*.

397   Common contaminants, such as human keratin, were detected in all sample types. This is not surprising

398   since this type of contaminants are typically detected by highly sensitive LC-MS/MS analysis in all types of

399   plastic ware (Frankenfield *et al.*, 2022). Furthermore we identified the bacterial protein "chaperonin GroEL",

400   from different bacterial taxa, in all sample types (FW, SW and UW). Interestingly, in FW and UW, GroEL

401   from the genus Ralstonia was identified. Ralstonia is known to be a common contaminant in laboratory kits

402   or reagents (e.g. DNA extraction kits) (Salter *et al.*, 2014), and therefore can be excluded to originate from

403   the eco-corona. Besides peptides of contaminants also peptides from bacteria and algae were unambiguously

404   identified. Strikingly, the most proteins were identified in the SW incubated samples (71 unique peptides for

405   bacteria, 28 unique peptides for algae) which could be assigned to 19 bacterial proteins and 13 algae proteins,

406   respectively. From the algae database, nearly all identified proteins were annotated as "unnamed protein

407   product" and not to specific protein classes, characteristic for these types of organisms. Furthermore, we

408   identified several proteins for the genus Marivita in the SW samples. The genus Marivita belongs to the

409   Roseobacter clade (within the Rhodobacteraceae family), which represent some of the most abundant

410   organisms in the oceanic environment and is also known to play key roles in many marine biochemical

411   processes (R. Budinoff *et al.*, 2011; Pujalte *et al.*, 2014; Bentzon-Tilia and Gram, 2017). However, due to the

412   fact that the databases, which are needed to identify proteins from MS/MS experiments, lack sequences

413   from the broad majority of FW and SW microorganisms, an in-depth analysis including the identification

414   of further peptides/proteins and the assignment of proper taxa is error prone and, in this case, not

415   expedient.

416

Discussion

417

418   Here we show that microplastic particles coated with an eco-corona have a stronger adhesion to cells, a

419   higher number of particle-cell interactions, and subsequently become more often internalized than particles

420   without an eco-corona in agreement with our previous observations (Ramsperger *et al.*, 2020). Furthermore,

421   by analyzing the proteinaceous components of an eco-corona and inhibiting the most common

422   internalization mechanisms for 3 μm sized particles, we shed some light on the underlying mechanisms of

423   the interactions of cells with microplastic particles coated with an eco-corona.

424   When a particle encounters a cell, it can bind to the cellular membrane. This binding can depend on the

425   biological identity of a particle initiating receptor-mediated interactions and the physico-chemical properties

426   of a particle initiating the interaction via electrostatic forces (Forest, Cottier and Pourchez, 2015; Ramsperger

427   *et al.*, 2021). The physico-chemical properties of particles determine not only their interaction with cells but

428   also their interaction with the surrounding environment in general. Only the environment, namely FW and

429   SW, differs between treatments in our experimental eco-corona setup. Our LC-MS/MS results show that

430   the proteinaceous composition of the eco-corona on particles incubated either in FW or SW is distinct from

431   each other. However, the most prominent kinds of proteins found in both eco-coronas are associated with

432   prokaryotic cellular membranes. Macrophages represent the forefront of the innate immune defence against

433   foreign particulate matter such as bacterial invaders (Weiss and Schaible, 2015). Therefore, we conclude that

434   the bacterial membrane-associated proteins are one driver for the enhanced relative attachment of particles

435   to macrophages, the higher number of particle-cell-interactions and subsequently, the higher number of

436   internalized particles coated with an eco-corona.

437   An eco-corona could change the biological properties of a microplastic particle in such a way that some

438   proteins of the eco-corona may expose ligands that can be recognized by membrane receptors facilitating

439   particle internalization (Forest, Cottier and Pourchez, 2015). However, many membrane receptors have dual

440   functions like the mediation of the particle attachment as well as the particle internalization. Those adhesion

441   and internalization receptors can also activate and inhibit each other's functions (Aderem and Underhill,

442   1999). Therefore, the proteinaceous components of the eco-corona can alter the particles' adhesion to cells

443   and their internalization. We show that microplastic particles coated with an eco-corona derived from SW

444   most likely become internalized accidentally via macropinocytosis, not phagocytosis. Particulate

445   internalization via macropinocytosis is not initiated by the direct interaction of ligands on the particle surface

446   with cell membrane receptors but rather randomly (Kerr and Teasdale, 2009; Mylvaganam, Freeman and

447   Grinstein, 2021). Cells of the innate immune system constitutively perform membrane ruffling (Swanson *et*

448   *al.*, 1995; Canton, 2018), making the internalization of microplastic particles adhering to cellular membranes

449   via electrostatic forces more likely. Furthermore, growth factors increase membrane ruffling and,

450   consequently, macropinocytosis (Swanson *et al.*, 1995). Therefore, we cannot exclude that growth factors

451   are present in the eco-corona from SW, initiating increased membrane ruffling and, therefore, higher

452   internalization compared to pristine particles.

453   Another explanation that microplastic particles coated with an eco-corona from SW seem to mainly become

454   internalized via macropinocytosis is the presence of salts within the eco-corona (Ramsperger *et al.*, 2020).

455   The salt concentration in the salt water incubation media is 3.5%; therefore, salts may also be present in the

456   eco-corona. Interestingly extracellular calcium can drive constitutive macropinocytosis in human monocyte-

457   derived macrophages (Canton, 2018). Calcium is the fifth most abundant salt in our incubation medium

458   (460mg/L), suggesting that calcium is also present in the eco-corona, initiating the process of membrane

459   ruffling. Thus, macropinocytosis might be the main internalization pathway for microplastic particles coated

460   with an eco-corona from SW. For the other particle types, the internalization process is most probably a

461   combination of both mechanisms, receptor-mediated endocytosis and macropinocytosis.

462   Particles opsonized with IgG highly specifically bind to the Fcγ-receptors, and therefore, the main

463   internalization pathway for particles opsonized with IgG is receptor-mediated phagocytosis (Nimmerjahn

464   and Ravetch, 2008). The strong binding of IgG to Fcγ-receptors is also shown by the strong adhesion

465   between the IgG-coated particles and cells (relative attachment > 1). In principle, the relative attachment
466   should not exceed the value of 1.0. However, we assume that IgG-coated particles that were not attached
467   to cells were attached after flushing, indicating that non-attached IgG particles got washed onto cells and
468   immediately attached to cellular membranes due to their high reactivity with membrane receptors. In our
469   microfluidic microscopy platform, the incubation times are < 10min to exclude the possibility of particle
470   internalization and focus on the initial interaction of a particle with the cellular membrane. The particle-cell-
471   interaction, on the other hand, give a broad overview of how often an interaction occurs and how many
472   particles of these interactions were consequently internalized within 2 hours. However, since
473   macropinocytosis is constitutive in macrophages, this may explain the combination of both mechanisms,
474   macropinocytosis and phagocytosis, not only for the particles with an eco-corona from FW or particles
475   without an eco-corona but also for particles opsonized with IgG.

476   Furthermore, not only the combination of both mechanisms may explain our results but also the type of
477   inhibitors used. For instance, Amiloride was described in several studies to effectively inhibit
478   macropinocytosis (Kerr and Teasdale, 2009; Gould, Min and Day, 2011; Dutta and Donaldson, 2012;
479   Bannunah *et al.*, 2014). Amiloride impairs the Na+/H+ exchange resulting in a dysregulation of the
480   submembranous pH. However, Canton (2018) highlighted that this effect is not specific to
481   macropinocytosis and is only marginally sensitive to the constitutive form of macropinocytosis.
482   Furthermore, other effects not related to the inhibition of macropinocytosis can be involved (Gould, Min
483   and Day, 2011), such as the inhibition of actin polymerization (Lagana *et al.*, 2000). Therefore, our results
484   further highlight that Amiloride cannot serve as a specific inhibitor for macropinocytosis.

485   Microplastic particles without an eco-corona only very occasionally bound to cellular membranes or became
486   internalized. However, the small number of particles interacting with cells and becoming internalized may
487   occur for different reasons. The LC-MS/MS analysis depicted slight proteinaceous contaminats in all
488   incubated particle types, especially from *Ralstonia* bacteria. Proteins from this order were described as
489   common contamination in LC-MS/MS analysis (Salter *et al.*, 2014). Therefore, the proteins detected on the
490   particles without an eco-corona originating from contamination may already be sufficient to cause weak
491   adhesion and a small number of internalizations. Furthermore, although the particles were added to the
492   experimental setup in a pristine form without an eco-corona, proteins and other biomolecules from the
493   surrounding cell media can adsorb to the surface of the particles (Lundqvist *et al.*, 2011) without an eco-
494   corona explaining the small number of interactions, which is highly significantly smaller than for both
495   particle types coated with an eco-corona. This, even more, highlights that the coating with an eco-corona
496   effectively enhances their adhesion to cells, the number of particle-cell-interactions and subsequent
497   internalization.

498

499   **Conclusion**

500   Our results show that microplastic particles coated with an eco-corona significantly stronger adhere to cell

501   membranes than microplastic particles without an eco-corona. Furthermore, the eco-corona enhances the

502   number of particle-cell interactions and the number of internalized particles, which agrees with our previous

503   observation (Ramsperger *et al.*, 2020). To understand better the process of particle internalization, we

504   inhibited the internalization mechanisms, macropinocytosis and phagocytosis. We found that particles

505   coated with an eco-corona from SW mainly become internalized via macropinocytosis, whereas the other

506   particle types seem to be internalized via both mechanisms. LC-MS/MS measurements unravelled that the

507   compositions of the two different eco-coronas, FW and SW, are distinct from each other, which might

508   explain their differences in cellular internalization mechanisms. Our results help to understand better which

509   properties of environmentally exposed microplastic particles lead to cellular internalization, which is one

510   major pathway of microplastic particle translocation into tissues.

511

512

523   **Author contributions:**

524   AFRMR, CL and HK initiated the research

525   All authors planned the research

526   AFRMR and SW performed the microplastic particle incubation experiments

527   AFRMR and SW prepared the SEM samples and SW imaged the SEM samples

528   AFRMR performed the cell experiments regarding particle-cell interactions, internalization and
529   inhibition of internalization mechanisms

530   SW performed the particle adhesion experiments

531   LVW performed LC-MS/MS experiments and data evaluation

532   AFRMR, SW and LVW wrote the first draft of the manuscript

533   AFRMR, SW, LVW, TF, HK and CL reviewed and edited the manuscript

534   **Competing interests:** Authors declare that they have no competing interests

535   **Data availability:** All data and materials used in the analysis are available from the corresponding authors

536   upon request.

537   Literature:

538   Aderem, A and Underhill, D. M. (1999) 'Mechanisms of phagocytosis in macrophages.', *Annual review of*

539   *immunology*, 17, pp. 593–623. doi: 10.1146/annurev.immunol.17.1.593.

540   Arthur, C., Baker, J. and Bamford, H. (2009) 'Proceedings of the International Research Workshop on the

541   Occurrence , Effects , and Fate of Microplastic Marine Debris', *Group*, (January), p. 530.

542   Bannunah, A. M. *et al.* (2014) 'Mechanisms of nanoparticle internalization and transport across an

543   intestinal epithelial cell model: Effect of size and surface charge', *Molecular Pharmaceutics*, 11(12), pp. 4363–

544   4373. doi: 10.1021/mp500439c.

545   Bentzon-Tilia, M. and Gram, L. (2017) 'Biotechnological Applications of the Roseobacter Clade BT -

546   Bioprospecting: Success, Potential and Constraints', in Paterson, R. and Lima, N. (eds). Cham: Springer

547   International Publishing, pp. 137–166. doi: 10.1007/978-3-319-47935-4_7.

548   Berghoff, K. *et al.* (2021) 'Using blinking optical tweezers to study cell rheology during initial cell-particle

549   contact', *Biophysical Journal*, 120(16), pp. 3527–3537. doi: 10.1016/j.bpj.2021.04.034.

550   Brehm, J. *et al.* (2022) 'In-depth characterization revealed polymer type and chemical content specific

551   effects of microplastic on Dreissena bugensis', *Journal of Hazardous Materials*, 437(March). doi:

552   10.1016/j.jhazmat.2022.129351.

553   Browne, M. a. *et al.* (2008) 'Ingested microscopic plastic translocates to the circulatory system of the

554   mussel, Mytilus edulis (L.)', *Environmental Science and Technology*, 42(13), pp. 5026–5031. doi:

555   10.1021/es800249a.

556   Canton, J. (2018) 'Macropinocytosis: New insights into its underappreciated role in innate immune cell

557   surveillance', *Frontiers in Immunology*, 9(OCT), pp. 1–8. doi: 10.3389/fimmu.2018.02286.

558   Doherty, G. J. and McMahon, H. T. (2009) 'Mechanisms of Endocytosis', *Annual Review of Biochemistry*,

559   78(1), pp. 857–902. doi: 10.1146/annurev.biochem.78.081307.110540.

560   Dong, X. *et al.* (2023) 'From natural environment to animal tissues: A review of

561   microplastics(nanoplastics) translocation and hazards studies', *Science of The Total Environment*, 855, p.

562   158686. doi: https://doi.org/10.1016/j.scitotenv.2022.158686.

563   Dris, R. *et al.* (2015) 'Beyond the ocean : Contamination of freshwater ecosystems with (micro-) plastic

564   particles', *Environmental Chemistry*, (MARCH), p. A-L. doi: 10.1071/EN14172.

565   Dutta, D. and Donaldson, J. G. (2012) 'Intended specificity and unintended consequences.', *Cellular*

566   *Logistics*, 2(4), pp. 203–208.

567   Forest, V., Cottier, M. and Pourchez, J. (2015) 'Electrostatic interactions favor the binding of positive

568   nanoparticles on cells: A reductive theory', *Nano Today*, 10(6), pp. 677–680. doi:

569   10.1016/j.nantod.2015.07.002.

570   Frankenfield, A. M. *et al.* (2022) 'Protein Contaminants Matter: Building Universal Protein Contaminant
571   Libraries for DDA and DIA Proteomics', *Journal of Proteome Research*, 21(9), pp. 2104–2113. doi:
572   10.1021/acs.jproteome.2c00145.

573   Galloway, T. S., Cole, M. and Lewis, C. (2017) 'Interactions of microplastic debris throughout the marine
574   ecosystem', *Nature Ecology & Evolution*, 1(5), p. 0116. doi: 10.1038/s41559-017-0116.

575   Garcia Gil, M. and Sanchez Crespo, M. (1983) 'Dansylcadaverine and rimantadine inhibition of
576   phagocytosis, PAF-acether release, and phosphatidylcholine synthesis in human polymorphonuclear
577   leukocytes', *Immunopharmacology*, 6(4), pp. 317–325. doi: 10.1016/0162-3109(83)90037-1.

578   Gould, N. S., Min, E. and Day, B. J. (2011) 'Macropinocytosis of extracellular glutathione ameliorates
579   tumor necrosis factor α release in activated macrophages', *PLoS ONE*, 6(10). doi:
580   10.1371/journal.pone.0025704.

581   Greenberg, S., Burridge, K. and Silverstein, S. C. (1990) 'Colocalization of F-actin and talin during Fc
582   receptor-mediated phagocytosis in mouse macrophages.', *The Journal of experimental medicine*, 172(6), pp.
583   1853–1856. doi: 10.1084/jem.172.6.1853.

584   Imhof, H. K. *et al.* (2017) 'Do microplastic particles affect Daphnia magna at the morphological , life
585   history and molecular level ?', pp. 1–20. doi: 10.5061/dryad.9d84j.

586   Irmscher, M. *et al.* (2013) 'A method for time-resolved measurements of the mechanics of phagocytic
587   cups.', *Journal of the Royal Society, Interface / the Royal Society*, 10(82), p. 20121048. doi: 10.1098/rsif.2012.1048.

588   Jonkman, J. E. N. *et al.* (2003) 'Resolution in optical microscopy', *Methods in Enzymology*, 360, pp. 416–446.
589   doi: 10.1016/S0076-6879(03)60122-9.

590   Keller, S., Berghoff, K. and Kress, H. (2017) 'Phagosomal transport depends strongly on phagosome size',
591   *Scientific Reports*, 7(1), pp. 1–15. doi: 10.1038/s41598-017-17183-7.

592   Kerr, M. C. and Teasdale, R. D. (2009) 'Defining macropinocytosis', *Traffic*, 10(4), pp. 364–371. doi:
593   10.1111/j.1600-0854.2009.00878.x.

594   Koivusalo, M. *et al.* (2010) 'Amiloride inhibits macropinocytosis by lowering submembranous pH and
595   preventing Rac1 and Cdc42 signaling', *Journal of Cell Biology*, 188(4), pp. 547–563. doi:
596   10.1083/jcb.200908086.

597   Lagana, A. *et al.* (2000) 'Regulation of the formation of tumor cell pseudopodia by the Na+/H+
598   exchanger NHE1', *Journal of Cell Science*, 113(20), pp. 3649–3662.

599   Lundqvist, M. *et al.* (2011) 'The evolution of the protein corona around nanoparticles: A test study', *ACS
600   Nano*, 5(9), pp. 7503–7509. doi: 10.1021/nn202458g.

601   MacLeod, M. *et al.* (2021) 'The global threat from plastic pollution', *Science*, 373(6550), pp. 61–65. doi:
602   10.1126/science.abg5433.

603   Mylvaganam, S., Freeman, S. A. and Grinstein, S. (2021) 'The cytoskeleton in phagocytosis and
604   macropinocytosis', *Current Biology*, 31(10), pp. R619–R632. doi: 10.1016/j.cub.2021.01.036.

605   Nimmerjahn, F. and Ravetch, J. V. (2008) 'Fcγ receptors as regulators of immune responses', *Nature*
606   *Reviews Immunology*, 8(1), pp. 34–47. doi: 10.1038/nri2206.

607   Pujalte, M. J. *et al.* (2014) 'The Family Rhodobacteraceae BT - The Prokaryotes: Alphaproteobacteria and
608   Betaproteobacteria', in Rosenberg, E. et al. (eds). Berlin, Heidelberg: Springer Berlin Heidelberg, pp. 439–
609   512. doi: 10.1007/978-3-642-30197-1_377.

610   Puskic, P. S., Lavers, J. L. and Bond, A. L. (2020) 'A critical review of harm associated with plastic
611   ingestion on vertebrates', *Science of the Total Environment*, 743(October 2021). doi:
612   10.1016/j.scitotenv.2020.140666.

613   R. Budinoff, C. *et al.* (2011) '<I>Marivita roseacus </I>sp. nov., of the family
614   <I>Rhodobacteraceae</I>, isolated from a temperate estuary and an emended description of the genus
615   <I>Marivita</I>', *The Journal of General and Applied Microbiology*, 57(5), pp. 259–267. doi:
616   10.2323/jgam.57.259.

617   Ramsperger, A. F. R. M. *et al.* (2020) 'Environmental exposure enhances the internalization of microplastic
618   particles into cells', *Science Advances*, 6(50), pp. 1–10. doi: 10.1126/sciadv.abd1211.

619   Ramsperger, A. F. R. M. *et al.* (2021) 'Supposedly identical microplastic particles substantially differ in their
620   material properties influencing particle-cell interactions and cellular responses', *Journal of Hazardous*
621   *Materials*, 425(November 2021), p. 127961. doi: 10.1016/j.jhazmat.2021.127961.

622   Ramsperger, A. F. R. M. *et al.* (2023) 'NanoImpact Nano- and microplastics : a comprehensive review on
623   their exposure routes , translocation , and fate in humans', 29(May 2022). doi:
624   10.1016/j.impact.2022.100441.

625   Ritschar, S. *et al.* (2022) 'Taking advantage of transparency: A proof-of-principle for the analysis of the
626   uptake of labeled microplastic particles by organisms of different functional feeding guilds using an
627   adapted CUBIC protocol', *Science of The Total Environment*, 832, p. 154922. doi:
628   https://doi.org/10.1016/j.scitotenv.2022.154922.

629   Rohrbach, A. *et al.* (2020) 'Measuring Stepwise Binding of Thermally Fluctuating Particles to Cell
630   Membranes without Fluorescence', *Biophysical Journal*, 118(8), pp. 1850–1860. doi:
631   10.1016/j.bpj.2020.03.005.

632   Salter, S. J. *et al.* (2014) 'Reagent and laboratory contamination can critically impact sequence-based
633   microbiome analyses', *BMC Biology*, 12(1), p. 87. doi: 10.1186/s12915-014-0087-z.

634   Schmidt, A. and Hall, M. N. (1998) 'SIGNALING TO THE ACTIN'.

635   Shahul Hamid, F. *et al.* (2018) 'Worldwide distribution and abundance of microplastic: How dire is the

636   situation?', *Waste Management and Research*, 36(10), pp. 873–897. doi: 10.1177/0734242X18785730.

637   Stock, V. *et al.* (2019) 'Uptake and effects of orally ingested polystyrene microplastic particles in vitro and
638   in vivo', *Archives of Toxicology*. doi: 10.1007/s00204-019-02478-7.

639   Stock, V. *et al.* (2021) 'Uptake and cellular effects of PE, PP, PET and PVC microplastic particles',
640   *Toxicology in Vitro*, 70(June 2020), p. 105021. doi: 10.1016/j.tiv.2020.105021.

641   Stricker, J., Falzone, T. and Gardel, M. L. (2010) 'Mechanics of the F-actin cytoskeleton', *Journal of*
642   *Biomechanics*, 43(1), pp. 9–14. doi: 10.1016/j.jbiomech.2009.09.003.

643   Swanson, J. *et al.* (1995) 'Macropinocytosis', 5(November), pp. 424–428.

644   Weiss, G. and Schaible, U. E. (2015) 'Macrophage defense mechanisms against intracellular bacteria',
645   *Immunological Reviews*, 264(1), pp. 182–203. doi: 10.1111/imr.12266.

646   Witzmann, T. *et al.* (2022) 'Repulsive Interactions of Eco-corona-Covered Microplastic Particles
647   Quantitatively Follow Modeling of Polymer Brushes', *Langmuir*, 38(29), pp. 8748–8756. doi:
648   10.1021/acs.langmuir.1c03204.

649   Wright, S. L. and Kelly, F. J. (2017) 'Plastic and Human Health: A Micro Issue?', *Environmental Science and*
650   *Technology*, 51(12), pp. 6634–6647. doi: 10.1021/acs.est.7b00423.

651
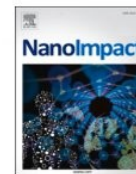
Article 7

**Nano- and microplastics: a comprehensive review on their exposure
routes, translocation, and fate in humans**

Nano- and microplastics: a comprehensive review on their exposure routes, translocation, and fate in humans

Anja F.R.M. Ramsperger [a,n], Enrico Bergamaschi [b], Marco Panizzolo [b], Ivana Fenoglio [c], Francesco Barbero [c], Ruud Peters [d], Anna Undas [d], Sebastian Purker [e], Bernd Giese [e], Carina R. Lalyer [e], Alba Tamargo [f], M. Victoria Moreno-Arribas [f], Hans-Peter Grossart [g,h], Dana Kühnel [i], Jana Dietrich [j], Friedrich Paulsen [j], Anani K. Afanou [k], Shan Zienolddiny-Narui [k], Stine Eriksen Hammer [k], Torunn Kringlen Ervik [k], Pål Graff [k], Bendik C. Brinchmann [k,l], Karl-Christian Nordby [k], Håkan Wallin [k], Matteo Nassi [m], Federico Benetti [m], Michela Zanella [m], Julian Brehm [a], Holger Kress [n], Martin G.J. Löder [a], Christian Laforsch [a,*]

[a] Animal Ecology I & BayCEER, University of Bayreuth, Bayreuth, Germany
[b] Department of Public Health and Pediatrics, University of Turin, Turin, Italy
[c] Department of Chemistry, University of Turin, Turin, Italy
[d] Wageningen Food Safety Research, Wageningen University & Research, Wageningen, the Netherlands
[e] Institute of Safety and Risk Sciences (ISR), University of Natural Resources and Life Sciences, Vienna, Austria
[f] Institute of Food Science Research (CIAL), CSIC-UAM, Madrid, Spain
[g] Plankton and Microbial Ecology, Leibniz Institute for Freshwater Ecology and Inland Fisheries (IGB), Berlin, Germany
[h] Biochemistry and Biology, Potsdam University, Potsdam, Germany
[i] Helmholtz Centre for Environmental Research GmbH - UFZ, Leipzig, Germany
[j] Institute of Functional and Clinical Anatomy, Friedrich-Alexander-Universität Erlangen-Nürnberg, Erlangen, Germany
[k] National Institute of Occupational Health, Oslo, Norway
[l] Section of Air Pollution and Noise, Department of Environment and Health, Norwegian Institute of Public Health, Oslo, Norway
[m] Ecamricert srl, Monte di Malo, Vicenza, Italy
[n] Biological Physics, University of Bayreuth, Bayreuth, Germany

ARTICLE INFO

ABSTRACT

Contamination of the environment with nano-and microplastic particles (NMPs) and its putative adverse effects on organisms, ecosystems, and human health is gaining increasing scientific and public attention. Various studies show that NMPs occur abundantly within the environment, leading to a high likelihood of human exposure to NMPs. Here, different exposure scenarios can occur. The most notable exposure routes of NMPs into the human body are via the airways and gastrointestinal tract (GIT) through inhalation or ingestion, but also via the skin due to the use of personal care products (PCPs) containing NMPs. Once NMPs have entered the human body, it is possible that they are translocated from the exposed organ to other body compartments. In our review article, we combine the current knowledge on the (1) exposure routes of NMPs to humans with the basic understanding of the potential (2) translocation mechanisms into human tissues and, consequently, their (3) fate within the human body. Regarding the (1) exposure routes, we reviewed the current knowledge on the occurrence of NMPs in food, beverages, personal care products and the air (focusing on indoors and workplaces) and found that the studies suggest an abundant presence of MPs within the exposure scenarios. The overall abundance of MPs in exposure matrices relevant to humans highlights the importance of understanding whether NMPs have the potential for tissue translocation. Therefore, we describe the current knowledge on the potential (2) translocation pathways of NMPs from the skin, GIT and respiratory systems to other body compartments. Here, particular attention was paid to how likely NMPs can translocate from the primary exposed organs to secondary organs due to naturally occurring defence mechanisms against tissue translocation. Based on the current understanding, we conclude that a dermal translocation of NMPs is rather unlikely. In contrast, small MPs and NPs can generally translocate from the GIT and respiratory system to other tissues. Thus, we reviewed the existing literature on the (3) fate of

NMPs within the human body. Based on the current knowledge of the contamination of human exposure routes and the potential translocation mechanisms, we critically discuss the size of the detected particles reported in the fate studies. In some cases, the particles detected in human tissue samples exceed the size of a particle to overcome biological barriers allowing particle translocation into tissues. Therefore, we emphasize the importance of critically reading and discussing the presented results of NMP in human tissue samples.

1. Introduction

The overall increase in single-use throw-away plastic products and packaging has led to a tenfold increase in plastics in municipal solid waste from 1960 until 2005 (Geyer et al., 2017; Jambeck et al., 2015; Lebreton and Andrady, 2019), and has even accelerated during the SARS-CoV-2 pandemic (Klemeš et al., 2020; Vanapalli et al., 2021). This increase in plastic waste is further accompanied by more plastic litter in the environment (GESAMP, 2016; Katare et al., 2022).

Once plastics enter the environment, the properties which make them useful turn into a threat to the environment. For instance, the longevity of plastics leads to plastic accumulation in the environment that is expected to persist for hundreds to thousands of years depending on the plastic type (Barnes et al., 2009). However, due to UV radiation, mechanical and biological degradation, larger plastic items can brittle into ever smaller particles (Barnes et al., 2009). Recently, it has been shown that degradation, for instance of polystyrene (PS), is a two-stage process where photooxidation at the near-surface layer is the first step followed by microcrack formation and particle rupturing, leading to the formation of a multitude of even smaller particles (Meides et al., 2021). Thompson et al., 2004 introduced the term microplastics (MPs), which has later been described as all plastic particles smaller than 5 mm in diameter (Arthur et al., 2009). Although there is no official lower size limit of MPs, 1 μm is widely accepted nowadays, and particles smaller than 1 μm are usually termed nanoplastics (NPs) (Gigault et al., 2018; Hartmann et al., 2019). Although MPs have been detected abundantly in the environment, detection and identification of NPs is still very challenging, mainly due to methodological and analytical limitations for detecting NMPs in environmental samples and biological matrices. This aspect has been comprehensively reviewed elsewhere (e.g., Chen et al., 2020; Möller et al., 2020; O'Connor et al., 2019; Schwaferts et al., 2019).

However, the number of NMPs occurring in nature increases with decreasing particle sizes (Hale et al., 2020). Yet, the overall occurrence of NMPs and their small sizes is a potential health risk for organisms. The risk of accidental ingestion or inhalation is much greater for smaller particles than larger particles. In addition, as particle size decreases, the surface area to mass ratio increases. Consequently, the reactivity and toxicity of particles increases, making subsequent interactions with biological barriers more likely (Buzea et al., 2007). Although NMPs have been present in the environment for several decades (Carpenter and Smith, 1972), they are regarded as a rather newly introduced environmental particulate stressors. Furthermore, as NMPs are a highly diverse group of contaminants with various physicochemical properties, overall conclusions on the potential adverse health effects of NMPs are challenging. However, first attempts to perform a risk assessment of NMPs for humans were conducted, which will be discussed later.

Studies on ingestion and subsequent translocation of NMPs in different organisms in nature (Barboza et al., 2020) and laboratory studies (Galloway et al., 2017; Yong et al., 2020) have raised concern about putative adverse effects of NMPs, even to humans (Prata et al., 2020; Wright and Kelly, 2017). Prata et al. (2020) highlighted that upon exposure and uptake, the potential toxicity of NMPs may result from oxidative stress and inflammation, which consequently could disrupt the immune and nervous system. NMPs from the environment may not solely be coated with an eco-corona which is known for enhancing the cellular uptake (Ramsperger et al., 2020) but also with potentially pathogenic microorganisms (Gkoutselis et al., 2021; Kettner et al., 2019; Kirstein et al., 2016; Weig et al., 2021). The accumulation of pathogens

on the surface of NMPs, exceeding the concentration of the surrounding media, may lead to a health threat upon uptake of an increased pathogen load on the particles by organisms.

The number of studies concerning the potential effects of NMPs on an environmental and organismal level steadily increases (Gabriel et al., 2015). In contrast, research on human exposure and toxicity is a relatively new field in NMP research. Nevertheless, there is a growing number of articles addressing the exposure of humans to NMP (Cox et al., 2019; Senathirajah et al., 2021) and their potential health risks (see, e.g. Prata et al., 2020; Rahman et al., 2021; Wright and Kelly, 2017). However, most review articles either focus on a specific exposure route (e.g., Chen et al., 2019; Danopoulos et al., 2020; Mercogliano et al., 2020; Peixoto et al., 2019; Yuan et al., 2022; Zhang et al., 2020) or the potential adverse health effects of NMP to humans upon exposure (Campanale et al., 2020; Danopoulos et al., 2021; Huang et al., 2021; Vethaak and Legler, 2021). In our review article, we combine the current knowledge on the contamination levels of the three major (1) exposure routes of NMPs to humans with the basic understanding of the potential (2) translocation mechanisms into human tissues and, consequently, their (3) fate within the human body. Regarding the (1) exposure scenarios, we reviewed the current knowledge on the occurrence of NMPs in food, beverages, personal care products (PCPs) and the air (focusing on indoors and workplaces). To avoid redundancies to other review articles describing the exposure levels of NMPs to humans, we focused on studies published after 2015. Furthermore, we describe the current knowledge on the potential (2) translocation pathways of NMPs from the primarily exposed organs (skin, gastrointestinal tract (GIT) and lung) into human tissues. Particular attention was paid to the mechanisms that allow particles to translocate into tissues and how likely the translocation from the primary exposed organs to secondary organs is. Based on the presented results of the NMP contamination in the different exposure scenarios and the current understanding of the potential translocation pathways, we critically discuss the significance of the described NMP in the (3) fate studies.

Since there is little to no data on the contamination of the environment and organisms with NPs, we mainly refer to MPs in our review article. We use the abbreviations MPs (5 mm – 1 μm) or NPs (<1 μm) to indicate the size class in the respective sections summarized and discussed. For more general statements, we use the abbreviation NMPs.

2. Methods of literature research

To avoid redundancy to other review articles, we only included studies from 2015 for the (1) exposure scenarios. To describe the potential (2) translocation mechanisms of NMPs from primary exposed organs (lung, GIT and skin) to other tissues and secondary organs, we did not set a threshold for the year of publication since the general understanding of the mechanisms requires fundamental literature. Since the topic of the (3) fate of NMPs in human tissue samples is a relatively new field of research, we included all studies published so far in the sense of NMPs.

We used *Google Scholar, ISI Web of Knowledge/Web of Science, Scopus, PubMed*, and *Embase* as databases. The common search terms for all chapters were: *microplastic*, nanoplastic**, and *human exposure*. For the more specific chapters, we included the following search terms: *drinking water and beverages* for NMP in drinking water; *meat, fish, seafood, edible tissue, vegetables, milk, egg, roots and tubers, plants and herbs, confectionary, honey, sugar, salt, cereal, rice, maize, wheat, barky, spelt, rye, oat,*

2

sorghum, millet, teabag, oil, olive oil, vegetable oil, and *palm oil* for the NMP in food chapter; *atmosphere, atmospheric,* and *air* in the NMP inhalation chapter; and *cosmetics, personal care products, contraceptive, eye, contact lenses,* and *ocular surface* for the PCP chapter. We were using the additional search terms *human tissue* and *organs* in the fate chapter. No studies were excluded.

3. Human exposure to NMPs

Since MPs have been detected abundantly in the environment, the exposure of human beings to NMPs is highly likely (Prata et al., 2021). There are numerous routes of exposure through which humans can come into contact with NMPs. Here we summarize the current knowledge on the contamination with NMPs of drinking water and beverages, the most relevant food items, and indoor air. Furthermore, we address polymers intentionally added as ingredient in PCPs designed for direct application on the human body.

3.1. Drinking water and beverages

Water is essential to sustain human life, and we consume water as plain drinking water as well as in other beverages and in food. Although there are guidelines for drinking water quality (WHO, 2017), contamination with NMPs has yet not been implemented. In the report on microplastics in drinking water by the World Health Organization (WHO) (Organization, 2019), it was described that MP should, in principle, be effectively removed since drinking water treatment is designed to remove particulate matter from drinking water sources. However, it is assumed that the contamination of drinking water with MPs could stem from the raw water used for its generation due to inefficient removal of the particles (Pivokonsky et al., 2018). Zhang et al. (2020) described that the efficiency of removing particles >50 μm ranges from 25--90%, depending on the treatment technologies of the respective drinking water treatment plants. Since many bottled water and other beverages contain filtered municipal tap water, the contamination with particles <50 μm could originate from the drinking water used to produce them. However, Mason et al. (2018) compared bottled water from the same brand available in glass or plastic bottles, and the contribution of the plastic bottle to the NMPs load is larger than that stemming from the water directly. Therefore, another potential source of the NMP contamination of bottled water may derive from the production processes, like packaging (Zhang et al., 2020). Furthermore, one potential reason for the higher contamination of plastic bottled water could be the repeated mechanical stress of opening and closing the bottles, increasing MPs release (Winkler et al., 2019).

Several studies investigated drinking water and beverages contamination with MPs, and other review articles have already summarized the current knowledge of MPs in drinking water (e.g. Danopoulos et al., 2020; Eerkes-Medrano et al., 2018; Koelmans et al., 2019). MPs were detected in drinking water, beverages like beer, refreshments, and wine across the globe (Kankanige and Babel, 2020; Makhdoumi et al., 2021; Mason et al., 2018; Shruti et al., 2021). Schymanski et al. (2018) describe that 80% of the detected particles have a size distribution of 5–20 μm and Oßmann et al. (2018) highlighted that more than 90% of the detected particles in their study were even smaller than 5 μm. Consequently, most MPs in drinking water and beverages are not visible to the naked eye.

However, there is a consensus on the occurrence of MPs in bottled drinking water and beverages produced for human consumption, although the actual amount of NMPs within drinking water is still to be evaluated. Based on 10 publications reviewed, Zhang et al. (2020) calculated a human microplastic intake of up to 4.7×10^3 particles per person per year. Finally, it's worth of note that drinking water is not solely used for direct consumption but also for further food processing. Therefore, it could contribute to the NMP content in processed food items.

3.2. Food

One of the main uptake routes of NMPs by humans is through food. To obtain a comprehensive picture of NMPs contamination in raw and processed food, we used food categories based on a technical report published by the European Food Safety Authority (EFSA) (EFSA CONTAM Panel, 2016; Food and Authority, 2011) and the classification and description system FoodEx2 (revision 2) (European Food Safety Authority, 2015, 2021) (see Table 1).

Amongst the major food commodities for humans are eggs, meat, milk, cereal and roots (FAO, 2013). Approximately 19% of the global population use seafood as their primary source of animal protein, which indicates how heavily reliant humans are on the oceans' life as protein source (Beaumont et al., 2019; Golden et al., 2016). Over the last 70 years, the global fishery capture production increased by a factor of ~5 (1950: 19 million tons living weight; 2019: 94 million tons living weight), whereas the global aquaculture production increased by a factor of ~200 (1950: 6×10^5 tons living weight; 2019: 120 million tons living weight) (FAO, 2020; FishStatJ software v4.02.04, 2022), to meet the increase in protein needs caused by a growing world population. Therefore, we first summarize the current knowledge of NMPs contamination in 'blue meat', a term introduced by Naylor et al. (2021) defining aquatic foods captured from or cultivated in marine and freshwater ecosystems. It must be noted that within this review, we only consider studies focusing on NMPs content in edible parts of the animals, starting with the findings on species consumed as a whole organism.

Mussels are filter feeders and therefore inadvertently ingest NMPs with their food. As a protein source for humans, they thus represent a potential vector of NMPs (Gündoğdu et al., 2020; Nalbone et al., 2021; Ribeiro et al., 2020; Sparks et al., 2021; Kumar et al., 2021; Wakkaf et al., 2020). The contamination of mussels with MPs was mainly stated in MPs per gram of wet weight (MPs/g w.w.) of the mussels and ranged from 0.040 ± 0.003 MPs/g w.w. up to 0.9 ± 0.1 MPs/g w.w. (Gündoğdu et al., 2020; Nalbone et al., 2021; Ribeiro et al., 2020; Sparks et al., 2021; Kumar et al., 2021), whereas one study estimated a higher value of 2.4 MPs/g w.w. (Wakkaf et al., 2020). Different polymer types with different shapes and sizes were detected in mussel tissues (Table 2). Next to mussels, other species consumed in whole may be relevant vectors of NMPs to humans. Ribeiro et al. (2020) analyzed wild and farm seafood (i.e., prawns, squids, sardines) and highlighted a high variability of polymers depending on the studied species. Furthermore, the occurrence of MPs in other commercially relevant marine species was evaluated in edible tissue of crab (Akhbarizadeh et al., 2019; Daniel et al., 2020a; Ribeiro et al., 2020; Zhang et al., 2021), sea urchin (Feng et al., 2020), shrimp (Daniel et al., 2020b, 2021), prawn (Akhbarizadeh et al., 2019; Ribeiro et al., 2020) and squid (Daniel et al., 2021; Ribeiro et al., 2020). Most studies showed that the percentage of MPs in edible tissues is generally lower than in the inedible ones, like the organisms' digestive tract (Daniel et al., 2020a; Wakkaf et al., 2020; Zhang et al., 2021). This implements that animals that are eaten whole, including their digestive

Table 1
Grouping of food categories used in the present chapter.

CATEGORY	subgroup
Cereals	A0EZF, A0EZV
Fruit and Vegetable	A07XJ, A0EZG, A0EZN, A0EZH
Oils	A015E
Roots and Tubers	A00ZS
Other plants and herbs	A010R, A0EZM
Terrestrial Meat	A0EZS, A0EZT
Marine Meat	A0EZR, A0EZQ
Milk	A0BXZ
Eggs	A031E
Confectionery	A04PE
Particular food	A03TD, A03PV, A03RR
Other	A03VA, A042N
isolated purified ingredients	A0BXX

3

Table 2

Overview of MPs found in selected animal food products. Cellulose Acetate (CA), Cellophane (CE), Ethylene Propylene diene monomer rubber (EPDM), Extruded PS (EPS), Ethylene-vinyl acetate (EVA), Polyamide (PA), Polyacrylamide (PAAm), Polyacrylonitrile (PAN), Polybutylene terephthalate (PBT), Polyethylene (PE), High-density PE (HDPE), Low-density PE (LDPE), Polyethylene terephthalate (PET), Polyethersulfone (PES), Poly(methyl methacrylate) (PMMA), Polypropylene (PP), Polystyrene (PS), Polysulfone (PSU), Polytetrafluoroethylene (PTFE), Polyurethan (PU), Polyvinyl acetate (PVA), Polyvinyl chloride (PVC). ATR-FTIR = Attenuated Total Reflection- Fourier-transform infrared spectroscopy, FPA = Focal Plane Array detector, FE-SEM = Field Emission- Scanning Electron Microscopy, EDX = Energy-dispersive X-ray spectroscopy, Py-GCMS = Pyrolysis–gas chromatography–mass spectrometry. Raw data rounded.

Food matrix	Polymer types found	NMP size	Detected concentrations	Analytical Method	Ref.
Mussel	- PET - Latex - PS-cotton - PVC - CA - EVA - HDPE - Nylon	500 µm – 2000 µm	0.040 ± 0.003 MPs/g wet weight (w.w.) 87% of mussels contained MPs	Stereomicroscope sorting FTIR-ATR	Sparks et al., 2021
Mussel	- PE - PP - PET - PVC	~ 500–1500 µm	Fresh mussels: 0.20 ± 0.24 MPs/g w.w. Processed mussels: 0.9 ± 0.1 MPs/g w.w. 61 % of mussels contained MPs	Stereomicroscope sorting FTIR	Nalbone et al., 2021,
Mussel	- PE - PP - CE	not specified	0.7 ± 0.5 – 3.5 ± 0.3 MPs/g w.w. 97% of mussels contained MPs	Stereomicroscope sorting FTIR	Wakkaf et al., 2020
Mussel	- PE - PP - Nylon - EVA - PET - p-acrylic acid	mean 1.7 ± 0.1 mm	Mean 0.06 MPs/g w.w Range 0.03–0.09 MPs/g w.w. 92% of vendors sold mussels that contained MPs	Stereomicroscope sorting µ-Raman	Gündoğdu et al. (2020)
Mussel	FTIR: - PP - PET - PAN - PE - PA - PU - PS - PBT Raman: - PA - PP - PE - PAN - PU - PET - PS - PMMA	3–60 µm (Raman analysis) Mostly <100 µm (FTIR analysis)	0.63 ± 0.59 MPs/g w.w.	FPA-based µ-FTIR µ-Raman	Kumar et al. (2021)
Mussel	- PVC	not specified	Range 0–24 µg/g	Py-GC/MS	Ribeiro et al. (2020)
Shrimp	Not detected			Stereomicroscope sorting FTIR	Daniel et al. (2021)
Shrimp	- PS - PA - PE - PP	150–1000 µm (72% of total) <500 µm (less than 25%)	0.04 ± 0.07 MPs/g w.w. 31% of the shrimps were contaminated with MPs	Stereomicroscope sorting FTIR	Daniel et al. (2020b)
Prawn	- PVC - PP - PMMA	not specified	PVC: 0–16 µg/g PP: 0-15 µg/g	Py-GC/MS	Ribeiro et al. (2020)
Prawn	not identified	Mainly <50 µm in muscle	0.36 MPs/g w.w. (muscle) 0.77 MPs/g w.w. (gill)	Stereomicroscope sorting FTIR	Akhbarizadeh et al. (2019)
Squid	- PP - PS - PE	~100–400 µm	0.008 ± 0.02 MPs/g w.w.	Stereomicroscope sorting FTIR	Daniel et al. (2021)
Squid	- PVC - PP	not specified	PVC: 0–11 µg/g PP: 0–24 µg/g	Py-GC/MS	Ribeiro et al. (2020)
Crab	- PP - PS - PE	~100–400 µm	0.003 ± 0.01 MPs/g w.w. 13 % of edible tissue contained MPs	Stereomicroscope sorting FTIR	Daniel et al. (2021)
Crab	- CE - PET - PE - PP - PA	20–5000 µm	0.80 ± 1.1 – 23 ± 25 MPs/g w.w. No MPs were found in crab's muscles.	Stereomicroscope sorting µ-FTIR	Zhang et al. (2021)
Crab	- PS - PE	not specified	PS: 0.28–8.1 µg/g PE: 0–40 µg/g	Py-GC/MS	Ribeiro et al. (2020)

4

Table 2 (*continued*)

Food matrix	Polymer types found	NMP size	Detected concentrations	Analytical Method	Ref.
Crab	- PVC - PP - PMMA not identified	Mainly <50 µm in muscle	PVC: 1.2–39 µg/g PP: 2.5–26 µg/g PMMA: 0–4.5 µg/g 0.26 MPs/g w.w. (muscle) 0.86 MPs/g w.w. (gill)	Stereomicroscope sorting Hot probe testing SEM-EDX	Akhbarizadeh et al. (2019)
Urchin	- CE - PET:PS - PE - PP - PP:PE - PA - ryon - PAN - PU - PVA:PE	7–1000 µm (60% of total) (range 30–4700 µm)	From 0.16 ± 0.09 MPs/g w.w to 2.3 ± 1.7 MPs/g w.w. ~90% of urchins contained MPs	Stereomicroscope sorting FTIR	Feng et al. (2020)
Fish	-PS -PE -PVC -PP -PMMA	not specified	PS: 0–100 µg/g PE: 0–2400 µg/g PVC: 0–10 µg/g PP: 0–60 µg/g PMMA: 0–30 µg/g	Py-GC/MS	Ribeiro et al. (2020)
Fish	- PE - PP - EPDM - PS	100-200 µm in edible tissue (range 115–210 µm) 200–400 µm in inedible tissue (range 136–4010 µm)	Edible: 0.005 ± 0.02 MPs/g w.w. 7% of fishes had MPs in edible parts. Inedible: 0.05 ± 0.01 MPs/g w.w. 41% of fishes had MPs in inedible parts.	Stereomicroscope sorting FTIR	Daniel et al. (2020a)
Fish	not identified	Mainly < 50 µm in muscle	0.16–0.28 MPs/g w.w. (muscle) 0.25 MPs/g w.w. (gill)	Stereomicroscope sorting Hot probe testing SEM-EDX	Akhbarizadeh et al. (2019)
Fish	- PP - PET - PE - PVC	mean: 1100 ± 940 µm (range 190–3800 µm)	Total 6 MPs found	Stereomicroscope sorting Raman FESEM-EDX	Karami et al. (2018)
Fish	- PP - PE - PS - PET - PA-6	not specified	29 MPs in eviscerated flesh and 7 MPs in organs	Stereomicroscope sorting Raman FESEM-EDX	Karami et al. (2017a)
Chicken	- PE - PS	1–10 mm	Gizzard: mean 46 ± 43 MPs/gizzard Crop: mean 11 ± 15 MPs/crop	Stereomicroscope	Lwanga et al. (2017)
Chicken meat	- EPS - Fibers (not specified)	130–450 µm	4-19 MPs/kg packaged meat	Stereomicroscope sorting ATR-FTIR	Kedzierski et al. (2020)
Milk	- PES - PSU	Fibers and fragments of <500 µm – 5 mm	3–11 MPs/L milk	Stereomicroscope SEM-EDS µ-Raman	Kutralam-Muniasamy et al. (2020)
Milk	- PP - HDPE - LDPE - PAAm	Fibers: 30 – 6740 µm Fragments: 2–180 µm	Fibers: 30–250 MPs/L milk Fragments: 100–280 MPs/L milk	Stereomicroscope sorting FTIR	Diaz-Basantes et al. (2020)
Milk	- PP - PE - PES - PS - PTFE - PU - PSU - PVA	69–99% <50 µm²	Samples ranged from 800–9700 MPs/L milk	µ-Raman SEM-EDX	Costa Filho et al. (2021)

tract, are a potentially larger vector for NMPs than when only parts of the animals are consumed. For instance, larger fish are usually not eaten whole, but mainly the fillet is consumed by humans. Here, the translocation of MPs from the digestive tract into edible tissues like fish fillet has already been shown in a laboratory study (Zeytin et al., 2020) and also in fish captured in nature for human consumption (Daniel et al., 2020a; Gabriel et al., 2015; Karami et al., 2017a). Therefore, both marine animals eaten as a whole, and saltwater fish fillet consumption can serve as a vector for human consumption of NMPs. However, 12.5% of the total share of captured fish derives from inland freshwater ecosystems (FAO, 2020). Although there are no studies demonstrating NMPs in the fillet of freshwater fish for human consumption, it has been described that freshwater fish also ingest MPs (Galafassi et al., 2021; Parker et al., 2021). Consequently, fillet of freshwater fish might be an additional vector of NMPs to humans.

The total protein requirement of humans is not only met by blue meat but also by a high proportion of meat. Poultry consumption, in particular, has increased over the last 60 years, even overtaking beef consumption (Naylor et al., 2021). However, only little information on MPs levels in meat have been published. First attempts were made to analyze the MPs content in chicken (Huerta Lwanga et al., 2017; Kedzierski et al., 2020). Both studies showed that MPs were attached to chicken tissues. Kedzierski et al. (2020) highlighted that the MPs associated with the washed chicken meat mainly derived from the packaging

5

itself. Huerta Lwanga et al. (2017) found MPs >1 mm in size in the gizzard of dissected chickens. The authors state that even a thorough washing of the gizzard would not guarantee the complete removal of MPs and calculated possible annual ingestion of 840 MPs per person per year in Mexico. However, to our best knowledge, MPs were not detected within the meat fillet mainly used for human consumption. This lack of knowledge may depend on time- and cost-consuming approaches like enzymatic digestion (Löder et al., 2017) that would be needed prior to analysis of the meat. Recently, Huang et al. (2020) used a non-disruptive method, namely mid-infrared spectroscopy, to detect MPs within chicken meat without destroying the meat matrix. However, the method's sensitivity for detecting MPs is very low (between 1% and 10% (w/w)) and needs to be improved to apply it to real samples.

Another important source of nutrients for humans are milk and dairy products. Milk is not solely used as a raw product but also for many processed food items, like butter, cheese, cream, and ready-made products.

A few studies have already investigated the contamination of MPs in milk (Table 2). For example, Kutralam-Muniasamy et al. (2020) detected MPs in branded milk from Mexico, reporting 3-11 MPs/L, and Diaz-Basantes et al. (2020) reported higher levels of average 40 MPs/L in milk from Ecuador. However, Costa Filho et al. (2021) reported much higher contamination levels, with 88 MPs/L in raw milk and 694 MPs/L in powdered milk. Therefore, although it is premature to conclude on MPs levels in milk, the results of Costa Filho et al. (2021) suggest that MPs' presence increases with milk processing.

In addition, humans consume and also need carbohydrates, with cereals accounting for the largest proportion. The FAO estimates that cereals are mainly produced for direct human consumption (41%) and animal feed (45%), the remaining percentages for industrial applications (brewing, biofuels, etc.). Cereals contribute 55-70% of the total diets of developing countries, with 2/3 represented by corn and wheat. Corn, oats, barley, wheat and sorghum are the main grains used in animal feeding globally (Kleih et al., 2006; World Trade Organization, 2019). Therefore, MP- containing cereals may serve as a direct vector when consumed by humans or indirectly by consuming animal products containing NMPs. There is growing evidence for the contamination of the terrestrial environment, with increasing attention drawn on agricultural soils for food production. However, if this leads to the contamination of cereals is not known to date. Possible transfer of NMPs to cereals may stem from agricultural soils (Harms et al., 2021; Rillig et al., 2017; Steinmetz et al., 2016; Wang et al., 2021), irrigation of cereal crops with contaminated waters (Domenech and Marcos, 2021), and fertilization with sewage sludge and polymer-coated fertilizer (Corradini et al., 2019; Lian et al., 2021; van den Berg et al., 2020; Weithmann et al., 2018). It is not known whether NMPs can enter the crop plant tissue grown on agricultural fields. However, in laboratory studies, it was shown that vascular plants could act as sinks for model NMPs as their surfaces can adsorb them (Taylor et al., 2020) or even be

taken up into the plant's tissues (Austen et al., 2022; Bosker et al., 2019; Dong et al., 2021; Li et al., 2021; Lian et al., 2021; Yin et al., 2021; Zhou et al., 2021). Nevertheless, most studies have focused on the potential effects of NMPs on plant physiology (Dong et al., 2020; Pehlivan and Gedik, 2021; Urbina et al., 2020; Wu et al., 2022).

Furthermore, industrial processing and packaging may lead to NMPs contamination of cereals (Dessì et al., 2021). Despite the high proportion of human consumption of cereals, very little data on their contamination by NMPs exists. We observed only one study investigating the MPs contamination of rice produced for human consumption (Table 3). Dessì et al. (2021) investigated the mass concentration of MPs in store-bought rice and found 45-322 µg/g dry weight. The authors found no difference between paper and plastic packaging of the rice. However, washing the rice before further processing reduced the mass of MPs within the samples. Noteworthy, pre-cooked rice contained a fourfold higher concentration of MPs, suggesting that industrial processes may be the primary source of MPs contamination.

Next to cereals, fruits and vegetables contribute to the overall consumption of carbohydrates. There is little information about NMPs' presence in commercial vegetables and fruits produced for human consumption. To our best knowledge, only Oliveri Conti et al. (2020) quantified MPs in several Italian fruits and vegetables produced for human consumption of different contamination levels, with fruit samples being generally more contaminated than vegetables (Table 3). However, the accumulation of NMPs has been described in edible tissues of radish (Tympa et al., 2021) or cucumber (Li et al., 2021) in plants grown under laboratory conditions.

Furthermore, the usual diet of humans also contains processed foods, reported in our used classification system (Table 1) as oil, confectionary, teabags, honey & sugar and salt (Table 4). To date, no studies are available reporting NMPs in confectionary or oil. However, some studies were published investigating NMPs in other processed foods. For instance, Li et al. (2020) detected MPs in packed Nori seaweed, and other edible macroalgae were discussed to be potential vectors for NMPs to humans (Yang et al., 2021). Some studies documented the presence of MPs and other fibers in honey (Diaz-Basantes et al., 2020; Liebezeit and Liebezeit, 2013, 2015; Mühlschlegel et al., 2017) and sugar (Liebezeit and Liebezeit, 2013, 2015) and several studies detected MPs in salt samples (Fadare et al., 2021; Fischer et al., 2019; Gündoğdu, 2018; Iñiguez et al., 2017; Karami et al., 2017b; Kim et al., 2018; Kosuth et al., 2018; Lee et al., 2019; Nithin et al., 2021; Renzi et al., 2019; Renzi and Blaŝković, 2018; Seth and Shriwastav, 2018; Tahir et al., 2019; Yang et al., 2015) (Table 4). Furthermore, two studies detected the release of MPs from commercial teabags during a typical steeping process (Hernandez et al., 2019; Xu et al., 2021). These results indicate that raw and processed food items may potentially contribute to human exposure to NMPs via ingestion.

Table 3
Overview of MPs found in rice, vegetables and fruits. Cellulose Acetate (CA), Cellophane (CE), Ethylene Propylene diene monomer rubber (EPDM), Extruded PS (EPS), Ethylene-vinyl acetate (EVA), Polyamide (PA), Polyacrylamide (PAAm), Polyacrylonitrile (PAN), Polybutylene terephthalate (PBT), Polyethylene (PE), High-density PE (HDPE), Low-density PE (LDPE), Polyethylene terephthalate (PET), Polyethersulfone (PES), Poly(methyl methacrylate) (PMMA), Polypropylene (PP), Polystyrene (PS), Polysulfone (PSU), Polytetrafluoroethylene (PTFE), Polyurethan (PU), Polyvinyl acetate (PVA), Polyvinyl chloride (PVC). SEM= Scanning Electron Microscopy, EDX= Energy-dispersive X-ray spectroscopy, Py-GCMS= Pyrolysis–gas chromatography–mass spectrometry. Raw data rounded.

Food matrix	Polymer types found	NMP size	Reported concentrations	Analytical methods	Ref.
Rice	- PE - PP - PET	Not determined	Dry rice: 67 ± 26 µg/g dry weight (d.w.) Washed rice: 52 ± 5 µg/g dw Dry instant rice: 280 ± 50 µg/g dw Washed instant rice: 170 ± 41 µg/g dw	Py-GC/MS	Dessì et al. (2021)
Fruit and vegetable	not specified	1.5–2.5 µm	Apples $1.96 \times 10^5 \pm 1.3 \times 10^5$ MPs/g Pears $1.90 \times 10^5 \pm 1.1 \times 10^5$ MPs/g Broccoli $1.26 \times 10^5 \pm 8.0 \times 10^4$ MPs/g Lettuce $5.10 \times 110^4 \pm 2.5 \times 10^4$ MPs/g Carrot: $1.02 \times 10^5 \pm 4.4 \times 10^4$ MPs/g	SEM-EDX	Oliveri Conti et al. (2020)

6

Table 4

Overview of MPs found in processed foods. Cellulose Acetate (CA), Cellophane (CE), Ethylene Propylene diene monomer rubber (EPDM), Extruded PS (EPS), Ethylene-vinyl acetate (EVA), Isobutyl Vinyl Ether (IBVE), Polyamide (PA), Polyacrylamide (PAAm), Polyacrylonitrile (PAN), Poly(butyl methacrylate) (PBMA), Polybutylene terephthalate (PBT), Polyethylene (PE), High-density PE (HDPE), Low-density PE (LDPE), Polyetherimide (PEI), Polyethylene terephthalate (PET), Polyethersulfone (PES), Poly(methyl methacrylate) (PMMA), Polyoxymethylene (POM), Polypropylene (PP), Polystyrene (PS), Polysulfone (PSU), Polytetrafluoroethylene (PTFE), Polyurethan (PU), Polyvinyl acetate (PVA), Polyvinyl chloride (PVC). ATR-FTIR = Attenuated Total Reflection- Fourier-transform infrared spectroscopy, FPA= Focal Plane Array detector, FE-SEM = Field Emission- Scanning Electron Microscopy, EDX = Energy-dispersive X-ray spectroscopy, Py-GCMS = Pyrolysis–gas chromatography–mass spectrometry, XPS = X-Ray Photoelectron Spectroscopy, NTA = Nanoparticle Tracking Analysis, NIR = Near-Infrared spectroscopy. Raw data rounded.

Food matrix	Polymer types found	NMP size	Reported concentrations	Analytical method	Ref.
Nori seaweed	- not specified	not specified	0.9–3 MPs/g	Stereomicroscope μ-FTIR	Li et al. (2020)
Honey, Sugar	- not specified	not specified	Honey, fibers 170 ± 150 MPs/kg, fragments 9 ± 9 MPs/kg Sugar, fibers 220 ± 120 MPs/kg, fragments 32 ± 7 MPs/kg Unrefined sugar, fibers 560 MPs/kg, fragments 540 MPs/kg	Stereomicroscope	Liebezeit and Liebezeit (2013)
Honey	- not specified	not specified	Fibers 10–340 MPs/kg, fragments 2–82 MPs/kg.	Stereomicroscope	Liebezeit and Liebezeit (2015)
Honey	- PET	>30 μm	0–8.3 MPs/kg (mean 3.8 MPs/kg)	Raman FTIR-ATR	Mühlschlegel et al. (2017)
Honey	- PP - HDPE/LDPE - PAAm	Fibers 67–2700 μm, fragments 5–230 μm	Fibers 20–180 MPs/L, fragments 190–830 MPs/L.	Stereomicroscope sorting FTIR	Diaz-Basantes et al. (2020)
Salt	- not specified	4–4600 μm	1600–3 × 10^4 MPs/kg	Stereomicroscope sorting μ-FTIR	Renzi and Blašković (2018)
Salt	- not specified	100–5000 μm	47–800 MPs/kg (mean 210 MPs/kg)	Stereomicroscope	Kosuth et al. (2018)
Salt	- PVA - PP - PE	4–4700 μm	0.67 ± 1.2–3.4 ± 4.9 MPs/kg	Stereomicroscope sorting FTIR	Fadare et al. (2021)
Salt	- Nylon - LDPE - PP - PET	not specified	470 ± 120–1600 ± 150 MPs/kg	FTIR	Nithin et al. (2021)
Salt	- PP - PE - PS - PEI - PET - POM	90–1500 μm	9.8 MPs/kg	Stereomicroscope sorting FTIR	Lee et al. (2019)
Salt	- PET - PVC - PA6 - PE - PS - IBVE - PA - PC - PP - PBMA - PU - Viscose	10–150 μm	170–320 MPs/kg (IT); 70–220 MPs/kg (CRO)	FTIR ATR	Renzi et al. (2019)
Salt	- PVA - PE - PS	390–9400 μm	6.7 - 53 MPs/kg	FTIR	Tahir et al. (2019)
Salt	- PES - PS - PA - PE - PET	80% of fragments and fibers were smaller than 500 and 2000 μm resp.	103±39 - 56±49 MPs/kg; 64 μg/kg	Stereomicroscope sorting μ-FTIR	Seth and Shriwastav (2018)
Lake salt, Rock salt, Sea salt	Lake salt: - PP - PE - Teflon - PET Rock salt: - PET - PE - PP Sea salt: - PE - PP - PET	100–5000 μm	Lake salt: 28–460 MPs/kg (mean 250 ± 310 part/kg) Rock salt: 0–150 MPs/kg (mean 38 ± 55 MPs/kg) Sea salt: 0–1700 MPs/kg (mean 680 ± 2600 MPs/kg)	Stereomicroscope sorting FTIR	Kim et al. (2018)
Sea salt, well salt		30–3500 μm	Sea salt: 50–280 MPs/kg Well salt: 120–190 MPs/kg		Iñiguez et al. (2017)

7

Table 4 (*continued*)

Food matrix	Polymer types found	NMP size	Reported concentrations	Analytical method	Ref.
Lake salt, Rock salt, Sea salt	-PET - PP - PE - PET - PES - PE - PB - PP - CE	45–4300 μm	Lake salt: 43–360 MPs/kg Rock salt: 7–200 MPs/kg Sea salt: 550–680 MPs/kg.	Stereomicroscope sorting FTIR Stereomicroscope sorting μ-FTIR	Yang et al. (2015)
Lake salt, Rock salt, Sea salt	Lake salt: - PE - PP - PU - PET - PMMA - PVC - PA-6 Rock salt: - PP Sea salt: - PU - PET - PP - PE - PVC - PA-6	not specified	Lake salt: 8–100 MPs/kg (mean 38 ± 14 MPs/kg) Rock salt: 9–16 MPs/kg (mean 12 ± 1.2 MPs/kg) Sea salt: 16–84 MPs/kg (mean 46 ± 13 MPs/kg).	Stereomicroscope sorting μ-Raman	Gündoğdu (2018)
Salt	- PP - PE - PET - polyisoprene: PS (copolymer) - PAN - PA-6	160–980 μm	10 MPs/kg	Stereomicroscope sorting Raman	Karami et al. (2017b)
Salt	- PP - PET - PE - PS - PVC - PUR - PA - PMMA - PC	-	140-2000 μg/kg	Py-GC/MS	Fischer et al. (2019)
Teabags	- PET - nylon	50−100 μm and 10−400 nm 1−50 μm and 50–600 nm	Estimation of 2.3 million micron-sized and 14.7 billion submicron particles per cup of tea	SEM XPS FTIR NTA	Hernandez et al. (2019)
Teabags	- nylon	500 nm to 100 μm.	Not stated	NIR FTIR	Xu et al. (2021)

3.3. Inhalation

Several comprehensive review articles on the contamination of the atmosphere and breathable ambient air with NMPs already exist (Amato-Lourenço et al., 2020; Bianco and Passananti, 2020; Chen et al., 2019; Wieland et al., 2022; Zhang et al., 2020). A recent study extrapolated wet and dry deposition data to the whole area of the River Weser catchment and reported a total MPs deposition of 232 tons. Furthermore the authors report a MP concentration of 500 MPs per m^3 even in outdoor environments (Kernchen et al., 2021). Although these numbers already seem to be relatively high, most studies indicate that exposure to indoor air seems to comprise a higher likelihood of inhaling NMPs than that of outdoor air (Dris et al., 2017; Liu et al., 2019; Wieland et al., 2022). Interestingly, Liao et al. (2021) reported that the mean values of MPs in indoor air samples were an order of magnitude higher than in outdoor samples. The United States Environmental Protection Agency (EPA) described the concentration of chemicals in indoor environments as 2 to 5 times higher than outdoor concentrations (EPA, 1987). Although the current data suggest that this seems to apply to the concentration of NMP, this needs further investigation. However, since the

EPA and the WHO estimate that European citizens usually spend approximately 90 % of their time indoors (Sarigiannis, 2014; US Environmental Protection Agency, 1986), in this review, we focus on the contamination of indoor environments with NMPs.

First attempts to estimate the inhalation of NMPs from indoor air were made using different methods (Table 5). One way to assess the contamination with airborne NMPs is by directly filtering the ambient air (Dris et al., 2017; Liao et al., 2021) or using a breathing mannikin (Vianello et al., 2019). In addition, passive sampling is another approach to assess the contamination with NMPs, for instance, via microparticle sedimentation into openly placed glass wear (Jenner et al., 2021; Soltani et al., 2021) or collecting dust samples (Dris et al., 2017; Zhang et al., 2020). To date, there is no doubt of the presence of NMPs in indoor air, and Wieland et al. (2022) estimated that humans might inhale more than 48,000 MPs per day.

The abundance of NMPs in indoor environments is likely influenced by the use of plastics in diverse human activities. Flooring, synthetic garments, textile and household furniture seem to be the significant determinants for NMPs contamination of the air as reviewed by Facciolà et al. (Facciolà et al., 2021). The highest concentrations of indoor

8

Table 5

Overview of airborne MPs in indoor environments. Polyamide (PA), Polyacrylonitrile (PAN), Polyethylene (PE), Polyethylene terephthalate (PET), Poly(methyl methacrylate) (PMMA), Polypropylene (PP), Polyvinyl (PV). ATR-FTIR = Attenuated Total Reflection- Fourier-transform infrared spectroscopy, FPA = Focal Plane Array detector, HPLC = High-performance liquid chromatography Raw data rounded.

Indoor sample	Polymer types found	NMP size	Reported concentrations	Analytical method	Ref.
Filtering, passive sampling & dust samples from a vacuum cleaner	- PP - PA-cotton mixture	Dust samples: 4700–4900 μm Indoor air: <3300 μm	Filtering: range 0.4–59 fibers/m^3 with a median value of 5.4 fibers/m^3 Passive sampling: range 2.7 to 20 fibers/day, corresponding to a deposition rate between 1600 and 11,000 fibers/day/m^2 Collected bags of vacuum cleaners: ranged 190 and 670 fibers/mg dust samples.	Stereomicroscope sorting FTIR-ATR	Dris et al. (2017)
Filtering & passive sampling	- PE - PA - PP	Fibers: 60 ± 2.7%: 5–30 μm 29 ± 2.3%: 30–100 μm 11%: >100 μm	Mean concentration: 1600 ± 1200 MPs/m^3	Stereomicroscope sorting μ-FTIR	Liao et al. (2021)
Filtering	- PE - PET - nylon - PP	Fibers: 13% Fragments 87% Size distribution 37-240 μm with a D$_{50}$ of 21-36 μm	Total number of inhaled MPs: 270 MPs The average number of inhaled MPs per unit volume: 9.3 ± 5.8 MP/m^3	FPA-μFTIR-	Vianello et al. (2019)
Passive sampling	- PET - PC	-	PET concentrations in the range of 29–1.1 × 10^5 μg/g dust sample PC concentrations in the range of <0.11–1700 μg/g dust sample	HPLC	Zhang et al. (2020)
Passive sampling	- PET - PA - acrylates - PP - co-polymer blends - PAN - PE - PMMA	Fibers (90%) Fragments (8%) Film (1%) Sphere (1%) Foam (<1%) Size not stated	Mean MPs concentration: 1400 ± 1000 MPs/m^2 per day	μ-FTIR	Jenner et al. (2021)
Passive sampling	- PE - PE:PET - PA - PV	Fibers: - 50–200 μm (5%) - 200–400 μm (19%) - 400–600 μm (17%) Fragments: - 686 μm (average) Films: -100 μm (average)	In total, 7400 fibers, 64 fragments and 18 films were collected. The deposition rate of fibrous MPs ranged from 22 to 6200 fibers/m^2 per day with an average of 3100 fibers/m^2 per day	Stereomicroscope sorting FTIR	Soltani et al. (2021)

airborne MPs (1600 ± 1200 MPs/m^3) were reported by Liao et al. (2021) by active air filtering. They reported that 2/3 of the number of all particles collected were smaller than 30 μm (Liao et al., 2021). Therefore, we can speculate that smaller particles dominate airborne MPs, which is plausible considering that smaller particles remain suspended in the air longer than larger particles. However, to date, there are no data on the occurrence and prevalence of MPs smaller than 5 μm in private indoor environments. Therefore, reliable statements regarding the potential exposure to small MPs or NPs cannot be made.

In some working environments, the potential of being exposed to NMPs generated during mechanical and environmental degradation of plastic goods or by NMPs being added as ingredients to, for example, printer inks, spray paints, injection mouldings, and abrasive may be enhanced (Murashov et al., 2020, https://blogs.cdc.gov/niosh-science-blog/2020/02/19/microplastics/; Bitounis et al., 2022; Getzlaff et al., 2019). However, to date, the occurrence and emission sources of NMPs at workplaces have received little attention. Wieland et al. (2022) compared workplace concentrations of different airborne microparticles and associated occupational diseases. As for many particles and fibers, the physicochemical properties like size, shape, ζ-potential, adsorbed molecules and pathogens, and the MPs' bio-persistence should be regarded as possible drivers of MPs' toxicity (Ramsperger et al., 2020, 2021; Wieland et al., 2022). The US National Institute for Occupational Safety and Health (NIOSH) has defined exposure limits for workers for other airborne particles, such as asbestos or silica dust (Wieland et al., 2022; NIOSH 2020, https://blogs.cdc.gov/niosh-science-blog/2020/02/19/microplastics/). To date, NMPs are considered nuisance dust with a permissible exposure limit (PEL) of 5 mg/m^3 for respirable dust (Bartley and Feldman, 1984, guideline 0600 Issue 3). However, NMP-associated diseases in occupational settings have already been described and summarized (Burkhart et al., 1999; Prata, 2018; Wieland et al., 2022). For instance, the exposure of workers to vinyl chloride monomers used for the production of PVC induce DNA damage in lymphocytes of plastic industry workers (Awara et al., 1998). In addition to the production of the plastic material itself the processing industry may pose a potential hazard to workers. Burkhart et al. (1999) analyzed the workers' particulate exposure during nylon flocking (applying short fibers to adhesive-coated surfaces) and found an average respirable particulate matter of 2.2 mg/m^3. Although this value is below the NIOSH PEL set for nuisance dust, cases of interstitial lung disease were suggested to be linked to the detected respirable particles (Burkhart et al., 1999).

NMPs may be generated via flocking or degradation and from a bottom-up production mechanism during high energy or high heat processes. One example is 3D printing, which is becoming popular in offices and at home, and releases potentially harmful volatile organic compounds and ultrafine particles into the air (Du Preez et al., 2018). Some studies compared the particulate release of 3D printers with PLA

9

and Acrylonitrile-Butadiene-Styrol-Copolymer (ABS) filaments (Stephens et al., 2013; Vance et al., 2017; Zhang et al., 2019). Zhang et al. (2019) suggested that particles released from PLA filament 3D printers were mainly composed of PLA bulk material, whereas particles from ABS 3D printers differed from the bulk material. In all reported studies investigating the emission of NMPs during 3D printing, several million particles were described to be released. For instance, Stephens et al. (2013) estimated that approximately 2.0×10^{10} and 1.9×10^{11} particles, mainly consisting of particles in the fine to ultrafine range (<0.2–0.1 μm), are released every minute for a 3D printer utilizing a PLA and ABS feedstock, respectively. Although it is currently unclear whether the particles consist purely of the bulk material of the filament, these numbers are alarming, especially given the duration of the printing processes. Next to 3D printers, laser toner printers are known to emit high numbers of nanoparticles, including NP (Bello et al., 2021; Getzlaff et al., 2019). As most of the printing devices are currently sold as stand-alone devices without any exhaust ventilation or filtering accessories, the results suggest that caution should be taken when operating in inadequately ventilated or unfiltered indoor environments. Especially because the emitted particles are so small that they can deposit in the deep alveolar region of the lungs upon inhalation (Stephens et al., 2013) and were discussed to be a severe health threat (Bello et al., 2021; Bitounis et al., 2022).

3.4. Personal care products (PCPs)

The term PCPs is often used synonymously for cosmetics, although there is a slight but essential difference. The European Commission defined cosmetics as follows: "Any substance or preparation intended to be placed in contact with the external parts of the human body (epidermis, hair system, nails, lips and external genital organs) or with the teeth and the mucous membranes of the oral cavity with a view exclusively or mainly to cleaning them, perfuming them, changing their appearance, protecting them, keeping them in good condition or correcting body odours." (European Commission, 2013). However, the term PCPs is not defined by law, but most PCPs are regulated as cosmetics, although some PCPs can be regulated as drugs. For instance, the Food & Drug Administration (FDA) listed PCP drugs as "(…) skin protectants (such as lip balms and diaper ointments), mouthwashes marketed with therapeutic claims, antiperspirants, and treatments for dandruff or acne." (FDA, 2016). Since both PCPs cosmetics and PCPs drugs are intentionally applied onto the human body, we decided to not separate them further concerning NMPs.

The European Commission initiated a restriction procedure on MPs in cosmetics in January 2018. Although an adopted restriction (if agreed by the member states) for the European Union is expected by 2022 (Anagnosti et al., 2021; https://www.europarl.europa.eu/doceo/document/E-9-2021-003388_EN.html), several European countries have already banned the intentional use of MPs in PCPs (Kentin and Kaarto, 2018). However, one of the main difficulties in proposing a general restriction of MPs in PCPs is the lack of a definition of the size range of MPs (Kentin and Kaarto, 2018). In the initiated proposal, the size of MPs was set to be lower than 5 mm in size without a lower threshold (ECHA 2021, https://www.europarl.europa.eu/doceo/document/E-9-2021-003388_EN.html). Although the industry has already responded to the pressure from non-governmental organizations and the concerned public by excluding MPs from several products (Anagnosti et al., 2021), the use of MPs is neither restricted in the European Union nor worldwide. Therefore, PCPs can still contain NMPs.

MPs are intentionally added to PCPs for different functions like viscosity regulators, emulsifiers, glitters, skin conditioning, exfoliants, abrasives, and many more (UNEP, 2015; Yurtsever, 2019). Depending on the desired function of the added MPs to PCPs, different polymer types, shapes, and sizes are used. The most often used polymer type is PE in various shapes and sizes (Gouin and Brunning, 2015; UNEP, 2015). Interestingly, the information on the main size ranges found in the

literature is highly heterogeneous and depends on the intended function of the added polymer. For example, Gouin and Brunning (2015) summarized that particles smaller than 60 μm are ineffective as abrasion and exfoliation and the optimum size is around 450 μm. However, Sun et al. (2020) propose that the diameters of MPs added to PCPs range from 24 μm to 2 mm, with more than 95% smaller than 350 μm. The United Nations Environment Programme (UNEP, 2015) highlighted that the primary size of MPs in PCPs lays in between 1 and 50 μm. The size of the added MPs seems to depend on the product type (Sun et al., 2020). For example, in toothpaste, the reported sizes range from 4 - 20 μm (Ustabasi and Baysal, 2019) and 3–145 μm (Praveena et al., 2018). In facial scrubs, sizes were reported between 10–178 μm (Praveena et al., 2018) and 313 ± 130 μm (Lei et al., 2017) and in shower gels of about 422 ± 185 μm (Lei et al., 2017).

Next to the variations in size, MP concentrations are also highly different in PCPs. Variations from less than 1 % (Ustabasi and Baysal, 2019) up to 90 % were reported (UNEP, 2015). Sun et al. (2020) described the concentrations of MPs in PCPs and found the documented concentrations ranging from 2.15 particles per gram up to 3.11×10^6 particles per gram.

Besides the fact that MPs intentionally added to PCPs contribute to overall environmental pollution (Gouin and Brunning, 2015; Praveena et al., 2018), when washed off the body, the direct exposure of humans to the particles is a potential pathway of MPs entering the human body. Especially MPs in toothpaste and other cosmetics applied on mucosa may potentially translocate directly into the human body. For example, swallowing or incomplete rinsing of the mouth after tooth brushing leads to a transfer of MPs into the GIT. Another vulnerable area where PCPs contact the human body is the eye. The skin is relatively thin, and the mucous membrane interacts directly with the environment when the eye is open. Potential contact of the eye's mucous membrane with NMPs can occur through eye shadow and other cosmetic products, contact lenses, and NMPs in the air. As the global PCPs market and the use of contact lenses continue to increase, it is essential to investigate eye and eye care products as a potential gateway for NMPs into our bodies and the environment (https://www.statista.com/statistics/297070/growth-rate-of-the-global-cosmetics-market/; https://www.statista.com/study/48868/contact-lenses-report/). Contact lenses could release NMPs themselves when worn, as they are often made of hydrogel polymers, on the other hand, NMPs from the air could stick to the contact lenses and thus be taken up by ocular surface epithelial cells through prolonged contact time (Burgener and Bhamla, 2021). In addition, glitter, commonly used in eye shadow, can be identified as a primary source of MPs entering the environment and possibly the human body. Glitter, usually in hexagonal form, consists of a core polymer of PET coated with colored aluminum and a transparent polymer, which produces the typical sparkle (Tagg and Ivar do Sul, 2019; Yurtsever, 2019). There are no studies examining the uptake of NMPs by ocular epithelial cells, nor are there any studies showing the presence or accumulation of NMPs in ocular tissues. Hence the relevance of this translocation pathway is unclear.

Other PCPs used by a large part of society are contraceptives and period products. For instance, condoms are a relatively safe, effective, user-controlled contraceptive method that is easy to use and relatively inexpensive. Although the highest share of condom material used on the market are latex, condoms made of polyurethan (PU) or elastomers have already been introduced to the market in the early 1990s (Gallo et al., 2006). Furthermore, Munoz et al. (2022) recently showed that 12 of 24 period products directly in contact with the vaginal wall contained plastic. These products released fibers during *in vitro* tests and fragmented to release up to 17 billion NPs per tampon. A relatively high number of condoms (Lambert et al., 2013) and period products are disposed of down the toilet entering waste water treatment plants or are released to the environments via improper waste disposal, where they may release a substantial number of NMPs. Besides their contribution to environmental pollution with NMPs, it has not been shown whether

condoms made of plastic or plastic containing period products release NMPs during usage and whether potentially released particles may interact with the respective tissues.

4. Translocation of NMPs into human tissues

The translocation of NMPs to our body compartments may occur after applying NMPs-containing PCPs to the skin or after ingestion and inhalation. The potential translocation pathways for the respective primarily exposed organs are described in the following. Since the translocation mechanisms of particulate matter through the human skin is distinct from those within the GUT and lung, we decided to describe the mechanisms separately.

4.1. Human skin

Applying PCPs-containing NMPs onto our skin can directly facilitate the particles translocating from the skin into deeper tissue layers. However, the translocation of particulate matter into the skin is complex (Schneider et al., 2009). The human skin comprises four layers: the stratum corneum, the viable dermis, the dermis and the subcutaneous connective tissue (Desai et al., 2010). The stratum corneum is the outermost layer and provides an effective defensive barrier against particulate matter and pathogens in a healthy status. Schneider et al. (2009) comprehensively reviewed the reported translocation of nanoparticles through the human skin. One potential pathway to how particulate matter could be transported through the skin barrier is via the transappendageal pathway across hair follicles, sebaceous glands, and sweat glands (Desai et al., 2010; Schneider et al., 2009). Vogt et al. (2006) detected a high density of Langerhans cells (dendritic cells) around hair follicles, capable of internalizing nanoparticles of various sizes, whereas the transport across the epidermis was restricted to 40 nm particles in their experimental setup. However, it has to be noted that the transappendageal pathway is restricted to a relatively small area since the total amount of openings amounts between 0.1 and 1.3% of the entire skin (Bos and Meinardi, 2000; Schneider et al., 2009). Nevertheless, keeping in mind the very high concentration of NMPs in some PCPs described above, the translocation of NMPs via the transappendageal pathway might be relevant to consider.

Bos and Meinardi (2000) proposed the 500 Dalton rule by investigating the molecular weight of common contact allergens and topical drugs. They conclude that a molecular weight increasing over 500 Dalton leads to a rapid decline in human skin absorption. Assuming a spherical PS particle with a density of 1.05 g/cm^3, it should not exceed a size of 1.15 nm to be absorbed directly by the skin. However, Schneider et al. (2009) proposed that next to the size, the particles' properties and skin's health status are important factors for translocation. Kohli and Alpar (2004) tested differently charged PS particles of different sizes (50, 100, 200 and 500 nm, positive, negative and neutral charge). They showed that only 50 and 500 nm negatively charged particles penetrated the investigated pigskin. They assume that the density of the negative charges of the 50 and 500 nm particles is higher (50 nm because of the high surface ratio and 500 nm because of a higher number of functional groups) compared to the 100 and 200 nm particles, enabling the interaction and translocation through the skin (Kohli and Alpar, 2004). However, the skin was mechanically stressed, which could impede the barrier function and allow the particles' translocation. Furthermore, the human skin has unique properties, and translocation studies performed in animal models are of limited use for understanding the human skin barrier (Bos and Meinardi, 2000). Larese Filon et al. (2015) comprehensively reviewed the size-dependent translocation of nanoparticles across the human skin. They conclude that nanoparticles can cross the intact skin if their sizes do not exceed 4 nm, nanoparticles between 4–20 nm can potentially cross intact and damaged skin, nanoparticles between 21 and 45 nm can cross only damaged skin, and nanoparticles with sizes >45 nm cannot translocate through the human

skin. However, they also highlighted that the material properties (metal or non-metal nanoparticles) are important factors (Larese Filon et al., 2015). No studies are reporting the translocation of NMPs through the human skin to our best knowledge.

4.2. Gastrointestinal tract

NMPs entering the human body via ingestion will encounter different defense mechanisms against tissue translocation. The first line of defense a particle would experience after entering the GIT is the mucus layer produced by the enterocytes in the form of membrane-bound mucins and the goblet cells in the form of secretory mucins. The mucus layer coats the interior surface of the digestive tract and is essential in the maintenance of intestinal homeostasis (Herath et al., 2020). In a healthy GIT, the mucus layer serves as a permeable barrier allowing the absorption of nutrients but limiting the transport of pathogens and microorganisms to the gut epithelial cells (Rackaityte and Lynch, 2020; Vancamelbeke and Vermeire, 2018). However, in vivo experiments with mice showed that due to oral exposure to NMPs, the intestinal microbiome's composition can be altered, leading to dysbiosis (Lu et al., 2018). Dysbiosis can change the thickness of the mucus layer and could result in abnormal mucus invasion and epithelial adherence of pathogens (Herath et al., 2020) or may even allow NMPs to interact with the epithelial layer directly. Moreover, the intestinal microbiota is considered a metabolic organ that may contribute to the metabolic health of the human host and, when imbalanced, to the pathogenesis of different disorders. Tamargo et al. (2022) evaluated the effects of the digestion of MPs on the human gut microbiota using feces from healthy donors and the internationally validated Dynamic Gastrointestinal Simulator simgi® model that represents the main functional sections of the digestive tract. The feeding with MPs altered human microbial colonic community composition, promoting the formation of biofilms and MPs biodegradation through digestion by intestinal bacteria (Tamargo et al., 2022).

4.3. Lung

The defense mechanisms associated with the ingestion of NMPs do not seem to depend as closely on particle sizes, as is the case for NMPs inhalation, the first line of defense depends on the particle sizes. The exposure to airborne particles is usually classified by the particles' aerodynamic diameter, with PM$_{10}$ (coarse particles ≤ 10 μm), PM$_{2.5}$ (fine particles ≤ 2.5 μm) and PM$_{0.1}$ (ultrafine particles ≤ 0.1 μm). The occurrence of atmospheric MPs of PM$_{10}$ have already been reported (Kernchen et al., 2021) and the inhalation of NMP is therefore generally possible. PM$_{10}$ are usually trapped in the nasopharyngeal area by hair and mucus, whereas PM$_{2.5}$ can reach the bronchioles and alveoli. PM$_{0.1}$ can directly translocate transcellularly across the alveolar epithelium (Cooper and Loxham, 2019; Schraufnagel, 2020). However, defensive mechanisms against PM$_{2.5-0.1}$ also occur within the respiratory system. The epithelial layer contains, similar to the GIT, goblet cells contributing to a mucus layer entrapping inhaled particles. By ciliary beating (the so-called mucociliary escalator mechanism), even PM$_{0.1}$ can be transported within the mucus towards the mouth, where the mucus can be expelled or swallowed (Schraufnagel, 2020).

4.4. Transport of NMP across the biological barriers of the GIT and lung

When entrapped within the mucus of the respiratory system or the GIT, a particle can also be transported towards the epithelial layer (Hussain et al., 2001). Here, two potential pathways for the transport from one side of the epithelium to the other can occur. In epithelial cells, small particles (<100 nm) are more easily transported transcellularly through the epithelium by endocytosis than larger particles (in the lower micrometer range), which are transported paracellularly (Boland et al., 1999; Volkheimer, 1975, 1977; Zeytin et al., 2020). The paracellular

11

transport is mainly regulated through the presence of junctional complexes, like tight junctions, adherence junctions and desmosomes. Tight junctions are the apical-most adhesive complexes sealing the intercellular space (Vancamelbeke and Vermeire, 2018) and make the paracellular transport of particles challenging. However, goblet cells interrupt the network of tight junctions, loosening the tight junctions between epithelial and neighboring goblet cells, consequently allowing the transport of particulate matter in a paracellular manner (Volkheimer, 1977). Within the GIT, the transcellular pathway is also involved in internalizing larger molecules, pathogens and microorganisms (Vancamelbeke and Vermeire, 2018). Once NMPs may have crossed the epithelial layer of the lung, gastrointestinal tract or skin, there is another line of defense. Underneath the dermis of the skin, the interstitium of the lung or the lamina propria in the GIT, i.e. all corresponding tissues directly under the epithelial layer, there are various immune cells such as macrophages, dendritic cells, T and B lymphocytes, eosinophils and mast cells.

The *lamina propria* of the entire GIT is richly populated with diffusely distributed immune cells of different type. Furthermore, it additionally contains situated solitary lymphoid follicles, covered by the so-called follicle-associated epithelium (FAE). Whole aggregates of lymphoid follicles, mainly found in the wall of the ileum and appendix vermiformis, are called aggregated lymph follicles or Peyer's patches. The surface of each follicle is domed by propria tissue and covered with FAE (so-called dome epithelium). Intestinal villi and crypts are missing here, there are no goblet cells, and the mucus is very thin or missing. Instead, M-cells (M = microfold, this cell type is named after its' physiological appearance as the cells have no microvilli but only short microplicae. M-cells can amount 10-15% of the cells in the FAE) are firmly anchored within the epithelium in between enterocytes and can internalize particulate matter, even the size of bacteria (Foged et al., 2005; Hussain et al., 2001; Owen, 1999). M cells transport molecules and particulate matter into pockets, in which migrating lymphocytes, macrophages, and dendritic cells are found (Owen, 1999). With the initiation of an immune response activated B-lymphocytes differentiate into plasma cell precursors on site or in neighboring mesentery lymph nodes where the immune response is further set in motion. The plasma cell precursors differentiate to mature Immunoglobulin A-producing plasma cells that produce an antibody directed against the initial antigen. In addition, dendritic cells push - outside the FAE regions - long projections between the enterocytes into the intestinal lumen to further sense for pathogens or release cytokines (Scott et al., 2005). Furthermore, dendritic cells are in principle capable of internalizing PS particles up to 15 μm in size (Foged et al., 2005).

If, for example, microorganisms or NMP penetrate the mucus and epithelial layer of the GIT, they may be phagocytosed by macrophages in the *lamina propria* (Grainger et al., 2017). These are ideally positioned to ingest and eliminate any bacteria that have passed through (Bain and Schridde, 2018). In principle, macrophages in the lamina propria can trigger the described inflammatory responses, but usually show a silent response to the invader in a healthy organism (Bain and Schridde, 2018; Grainger et al., 2017). However, if specific antigens are perceived or there is increased invasion with pathogens, the immune cells (especially macrophages and dendritic cells) can trigger an inflammatory process by releasing cytokines or migrating into the mesenteric lymph nodes and initiating an immune response. After initiation of the immune response, cells reach the blood circulation via the lymph vessels, lymph nodes and finally the thoracic duct, to be distributed throughout the whole organism (Hampton and Chtanova, 2019; Owen, 1999).

The actual transport of NMPs across biological barriers that may trigger inflammatory responses has not yet been demonstrated. However, *in vitro* experiments showed that macrophages are in principle able to internalize MPs (Ramsperger et al., 2021; Stock et al., 2021), which is even enhanced in the case of environmentally exposed particles coated with an eco-corona (Ramsperger et al., 2020). After particle interaction, NMPs have been shown to trigger inflammatory responses in epithelial

cells (Wu et al., 2020) and macrophages (Völkl et al., 2022). The transport of NMPs across more realistic biological barrier models was shown by using single cell culture approaches (Xu et al., 2019) and coculture of cell lines representing small intestinal barrier models (Stock et al., 2021, DeLoid et al., 2021; Hesler et al., 2019). Furthermore, first attempts were made to estimate the uptake and potential effects of MP on organoid structures of the lung (Song et al., 2022) and intestine (Hou et al., 2022). Here, although MP fibers showed no adverse effects on mature organoids the development of lung organoids was hampered by the presence of MP fibers. The authors state, that the development of lung tissue of young children may be affected by airborne NMP, however, this needs further investigations (Song et al., 2022). The exposure of NP to intestinal organoids resulted in an accumulation of NP mainly in goblet, Paneth and endocrine cells, which consequently induced apoptosis and inflammatory responses (Hou et al., 2022).

Furthermore, *in vivo* studies using mouse model systems revealed the translocation of model nanoparticles from the lungs to the systemic circulation (Campagnolo et al., 2017; Miller et al., 2017; Raftis and Miller, 2019; Stapleton et al., 2012). Miller et al. (2017) and Raftis and Miller (2019) exposed healthy human volunteers to 5 nm gold nanoparticles via inhalation and detected the particles in the blood even three months after exposure. This retention indicates that for small NPs, translocation from the respiratory system in healthy human beings into the blood circulation may be possible. Interestingly, Burkhart et al. (1999) linked the workers' exposure to plastic products with interstitial lung diseases, suggesting that the transport of NMPs and the subsequent inflammatory response are generally possible in human.

To our best knowledge, no empirical *in vivo* studies with volunteer human beings exposed to NMPs either via inhalation, ingestion or dermal exposure were conducted. Therefore, we reviewed the fate of NMPs in different human tissue samples to estimate the amount of NMP present in human tissues and their overall translocation within the human body.

5. The fate of NMPs within the human body

There is a lack of scientific literature documenting the occurrence of NMPs in humans. However, already more than twenty years ago, Pauly et al. (1998) described the presence of fibers in cancerous and non-pathologic human lung tissues. They found fibers in 87% of human lung specimens and discussed that some fibers were made of plastic due to their shape and structure. Since the aim of the study was not to primarily distinguish between natural and plastic fibers, the polymeric composition was not investigated spectroscopically (Pauly et al., 1998). In a more recent study, applying Raman spectroscopy on 20 routine coroner autopsy samples from individuals living in São Paulo, polymeric particles and fibers were detected in 13 samples (Amato-Lourenço et al., 2021). In total, 31 MPs were detected, of which 88% were fragments (mean size: 3.9 ± 0.7 μm) and 13% fibers (mean fiber length: 11 ± 2 μm). Although PM_{10} is usually trapped in the nasopharyngeal region (Cooper and Loxham, 2019; Schraufnagel, 2020), smaller particles may potentially be inhaled, entering deeper lung regions. However, a recent study found MP much larger than PM_{10} in different regions of the human lung (mean particle length: 105.22 ± 92.82 μm, mean particle width: 34.44 ± 22.61 μm) (Jenner et al., 2022). Furthermore, Huang et al. (2022) indirectly measured the contamination of the human lung with NMPs using sputum samples of 22 volunteers. They found different polymer types mainly smaller than 500 μm (median: 75.43 μm). To monitor potential procedural contamination, they conducted one blank sample. Subsequently, the authors corrected the sputum samples with the blank sample value and found a median number of 39.5 MPs/10 mL sputum.

Two pilot studies on the contamination of the human placenta with NMPs were conducted (Braun et al., 2021; Ragusa et al., 2021). Both studies showed the contamination of human placenta samples from vaginal (Ragusa et al., 2021) and cesarean delivery (Braun et al., 2021).

12

Furthermore, one study investigated MPs in human colon tissue samples (Ibrahim et al., 2021). They found a mean of 28 MPs/g colon sample, with 96% of all MPs being fibers of approximately 1 mm length. Interestingly, the authors found mainly fibers in their samples, whereas in human stool samples, mainly fragment- and film-shaped MPs were detected (Schwabl et al., 2019). A second study confirmed the presence of MPs in human stool samples but unfortunately no information regarding the shape of the MPs were given (N. Zhang et al., 2021). Therefore, we can only speculate that the differences in the observed shapes from colon and stool samples could either derive from differences in the sample collection, procedure, and subsequent measurements or by the fact that fibers are more likely to stick to the colon tissues than fragments and films that are more easily released. However, this is highly speculative and needs further investigation. Just recently, Horvatits et al. (2022) described the presence of MPs in human liver, spleen and kidney samples. Out of 17 tissue samples, the authors found six MPs ranging from 4–30 μm in size. Another study investigated NMPs in human blood samples (Leslie et al., 2022). The authors found a mean NMPs concentration of 1.6 μg/mL of blood by using Py-GCMS. It has to be noted that the particle size distribution is defined by the opening of the venipuncture (0.5 mm, upper limit) and the filter mesh size (700 nm, lower limit). The authors aimed to detect five different polymer types (PET, PE, PS, PMMA and PP). All polymer types were detected except for PP.

At this point, we would like to emphasise that in both the exposure studies and the fate studies different sampling procedures and analytical techniques have been applied while quality assurance and quality control (QA/QC) measures are often lacking. A few studies investigated the quality and reliability of data and whether a proper risk assessment can be performed based on current knowledge. For instance, Koelmans et al. (2019) determined the reliability of studies using nine quality control criteria in a systematic review, including 50 publications on NMPs in freshwater, wastewater and drinking water. They concluded that out of the 50 publications, only 4 scored positive in all criteria and can be considered reliable data. Furthermore, Coffin et al. (2022) aimed to develop and evaluate the feasibility and confidence in deriving a human health-based threshold value for MPs in drinking water. The authors scored the quality of the reviewed publications and concluded that currently, the uncertainties in the data are too high to develop a human health-based threshold for drinking water quality. The conclusion of Coffin et al. (2022) is in great agreement with the WHO report (2022), indicating that "(…) the available data are of only very limited use for assessing the risk of NMP to human health".

Therefore, we would like to highlight that the comparability between studies is challenging and the interpretation of the presented results above should be taken with caution.

6. Reasons why reported studies should be interpreted critically

In our review article, we described the current knowledge of the NMP contamination of the most relevant (1) exposure routes to humans, the potential (2) translocation mechanisms of NMP across biological barriers and summarized the studies of the (3) fate of NMP in human tissues and fluids. Although our review article did not aim to compare contamination levels of NMP in the different studies investigating exposure scenarios and the fate of NMP in human tissues, it is essential to keep several aspects in mind. Other review articles have already addressed the analytical challenges for assessing NMPs in matrices relevant to human exposure and described the crucial steps during sample collection and processing (Alexy et al., 2020; Koelmans et al., 2020; Noventa et al., 2021; Van Raamsdonk et al., 2020; Toussaint et al., 2019; Wright and Kelly, 2017). Especially sufficient QA/QC in NMP analysis are essential. Considering that NMPs are usually found everywhere in the laboratory environment, the possible contamination of a sample (exposure template or human tissues and fluids) should be kept in mind. In brief, using procedural blank samples in every step is critical

to monitor potential contamination during sampling and sample processing. Further information on how to sufficiently perform QA/QC in NMP research can be found elsewhere (Brander et al., 2020; Enders et al., 2020; Möller et al., 2020). However, even if QA/QC measures have been addressed, studies must be critically viewed. For instance, in Ragusa et al. (2021), the authors state that they performed procedural blanks and corrected the samples with the blank values; however, the numbers of particles found in the blanks are not stated and therefore, it is hard to interpret the data. Furthermore, they state that they have excluded fibers from their analysis as they could not use laminar airflow cabinets during sample processing. However, NMP fragments also occur in the ambient air and may contribute to the potential airborne contamination of the samples. Another example is the Study of Ibrahim et al. (2021). The authors followed several steps to prevent airborne plastic contamination: E.g. cotton lab wear was worn, liquid reagents were prefiltered before usage (although no mesh sizes were stated), test devices were pre-cleaned, and the use of plastic items for sample processing was kept to a minimum. Here it must be noted that although the authors used blank samples during microscopy, they did not describe the use of blanks during sample collection but have pre-checked the formalin fixative and filters for plastic contamination (Ibrahim et al., 2021).

Given the limitations of state-of-the-art analytical methods, particle numbers and sizes found in exposure matrices and in human tissues and fluids may not reflect accurate numbers. Möller et al. (2020) summarized the advantages and disadvantages of the different techniques used in NMP identification. In brief, visual sorting or hot needle tests are highly error-prone and not recommended. In contrast, vibrational spectroscopy and chromatographic techniques are state-of-the-art and suitable MP identification techniques. Vibrational techniques include Raman or Fourier transform infrared (FTIR) spectroscopy and allow the precise identification of different polymer types. However, it must be noted that a particle's detection limit is at ~1 μm for Raman and ~10 μm for FTIR (depending on the instrument); therefore, smaller MP and NP cannot be detected.

On the other hand, chromatographic techniques such as pyrolysis-gas chromatography-mass spectrometry (py-GCMS) or thermal extraction desorption GCMS (TED-GCMS) can identify MP and even NP within a non-treated sample. However, both methods can only measure relatively small sample sizes and are destructive. Therefore, no information can be given about the number of particles, size and shape (Möller et al., 2020). However, by comparing different particulate contaminants, Wieland et al. (2022) concluded that the size, shape and surface properties play a decisive role in particle toxicity and should be considered. In principle, to determine the size of NMP, the samples could be filtered and therefore grouped in different size classes and subsequently analyzed with py- or TED-GCMS. However, due to the pre-processing of the sample, the decisive advantage that no sample preparation is necessary for chromatographic methods is lost, and the prior processing of the samples create the risk of sample contamination or loss of particles.

Another commonly used method in the presented studies is scanning electron microscopy coupled with energy dispersive X-ray spectroscopy (SEM-EDS) emission detection. However, an accurate interpretation of the spectra is only possible for flat-polished samples or thin films with irrelevant topography (Girão, 2020). Therefore, due to the different limitations of the various methods as well as the potential contamination of a sample, both the numbers and the polymer types should be critically viewed in the reported studies.

If one considers the translocation mechanisms described earlier in our review article, the size of the particles seems to be one of the driving factors for tissue translocation. For instance, the translocation of particles in healthy human skin is determined by their size, which should not exceed the lower nanometer size range. For the GI and lung, the particles should not exceed sizes of the lower micrometre size range, namely <10 μm or even smaller, with an increasing translocation potential with

decreasing particle sizes. Particulate matter's size-related transport across biological barriers was investigated *in vitro* and *in vivo*. In rodent models, it was shown *in vivo* that radioactive-labelled NPs are more likely to be translocated within the GIT mucosa than MPs. The smaller NPs (50 and 100 nm) showed a higher adsorption rate than 1 μm MP particles (33, 26 and 4.5%, respectively) (Jani et al., 1990). Furthermore, after intratracheal exposure of mice to 20 nm rhodamine-labelled polystyrene NPs the particles could be detected in maternal and fetal tissues (Fournier et al., 2020). However, it has to be noted that it cannot entirely be ruled out that the labelling of the used particles may have leached, and it was not the particles per se being detected. Furthermore, using an *in vitro* model of the small intestinal epithelium, DeLoid et al. (2021) showed significantly higher uptake of small NPs (25 nm carboxylated PS spheres) than larger particles. However, Stock et al. (2019), using a similar epithelial model, demonstrated that the uptake of MP (1, 4 and 10 μm) is generally possible.

Keeping the potential for tissue translocation in mind, most particle sizes detected in the exposure matrices are much larger than the described particle sizes for translocation mechanisms. For instance, the smallest NMP sizes described in the exposure scenario studies presented in this review are in the lower micrometre size range: 1–50 μm (Hernandez et al., 2019), 1.5–2.5 μm (Oliveri Conti et al., 2020), 2–180 μm (Diaz-Basantes et al., 2020), 3–60 μm (Kumar et al., 2021), 3–145 μm (Praveena et al., 2018), 4–20 μm (Ustabasi et al. 2019), <5 μm (Oßmann et al., 2018) and 5–20 μm (Schymanski et al., 2018). However, not all studies present clear evidence that the small fraction of the reported NMP in the exposure matrices are indeed plastic particles. For instance, Praveena et al. (2018) performed FTIR analysis only on the larger fraction of isolated NMPs. Ustabasi and Baysal (2019) did not perform FTIR analysis on single particles but measured a film consisting of particle aggregates. Diaz-Basantes et al. (2020) used FTIR to identify the polymeric composition of 10 particles per sample. The particles must be larger than the instrument's detection limits; therefore, the authors cannot conclude the presence of small NMPs.

In the fate studies, very small MPs (<3 μm) or NPs were also not reported or insufficiently identified. The smallest particles found in human tissues were 2 μm in the lung (Amato-Lourenço et al., 2021), 3.3 μm in liver (Horvatits et al., 2022), and 5–10 μm in human placenta (Ragusa et al., 2021). Horvatits et al. (2022) stained the isolated particulate matter with Nile Red and measured only a few particles with Raman spectroscopy. The authors do not state the size of the identified MP; therefore, no conclusions can be drawn whether all small particles are of polymeric origin.

Next to the size and shape of NMPs, their concentration plays a decisive role. For instance, the concentration of NMP found in blood samples seems to be rather high since concentrations reported in surface waters or bottled waters were by a factor of 22 and 8.300 lower (1.6 μg/mL in blood (Leslie et al., 2022), 0.073 μg/mL in surface waters and 0.000193 μg/mL in bottled drinking water (only PET detected) (Braun et al., 2021). One may assume that the constant exposure of humans to NMP may lead to their accumulation in tissues and blood, even exceeding environmental concentrations. However, whether an accumulation of NMP in human tissues and blood is realistic needs further investigation.

Here would like to emphasise that particle properties other than size or shape are rearly reported in these studies, although different properties can contribute to the particles' potential to cross biological barriers. To date, most studies used model NMP particles, like polystyrene spheres which do not resemble particles present within the exposure matrices. Environmentally relevant NMPs have various sizes and shapes with different surface modifications and are not uniform spherical particles of homogenous sizes. Furthermore, the use of model NMPs in effect studies has been considered insufficient since the choice of the commercial source of the model NMPs can significantly affect the experimental output, and the particles should be characterized in detail (Ramsperger et al., 2021). In contrast, weathered NMPs should be used

since it has been shown that an eco-corona (Ramsperger et al., 2020) or the artificial UV-aging of particles (Völkl et al., 2022) alters the surface of the particle leading to differences in the particle-cell interactions and cellular responses. This aspect is also highlighted by the fact that the MP found in human tissue samples is irregular, like fragments or fibres. To date, we have a discrepancy between the studies on the transport of spherical NMP across biological barriers and the properties of the particles described in the fate studies. Therefore, reliable statements of how non-spherical particles can potentially enter the tissues and whether the concentrations found in the tissues are meaningful cannot be made to date.

6.1. Risk assessments of NMP exposure to humans

The presence of NMP may cause oxidative stress and cytotoxicity, either due to the particles' physical or chemical properties or the exposed tissue's response (Prata et al., 2020). Altered metabolism, neurotoxicity, reproductive toxicity, and immune function disruption are also potential health risks (Prata et al., 2020; Rahman et al., 2021). However, these assumptions are predominantly based on observations in animal models or *in vitro* approaches. It remains unclear whether the toxicological effects observed in animal models are transferable to humans (SAPEA, 2019).

In general, it is doubted that without extensive standardization, representative reference materials, and inclusion of physicochemical properties and associated substances, a realistic assessment of human health risks is possible (Brachner et al., 2020; Vethaak and Legler, 2021). Toxic effects may also depend on specific properties such as shape, surface charge or residual monomers of the plastic particles. Kooi and Koelmans, therefore, propose to consider continuous scales for probabilistic risk assessment of microplastics (Kooi and Koelmans, 2019). Ultimately, however, the complex mixtures of different chemicals found in environmental samples of NMPs may present too high a hurdle to separate the different effects of combinations of chemicals and particles (Gouin et al., 2022). Recent studies pointed to the need for adopting tools and models to estimate the exposure and fate of NMPs to perform a risk assessment. For example, modelling human exposure to MP and the associated chemicals needs to consider MPs' characteristics and leaching rates of chemicals in a combined manner for a holistic risk assessment (e.g., Mohamed Nor et al., 2021). Screening and prioritization tools for hazard data are also needed to ensure the use of fit-for-purpose data for risk assessment (Gouin et al., 2022).

Overall, promising steps have been made toward identifying and prioritizing major research needs, limitations in microplastic risk assessment, and the development of the respective tools and models (Gouin et al., 2019; Mehinto et al., 2022). However, a fully operational human health risk assessment is not available to date. Even if only small fractions of NMP can overcome epithelial barriers, the long-term effects of persistent particles and associated chemicals should not be underestimated (Vethaak and Legler, 2021).

7. Conclusion

We describe in this review the various sources and exposure routes of how humans can come into contact with NMPs. We detected three main pathways of how NMPs enter food: First, the contamination of the environment with NMPs determines the contamination of food items (e. g., the contaminated waters determine the contamination of blue meat). Secondly, NMPs can enter food through industrial processing and thirdly, NMPs can enter food through packaging and atmospheric deposition. Concerning the sources, in almost all matrices, NMPs were detected, emphasizing various human exposure sources via drinking water, food, air and PCPs. It is widely accepted that as particle size decreases, interaction with tissue and individual cells increases. From the three exposure routes of NMPs to humans, size-dependent defence mechanisms occur for the skin and inhalation, whereas in principle

NMPs of any size can be ingested. The translocation through the skin is either restricted to particles in the lower nanometer size range or may occur via the transappendageal pathway, restricted to a very small percentage of the skin area (up to 1.3%). As described above, the respiratory system of humans is also equipped with size-dependent defense mechanisms, usually retaining larger NMPs before entering the deeper lung tissue. However, to date, the few studies on the fate of MPs in human tissues, also within the lung, detected particles in a size range of a few micrometers. The fact that it is often not stated in the presented studies which, or if, QA/QC measures were taken, makes it difficult to draw conclusions on the actual exposure level of biologically relevant particle sizes and whether the NMP found in human tissues and fluids are meaningful. Although first studies indicate the presence of small NMP in exposure matrices and human tissues and fluids, we highly recommend, to critically read and interpretate current literature, to not overinterpret the current understanding in NMP research regarding human health. Research into very small MPs and NPs is still in its infancy. Consistently further development of reliable methods for the isolation, purification and analysis of small MPs and NPs is urgently needed to make accurate statements regarding the exposure and fate of NMPs within the human body.

Author statement

All authors contributed to conceptualization, resources and funding acquisition. AFRMR, HK, JB, MGJL, CL, BG, CRL, SP and HPG wrote the introduction. AFRMR, MGJL, CL, HPG and DK wrote the chapter of NMP in drinking water. AFRMR, HK, JB, MGJL, CL, RP, AU, EB, MP, IF, FBa, FBe, MZ, AT and VM wrote the chapter of NMP in food. AFRMR, MGJL, CL, JD and FP wrote the chapter of NMP in PCPs. AFRMR, HK, JB, MGJL, CL, FBe, MZ, MN, HW, AKA, SZN, SEH, TKE, PG, BCB, KCN, EB, MP, IF and FBa wrote the chapter of NMP in indoor air and workplaces. AFRMR, HK, JB, MGJL, CL, FP, HW, AKA, SZN, SEH, TKE, PG, BCB and KCN wrote the chapter of NMP translocation. AFRMR, HK, JB, MGJL, CL wrote the chapter of NMP fate in the human body, abstract and conclusion. AFRM, JB, MGJL, CL, DK, BG, CRL and SP wrote the Reasons why reported studies should be interpreted critically and risk assessment. AFRMR, HK, JB, MGJL, CL wrote the first draft of the manuscript and all authors reviewed and edited the manuscript. JB and AFRMR designed the graphical abstract.

Declaration of Competing Interest

The authors declare no competing interests.

Data availability

No data was used for the research described in the article.

Acknowledgments:

References

Akhbarizadeh, R., Moore, F., Keshavarzi, B., 2019. Investigating microplastics bioaccumulation and biomagnification in seafood from the Persian Gulf: a threat to human health? Food Addit. Contam. - Part A Chem. Anal. Control. Expo. Risk Assess. 36, 1696–1708. https://doi.org/10.1080/19440049.2019.1649473.

Alexy, P., Anklam, E., Emans, T., Furfari, A., Galgani, F., Hanke, G., Koelmans, A., Pant, R., Saveyn, H., Sokull, B., Alexy, P., Anklam, E., Emans, T., Furfari, A., Galgani, F., Hanke, G., Koelmans, A., Pant, R., Saveyn, H., Kluettgen, B.S., 2020. Food additives & contaminants: part a managing the analytical challenges related to micro- and nanoplastics in the environment and food: filling the knowledge gaps.

Food Addit. Contam. Part A 37, 1–10. https://doi.org/10.1080/19440049.2019.1673905.

Amato-Lourenço, L.F., dos Santos Galvão, L., de Weger, L.A., Hiemstra, P.S., Vijver, M.G., Mauad, T., 2020. An emerging class of air pollutants: potential effects of microplastics to respiratory human health? Sci. Total Environ. 749, 141676 https://doi.org/10.1016/j.scitotenv.2020.141676.

Amato-Lourenço, L.F., Carvalho-Oliveira, R., Júnior, G.R., dos Santos Galvão, L., Ando, R.A., Mauad, T., 2021. Presence of airborne microplastics in human lung tissue. J. Hazard. Mater. 416 https://doi.org/10.1016/j.jhazmat.2021.126124.

Anagnosti, L., Varvaresou, A., Pavlou, P., Protopapa, E., 2021. Worldwide actions against plastic pollution from microbeads and microplastics in cosmetics focusing on European policies. Has the issue been handled effectively? Mar. Pollut. Bull. 162, 111883 https://doi.org/10.1016/j.marpolbul.2020.111883.

Arthur, C., Baker, J., Bamford, H., 2009. Proceedings of the International Research Workshop on the Occurrence, Effects, and Fate of Microplastic Marine Debris. Group 530.

Austen, K., MacLean, J., Balanzategui, D., Hölker, F., 2022. Microplastic inclusion in birch tree roots. Sci. Total Environ. 808 https://doi.org/10.1016/j.scitotenv.2021.152085.

Awara, W.M., El-Nabi, S.H., El-Gohary, M., 1998. Assessment of vinyl chloride-induced DNA damage in lymphocytes of plastic industry workers using a single-cell gel electrophoresis technique. Toxicology 128, 9–16. https://doi.org/10.1016/S0300-483X(98)00008-0.

Bain, C.C., Schridde, A., 2018. Origin, differentiation, and function of intestinal macrophages. Front. Immunol. 9, 1–15. https://doi.org/10.3389/fimmu.2018.02733.

Barboza, L.G.A., Lopes, C., Oliveira, P., Bessa, F., Otero, V., Henriques, B., Raimundo, J., Caetano, M., Vale, C., Guilhermino, L., 2020. Microplastics in wild fish from North East Atlantic Ocean and its potential for causing neurotoxic effects, lipid oxidative damage, and human health risks associated with ingestion exposure. Sci. Total Environ. 717, 134625 https://doi.org/10.1016/j.scitotenv.2019.134625.

Barnes, D.K.A., Galgani, F., Thompson, R.C., Barlaz, M., 2009. Accumulation and fragmentation of plastic debris in global environments. Philos. Trans. R. Soc. Lond. Ser. B Biol. Sci. 364, 1985–1998. https://doi.org/10.1098/rstb.2008.0205.

Bartley, David L., Feldman, Ray, 1984. Particulates not otherwise regulated, respirable. Method 0600 (3). https://www.cdc.gov/niosh/docs/2003-154/pdfs/0600.pdf.

Beaumont, N.J., Aanesen, M., Austen, M.C., Börger, T., Clark, J.R., Cole, M., Hooper, T., Lindeque, P.K., Pascoe, C., Wyles, K.J., 2019. Global ecological, social and economic impacts of marine plastic. Mar. Pollut. Bull. 142, 189–195. https://doi.org/10.1016/j.marpolbul.2019.03.022.

Bello, D., Chanetsa, L., Cristophi, C.A., Poh, T.Y., Singh, D., Setyawati, M.I., Christiani, D., Chotirmall, S.H., Ng, K.W., Demokritou, P., 2021. Chronic upper airway and systemic inflammation from copier emitted particles in healthy operators at six Singaporean workplaces. NanoImpact 22, 100325. https://doi.org/10.1016/j.impact.2021.100325.

van den Berg, P., Huerta-Lwanga, E., Corradini, F., Geissen, V., 2020. Sewage sludge application as a vehicle for microplastics in eastern Spanish agricultural soils. Environ. Pollut. 261, 114198 https://doi.org/10.1016/j.envpol.2020.114198.

Bianco, A., Passananti, M., 2020. Atmospheric micro and nanoplastics: An enormous microscopic problem. Sustain. 12 https://doi.org/10.1016/j.scitotenv.2020.141676.

Bitounis, D., Huang, Q., Toprani, S.M., Setyawati, M.I., Oliveira, N., Wu, Z., Tay, C.Y., Ng, K.W., Nagel, Z.D., Demokritou, P., 2022. Printer center nanoparticles alter the DNA repair capacity of human bronchial airway epithelial cells. NanoImpact 25, 100379. https://doi.org/10.1016/j.impact.2022.100379.

Boland, S., Baeza-Squiban, A., Fournier, T., Houcine, O., Gendron, M.C., Chévrier, M., Jouvenot, G., Coste, A., Aubier, M., Marano, F., 1999. Diesel exhaust particles are taken up by human airway epithelial cells in vitro and alter cytokine production. Am. J. Phys. Lung Cell. Mol. Phys. 276 https://doi.org/10.1152/ajplung.1999.276.4.l604.

Bos, J.D., Meinardi, M.M.H.M., 2000. The 500 Dalton rule for the skin penetration of chemical compounds and drugs. Exp. Dermatol. 9, 165–169. https://doi.org/10.1034/j.1600-0625.2000.009003165.x.

Bosker, T., Bouwman, L.J., Brun, N.R., Behrens, P., Vijver, M.G., 2019. Microplastics accumulate on pores in seed capsule and delay germination and root growth of the terrestrial vascular plant Lepidium sativum. Chemosphere 226, 774–781. https://doi.org/10.1016/j.chemosphere.2019.03.163.

Brachner, A., Fragouli, D., Duarte, I.F., Farias, P.M.A., Dembski, S., Ghosh, M., Barisic, I., Zdzieblo, D., Vanoirbeek, J., Schwabl, P., Neuhaus, W., 2020. Assessment of human health risks posed by nano-and microplastics is currently not feasible. Int. J. Environ. Res. Public Health 17, 1–10. https://doi.org/10.3390/ijerph17238832.

Brander, S.M., Renick, V.C., Foley, M.M., Steele, C., Woo, M., Lusher, A., Carr, S., Helm, P., Box, C., Cherniak, S., Andrews, R.C., Rochman, C.M., 2020. Sampling and quality assurance and quality control: a guide for scientists investigating the occurrence of microplastics across matrices. Appl. Spectrosc. 74, 1099–1125. https://doi.org/10.1177/0003702820945713.

Braun, T., Ehrlich, L., Henrich, W., Koeppel, S., Lomako, I., Schwabl, P., Liebmann, B., 2021. Detection of microplastic in human placenta and meconium in a clinical setting. Pharmaceutics 13, 1–12. https://doi.org/10.3390/pharmaceutics13070921.

Burgener, K., Bhamla, M.S., 2021. A polymer-based technique to remove pollutants from soft contact lenses. Contact Lens Anterior Eye 44. https://doi.org/10.1016/j.clae.2020.05.004, 0–1.

Burkhart, J., Piacitelli, C., Schwegler-Berry, D., Jones, W., 1999. Environmental study of nylon flocking process. J. Toxicol. Environ. Heal. - Part A 57, 1–23. https://doi.org/10.1080/009841099157836.

Buzea, C., Pacheco, I.I., Robbie, K., 2007. Nanomaterials and nanoparticles: sources and toxicity. Biointerphases 2. https://doi.org/10.1116/1.2815690. MR17–MR71.

15

Campagnolo, L., Massimiani, M., Vecchione, L., Piccirilli, D., Toschi, N., Magrini, A., Bonanno, E., Scimeca, M., Buonanno, G., Stabile, L., Cubadda, F., Fokkens, P.H.B., Kreyling, W.G., Cassee, F.R., 2017. ce pt. Nanotoxicology 0, 000. https://doi.org/10.1080/17435390.2017.1343875.

Campanale, C., Massarelli, C., Savino, I., Locaputo, V., Uricchio, V.F., 2020. A detailed review study on potential effects of microplastics and additives of concern on human health. Int. J. Environ. Res. Public Health 17. https://doi.org/10.3390/ijerph17041212.

Carpenter, E.J., Smith, K.L., 1972. Plastics on the Sargasso Sea Surface. Science (80-.) 175, 1240–1241. https://doi.org/10.1126/science.175.4027.1240.

Chen, G., Feng, Q., Wang, J., 2019. Mini-review of microplastics in the atmosphere and their risks to humans. Sci. Total Environ. 135504 https://doi.org/10.1016/j.scitotenv.2019.135504.

Chen, G., Fu, Z., Yang, H., Wang, J., 2020. An overview of analytical methods for detecting microplastics in the atmosphere. TrAC - Trends Anal. Chem. 130, 115981 https://doi.org/10.1016/j.trac.2020.115981.

Coffin, S., Bouwmeester, H., Brander, S., Damdimopoulou, P., Gouin, T., Hermabessiere, L., Khan, E., Koelmans, A.A., Lemieux, C.L., Teerds, K., Wagner, M., Weisberg, S.B., Wright, S., 2022. Development and application of a health-based framework for informing regulatory action in relation to exposure of microplastic particles in California drinking water. Microplast. Nanoplast. 2 https://doi.org/10.1186/s43591-022-00030-6.

Cooper, D.M., Loxham, M., 2019. Particulate matter and the airway epithelium: the special case of the underground? Eur. Respir. Rev. 28 https://doi.org/10.1183/16000617.0066-2019.

Corradini, F., Meza, P., Eguiluz, R., Casado, F., Huerta-Lwanga, E., Geissen, V., 2019. Evidence of microplastic accumulation in agricultural soils from sewage sludge disposal. Sci. Total Environ. 671, 411–420. https://doi.org/10.1016/j.scitotenv.2019.03.368.

Costa Filho, P.A., Andrey, D., Eriksen, B., Peixoto, R., Carreres, B.M., Ambühl, M., Descarrega, J.B., Dubascoux, S., Zbinden, P., Panchaud, A., Poitevin, E., 2021. Detection and characterization of small-sized microplastics (≥4 μm) in milk products (Pre-Proof). Res. Sq. 1–19 https://doi.org/10.21203/rs.3.rs-257514/v1.

Cox, K.D., Covernton, G.A., Davies, H.L., Dower, J.F., Juanes, F., Dudas, S.E., 2019. Human consumption of microplastics. Environ. Sci. Technol. 53, 7068–7074. https://doi.org/10.1021/acs.est.9b01517.

Daniel, D.B., Ashraf, P.M., Thomas, S.N., 2020a. Microplastics in the edible and inedible tissues of pelagic fishes sold for human consumption in Kerala. India. Environ. Pollut. 266, 115365 https://doi.org/10.1016/j.envpol.2020.115365.

Daniel, D.B., Ashraf, P.M., Thomas, S.N., 2020b. Abundance, characteristics and seasonal variation of microplastics in Indian white shrimps (Fenneropenaeus indicus) from coastal waters off Cochin, Kerala. India. Sci. Total Environ. 737, 139839 https://doi.org/10.1016/j.scitotenv.2020.139839.

Daniel, D.B., Ashraf, P.M., Thomas, S.N., Thomson, K.T., 2021. Microplastics in the edible tissues of shellfishes sold for human consumption. Chemosphere 264, 128554. https://doi.org/10.1016/j.chemosphere.2020.128554.

Danopoulos, E., Twiddy, M., Rotchell, J.M., 2020. Microplastic contamination of drinking water: a systematic review. PLoS One 15, 1–23. https://doi.org/10.1371/journal.pone.0236838.

Danopoulos, E., Twiddy, M., West, R., Rotchell, J.M., 2021. A rapid review and meta-regression analyses of the toxicological impacts of microplastic exposure in human cells. J. Hazard. Mater. 127861 https://doi.org/10.1016/j.jhazmat.2021.127861.

DeLoid, G.M., Cao, X., Bitounis, D., Singh, D., Llopis, P.M., Buckley, B., Demokritou, P., 2021. Toxicity, uptake, and nuclear translocation of ingested micro-nanoplastics in an in vitro model of the small intestinal epithelium. Food Chem. Toxicol. 158, 112609 https://doi.org/10.1016/j.fct.2021.112609.

Desai, P., Patlolla, R.R., Singh, M., 2010. Interaction of nanoparticles and cell-penetrating peptides with skin for transdermal drug delivery. Mol. Membr. Biol. 27, 247–259. https://doi.org/10.3109/09687688.2010.522203.

Dessì, C., Okoffo, E.D., O'Brien, J.W., Gallen, M., Samanipour, S., Kaserzon, S., Rauert, C., Wang, X., Thomas, K.V., 2021. Plastics contamination of store-bought rice. J. Hazard. Mater. 416, 125778 https://doi.org/10.1016/j.jhazmat.2021.125778.

Diaz-Basantes, M.F., Conesa, J.A., Fullana, A., 2020. Microplastics in honey, beer, milk and refreshments in Ecuador as emerging contaminants. Sustain. 12 https://doi.org/10.3390/SU12145514.

Domenech, J., Marcos, R., 2021. Pathways of human exposure to microplastics, and estimation of the total burden. Curr. Opin. Food Sci. 39, 144–151. https://doi.org/10.1016/j.cofs.2021.01.004.

Dong, Y., Gao, M., Song, Z., Qiu, W., 2020. Microplastic particles increase arsenic toxicity to rice seedlings. Environ. Pollut. 259, 113892 https://doi.org/10.1016/j.envpol.2019.113892.

Dong, Y., Gao, M., Qiu, W., Song, Z., 2021. Uptake of microplastics by carrots in presence of As (III): combined toxic effects. J. Hazard. Mater. 411, 125055 https://doi.org/10.1016/j.jhazmat.2021.125055.

Dris, R., Gasperi, J., Mirande, C., Mandin, C., Guerrouache, M., Langlois, V., Tassin, B., 2017. A first overview of textile fibers, including microplastics, in indoor and outdoor environments. Environ. Pollut. 221, 453–458. https://doi.org/10.1016/j.envpol.2016.12.013.

Du Preez, J., Johnson, A., LeBouf, R.F., Linde, S.J.L., Stefaniak, A.B., Du Plessis, J., 2018. Exposures during industrial 3-D printing and post-processing tasks. Rapid Prototyp. J. 24, 865–871. https://doi.org/10.1108/RPJ-03-2017-0050.

Eerkes-medrano, D., Leslie, H.A., Quinn, B., 2018. SC. Curr. Opin. Environ. Sci. Heal. https://doi.org/10.1016/j.coesh.2018.12.001.

EFSA CONTAM Panel, 2016. Statement on the presence of microplastics and nanoplastics in food, with particular focus on seafood. EFSA J. 14 (4501), 30pp. https://doi.org/10.2903/j.efsa.2016.4501.

Enders, K., Lenz, R., Ivar do Sul, J.A., Tagg, A.S., Labrenz, M., 2020. When every particle matters: a QuEChERS approach to extract microplastics from environmental samples. MethodsX 7, 100784. https://doi.org/10.1016/j.mex.2020.100784.

EPA, 1987. The Total Exposure Assessment Methodology (TEAM) Study.

European Commission, 2013. Glossary and Acronyms Related to Cosmetics Legislation. European Commission, Brussels, Belgium. Ref. Ares(2015)4230487 - 12/10/2015.

European Food Safety Authority, 2015. The food classification and description system FoodEx 2 (revision 2). EFSA Support. Publ. 12, 1–90. https://doi.org/10.2903/sp.efsa.2015.en-804.

European Food Safety Authority, 2021. FoodEx2 maintenance 2020. EFSA Support. Publ. 18 https://doi.org/10.2903/sp.efsa.2021.en-6507.

Facciolà, A., Visalli, G., Ciarello, M.P., Di Pietro, A., 2021. Newly emerging airborne pollutants: current knowledge of health impact of micro and nanoplastics. Int. J. Environ. Res. Public Health 18, 1–17. https://doi.org/10.3390/ijerph18062997.

Fadare, O.O., Okoffo, E.D., Olasehinde, E.F., 2021. Microparticles and microplastics contamination in African table salts. Mar. Pollut. Bull. 164, 112006 https://doi.org/10.1016/j.marpolbul.2021.112006.

FAO, 2013. Milk and dairy products in human nutrition. Nutrit. Biochem. Milk/Mainten. https://doi.org/10.1016/b978-0-12-436703-6.50013-2.

FAO, 2020. The state of world fisheries and aquaculture 2020. Sustainability in action. https://doi.org/10.4060/ca9229en.

FDA, 2016. Are all personal care products regulated as cosmetics? U.S. Food Drug Adm., p. 2005076

Feng, Z., Wang, R., Zhang, T., Wang, J., Huang, W., Li, J., Xu, J., Gao, G., 2020. Microplastics in specific tissues of wild sea urchins along the coastal areas of northern China. Sci. Total Environ. 728, 138660 https://doi.org/10.1016/j.scitotenv.2020.138660.

Fischer, M., Goßmann, I., Scholz-Böttcher, B.M., 2019. Fleur de Sel—An interregional monitor for microplastics mass load and composition in European coastal waters? J. Anal. Appl. Pyrolysis 144. https://doi.org/10.1016/j.jaap.2019.104711.

Foged, C., Brodin, B., Frokjaer, S., Sundblad, A., 2005. Particle size and surface charge affect particle uptake by human dendritic cells in an in vitro model. Int. J. Pharm. 298, 315–322. https://doi.org/10.1016/j.ijpharm.2005.03.035.

Food, E., Authority, S., 2011. Report on the development of a food classification and description system for exposure assessment and guidance on its implementation and use. EFSA J. 9, 1–84. https://doi.org/10.2903/j.efsa.2011.2489.

Fournier, S.B., D'Errico, J.N., Adler, D.S., Kollontzi, S., Goedken, M.J., Fabris, L., Yurkow, E.J., Stapleton, P.A., 2020. Nanopolystyrene translocation and fetal deposition after acute lung exposure during late-stage pregnancy. Part. Fibre Toxicol. 17, 1–11. https://doi.org/10.1186/s12989-020-00385-9.

Gabriel, L., Barboza, A., Carolina, B., Gimenez, G., 2015. Microplastics in the marine environment: current trends and future perspectives. Mar. Pollut. Bull. 97, 5–12. https://doi.org/10.1016/j.marpolbul.2015.06.008.

Galafassi, S., Campanale, C., Massarelli, C., Uricchio, V.F., Volta, P., 2021. Do freshwater fish eat microplastics? A review with a focus on effects on fish health and predictive traits of mps ingestion. Water (Switzerland) 13, 1–20. https://doi.org/10.3390/w13162214.

Gallo, M.F., Grimes, D.A., Lopez, L.M., Schulz, K.F., 2006. Nonlatex versus latex male condoms for contraception. Cochrane Database Syst. Rev. https://doi.org/10.1002/14651858.cd003550.pub2.

Galloway, T.S., Dogra, Y., Garrett, N., Rowe, D., Tyler, C.R., Moger, J., Lammer, E., Landsiedel, R., Sauer, U.G., Scherer, G., Wohlleben, W., Wiench, K., 2017. Ecotoxicological assessment of nanoparticle-containing acrylic copolymer dispersions in fairy shrimp and zebrafish embryos. Environ. Sci. Nano 4, 1981–1997. https://doi.org/10.1039/c7en00385d.

GESAMP Joint Group of Experts on the Scientific Aspects of Marine Environmental Protection, 2016. Sources, Fate and Effects of Microplastics in the Marine Environment: Part 2 of a global Assessment. Reports Stud. GESAMP. No. 93, 96 p. 93.

Getzlaff, M., Leifels, M., Weber, P., Kökcam-Demir, Janiak, C., 2019. Nanoparticles in toner material. SN Appl. Sci. 1, 1–14. https://doi.org/10.1007/s42452-019-0501-9.

Geyer, R., Jambeck, J.R., Law, K.L., 2017. Production, use, and fate of all plastics ever made. Sci. Adv. 3, 25–29. https://doi.org/10.1126/sciadv.1700782.

Gigault, J., Halle, Ater, Baudrimont, M., Pascal, P.Y., Gauffre, F., Phi, T.L., El Hadri, H., Grassl, B., Reynaud, S., 2018. Current opinion: What is a nanoplastic? Environ. Pollut. 235, 1030–1034. https://doi.org/10.1016/j.envpol.2018.01.024.

Girão, A.V., 2020. SEM/EDS and Optical Microscopy Analysis of Microplastics. In: Rocha-Santos, T., Costa, M., Mouneyrac, C. (Eds.), Handb. Microplastics Environ. Springer, Cham. https://doi.org/10.1007/978-3-030-10618-8_7-1.

Gkoutselis, G., Rohrbach, S., Harjes, J., Obst, M., Brachmann, A., Horn, M.A., Rambold, G., 2021. Microplastics accumulate fungal pathogens in terrestrial ecosystems. Sci. Rep. 11, 1–13. https://doi.org/10.1038/s41598-021-92405-7.

Golden, C.D., Allison, E.H., Cheung, W.W.L., Dey, M.M., Halpern, B.S., McCauley, D.J., Smith, M., Vaitla, B., Zeller, D., Myers, S.S., 2016. Nutrition: Fall in fish catch threatens human health. Nature 534, 317–320. https://doi.org/10.1038/534317a.

Gouin, T., Brunning, I., 2015. Use of Micro-Plastic Beads in Cosmetic Products in Europe and Their Estimated Emissions to the North Sea Environment.

Gouin, T., Becker, R.A., Collot, A.G., Davis, J.W., Howard, B., Inawaka, K., Lampi, M., Ramon, B.S., Shi, J., Hopp, P.W., 2019. Toward the development and application of an environmental risk assessment framework for microplastic. Environ. Toxicol. Chem. 38, 2087–2100. https://doi.org/10.1002/etc.4529.

Gouin, T., Ellis-Hutchings, R., Thornton Hampton, L.M., Lemieux, C.L., Wright, S.L., 2022. Screening and prioritization of nano- and microplastic particle toxicity studies

16

for evaluating human health risks – development and application of a toxicity study assessment tool. Microplast. Nanoplast. 2 https://doi.org/10.1186/s43591-021-00023-x.

Grainger, J.R., Konkel, J.E., Zangerle-Murray, T., Shaw, T.N., 2017. Macrophages in gastrointestinal homeostasis and inflammation. Pflugers Arch. - Eur. J. Physiol. 469, 527–539. https://doi.org/10.1007/s00424-017-1958-2.

Gündoğdu, S., 2018. Contamination of table salts from Turkey with microplastics. Food Addit. Contam. Part A 35, 1006–1014. https://doi.org/10.1080/19440049.2018.1447694.

Gündoğdu, S., Çevik, C., Ataş, N.T., 2020. Stuffed with microplastics: Microplastic occurrence in traditional stuffed mussels sold in the Turkish market. Food Biosci. 37, 100715 https://doi.org/10.1016/j.fbio.2020.100715.

Hale, R.C., Seeley, M.E., La Guardia, M.J., Mai, L., Zeng, E.Y., 2020. A global perspective on microplastics. J. Geophys. Res. Ocean. 125, 1–40. https://doi.org/10.1029/2018JC014719.

Hampton, H.R., Chtanova, T., 2019. Lymphatic migration of immune cells. Front. Immunol. 10, 19–23. https://doi.org/10.3389/fimmu.2019.01168.

Harms, I.K., Diekötter, T., Troegel, S., Lenz, M., 2021. Amount, distribution and composition of large microplastics in typical agricultural soils in Northern Germany. Sci. Total Environ. 758, 143615 https://doi.org/10.1016/j.scitotenv.2020.143615.

Hartmann, N.B., Hüffer, T., Thompson, R.C., Hassellöv, M., Verschoor, A., Daugaard, A. E., Rist, S., Karlsson, T., Brennholt, N., Cole, M., Herrling, M.P., Hess, M.C., Ivleva, N. P., Lusher, A.L., Wagner, M., 2019. Are we speaking the same language? Recommendations for a definition and categorization framework for plastic Debris. Environ. Sci. Technol. 53, 1039–1047. https://doi.org/10.1021/acs.est.8b05297.

Herath, M., Hosie, S., Bornstein, J.C., Franks, A.E., Hill-Yardin, E.L., 2020. The Role of the gastrointestinal mucus system in intestinal homeostasis: implications for neurological disorders. Front. Cell. Infect. Microbiol. 10 https://doi.org/10.3389/fcimb.2020.00248.

Hernandez, L.M., Xu, E.G., Larsson, H.C.E., Tahara, R., Maisuria, V.B., Tufenkji, N., 2019. Plastic teabags release billions of microparticles and nanoparticles into tea. Environ. Sci. Technol. 53, 12300–12310. https://doi.org/10.1021/acs.est.9b02540.

Hesler, M., Aengenheister, L., Ellinger, B., Drexel, R., Straskraba, S., Jost, C., Wagner, S., Meier, F., von Briesen, H., Büchel, C., Wick, P., Buerki-Thurnherr, T., Kohl, Y., 2019. Multi-endpoint toxicological assessment of polystyrene nano- and microparticles in different biological models in vitro. Toxicol. in Vitro 61, 104610. https://doi.org/10.1016/j.tiv.2019.104610.

Horvatits, T., Tamminga, M., Liu, B., Sebode, M., Kerstin, E., 2022. Articles Microplastics Detected in Cirrhotic Liver Tissue, 82, pp. 1–10. https://doi.org/10.1016/j.ebiom.2022.104147.

Hou, Z., Meng, R., Chen, G., Lai, T., Qing, R., Hao, S., Deng, J., Wang, B., 2022. Distinct accumulation of nanoplastics in human intestinal organoids. Sci. Total Environ. 155811 https://doi.org/10.1016/j.scitotenv.2022.155811.

Huang, S., Huang, X., Bi, R., Guo, Q., Yu, X., Zeng, Q., Huang, Z., Liu, T., Wu, H., Chen, Y., Xu, J., Wu, Y., Guo, P., 2022. Detection and analysis of microplastics in human sputum. Environ. Sci. Technol. https://doi.org/10.1021/acs.est.1c03859.

Huang, Y., Chapman, J., Deng, Y., Cozzolino, D., 2020. Rapid measurement of microplastic contamination in chicken meat by mid infrared spectroscopy and chemometrics: a feasibility study. Food Control 113, 107187. https://doi.org/10.1016/j.foodcont.2020.107187.

Huang, Z., Weng, Y., Shen, Q., Zhao, Y., Jin, Y., 2021. Microplastic: A potential threat to human and animal health by interfering with the intestinal barrier function and changing the intestinal microenvironment. Sci. Total Environ. 785, 147365 https://doi.org/10.1016/j.scitotenv.2021.147365.

Huerta Lwanga, E., Mendoza Vega, J., Ku Quej, V., Chi, J. de los A., Sanchez del Cid, L., Chi, C., Escalona Segura, G., Gertsen, H., Salánki, T., van der Ploeg, M., Koelmans, A. A., Geissen, V., 2017. Field evidence for transfer of plastic debris along a terrestrial food chain. Sci. Rep. 7, 1–7. https://doi.org/10.1038/s41598-017-14588-2.

Hussain, N., Jaitley, V., Florence, A.T., 2001. Recent advances in the understanding of uptake of microparticulates across the gastrointestinal lymphatics. Adv. Drug Deliv. Rev. 50, 107–142. https://doi.org/10.1016/S0169-409X(01)00152-1.

Ibrahim, Y.S., Anuar, S.T., Azmi, A.A., Mohd, W., Lehata, S., Hamzah, S.R., Ma, Z.F., Dzulkarnaen, A., Zakaria, Z., Mustaffa, N., Emilia, S., Sharif, T., Lee, Y.Y., 2021. Detection of Microplastics in Human Colectomy Specimens, 5, pp. 116–121. https://doi.org/10.1002/jgh3.12457.

Iñiguez, M.E., Conesa, J.A., Fullana, A., 2017. Microplastics in spanish table salt. Sci. Rep. 7, 1–7. https://doi.org/10.1038/s41598-017-09128-x.

Jambeck, J.R., Geyer, R., Wilcox, C., Siegler, T.R., Perryman, M., Andrady, A., Narayan, R., Law, K.L., 2015. Plastic waste inputs from land into the ocean. Science (80) 347. https://doi.org/10.1126/science.1260352.

Jani, P., Halbert, G.W., Langridge, J., Florence, A.T., 1990. Nanoparticle uptake by the rat gastrointestinal mucosa: quantitation and particle size dependency. J. Pharm. Pharmacol. 42, 821–826. https://doi.org/10.1111/j.2042-7158.1990.tb07033.x.

Jenner, L.C., Sadofsky, L.R., Danopoulos, E., Rotchell, J.M., 2021. Household indoor microplastics within the Humber region (United Kingdom): Quantification and chemical characterisation of particles present. Atmos. Environ. 259, 118512 https://doi.org/10.1016/j.atmosenv.2021.118512.

Jenner, L.C., Rotchell, J.M., Bennett, R.T., Cowen, M., Tentzeris, V., Sadofsky, L.R., 2022. Detection of microplastics in human lung tissue using μFTIR spectroscopy. Sci. Total Environ. 831, 154907 https://doi.org/10.1016/j.scitotenv.2022.154907.

Kankanige, D., Babel, S., 2020. Smaller-sized micro-plastics (MPs) contamination in single-use PET-bottled water in Thailand. Sci. Total Environ. 717, 137232 https://doi.org/10.1016/j.scitotenv.2020.137232.

Karami, A., Golieskardi, A., Choo, C.K., Larat, V., Karbalaei, S., Salamatinia, B., 2018. Microplastic and mesoplastic contamination in canned sardines and sprats. Science

of The Total Environment 612, 1380–1386. https://doi.org/10.1016/j.scitotenv.2017.09.005. ISSN 0048-9697.

Karami, A., Golieskardi, A., Ho, Y. Bin, Larat, V., Salamatinia, B., 2017a. Microplastics in eviscerated flesh and excised organs of dried fish. Sci. Rep. 7, 1–9. https://doi.org/10.1038/s41598-017-05828-6.

Karami, A., Golieskardi, A., Keong Choo, C., Larat, V., Galloway, T.S., Salamatinia, B., 2017b. The presence of microplastics in commercial salts from different countries. Sci. Rep. 7, 46173. https://doi.org/10.1038/srep46173.

Katare, Y., Singh, P., Sankhla, M.S., Singhal, M., Jadhav, E.B., Parihar, K., Nikalje, B.T., Trpathi, A., Bhardwaj, L., 2022. Microplastics in aquatic environments: sources, ecotoxicity, detection & remediation. Biointerface Res. Appl. Chem. 12, 3407–3428. https://doi.org/10.33263/BRIAC123.34073428.

Kedzierski, M., Lechat, B., Sire, O., Le Maguer, G., Le Tilly, V., Bruzaud, S., 2020. Microplastic contamination of packaged meat: occurrence and associated risks. Food Packag. Shelf Life 24, 100489. https://doi.org/10.1016/j.fpsl.2020.100489.

Kentin, E., Kaarto, H., 2018. An EU ban on microplastics in cosmetic products and the right to regulate. Rev. Eur. Comp. Int. Environ. Law 27, 254–266. https://doi.org/10.1111/reel.12269.

Kernchen, S., Löder, M.G.J., Fischer, F., Fischer, D., Moses, S.R., Georgi, C., Nölscher, A. C., Held, A., Laforsch, C., 2021. Airborne microplastic concentrations and deposition across the Weser River catchment. Sci. Total Environ. 151812 https://doi.org/10.1016/j.scitotenv.2021.151812.

Kettner, M.T., Oberbeckmann, S., Labrenz, M., Grossart, H.P., 2019. The eukaryotic life on microplastics in brackish ecosystems. Front. Microbiol. 10 https://doi.org/10.3389/fmicb.2019.00538.

Kim, J.S., Lee, H.J., Kim, S.K., Kim, H.J., 2018. Global pattern of microplastics (MPs) in commercial food-grade salts: sea salt as an indicator of seawater MP pollution. Environ. Sci. Technol. 52, 12819–12828. https://doi.org/10.1021/acs.est.8b04180.

Kirstein, I.V., Kirmizi, S., Wichels, A., Garin-Fernandez, A., Erler, R., Löder, M., Gerdts, G., 2016. Dangerous hitchhikers? Evidence for potentially pathogenic Vibrio spp. on microplastic particles. Mar. Environ. Res. 120, 1–8. https://doi.org/10.1016/j.marenvres.2016.07.004.

Kleih, P.U., Greenhalgh, P., Marter, A., Peacock, N., Fisheries, N.A.P., 2006. Sustainability Impact Assessment of Proposed Wto Negotiations Final Report for the 2005.

Klemeš, J.J., Fan, Y.V., Jiang, P., 2020. Plastics: friends or foes? The circularity and plastic waste footprint. Util. Environ. Eff. 00, 1–17. https://doi.org/10.1080/15567036.2020.1801906.

Koelmans, A.A., Mohamed Nor, N.H., Hermsen, E., Kooi, M., Mintenig, S.M., De France, J., 2019. Microplastics in freshwaters and drinking water: critical review and assessment of data quality. Water Res. 155, 410–422. https://doi.org/10.1016/j.watres.2019.02.054.

Koelmans, A.A., Redondo-hasselerharm, P.E., Hazimah, N., Nor, M., Kooi, M., 2020. Solving the Nonalignment of Methods and Approaches Used in Microplastic Research to Consistently Characterize Risk. https://doi.org/10.1021/acs.est.0c02982.

Kohli, A.K., Alpar, H.O., 2004. Potential use of nanoparticles for transcutaneous vaccine delivery: Effect of particle size and charge. Int. J. Pharm. 275, 13–17. https://doi.org/10.1016/j.ijpharm.2003.10.038.

Kooi, M., Koelmans, A.A., 2019. Simplifying microplastic via continuous probability distributions for size, shape,and density. Environ. Sci. Technol. Lett. 6, 551–557. https://doi.org/10.1021/acs.estlett.9b00379.

Kosuth, M., Mason, S.A., Wattenberg, E.V., 2018. Anthropogenic contamination of tap water, beer, and sea salt. PLoS One 13, 1–18. https://doi.org/10.1371/journal.pone.0194970.

Kumar, B.N.V., Löschel, Lena A., Imhof, Hannes K., Löder, Martin G.J., Laforsch, Christian, 2021. Analysis of microplastics of a broad size range in commercially important mussels by combining FTIR and Raman spectroscopy approaches. Environmental Pollution 269, 116147. https://doi.org/10.1016/j.envpol.2020.116147. ISSN 0269-7491.

Kutralam-Muniasamy, G., Pérez-Guevara, F., Elizalde-Martínez, I., Shruti, V.C., 2020. Branded milks – Are they immune from microplastics contamination? Sci. Total Environ. 714, 136823 https://doi.org/10.1016/j.scitotenv.2020.136823.

Lambert, S., Johnson, C., Keller, V.D.J., Sinclair, C.J., Williams, R.J., Boxall, A.B.A., 2013. Do natural rubber latex condoms pose a risk to aquatic systems? Environ Sci Process Impacts 15, 2312–2320. https://doi.org/10.1039/c3em00422h.

Larese Filon, F., Mauro, M., Adami, G., Bovenzi, M., Crosera, M., 2015. Nanoparticles skin absorption: new aspects for a safety profile evaluation. Regul. Toxicol. Pharmacol. 72, 310–322. https://doi.org/10.1016/j.yrtph.2015.05.005.

Lebreton, L., Andrady, A., 2019. Future scenarios of global plastic waste generation and disposal. Palgrave Commun. 5, 1–11. https://doi.org/10.1057/s41599-018-0212-7.

Lee, H., Kunz, A., Shim, W.J., Walther, B.A., 2019. Microplastic contamination of table salts from Taiwan, including a global review. Sci. Rep. 9, 1–9. https://doi.org/10.1038/s41598-019-46417-z.

Lei, K., Qiao, F., Liu, Q., Wei, Z., Qi, H., Cui, S., Yue, X., Deng, Y., 2017. Microplastics releasing from personal care and cosmetic products in China. Mar. Pollut. Bull. 0–1 https://doi.org/10.1016/j.marpolbul.2017.09.016.

Leslie, H.A., van Velzen, M.J.M., Brandsma, S.H., Vethaak, A.D., Garcia-Vallejo, J.J., Lamoree, M.H., 2022. Discovery and quantification of plastic particle pollution in human blood. Environ. Int. 163, 107199 https://doi.org/10.1016/j.envint.2022.107199.

Li, Q., Feng, Z., Zhang, T., Ma, C., Shi, H., 2020. Microplastics in the commercial seaweed nori. J. Hazard. Mater. 388, 122060 https://doi.org/10.1016/j.jhazmat.2020.122060.

17

Li, Z., Li, Q., Li, R., Zhou, J., Wang, G., 2021. The distribution and impact of polystyrene nanoplastics on cucumber plants. Environ. Sci. Pollut. Res. 28, 16042–16053. https://doi.org/10.1007/s11356-020-11702-2.

Lian, J., Liu, W., Meng, L., Wu, J., Zeb, A., Cheng, L., Lian, Y., Sun, H., 2021. Effects of microplastics derived from polymer-coated fertilizer on maize growth, rhizosphere, and soil properties. J. Clean. Prod. 318, 128571 https://doi.org/10.1016/j.jclepro.2021.128571.

Liao, Z., Ji, X., Ma, Y., Lv, B., Huang, W., Zhu, X., 2021. Airborne microplastics in indoor and outdoor environments of a coastal city in Eastern China. J. Hazard. Mater. 417, 126007 https://doi.org/10.1016/j.jhazmat.2021.126007.

Liebezeit, G., Liebezeit, E., 2013. Non-pollen particulates in honey and sugar. Food Addit. Contam. - Part A Chem. Anal. Control. Expo. Risk Assess. 30, 2136–2140. https://doi.org/10.1080/19440049.2013.843025.

Liebezeit, G., Liebezeit, E., 2015. Origin of synthetic particles in honeys. Polish J. Food Nutr. Sci. 65, 143–147. https://doi.org/10.1515/pjfns-2015-0025.

Liu, C., Li, J., Zhang, Y., Wang, L., Deng, J., Gao, Y., Yu, L., Zhang, J., Sun, H., 2019. Widespread distribution of PET and PC microplastics in dust in urban China and their estimated human exposure. Environ. Int. 128, 116–124. https://doi.org/10.1016/j.envint.2019.04.024.

Löder, M.G.J., Imhof, H.K., Ladehoff, M., Löschel, L.A., Lorenz, C., Mintenig, S., Piehl, S., Primpke, S., Schrank, I., Laforsch, C., Gerdts, G., 2017. Enzymatic purification of microplastics in environmental samples. Environ. Sci. Technol. 51, 14283–14292. https://doi.org/10.1021/acs.est.7b03055.

Lu, L., Wan, Z., Luo, T., Fu, Z., Jin, Y., 2018. Polystyrene microplastics induce gut microbiota dysbiosis and hepatic lipid metabolism disorder in mice. Sci. Total Environ. 631–632, 449–458. https://doi.org/10.1016/j.scitotenv.2018.03.051.

Makhdoumi, P., Amin, A.A., Karimi, H., Pirsaheb, M., Kim, H., Hossini, H., 2021. Occurrence of microplastic particles in the most popular Iranian bottled mineral water brands and an assessment of human exposure. J. Water Process Eng. 39, 101708 https://doi.org/10.1016/j.jwpe.2020.101708.

Mason, S.A., Welch, V.G., Neratko, J., 2018. Synthetic polymer contamination in bottled water. Front. Chem. 6 https://doi.org/10.3389/fchem.2018.00407.

Mehinto, A.C., Coffin, S., Koelmans, A.A., Brander, S.M., Wagner, M., Thornton Hampton, L.M., Burton, A.G., Miller, E., Gouin, T., Weisberg, S.B., Rochman, C.M., 2022. Risk-based management framework for microplastics in aquatic ecosystems. Microplast. Nanoplast. 2 https://doi.org/10.1186/s43591-022-00033-3.

Meides, N., Menzel, T., Poetzschner, B., Löder, M.G.J., Mansfeld, U., Strohriegl, P., Altstaedt, V., Senker, J., 2021. Reconstructing the environmental degradation of polystyrene by accelerated weathering. Environ. Sci. Technol. 55, 7930–7938. https://doi.org/10.1021/acs.est.0c07718.

Mercogliano, R., Avio, C.G., Regoli, F., Anastasio, A., Colavita, G., Santonicola, S., 2020. Occurrence of microplastics in commercial seafood under the perspective of the human food chain. A review. J. Agric. Food Chem. 68, 5296–5301. https://doi.org/10.1021/acs.jafc.0c01209.

Miller, M.R., Raftis, J.B., Langrish, J.P., McLean, S.G., Samutrtai, P., Connell, S.P., Wilson, S., Vesey, A.T., Fokkens, P.H.B., Boere, A.J.F., Krystek, P., Campbell, C.J., Hadoke, P.W.F., Donaldson, K., Cassee, F.R., Newby, D.E., Duffin, R., Mills, N.L., 2017. Inhaled nanoparticles accumulate at sites of vascular disease. ACS Nano 11, 4542–4552. https://doi.org/10.1021/acsnano.6b08551.

Mohamed Nor, N.H., Koelmans, A., Kooi, M., Diepens, N., 2021. Lifetime accumulation of microplastic in children and adults. Environ. Sci. Technol. 55, 5084–5096. https://doi.org/10.1021/acs.est.0c07384.

Möller, J.N., Löder, M.G.J., Laforsch, C., 2020. Finding microplastics in soils: a review of analytical methods. Environ. Sci. Technol. 54, 2078–2090. https://doi.org/10.1021/acs.est.9b04618.

Mühlschlegel, P., Hauk, A., Walter, U., Sieber, R., 2017. Lack of evidence for microplastic contamination in honey. Food Addit. Contam. - Part A Chem. Anal. Control. Expo. Risk Assess. 34, 1982–1989. https://doi.org/10.1080/19440049.2017.1347281.

Munoz, L.P., Baez, A.G., Purchase, D., Jones, H., Garelick, H., 2022. Release of microplastic fibres and fragmentation to billions of nanoplastics from period products: preliminary assessment of potential health implications. Environ. Sci. Nano 9, 606–620. https://doi.org/10.1039/D1EN00755F.

Murashov, V., Geraci, C.L., Schulte, P., Howard, J., 2020. Are There Nano- and Microplastics in the Workplace?.

Nalbone, L., Cincotta, F., Giarratana, F., Ziino, G., Panebianco, A., 2021. Microplastics in fresh and processed mussels sampled from fish shops and large retail chains in Italy. Food Control 125, 108003. https://doi.org/10.1016/j.foodcont.2021.108003.

Naylor, R.L., Kishore, A., Sumaila, U.R., Issifu, I., Hunter, B.P., Belton, B., Bush, S.R., Cao, L., Gelcich, S., Gephart, J.A., Golden, C.D., Jonell, M., Koehn, J.Z., Little, D.C., Thilsted, S.H., Tigchelaar, M., Crona, B., 2021. Blue food demand across geographic and temporal scales. Nat. Commun. 12, 1–14. https://doi.org/10.1038/s41467-021-25516-4.

Nithin, A., Sundaramanickam, A., Surya, P., Sathish, M., Soundharapandiyan, B., Balachandar, K., 2021. Microplastic contamination in salt pans and commercial salts – A baseline study on the salt pans of Marakkanam and Parangipettai, Tamil Nadu, India. Mar. Pollut. Bull. 165, 112101 https://doi.org/10.1016/j.marpolbul.2021.112101.

Noventa, S., Boyles, M.S.P., Seifert, A., Belluco, S., Jiménez, A.S., Johnston, H.J., Tran, L., Fernandes, T.F., Mughini-gras, L., Orsini, M., Corami, F., 2021. Paradigms to Assess the Human Health Risks of Nano- and Microplastics, 1, pp. 1–27. https://doi.org/10.1186/s43591-021-00011-1 (2021).

O'Connor, J.D., Mahon, A.M., Ramsperger, A.F.R.M., Trotter, B., Redondo-Hasselerharm, P.E., Koelmans, A.A., Sinead, M., 2019. Microplastics in freshwater biota: a critical review of isolation, characterization and assessment methods. Glob. Challenges. https://doi.org/10.1002/gch2.201800118, 1800118.

Oliveri Conti, G., Ferrante, M., Banni, M., Favara, C., Nicolosi, I., Cristaldi, A., Fiore, M., Zuccarello, P., 2020. Micro- and nano-plastics in edible fruit and vegetables. The first diet risks assessment for the general population. Environ. Res. 187, 109677 https://doi.org/10.1016/j.envres.2020.109677.

Organization, W.H., 2019. Microplastics in drinking-water. World Health Organization, Geneva PP - Geneva.

Oßmann, B.E., Sarau, G., Holtmannspötter, H., Pischetsrieder, M., Christiansen, S.H., Dicke, W., 2018. Small-sized microplastics and pigmented particles in bottled mineral water. Water Res. 141, 307–316. https://doi.org/10.1016/j.watres.2018.05.027.

Owen, R.L., 1999. Uptake and transport of intestinal macromolecules and microorganisms by M cells in Peyer's patches: a personal and historical perspective. Semin. Immunol. 11, 157–163. https://doi.org/10.1006/smim.1999.0171.

Parker, B., Andreou, D., Green, I.D., Britton, J.R., 2021. Microplastics in freshwater fishes: occurrence, impacts and future perspectives. Fish Fish. 22, 467–488. https://doi.org/10.1111/faf.12528.

Pauly, J.L., Stegmeier, S.J., Allaart, H.A., Cheney, R.T., Zhang, P.J., Mayer, A.G., Streck, R.J., 1998. Inhaled cellulosic and plastic fibers found in human lung tissue. Cancer Epidemiol. Biomark. Prev. 7, 419–428.

Pehlivan, N., Gedik, K., 2021. Particle size-dependent biomolecular footprints of interactive microplastics in maize. Environ. Pollut. 277, 116772 https://doi.org/10.1016/j.envpol.2021.116772.

Peixoto, D., Pinheiro, C., Amorim, J., Oliva-Teles, L., Guilhermino, L., Vieira, M.N., 2019. Microplastic pollution in commercial salt for human consumption: a review. Estuar. Coast. Shelf Sci. 219, 161–168. https://doi.org/10.1016/j.ecss.2019.02.018.

Pivokonsky, M., Cermakova, L., Novotna, K., Peer, P., Cajthaml, T., Janda, V., 2018. Occurrence of microplastics in raw and treated drinking water. Sci. Total Environ. 643, 1644–1651. https://doi.org/10.1016/j.scitotenv.2018.08.102.

Prata, J.C., 2018. Airborne microplastics: consequences to human health? Environ. Pollut. 234, 115–126. https://doi.org/10.1016/j.envpol.2017.11.043.

Prata, J.C., da Costa, J.P., Lopes, I., Duarte, A.C., Rocha-Santos, T., 2020a. Environmental exposure to microplastics: an overview on possible human health effects. Sci. Total Environ. 702, 134455 https://doi.org/10.1016/j.scitotenv.2019.134455.

Prata, J.C., Reis, V., da Costa, J.P., Mouneyrac, C., Duarte, A.C., Rocha-Santos, T., 2021. Contamination issues as a challenge in quality control and quality assurance in microplastics analytics. J. Hazard. Mater. 403 https://doi.org/10.1016/j.jhazmat.2020.123660.

Praveena, S.M., Norashikin, S., Shaifuddin, M., Akizuki, S., 2018. Exploration of microplastics from personal care and cosmetic products and its estimated emissions to marine environment: an evidence from Malaysia. Mar. Pollut. Bull. 136, 135–140. https://doi.org/10.1016/j.marpolbul.2018.09.012.

Rackaityte, E., Lynch, S.V., 2020. The human microbiome in the 21st century. Nat. Commun. 11, 19–21. https://doi.org/10.1038/s41467-020-18983-8.

Raftis, J.B., Miller, M.R., 2019. Nanoparticle translocation and multi-organ toxicity: a particularly small problem. Nano Today 26, 8–12. https://doi.org/10.1016/j.nantod.2019.03.010.

Ragusa, A., Svelato, A., Santacroce, C., Catalano, P., Notarstefano, V., Carnevali, O., Papa, F., Rongioletti, M.C.A., Baiocco, F., Draghi, S., D'Amore, E., Rinaldo, D., Matta, M., Giorgini, E., 2021. Plasticenta: first evidence of microplastics in human placenta. Environ. Int. 146, 106274 https://doi.org/10.1016/j.envint.2020.106274.

Rahman, A., Sarkar, A., Yadav, O.P., Achari, G., Slobodnik, J., 2021. Potential human health risks due to environmental exposure to nano- and microplastics and knowledge gaps: a scoping review. Sci. Total Environ. 757, 143872 https://doi.org/10.1016/j.scitotenv.2020.143872.

Ramsperger, A.F.R.M., Narayana, V.K.B., Gross, W., Mohanraj, J., Thelakkat, M., Greiner, A., Schmalz, H., Kress, H., Laforsch, C., 2020. Environmental exposure enhances the internalization of microplastic particles into cells. Sci. Adv. 6, 1–10. https://doi.org/10.1126/sciadv.abd1211.

Ramsperger, A.F.R.M., Jasinski, J., Völkl, M., Witzmann, T., Meinhart, M., Jérôme, V., Kretschmer, W.P., Freitag, R., Senker, J., Fery, A., Kress, H., Scheibel, T., Laforsch, C., 2021. Supposedly identical microplastic particles substantially differ in their material properties influencing particle-cell interactions and cellular responses. J. Hazard. Mater. 425, 127961 https://doi.org/10.1016/j.jhazmat.2021.127961.

Renzi, M., Blašković, A., 2018. Litter & microplastics features in table salts from marine origin: Italian versus croatian brands. Mar. Pollut. Bull. 135, 62–68. https://doi.org/10.1016/j.marpolbul.2018.06.065.

Renzi, M., Grazioli, E., Bertacchini, E., Blašković, A., 2019. Microparticles in table salt: Levels and chemical composition of the smallest dimensional fraction. J. Mar. Sci. Eng. 7, 1–14. https://doi.org/10.3390/jmse7090310.

Ribeiro, F., Okoffo, E.D., O'Brien, J.W., Fraissinet-Tachet, S., O'Brien, S., Gallen, M., Samanipour, S., Kaserzon, S., Mueller, J.F., Galloway, T., Thomas, K.V., 2020. Quantitative analysis of selected plastics in high-commercial-value australian seafood by pyrolysis gas chromatography mass spectrometry. Environ. Sci. Technol. 54, 9408–9417. https://doi.org/10.1021/acs.est.0c02337.

Rillig, M.C., Ingraffia, R., de Souza Machado, A.A., 2017. Microplastic incorporation into soil in agroecosystems. Front. Plant Sci. 8, 8–11. https://doi.org/10.3389/fpls.2017.01805.

SAPEA, 2019. A Scientific Perspective on Microplastics in Nature and Society. Berlin.

Sarigiannis, D.A., 2014. Combined or Multiple Exposure to Health Stressors in Indoor Built Environments. World Heal. Organ. Rep. Eur, p. 82.

Schneider, M., Stracke, F., Hansen, S., Schaefer, U.F., 2009. Nanoparticles and their interactions with the dermal barrier. Dermatoendocrinol 1, 197–206.

Schraufnagel, D.E., 2020. The health effects of ultrafine particles. Exp. Mol. Med. 52, 311–317. https://doi.org/10.1038/s12276-020-0403-3.

18

Schwabl, P., Koppel, S., Konigshofer, P., Bucsics, T., Trauner, M., Reiberger, T., Liebmann, B., 2019. Detection of various microplastics in human stool: a prospective case series. Ann. Intern. Med. 171, 453–457. https://doi.org/10.7326/M19-0618.

Schwaferts, C., Niessner, R., Elsner, M., Ivleva, N.P., 2019. Methods for the analysis of submicrometer- and nanoplastic particles in the environment. TrAC - Trends Anal. Chem. 112, 52–65. https://doi.org/10.1016/j.trac.2018.12.014.

Schymanski, D., Goldbeck, C., Humpf, H.U., Fürst, P., 2018. Analysis of microplastics in water by micro-Raman spectroscopy: release of plastic particles from different packaging into mineral water. Water Res. 129, 154–162. https://doi.org/10.1016/j.watres.2017.11.011.

Scott, K., Manunta, M., Germain, C., Smith, P., Jones, M., Mitchell, P., Dessi, D., Branigan, K., Lechler, R.I., Fiori, L., Foster, G.R., Lombardi, G., 2005. Qualitatively Distinct Patterns of Cytokines are Released by Human Dendritic Cells in Response to Different Pathogens. https://doi.org/10.1111/j.1365-2567.2005.02218.x.

Senathirajah, K., Attwood, S., Bhagwat, G., Carbery, M., Wilson, S., Palanisami, T., 2021. Estimation of the mass of microplastics ingested – A pivotal first step towards human health risk assessment. J. Hazard. Mater. 404, 124004 https://doi.org/10.1016/j.jhazmat.2020.124004.

Seth, C.K., Shriwastav, A., 2018. Contamination of Indian sea salts with microplastics and a potential prevention strategy. Environ. Sci. Pollut. Res. 25, 30122–30131. https://doi.org/10.1007/s11356-018-3028-5.

Shruti, V.C., Pérez-Guevara, F., Elizalde-Martínez, I., Kutralam-Muniasamy, G., 2021. Toward a unified framework for investigating micro(nano)plastics in packaged beverages intended for human consumption. Environ. Pollut. 268, 115811 https://doi.org/10.1016/j.envpol.2020.115811.

Soltani, S.N., Taylor, M.P., Wilson, S.P., 2021. Quanti Fication and Exposure Assessment of Microplastics in Australian Indoor House Dust * 283. https://doi.org/10.1016/j.envpol.2021.117064.

Song, S., Van Dijk, F., Eck, G., Wu, X., Bos, S., Boom, D., Kooter, I., Wardenaar, R., Spierings, D., Cole, M., Salvati, A., Gosens, R., Melgert, B., 2022. Inhalable textile microplastic fibers impair lung repair. ERJ Open Res. 8 https://doi.org/10.1183/23120541.LSC-2022.69.

Sparks, C., Awe, A., Maneveld, J., 2021. Abundance and characteristics of microplastics in retail mussels from Cape Town, South Africa. Mar. Pollut. Bull. 166, 112186 https://doi.org/10.1016/j.marpolbul.2021.112186.

Stapleton, P.A., Minarchick, V.C., Cumpston, A.M., Mckinney, W., 2012. Impairment of Coronary Arteriolar Endothelium-Dependent Dilation after Multi-Walled Carbon Nanotube Inhalation: A Time-Course Study 13781–13803. https://doi.org/10.3390/ijms131113781.

Steinmetz, Z., Wollmann, C., Schaefer, M., Buchmann, C., David, J., Tröger, J., Muñoz, K., Frör, O., Schaumann, G.E., 2016. Plastic mulching in agriculture. Trading short-term agronomic benefits for long-term soil degradation? Sci. Total Environ. 550, 690–705. https://doi.org/10.1016/j.scitotenv.2016.01.153.

Stephens, B., Azimi, P., El Orch, Z., Ramos, T., 2013. Ultrafine particle emissions from desktop 3D printers. Atmos. Environ. 79, 334–339. https://doi.org/10.1016/j.atmosenv.2013.06.050.

Stock, V., Böhmert, L., Lisicki, E., Block, R., Cara-Carmona, J., Pack, L.K., Selb, R., Lichtenstein, D., Voss, L., Henderson, C.J., Zabinsky, E., Sieg, H., Braeuning, A., Lampen, A., 2019. Uptake and effects of orally ingested polystyrene microplastic particles in vitro and in vivo. Arch. Toxicol. 93, 1817–1833. https://doi.org/10.1007/s00204-019-02478-7.

Stock, V., Laurisch, C., Franke, J., Dönmez, M.H., Voss, L., Böhmert, L., Braeuning, A., Sieg, H., 2021. Uptake and cellular effects of PE, PP, PET and PVC microplastic particles. Toxicol. in Vitro 70, 105021. https://doi.org/10.1016/j.tiv.2020.105021.

Sun, Q., Ren, S.Y., Ni, H.G., 2020. Incidence of microplastics in personal care products: An appreciable part of plastic pollution. Sci. Total Environ. 742, 140218 https://doi.org/10.1016/j.scitotenv.2020.140218.

Tagg, A.S., Ivar do Sul, J.A., 2019. Is this your glitter? An overlooked but potentially environmentally-valuable microplastic. Mar. Pollut. Bull. 146, 50–53. https://doi.org/10.1016/j.marpolbul.2019.05.068.

Tahir, A., Taba, P., Samawi, M.F., Werorilangi, S., 2019. Microplastics in water, sediment and salts from traditional salt producing ponds. Glob. J. Environ. Sci. Manag. 5, 431–440. https://doi.org/10.22034/gjesm.2019.04.03.

Tamargo, A., Molinero, N., Reinosa, J.J., Alcolea-Rodriguez, V., Portela, R., Bañares, M.A., Fernández, J.F., Moreno-Arribas, M.V., 2022. PET microplastics affect human gut microbiota communities during simulated gastrointestinal digestion, first evidence of plausible polymer biodegradation during human digestion. Sci. Rep. 12, 1–15. https://doi.org/10.1038/s41598-021-04489-w.

Taylor, S.E., Pearce, C.I., Sanguinet, K.A., Hu, D., Chrisler, W.B., Kim, Y.M., Wang, Z., Flury, M., 2020. Polystyrene nano-A nd microplastic accumulation at Arabidopsis and wheat root cap cells, but no evidence for uptake into roots. Environ. Sci. Nano 7, 1942–1953. https://doi.org/10.1039/d0en00309c.

Thompson, R.C., Olsen, Ylva, Mitchell, R.P., Davis, A., Rowland, S.J., John, A.W.G., McGonigle, D., Russel, A.E., 2004. Lost at sea: where is all the plastic? Science (80) 304, 838. https://doi.org/10.1126/science.1094559.

Toussaint, B., Raffael, B., Angers-Loustau, A., Gilliland, D., Kestens, V., Petrillo, M., Rio-Echevarria, I.M., Van den Eede, G., 2019. Review of micro- and nanoplastic contamination in the food chain. Food Addit. Contam. - Part A Chem. Anal. Control. Expo. Risk Assess. 36, 639–673. https://doi.org/10.1080/19440049.2019.1583381.

Tympa, L.E., Katsara, K., Moschou, P.N., Kenanakis, G., Papadakis, V.M., 2021. Do microplastics enter our food chain via root vegetables? A raman based spectroscopic study on raphanus sativus. Materials (Basel). 14, 1–11. https://doi.org/10.3390/ma14092329.

UNEP, 2015. Are We Polluting the Environment Through Our Personal care?.

Urbina, M.A., Correa, F., Aburto, F., Ferrio, J.P., 2020. Adsorption of polyethylene microbeads and physiological effects on hydroponic maize. Sci. Total Environ. 741, 140216 https://doi.org/10.1016/j.scitotenv.2020.140216.

US Environmental Protection Agency, 1986. Assessment and Control of Indoor Air Pollution.

Ustabasi, G.S., Baysal, A., 2019. Occurrence and risk assessment of microplastics from various toothpastes. Environ. Monit. Assess. 191, 438. https://doi.org/10.1007/s10661-019-7574-1.

Van Raamsdonk, L.W.D., Van Der Zande, M., Koelmans, A.A., 2020. and Potential Health E ff ects of Microplastics Present in the Food Chain.

Vanapalli, K.R., Sharma, H.B., Ranjan, V.P., Samal, B., Bhattacharya, J., Dubey, B.K., Goel, S., 2021. Challenges and strategies for effective plastic waste management during and post COVID-19 pandemic. Sci. Total Environ. 750, 141514 https://doi.org/10.1016/j.scitotenv.2020.141514.

Vancamelbeke, M., Vermeire, S., 2018. The Intestinal Barrier: A Fundamental Role in Health and Disease, 11, pp. 821–834. https://doi.org/10.1080/17474124.2017.1343143.

Vance, M.E., Pegues, V., Van Montfrans, S., Leng, W., Marr, L.C., 2017. Aerosol emissions from fuse-deposition modeling 3D printers in a chamber and in real indoor environments. Environ. Sci. Technol. 51, 9516–9523. https://doi.org/10.1021/acs.est.7b01546.

Vethaak, A.D., Legler, J., 2021. Microplastics and human health. Science (80) 371, 672–674. https://doi.org/10.1126/science.abe5041.

Vianello, A., Jensen, R.L., Liu, L., Vollertsen, J., 2019. Simulating human exposure to indoor airborne microplastics using a Breathing Thermal Manikin. Sci. Rep. 9, 1–11. https://doi.org/10.1038/s41598-019-45054-w.

Vinay Kumar, B.N., Löschel, L.A., Imhof, H.K., Löder, M.G.J., Laforsch, C., 2021. Analysis of microplastics of a broad size range in commercially important mussels by combining FTIR and Raman spectroscopy approaches. Environ. Pollut. 269, 116147 https://doi.org/10.1016/j.envpol.2020.116147.

Vogt, A., Combadiere, B., Hadam, S., Stieler, K.M., Lademann, J., Schaefer, H., Autran, B., Sterry, W., Blume-Peytavi, U., 2006. 40 nm, but not 750 or 1,500 nm, nanoparticles enter epidermal CD1a+ cells after transcutaneous application on human skin. J. Invest. Dermatol. 126, 1316–1322. https://doi.org/10.1038/sj.jid.5700226.

Volkheimer, G., 1975. Hematogenous Dissemination of Ingested Polyvinyl-Chloride Particles. Ann. N. Y. Acad. Sci. 246, 164. https://doi.org/10.1111/j.1749-6632.1975.tb51092.x.

Volkheimer, G., 1977. Particles: Physiology and Pharmacology. https://doi.org/10.1016/S1054-3589(08)60188-X.

Völkl, M., Jerome, V., Weig, A.R., Jasinski, Julia, Meides, N., Strohriegl, P., Scheibel, T., Freitag, R., 2022. Pristine and Artificially-aged Polystyrene Microplastic Particles Differ in Regard to Cellular Response, p. 435.

Wakkaf, T., El Zrelli, R., Kedzierski, M., Balti, R., Shaiek, M., Mansour, L., Tlig-Zouari, S., Bruzaud, S., Rabaoui, L., 2020. Microplastics in edible mussels from a southern Mediterranean lagoon: Preliminary results on seawater-mussel transfer and implications for environmental protection and seafood safety. Mar. Pollut. Bull. 158 https://doi.org/10.1016/j.marpolbul.2020.111355.

Wang, J., Li, J., Liu, S., Li, H., Chen, X., Peng, C., Zhang, P., Liu, X., 2021. Distinct microplastic distributions in soils of different land-use types: a case study of Chinese farmlands. Environ. Pollut. 269, 116199 https://doi.org/10.1016/j.envpol.2020.116199.

Weig, A., Löder, M.G.J., Ramsperger, A.F.R.M., Laforsch, C., 2021. In situ Prokaryotic and Eukaryotic Communities on Microplastic Particles in a Small Headwater Stream in Germany, 12, pp. 1–14. https://doi.org/10.3389/fmicb.2021.660024.

Weithmann, N., Möller, J.N., Löder, M.G.J., Piehl, S., Laforsch, C., Freitag, R., 2018. Organic fertilizer as a vehicle for the entry of microplastic into the environment. Sci. Adv. 4, 1–7. https://doi.org/10.1126/sciadv.aap8060.

WHO, 2017. Guidelines for Drinking-water Quality.

WHO, 2022. Dietary and Inhalation Exposure to Nano- and Microplastic Particles and Potential Implications for Human Health.

Wieland, S., Balmes, A., Bender, J., Kitzinger, J., Meyer, F., Ramsperger, A.F., Roeder, F., Tengelmann, C., Wimmer, B.H., Laforsch, C., Kress, H., 2022. From properties to toxicity: comparing microplastics to other airborne microparticles. J. Hazard. Mater. https://doi.org/10.1016/j.jhazmat.2021.128151. Elsevier.

Winkler, A., Santo, N., Ortenzi, M.A., Bolzoni, E., Bacchetta, R., Tremolada, P., 2019. Does mechanical stress cause microplastic release from plastic water bottles? Water Res. 166, 115082 https://doi.org/10.1016/j.watres.2019.115082.

World Trade Organization, 2019. World Trade Statistical Review. World Trade Stat. Rev. 12, 120.

Wright, S.L., Kelly, F.J., 2017. Plastic and human health: a micro issue? Environ. Sci. Technol. 51, 6634–6647. https://doi.org/10.1021/acs.est.7b00423.

Wu, S., Wu, M., Tian, D., Qiu, L., Li, T., 2020. Effects of polystyrene microbeads on cytotoxicity and transcriptomic profiles in human Caco-2 cells. Environ. Toxicol. 35, 495–506. https://doi.org/10.1002/tox.22885.

Wu, X., Hou, H., Liu, Y., Yin, S., Bian, S., Liang, S., Wan, C., Yuan, S., Xiao, K., Liu, B., Hu, J., Yang, J., 2022. Microplastics affect rice (Oryza sativa L.) quality by interfering metabolite accumulation and energy expenditure pathways: a field study. J. Hazard. Mater. 422, 126834 https://doi.org/10.1016/j.jhazmat.2021.126834.

Xu, J.-L., Lin, X., Hugelier, S., Herrero-Langreo, A., Gowen, A.A., 2021. Spectral imaging for characterization and detection of plastic substances in branded teabags. J. Hazard. Mater. 418, 126328 https://doi.org/10.1016/j.jhazmat.2021.126328.

Xu, M., Halimu, G., Zhang, Q., Song, Y., Fu, X., Li, Yongqiang, Li, Yansheng, Zhang, H., 2019. Internalization and toxicity: a preliminary study of effects of nanoplastic particles on human lung epithelial cell. Sci. Total Environ. 694, 133794 https://doi.org/10.1016/j.scitotenv.2019.133794.

19

Yang, D., Shi, H., Li, L., Li, J., Jabeen, K., Kolandhasamy, P., 2015. Microplastic pollution in table salts from China. Environ. Sci. Technol. 49, 13622–13627. https://doi.org/10.1021/acs.est.5b03163.

Yang, X., Wang, H., Zhang, L., Kong, L., Chen, Y., He, Q., Li, L., Grossart, H.P., Ju, F., 2021. Marine algae facilitate transfer of microplastics and associated pollutants into food webs. Sci. Total Environ. 787, 147535 https://doi.org/10.1016/j.scitotenv.2021.147535.

Yin, L., Wen, X., Huang, D., Du, C., Deng, R., Zhou, Z., Tao, J., Li, R., Zhou, W., Wang, Z., Chen, H., 2021. Interactions between microplastics/nanoplastics and vascular plants. Environ. Pollut. 290, 117999 https://doi.org/10.1016/j.envpol.2021.117999.

Yong, C.Q.Y., Valiyaveetill, S., Tang, B.L., 2020. Toxicity of microplastics and nanoplastics in Mammalian systems. Int. J. Environ. Res. Public Health 17. https://doi.org/10.3390/ijerph17051509.

Yuan, Z., Li, H.-X., Lin, L., Pan, Y.-F., Liu, S., Hou, R., Xu, X.-R., 2022. Occurrence and human exposure risks of atmospheric microplastics: a review. Gondwana Res. 108, 200–212. https://doi.org/10.1016/j.gr.2022.02.001.

Yurtsever, M., 2019. Tiny, shiny, and colorful microplastics: are regular glitters a significant source of microplastics? Mar. Pollut. Bull. 146, 678–682. https://doi.org/10.1016/j.marpolbul.2019.07.009.

Zeytin, S., Wagner, G., Mackay-roberts, N., Gerdts, G., Schuirmann, E., Klockmann, S., Slater, M., 2020. Quantifying microplastic translocation from feed to the fi llet in European sea bass Dicentrarchus labrax. Mar. Pollut. Bull. 156, 111210 https://doi.org/10.1016/j.marpolbul.2020.111210.

Zhang, N., Li, Y. Bin, He, H.R., Zhang, J.F., Ma, G.S., 2021a. You are what you eat: microplastics in the feces of young men living in Beijing. Sci. Total Environ. 767, 144345 https://doi.org/10.1016/j.scitotenv.2020.144345.

Zhang, Q., Pardo, M., Rudich, Y., Kaplan-Ashiri, I., Wong, J.P.S., Davis, A.Y., Black, M.S., Weber, R.J., 2019. Chemical composition and toxicity of particles emitted from a consumer-level 3D printer using various materials. Environ. Sci. Technol. 53, 12054–12061. https://doi.org/10.1021/acs.est.9b04168.

Zhang, J., Wang, L., Kannan, K., 2020. Microplastics in house dust from 12 countries and associated human exposure. Environment International 134, 105314. https://doi.org/10.1016/j.envint.2019.105314. ISSN 0160-4120.

Zhang, Q., Xu, E.G., Li, J., Chen, Q., Ma, L., Zeng, E.Y., Shi, H., 2020. A review of microplastics in table salt, drinking water, and air: direct human exposure. Environ. Sci. Technol. 54, 3740–3751. https://doi.org/10.1021/acs.est.9b04535.

Zhang, Q., Zhao, Y., Du, F., Cai, H., Wang, G., Shi, H., 2020. Microplastic fallout in different indoor environments. Environ. Sci. Technol. 54, 6530–6539. https://doi.org/10.1021/acs.est.0c00087.

Zhang, T., Sun, Y., Song, K., Du, W., Huang, W., Gu, Z., Feng, Z., 2021. Microplastics in different tissues of wild crabs at three important fishing grounds in China. Chemosphere 271, 129479. https://doi.org/10.1016/j.chemosphere.2020.129479.

Zhou, C.-Q., Lu, C.-H., Mai, L., Bao, L.-J., Liu, L.-Y., Zeng, E.Y., 2021. Response of rice (Oryza sativa L.) roots to nanoplastic treatment at seedling stage. J. Hazard. Mater. 401, 123412 https://doi.org/10.1016/j.jhazmat.2020.123412.

Article 8

Structural Diversity in Early-Stage Biofilm Formation on Microplastics Depends on Environmental Medium and Polymer Properties

water

MDPI

Structural Diversity in Early-Stage Biofilm Formation on Microplastics Depends on Environmental Medium and Polymer Properties

Anja F. R. M. Ramsperger [1,4], **Anja C. Stellwag** [1], **Anja Caspari** [2], **Andreas Fery** [2], **Tillmann Lueders** [3], **Holger Kress** [4], **Martin G. J. Löder** [1] and **Christian Laforsch** [1,*]

[1] Animal Ecology I, University of Bayreuth, 95447 Bayreuth, Germany; anja.ramsperger@uni-bayreuth.de (A.F.R.M.R.); anja.stellwag@uni-bayreuth.de (A.C.S.); martin.loeder@uni-bayreuth.de (M.G.J.L.)

[2] Institut für Physikalische Chemie und Physik der Polymere, Leibniz Institut für Polymerfoschung Dresden e.V., 01069 Dresden, Germany; caspari@ipfdd.de (A.C.); fery@ipfdd.de (A.F.)

[3] Ecological Microbiology, University of Bayreuth, 95447 Bayreuth, Germany; tillmann.lueders@uni-bayreuth.de

[4] Biological Physics, University of Bayreuth, 95447 Bayreuth, Germany; holger.kress@uni-bayreuth.de

[*] Correspondence: Christian.laforsch@uni-bayreuth.de; Tel.: +49-921-552650

check for
updates

Abstract: Plastics entering the environment can not only undergo physical degradation and fragmentation processes, but they also tend to be colonized by microorganisms. Microbial colonization and the subsequent biofilm formation on plastics can alter their palatability to organisms and result in a higher ingestion as compared to pristine plastics. To date, the early stage of biofilm formation on plastic materials has not been investigated in context of the environmental medium and polymer properties. We explored the early-stage biofilm formation on polyamide (PA), polyethylene terephthalate (PET), and polyvinyl chloride (PVC) after incubation in freshwater and artificial seawater and categorized the structural diversity on images obtained via scanning electron microscopy. Furthermore, by the measurement of the initial ζ-potential of the plastic materials, we found that PA with the highest negative ζ-potential tended to have the highest structural diversity, followed by PET and PVC after incubation in freshwater. However, PVC with the lowest negative ζ-potential showed the highest structural diversity after incubation in seawater, indicating that the structural diversity is additionally dependent on the incubation medium. Our results give insights into how the incubation medium and polymer properties can influence the early-stage biofilm formation of just recently environmentally exposed microplastics. These differences are responsible for whether organisms may ingest microplastic particles with their food or not.

Keywords: microplastic; plastic; biofilm; SEM; ζ-potential; EPS

1. Introduction

Plastic materials have a considerable number of favorable properties, amongst others their lightweight, versatility, and longevity [1]. However, once plastics enter the environment, their longevity is a disadvantage that prevents their degradation and promotes their accumulation in the environment [2]. There, most plastic items break down into smaller pieces. Those smaller plastic particles are defined as microplastic particles [3] if their size is smaller than 5 mm [4]. Meanwhile, microplastic particles are detected in all environmental compartments, ranging from marine [5] and limnetic environments [6] over soils [7] up to the atmosphere [8,9]. The occurrence of microplastic particles in the environment is not necessarily restricted to areas of high human activities such as

in urban areas because microplastic particles are also found in remote mountain lakes [10], remote islands [11], the Antarctica [12], and even in the deep sea [13]. Once plastics enter an environmental compartment, they may pose a risk to the associated organisms, for example due to the ingestion of plastic items [14]. Already thirty years ago, Harper and Fowler [15] described the ingestion of plastic items by sea birds. By now, the ingestion of microplastic particles has been shown in a variety of organisms within the food web, starting at the bottom with zooplankton [10,16] and mussels [17,18] going up to vertebrates such as fish [14,19,20] and right up to humans [9,21,22]. Although there is no broad evidence for plastic ingestion-related mortality [14], internal blockage or lesions of the digestive tract and a false feeling of satiation due to indigestible plastic filling up the stomach was described to negatively affect associated organisms and may lead to their death [20,23]. In addition to those physical risks, microplastics are controversially discussed to act as vectors for adsorbed hazardous chemicals [24] or pathogenic microorganisms [25]. The ingestion of microplastic particles has been found to be enhanced for weathered particles [26,27], i.e., particles exposed longer to environmental influences, thereby undergoing degradation and fragmentation processes [2,28]. Next to those physicochemical changes, plastics released to the environment are typically also rapidly colonized by microbes. The observed enhanced ingestion by organisms after the aging of microplastics was suggested to be due to the presence of a biofilm masking the plastics by mimicking an organic origin and thus altering the palatability of the particles [27]. Unfortunately, the exposure time for microplastics collected from the environment cannot be determined but can theoretically be decades or longer. Biofilms on plastic materials have already been described in exposure experiments in the environment [29,30] and on plastic materials collected directly from nature [30,31]. Such exposure experiments ranged from short time scales of days [32] and weeks [29,30] up to longer time scales of months [33,34] and years [35].

An initial coating with microbes is considered to occur within minutes to hours after the exposure in marine waters [36]. Renner and Weibel [37] described the five typical successive steps of biofilm formation as follows: First, microorganisms reversibly attach to surfaces via pili, flagella, or membrane proteins. By extruding extracellular polymeric substances (EPS), the second step of biofilm formation is initiated. At this point, microorganisms have already irreversibly attached to the surfaces, which can be defined as the early stage of a biofilm formation. In the third step, microorganisms embedded in the EPS proliferate, form smaller colonies, and release additional EPS. The microbial communities further proliferate and form three-dimensional structures described as the maturing of a substantial biofilm within the fourth step. Lastly, in the fifth step, cells can again detach from the biofilm and colonize newly available surfaces [37]. This description highlights that a mature biofilm is a highly complex and dynamic system controlled in addition to abiotic factors by many different biotic factors, including microbial interactions and competition [38]. Rummel et al. [39] emphasize in their comprehensive review that the surface properties of polymers, such as their roughness, surface energy, and charge or hydrophobicity may be relevant for biofilm formation. In this context, Hossain et al. [34] showed that the formation of a biofilm on microplastics in freshwater mesocosms that have been enriched with bacterial strains was dependent on the polymer type.

It has further been shown that an incubation period of two months already alters the initial polymers' physicochemical properties by microbial attachment [34]. However, to date, it has not been investigated whether the initial surface properties of different polymer types predefine the colonization in the early stage of a biofilm formation, or if colonization patterns of the same polymer differ between different environmental media. To fill this gap and to correlate the initial surface properties with the biofilm formation, we monitored the very early stage of biofilm formation (0 h up to 14 days) in freshwater and artificial seawater on the surfaces of polyamide (PA), polyethylene terephthalate (PET), and polyvinyl chloride (PVC) fragments, which are three polymers that are produced in high amounts [40]. The chosen polymers highly differ in their chemical composition (PA-containing amid groups, PET-containing ester groups and PVC-containing chloride) resulting in different physicochemical properties, which allows a correlation of the early-stage biofilm formation

with the polymers' properties. We visualized microorganisms and associated structures on the microplastic fragments' surfaces by using scanning electron microscopy (SEM). We compared the structural diversity of the biofilms by determining microbial and non-microbial structures on the polymer fragments for different incubation times and incubation media. To evaluate how the fragments' surface properties may influence the early stage biofilm formation, we measured the pH-dependent initial ζ-potential of the three polymer types. Additionally, the structural diversity on mature biofilms from a very late stage of biofilm formation (more than two years) on the surface of PA incubated in either freshwater or seawater was compared to the very early stage biofilm formation in our experiments. We hypothesize that due to the different initial properties of the chosen polymers, the very early stage of biofilm formation differs between polymers and incubation media and changes over time.

2. Materials and Methods

2.1. Microplastic Particles

Polymers were purchased as raw pellets from different suppliers (PA Pellets: Leibniz-Institut für Polymerforschung Dresden e.V.; Polymers used for fragments: PA: BASF, PET: Neogroup and PVC: Vinnolit; see Table 1). For long-term incubation of PA, the whole pellets were incubated without further processing. To obtain the microplastic fragments for the time-series incubation, the raw pellets were ground in an ultra-centrifugal mill (ZM 200 Retsch, Haan, Germany) with a 12-tooth rotor and a sieve size of 1000 µm with 18,000 U/min. The milling was performed in liquid nitrogen to prevent the conglutination of the fragments. Subsequently, 10 g of the fragments were sieved using an Alpine air jet sieve (E200LS, Hosokawa Alpine, Augsburg, Germany) with mesh sizes of 125 µm and 4000 Pa for 15 min.

Table 1. Summary of the used polymers. The suppliers, the corresponding trading names, and size in µm after milling.

Polymer Type	Supplier	Trade Name	Size Distribution [µm]
Polyamide pellet *	Leibniz-Institut für Polymerforschung Dresden e.V.	-	2000–2500
Polyamid fragments	BASF, Ludwigshafen, Germany	Ultramid®, A3K, PA66	<500
Polyethylene terephtalate fragments	Neogroup, Klaipeda district, Lithuania	Neopet 80	<500
Polyvinyl chloride fragments	Vinnolit GmbH & Co.KG, Ismaning, Germany	®Vinnolit S 3268	< 500

* The polyamide pellet for the long-term experiment was not milled.

2.2. Incubation of Microplastic Particles in Environmental Media

PA pellets that were incubated in freshwater and seawater for approximately two years in a long-term experiment were used to investigate a mature late-stage biofilm on the surface of a microplastic particle for comparison with the biofilms of the short-term experiments. To monitor the early stage of biofilm formation, the polymer fragments were incubated in two environmental media, freshwater and seawater. Prior to incubation, the produced fragments of each polymer type were washed thoroughly in ultrapure water (Purelab Flex Elga, Veolia Water Technologies, Celle, Germany) to remove possible contamination from milling: 250 mg of each polymer fragments were transferred to a 15 mL tube (CELLSTAR®, Greiner Bio-One GmbH, Frickenhausen, Germany) and filled up with 10 mL ultrapure water. After carefully mixing for 30 seconds (Reax 2000, Heidolph Instruments GmbH & Co. KG, Schwabach, Germany, pace 8), all polymers were homogeneously suspended. Subsequently, the samples were centrifuged (2500 g, 20 min, room temperature), the supernatant was removed via pipetting, and the samples were resuspended in 10 mL of the respective environmental media. Before incubating each polymer type in the respective environmental media, samples were prepared for SEM images as a control. The freshwater for incubation was obtained

from an artificial pond at the University of Bayreuth (49°55′44.1″ N; 11°34′60.0″ E), and seawater was obtained from a marine aquarium facility of the University of Bayreuth (sampling sites of the environmental media in Figure S1).

To analyze the time-dependent development of a biofilm, we sampled the fragments after 0, 0.5, 1, 2, 5, 7, 11, and 14 days of incubation from the respective tube. For maintaining a vital microbial community during the incubation series, the respective media in the incubation tubes were exchanged three times per week after centrifugation, as described above. To avoid sedimentation of the microplastic fragments and obtain a homogeneous development of a biofilm on the particles' surface, the 15 mL tubes were placed in a hybridization furnace and continuously agitated to prevent sedimentation (26.5 ± 0.5 °C, 9 rpm).

2.3. Sample Preparation for Scanning Electron Microscopy

To visualize biofilm formation, the samples were analyzed using a scanning electron microscope (SEM, LEO1530 Zeiss, Oberkochen, Germany, magnification 500×–50,000×, 2–3 kV, SE2 detector). From each sample, 20 µL were pipetted onto carbon conductive tabs (Ø 12 mm Plano GmbH, Wetzlar, Germany) fixed to aluminum stubs (Ø 12 mm, Plano GmbH, Wetzlar, Germany). Then, the stubs were transferred into a desiccator, vacuum-dried, and stored until the images were acquired. Samples were subsequently sputter-coated with a two nm-thick platinum layer (208HR sputter coater, Cressington, Watford, UK) and visualized using the SEM. The structural diversity was further compared with SEM images from the literature [12,31,41–53]. Additionally, we investigated both incubation media, freshwater and seawater, as a blank for comparison with the samples. To do so, 20 µL of the respective pure media without microplastics were pipetted onto the carbon conductive tabs and further processed as described.

2.4. Classification of Observed Structural Diversity via SEM Images

We compared the microorganismal and non-microorganismal structures in the SEM images and compared them with typical microbial structures found in the literature [12,31,41–53]. For instance, spherical structures resembling coccoid cellular structures were defined as coccoid bacteria (cc). A summary of all detected structures can be found in Table 2.

The overall number of different structures observed within the 14-day incubation were counted and defined as the biofilms' structural diversity. We categorized the structural diversity into low, medium, and high structural diversity (0–3, 4–6, and 7–9 numbers of different structures, respectively), depending on the number of the observed different structures.

Table 2. Summary of the biofilm structures. Abbreviations and associated structures from late and early stage biofilm formation were observed in SEM images.

	Biofilm Structures	
	Abbreviation	**Associated Structure**
late-stage biofilm	compf	compartmented filaments
	edia	elongated diatoms
	f	filamentous
	flag	flagella-like
	mc	multicellular
	media	marine elongated diatoms
	pEPS	particulate EPS
	res	rough elliptical structure
	sp	sporous
	tmf	thin mucus-like film
	tub	tubular

Table 2. *Cont.*

	Biofilm Structures	
	Abbreviation	**Associated Structure**
	a	non-assignable/exceptional microorganismal structure
	cc	coccoid bacteria
	cd	centric diatom
	d	diatom
	f	filamentous structure
early stage biofilm	mc	multicellular
	p	platelet
	rp	round platelet
	rod	rod-/vibrio-shaped bacteria
	rodf	rod-/vibrio-shaped bacteria with flagella
	sf	solid film
	tf	thin film
	uc	unicellular

2.5. ζ-Potential

The ζ-potential gives information about the electrostatic potential at the surfaces of the polymer of hydrodynamic shear or slipping plain surrounding a polymer particle and helps to predict how a particle may interact with other surfaces or soluble [54]. The ζ-potential measurements were performed as recently described [55]. In brief, 200 mg of each polymer type's fragments were investigated with the Electrokinetic Analyzer EKA (Anton Paar GmbH, Austria). The fragments were packed densely in a cylindrical powder cell with a diameter 12 mm and height 2 mm and covered at both ends with a 20 μm pore sized membrane. After mounting the powder cells, 0.001 M KCl was streamed through the samples until an equilibrium was reached. The pH value was adjusted by adding 0.1 M HCl or 0.1 M KOH solution. The ζ-potential was calculated as described in Drechsler et al. [55], without the correction for the surface conductivity, as the particle geometry was unknown for fragments.

3. Results

3.1. Surface Properties—ζ-Potential

We measured the initial ζ-potential via a pH titration, ranging from an acidic pH of 2 up to an alkaline pH of 9. In the acidic pH range, PET showed the highest ζ-potential, followed by PA and the lowest ζ-potential for PVC. Within the pH titration, we observed the highest drop in ζ-potential for PA (from +12 ± 0.1 mV at pH 2.5 to −55 ± 1 mV at pH 8.9), followed by PET (from +15 ± 0.1 mV at pH 2.6 to −39 ± 1 mV at pH 8.8) and PVC showing the smallest drop in ζ-potential (from +3 ± 1 mV at pH 2.5 to −17 ± 2 mV at pH 8.9) (Figure 1). Table 3 shows the ζ-potential at pH 8 which refers to the pH of both incubation media with PA showing the highest negative ζ-potential, followed by PET and PVC showing the lowest negative ζ-potential (−55 ± 1 mV, −43 ± 1 mV and −15 ± 1 mV, respectively).

Table 3. ζ-potential at pH 8, contact angles, and the overall number of structural diversities on the surfaces of the three polymers after the incubation in freshwater (FW) and seawater (SW) within two weeks.

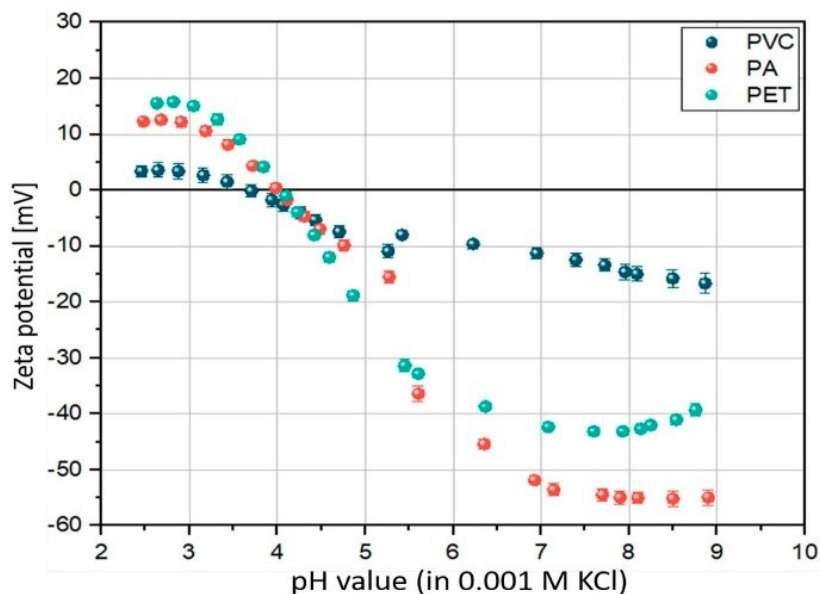| Polymer Type	ζ-Potential (pH 8)	Contact Angle [56]	Environmental Media	Biofilm Structural Diversity [14 Days]
PA	−55 mV	70°	FW	9
			SW	7
PET	−43 mV	81°	FW	6
			SW	6
PVC	−15 mV	87°	FW	3
			SW	8

Figure 1. Zeta potential values of the three polymers versus pH value. The zeta potential was measured for polyvinyl chloride (PVC) (blue), polyamide (PA) (red), and polyethylene terephthalate (PET) (green) via pH titration in 0.001M KCl. Values indicate means ± standard error of the mean.

3.2. Structural Diversity of the Early-Stage Biofilm

We found differences in the numbers of structural diversities depending on the polymer type and incubation medium. After incubating the polymers in freshwater, we found the highest structural diversity on PA followed by a medium structural diversity on surfaces of PET and a low structural diversity on PVC. However, in seawater, PVC showed the highest structural diversity followed by a high structural diversity of PA and a medium structural diversity of PET (see Table 3).

We did not find any structures resembling microorganismal or non-microorganismal origin forming a biofilm on any control image of the non-incubated polymers (see Figure S2). In botch incubation media, freshwater and seawater, microorganisms, and non-microorganismal structures were abundant (see Figures S3 and S4).

3.3. Morphological Strcutures Within Late-Stage Biofilms

For comparison with the early stage biofilms we first investigated PA pellets incubated in freshwater and seawater for approximately two years for a clear idea of the structures forming a mature biofilm. The mature biofilm on PA pellets incubated in freshwater (Figure 2) showed a relatively smooth surface consisting of filamentous (f), compartmented multicellular (compf, mc), and smooth tubular (tub) structures with embedded elongated diatoms (edia). Figure 3 shows a mature biofilm on a PA pellet incubated in seawater, with microorganismal structures and marine diatoms (media) embedded in reticulate structures with a relatively rough surface. The overall structural diversity on the PA pellets after two years was higher in freshwater compared to the structural diversity observed in seawater (eight and four morphological structures, respectively).
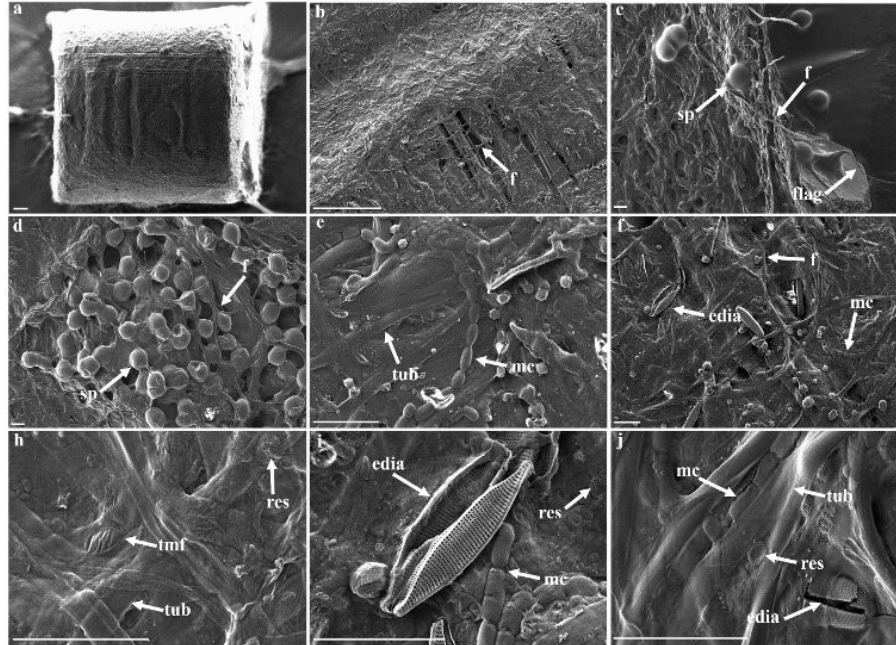
Figure 2. Scanning electron microscopy images of PA pellet incubated in freshwater for two years. Filamentous structures (**f**) almost completely cover the PA pellet (**a**,**b**). (**c**–**j**) show higher magnifications of smooth late-stage biofilm. Sporous (sp), multicellular (mc), and tubular (tub) structures form the coalesced reticular structure of the biofilm. Elongated diatoms (edia) as exceptional rough elliptical structures (res) are on top and embedded within the biofilm. Furthermore, exceptional thin mucus-film-like (tmf) and flagella-like structures (flag) are highlighted. Scale bars: (**a**,**b**) 100 μm, (**c**–**j**) 10 μm.
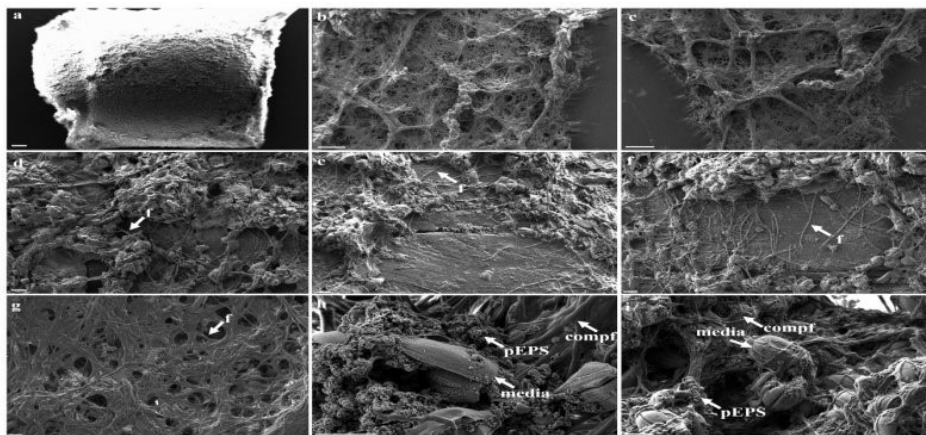
Figure 3. Scanning electron microscopy images of PA pellet incubated in seawater for two years. (**a**–**j**) Reticulate structures forming a mature biofilm consisting of (**e**–**g**) filamentous structures (**f**) and marine elongated diatoms (media). pEPS indicate particulate EPS. Higher magnification reveals filamentous cells being compartmented filaments (compf) resembling filamentous unbranched algae or cable bacteria. Scale bars: (**a**–**c**) 100 μm, (**d**–**i**) 10 μm.

3.4. Morphological Strcutures Within Early-Stage Biofilms

All polymers incubated in seawater showed increasing amounts of salt crystals with increasing incubation time, which we could not detect for the polymers incubated in freshwater. Nevertheless, there were no obvious differences in the roughness or overall appearance for all polymer types from both incubation media for incubation times less than eleven days. However, we observed marked differences in structural diversity of early-stage biofilms for all polymer types, time points, and incubation media (Figures 4–9).

Although elongated diatoms (*edia*, bilateral, mostly sessile [57]) occurred in both late-stage biofilms from fresh- and seawater, diatoms (*d*) were only observed once in the early-stage biofilms of PA after two weeks of incubation in freshwater (Figure 4). Interestingly, centric diatoms (*cd*, radial, mostly planktonic [57]) exclusively occurred in early-stage biofilms originating from seawater and were found on all polymer type surfaces but not in late-stage biofilms on PA pellets.

Small coccoid and platelet-shaped structures (*cc*, see e.g., Figure 6 after seven days of incubation) occurred in both incubation media on all polymer types. Whereas the round platelet (*rp*) structures, which were also present in the pure incubation media (see Figure S3 and S4), were exclusively found on PA and PET in early-stage freshwater biofilms (see e.g., Figure 4 after two days of incubation and Figure 6 after seven days of incubation) but not on PVC at any time. Another interesting finding was that rod- and vibrio-shaped bacteria (*rod*, see e.g., Figure 7 after one day of incubation) were found on all polymer types incubated in both media, except for PVC incubated in freshwater (which was mainly covered by platelet-shaped (*p*) and coccoid (*cc*) structures). Albeit, the rod- and vibrio-shaped bacteria, which seemed to have a long flagellum (*rodf*, see e.g., Figure 5 after eleven days of incubation), only occurred on the surfaces of PA microplastic fragments independent of the incubation medium. Filamentous (*f*) structures on PVC microplastic fragments incubated in freshwater after two weeks could possibly resemble flagella (see e.g., Figure 8 after 14 days of incubation), or also other bacterial appendices. In addition to the unicellular (*uc*) structures (see e.g., Figure 7 after eleven days of incubation) observed on all polymer types incubated in seawater, the multicellular (*mc*) structures were only observed on surfaces of PA and PET microplastic particles incubated for eleven days in freshwater (Figures 4 and 6). A comparison of the found morphological structures of both late and early stage biofilms with descriptions of biofilms from the literature is given in the following Section 4.
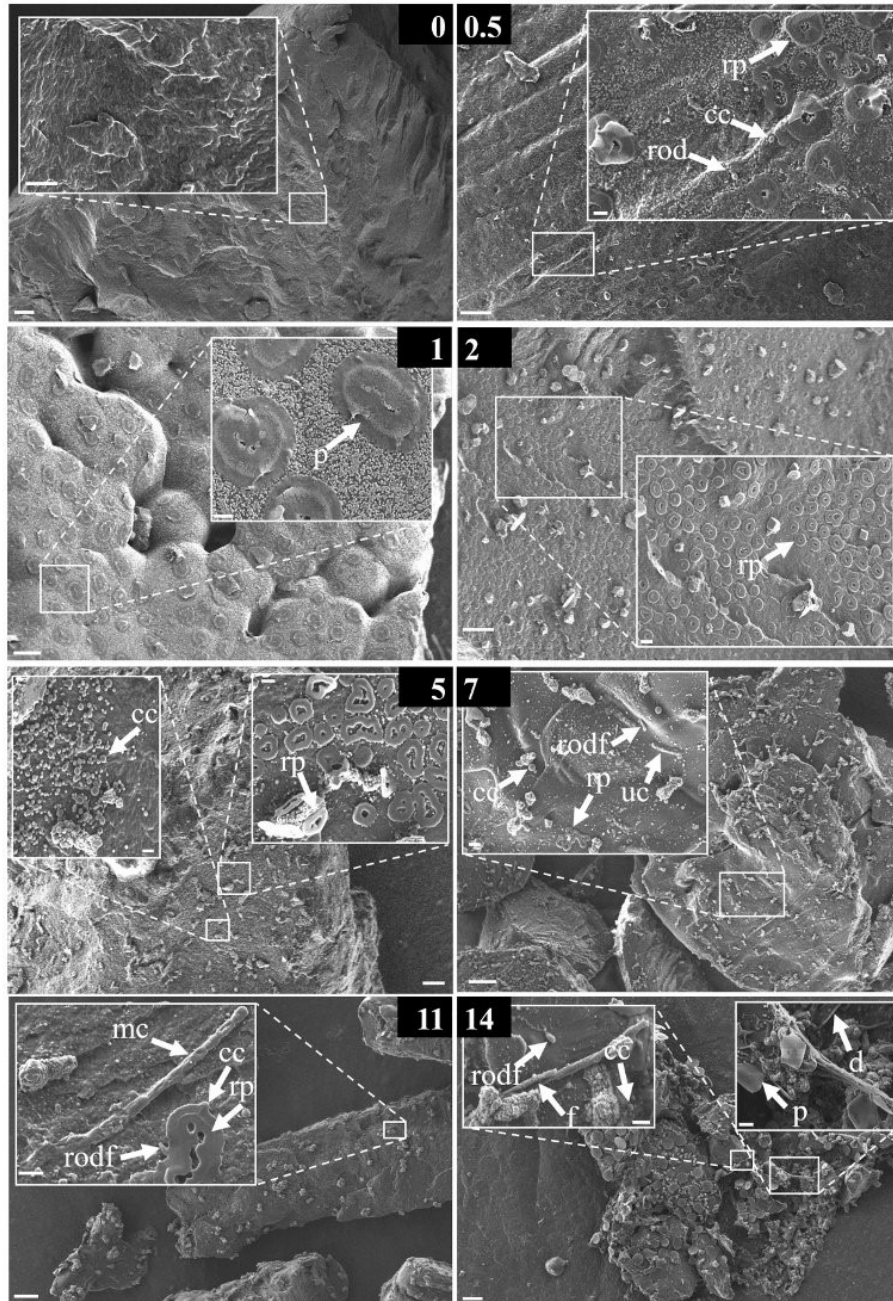
Figure 4. Scanning electron microscopy images of PA incubated in freshwater. Numbers in black boxes indicate incubation times in days (0 = raw material, 0.5 = half day, 1 = one day, 2 = two days, 5 = five days, 7 = seven days, 11 = eleven days, 14 = 14 days of incubation). Microorganismal structures are highlighted with arrows. rod= rod/vibrio-shaped bacteria, rodf = rod/vibrio-shaped bacteria with long flagella, cc = coccoid bacteria, d = diatom, f = filamentous structure, mc = multicellular structure, rp = round platelet structure, p = platelet structure, uc = unicellular structure. Scale bar: Large image 10 μm, magnified image 2 μm.
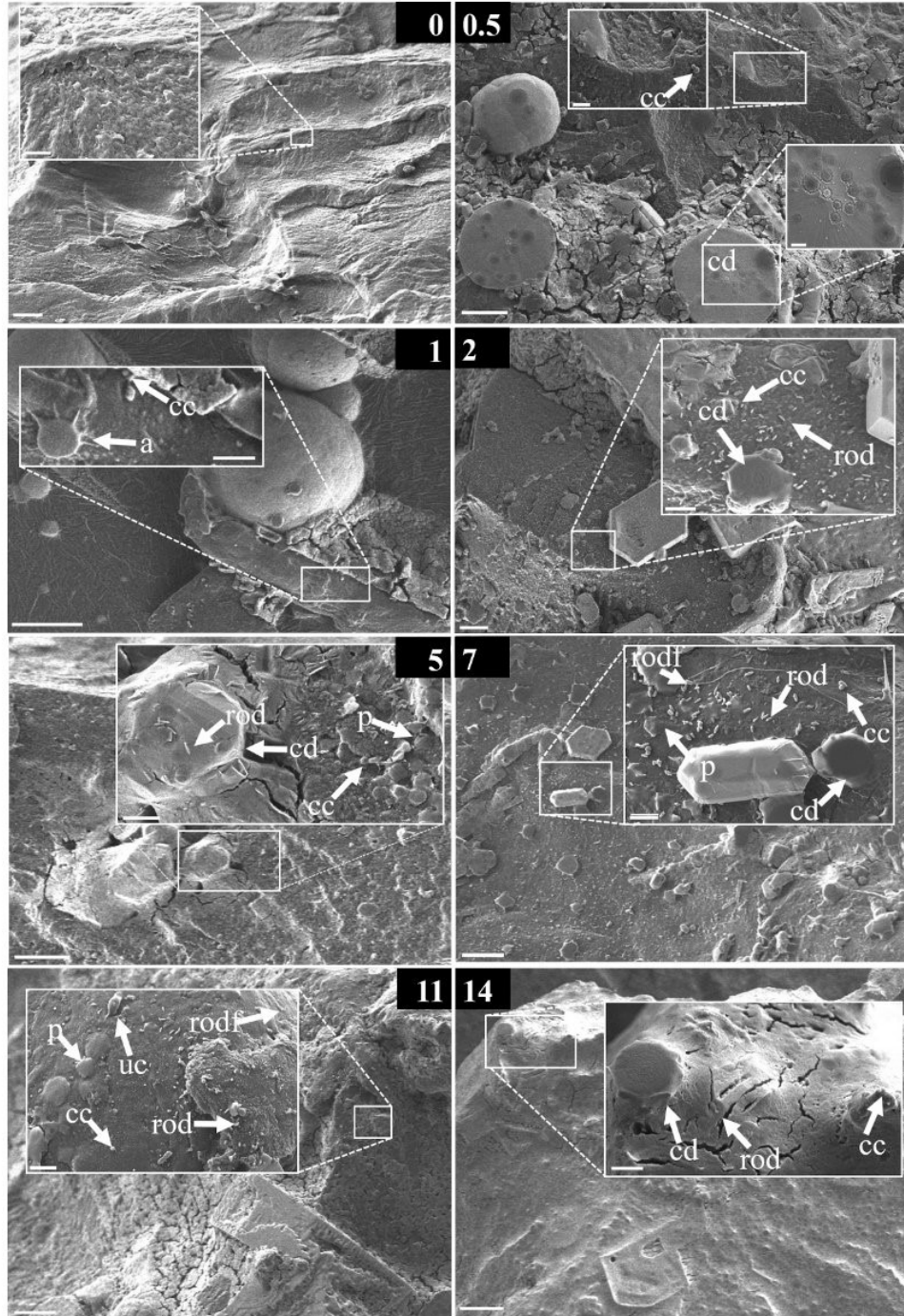
Figure 5. Scanning electron microscopy images of PA incubated in seawater. Numbers in black boxes indicate incubation times in days (0 = raw material, 0.5 = half day, 1 = one day, 2 = two days, 5 = five days, 7 = seven days, 11 = eleven days, 14 = 14 days of incubation). Microorganismal structures are highlighted with arrows. a = non-assignable structure, rod= rod-/vibrio-shaped bacteria, rodf = rod-/vibrio-shaped bacteria with long flagella, cc = coccoid bacteria, cd = centric diatom, p = platelet structure, uc = unicellular structure. Scale bar: Large image 10 μm, magnified image 2 μm.
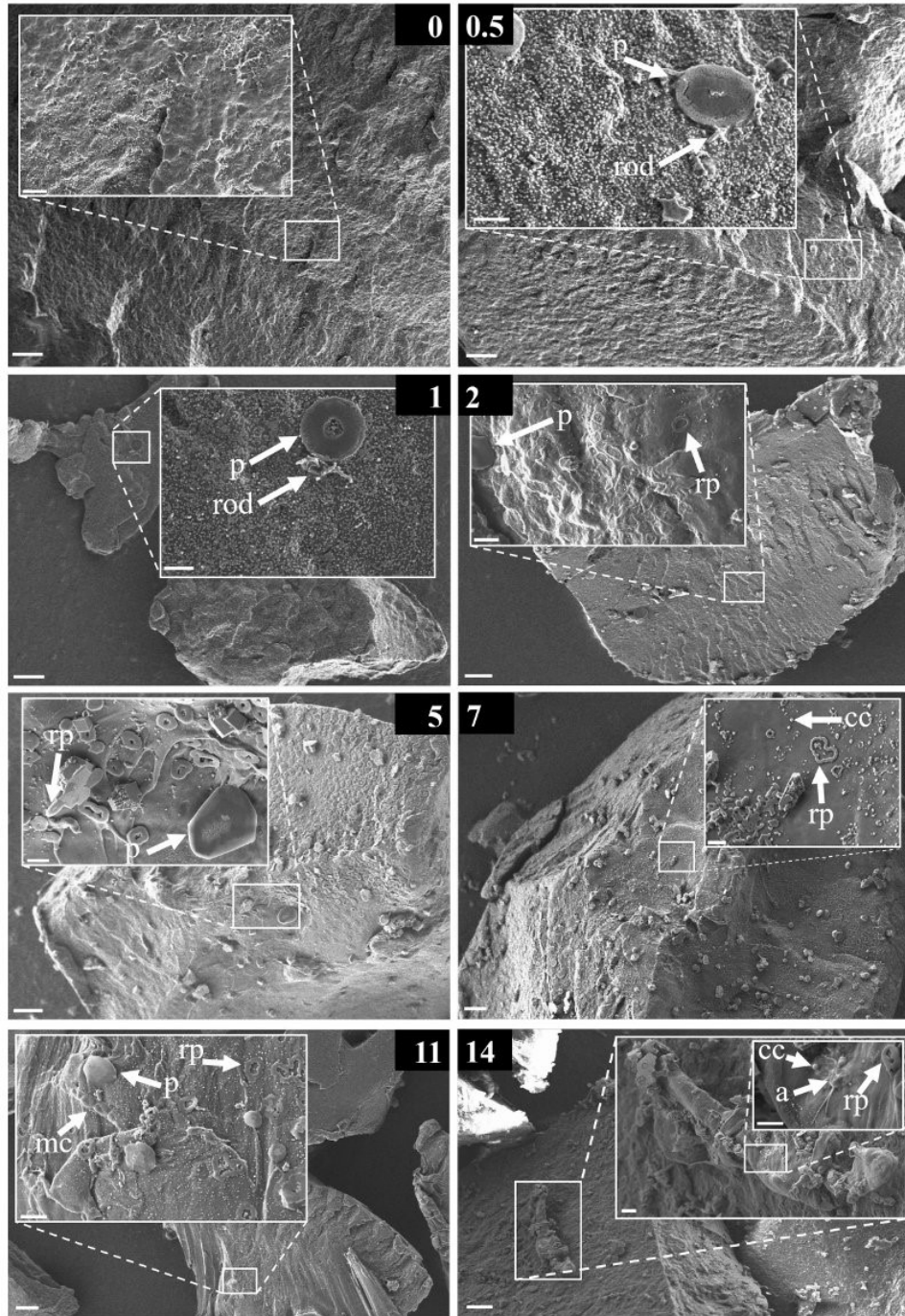
Figure 6. Scanning electron microscopy images of PET incubated in freshwater. Numbers in black boxes indicate incubation times in days (0 = raw material, 0.5 = half day, 1 = one day, 2 = two days, 5 = five days, 7 = seven days, 11 = eleven days, 14 = 14 days of incubation). Microorganismal structures are highlighted with arrows. a = non-assignable structure, rod= rod/vibrio-shaped bacteria, cc = coccoid bacteria, mc = multicellular structure, p = platelet structure, rp = round platelet structure. Scale bar: Large image 10 μm, magnified image 2 μm.
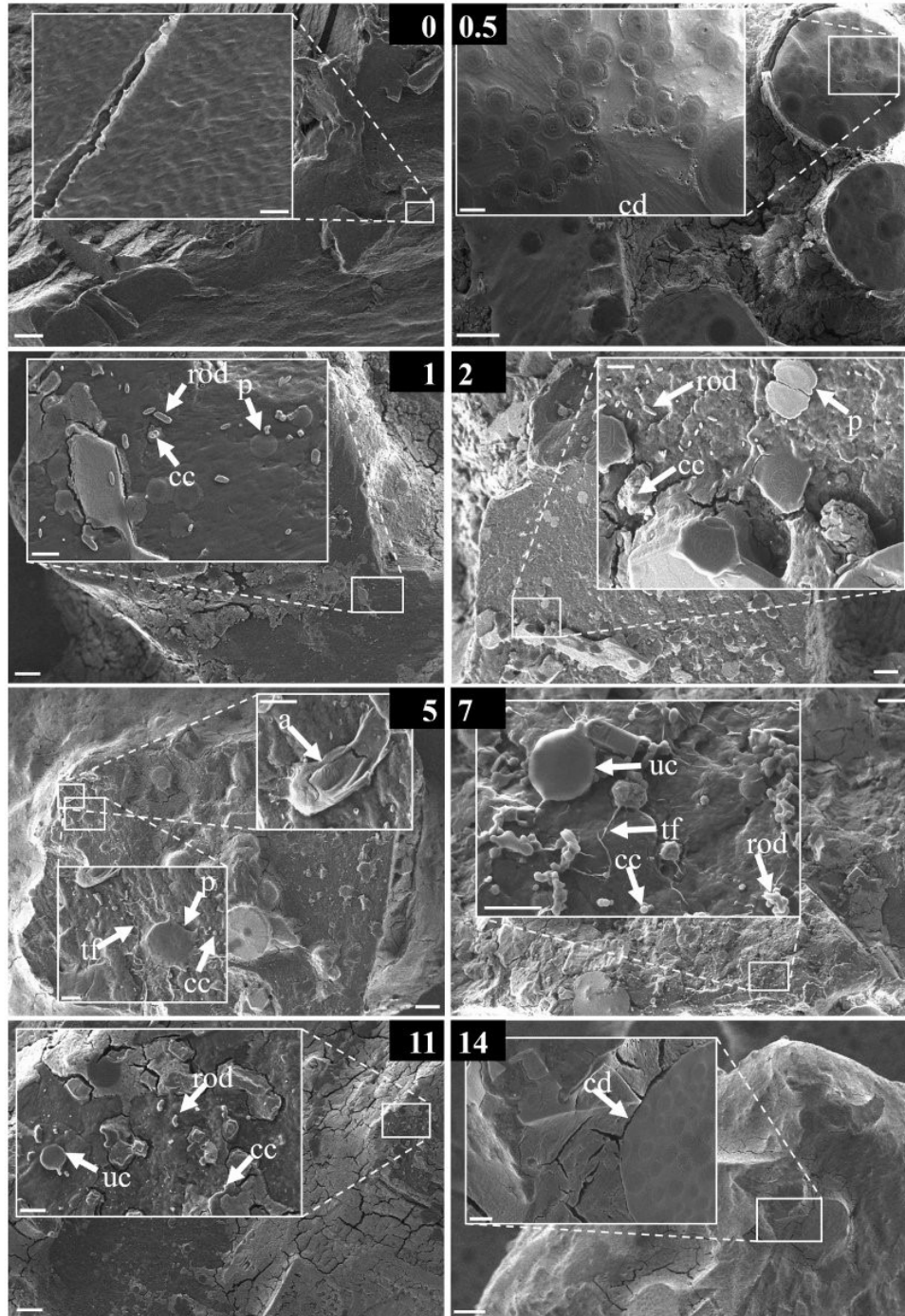
Figure 7. Scanning electron microscopy images of PET incubated in seawater. Numbers in black boxes indicate incubation times in days (0 = raw material, 0.5 = half day, 1 = one day, 2 = two days, 5 = five days, 7 = seven days, 11 = eleven days, 14 = 14 days of incubation). Microorganismal structures are highlighted with arrows. a = non-assignable structure, rod= rod/vibrio-shaped bacteria, cc = coccoid bacteria, p = platelet structure, tf = thin film, uc = unicellular structure. Scale bar: Large image 10 µm, magnified image 2 µm.
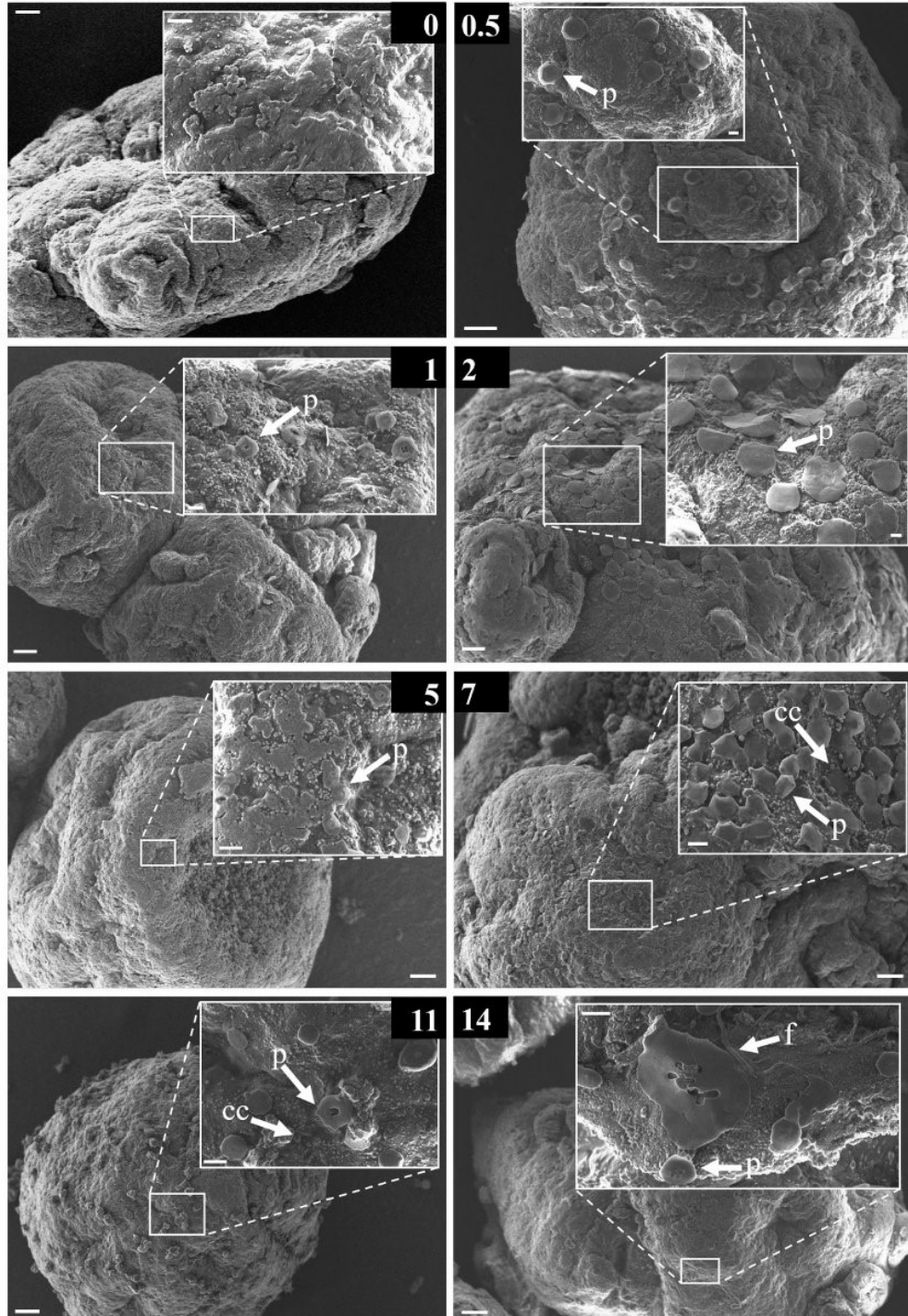
Figure 8. Scanning electron microscopy images of PVC incubated in freshwater. Numbers in black boxes indicate incubation times in days (0 = raw material, 0.5 = half day, 1 = one day, 2 = two days, 5 = five days, 7 = seven days, 11 = eleven days, 14 = 14 days of incubation). Microorganismal structures are highlighted with arrows. cc = coccoid bacteria, f = filamentous structure, p = platelet structure. Scale bar: Large image 10 μm, magnified image 2 μm.
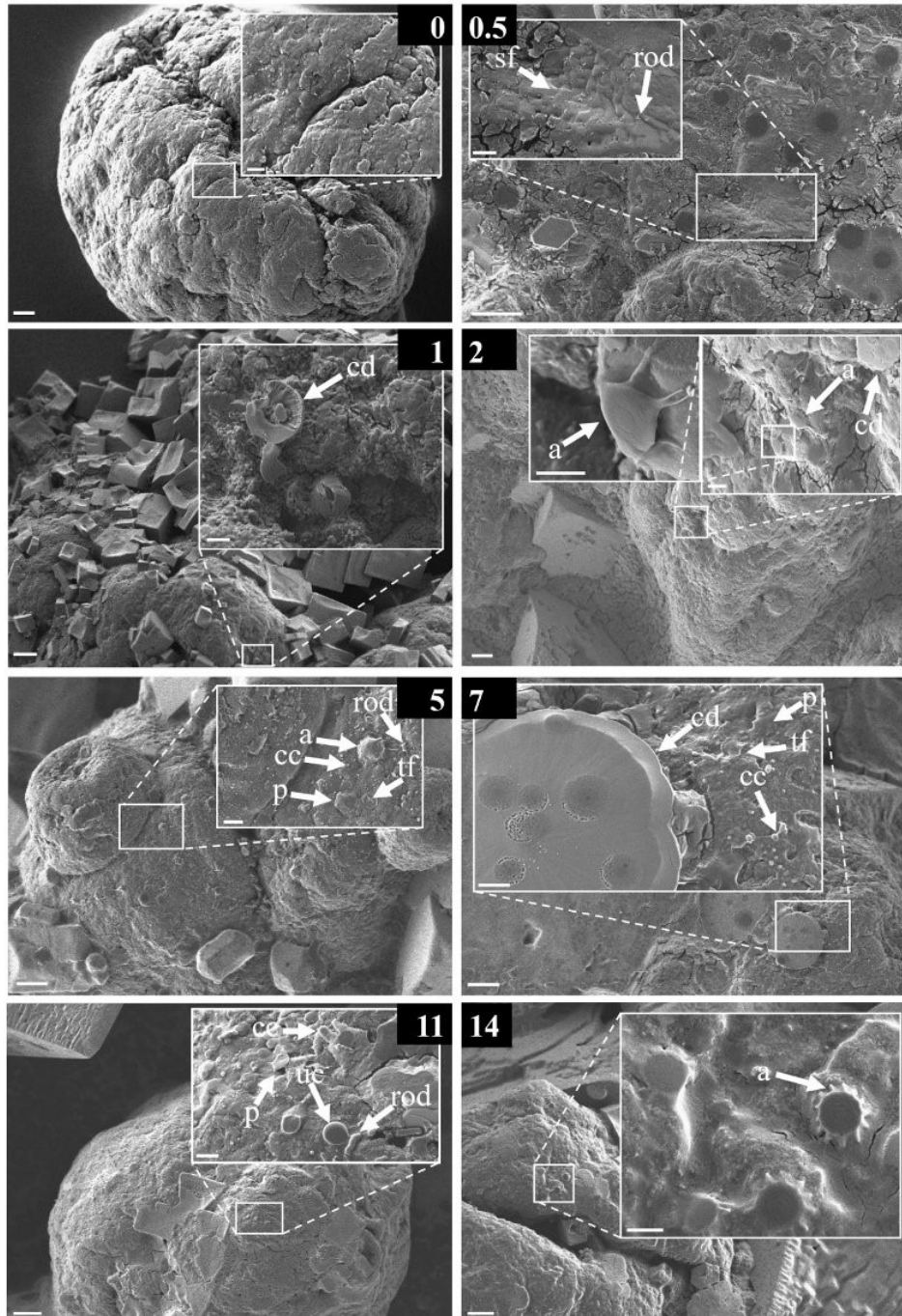
Figure 9. Scanning electron microscopy images of PVC incubated in seawater. Numbers in black boxes indicate incubation times in days (0 = raw material, 0.5 = half day, 1 = one day, 2 = two days, 5 = five days, 7 = seven days, 11 = eleven days, 14 = 14 days of incubation). Microorganismal structures are highlighted with arrows. a = non-assignable structure, rod= rod/vibrio-shaped bacteria, cc = coccoid bacteria, cd = centric diatom, p = platelet structure, sf = solid film, tf = thin film, uc= unicellular structure. Scale bar: Large image 10 µm, magnified image 2 µm.

4. Discussion

4.1. Correlation of Structural Diversity of Early-Stage Biofilms and Polymer Properties

It has already been shown that several factors are influencing the results from ζ-potential measurements, such as the pH, particle concentration, and additionally the ionic strength of the measurement media [58]. The freshwater and artificial seawater medium used for incubation in our experiments both had a pH value of around 8. Interestingly, within this pH range, PA has the highest negative ζ-potential followed by PET and PVC, showing the lowest negative ζ-potential (see Table 3). It must be considered that beside the similar pH values of freshwater and seawater, the ionic strength may be different. Due to a higher amount of solved salts in seawater, the ionic strength is described to be 500 times higher than in freshwater [59]. As soon as the polymers face either freshwater or seawater, their surfaces may interact with available ions, influencing their ζ-potential immediately. Therefore, we conducted a time-series incubation to monitor the time-dependent development of an early-stage biofilm formation and if this correlates with the initial ζ-potential of the polymers. We found a clear correlation between the higher negative initial ζ-potential and the highest structural diversity observed for PA when incubating the polymers for two weeks in freshwater, indicating that a negative charge of the polymer surface facilitates or triggers the settlement of microorganisms in freshwater. The latter correlation holds not true for the polymers incubated in seawater, as we found the highest structural diversity on PVC with the lowest negative ζ-potential, followed with a high structural diversity on PA and PET showing medium structural diversities (see Table 3). This indicates that other surface properties than ζ-potential may also play a role in the early stage biofilm formation in seawater.

Sanni et al. [60] describe that the settlement of bacteria on the polymer surface is strongly correlated with the polymer's morphology. The morphologies of the pristine polymers (before the incubation) visualized with SEM differed only slightly. PA and PET fragments showed similar, relatively smooth surfaces with some cracks, whereas PVC particles were relatively spherical with a slightly rougher surface and deeper cracks (see Figure S2). In addition to the morphology and initial ζ-potential of the particles, the settlement of bacteria on the polymer surface is also correlated with the polymer's hydrophobicity [60]. The hydrophobicity of polymers can be measured via determining the contact angle of a liquid drop in contact with a solid surface [61]. The larger the contact angle, the larger the hydrophobicity of the solid surface. It was found that the contact angles for PA, PET, and PVC are 70°, 81°, and 87°, respectively [56]. Contact angles smaller than 90° are usually associated with hydrophilic surfaces. This indicates that all polymers used in our experiments have hydrophilic surfaces, with PA being the most and PVC the least hydrophilic polymer. Nevertheless, contact angles are usually measured by applying a water drop on the polymers' clean and flat surfaces, which makes it difficult to measure the contact angle for irregularly shaped microplastic particles [56], such as those we used in our experiments. Next to the different initial ζ-potential, morphology, and hydrophobicity of the three polymers used, the nature of the polymer itself may play an additional role. For instance, it has already been described that PVC has a low binding affinity to Staphylococci, which may also be true for other microorganisms because of its chloride content and the high content of plasticizers [62]. Interestingly, the structural diversity on PVC surfaces incubated in seawater was the highest observed, which is probably due to the fact that microorganisms from seawater are better adapted to higher chloride concentrations than freshwater microorganisms. This is most probably related to the overall higher salinity of seawater compared to freshwater, with sodium chloride being amongst the most common salts in the marine environment [63].

4.2. Descriptive Analysis of the Observed Morphological Structures Forming a Late-Stage Biofilm

The smooth tubular structures (*tub*, see Figure 2e) observed on the PA pellet incubated in freshwater for 2 years strongly resembled fungal hyphae [41], with indications of spore formation (*sp*, see Figure 2d). Structures (Figure 3e) observed on PA incubated in seawater resemble the microbial cells that Zettler et al. [31] found on marine plastic debris (see Zettler et al. [31], Figure 2d), although

in our case, the cells seemed attached to, instead of pitting into, the PA surface. The differences between seawater and freshwater in the late-stage biofilm structures may relate to different types of EPS and the differences in salinity of the incubation media. Two types of EPS are typically described, which are defined as dissolved and particulate EPS (*pEPS*, Figure 3 h) [42,43]. For instance, diatoms show different morphological forms of EPS, such as highly crystalline and rigid fibrils (rough) up to highly hydrated and mucilaginous capsules (smooth) [43,44]. We observed diatoms in both biofilms originating from freshwater and seawater, which may explain the structural differences in the late-stage biofilms. The observed rough surface of the biofilm originating from seawater may be a combination of a higher proportion of particulate EPS and the higher salinity of seawater, resulting in salt crystals' embedment during the sample drying.

4.3. Descriptive Analysis of the Observed Morphological Structures Forming an Early-Stage Biofilm

The abundant platelet-shaped structures (*p*, e.g., Figure 4) observed already after one-day incubation on all polymer surfaces independent of the incubation medium were likely not of biological origin. While they remain unidentified and could indicate desorption or outcropping processes within polymers, some resembled triangular scales of the testate amoeba *Penardeugenia* [45] and scales of other protists of the genera *Thaumatomastix* and *Reckertia* [46]. However, the platelet-shaped structures may also originate from polygonal cells [53] or damaged *Staphylococcus aureus*-like cells [47], as we found small coccoid structures (*cc*, see e.g., Figure 6 after seven days of incubation) in both incubation media and on all polymer types, just as the platelet-shaped structures. Bacterial cocci are typically 0.5–1.5 μm in size [64], which is about the size range of the coccoid-shaped structures we observed. Interestingly, round platelet (*rp*) structures were exclusively found on PA and PET in early-stage freshwater biofilms (see e.g., Figure 4 after two days of incubation and Figure 6 after seven days of incubation). We did not observe round platelet structures on PVC, but at any time in the pure freshwater incubation medium (SEM images of both incubation media, see Figure S3 and S4), we can exclude that these structures originate from drying effects or from the early degradation processes of the polymers. The round platelet structures also resembled scales from planktonic algae such as silica-scaled chrysophytes [48], but their early appearance and very regular distribution make them unlikely to be of microorganismal but rather inorganic origin or drying effects.

The multicellular structures found in the early-stage biofilms resemble those found in the late-stage freshwater biofilms, indicating that these organisms may attach to surfaces already after less than two weeks of incubation and further develop a mature biofilm. The multicellular structures could be of diverse origin but resemble filamentous microorganisms such as cable bacteria [49] or multicellular Cyanobacteria [50]. Abundantly found on the surfaces of polymers incubated in seawater were structures resembling centric diatoms [12,44] (cd, see e.g., Figure 9 after one day of incubation). In their comprehensive review, Hoagland et al. [44] described different mechanisms for the attachment of elongated and centric diatoms on surfaces using EPS in the form of stalks, tubes, apical pads, adhering films, fibrils, or cell coatings. We observed some structures in the very early-stage of biofilm formation, which we named exceptional microorganismal structures (e.g., in Figure 5 after one day of incubation). These were exclusively found in seawater treatments and may be centric diatoms forming fibrils or stalks [44]. However, these structures with about 3 μm in diameter are at the lower size range of small centric diatoms [51,52]. Furthermore, we found film-like structures on PET and PVC incubated in seawater that may be part of extruded EPS (Figures 7 and 9). On PET, we found exclusively thin and smooth films (tf, see e.g., Figure 7 after seven days of incubation), which were additionally accompanied by a solid film (sf, see e.g., Figure 9 after half a day of incubation) on PVC. When considering the five successive steps of biofilm formation described by Renner and Weibel [37], EPS's excretion initiates the second step of biofilm formation, which starts the formation of a mature biofilm. This means that for PET and PVC incubated in seawater, five days and one week of incubation, respectively, initiates the maturing of a biofilm. Furthermore, our observations demonstrate that the structural diversity on the surfaces of the three polymers from either freshwater or seawater differed, although

the same experimental conditions were chosen for each polymer–environmental medium combination. This highlights that the properties of a polymer itself may play a crucial role for the formation of a very early-stage biofilm on different plastics.

4.4. Potential Ecological Implications of Our Findings

De Tender et al. [65] showed the temporal dynamics of bacterial and fungal colonization on plastic materials within almost one year in the marine environment. They found community changes by using genetic screening methods and additionally visualized the development of the late-stage biofilm. Within the observed time periods of one month, the maturing of a biofilm was macroscopically visible [65]. For plastics incubated in seawater, it has already been shown that biofilms enhance polymer palatability by mimicking an organic origin [26,27]. Exposure of polystyrene beads to filtered seawater for three weeks [26] and polyethylene for one month of incubation directly in the marine environment [27] increased the ingestion, possibly increasing the physical and chemical risks from plastic particles to the tested organisms. However, this phenomenon has not been shown for other polymer types incubated for shorter time periods or incubated in freshwater. Hence, our results indicate that even short-term environmental exposure may be sufficient that a variety of organisms from different ecosystems mistake microplastics with food.

5. Conclusions

Here, we show that already, half a day of incubation in either freshwater or seawater initiates the formation of an early-stage biofilm by the attachment of microbial structures, but possibly also the appearance of non-microbial structures. The overall structural diversity of biofilm structures increased within two weeks for all polymer types in both incubation media. We show that a mature biofilm on PA differs in its composition depending on the incubation medium and found that the early-stage biofilm formation on three different polymers depends on the incubation medium and is most probably related to the polymers' surface properties. In freshwater, we found a correlation of the initial ζ-potential of the particles with the structural diversity on the polymer's surfaces. PA, with the highest negative initial ζ-potential, showed the highest structural diversity and PVC with the lowest negative initial ζ-potential showed the lowest structural diversity. However, in seawater, PVC showed the highest structural diversity with the lowest negative initial ζ-potential. For seawater, we did not find a clear correlation with the initial ζ-potential, as there were not such apparent differences between PET and PA. Furthermore, we show that the early-stage biofilm formation on polymers seems additionally being dependent on the polymers' surface morphology and the polymers' chemical composition. Our findings emphasize the complexity that can be related to research on microplastic biofilms and show that not solely the polymer type but also the incubation medium, time, and the initial surface properties of the used polymers may play an important role for the initial colonization of plastic surfaces.

References

1. Andrady, A.L.; Neal, M.A. Applications and societal benefits of plastics. *Philos. Trans. R. Soc. B Biol. Sci.* **2009**, *364*, 1977–1984. [CrossRef]

2. Barnes, D.K.A.; Galgani, F.; Thompson, R.C.; Barlaz, M. Accumulation and fragmentation of plastic debris in global environments. *Philos. Trans. R. Soc. Lond. B Biol. Sci.* **2009**, *364*, 1985–1998. [CrossRef]

3. Thompson, R.C.; Olsen, Y.; Mitchell, R.P.; Davis, A.; Rowland, S.J.; John, A.W.J.; McGonigle, D.; Russell, A.E. Lost at sea: Where is all the plastic. *Science* **2004**, *304*, 838. [CrossRef]

4. Arthur, C.; Baker, J.; Bamford, H. Proceedings of the International Research Workshop on the Occurrence, Effects, and Fate of Microplastic Marine Debris. In *Conference Proceedings*; Environmental Science: Silver Spring, MD, USA, 2008; p. 530.

5. Andrady, A.L. The plastic in microplastics: A review. *Mar. Pollut. Bull.* **2017**, *119*, 12–22. [CrossRef]

6. Dris, R.; Imhof, H.; Sanchez, W.; Gasperi, J.; Galgani, F.; Tassin, B.; Laforsch, C. Beyond the ocean: Contamination of freshwater ecosystems with (micro-) plastic particles. *Environ. Chem.* **2015**. [CrossRef]

7. Piehl, S.; Leibner, A.; Löder, M.G.J.; Dris, R.; Bogner, C.; Laforsch, C. Identification and quantification of macro- and microplastics on an agricultural farmland. *Sci. Rep.* **2018**, *8*, 17950. [CrossRef] [PubMed]

8. Dris, R.; Gasperi, J.; Saad, M.; Mirande, C.; Tassin, B. Synthetic fibers in atmospheric fallout: A source of microplastics in the environment? *Mar. Pollut. Bull.* **2016**, *104*, 290–293. [CrossRef] [PubMed]

9. Gasperi, J.; Wright, S.L.; Dris, R.; Collard, F.; Mandin, C.; Guerrouache, M.; Langlois, V.; Kelly, F.J.; Tassin, B. Microplastics in air: Are we breathing it in? *Curr. Opin. Environ. Sci. Health* **2018**, *1*, 1–5. [CrossRef]

10. Imhof, H.K.; Ivleva, N.P.; Schmid, J.; Niessner, R.; Laforsch, C. Contamination of beach sediments of a subalpine lake with microplastic particles. *Curr. Biol.* **2013**, *23*, R867–R868. [CrossRef]

11. Imhof, H.K.; Sigl, R.; Brauer, E.; Feyl, S.; Giesemann, P.; Klink, S.; Leupolz, K.; Löder, M.G.J.; Löschel, L.A.; Missun, J.; et al. Spatial and temporal variation of macro-, meso- and microplastic abundance on a remote coral island of the Maldives, Indian Ocean. *Mar. Pollut. Bull.* **2017**, *116*, 340–347. [CrossRef]

12. Lacerda, A.L.d.F.; Rodrigues, L. dos S.; van Sebille, E.; Rodrigues, F.L.; Ribeiro, L.; Secchi, E.R.; Kessler, F.; Proietti, M.C. Plastics in sea surface waters around the Antarctic Peninsula. *Sci. Rep.* **2019**, *9*, 3977. [CrossRef] [PubMed]

13. Woodall, L.C.; Sanchez-Vidal, A.; Canals, M.; Paterson, G.L.J.; Coppock, R.; Sleight, V.; Calafat, A.; Rogers, A.D.; Narayanaswamy, B.E.; Thompson, R.C. The deep sea is a major sink for microplastic debris. *R. Soc. Open Sci.* **2014**, *1*. [CrossRef]

14. Laist, D. Impacts of marine debris: Entanglement of marine life in marine debris including a comprehensive list of species with entanglement and ingestion records. In *Marine Debris—Sources, Impacts Solutions*; Coe, J.M., Rogers, D.B., Eds.; Springer: New York, NY, USA, 1997; pp. 99–139. [CrossRef]

15. Harper, P.C.; Fowler, J.A. Plastic pellets in New Zealand storm-killed prions (*Pachyptila* spp.) 1958–1977. *Notornis* **1987**, *34*, 65–70.

16. Cole, M.; Lindeque, P.; Fileman, E.; Halsband, C.; Goodhead, R.; Moger, J.; Galloway, T.S. Microplastic ingestion by zooplankton. *Environ. Sci. Technol.* **2013**, *47*, 6646–6655. [CrossRef] [PubMed]

17. Browne, M.A.; Dissanayake, A.; Galloway, T.S.; Lowe, D.M.; Thompson, R.C. Ingested microscopic plastic translocates to the circulatory system of the mussel, *Mytilus edulis* (L.). *Environ. Sci. Technol.* **2008**, *42*, 5026–5031. [CrossRef]

18. von Moos, N.; Burkhardt-Holm, P.; Koehler, A. Uptake and Effects of Microplastics on Cells and Tissue of the Blue Mussel *Mytilus edulis* L. after an Experimental Exposure. *Environ. Sci. Technol.* **2012**, *46*, 327–335. [CrossRef]

19. Lu, Y.; Zhang, Y.; Deng, Y.; Jiang, W.; Zhao, Y.; Geng, J.; Ding, L.; Ren, H. Uptake and Accumulation of Polystyrene Microplastics in Zebrafish (Danio rerio) and Toxic Effects in Liver. *Environ. Sci. Technol.* **2016**, *50*, 4054–4060. [CrossRef]

20. Rummel, C.D.; Löder, M.G.J.; Fricke, N.F.; Lang, T.; Griebeler, E.; Janke, M.; Gerdts, G. Plastic ingestion by pelagic and demersal fish from the North Sea and Baltic Sea. *Mar. Pollut. Bull.* **2015**. [CrossRef]

21. Prata, J.C.; da Costa, J.P.; Lopes, I.; Duarte, A.C.; Rocha-Santos, T. Environmental exposure to microplastics: An overview on possible human health effects. *Sci. Total Environ.* **2020**, *702*, 134455. [CrossRef]

22. Welden, N.A.; Lusher, A.L. *Microplastics: From Origin to Impacts*; Elsevier Inc.: New York, NY, USA, 2020; Volume 32, ISBN 9780128178805. [CrossRef]

23. Ryan, P.G. Effects of ingested plastic on seabird feeding: Evidence from chickens. *Mar. Pollut. Bull.* **1988**, *19*, 125–128. [CrossRef]

24. Koelmans, A.A.; Bakir, A.; Burton, G.A.; Janssen, C.R. Microplastic as a Vector for Chemicals in the Aquatic Environment: Critical Review and Model-Supported Reinterpretation of Empirical Studies. *Environ. Sci. Technol.* **2016**, *50*, 3315–3326. [CrossRef] [PubMed]

25. Kirstein, I.V.; Kirmizi, S.; Wichels, A.; Garin-Fernandez, A.; Erler, R.; Löder, M.; Gerdts, G. Dangerous hitchhikers? Evidence for potentially pathogenic Vibrio spp. on microplastic particles. *Mar. Environ. Res.* **2016**, *120*, 1–8. [CrossRef] [PubMed]

26. Vroom, R.J.E.; Koelmans, A.A.; Besseling, E.; Halsband, C. Aging of microplastics promotes their ingestion by marine zooplankton. *Environ. Pollut.* **2017**, *231*, 987–996. [CrossRef] [PubMed]

27. Hodgson, D.J.; Bréchon, A.L.; Thompson, R.C. Ingestion and fragmentation of plastic carrier bags by the amphipod Orchestia gammarellus: Effects of plastic type and fouling load. *Mar. Pollut. Bull.* **2018**, *127*, 154–159. [CrossRef] [PubMed]

28. Liu, P.; Zhan, X.; Wu, X.; Li, J.; Wang, H.; Gao, S. Effect of weathering on environmental behavior of microplastics: Properties, sorption and potential risks. *Chemosphere* **2020**, *242*. [CrossRef]

29. Lobelle, D.; Cunliffe, M. Early microbial biofilm formation on marine plastic debris. *Mar. Pollut. Bull.* **2011**, *62*, 197–200. [CrossRef]

30. Oberbeckmann, S.; Loeder, M.G.J.; Gerdts, G.; Osborn, A.M. Spatial and seasonal variation in diversity and structure of microbial biofilms on marine plastics in Northern European waters. *FEMS Microbiol. Ecol.* **2014**, *2*, 478–492. [CrossRef]

31. Zettler, E.R.; Mincer, T.J.; Amaral-zettler, L.A. Life in the ' Plastisphere ': Microbial communities on plastic marine debris. *Environ. Sci. Technol.* **2013**, *47*, 7137–7146. [CrossRef]

32. Dang, H.; Li, T.; Chen, M.; Huang, G. Cross-ocean distribution of Rhodobacterales bacteria as primary surface colonizers in temperate coastal marine waters. *Appl. Environ. Microbiol.* **2008**, *74*, 52–60. [CrossRef]

33. Webb, H.K.; Crawford, R.J.; Sawabe, T.; Ivanova, E.P. Poly(ethylene terephthalate) polymer surfaces as a substrate for bacterial attachment and biofilm formation. *Microbes Environ.* **2009**, *24*, 39–42. [CrossRef]

34. Hossain, M.R.; Jiang, M.; Wei, Q.H.; Leff, L.G. Microplastic surface properties affect bacterial colonization in freshwater. *J. Basic Microbiol.* **2019**, *59*, 54–61. [CrossRef] [PubMed]

35. Artham, T.; Sudhakar, M.; Venkatesan, R.; Madhavan Nair, C.; Murty, K.V.G.K.; Doble, M. Biofouling and stability of synthetic polymers in sea water. *Int. Biodeterior. Biodegrad.* **2009**, *63*, 884–890. [CrossRef]

36. Loeb, G.; Neihof, R. Marine conditioning films. *Adv. Chem.* **1975**, *145*, 319–335. [CrossRef]

37. Renner, L.D.; Weibel, D.B. Physicochemical regulation of biofilm formation. *MRS Bull.* **2011**, *36*, 347–355. [CrossRef] [PubMed]

38. Sutherland, I.W. The biofilm matrix—An immobilized but dynamic microbial environment. *Trends Microbiol.* **2001**, *9*, 222–227. [CrossRef] [PubMed]

39. Rummel, C.D.; Jahnke, A.; Gorokhova, E.; Kühnel, D.; Schmitt-Jansen, M. The Impacts of Biofilm Formation on the Fate and Potential Effects of Microplastic in the Aquatic Environment. *Environ. Sci. Technol. Lett.* **2017**. [CrossRef]

40. PlasticsEurope (Association of Plastic Manufacturers). *Conversio Market & Strategy GmbH Plastics—The Facts 2019*; PlasticsEurope (Association of Plastic Manufacturers): Brussels, Belgium, 2019.

41. González-Ramírez, A.I.; Ramírez-Granillo, A.; Medina-Canales, M.G.; Rodríguez-Tovar, A.V.; Martínez-Rivera, M.A. Analysis and description of the stages of Aspergillus fumigatus biofilm formation using scanning electron microscopy. *BMC Microbiol.* **2016**, *16*, 243. [CrossRef]

42. Solmaz, K.; Ozcan, Y.; Mercan Dogan, N.; Bozkaya, O.; Ide, S. Characterization and Production of Extracellular Polysaccharides (EPS) by Bacillus Pseudomycoides U10. *Environments* **2018**, *5*, 63. [CrossRef]

43. Zhang, S.; Xu, C.; Santschi, P.H. Chemical composition and 234Th (IV) binding of extracellular polymeric substances (EPS) produced by the marine diatom *Amphora* sp. *Mar. Chem.* **2008**, *112*, 81–92. [CrossRef]
44. Hoagland, K.D.; Rosowski, J.R.; Gretz, M.R.; Roemer, S.C. Diatom extracellular polymeric substances: Function, fine structure, chemistry, and physiology. *J. Phycol.* **1993**, *29*, 537–566. [CrossRef]
45. Dumack, K.; Siemensma, F.; Bonkowski, M. Rediscovery of the Testate Amoeba Genus Penardeugenia (Thaumatomonadida, Imbricatea). *Protist* **2018**, *169*, 29–42. [CrossRef] [PubMed]
46. Nicholls, K.H. New and little-known marine and freshwater species of the silica-scaled genera Thaumatomastix and Reckertia (Cercozoa: Thaumatomonadida). *J. Mar. Biol. Assoc. UK* **2013**, *93*, 1231–1244. [CrossRef]
47. Saraeva, I.; Kudryashov, S.I.; Danilov, P.; Busleev, N.; Tolordava, E.R.; Rudenko, A.A.; Zayarny, D.; Ionin, A.; Romanova, Y.M. Polarization-Sensitive Surface-Enhanced In Situ Photoluminescence Spectroscopy of S. aureus Bacteria on Gold Nanospikes. *Sensors* **2020**, *20*, 2466. [CrossRef]
48. Bessudova, A.Y.; Domysheva, V.M.; Firsova, A.D.; Likhoshway, Y.V. Silica-scaled chrysophytes of Lake Baikal. *Acta Biol. Sib.* **2017**, *3*, 47. [CrossRef]
49. Reimers, C.E.; Li, C.; Graw, M.F.; Schrader, P.S.; Wolf, M. The identification of cable bacteria attached to the anode of a benthic microbial fuel cell: Evidence of long distance extracellular electron transport to electrodes. *Front. Microbiol.* **2017**, *8*, 2055. [CrossRef]
50. Koon, M.A.; Almohammed Ali, K.; Speaker, R.M.; McGrath, J.P.; Linton, E.W.; Steinhilb, M.L. Preparation of prokaryotic and eukaryotic organisms using chemical drying for morphological analysis in scanning electron microscopy (SEM). *J. Vis. Exp.* **2019**, *2019*, 1–10. [CrossRef]
51. Margalef, R. Size of centric diatoms as an ecological indicator. *SIL Commun. 1953–1996* **1969**, *17*, 202–210. [CrossRef]
52. Wu, Y.; Li, Z.; Du, W.; Gao, K. Physiological response of marine centric diatoms to ultraviolet radiation, with special reference to cell size. *J. Photochem. Photobiol. B Biol.* **2015**, *153*, 1–6. [CrossRef]
53. Oliver, P.G.; Rodrigues, C.F. Thyasiridae (mollusca: Bivalvia) from the Kemp caldera hydrothermal site, south sandwich islands, Antarctica. *J. Conchol.* **2017**, *42*, 267–282. [CrossRef]
54. Lowry, G.V.; Hill, R.J.; Harper, S.; Rawle, A.F.; Hendren, C.O.; Klaessig, F.; Nobbmann, U.; Sayre, P.; Rumble, J. Guidance to improve the scientific value of zeta-potential measurements in nanoEHS. *Environ. Sci. Nano* **2016**, *3*, 953–965. [CrossRef]
55. Drechsler, A.; Caspari, A.; Synytska, A. Influence of roughness and capillary size on the zeta potential values obtained by streaming potential measurements. *Surf. Interface Anal.* **2020**, 1–5. [CrossRef]
56. Heinrich, P.; Hanslik, L.; Kämmer, N.; Braunbeck, T. The tox is in the detail: Technical fundamentals for designing, performing, and interpreting experiments on toxicity of microplastics and associated substances. *Environ. Sci. Pollut. Res.* **2020**, *27*, 22292–22318. [CrossRef]
57. Chiovitti, A.; Dugdale, T.M.; Wetherbee, R. Diatom Adhesives: Molecular and Mechanical Properties. *Biol. Adhes.* **2006**, *1*, 79–103. [CrossRef]
58. Bhattacharjee, S. DLS and zeta potential—What they are and what they are not? *J. Control. Release* **2016**, *235*, 337–351. [CrossRef]
59. Chepkwony, N.K.; Berne, C.; Brun, Y.V. Comparative analysis of ionic strength tolerance between freshwater and marine Caulobacterales adhesins. *J. Bacteriol.* **2019**, *201*, 18. [CrossRef]
60. Sanni, O.; Chang, C.Y.; Anderson, D.G.; Langer, R.; Davies, M.C.; Williams, P.M.; Williams, P.; Alexander, M.R.; Hook, A.L. Bacterial attachment to polymeric materials correlates with molecular flexibility and hydrophilicity. *Adv. Healthc. Mater.* **2015**, *4*, 695–701. [CrossRef]
61. Dwivedi, C.; Pandey, I.; Himanshu, P.; Ramteke, P.W.; Pandey, A.C.; Mishra, S.B.; Patil, S. *Electrospun Nanofibrous Scaffold as a Potential Carrier of Antimicrobial Therapeutics for Diabetic Wound Healing and Tissue Regeneration*; Elsevier Inc.: New York, NY, USA, 2017; ISBN 9780323527279. [CrossRef]
62. Frank, E.; Merete, W.; Lotte, C.; Anne-lise, H.; Vibke, T.R.; Clemmensen, I. Attachment of staphylococci to different plastic tubes in vitro. *Med. Microbiol.* **1994**, *40*, 37–42. [CrossRef]
63. Gorrell, H.A. Classification of Formation Waters Based on Sodium Chloride Content: GEOLOGICAL NOTES. *Am. Assoc. Pet. Geol. Bull.* **1958**, *42*, 2522. [CrossRef]

64. Harris, L.G.; Foster, S.J.; Richards, R.G.; Lambert, P.; Stickler, D.; Eley, A. An introduction to Staphylococcus aureus, and techniques for identifyingand quantifying S. aureus adhesins in relation to adhesion to biomaterials:Review. *Eur. Cells Mater.* **2002**, *4*, 39–60. [CrossRef]

65. De Tender, C.; Devriese, L.I.; Haegeman, A.; Maes, S.; Vangeyte, J.; Cattrijsse, A.; Dawyndt, P.; Ruttink, T. Temporal Dynamics of Bacterial and Fungal Colonization on Plastic Debris in the North Sea. *Environ. Sci. Technol.* **2017**, *51*, 7350–7360. [CrossRef]

water

MDPI

Supplementary Information

Structural diversity in early-stage biofilm formation on microplastics depends on environmental medium and polymer properties

Anja FRM Ramsperger [1,4], Anja C Stellwag [1], Anja Caspari[2], Andreas Fery[2], Tillmann Lueders[3], Holger Kress [4], Martin GJ Löder [1], and Christian Laforsch [1,*]

[1] Animal Ecology I, University of Bayreuth, Germany;
[2] Institut für Physikalische Chemie und Physik der Polymere, Leibniz Institut für Polymerfoschung Dresden e.V., Germany;
[3] Ecological Microbiology, University of Bayreuth, Germany;
[4] Biological Physics, University of Bayreuth, Germany;
* Correspondence: Christian.laforsch@uni-bayreuth.de;

Content:

19

20

21 **Figure S1: Photographs of the sampling sites for the incubation media.** a) Freshwater from an
22 artificial pond (49°55'44.1" N; 11°34'60.0" E) and b) saltwater obtained from a marine aquaria facility.
23 Photo Credit: Anja C. Stellwag, University of Bayreuth.
24
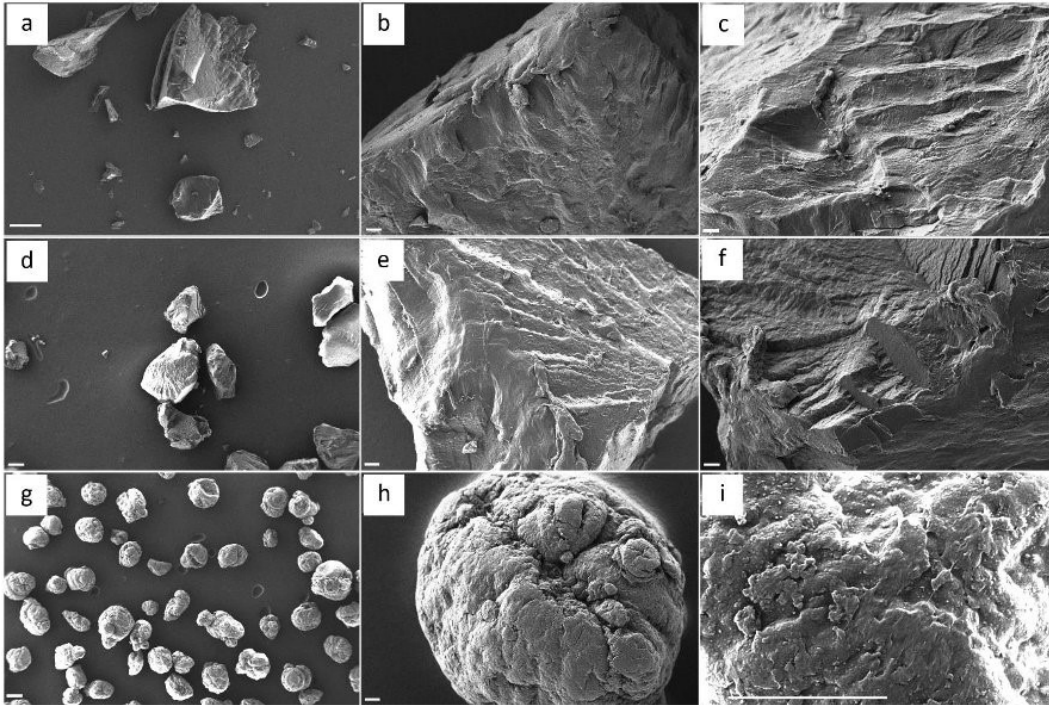
25
26   **Figure S2: Scanning electron microscopy images of the three polymer raw materials.** Surfaces of
27   the PA fragments are shown from a-c, PET surfaces from d-f and the slightly rougher surface of PVC
28   from g-i. Scale bars: a, d, g = 100µm, b, c, e, f, h, i = 10µm.
29
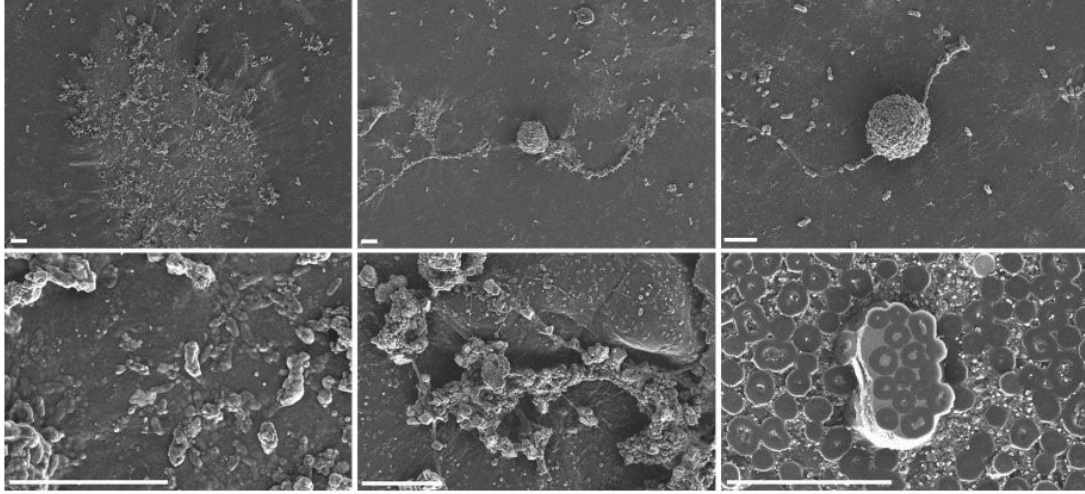
30
31 **Figure S3: Scanning electron microscopy images of the freshwater incubation medium after**
32 **evaporation of water.** Images show microorganismal and non-microorganismal structures occurring
33 in the freshwater incubation medium. Scale bars 10μm.
34
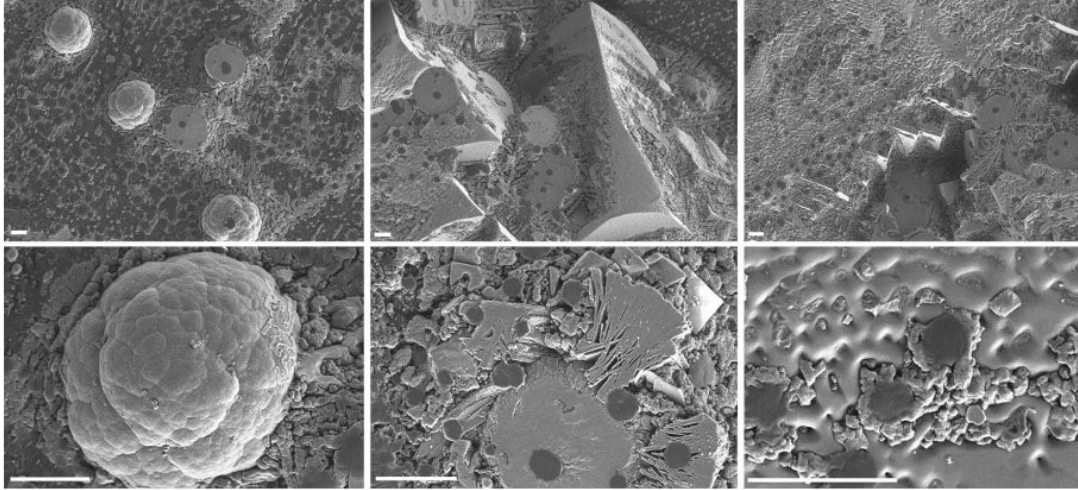
35
36 **Figure S4: Scanning electron microscopy images of the saltwater incubation medium after**
37 **evaporation of water.** Images show microorganismal and non-microorganismal structures occurring
38 in the freshwater incubation medium. Scale bars 10μm.
39

Article 9

In situ Prokaryotic and Eukaryotic Communities on Microplastic Particles in a Small Headwater Stream in Germany

In situ Prokaryotic and Eukaryotic Communities on Microplastic Particles in a Small Headwater Stream in Germany

Alfons R. Weig[1]*, Martin G. J. Löder[2], Anja F. R. M. Ramsperger[2,3] and Christian Laforsch[2]

[1] Genomics and Bioinformatics, Bayreuth Center of Ecology and Environmental Research, University of Bayreuth, Bayreuth, Germany, [2] Animal Ecology, Bayreuth Center of Ecology and Environmental Research, University of Bayreuth, Bayreuth, Germany, [3] Biological Physics, University of Bayreuth, Bayreuth, Germany

The ubiquitous use of plastic products in our daily life is often accompanied by improper disposal. The first interactions of plastics with organisms in the environment occur by overgrowth or biofilm formation on the particle surface, which can facilitate the ingestion by animals. In order to elucidate the colonization of plastic particles by prokaryotic and eukaryotic microorganisms *in situ*, we investigated microbial communities in biofilms on four different polymer types and on mineral particles in a small headwater stream 500 m downstream of a wastewater treatment plant in Germany. Microplastic and mineral particles were exposed to the free-flowing water for 4 weeks in spring and in summer. The microbial composition of the developing biofilm was analyzed by 16S and 18S amplicon sequencing. Despite the expected seasonal differences in the microbial composition of pro- and eukaryotic communities, we repeatedly observed polymer type-specific differentiation in both seasons. The order of polymer type-specific prokaryotic and eukaryotic community distances calculated by Robust Aitchison principal component analysis (PCA) was the same in spring and summer samples. However, the magnitude of the distance differed considerably between polymer types. Prokaryotic communities on polyethylene particles exhibited the most considerable difference to other particles in summer, while eukaryotic communities on polypropylene particles showed the most considerable difference to other spring samples. The most contributing bacterial taxa to the polyethylene-specific differentiation belong to the Planctomycetales, Saccharimonadales, Bryobacterales, uncultured Acidiomicrobia, and Gemmatimonadales. The most remarkable differences in eukaryotic microorganism abundances could be observed in several distinct groups of Ciliophora (ciliates) and Chlorophytes (green algae). Prediction of community functions from taxonomic abundances revealed differences between spring and summer, and – to a lesser extent – also between polymer types and mineral surfaces. Our results show that different microplastic particles were colonized by different biofilm communities. These findings may be used for advanced experimental designs to investigate the role of microorganisms on the fate of microplastic particles in freshwater ecosystems.

Keywords: biofilm, prokaryote community, eukaryote community, freshwater stream, microplastics

INTRODUCTION

Plastic materials are widely used in all areas of human life due to their outstanding material properties such as lightweight, stability, corrosion resistance, insulating properties, and moldability. Global plastic production increased from 1.5 million tons in 1950 to 367 million tons in 2020 (Statistica, 2021). The primary uses for plastics in Europe are packaging (39.6%), followed by building and construction, automotive, electrical/electronic, household/leisure/sports, and agriculture (PlasticsEurope, 2020). The polymer types used for the production of packaging materials are mainly polyethylene (PE; in different densities), polypropylene (PP), and polyethylene terephthalate (PET), and to a lesser extent polystyrene (PS) and polyvinylchloride (PVC). The often short-time use of plastics in packaging contributes mainly to the enormous increase of plastic waste. Of the plastic waste that was collected appropriately in Europe in 2018, only 32.5% entered the recycling process, while the rest of the collected waste was used for energy recovery by incineration (42.6%) or disposed in landfills (24.9%) (PlasticsEurope, 2020). However, it is estimated that 33% of global waste is not collected appropriately but openly dumped or littered, imposing unforeseen risks to public and environmental health (Kaza et al., 2018).

Once plastic material enters the environment, it fragments into smaller particles (microplastics smaller than 5 mm) (Arthur et al., 2009). The fragmentation and eventually degradation processes depend on various physicochemical factors such as mechanical forces, temperature, UV radiation, pH, and additives present in the plastic and varies between different polymer types (Barnes et al., 2009). In addition, plastic degradation by environmental (micro-)organisms can add to the overall degradation process (Restrepo-Montoya et al., 2011), a fact summarized by Yuan et al. (2020) in a recent review. Therefore, the direct interaction of microorganisms with plastics could be of key importance for the fate of plastic in the environment, as it has been shown for PET-and polyurethane (PU)-degrading bacteria (Nakajima-Kambe et al., 1999; Yoshida et al., 2016) as well as for PU- and PE-degrading fungi (Brunner et al., 2018; Sangale et al., 2019).

The composition of biofilms on plastic particles in natural environments, the so-called "plastisphere" (Zettler et al., 2013), has been investigated in aquatic (e.g., marine or freshwater) and terrestrial environments (for reviews, see Oberbeckmann et al., 2015; Oberbeckmann and Labrenz, 2020). Recently, a thorough meta-analysis of studies describing the global diversity of the plastisphere published between 2010 and 2019 revealed the large variety of experiments (Wright et al., 2021): of the 35 studies selected for the meta-analysis, only 6 studies included field studies in the water column of freshwater habitats (Hoellein et al., 2014, 2017; McCormick et al., 2014, 2016; Arias-Andres et al., 2018; Parrish and Fahrenfeld, 2019), sometimes combined with laboratory experiments and/or exposition experiments in sediments. However, reports on plastisphere biofilms from small headwater streams (in contrast to rivers and lakes) are rare (Kaevska et al., 2016), even though those seemingly pristine aquatic habitats receive plastic particles, e.g., via

runoff (Piehl et al., 2018), aerial deposition (Zhang et al., 2020), or discharge of sewage effluents. Moreover, in addition to compositional and functional analyses of plastisphere biofilms, the spatial structure of microorganisms has been investigated by advanced confocal microscopy and illustrated analytical access to biofilm development at micrometer scales (Schlundt et al., 2020).

Biofilms are composed of microorganisms, mainly bacteria, although fungi and other micro-eukaryotes can contribute to and be enclosed in biofilms, bound in a mucilaginous matrix of an extracellular polymeric material such as exopolysaccharides (Flemming and Wingender, 2010). Biofilms represent key sites for enzymatic activity, organic matter cycling, respiration, and primary production; and the influence of environmental processes on biofilm formation has been reviewed recently (Battin et al., 2016; Wagner and Lambert, 2018). The formation of a biofilm leads to several advantages for single planktonic cells. Amongst others, the biofilm matrix enables bacterial cells to perform cell–cell interactions/communication and exchange of DNA; the matrix stores nutrients and can act as a barrier against desiccation and serves as a defense mechanism against predation.

Biofilms are part of the aquatic food web and were characterized in a recent review by three major elements: energy pathways/subsidization from plankton, horizontal complexity of the basal food web, and the vertical food web complexity/food chain length (Weitere et al., 2018). Laboratory experiments showed that microplastic particles coated with a biofilm preferentially become ingested by organisms compared with pristine particles (Vroom et al., 2017; Hodgson et al., 2018), which renders biofilm-coated plastic materials a potentially enhanced environmental and organismal health risk (Ramsperger et al., 2020b). Furthermore, bacterial and fungal pathogens have been identified in the plastisphere of freshwater and terrestrial habitats, where microplastic particles can serve as vectors for pathogen distribution (Wu et al., 2019; Gkoutselis et al., 2021).

In the last couple of years, studies showed that emigration, dispersal, and immigration also play a major role for biofilm microorganisms (Augspurger et al., 2010), indicating that differences in the colonization of various plastic types may also account for the composition of microbial communities. Further, microbial communities in natural environments, contrary to laboratory conditions, undergo considerable seasonal dynamics as shown for headwater streams and small rivers in Central Europe (Kaevska et al., 2016) and account for the formation and composition of biofilm microbiomes. However, the few publications from natural freshwater habitats show that only little is known about the colonization and biofilm formation on different polymer types in freshwater ecosystems, which holds even more true for small headwater streams.

To explore the pro- and eukaryotic microbial communities on microplastic particles in a headwater stream, we directly exposed particles of various polymer types for 4 weeks in a small headwater stream in Northern Bavaria, Germany, in two independent experiments (spring and summer) to compensate for seasonal dynamics of freshwater microbiomes. We analyzed the prokaryotic community by 16S amplicon sequencing to elucidate bacterial community differences in colonization and potential degradation of polymer particles. Since prokaryotic

biofilms attract eukaryotic predators such as protists and small metazoans, 18S amplicon sequencing was chosen to investigate eukaryotic community dynamics on the biofilms. We investigated whether differences in community functions can be inferred from taxonomic abundances of prokaryotic communities in a seasonal and/or particle-type specific manner. Furthermore, the presence of pathogenic bacteria was analyzed in biofilm and stream water samples.

MATERIALS AND METHODS

Exposition of Plastic Particles in a Freshwater Stream

Plastic particles (approximately 3 mm in diameter) were exposed in the freshwater stream Truppach in northern Bavaria, Germany (lat. 11.36459, lon. 49.89573), about 500 m downstream a local wastewater treatment plant (WWTP) from May 2, 2016, to May 30, 2016 (spring experiment), and from August 13, 2016, to September 9, 2016 (summer experiment), respectively. Water samples of the headwater stream were taken on September 9, 2016, at two locations: the site of the *in situ* exposition experiment and at a site approximately 500 m upstream of the outlet of the WWTP (lat. 11.37370, lon. 49.90627). The water temperature of streams and rivers in this area is monitored by the Bavarian Environment Agency[1] at a nearby monitoring station at Hollfeld, Bavaria, Germany, and ranged from ca. 11.2 to 13.1°C (spring experiment) and from 13.2 to 13.8°C (summer experiment). The WWTP receives mainly private household wastewater for mechanical and biological (nitrification and denitrification) treatment. The efflux of the WWTP is not sterilized and constituted 3.75% (annual average) of the streamflow in the year of exposition (source: www.lfu.bayern.de and personal communication with the operator of the WWTP). The area next to the sampling site is agriculturally used grassland (partly pasture) and protected by the Flora–Fauna–Habitats directive of the European Commission (Council Directive 92/43/EEC). The properties of the particles used in the exposure experiment are summarized in **Table 1**. The polymer particles were taken from the original container but were not sterilized prior to the experiment to avoid thermal modification of the particles. The quartz particles were thoroughly rinsed with deionized water to remove quartz dust and were autoclaved. The experimental design was as follows: for each particle type, one basket (ball-shaped stainless-steel sieve, about 4.5 cm in diameter, mesh size ca. 0.65 mm) containing approximately 50 particles was used to expose particles to the stream water, prohibiting contact of particles with floating debris (e.g., branches and litter) as well as access of feeding macrofauna of the stream (e.g., fishes, snails, and insect larvae) to the developing biofilm. The baskets were attached to a wooden raft, held in place by a rope, and always free-floating in the stream at a depth of approximately 20 cm below the water surface without touching the streambed at any time. After the exposure period, the particles were collected separately for each particle type and washed three times with

tap water to remove stream water and loosely attached debris from the developing biofilm. Ten particles were randomly taken two times from each particle type pool (unit of replication: 10 particles), transferred to an extraction vial, and kept at 4°C overnight until DNA extraction on the following day. The same experimental design was used for the repetition of the experiment in August/September 2016. Potential microbial contamination of the tap water (used for the initial washing step) was analyzed by amplification of 16S fragments and high-resolution capillary electrophoresis. No 16S amplification products could be detected in any tap water samples, while stream water samples showed specific 16S amplification products (data not shown).

DNA Extraction From Biofilm and Water Samples

Metagenomic DNA of the biofilms was extracted independently (representing technical replicates) using the "PowerBiofilm DNA Isolation Kit" (MO-BIO[2]) as recommended by the manufacturer. In addition, metagenomic DNA was extracted from water samples by ethanol precipitation (Ficetola et al., 2008). The amount of DNA was quantified using the dsDNA High-Sensitivity Assay Kit on a Qubit 3 fluorometer (Fisher Scientific[3]).

High-Throughput Sequencing of 16S- and 18S-rDNA Amplification Products

The replicate samples of metagenomic DNA were sent to LGC Genomics GmbH[4] for library preparation and high-throughput sequencing. Briefly, 16S-rDNA fragments were amplified using primer pair Bakt_341F and modified Bakt_805R (GACTACHVGGGTATCTAAKCC, after Herlemann et al., 2011), and 18S-rDNA fragments were amplified using primer pair TAReuk454FWD1 and modified TAReukREV3 (Stoeck et al., 2010; Piredda et al., 2017). PCR amplicons were sequenced in the 300-bp paired-end mode using Illumina's MiSeq V3 chemistry and instrument. Raw sequence reads were demultiplexed, adapter remnants were clipped from all reads, and forward and reverse primers were removed from the sequences. The sequences were deposited in National Center for Biotechnology Information's (NCBI's) Sequence Read Archive (SRA) under project number PRJNA680706.

Bioinformatics and Statistical Analyses

The microbial composition of the samples was analyzed using the Qiime2 package; a description of the applied workflow is encoded in the provenance tab of Qiime2 **Supplementary Data File** (a short description on how to view Qiime2 data files is given in a Qiime2 instruction file in **Supplementary Material**). Briefly, the primer-clipped reads were loaded into the Qiime2 pipeline. The paired-end reads were quality-filtered (including a 3′-end trimming at position 250, where the average read qualities fell below the quality score of Q25 for 16S reads, and Q30 for 18S reads), denoised, and

---

[1]www.lfu.bayern.de

[2]www.mobio.com
[3]www.fishersci.co.uk
[4]www.lgcgroup.com

TABLE 1 | Characteristics of particles used in the experiments.

Particle type	Trade name	Article no.	Supplier	Diameter (mm)
Low-density polyethylene (PE)	Lupolen	6031M	Pro-Plast Kunststoff GmbH, Weiterstadt, Germany	3
Polypropylene (PP)	Moplen	HP570M	Pro-Plast Kunststoff GmbH, Weiterstadt, Germany	3
Polystyrene (PS)	–	158K KG2	BASF SE, Ludwigshafen, Germany	3
Polyvinyl chloride (PVC)	Troilit	VB537-HE	Granulat GmbH, Troisdorf, Germany	3
Quartz-based gravel (Q, reference particles)	Color Gravel Super White	50260	Colorstone, Rudolstadt, Germany	2–3

joined by DADA2 (Callahan et al., 2016), yielding so-called amplicon sequence variants (ASVs) (Callahan et al., 2017). Low-abundant ASVs were filtered out based on the median frequency per ASV of 16 (bacterial amplicons) and 17 (18S amplicons). The remaining ASVs were taxonomically classified using "naïve-Bayes" trained taxonomic classifiers based on the SILVA reference database (version 138), containing 16S and 18S reference sequences. Throughout this article, we adhere to the taxonomic nomenclature of the GTDB (prokaryotes) and UniEuk (eukaryotes), which has been adopted with the SILVA v138 reference database release.[5] Phylogenetic trees were constructed by sequence alignments of 16S and 18S ASVs using MAFFT, followed by masking phylogenetically uninformative or ambiguously aligned columns; FastTree was used to infer phylogenetic trees, which were subsequently rooted at their midpoints. Alpha diversity analyses were performed using core-metrics-phylogenetic workflow of Qiime2, producing several alpha diversity measures (Faith's PD, evenness, observed ASVs, and Shannon). Beta diversity analyses between sample groups were calculated by DEICODE (Martino et al., 2019) and visualized by QURRO (Fedarko et al., 2020). Statistical differences between sample groups were calculated by ANOSIM and PERMANOVA implemented in Qiime2. Alpha rarefaction curves were generated from the frequency information of the representative ASVs in each sample. The functional prediction tool FAPROTAX (Louca et al., 2016) was used to predict metagenome function from 16S marker gene sequencing profiles. Therefore, taxonomic features obtained by the Qiime2 pipeline were collapsed at the species level. The resulting frequency table was used to predict functional profiles in biofilm, and water samples from the FAPROTAX database provided together with a python script.[6] Pathogenic bacteria were identified from 16S amplicon reads using the 16sPIP tool (Miao et al., 2017). The 16sPIP package was obtained from the GitHub repository[7] and run in the sensitive mode with the pair of forward and reverse reads in fastq format for each sample.

RESULTS

Amplicon Sequencing Data Overview

Amplicon sequencing of 20 biofilm and 4 water samples obtained from the experiments in spring and summer 2016 resulted in

[5]https://www.arb-silva.de/documentation/release-1381/
[6]http://www.loucalab.com/archive/FAPROTAX/
[7]github.com/jjmiao1314/16sPIP

1.95 million (16S) and 2.94 million (18S) paired-end reads, respectively. The DADA2 plugin (Qiime2) was used to denoise and merge paired-end reads, detect putative chimera, and identify representative ASVs. After rare ASVs were filtered, a final number of 2,521 (16S) and 3,190 (18S) representative ASVs were obtained and used for downstream analyses. Rarefaction analysis of the denoised, chimera-, and quality-filtered reads showed that the remaining sequences were enough to reach saturation for each sample. For alpha and beta diversity analyses of biofilm communities, data corresponding to stream water samples were filtered out from the full dataset.

Taxonomic Classification of Bacterial and Eukaryotic Amplicon Sequence Variants

Representative ASVs were classified using a naïve-Bayes classifier trained on the SILVA 138 reference sequence database (Bokulich et al., 2018; Robeson et al., 2020). The relative frequency of prokaryotic and eukaryotic taxa of biofilm samples differed from microbial communities of the stream water (**Figure 1** and Qiime2 taxa bar plots in **Supplementary Material**). The 10 most abundant orders of bacteria (based on global abundance across all samples) were Burkholderiales, Sphingomonadales, Rhizobiales, Flavobacteriales, Chitinophagales, Rhodobacterales, Pirellulales, Cytophagales, Verrucomicrobiales, and plant chloroplasts (mainly from algae), which contributed to about 40–80% of relative abundance of each sample (**Figure 1A**).

The number of observed bacterial taxa in biofilm samples ranged from ca. 325 to 583 taxa per particle type and did not differ considerably between May and August samples. PE particles always showed the most detectable bacterial taxa (**Table 2A**). The evenness of the bacterial microbiome was above 0.9 (Pielou's index) for most of the samples, indicating that no dominant bacterial group was present (**Table 2A**). Shannon's biodiversity index ranged from ca. 7.65 to 8.38 for bacterial taxa, and no remarkable differences were observed between spring and summer samples.

The number of observed eukaryotic taxa ranged from 237 to 718 taxa in biofilm samples, with a clear tendency for more detectable taxa in spring samples (**Table 2B**). The 10 most abundant eukaryotic orders were Conthreep, Spirotrichea, Bacillariophyceae, Chaetonotida, Craspedida, unclassified Eukaryota, Litostomatea, Bicosoecida, Chlorophyceae, and Ulvophyceae, which summed up to about 60–90% of relative abundance on the particles (**Figure 1B**). Pielou's evenness and Shannon's biodiversity indices were lower for

FIGURE 1 | Taxonomy bar plot displaying the relative frequency (%) of prokaryotic **(A)** and eukaryotic **(B)** orders based on taxonomic classification of 16S and 18S rRNA gene fragments. Only the 20 most frequent orders are shown in the legend and are arranged from the most frequent (top) to less frequent taxa (down). The higher taxonomic level is used when the order level is not annotated in the reference database. Biofilm samples are indicated on the horizontal axis as "season-particle" next to water samples taken from the *in situ* exposition site (Wdn) and upstream of the WWTP outlet (Wup).

the eukaryotic samples compared with bacterial samples, ranging from ca. 0.585 to 0.770 (evenness) and from 4.61 to 7.14 (Shannon), respectively (**Table 2B**). Although alpha diversity evenness did not show differences between spring and summer experiments, lower numbers of detectable taxa and lower Shannon's indices could be seen in the summer samples compared with the spring samples. Alpha rarefaction curves of the eukaryotic dataset showed that the lower number of taxa in the summer samples did not result from insufficient sampling depth as rarefaction curves reached almost saturation even at the sequencing depth of the smallest sample (data not shown).

Seasonal and Plastic Type-Dependent Differences in Microbial Community Composition

The microbial compositions in biofilms between sample groups (beta diversity) were analyzed by the "Robust Aitchison PCA"

(RPCA; implemented in the Qiime2 DEICODE plugin) to address the sparsity and compositional nature of the 16S and 18S datasets (Martino et al., 2019). First, bacterial and eukaryotic microbial communities of the spring and summer exposition experiments exhibit statistically significant separation along RPCA axis 1 (explaining 69 and 64% of the data) in the 16S and 18S dataset (**Table 3**); the overall direction of community shifts was very similar for all polymer and reference particle types (**Figure 2**; Qiime2 RPCA plots in **Supplementary Material**). Second, pro- and eukaryotic microbial communities of the different particle types showed an additional separation along RPCA axis 2, perpendicular to seasonal axis 1 (explaining ca. 26 and 31% of the 16S and 18S data, respectively; **Figure 2**; Qiime2 RPCA plots in **Supplementary Material**). Pairwise differences between some particle groups were statistically significant, while other groups overlapped with each other (**Table 3**).

A common observation was that reference samples were always found on one side of axis 2 in both seasons and

TABLE 2 | Alpha-biodiversity metrics of (A) pro- and (B) eukaryotic biofilm microbiomes for the spring and summer experiments (mean of replicate samples).

Particle type	Pielou			ASV			Shannon		
	Spring	Summer	Statistics	Spring	Summer	Statistics	Spring	Summer	Statistics
(A) Prokaryota									
PE	0.912	0.916	a	583	558	a	8.38	8.36	a
PP	0.907	0.925	a	507	438	b	8.14	8.06	a,b
PS	0.925	0.929	a	449	332	b	8.14	7.65	B
PVC	0.897	0.901	b	462	431	b	7.94	7.86	b
Q	0.924	0.930	a	509	325	b	8.31	7.52	a,b
Statistics	a	a		a	a		a	a	
(B) Eukaryota									
PE	0.747	0.697	a	557	289	a	6.82	5.70	a
PP	0.696	0.719	a	718	354	a	6.60	6.07	a
PS	0.770	0.725	a	635	459	a	7.14	6.22	a
PVC	0.757	0.638	a	522	286	a	6.83	5.20	a
Q	0.706	0.585	a	700	237	a	6.67	4.61	a
Statistics	a	b		a	b		a	b	

Calculations were performed by the diversity plugin of Qiime2. Statistical test: Kruskal–Wallis (pairwise) between particle types and seasonal groups; groups with significant difference ($p < 0.05$) are indicated with different letters. PE, polyethylene; PP, polypropylene; PS, polystyrene; PVC, polyvinyl chloride; Q, quartz-based gravel.

TABLE 3 | Results of pairwise statistical tests of sample groups from 16S and 18S datasets.

Groups	PERMANOVA		ANOSIM	
	p-Value	Pseudo-*F*	*p*-Value	Rho
16S (prokaryotes)				
Spring–summer	0.001	14.9	0.001	0.634
PE–PS	0.032	5.47	0.027	0.594
PE–Q	0.024	8.1	0.04	0.718
18S (eukaryotes)				
Spring–summer	0.001	16.1	0.001	0.737
PE–Q	*0.055*	*3.82*	*0.067*	*0.427*
PP–PVC	*0.06*	*3.15*	*0.063*	*0.354*
PP–Q	0.028	6.83	0.03	0.667

Pairwise tests of spring–summer groups included all particle types (n = 10), and pairwise tests between particle types included both seasons (n = 4). Test results, close to but not reaching the "p < 0.05" criteria, are shown in italics. PE, polyethylene; PP, polypropylene; PS, polystyrene; PVC, polyvinyl chloride; Q, quartz-based gravel.
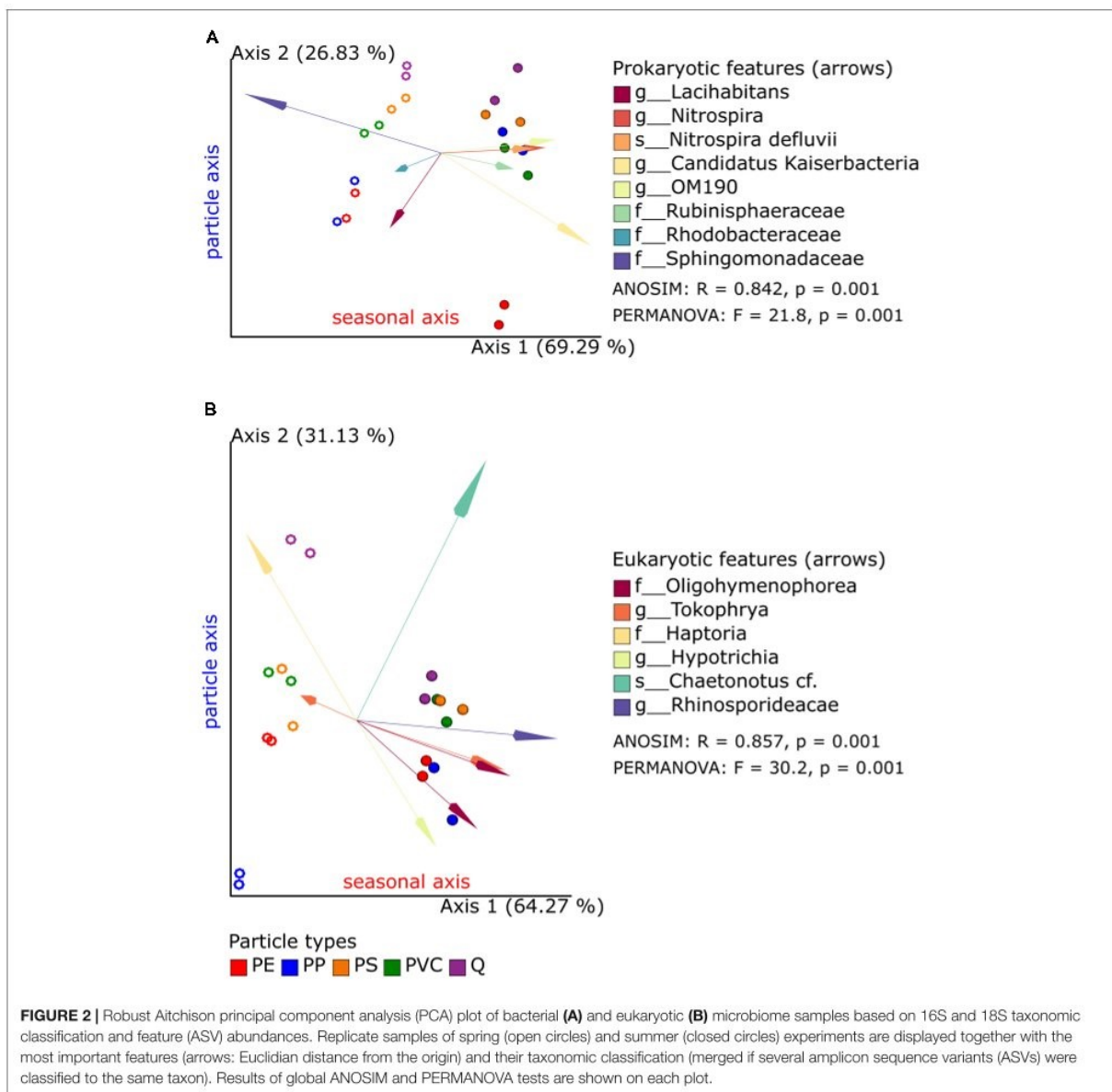
the 16S and 18S datasets. Significant differences to quartz samples were found for PE (in 16S data) and PP samples (in 18S data). Although the significance level of 0.05 has not been reached for the PE–Q pair in 18S datasets, the observed p-values close to this threshold indicate a putative separation also between these biofilm communities. PS and PVC samples clustered next to each other and in close vicinity to reference samples in the 16S dataset and, therefore, do not show significant differences. This was also true for the 18S dataset in summer experiments, but not for the spring data: here, the PS and PVC samples cluster in the same range of axis 2, while the reference samples are placed apart from these two polymer samples. Finally, pairwise differences within polymer samples could be also observed in the 16S dataset

(PE–PS, statistically significant) and in the 18S dataset (PP–PVC, tendency with $p = 0.060$ and $p = 0.063$), respectively. Since axes 1 and 2 together explain over 95% of the data in 16S and 18S RPCA plots, respectively, season and particle types are the most determining factors for microbial diversity in biofilm samples.

Seasonal Effects on Bacterial and Eukaryotic Microbiomes

A key benefit of RPCA is that sample and feature loadings can be accessed by the QURRO plugin to identify those ASVs at the ends of ordinations, which are the most contributing to the clustering of samples along RPCA axes. Spring and summer samples could be separated along axis 1 in RPCA plots in 16S and 18S datasets. A selection of each 1% from the top and the bottom of ranked features (ASVs) was chosen to retrieve lists of bacterial and eukaryotic taxa, respectively (**Supplementary Tables 1A**, **2A** and **Supplementary Figure 1**), which differed significantly between spring and summer samples (**Supplementary Tables 1B, 2B**).

In spring biofilms, most of these top-/bottom-ranked bacterial ASVs were classified as Sphingomonadales and Burkholderiales, in addition to Armatimonadales, Chitinophagales, Flavobacteriales, and Verrucomicrobiales. Furthermore, 16S sequences from plant chloroplasts were also abundant in spring samples (**Supplementary Table 1A**). In summer biofilms, ASVs were classified to Oligoflexales, Nitrospirales, Pirellulales, Planctomycetales, Sphingomonadales, Burkholderiales (different ASVs as the above ones), Steroidobacterales, and Verrucomicrobiales, as well as Candidatus Kaiserbacteria and Candidatus Nomurabacteria; and two clone references were more abundant.

266

FIGURE 2 | Robust Aitchison principal component analysis (PCA) plot of bacterial **(A)** and eukaryotic **(B)** microbiome samples based on 16S and 18S taxonomic classification and feature (ASV) abundances. Replicate samples of spring (open circles) and summer (closed circles) experiments are displayed together with the most important features (arrows: Euclidian distance from the origin) and their taxonomic classification (merged if several amplicon sequence variants (ASVs) were classified to the same taxon). Results of global ANOSIM and PERMANOVA tests are shown on each plot.

A comparable selection of the most contributing features (1% top/bottom) to RPCA axis 1 of the eukaryotic dataset showed that spring and summer sample groups could be distinguished. The largest eukaryotic group characterizing the spring samples belonged to the phylum Diatomea, e.g., Bacillariophyceae. Furthermore, the phyla Ciliophora, Holozoa, Chlorophyta, and Bicosoecida were identified with two or more ASVs, next to phyla represented by single ASVs (**Supplementary Table 2A**). Abundant taxa in summer samples belonged mainly to Ciliophora (16 of 28 ASVs), particularly to the two families Oligohymenophorea and Phyllopharyngea, and the phyla Cryptomycota (LKM11), Gastrotricha, and Holozoa.

It should be noted that other thresholds can be applied to the datasets at the reader's choice using the Qiime2 QURRO visualization files provided as electronic supplements.

Identification of Polymer-Specific Taxa Within Bacterial and Eukaryotic Biofilms

Particle type-dependent differences in microbial communities occurred mainly along RPCA axis 2, and significant differences between quartz and some polymer-specific communities have been shown above (**Table 3**). Taxonomic groups responsible for the positioning of each sample along axis 2 of the RPCA plots

were identified by QURRO in the same way as described above for seasonal differences along axis 1 in prokaryotic and eukaryotic datasets. The most contributing taxonomic groups were filtered from ranked features (ASVs) of the complete prokaryotic and eukaryotic datasets (using a 3% top/bottom threshold) but also from pairwise datasets composed of each of the polymer types and the reference samples (Q-PE, Q-PP, Q-PS, and Q-PVC; using a 2% top/bottom threshold, accounting for the slightly lower numbers of ASVs present in pairwise subsets). The resulting prokaryotic and eukaryotic taxonomic groups were combined in non-redundant tables, and the association of features (ASVs) to the polymer or the reference sample end of axis 2 was color-coded in these tabular overviews (**Supplementary Tables 3A, 4A**). Pairwise *t*-tests using the current log-ratio values corresponding to the most contributing taxa between all particle groups confirmed significant differences (and indicated tendencies at slightly higher *p*-values) between those groups, which have been already detected permutation tests on the full 16S and 18S datasets but also revealed considerable overlap between other groups (**Supplementary Tables 3B, 4B**).

Bacterial Taxa on Microplastic Particles

The list of bacterial taxa contributing to axis 2 of the full and the pairwise datasets consisted of 207 non-redundant ASVs. Thus, a considerable overlap of 47 ASVs could be identified that were present in full and in any of the four pairwise datasets (**Supplementary Table 3A**). Furthermore, log-ratio plots calculated from selected taxa showed that the sample groups (particle, season) differed considerably (**Supplementary Figure 2A**): PE samples always showed more negative log-ratio values than other particles, indicating that the denominator taxa were more abundant as compared with the numerator taxa. However, it should be noted that the reference samples (as the most contrasting samples) received log-ratio values in the range from −0.5 to 0, which means that numerator and denominator taxa were present in comparable amounts in these samples (based on RPCA). Interestingly, the log-ratio values of particle groups showed a shift to more negative values in summer samples, which can be caused by either a decrease of the numerator taxa or an increase in the denominator taxa used for log-ratio calculations.

Analysis of pairwise subsets of bacterial data showed a similar trend based on unique selections of taxa from each subset: each particular selection of taxa resulted in a clear separation of microplastic biofilms from the mineral reference biofilms in the spring and summer experiments (for details of pairwise analyses, see QURRO visualizations of pairwise prokaryotic datasets in **Supplementary Material**).

The non-redundant list of the selected taxa (207 ASVs) is assigned to the orders Chitinophagales, Cytophagales, Flavobacteriales, Candidatus Kaiserbacteria, Pirellulales, Planctomycetales, Rhizobiales, Rhodobacterales, Sphingomonadales, Burkholderiales, and Verrucomicrobiales (containing at least 5 ASVs) and 48 orders with less than 5 ASVs (**Supplementary Table 3A**). Within Chitinophagales, ASVs classified as Chitinophagaceae (family) were exclusively found in the numerator group (reference particle end). In contrast, some of the Saprospiraceae ASVs were clustering with reference

particles and others with polymer particles. Ten ASVs classified to the order of Pirellulales were found exclusively at the polymer particle end of feature rankings. Only one ASV of this order was found within the reference particle end. ASVs of the family Comamonadaceae (order Burkholderiales) represent another taxa example filtered out mainly from the polymer particle end of feature rankings (16 ASVs). Only two belong to the reference particle end.

Eukaryotic Taxa on Microplastic Particles

The list of eukaryotic taxa extracted from axis 2 of the full and the pairwise RPCA ordination (same percentage filtering as for bacterial data) resulted in 226 non-redundant ASVs with complete overlap of 90 ASVs (**Supplementary Table 4A**). Log-ratio plots of the selected taxa from the entire dataset showed that the "denominator" taxa are more abundant in PP biofilms (spring and summer) and PE biofilms (summer) in comparison with the "nominator" taxa (**Supplementary Figure 2B**). Quartz (Q) samples differed most from PP samples with log-ratio values above 3 in spring samples and ca. 0.8 in summer samples. As previously observed for bacterial microbiomes, a shift to more negative log-ratio values could also be observed in the summer experiments for eukaryotic samples.

Log-ratio calculations using taxa obtained from pairwise analyses showed clear separation of most polymer samples from reference samples within each season, except for Q and PVC samples in the summer experiment (see QURRO visualizations of pairwise prokaryotic datasets in **Supplementary Material**).

The largest taxonomic groups found within the selected taxa (whole and pairwise datasets) were ciliates, e.g., the Conthreep clade, and the orders Litostomatea and Spirotrichea (**Supplementary Table 4A**). Within the Conthreep clade, ASVs of the family Oligohymenophorea were predominately associated with polymer samples, while ciliates of the families Phyllopharyngea, Prostomatea, Haptoria, and Hypotrichia cluster more with reference samples as well as the family Heterotrichea, another ciliate group assigned to the class Postciliodesmatophora. Several ASVs assigned to green algae (unfortunately with incomplete taxonomic classification from order to genus levels in the SILVA reference database) were also enriched in polymer biofilms (e.g., *Chaetophora incrassata*, *Microspora* sp., *Oedocladium prescottii*, and *Radiococcus* sp. in addition to two ASVs with lacking classification). Several ASVs of the phylum Peronosporomycetes were identified from Q-PVC datasets, indicative of PVC samples. However, the available taxonomic classification is incomplete in SILVA; this group was previously called Oomycota and belongs to the SAR clade of primarily unicellular eukaryotes. A few other groups were enriched in reference samples, such as Nematodes of the order Diplogasterida and Monhysterida, except for one ASV of the order Chromadoria was identified in full and all four pairwise datasets as indicative for polymer particles. A large group of nine ASVs was classified as Rotifera, multicellular animals present in almost all habitats, six of them from the reference particle end of feature rankings, two from PS/PVC specific rankings, and one

FIGURE 3 | Prediction of metabolic and ecologically relevant functions from 16S taxa abundances by FAPROTAX in different biofilm and planktonic samples.

each from Q (whole dataset) and PVC (Q-PVC dataset) ranking (**Supplementary Table 4A**).

Functions of Bacterial Communities

The functions of bacterial communities were predicted by FAPROTAX (Louca et al., 2016) and revealed a broad range of functional similarities between the biofilm and stream water communities but showed also differences in relative abundance between different polymer, quartz, and water samples, as well as between spring and summer experiments. Functions detected in biofilm, but not in water samples, were aerobic nitrite oxidation, chitinolysis, manganese oxidation, and nitrification. Some functions are more abundant in spring samples within these groups, such as nitrification and aerobic nitrite oxidation. In contrast, other closely related functions such as photosynthetic cyanobacteria, photoautotrophy, and oxygenic photoautotrophy were more abundant in biofilm samples collected in summer. Discriminating functions between polymer and quartz samples are rare, except for aromatic compound degradation and photosynthetic cyanobacteria/oxygenic photoautotrophy, which were not detected on quartz samples. Although many functions detected in stream water communities were also observed in biofilm communities, some functions were prevalent to stream water communities, such as dark oxidation of sulfur compounds, dark sulfite oxidation, and iron respiration, and – more restricted to water samples collected downstream of the WWTP outlet (the site of the exposition experiment) – functions related to xylanolysis, animals, and the human gut, respectively (**Figure 3**).

Pathogen Identification in Biofilm Communities

In addition to the taxonomy-based identification of potential human pathogens by FAPROTAX (see above), a sequence-based identification of putative pathogens was performed using the 16sPIP tool and a manually curated pathogen database (Miao et al., 2017). Sixty-nine putative pathogenic bacteria were identified in at least one biofilm or water sample (34 taxa overlapping between biofilm and water samples, 21 taxa only detected in biofilm samples, and 14 taxa only detected in water samples). The most abundant putative pathogen, *Enterobacter ludwigii*, was detected in all samples but exhibited higher relative abundance (up to 0.173%) in biofilm samples than water samples. The seven most abundant pathogens (*E. ludwigii, Aeromonas hydrophila, Nocardia farcinica, Afipia broomeae, Pseudomonas aeruginosa, Acinetobacter lwoffii,* and *Klebsiella pneumoniae*) represented together over 80% of the sequence reads of putative pathogenic bacteria (**Supplementary Figure 3**).

DISCUSSION

Our study investigated whether prokaryotic and eukaryotic biofilm communities differ in their microbial composition between particle types (polymers and quartz) and between two experimental timepoints (seasons) within 1 year. We could show that bacterial and eukaryotic microbiomes cluster between biofilms by only two factors, a seasonal factor and a particle

type-specific factor, both together explaining approximately 95% of data variation. Notably, the relative position of biofilm samples along the particle type-specific factor exhibited strong similarities between spring and summer samples, suggesting that substrate characteristics were responsible for biofilm formation in independent experiments.

It has to be noted that the species composition of biofilms is difficult to compare between different studies. Next to the influence of season, the initial species composition may be highly different between ecosystems, or even similar ecosystems may differ in their microbial species compositions due to different biotic and abiotic factors and, thus, influence biofilm formation and composition (see Figure 4 in Battin et al., 2016). Furthermore, *in situ* exposure experiments are hardly comparable with laboratory studies concerning species composition. Microbial species of sampled water represent a one-time inoculum and differ considerably from the dynamic inoculum of streams. The exposition site selected for our experiments is located ca. 500 m downstream of the outlet of a WWTP, which is the first plant along this headwater stream (source: urban wastewater map at www.thru.de). Having these thoughts in mind, we attempt to compare our results with similar studies in the following sections.

The most abundant prokaryotic phyla in biofilm samples were Proteobacteria, Bacteridota, and Planctomycetota, representing up to 80% of the relative abundance in these samples. On the other hand, planktonic water samples differed mainly from biofilm samples by the relatively high abundance of the class Actinobacteria and the lower relative abundance of Planctomycetes. The overall prokaryotic composition of biofilm and planktonic samples in our study largely coincides with results of a recent meta-analysis of plastisphere communities from different environments, including freshwater plastisphere and plankton (Wright et al., 2021).

Applying the high resolution power of RPCA (Martino et al., 2019) on sparse compositional microbiome datasets and filtering ranked ASVs from the ordination ends, we could show in our study that prokaryotic taxa of the Saprospiraceae (Bactegroidia), Pirellulales (Planctomycetota), and Comamonadaceae (Gammaproteobacteria) were detected multiple times (independent ASVs) as enriched taxa on microplastic particles compared with reference particles. Recently, a laboratory study of developing biofilms on PE, PP, and other natural particles incubated in sampled freshwater from Xuanwu lake (China) revealed Gammaproteobacteria as one of the bacterial groups that were more abundant (based on relative frequency) on PE particles compared with other particles (Miao et al., 2019). This observation agrees in part with our findings from exposure experiments performed in a natural environment, as the ASVs of the Comamonadaceae (Gammaproteobacteria) were highly indicative for polymer-specific biofilms. In contrast, other Gammaproteobacteria taxa were more indicative for reference samples.

The most abundant eukaryotic taxa detected in our experiments were Ciliophora, Diatomea, Holozoa, and Gastrotricha, representing ca. 60–85% of relative frequencies

in the samples. These findings overlap in part with eukaryotic taxa found on plastic particles in brackish ecosystems (Kettner et al., 2019), despite that freshwater streams and brackish coastal water constitute quite different environments. A potential eukaryotic key taxon for PE biofilms in brackish water has been identified as an unclassified Monogononta (phylum Rotifera) by Kettner et al. (2019). Still, it remains unclear whether the corresponding 18S sequence is similar/identical to any of the Rotifera ASVs identified in our experiments. Furthermore, additional ASVs classified as Rotifera were enriched on reference particles, and only two ASVs (order Ploimidia, class Monogononta) were more abundant on PS and PVC samples. Eukaryotic biofilms on low-density PE (LDPE) membranes have also been investigated by ARISA and sequencing clone libraries in the Marne river (Fechner et al., 2010). Although the sequencing depth is not comparable with 18S metabarcoding, the obtained 5.8S sequences also represented mainly diatoms and ciliates.

In our study, many ASVs assigned to Ciliophora have been identified as accountable taxa to the clustering of samples along the polymer axis of the RPCA plot. This phylum diverged from other eukaryotes approximately 1,143 Ma ago and split into large classes such as CONThreeP (in SILVA: Conthreep) and Spirotrichea (Fernandes and Schrago, 2019). Although ciliates were ubiquitously identified on polymer and reference particles, members of the Oligohymenophorea family (Conthreep clade) were more associated with polymer particles, in particular PE and PP, while members of the families Phyllopharyngea and Prostomatea (Contreep clade), Haptoria (order Litostomatea), and Hypotrichia (order Spirotrichea) were equally distributed or even more often associated with reference particles (Q). An extensive review on the functional diversity of aquatic ciliates (Weisse, 2017) has shown that ciliates cover many ecological niches and a broad range of trophic layers ranging from heterotrophs (bacterivores, herbivores, omnivores, carnivores, etc.) to symbionts (commensals, parasites, mixotrophs, and even photoautotrophs). The differential abundance of distinct ciliate taxa (distinct ASVs) in the different polymer-specific biofilms could possibly be explained by such a ciliate diversification into different ecological niches and shows that a complex biofilm community with different trophic layers has been developed even on a comparably young biofilm of only 4 weeks.

With respect to biofilms on different plastic types, the development and succession of biofilms of different plastic and glass substrates have been investigated in marine environments by scanning electron microscopy and 16S sequencing (Pinto et al., 2019). Significant differences in the bacterial communities were observed on PVC compared with other plastic types and glass surfaces after 10 days of exposure in this natural saltwater environment. This observation agrees well with recent findings that the early-stage biofilm formation on microplastics depends on environmental medium and polymer properties, particularly with the comparably high structural diversity of PVC samples in seawater compared with freshwater (Ramsperger et al., 2020a). If comparable fast colonization also occurred in our freshwater experiments, it is intriguing to

assume that slightly different bacterial communities on particles can influence the subsequent colonization of the particles by specified eukaryotic predators. Such trophic predator–prey interactions certainly occur multiple times in natural biofilms and highlight the need to investigate these interactions at the basis of the food web in much more detail to explore the fate and persistence of microplastics in the environment.

Prediction of functional abundances in bacterial communities of different polymer types and the surrounding water samples highlighted functional profiles that differed between water and biofilm samples, between the two seasons, and between various particle types. A possible contribution of the WWTP effluent to microbial communities could be detected in functions ascribed to mammalian gut bacteria and xylanolysis (occurring during digestion of plant material in the rumen), which were only found in water samples at the experiment site (downstream of the WWTP) but not in water samples collected upstream of the WWTP. However, gut-related functions were almost absent in biofilm communities of plastic and quartz particles, indicating that gut-related microbes present in stream water do hardly contribute to biofilm communities. Although the putative origin of gut-affiliated functions from the outflow of the WWTP is intriguing, other potential sources such as cattle grazing areas with surface water runoffs entering the stream upstream of the experiment site but downstream of the second water collection site cannot be ruled out. Furthermore, functions related to photoautotrophy, e.g., cyanobacteria, are more abundant in summer, suggesting an increase in photosynthetic microorganisms in biofilms as described for cyanobacterial bloom in rivers and lakes (Larsen et al., 2020). On the other side, nitrification (including aerobic nitrite oxidation) is more abundant in spring samples as it has been observed in freshwater lakes (Massé et al., 2019). Aerobic ammonia oxidation, another sub-function within nitrification, has not been detected by FAPROTAX in any sample, although included in the FAPROTAX database. Differentiation between organic polymers and inorganic quartz samples is weak and only detected with photosynthetic cyanobacteria/oxygenic photoautotrophy and for aromatic compound degradation. The latter function has also been described as an enriched function in the plastisphere of freshwater and saltwater (Li C. et al., 2021). However, more experiments are necessary to investigate whether metabolic processes of aromatic compounds correlate with organic (and potentially degradable) surfaces (in contrast to quartz particles).

Pathogenic bacteria, identified based on 16S sequence comparison (16sPIP tool), were detected in biofilm and water samples at the same abundances described for sewage and WWTP (Li D. et al., 2021). Few bacterial species dominated the profile of pathogenic bacteria in biofilm samples; the seven most abundant pathogenic bacteria already represented over 80% of the 69 identified pathogenic bacteria in biofilm samples. *E. ludwigii* has been recently identified in a case of catheter-associated bloodstream infection with massive aggregation of the bacterium outside the central venous catheter (Wagner et al., 2020). Other pathogens have also been reported as colonizers of PE and PP (*A. hydrophila*: Thomas et al., 2020),

as possible degraders of LDPE and as microplastic surface colonizers (*N. farcinica*: Soleimani et al., 2021; Yi et al., 2021), or were identified as so-called ultramicrocells from drinking water systems made of PVC pipes (*Afipia* sp.: Silbaq, 2009). Identifying pathogenic bacteria at similar percentages over a broad range of polymer and quartz surfaces suggests that these potentially harmful microorganisms can colonize many surfaces.

Our results contribute to the knowledge of microplastic biofilm communities, and it is to our best knowledge the first report of parallel analysis of prokaryotic and eukaryotic (mainly protists) communities on various polymers in headwater streams. We show that polymer-specific community differences can be identified from complex microbiome datasets despite the seasonal dynamics of biofilm communities. While functional differences in biofilm communities could be detected along the seasonal gradient, polymer- and quartz-specific functional differences are weak (but not absent) and should be further investigated in the future. Finally, a surprisingly strong correlation of polymer-specific clustering in prokaryotic and eukaryotic communities could be discovered, which could serve as a starting point for designing new experiments in microplastic research.

DATA AVAILABILITY STATEMENT

The datasets presented in this study can be found in online repositories. The names of the repository/repositories and accession number(s) can be found below: NCBI's Sequence Read Archive (SRA), Bioproject PRJNA680706.

AUTHOR CONTRIBUTIONS

AW and CL created the project idea. AW conducted the experiment, processed the samples, analyzed that data, and wrote the manuscript. ML, AR, and CL revised the manuscript. All authors contributed to the article and approved the submitted version.

FUNDING

ACKNOWLEDGMENTS

SUPPLEMENTARY MATERIAL

The Supplementary Material for this article can be found online at: https://www.frontiersin.org/articles/10.3389/fmicb.2021.660024/full#supplementary-material

REFERENCES

Arias-Andres, M., Klümper, U., Rojas-Jimenez, K., and Grossart, H.-P. (2018). Microplastic pollution increases gene exchange in aquatic ecosystems. *Environ. Pollut.* 237, 253–261. doi: 10.1016/j.envpol.2018.02.058

Arthur, C., Baker, J., and Bamford, H. (eds) (2009). *Proceedings of the International Research Workshop on the Occurrence, Effects, and Fate of Microplastic Marine Debris.* Springfield, VA: NOAA. Technical Memorandum NOS-OR&R-30.

Augspurger, C., Karwautz, C., Mussmann, M., Daims, H., and Battin, T. J. (2010). Drivers of bacterial colonization patterns in stream biofilms. *FEMS Microbiol. Ecol.* 72, 47–57. doi: 10.1111/j.1574-6941.2009.00830.x

Barnes, D. K. A., Galgani, F., Thompson, R. C., and Barlaz, M. (2009). Accumulation and fragmentation of plastic debris in global environments. *Philos. Trans. R. Soc. Lond. B Biol. Sci.* 364, 1985–1998. doi: 10.1098/rstb.2008.0205

Battin, T. J., Besemer, K., Bengtsson, M. M., Romani, A. M., and Packmann, A. I. (2016). The ecology and biogeochemistry of stream biofilms. *Nat. Rev. Microbiol.* 14, 251–263. doi: 10.1038/nrmicro.2016.15

Bokulich, N. A., Kaehler, B. D., Rideout, J. R., Dillon, M., Bolyen, E., Knight, R., et al. (2018). Optimizing taxonomic classification of marker-gene amplicon sequences with QIIME 2′s q2-feature-classifier plugin. *Microbiome* 6:90. doi: 10.1186/s40168-018-0470-z

Brunner, I., Fischer, M., Rüthi, J., Stierli, B., and Frey, B. (2018). Ability of fungi isolated from plastic debris floating in the shoreline of a lake to degrade plastics. *PLoS One* 13:e0202047. doi: 10.1371/journal.pone.0202047

Callahan, B. J., McMurdie, P. J., and Holmes, S. P. (2017). Exact sequence variants should replace operational taxonomic units in marker-gene data analysis. *ISME J.* 11, 2639–2643. doi: 10.1038/ismej.2017.119

Callahan, B. J., McMurdie, P. J., Rosen, M. J., Han, A. W., Johnson, A. J. A., and Holmes, S. P. (2016). DADA2: high-resolution sample inference from Illumina amplicon data. *Nat. Methods* 13, 581–583. doi: 10.1038/nmeth.3869

Fechner, L. C., Vincent-Hubert, F., Gaubert, P., Bouchez, T., Gourlay-Francé, C., and Tusseau-Vuillemin, M.-H. (2010). Combined eukaryotic and bacterial community fingerprinting of natural freshwater biofilms using automated ribosomal intergenic spacer analysis. *FEMS Microbiol. Ecol.* 74, 542–553. doi: 10.1111/j.1574-6941.2010.00968.x

Fedarko, M. W., Martino, C., Morton, J. T., González, A., Rahman, G., Marotz, C. A., et al. (2020). Visualizing 'omic feature rankings and log-ratios using Qurro. *NAR Genom. Bioinform.* 2:lqaa023. doi: 10.1093/nargab/lqaa023

Fernandes, N. M., and Schrago, C. G. (2019). A multigene timescale and diversification dynamics of Ciliophora evolution. *Mol. Phylogenet. Evol.* 139, 106521. doi: 10.1016/j.ympev.2019.106521

Ficetola, G. F., Miaud, C., Pompanon, F., and Taberlet, P. (2008). Species detection using environmental DNA from water samples. *Biol. Lett.* 4, 423–425. doi: 10.1098/rsbl.2008.0118

Flemming, H.-C., and Wingender, J. (2010). The biofilm matrix. *Nat. Rev. Microbiol.* 8, 623–633. doi: 10.1038/nrmicro2415

Gkoutselis, G., Rohrbach, S., Harjes, J., Obst, M., Brachmann, A., Horn, M. A., et al. (2021). Microplastics accumulate fungal pathogens in terrestrial ecosystems. *Sci. Rep.* 11:13214. doi: 10.1038/s41598-021-92405-7

Herlemann, D. P. R., Labrenz, M., Juergens, K., Bertilsson, S., Waniek, J. J., and Andersson, A. F. (2011). Transitions in bacterial communities along the 2000 km salinity gradient of the Baltic Sea. *ISME J.* 5, 1571–1579. doi: 10.1038/ismej.2011.41

Hodgson, D. J., Bréchon, A. L., and Thompson, R. C. (2018). Ingestion and fragmentation of plastic carrier bags by the amphipod *Orchestia gammarellus*: effects of plastic type and fouling load. *Mar. Pollut. Bull.* 127, 154–159. doi: 10.1016/j.marpolbul.2017.11.057

Hoellein, T., Rojas, M., Pink, A., Gasior, J., and Kelly, J. (2014). Anthropogenic litter in urban freshwater ecosystems: distribution and microbial interactions. *PLoS One* 9:e98485. doi: 10.1371/journal.pone.0098485

Hoellein, T. J., McCormick, A. R., Hittie, J., London, M. G., Scott, J. W., and Kelly, J. J. (2017). Longitudinal patterns of microplastic concentration and bacterial assemblages in surface and benthic habitats of an urban river. *Freshwater Sci.* 36, 491–507. doi: 10.1086/693012

Kaevska, M., Videnska, P., Sedlar, K., and Slana, I. (2016). Seasonal changes in microbial community composition in river water studied using 454-pyrosequencing. *SpringerPlus* 5:409. doi: 10.1186/s40064-016-2043-6

Kaza, S., Yao, L., Bhada-Tata, P., and van Woerden, F. (2018). *What a Waste 2.0: A Global Snapshot of Solid Waste Management to 2050.* Washington, DC: The World Bank.

Kettner, M. T., Oberbeckmann, S., Labrenz, M., and Grossart, H.-P. (2019). The eukaryotic life on microplastics in brackish ecosystems. *Front. Microbiol.* 10:538. doi: 10.3389/fmicb.2019.00538

Larsen, M. L., Baulch, H. M., Schiff, S. L., Simon, D. F., Sauvé, S., and Venkiteswaran, J. J. (2020). Extreme rainfall drives early onset cyanobacterial bloom. *FACETS* 5, 899–920. doi: 10.1139/facets-2020-0022

Li, C., Wang, L., Ji, S., Chang, M., Wang, L., Gan, Y., et al. (2021). The ecology of the plastisphere: microbial composition, function, assembly, and network in the freshwater and seawater ecosystems. *Water Res.* 202:117428. doi: 10.1016/j.watres.2021.117428

Li, D., van de Werfhorst, L. C., Rugh, M. B., Feraud, M., Hung, W.-C., Jay, J., et al. (2021). Limited bacterial removal in full-scale stormwater biofilters as evidenced by community sequencing analysis. *Environ. Sci. Technol.* 55, 9199–9208. doi: 10.1021/acs.est.1c00510

Louca, S., Parfrey, L. W., and Doebeli, M. (2016). Decoupling function and taxonomy in the global ocean microbiome. *Science* 353, 1272–1277. doi: 10.1126/science.aaf4507

Martino, C., Morton, J. T., Marotz, C. A., Thompson, L. R., Tripathi, A., Knight, R., et al. (2019). A novel sparse compositional technique reveals microbial perturbations. *mSystems* 4:13. doi: 10.1128/mSystems.00016-19

Massé, S., Botrel, M., Walsh, D. A., and Maranger, R. (2019). Annual nitrification dynamics in a seasonally ice-covered lake. *PLoS One* 14:e0213748. doi: 10.1371/journal.pone.0213748

McCormick, A., Hoellein, T. J., Mason, S. A., Schluep, J., and Kelly, J. J. (2014). Microplastic is an abundant and distinct microbial habitat in an urban river. *Environ. Sci. Technol.* 48, 11863–11871. doi: 10.1021/es503610r

McCormick, A. R., Hoellein, T. J., London, M. G., Hittie, J., Scott, J. W., and Kelly, J. J. (2016). Microplastic in surface waters of urban rivers: concentration, sources, and associated bacterial assemblages. *Ecosphere* 7:e01556. doi: 10.1002/ecs2.1556

Miao, J., Han, N., Qiang, Y., Zhang, T., Li, X., and Zhang, W. (2017). 16SPIP: a comprehensive analysis pipeline for rapid pathogen detection in clinical samples based on 16S metagenomic sequencing. *BMC Bioinformatics* 18:568. doi: 10.1186/s12859-017-1975-3

Miao, L., Wang, P., Hou, J., Yao, Y., Liu, Z., Liu, S., et al. (2019). Distinct community structure and microbial functions of biofilms colonizing microplastics. *Sci. Tot. Environ.* 650, 2395–2402. doi: 10.1016/j.scitotenv.2018.09.378

Nakajima-Kambe, T., Shigeno-Akutsu, Y., Nomura, N., Onuma, F., and Nakahara, T. (1999). Microbial degradation of polyurethane, polyester polyurethanes and polyether polyurethanes. *Appl. Microbiol. Biotechnol.* 51, 134–140. doi: 10.1007/s002530051373

Oberbeckmann, S., and Labrenz, M. (2020). Marine microbial assemblages on microplastics: diversity, adaptation, and role in degradation. *Ann. Rev. Mar. Sci.* 12, 209–232. doi: 10.1146/annurev-marine-010419-010633

Oberbeckmann, S., Löder, M. G. J., and Labrenz, M. (2015). Marine microplastic-associated biofilms – a review. *Environ. Chem.* 12:551. doi: 10.1071/EN15069

Parrish, K., and Fahrenfeld, N. L. (2019). Microplastic biofilm in fresh- and wastewater as a function of microparticle type and size class. *Environ. Sci. Water Res. Technol.* 5, 495–505. doi: 10.1039/c8ew00712h

Piehl, S., Leibner, A., Löder, M. G. J., Dris, R., Bogner, C., and Laforsch, C. (2018). Identification and quantification of macro- and microplastics on an agricultural farmland. *Sci. Rep.* 8:17950. doi: 10.1038/s41598-018-36172-y

Pinto, M., Langer, T. M., Hüffer, T., Hofmann, T., and Herndl, G. J. (2019). The composition of bacterial communities associated with plastic biofilms

differs between different polymers and stages of biofilm succession. *PLoS One* 14:e0217165. doi: 10.1371/journal.pone.0217165

Piredda, R., Tomasino, M. P., D'Erchia, A. M., Manzari, C., Pesole, G., Montresor, M., et al. (2017). Diversity and temporal patterns of planktonic protist assemblages at a mediterranean long term ecological research site. *FEMS Microbiol. Ecol.* 93:fiw200. doi: 10.1093/femsec/fiw200

PlasticsEurope (2020). *Plastics - the Facts 2020.* Available online at: https://www.plasticseurope.org/de/resources/publications/4312-plastics-facts-2020 (accessed January 20, 2021).

Ramsperger, A. F. R. M., Stellwag, A. C., Caspari, A., Fery, A., Lueders, T., Kress, H., et al. (2020a). Structural diversity in early-stage biofilm formation on microplastics depends on environmental medium and polymer properties. *Water* 12:3216. doi: 10.3390/w12113216

Ramsperger, A. F. R. M., Narayana, V. K. B., Gross, W., Mohanraj, J., Thelakkat, M., Greiner, A., et al. (2020b). Environmental exposure enhances the internalization of microplastic particles into cells. *Sci. Adv.* 6, eabd1211. doi: 10.1126/sciadv.abd1211

Restrepo-Montoya, D., Becerra, D., Carvajal-Patiño, J. G., Mongui, A., Niño, L. F., Patarroyo, M. E., et al. (2011). Identification of Plasmodium vivax proteins with potential role in invasion using sequence redundancy reduction and profile hidden Markov models. *PLoS One* 6:e25189. doi: 10.1371/journal.pone.0025189

Robeson, M. S., O'Rourke, D. R., Kaehler, B. D., Ziemski, M., Dillon, M. R., Foster, J. T., et al. (2020). RESCRIPt: reproducible sequence taxonomy reference database management for the masses. *bioRxiv* [preprint]. doi: 10.1101/2020.10.05.326504

Sangale, M. K., Shahnawaz, M., and Ade, A. B. (2019). Potential of fungi isolated from the dumping sites mangrove rhizosphere soil to degrade polythene. *Sci. Rep.* 9:5390. doi: 10.1038/s41598-019-41448-y

Schlundt, C., Mark Welch, J. L., Knochel, A. M., Zettler, E. R., and Amaral-Zettler, L. A. (2020). Spatial structure in the "Plastisphere": molecular resources for imaging microscopic communities on plastic marine debris. *Mol. Ecol. Resour.* 20, 620–634. doi: 10.1111/1755-0998.13119

Silbaq, F. S. (2009). Viable ultramicrocells in drinking water. *J. Appl. Microbiol.* 106, 106–117. doi: 10.1111/j.1365-2672.2008.03981.x

Soleimani, Z., Gharavi, S., Soudi, M., and Moosavi-Nejad, Z. (2021). A survey of intact low-density polyethylene film biodegradation by terrestrial *Actinobacterial species. Int. Microbiol.* 24, 65–73. doi: 10.1007/s10123-020-00142-0

Statistica (2021). *Global Plastic Production 1950-2020.* Available online at: https://www.statista.com/statistics/282732/global-production-of-plastics-since-1950/ (accessed October 19, 2021).

Stoeck, T., Bass, D., Nebel, M., Christen, R., Jones, M. D. M., Breiner, H.-W., and Richards, T. A. (2010). Multiple marker parallel tag environmental DNA sequencing reveals a highly complex eukaryotic community in marine anoxic water. *Mol. Ecol.* 19(Suppl. 1), 21–31. doi: 10.1111/j.1365-294X.2009.04480.x

Thomas, S. G., Glover, M. A., Parthasarathy, A., Wong, N. H., Shipman, P. A., and Hudson, A. O. (2020). Expression of a shiga-like toxin during plastic colonization by two multidrug-resistant bacteria, *Aeromonas hydrophila* RIT668 and *Citrobacter freundii* RIT669, isolated from endangered turtles (*Clemmys guttata*). *Microorganisms* 8:1172. doi: 10.3390/microorganisms8081172

Vroom, R. J. E., Koelmans, A. A., Besseling, E., and Halsband, C. (2017). Aging of microplastics promotes their ingestion by marine zooplankton. *Environ. Pollut.* 231, 987–996. doi: 10.1016/j.envpol.2017.08.088

Wagner, L., Bloos, F., and Vylkova, S. (2020). Bloodstream infection due to *Enterobacter ludwigii*, correlating with massive aggregation on the surface of a central venous catheter. *Infection* 48, 955–958. doi: 10.1007/s15010-020-01482-9

Wagner, M., and Lambert, S. (2018). *Freshwater Microplastics.* Cham: Springer International Publishing.

Weisse, T. (2017). Functional diversity of aquatic ciliates. *Eur. J. Protistol.* 61, 331–358. doi: 10.1016/j.ejop.2017.04.001

Weitere, M., Erken, M., Majdi, N., Arndt, H., Norf, H., Reinshagen, M., et al. (2018). The food web perspective on aquatic biofilms. *Ecol. Monogr.* 88, 543–559. doi: 10.1002/ecm.1315

Wright, R. J., Langille, M. G. I., and Walker, T. R. (2021). Food or just a free ride? a meta-analysis reveals the global diversity of the Plastisphere. *ISME J.* 15, 789–806. doi: 10.1038/s41396-020-00814-9

Wu, X., Pan, J., Li, M., Li, Y., Bartlam, M., and Wang, Y. (2019). Selective enrichment of bacterial pathogens by microplastic biofilm. *Water Res.* 165, 114979. doi: 10.1016/j.watres.2019.114979

Yi, M., Zhou, S., Zhang, L., and Ding, S. (2021). The effects of three different microplastics on enzyme activities and microbial communities in soil. *Water Environ. Res.* 93, 24–32. doi: 10.1002/wer.1327

Yoshida, S., Hiraga, K., Takehana, T., Taniguchi, I., Yamaji, H., Maeda, Y., et al. (2016). A bacterium that degrades and assimilates poly(ethylene terephthalate). *Science* 351, 1196–1199. doi: 10.1126/science.aad6359

Yuan, J., Ma, J., Sun, Y., Zhou, T., Zhao, Y., and Yu, F. (2020). Microbial degradation and other environmental aspects of microplastics/plastics. *Sci. Tot. Environ.* 715:136968. doi: 10.1016/j.scitotenv.2020.136968

Zettler, E. R., Mincer, T. J., and Amaral-Zettler, L. A. (2013). Life in the "plastisphere": microbial communities on plastic marine debris. *Environ. Sci. Technol.* 47, 7137–7146. doi: 10.1021/es401288x

Zhang, Y., Kang, S., Allen, S., Allen, D., Gao, T., and Sillanpää, M. (2020). Atmospheric microplastics: a review on current status and perspectives. *Earth-Sci. Rev.* 203:103118. doi: 10.1016/j.earscirev.2020.103118

Conflict of Interest: The authors declare that the research was conducted in the absence of any commercial or financial relationships that could be construed as a potential conflict of interest.

Publisher's Note: All claims expressed in this article are solely those of the authors and do not necessarily represent those of their affiliated organizations, or those of the publisher, the editors and the reviewers. Any product that may be evaluated in this article, or claim that may be made by its manufacturer, is not guaranteed or endorsed by the publisher.

274

Supplementary Material

1   List of Supplementary Material

1.1   Tables

- Table S1.xlsx: Excel spreadsheets containing the most contributing prokaryotic features along axis 1 (seasonal axis) including t-test results
- Table S2.xlsx: Excel spreadsheets containing the most contributing eukaryotic features along axis 1 (seasonal axis) including t-test results
- Table S3.xlsx: Excel spreadsheets containing the most contributing prokaryotic features along axis 2 (particle axis) including pairwise t-test results
- Table S4.xlsx: Excel spreadsheets containing the most contributing eukaryotic features along axis 2 (particle axis) including pairwise t-test results

1.2   Figures

- Figure S1.pdf: Current log-ratio plots for RPCA axis 1 (seasonal axis) for prokaryotic and eukaryotic data sets
- Figure S2.pdf: Current log-ratio plots for RPCA axis 2 (particle axis) for prokaryotic and eukaryotic data sets
- Figure S3.pdf: Pathogenic bacteria detected in biofilm and water samples

1.3   Qiime2 Information and Data Files

- Intruction_to_use_Qiime2_data.pdf: Instructions to open Qiime2 data by Qiime2view Web Interface (view.qiime2.org), including instructions how to access Qiime2 analysis parameters via the provenance tab;
- Taxonomic barplots:
    - taxa-barplot_Figure-1A_Prokaryotes2.qzv
    - taxa-barplot_Figure-1B_Eukaryotes2.qzv
- RPCA biplots
    - biplot_RPCA_Figure-2A_Prokaryotes.qzv
    - biplot_RPCA_Figure-2B_Eukaryotes.qzv
- QURRO plots
    - qurro-plot_full_Prokaryotes.qzv
    - qurro-plot_full_Eukaryotes.qzv
    - qurro-plot_Q-PE_Eukaryotes.qzv
    - qurro-plot_Q-PE_Prokaryotes.qzv
    - qurro-plot_Q-PP_Eukaryotes.qzv
    - qurro-plot_Q-PP_Prokaryotes.qzv
    - qurro-plot_Q-PS_Eukaryotes.qzv
    - qurro-plot_Q-PS_Prokaryotes.qzv
    - qurro-plot_Q-PVC_Eukaryotes.qzv
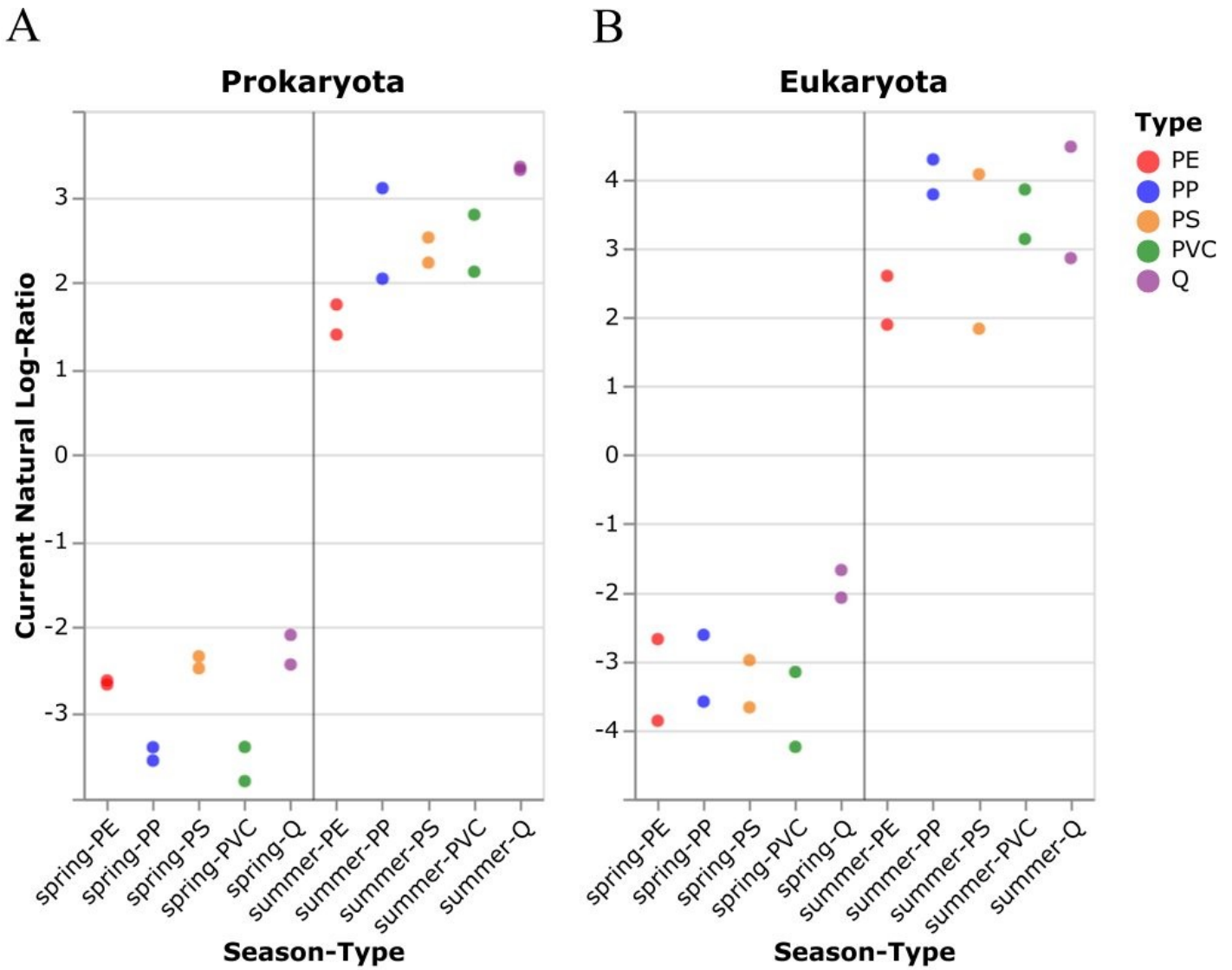   - qurro-plot_Q-PVC_Prokaryotes.qzv

Figure S1: Log-ratio calculations of most-contributing features of prokaryotic (A) and eukaryotic (B) data sets to the season-specific axis 1 in RPCA plots. The respective list of features (ASVs) were filtered from RPCA data files using a 1% autoselection threshold (QURRO plugin to Qiime).

Figure S2: Log-ratio calculations of most-contributing features of prokaryotic (A) and eukaryotic (B) data sets to the particle-specific axis 2 in RPCA plots. The respective list of features (ASVs) were filtered from RPCA data files using a 3% autoselection threshold (QURRO plugin to Qiime).
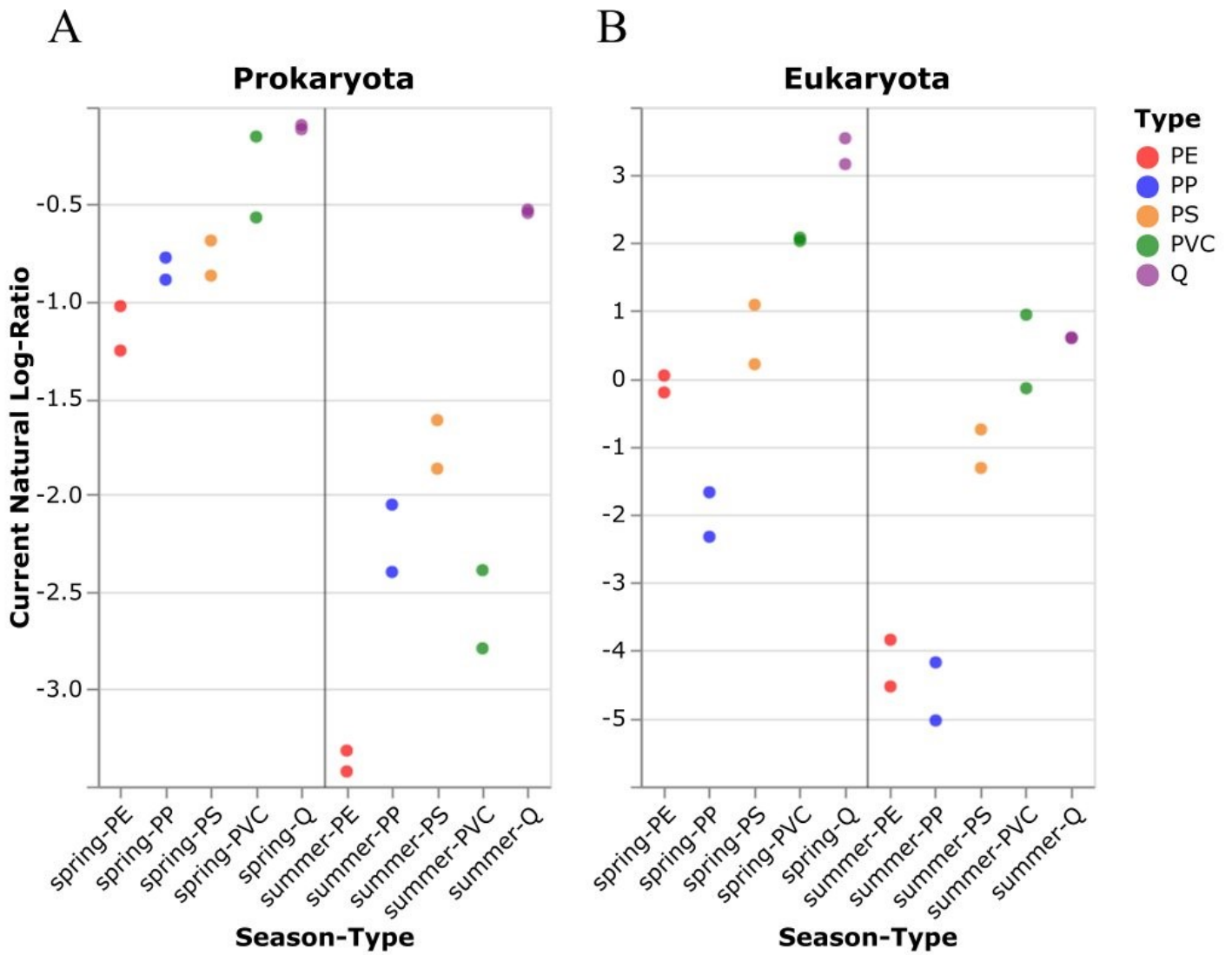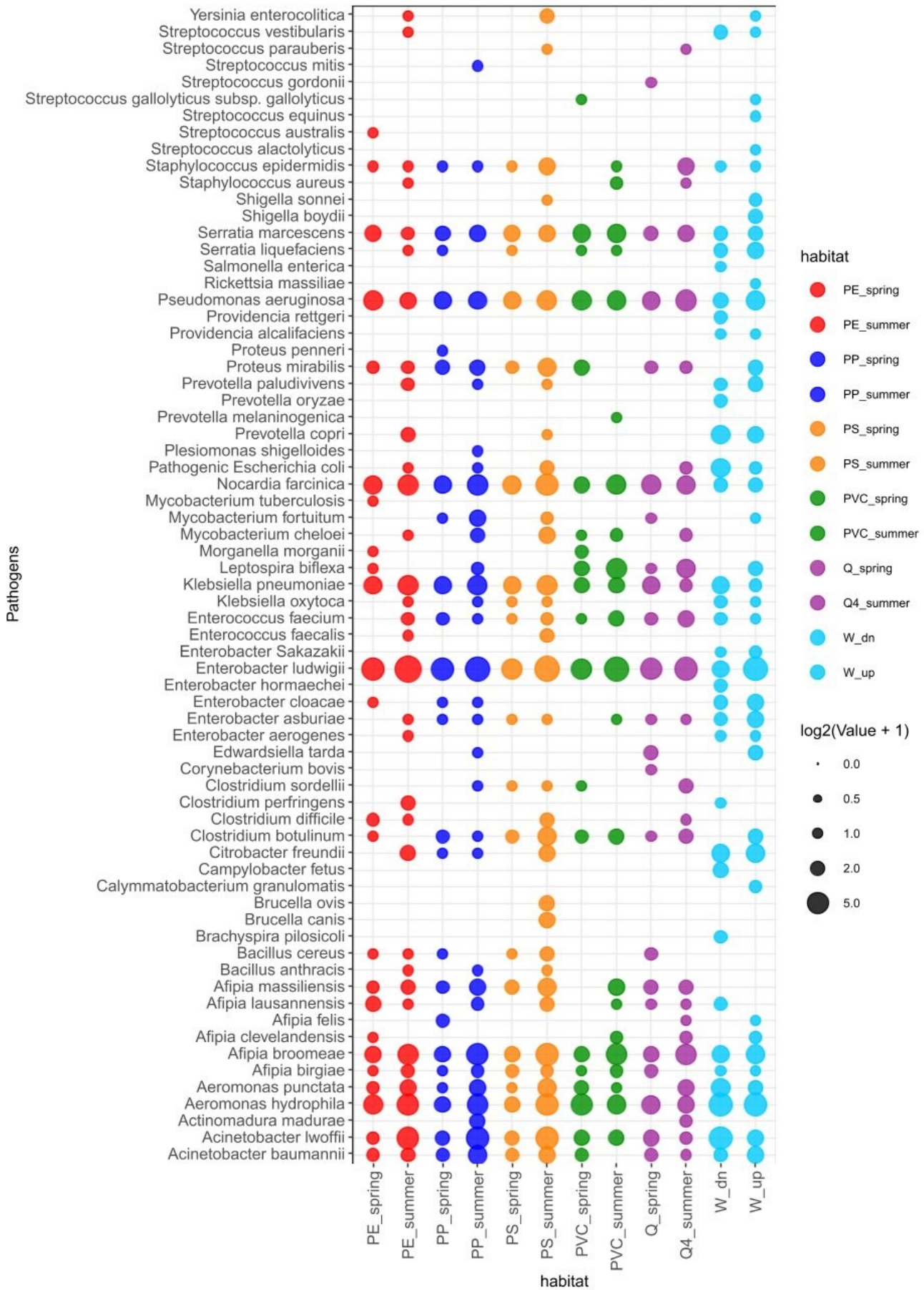
Figure S3: Potential pathogenic bacteria in biofilm and water samples, predicted by 16sPIP (Miao et al., 2017)

Article 10

Spatio-chemical analysis of the plastisphere using Raman spectroscopy

1 Manuscript

2 **Title**

3 Spatio-chemical analysis of the plastisphere using Raman spectroscopy

4

5 **Authors:**

6 Vinay Kumar Bangalore-Narayana[1], Anja FRM Ramsperger[1,2], Marvin Kiene[1], Julian Brehm[1], Martin GJ
7 Löder[1] & Christian Laforsch[1,#]

8

9 **Affiliations:**

10 [1] Animal Ecology I, University of Bayreuth, Bayreuth, Germany

11 [2] Biological Physics, University of Bayreuth, Bayreuth, Germany

12 [#] corresponding author

13   **Abstract:**

14   Microplastics (MPs; <5 mm) in the environment have in the recent years come to be increasingly scrutinized

15   as sites of colonization and interaction for different types of microorganisms. Different MPs polymer types

16   are known to harbour distinct microbial communities on their surface forming biofilms termed as the

17   plastisphere. To date, a detailed multimolecular profiling of the plastisphere on different MPs polymer types

18   in association with their native environment has not been established. Probing these profiles may help in

19   obtaining a quick snapshot of the contents of the plastisphere and may aid in the identification of

20   plastisphere fingerprints, which are specific to a MPs type. Specific plastisphere fingerprints on MPs would

21   allow the direct measurement of MPs within an environmental sample without the currently performed

22   pre-processing of a sample like the MP isolation and purification from the environmental matrix. Therefore,

23   we apply micro-Raman spectroscopy to achieve a label free and non-invasive investigation of the molecular

24   profiles of the plastisphere on the surface of 12 different synthetic polymer types. We incubated MPs pellets

25   (~3 mm) and glass pellets (as non-plastic control particles) in a microcosm consisting of freshwater (FW)

26   and artificial seawater (SW) for a duration of 30 days, and analysed those using micro-Raman spectroscopy

27   and scanning electron microscopy. Our investigations reveal morphologically diverse microorganismal

28   structures and a heterogeneous distribution of associated key molecular signatures as arising mainly from

29   extracellular polymeric substances (EPS). Our results highlight that the microbial diversity and biomass of

30   the plastisphere in FW incubated MPs is relatively higher in comparison to the SW incubated MPs.

31   Although there were no MPs specific plastisphere fingerprints detected with micro-Raman spectroscopy,

32   the plastisphere molecular profiles investigation allowed for the acquisition of spectral variants of MPs

33   influenced by the presence of microbial biomass on their surface. A microbial biofilm influenced MPs

34   spectral variant library is provided, for the utility of the MPs research community. This will help to

35   overcome the time- and cost-intensive complex pre-treatment of MPs in environmental matrices, which

36   enables the direct identification of environmental MPs.

37

38

40

1. Introduction

A scenario that is consistent with the current scheme of things related to the world's pollution is that the increased production of plastics leads to increased amounts of plastic litter in the environment (Andrady, 2011). This plastic litter may be compiled of different size classes such as the mega (>1 m), macro (>10 mm), meso (<10 mm), micro (MPs; <5 mm) all the way down to the nanoplastics (NPs; <1µm) size range (Hartmann et al., 2019; Imhof et al., 2017; Lusher et al., 2017). In the last decade, plastic pollution has developed into an issue that is a major cause of concern due to its impact on the environment (Klein et al., 2018; MacLeod et al., 2021; Rhodes, 2018; Takada et al., 2022). This led to an avalanche of research focussed primarily on MPs and NPs as these predominantly constitute the size fraction that can be adsorbed by primary producers and ingested by higher trophic level organisms like the zooplankton, birds, fish, mammals etc., across different environments (Arp et al., 2021; Gomes et al., 2022; Raju et al., 2021; Wright et al., 2013). With aspects like the sources of MPs and NPs, standardization and harmonization of extraction and analysis methodologies, abundances, spatial and temporal distribution and their ecotoxicological impacts on organisms in different environments are being rigorously investigated in research labs across the world (Banerjee and Shelver, 2021; Möller et al., 2020; Riveros et al., 2022; Talbot and Chang, 2022; Trotter et al., 2021; Wang et al., 2021). Along with the aforementioned aspects, a budding topic of interest has emerged in association with MPs, which is the selective colonization of microorganisms on its surfaces. A phenomenon described by Zettler et al. (2013), by the coinage of the term the "plastisphere" (Miao et al., 2021; Tiwari et al., 2022; Wright et al., 2021; Zettler et al., 2013).

The development of a plastisphere in general begins with the formation of a conditioning film, or the eco-corona, on the surfaces of MPs, which form within time periods of a few minutes to hours depending on the native environment and associated physico-chemical conditions (Bhagwat et al., 2021; Ramsperger et al., 2020; Rummel et al., 2017). The eco-corona may facilitate the arrival of the first colonizers, which will be followed by a dynamic development into a thick matrix of microorganisms and associated extracellular polymeric substances (EPS) on the MPs surface (Lawrence et al., 2016; Siboni et al., 2007). This complex organization of microorganisms associated with a surface can be collectively referred to as the biofilm (Flemming and Wingender, 2010). The biofilm may include a host of microorganisms ranging from bacteria, algae, fungi and viruses etc., differing in phylogeny and functionality embedded in a matrix composed of EPS (Flemming and Wingender, 2010; Gkoutselis et al., 2021; Rummel et al., 2017). In general, the biofilms are important for microorganisms to perform functions such as protection against UV light, nutrient accumulation, waste product removal, toleration of dehydration, antibiotic resistance, toxic substance removal and protection from grazers (Flemming and Wingender, 2010). MPs surface serve as an ideal substrate for microbial growth and biofilm formation due to its stability and persistence in the environment (Barros et al., 2020). Many studies have shown that the characteristics of MPs such as their inherent chemistry, surface roughness, hydrophobicity, surface free energy influence the presence of unique microbial species in the plastisphere (Xie et al., 2021; Zhang et al., 2022). Nevertheless, other physico-chemical parameters relevant to the environment such as light, salinity, pH, temperature, nutrient

78 concentration, oxygen levels, dissolved organic matter (DOM) and incubation period have also been shown

79 to play a major role (Barros and Seena, 2021; Basili et al., 2020; Harrison et al., 2018; Rummel et al., 2021).

80 However, it remains a matter of debate as to which of these factors may have more weightage and influence

81 in supporting the growth of specific microbial communities on different types of MPs (Coons et al., 2021).

82 Plastisphere in principle could potentially have negative effects for the environment, organisms and human

83 health. For example, pathogenic microbial species, persistent organic pollutants (POPs) and toxic metals

84 may hitchhike within the plastisphere and get transported to different trophic level organisms via the food

85 web (Strungaru et al., 2019; Weig et al., 2021; Zettler et al., 2013). Furthermore, the plastisphere may alter

86 the density of the MPs leading to differences in their sinking behaviour resulting in their transport within

87 the water column even reaching sediments leading to the underestimation of MPs abundances in the

88 aqueous environments (Lobelle et al., 2021). However, on the brighter side, the plastisphere may also

89 harbour microbial communities, that are capable of facilitating the degradation of plastic debris which can

90 be amongst a potential solution in the future for the removal of this debris from the environment (Vaksmaa

91 et al., 2021; Zhou et al., 2022).

92 The microbial communities in the plastisphere in freshwater (FW) and marine water environments were

93 analyzed either by incubating the particles for several months or years (Artham et al., 2009; Hossain et al.,

94 2019; Webb et al., 2009) or analysing microplastic particles isolated directly from the environment with

95 unknown incubation times (Oberbeckmann et al., 2014; Zettler et al., 2013). To date, the biodiversity and

96 structure of the plastisphere has been predominantly analysed using confocal laser scanning microscopy

97 (CLSM) in combination with the metagenomic sequencing analysis (Bartkova et al., 2021; Di Pippo et al.,

98 2020; Miao et al., 2021). Interestingly, it was described that there can occur distinct polymer-specific

99 microbial communities that are additionally different to natural surfaces like wood or glass, which were

100 discussed to origin from the physicochemical characteristics of the different polymers (Huang et al., 2022;

101 Ramsperger et al., 2020; Weig et al., 2021; Zettler et al., 2013; Zhang et al., 2022). However, an in-depth

102 multimolecular analysis of the aqueous plastisphere has so far not been performed.

103 To fill the current gap in lack of an in-depth multimolecular profiling of the plastisphere, we envision the

104 application of micro-Raman spectroscopy that allows a non-invasive monitoring of molecular signatures of

105 individual microorganisms and complex biofilms at a high spatial resolution (Cialla-May et al., 2022; Ivleva

106 et al., 2017, 2008; Kusić et al., 2015; Wagner et al., 2009). The technique has been applied in many studies

107 for non-destructively investigating the microbial biofilm heterogeneity and for its characterization,

108 respectively (Beier et al., 2012; Feng et al., 2015; Hrubanova et al., 2018; Kusić et al., 2015; Nag et al., 2021).

109 To date, it has not been investigated whether there are polymer-specific spatio-chemical compositions of

110 the plastisphere and whether differences in the chemical signatures could be used to distinguish between

111 different polymer types in a complex matrix, which may aid in the easier identification of MPs from complex

112 environmental matrices.

113

114 **2. Materials and Methods**

115 *Microplastic (MPs) and glass particles*

116 MPs and glass pellets were obtained from different sources and have been listed in **Table S1**. Representative
117 images of the particles are also visualized in **Fig. S1**.

118 *Microcosm setup*

119 *Sample collection and biofilm incubation*

120 Freshwater (FW) and artificial seawater (SW) samples were collected in July 2021, the FW samples were
121 collected from a stream wherein the water from the nearby waste water treatment plant (WWTP) located
122 in Bayreuth, Germany is channelled out and the SW were collected from the in-house marine aquarium
123 facility located at the Animal Ecology I department, University of Bayreuth. The water samples were
124 collected in 10L Teflon containers, which were thoroughly sterilized with 70% ethanol followed by rigorous
125 rinsing with distilled water and finally by rinsing thrice with the water from the source. These samples were
126 then filtered using 10 µm pore size (Whatmann filter papers) to remove any large debris and small organisms
127 prior to channelling of the water into sterilized 1L Erlen-Meyer flasks which serve as the microcosm (**Fig.**
128 **S2**). The FW and SW samples are the sole source of microorganisms for the formation of plastisphere.

129 A total of 26 microcosms were used. Each microcosm consisted of 1L of either FW or SW spiked with
130 one, out of 12, types of MPs or glass pellets with ~175-200 particles included in each individual microcosm.
131 Glass pellets were used as the non-polymer control or reference particles. Hence, 13 microcosms were
132 designated for FW incubation and 13 others were designated for SW incubation respectively. The
133 microcosms were incubated with continuous aeration in a climate chamber (20 °C + 1 °C) with a day-and-
134 night-simulating photoperiod (15h light; 9h darkness) for a time period of 30 days (**Fig. S2**). pH in the
135 microcosms was monitored on a weekly basis and no drastic changes were detected throughout the
136 incubation period (pH 7 ± 0.5).

137 **Micro-Raman instrumentation, sample preparation and Raman image analysis**

138 The Raman spectroscopic measurements were performed using a commercial micro-Raman instrument
139 Witec Alpha-300 RA+ (Witec, Ulm, Germany). A frequency doubled Nd-YAG laser with a wavelength of
140 532 nm was used as an excitation source, focal length of the spectrometer is 300 mm and is equipped with
141 a grating having a groove density of 600 lines per mm to give a spectral resolution of about ~ < 3 cm^{-1} and
142 a 50x magnification objective was used for the measurements (more details of the instrument can be found
143 elsewhere (Ritschar et al., 2020)). For the acquisition of Raman images, the sample particles were carefully
144 harvested from the microcosms using sterile, ungraduated, extra-long glass Pasteur pipettes (VWR) with a
145 custom made cut big enough to collect the particles. The particles were transferred directly into a Petri dish
146 filled with tap water. Following this step, the particles were picked using small soft hold steel spring forceps
147 and gently rinsed in tap water collected in two different Petri dishes to wash off the loosely bound

148   planktonic cells. Finally, the particles were transferred to a concavity glass slide consisting of a drop of tap

149   water and immediately used for Raman measurements (**Fig**. **S3**). The surface of the pellet was then searched

150   for the presence of clusters of biofilm-associated cells as an indicator of plastisphere on the surface. Raman

151   images were then acquired from these target regions by executing a large area z-stack scan based on point-

152   by-point spectral mapping method (100 ms per point exposure time) with a step size between ~ 400–500

153   nm covering an area of ~75 × 75 µm or more depending on the cell cluster size on the MPs surface in x

154   and y directions and 20 µm in the z direction. The spectral range was selected between 3600–500 cm^{-1}. The

155   step size in the z direction was set to 2 µm, resulting in the acquisition of 10 layers in the z-stack. Each

156   Raman image required an acquisition time of ~ 1-1.5 h and comprised of a data set constituting a total of

157   approximately 25,000 spectra. The Raman images were processed using the Witec integrated Project

158   software (version 5.3) and were subjected to true component analysis (TCA) coupled with spectral demixing

159   to visualize the spatial distribution of different components within the Raman image (example; MPs

160   signature and biomolecules signature). More details about TCA are described elsewhere (Ritschar et al.,

161   2020). The Raman spectrum of true components were pre-processed (baseline correction) using GNU R

162   versions (2.15.3 and 3.5.1) and OriginLab software version 8.5.. Inkscape (Version 2.0.1) was used for

163   visualization of data. Sample size is n = 2 (technical replicates), all measurements were performed on 2

164   different pellets corresponding to each type of MPs and glass pellet. 3D reconstruction; at each layer within

165   the 10 layers of the z-stack, a spectral point map was created by plotting the intensity of each of the spectral

166   component as a function of the position. These maps corresponding to unique spectral components were

167   then merged together using Fiji ImageJ software and 3D visualizations was created using the volume viewer

168   mode available within the Fiji ImageJ 3D plugin (Schmid et al., 2010). It is important to note that Raman

169   measurements have not been performed for PMMA MPs as the fluorescence signal of PMMA completely

170   masked the Raman signal of the plastisphere and the underlying MPs.

171   *Plastisphere_Raman MPs spectral variant library*

172   We provide the underlying pre-processed Raman spectral data acquired in this study together with the meta

173   data as an R package, the "RaMPP" lib. We further include a shiny app in this package to provide a simple

174   tool for visualization and comparison of the spectral variant data with other data from the library or a

175   spectrum recorded by the user. To achieve this, we used R version 4.0.3 (Core Development Team, 2020)

176   with the package shiny version 1.7.1. The app makes use of the packages ggplot2 for visualisation and

177   pracma version 2.3.6 for interpolating parts of user spectra, in case they have a lower resolution compared

178   to our data.

179   *Scanning Electron Microscopy (SEM) measurements*

180   Two particles for each treatment were sampled for scanning electron microscopy (SEM) investigations.

181   The particles were transferred into a 12 well plate (CellStar, Greiner Bio-One, Frickenhausen, Germany)

182   and fixed for 1 hour in 1mL Karnovsky's fixative (2% paraformaldehyde (PFA) and 2.5% glutaraldehyde

183   in 1x PBS). Subsequently, an ethanol series was conducted for dehydration of the biofilm. Therefore, the

184 fixative was replaced by 1mL of the corresponding ethanol concentration (1x 30% & 50% for 15min each

185 at 4°C, 1x 70% & 90% for 15min each at -20°C and 3x absolute ethanol for 20 min at -20°C). Then, the

186 samples were dried twice in 1mL hexamethyldisilazane (HMDS, Carl Roth GmbH) for 10min at room

187 temperature and stored in a desiccator until complete drying. The dry samples were placed on carbon

188 conductive tabs (Ø 12 mm, Plano GmbH, Wetzlar, Germany) fixed to aluminium stubs (Ø 12 mm, Plano

189 GmbH, Wetzlar, Germany) and sputter-coated with 2 nm carbon and 2 nm platinum (Leica EM ACE600,

190 Leica GmbH, Wetzlar, Germany). They were analysed with a scanning electron microscope (JSM-IT500,

191 Jeol, Joel GmbH, Freising, Germany) at 3-4 kV using an Everhart-Thornley Detector.

192

193 ## 3. Results

194

195 *Plastisphere morphology and distribution-SEM investigations*

196 SEM investigations indicated the presence of distinct differences in plastisphere morphology and

197 distribution on the surfaces of different MPs polymer types in association with the corresponding FW and

198 SW incubations. Firstly, with respect to the FW incubations, a thick layer of plastisphere was observed in

199 Polyamide (PA), Polyethyleneterepthalate (PET), Polystyrene (PS), Polyurethane (PU), Polycarbonate (PC),

200 Polyvinylchloride (PVC) and Acrylonitrile Butadiene Styrene (ABS) MPs surfaces respectively (**Fig. 1**). In

201 contrast to these MPs surfaces, a relatively minimal or less thick layer of plastisphere was observed on

202 Polyethylene (PE), Polypropylene (PP), Polymethylenemethacrylate (PMMA), Polyoxymethylene (POM),

203 and Styrene Acrylonitrile (SAN) MPs surfaces. Interestingly, the glass pellet surface in general showed no

204 prominent microorganismal structures, which was not adequate to indicate biofilm growth. Secondly, with

205 the SW incubations, the presence of a minimally thick plastisphere was observed in PET, PS, PU, PVC and

206 SAN MPs surfaces respectively. In contrast, all the other MPs surfaces only had a random distribution of

207 cells but not enough microbial growth to indicate the presence of a plastisphere. As in FW incubations, the

208 SW incubated glass pellet surface did not have any prominent microorganismal structures that were

209 indicative of biofilm formation (**Fig. 1**).

210 The prominent microorganismal structures detected on the surface of some of the MPs mentioned above

211 either show morphologies that resemble rod-shaped or coccoid-like bacteria (e.g. PE **Fig.1 (C, D)**),

212 rhombus and sphere shaped diatomic structures, dense tubular structures, etc. wherein all of these

213 structures are seen embedded into the EPS matrix (**Fig.1 C, G**). Elongated filament like structures

214 resembling hyphae and elongated chains of bacteria were also observed for example on PA and PC

215 incubated in FW (**Fig. 1**). All types of MPs incubated in FW generally highlighted the presence of a dense

216 and morphologically diverse plastisphere on its surfaces in comparison to their SW counterparts, which

217 indicated only minimal plastisphere presence or no presence of microorganismal structures at all. For

218 example: PA incubated in FW was almost entirely covered by microorganismal structures indicating the

219 presence of a dense plastisphere (**Fig. 1(I)**). In contrast, only planktonic cells were visible after the same

220 incubation time in SW on the surface of PA (**Fig. 1(J)**). This observation was also true for PET (**Fig. 1(G,**

221 **H)**), although the SW incubated PET plastisphere coverage was more pronounced in comparison to the

222 SW incubated PA. This pattern of results was consistent in all the other types of MPs (**Fig. 1**) except for

223 PE, PP, SAN, PMMA and POM MPs incubated in both the environmental media **(Fig. 1(C, D, K & L))**.

224 The latter showed a rather plain surface with microorganismal structures seen only in close proximity to

225 cracks of the MPs surface and were predominantly cells. The glass pellets surface interestingly showed no

226 microbial biomass coverage after the incubation in both environmental media (**Fig. 1 (A, B)**). The

227 molecular fingerprints of the plastispheres, which was seen to be composed of a diverse array of

228 microorganismal structures, was then investigated using micro-Raman spectroscopy.
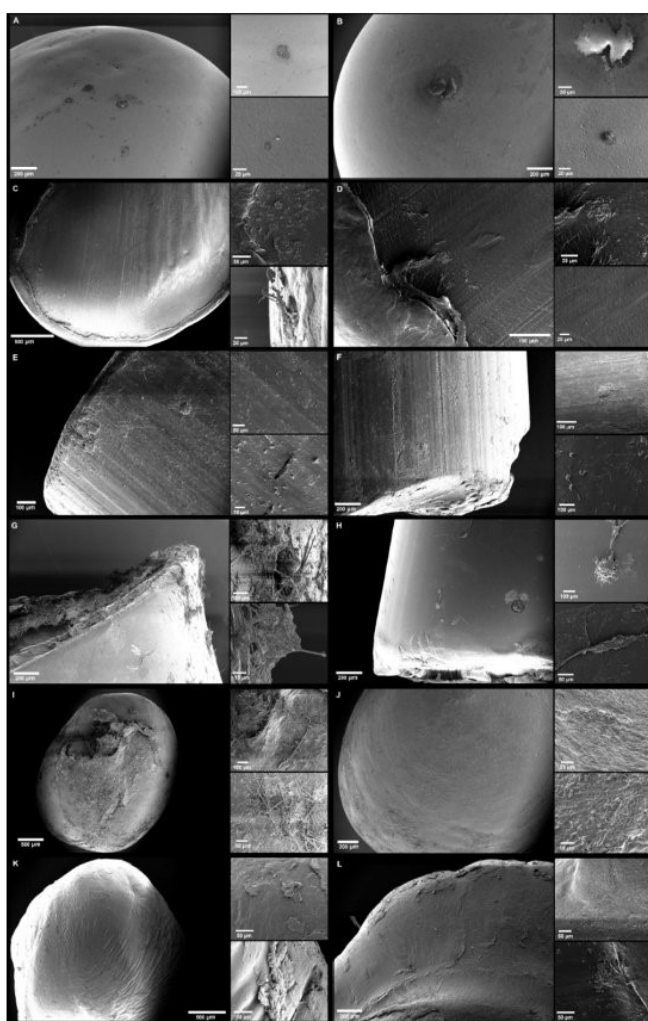
229

230 **Figure 1:** *Representative SEM images of the plastisphere on the surfaces of MPs incubated in FW and SW;*

231 A= glass pellets incubated in FW, B= glass pellets incubated in SW, C= PE incubated in FW, D= PE incubated in

232 SW, E= PS incubated in FW, F= PS incubated in SW, G= PET incubated in FW, H= PET incubated in SW, I= PA

233 incubated in FW, J= PA in SW, K= PP incubated in FW, L= PP incubated in SW. Each image shows the overview

234 of the MPs surfaces with two representative magnified images. Images were obtained at 3-4 kV using an Everhart-

235 Thornley detector.
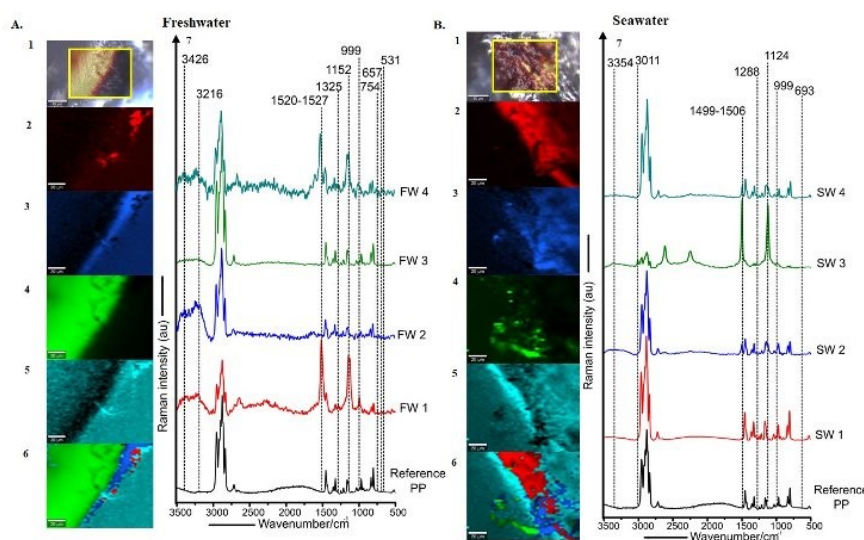
Molecular profiling of the plastisphere

237 Micro-Raman spectroscopic investigations revealed the spatio-chemical composition of the plastisphere on

238 the FW and SW incubated MPs, which indicated that the key molecular signatures in both environments

239 are predominantly a combination of polysaccharides, proteins, nucleic acids (extracellular DNA and RNA),

240 lipids and secondary metabolites like carotenoids. These molecules are indicative of a multispecies microbial

241 community constituting the plastisphere which may be composed of algae, fungi, diatoms, diverse types of

242 bacteria together with the associated EPS matrix corresponding to the respective incubation medium. These

243 molecular signatures are well associated with Raman spectroscopic characterization of biofilms (Feng et al.,

244 2015; Ivleva et al., 2017, 2008). In our study, the micro-Raman imaging investigations revealed a

245 heterogeneous and spatial distribution of these molecules (**Fig.2-7, Fig. S4-S9**). Raman images acquired

246 from the target regions on the surfaces of the pellets (region highlighted in yellow within the bright field

247 image) indicated the presence of unique spectral components corresponding to the plastisphere. Wherein,

248 each spectral component represents the presence of a unique representative plastisphere molecular

249 signature. Such as presence of nucleic acids in one spectral component vs presence of carotenoids in

250 another spectral component and likewise. This is represented in relation to one another and their pristine

251 or reference spectral counterpart (**Fig.2-7, Fig. S4-S9**).
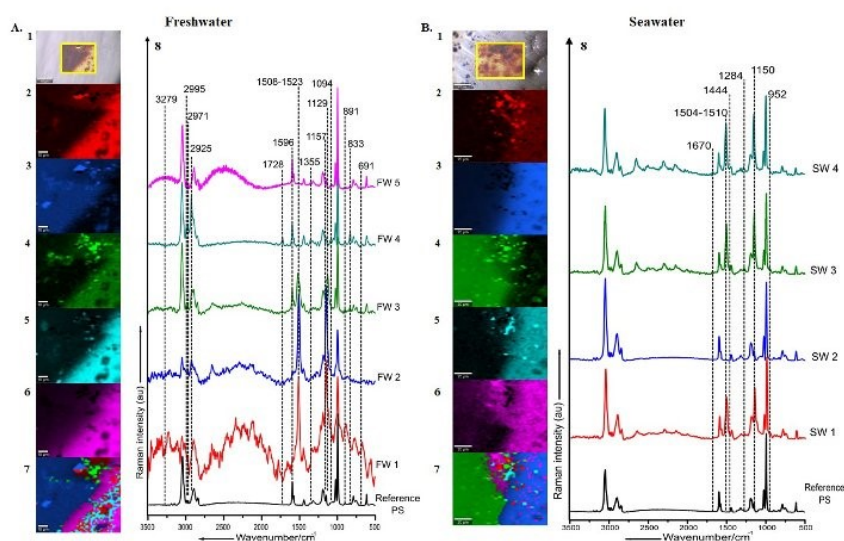
252

253 **Figure 2***: Molecular profiles of the plastisphere on the surface of PS MPs incubated in FW and SW as revealed*
254 *by micro-Raman imaging* (**A.**) FW incubation **{1}** Bright field microscopic image of the surface of the PS incubated
255 for 30 days with the inset representing the region of interest selected for imaging **{2-6}**. False coloured Raman images
256 of the collapsed stack indicating the differential intensity distribution of the respective demixed spectral components
257 **{7}** Combined image inclusive of all demixed spectral components **{6}** Mean spectrum of the respective demixed
258 spectral components compared with the pristine or reference PS spectrum (Ref, FW1-FW5) (**B.**) SW incubation **{1}**.
259 Bright field microscopic image of the surface of PS incubated in for 30 days with the inset representing the region of
260 interest selected for Raman imaging **{2,3,4,5}**. False coloured Raman images of the collapsed stack indicating the
261 spatial and differential intensity distribution of the respective demixed spectral components **{6}** Mean spectrum of the
262 respective demixed spectral components compared with the pristine glass pellet spectrum (Ref, SW 1-SW 4) The
263 spectral components represent the respective mean spectrum calculated from n=25,000 spectra constituting the
264 Raman images analysed via TCA coupled with spectral demixing. The Raman image has been visualized here is from
265 the surface of a single PS MPs sample (FW n=1 and SW n=1)

266 These spectral components show characteristic Raman bands corresponding to the plastisphere, which may

267 be observed in the wavenumber range of 500-3500 cm^{-1} respectively (**Fig. 2-7, Fig. S4-S9, Table S1. S2**).

268 Herein, the Raman bands at ~560, 891, 1094, 1280-1288, 1355 and 1380 cm^{-1} correspond to polysaccharides

269 (**Fig. 2-Fig. 7, Fig. S4-S9, Table S2. S3**). Raman bands at ~520, 531, 643, 665, 670, 677, 691, 696, 741,

270 746, 747, 833, 871, 876, 1004, 1203, 1540, 1564, 1586, 1661, 1668, 1670, 2924 and 2925 cm^{-1} correspond

271 to proteins. Nucleic acid (DNA/RNA) signatures appear at 693, 713, 754, 908, 952, 961, 962, 980, 1094

272 and 1570 cm^{-1} respectively. Lipid signatures were seen at ~592, 1302, 1320, 1325, 1334, 1339, 1420, 1426,

273 1437, 1444, 1452, 1724, 1728, 1775, 1787, 1793, 2835, 2853, 2866, 2958, 2966, 2971, 2995 and 3097 cm^{-1}

274 respectively. In addition to these signatures there were Raman bands at positions 1123, 1129 and 1580-96

275 cm^{-1} which indicated the presence of cytochrome molecules. Furthermore, carotenoid signatures were

276 predominantly seen in the wavenumber range 1150-1160 cm^{-1} and 1499-1528 cm^{-1} respectively. Finally,

277 signatures indicative of the presence of water molecules were seen between 3200-3500 cm^{-1} respectively.

278 The vibrational modes and functional groups corresponding to these Raman band assignments have been

279 listed in **Table S2, S3** (Brazhe et al., 2015; Ivleva et al., 2008; Talari et al., 2015). Overall, it may be stated

280 that a combination of all these molecular signatures determine the unique spectral components constituting

281 the molecular profiles of the plastisphere (**Fig.2-7, Fig. S4-S9**).

282

283 **Figure 3:** *Molecular profiles of the plastisphere on the surface of PP MPs incubated in FW and SW as*
284 *revealed by micro-Raman imaging* (**A.**) FW incubation **{1}** Bright field microscopic image of the surface of the PP
285 incubated for 30 days with the inset representing the region of interest selected for imaging **{2-5}** False coloured
286 Raman images of the collapsed stack indicating the spatial and differential intensity distribution of the respective
287 demixed spectral components **{6}** Combined image inclusive of all demixed spectral components **{7}** Mean spectrum
288 of the respective demixed spectral components compared with the pristine or reference PP spectrum (Ref, FW 1-FW
289 4) (**B.**) SW incubation **{1}** Bright field microscopic image of the surface of PP incubated in for 30 days with the inset
290 representing the region of interest selected for Raman imaging **{2-5}** False coloured Raman images of the collapsed
291 stack indicating the spatial and differential intensity distribution of the respective demixed spectral components **{6}**
292 Combined image inclusive of all demixed spectral components **{7}** Mean spectrum of the respective demixed spectral
293 components compared with the pristine PP spectrum (Ref, SW 1-SW 4) The spectral components represent the
294 respective mean spectrum calculated from n=25,000 spectra constituting the Raman images analysed via TCA coupled
295 with spectral demixing. The Raman image visualized here is from the surface of a single PP MPs sample (FW n=1
296 and SW n=1)

297   A deeper evaluation of the spectral components of the plastisphere indicates the presence of distinct

298   differences amongst the different types of MPs in relation to the incubation medium and also in relation to

299   the control glass pellet surface. For example, the molecular profiles acquired from the plastisphere on some

300   of the MPs such as PS, PET, PA, PE and PP, which are representative of some of the most commonly

301   used consumer plastics indicated the presence of several unique spectral components in both incubation

302   environments (**Fig. 2-6, Fig. S4-S9,** (Rhodes, 2018)) with the exception of PE and SAN, incubated in SW

303   (**Fig. 4B and Fig. S4B**). The Raman images corresponding to these spectral components represent the

304   spatial and relative intensity distribution of the Raman bands, constituting a specific spectral component,

305   which are uniquely colour coded and combined to provide a false colour visualization of the corresponding

306   plastisphere on the surface. The combination of Raman bands in the spectral components mainly indicated

307   the heterogeneous presence of nucleic acids, proteins, polysaccharides and lipid signatures along with

308   predominant carotenoid signatures, which were not observed on the molecular profiles acquired from the

309   glass pellet surface. This pattern of results was consistent with all other types of MPs with the only exception

310   of PE and SAN pellets incubated in SW, wherein the molecular profiles did not indicate any presence of

311   neither microbial growth nor the conditioning film, which was seen in the glass pellet surface (**Fig. 4B and**

312   **Fig. S4B, Fig. 7**).
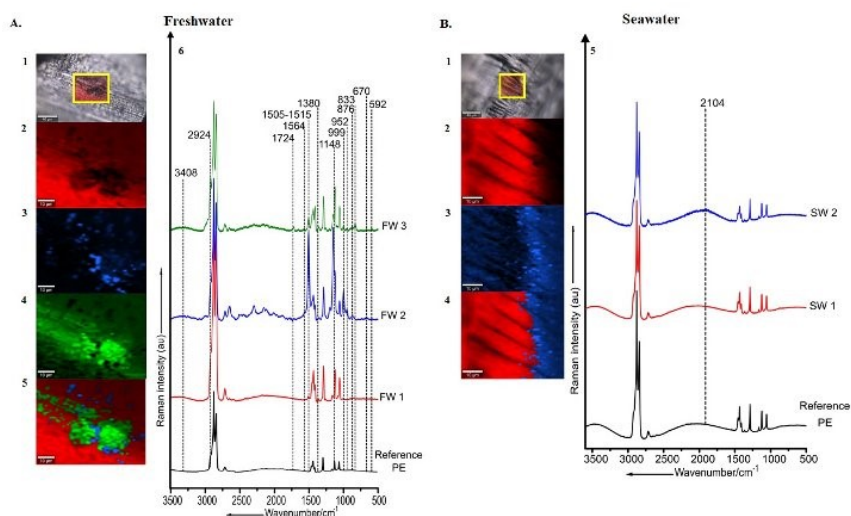
313

314   **Figure 4:** *Molecular profiles of the plastisphere on the surface of PE MPs incubated in FW and SW as*
315   *revealed by micro-Raman imaging* (**A.**) FW incubation {**1**} Bright field microscopic image of the surface of the PE
316   incubated for 30 days with the inset representing the region of interest selected for imaging {**2-4**} False coloured
317   Raman images of the collapsed stack indicating the spatial and differential intensity distribution of the respective
318   demixed spectral components {**5**} Combined image inclusive of all demixed spectral components {**6**} Mean spectrum
319   of the respective demixed spectral components compared with the pristine or reference PE spectrum (Ref, FW 1-FW
320   3) (**B.**) SW incubation {**1**} Bright field microscopic image of the surface of the PE incubated in for 30 days with the
321   inset representing the region of interest selected for Raman imaging {**2-3**} False coloured Raman images of the
322   collapsed stack indicating the spatial and differential intensity distribution of the respective demixed spectral
323   components {**4**} Combined image inclusive of all demixed spectral components {**5**} Mean spectrum of the respective
324   demixed spectral components compared with the pristine PE spectrum (Ref, SW 1-SW 2) The spectral components
325   represent the respective mean spectrum calculated from n=25,000 spectra constituting the Raman images analysed via
326   TCA coupled with spectral demixing. The Raman image visualized here is from the surface of a single PE MPs sample
327   (FW n=1 and SW n=1)

328   A comparison of the plastisphere molecular profiles of specific MPs type in correlation with the incubation

329   media alone also reveals distinct differences. For example, the molecular profiles of the plastisphere of PS

330   incubated in FW is composed of proteins, polysaccharides, lipids, cytochrome and carotenoid signatures.

331   In contrast, the plastisphere profile of the SW incubated PS counterpart is composed of nucleic acids, lipids,

332   polysaccharides and carotenoids respectively. These results may indicate that the plastisphere in the FW

333   incubated PS is more diverse in comparison to their SW counterpart and may contain a relatively higher

334   concentration of proteins (**Fig.2A-2B**). Similarly, PP plastisphere profiles revealed the presence of proteins,

335   nucleic acids, polysaccharides and carotenoids signatures in comparison to its SW counterpart, wherein the

336   nucleic acid signatures were not detected (**Fig.3A-3B**). Surprisingly, the plastisphere profile of PE incubated

337   in FW indicates the presence of signatures corresponding to nucleic acids, proteins, lipids and carotenoids

338   in comparison to its SW counterpart wherein the molecular profile was devoid of any microbial growth or

339   EPS indicator signatures (**Fig. 4A -Fig. 4B**). The molecular profiles of the plastisphere on the surfaces of

340   PVC, SAN, POM, ABS and PU MPs incubated in FW also followed this pattern of results wherein their

341   plastisphere was more diverse and more enriched in comparison to their SW counterparts (**Fig. S4-S9**).
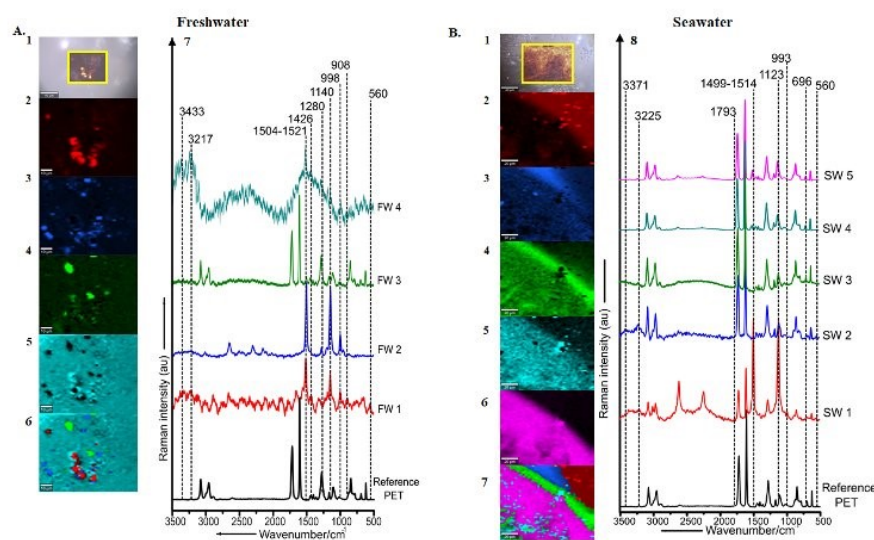
342

343 **Figure 5:** *Molecular profiles of the plastisphere on the surface of PET MPs incubated in FW and SW as*
344 *revealed by micro-Raman imaging* (**A.**) FW incubation {**1**} Bright field microscopic image of the surface of the
345 PET incubated for 30 days with the inset representing the region of interest selected for imaging {**2-5**} False coloured
346 Raman images of the collapsed stack indicating the spatial and differential intensity distribution of the respective
347 demixed spectral components {**6**} Combined image inclusive of all demixed spectral components {**7**} Mean spectrum
348 of the respective demixed spectral components compared with the pristine or reference PET spectrum (Ref, FW 1-
349 FW 4) (**B.**) SW incubation {**1**} Bright field microscopic image of the surface of the PET incubated for 30 days with
350 the inset representing the region of interest selected for Raman imaging {**2-6**} False coloured Raman images of the
351 collapsed stack indicating the spatial and differential intensity distribution of the respective demixed spectral
352 components {**7**} Combined image inclusive of all demixed spectral components {**8**} Mean spectrum of the respective
353 demixed spectral components compared with the pristine PET spectrum (Ref, SW 1-SW 5) The spectral components
354 represent the respective mean spectrum calculated from n=25,000 spectra constituting the Raman images analysed via
355 TCA coupled with spectral demixing. The Raman image visualized here is from the surface of a single PET MPs
356 sample (FW n=1 and SW n=1)

357

358   There was also another pattern of results wherein the SW incubated MPs plastisphere were more diverse

359   and enriched in comparison to their FW counterparts. For example, PET plastisphere of SW incubation

360   was composed of polysaccharides, nucleic acids, proteins, lipids and higher carotenoid diversity in

361   comparison to its FW counterpart, which lacked protein signatures indicating that the SW PET plastisphere

362   was more diverse (**Fig. 5A-5B**). Furthermore, PA also showed similar pattern of results, wherein the SW

363   incubated plastisphere showed higher diversity in carotenoids along with the presence of proteins,

364   polysaccharides and lipids signatures in comparison to its FW counterpart, which showed no diversity with

365   respect to carotenoids and further lacked lipid signatures (**Fig. 6A-6B**). The molecular profiles of the

366   plastisphere on the surface of PC MPs interestingly also showed the presence of nucleic acids and protein

367   signatures in the SW incubation environment alone indicating a higher diversity in biomolecular content in

368   comparison to its FW counterpart (**Fig. S9A-9B**). Although, there were these distinct pattern of results,

369   there was no MPs polymer-specific plastisphere fingerprint detected.
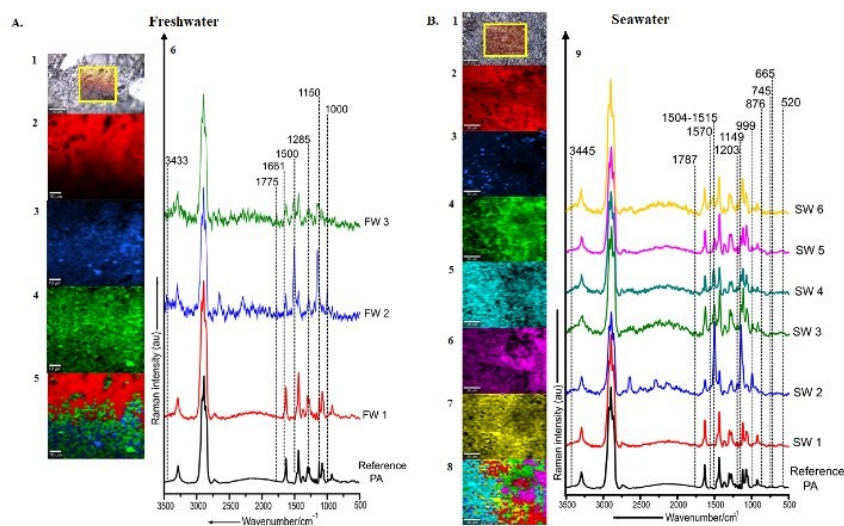
370

371 **Figure 6:** *Molecular profiles of the plastisphere on the surface of PA MPs incubated in FW and SW as*
372 *revealed by micro-Raman imaging* (**A.**) FW incubation {**1**} Bright field microscopic image of the surface of the PA
373 incubated for 30 days with the inset representing the region of interest selected for imaging {**2-4**} False coloured
374 Raman images of the collapsed stack indicating the spatial and differential intensity distribution of the respective
375 demixed spectral components {**5**} Combined image inclusive of all demixed spectral components {**6**} Mean spectrum
376 of the respective demixed spectral components compared with the pristine or reference PA spectrum (Ref, FW 1-FW
377 3) (**B.**) SW incubation {**1**} Bright field microscopic image of the surface of the PA incubated for 30 days with the inset
378 representing the region of interest selected for Raman imaging {**2-7**}. False coloured Raman images of the collapsed
379 stack indicating the differential intensity distribution of the respective demixed spectral components {**8**} Combined
380 image inclusive of all demixed spectral components {**9**} Mean spectrum of the respective demixed spectral
381 components compared with the pristine PA spectrum (Ref, SW 1-SW 6) The spectral components represent the
382 respective mean spectrum calculated from n=25,000 spectra constituting the Raman images analysed via TCA coupled
383 with spectral demixing. The Raman image visualized here is from the surface of a single PA MPs sample (FW n=1
384 and SW n=1)

385

386   Furthermore, in comparison to MPs mentioned above wherein several spectral components representing

387   unique plastisphere signatures were observed, the molecular profiles acquired from the glass pellet surface

388   incubated in both FW and SW indicate the presence of only two unique spectral components wherein the

389   Raman bands can be correlated to the presence of molecules like proteins, polysaccharides, lipids and

390   nucleic acids. In both the incubation environments, there were no prominent cell clusters observed on the

391   glass pellet surfaces, which indicated that these molecular signatures may be representative of the presence

392   of a conditioning film or an eco-corona (**Fig 7**) but no biofilm growth. This finding is in great agreement

393   with the observations of the SEM images.
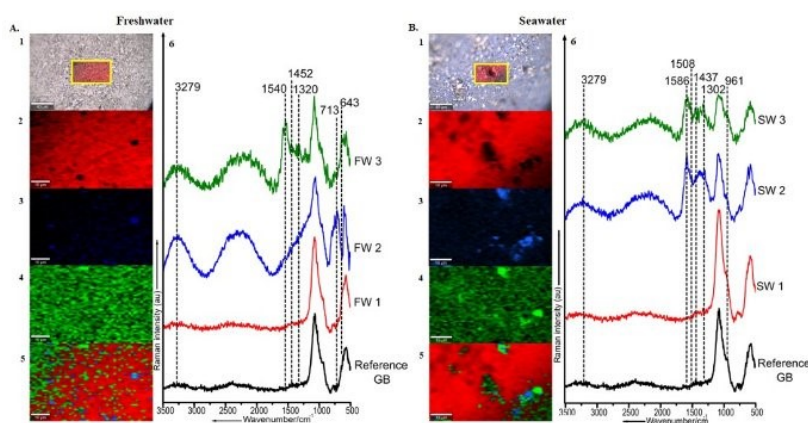
394

395   **Figure 7:** *Molecular profiles of the plastisphere on the surface of glass pellets incubated in FW and SW as*
396   *revealed by micro-Raman imaging* (**A.**) FW incubation **{1}** Bright field microscopic image of the surface of the
397   glass pellet incubated for 30 days with the inset representing the region of interest selected for imaging **{2-4}** False
398   coloured Raman images of the collapsed stack (Z=20 μm) indicating the spatial and differential intensity distribution
399   of the respective demixed spectral components **{5}** Combined image inclusive of all demixed spectral components
400   **{6}** Mean spectrum of the respective demixed spectral components compared with the pristine or reference glass
401   pellet spectrum (Ref, FW1-FW3) (**B.**) SW incubation **{1}** Bright field microscopic image of the surface of the glass
402   pellet incubated for 30 days with the inset representing the region of interest selected for Raman imaging **{2-4}**. False
403   coloured Raman images of the collapsed stack (Z=20 μm) indicating the spatial and differential intensity distribution
404   of the respective demixed spectral components **{5}** Combined image inclusive of all demixed spectral components
405   **{6}** Mean spectrum of the respective demixed spectral components compared with the pristine glass pellet spectrum
406   (Ref, SW1-SW3). The spectral components represent the respective mean spectrum calculated from n=25,000 spectra
407   constituting the Raman image analysed via TCA coupled with spectral demixing. The Raman image visualized here is
408   from the surface of a single glass pellet sample (FW n=1 and SW n=1)

409

410   *Plastisphere based generation of Raman spectral variants of MPs*

411   The above-described molecular profiles of the plastisphere investigated in this study consisted of unique

412   signatures that were corresponding to the underlying polymer surface. The visibility of these underlying

413   polymer signatures, in parallel with the plastisphere molecular signatures, was in principle dependent on the

414   thickness of the biological material, i.e. if the plastisphere is not dense then the underlying MPs surface

415   molecular signature is also visible along with the plastisphere molecular signature in the spectral

416   components. This phenomenon leads to several bands of the plastisphere spectrum to be also used as

417   spectral variants of specific MPs, which can be representatives of the spectral data of environmental MPs.

418   It is well known that the spectral data of environmental MPs, in most cases, do not establish an accurate

419   spectral match to its pristine counterpart (Munno et al., 2020).

420   Hence, we provide this Raman spectral data together with the meta data on the plastisphere with an R

421   package, labelled as *"RaMPP"*. We further include a shiny app in this package to provide a simple tool for

422   visualizing and comparing those spectra with each other, as well as with a user's spectral data. The data, as

423   well as the app, included in this package, will complement the known spectrum of pristine MPs with

424   additional information constituting plastisphere signatures and visualize as to how the spectrum of the

425   plastisphere infested MPs may change in comparison to its pristine counterpart. Below, we briefly describe

426   the functionality and usage of the app. To install the package, two lines of code have to be executed in

427   RStudio: *require(shiny)* and *runGitHub ("Shiny-MP-spectra", "Maki-science")*. The app will automatically start,

428   and the user interface is presented (**Fig. 8**).
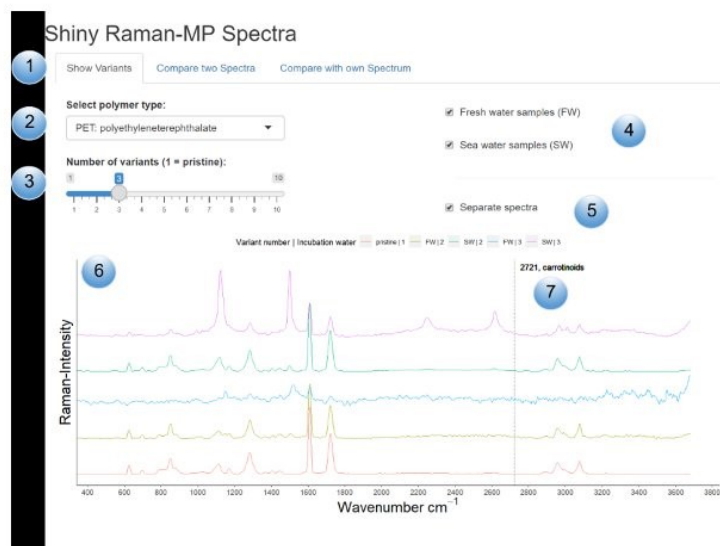
429

430   Figure 8: *User interface of the "RaMPPapp" representing plastisphere based MPs Raman spectral variants.*
431   There are three possible ways to access the spectral library, which are separated by three tabs at the top of the interface
432   (**1**). Below the three tabs the corresponding input panel is located. Here, the MPs type can be selected (**2**) and the
433   number of plastisphere MPs variants can be chosen (**3**), while 1 always represents the pristine MPs. On the right side
434   of the input panel, it can be chosen, whether to show variants of FW or SW incubated particles or both (**4**).
435   Additionally, there is the option to separate the spectrum along the y-axis for a better overview over many spectra,
436   like shown in this figure (**5**). Further below, Raman spectra will be shown in the selected configuration with the Raman
437   intensity as an arbitrary unit on the y-axis and the wavenumber on the x-axis (**6**). The legend at the top of the graph
438   informs the user about the colour code. Wavenumber range below 400 cm^{-1} are not shown, as there is no meaningful
439   information in this part of the spectrum. The colours indicate the different spectra. Additionally, meta data can be
440   accessed/provided, when moving the cursor over the graph (**7**). A vertical line will appear indicating the currently
441   selected wavenumber position. When meta data for a certain wavenumber is available, the wavenumber and additional
442   information are shown at the top of the vertical line, providing information about the substance class, that can be
443   found at this specific wavenumber. When moving the courser towards the corner of the graph, the vertical line will
444   disappear again. See the main text for further information.

445

446   There are three possible ways to access the spectral library, which are separated by three tabs at the top of

447   the interface: show the variants, compare two spectral variants and compare a spectrum with a user's own

448   spectrum. The interface should be widely self-explanatory and similar for all three ways. Herein we will just

449   explain the interface for the first and most complex way (**Fig. 8**). The first option provides the opportunity

450   to visualize the pristine spectrum and compare it to all corresponding spectral variants available in the

451   library. It is important to note that the number of variants for all MPs types are not equal. Therefore, if the

452   number selected, exceeds the number of available variants there will not be any changes in the

453   corresponding window. When two spectra should be compared in more detail, the second tab of the user

454   interface can used. This option provides almost the same functionality as before. In the third tab, the user

455   can provide their own MPs Raman spectrum, to compare with another selected spectrum in the library.

456   The data can be simply provided by copying and pasting an excel-file column (without header) into the text

457   field. We expect the user to use '.' as decimal sign. If the spectral resolution of the users' spectrum is higher

458   or lower compared to the resolution of the spectral data in the library, the spectrum will be fitted

459   accordingly. The data of the Raman spectra and the meta data information can be accessed by calling the

460   separate functions for using the data in other contexts.

461

462   **4. Discussion**

463   *Freshwater (FW) vs Artificial Seawater (SW) based plastisphere*

464   The SEM investigations reveal that the plastisphere is generally comprised of a heterogeneous distribution

465   of microbial communities on the surfaces of MPs. We detected similar morphological structures as

466   described in (Ramsperger et al., 2020), such as patches of filaments, chain of randomly distributed rod,

467   diatom, rhombic cube and spherically shaped morphological types. However, here the structures were

468   frequently embedded in a thick mesh like structure representing the EPS matrix (**Fig. 1**), which was not the

469   case in Ramsperger et al. (2020). One potential reason could be the differences in particle size (Chen et al.,

470   2020) and incubation technique, as well as the exposure time (here: 30 days, Ramsperger et al. consecutive

471   time series until 14 days of exposure).

472   However, the plastisphere heterogeneity and density or richness was consistently higher in the MPs

473   incubated in the FW incubation, projecting the presence of a relatively higher microbial biomass in

474   comparison to the SW incubated MPs. This may be due to the eutrophic nature of the FW utilized in this

475   study, which correlates to a higher abundance of microbial communities and hence providing a more

476   abundant sink of microbes for the formation of plastisphere. In comparison, SW collected from a marine

477   aquarium due to its stable and oligotrophic nature provided a relatively less abundant sink of microbes to

478   facilitate plastisphere formation in the 30-day incubation period. Interestingly, the SEM investigations also

479   clearly show that the microbial communities prefer to use the MPs surface as a growth substrate in

480   comparison to the glass pellet surface in both FW and SW incubations. This is not surprising as previously

481   mentioned; factors such as the material chemistry, surface roughness, hydrophobicity and surface free

482   energy will dictate such a preference of substrate by microbes. For example; porous, uneven, edgy and

483   rough surfaces of the MPs in comparison to the smooth glass surface may be one amongst the many factors

484   that influence preferential colonization (**Fig. S1**). Furthermore, the chemical composition of the MPs for

485   example; the presence of specific functional groups such as the carbonyl groups in PA, isocyanate groups

486   in PU, methyl groups in PP and PET, aromatic rings in PS, SAN, ABS and chlorine groups in PVC may

487   influence chemotactic selective colonization of specific microbial species, which could utilize them as a

488   carbon and energy source (Xie et al., 2021). The presence of functional groups is probably also contributing

489   to the microorganisms colonizing MPs surfaces preferentially, instead of the glass pellet surface.

490   In corroboration to the SEM investigations, molecular profiling via micro-Raman spectroscopy also

491   predominantly indicates a higher microbial diversity and biomolecular content in the plastisphere,

492   corresponding to the MPs incubated in FW in comparison to its SW counterparts. This can be deduced

493   based on the heterogeneity in the relative concentration and distribution of the most common biomolecular

494   signatures representing the plastisphere such as the proteins, extracellular nucleic acids, polysaccharides and

495   lipids in combination with the carotenoid secondary metabolite signatures (Ivleva et al., 2017; Kusić et al.,

496   2015). However, we could not detect MPs polymer-specific plastisphere fingerprints. It was seen that the

497   plastisphere signatures are predominantly constituted of the biomolecules mentioned above irrespective of

498   the polymer types of MPs but only the relative abundances of these molecules change in the respective

499   plastispheres. There were no exclusive signatures in the plastisphere that could be linked to a specific MPs

500   polymer type alone.

501   *Carotenoid signatures as an indicator of microbial diversity in the plastisphere*

502   Amongst the biomolecules constituting the plastisphere, the carotenoid signatures in specific can be utilized

503   to highlight the microbial diversity within the plastisphere. These molecules are chromophoric, lipid soluble

504   isoprenoid compounds that comprise a unique central polyene chain comprised of a conjugated double

505   bond system that is responsible for the coloration of a multitude of organisms in the ecosystem (Kumar B.

506   N. et al., 2015; Withnall et al., 2003). Carotenoids are taxonomically diverse. Currently, there are 1029

507   different types of carotenoids, which are known to be synthesized by bacteria (324 types assigned), archaea

508   (25 types assigned) and eukaryotic (680 types assigned) organisms. Amongst this classification there are 13

509   unique carotenoids synthesized by archaea, 262 by bacteria and 621 by the eukaryotes which makes them

510   an ideal marker for the characterization of microorganisms (Fernandes et al., 2018; Yabuzaki, 2017). Raman

511   spectroscopy can be used to detect and differentiate the different types of carotenoids in complicated

512   matrices such as the biofilm based on the position of two characteristic signatures, which occurs in the

513   (1100-1200 cm^{-1}) and (1400-1600 cm^{-1}) wavenumber region. The former region corresponds to the ν_1(C-C)

514   stretching mode and the latter to the ν_2(C=C) stretching mode representing the polyene chain structure of

515   the carotenoid molecule. The presence of different types of carotenoids in complex matrices can be

516   monitored based on the position of the ν_2(C=C-1400-1600 cm^{-1}) stretching mode signature as this band

517   position is directly related and sensitive to the length of the polyene chain in the carotenoids (Kumar B. N.

518   et al., 2015). As the length of the polyene chain in a carotenoid molecule increases the position of this band

519   moves to lower wavenumbers and *vice versa* due to electron-phonon coupling (Jehlička and Oren, 2013;

520   Withnall et al., 2003). The major carotenoid or the carotenoid having the highest concentration in a

521   particular focal volume will be detected via the resonance Raman effect. Several studies have utilized this

522   effect for the characterization of microorganisms based on carotenoid signatures such as in soil bacteria,

523   halophilic bacteria, cyanobacteria etc., (Jehlička and Oren, 2013; Kumar B. N. et al., 2015).

524   This phenomenon can be used to detect the presence of different carotenoids within the plastisphere, which

525   then directly relates to the presence of different microbial communities. The variation in the position of

526   the ν_2(C=C) Raman band within the spectral components representing the plastisphere highlights the

527   presence of microbial diversity within single type of MPs and between MPs (**Figure. 9)**. Among the MPs

528   incubated in FW; the plastisphere of PS, PET, PU, POM and PC had a higher variation in carotenoid

529   signatures in comparison to the other MPs. In contrast, the MPs incubated in SW; the plastisphere of PA

530   and PU had a higher variation in carotenoid signatures in comparison to the other MPs. Interestingly, the

531   plastisphere of PVC, SAN and PE MPs incubated in SW incubations did not show the presence of

532   carotenoids. Overall, based on the variation of molecular signatures of carotenoids it can be clearly

533   established that the microbial diversity of the plastisphere in FW incubated MPs could be higher than that

534   compared to the SW incubated MPs.
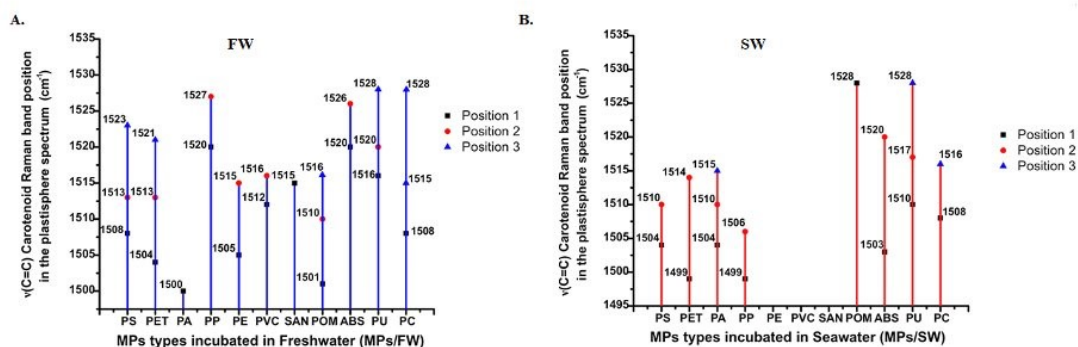
535

536   **Figure 9**: *Positional variation of the Raman band corresponding to the* ν**(C=C) stretching vibrational mode**
537   **of carotenoids in the plastisphere**; (**A.**) Carotenoid signatures corresponding to the plastisphere of the FW
538   incubations (**B.**) Carotenoid signatures corresponding to the plastisphere of the SW incubations. Position 1-3 indicate
539   the position of the ν_2 (C=C) Raman band deduced from the respective spectral components representing the
540   corresponding MPs plastisphere.

541

542   Carotenoiddb.jp database currently has a well-established list of microorganisms that synthesize carotenoids

543   under the three domains of life (http://carotenoiddb.jp., (Fernandes et al., 2018; Yabuzaki, 2017)). Previous

544   Raman studies have correlated the positions of ν_2 (C=C) Raman band observed in our study (**Figure. 9**) to

545   carotenoids like lycopene, sarcinaxanthin, bacterioruberin, astaxanthin, lutein, spirilloxanthin, torularhodin,

546   neurosporaxanthin, zeaxanthin, deinoxanthin and canthaxanthin respectively wherein the polyene chain in

547   these carotenoids are constituted of 9 to 13 conjugated double bonds (Jehlička and Oren, 2013; Kumar B.

548   N. et al., 2015; Pankin et al., 2021; Tao et al., 2011; Withnall et al., 2003). Some of the microbial sources

549   linked to the production of these carotenoids are for example; *Saccharomyces cerevisiae* (astaxanthin), *Chlorella*

550   *zofingiensis* (β-carotene), *Rhodotorula glutinis* (torularhodin), *Aspergillus carbonarius (*canthaxanthin), *Scenedesmus*

551   *bijugus* (lutein), *Dunaliella salina* (lycopene), *Micrococcus luteus* (sarcinaxanthin), *Kocuria rosea* (bacterioruberin),

552   *Oscillatoria limnetica* (zeaxanthin), *Rhodospirillum rubrum (spirilloxanthin), Deinococcus radiodurans* (deinoxanthin)

553 and *Fusarium fujikuroi* (neurosporaxanthin) etc. (Jehlička and Oren, 2013; Kot et al., 2018; Kumar B. N. et

554 al., 2015; Parra-Rivero et al., 2020). From this comparison, it may be deduced that the FW and SW

555 plastisphere of the MPs investigated in our study may be composed of a heterogeneous distribution of such

556 microbial communities. The drawback of resonance Raman technique is that the carotenoids having a

557 similar structure such as the same number of conjugated double bonds in the polyene chain cannot be

558 differentiated (Jehlička and Oren, 2013). Hence, due to this inherent limited molecular resolution it is not

559 possible to identify if different carotenoids are contributing to the plastisphere in MPs in FW in comparison

560 to the SW incubations. Gold standards such as UV-visible absorption and high performance liquid

561 chromatography (HPLC) technique needs to be used with the combination of molecular sequencing

562 approaches to establish such differences and the precise profiling of plastisphere associated carotenoid

563 producing microorganisms (Jehlička and Oren, 2013; Weig et al., 2021; Zhang et al., 2022).

564

565 *Influence of density, size and shape of the MPs towards plastisphere growth*

566 Our investigations indicate that the proportion of plastisphere growth on MPs seemed to be influenced by

567 factors such as the polymer type, density, size and surface topography of the MPs. For example, all MPs

568 used in this study except for PE, PP and ABS had densities higher than the FW and SW and sink to the

569 bottom in the microcosm. Hence the immobile bottom dwelling MPs, which are not affected by the

570 hydrodynamic shear forces resulting from the aeration provided in the microcosm are likely to support the

571 formation of a thicker plastisphere or a higher microbial abundance, for example as seen in the FW

572 incubated PET and PA MPs in comparison to the positively bouyant MPs like PE and PP (**Fig. 1**).

573 However, the factor of surface topography of the MPs may outrank the density factor. For example, glass

574 pellets have a density of ~1.6 g/cm^{-3} but also have a smooth surface topography, which may be a key factor

575 in addition to their surface chemistry difference compared to that of MPs, that may not allow the formation

576 of abundant microbial growth on their surfaces in the 30-day incubation timeline corroborated by the SEM

577 and Raman spectroscopic analysis (**Fig. 1, Fig. 2**). Similarly, all the FW incubated MPs, which were

578 spherical in shape (POM, ABS, PE and PP) except for PA harboured plastisphere that were relatively less

579 thick than the box or square shaped MPs, which may be due to a lower surface area, surface topography

580 and influence of hydrodynamic shear forces as the main influencing factors. (**Fig. 1, Fig. S1**). Furthermore,

581 the largest MPs used in our study were PS, PET, PVC and PU respectively (**Fig. S1**). Interestingly, Raman

582 spectral components representative of a pure plastisphere i.e. spectrum devoid of any underlying MP

583 signature was found only in these 4 MPs polymer types incubated in FW indicating that the plastisphere on

584 these MPs surface was thicker in relation to the other MPs (**Fig. 3A**, **Fig. 5A**, **Fig. S5A** and **Fig. S5A**).

585 Raman z-stack based 3D reconstructed visualization of the spatial distribution of the plastisphere specific

586 components in these MPs vs the MP specific spectral component (**Fig. 10**) indicates that the FW incubated

587 PET MPs and PU MPs harboured the thickest plastisphere in comparison to PVC and PS MPs. This could

588 possibly be due to the larger surface area to volume ratio as mentioned previously of both PET and PU

589 MPs in addition to the presence of significant crevices or pits on their surfaces (**Fig. S1),** which probably

590   is also facilitating a favourable adherence or attachment of the microorganisms onto these surfaces. These
591   results demonstrate that the plastisphere formation and thickness is highly likely to be influenced by particle
592   characteristics such as the polymer type, density, shape and surface structure of the MPs. These factors are
593   only a few amongst many other factors as previously mentioned, such as the local environment conditions
594   and physicochemical properties like temperature, salinity, pH, dissolved organic carbon, surface chemistry,
595   surface charge, elastic modulus, steric forces, etc. and finally the inherent physiologies of the colonizing
596   microorganisms itself that shape the formation and development of the plastisphere (Liao et al., 2015; Paerl,
597   1975; Rummel et al., 2021).

598
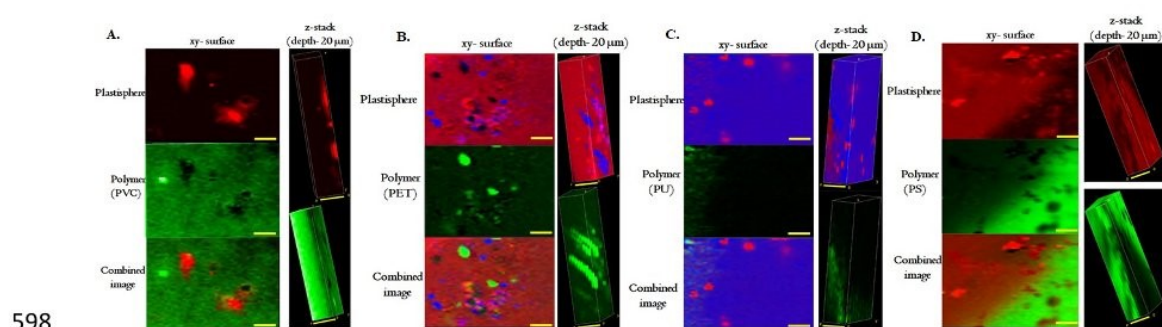
599   Figure 10: *Spatial distribution of the plastisphere in relation to the surface of the respective MPs visualized*
600   *via micro-Raman z-stack imaging;* (*xy-surface*) Collapsed stack indicating the distribution of the plastisphere on
601   the surface of the respective MPs with the spectral component specific to plastisphere colour coded in red and blue
602   depending on the number of unique plastisphere spectral components identified, spectral component corresponding
603   to the MPs is coded in green and the visualization of the components together via the combined image (scale bar
604   translates to **10 μm**), (**z-stack**) spatial distribution of the plastisphere versus the MPs surface in the z-direction (scale
605   bar translates to **20 μm**), changes in the colour intensity is dependent on the relative intensity changes in the Raman
606   bands corresponding to the respective spectral components. (**A**) Plastisphere spatial distribution in relation to the
607   PVC MPs surface, (**B**) Plastisphere spatial distribution in relation to the PET MPs surface, (**C**) Plastisphere spatial
608   distribution in relation to the PU MPs surface, (**D**) Plastisphere spatial distribution in relation to the PS MPs surface.

609

610   *Significance of the plastisphere based Raman spectral variants of MPs*

611   As mentioned previously, Raman spectral data of environmental MPs can be drastically altered in
612   comparison to its pristine reference counterpart (Munno et al., 2020). Environmental MPs predominantly
613   have organic and inorganic contaminants that also includes microbial biomass adsorbed to their surfaces,
614   which are one of the factors responsible for the changes in the MPs Raman spectrum. Our results from the
615   plastisphere based Raman spectral variants specifically highlights the changes due to the accumulation of
616   microbial biomass. As most studies use customized and commercially available spectral libraries for the
617   identification and characterization of environmental MPs, wherein the efficiency of spectral data matches
618   are directly dependent on the comprehensiveness of the libraries utilized. Hence, if the Raman MPs
619   databases in such libraries lack spectral data, which are not relevant to the environmental MPs, it can result
620   in a gross underestimation of MPs levels in samples due to misclassification or the inability to find an
621   appropriate spectral match with reference data (Munno et al., 2020). Furthermore, there are also possibilities
622   that the Raman bands from the plastisphere are incorrectly assumed to be originating from additives or

623   pigments inherent with the synthetic polymer constituting MPs instead of it being associated with the

624   microbial biofilms. Thereby, it is critical to establish spectral libraries of MPs taking microbial influences

625   into consideration, which can help to improve the efficiency of Raman spectroscopic characterization of

626   environmental MPs. We have taken a first step in this direction by providing the biofilm infested MPs

627   Raman spectral library RaMPP, constituting data acquired from 11 different (PMMA MPs were not

628   subjected to Raman spectroscopic investigations due to the strong fluorescence signal from the dye inherent

629   in these particles) synthetic polymer types by means of an "R" package and an app for the interactive

630   visualization and comparison of our data. Utilization of this library may aid in the direct and pre-treatment

631   free detection of large MPs in the size range of the particles like the ones used in our study, which has the

632   potential to be a critical improvement in the Raman spectroscopic analysis of environmental MPs.

633   Furthermore, it can also be highly advantageous when the goal is to achieve a rapid *in situ* characterization

634   of environmental MPs via Raman spectroscopy utilizing a portable Raman spectrometer, an emerging

635   application in the context of qualitative *in situ* and on-site analysis of MPs and macroplastics (Becucci et al.,

636   2022).

637

638   5. Conclusion

639   To the best of our knowledge, our investigations performed with a combination of non-invasive label free

640   Raman spectroscopy analysis and SEM reveals, for the first time, the molecular and morphological

641   composition of the plastisphere on several types of MPs incubated in a simulated aquatic environment

642   microcosm for a period of 30 days. SEM investigations clearly visualize the heterogeneity in

643   microorganismal structures representing different microbial communities constituting the plastisphere.

644   The Raman spectroscopic spatio-chemical analysis enabled the detection of the signatures of key molecular

645   components constituting the plastisphere along with their spatial distribution. Overall, the SEM and

646   Raman investigations allowed us to deduce that MPs surface are preferentially colonized by

647   microorganisms in comparison to the glass surface, and there is a relatively higher microbial biomass and

648   diversity in the FW incubated MPs plastisphere in comparison to the SW incubated MPs. There were no

649   MPs specific plastisphere fingerprints detected, but the presence of signatures like carotenoids in the

650   molecular profiles could be specifically utilized to highlight the microbial diversity in the plastisphere on

651   specific MPs types. We could also deduce from our results that the shape, surface area and surface

652   topography of the MPs seem to play an important role in the development of the plastisphere.

653   Furthermore, the plastisphere based Raman MPs spectral variant data may be utilized for the improved

654   detection of environmental MPs and also on-site characterization of environmental MPs and

655   macroplastics. Future work is required where in the MPs sample size and also the type of MPs should be

656   increased to include weathered particles produced as a result of UV irradiation, physical stress etc. And

657   more heterogeneity with regards to the physicochemical conditions in the simulated environments could

658   be included. In order to establish a wider array of plastisphere profiles and the simultaneous generation of

659   higher number of Raman MPs spectral variants. Such an extension of the Raman spectral library of MPs

660   can help to achieve improved detection and characterization of environment MPs. Furthermore, it can be

661   anticipated that the acquisition of the plastisphere profiles from an increased sample size specific to a MPs

662   type may increase the chances of the identification of polymer specific plastisphere fingerprints.

663

675

676   **Author contributions:**

677   VKBN, ML and CL initiated the research

678   All authors planned the research

679   VKNB performed the incubation experiments

680   AFRMR, JB and VKBN prepared and imaged the SEM samples and performed image analysis

681   VKNB performed Raman sample preparation, data acquisition, analysis and interpretation of the

682   data

683   MK developed the RaMPP R package

684   VKNB, AFRMR, JB and MK wrote the draft of the manuscript

685   All authors reviewed and edited the manuscript

686

687   **Competing interests:** Authors declare that they have no competing interests

688

689   **Data availability:** All data and materials used in the analysis are available from the corresponding

690   authors upon request.

691

692   **Code availability:** All code used in the analysis and development of the RaMPP are available from

693   the corresponding authors upon request.

694   **Literature**

695   Andrady, A.L., 2011. Microplastics in the marine environment. Mar. Pollut. Bull. 62, 1596–1605.
696   https://doi.org/10.1016/j.marpolbul.2011.05.030

697   Arp, H.P.H., Ku, D., Rummel, C., Macleod, M., Pottho, A., Reichelt, S., Rojo-nieto, E., Schmitt-jansen,
698   M., Sonnenberg, J., Toorman, E., 2021. Weathering Plastics as a Planetary Boundary Threat:
699   Exposure, Fate, and Hazards. https://doi.org/10.1021/acs.est.1c01512

700   Artham, T., Sudhakar, M., Venkatesan, R., Madhavan Nair, C., Murty, K.V.G.K., Doble, M., 2009.
701   Biofouling and stability of synthetic polymers in sea water. Int. Biodeterior. Biodegrad. 63, 884–890.
702   https://doi.org/10.1016/j.ibiod.2009.03.003

703   Banerjee, A., Shelver, W.L., 2021. Micro- and nanoplastic induced cellular toxicity in mammals: A review.
704   Sci. Total Environ. 755, 142518. https://doi.org/https://doi.org/10.1016/j.scitotenv.2020.142518

705   Barros, C.H.N. Fulaz, S., Vitale, S., Casey, E., Quinn, L., 2020. Interactions between functionalised silica
706   nanoparticles and P. fluorescens EPS: a focus on the proteins. Colloids Surfaces B Biointerfaces 1–
707   15. https://doi.org/10.1371/journal.pone.0236441

708   Barros, J., Seena, S., 2021. Plastisphere in freshwaters: An emerging concern. Environ. Pollut. 290,
709   118123. https://doi.org/https://doi.org/10.1016/j.envpol.2021.118123

710   Bartkova, S., Kahru, A., Heinlaan, M., Scheler, O., Miller, D., 2021. Techniques Used for Analyzing
711   Microplastics , Antimicrobial Resistance and Microbial Community Composition : A Mini-Review
712   12, 1–9. https://doi.org/10.3389/fmicb.2021.603967

713   Basili, M., Quero, G.M., Giovannelli, D., Manini, E., Vignaroli, C., Avio, C.G., Marco, R. De, Luna, G.M.,
714   Luna, G.M., 2020. Major Role of Surrounding Environment in Shaping Biofilm Community
715   Composition on Marine Plastic Debris 7, 1–12. https://doi.org/10.3389/fmars.2020.00262

716   Becucci, M., Mancini, M., Campo, R., Paris, E., 2022. Microplastics in the Florence wastewater treatment
717   plant studied by a continuous sampling method and Raman spectroscopy: A preliminary
718   investigation. Sci. Total Environ. 808, 152025.
719   https://doi.org/https://doi.org/10.1016/j.scitotenv.2021.152025

720   Beier, B.D., Quivey, R.G., Berger, A.J., 2012. Raman microspectroscopy for species identification and
721   mapping within bacterial biofilms. AMB Express 2, 35. https://doi.org/10.1186/2191-0855-2-35

722   Bhagwat, G., Connor, W.O., Grainge, I., Palanisami, T., 2021. Understanding the Fundamental Basis for
723   Biofilm Formation on Plastic Surfaces : Role of Conditioning Films 12, 1–10.
724   https://doi.org/10.3389/fmicb.2021.687118

725   Brazhe, N.A., Evlyukhin, A.B., Goodilin, E.A., Semenova, A.A., Novikov, S.M., Bozhevolnyi, S.I.,
726   Chichkov, B.N., Sarycheva, A.S., Baizhumanov, A.A., Nikelshparg, E.I., Deev, L.I., Maksimov,
727   E.G., Maksimov, G. V, Sosnovtseva, O., 2015. Probing cytochrome c in living mitochondria with
728   surface-enhanced Raman spectroscopy. Sci. Rep. 5, 13793. https://doi.org/10.1038/srep13793

729   Chen, B., Wu, Z., Tian, M., Feng, T., Yuanwei, C., Luo, X., 2020. Effect of surface morphology change of
730   polystyrene microspheres through etching on protein corona and phagocytic uptake. J. Biomater.
731   Sci. Polym. Ed. 31. https://doi.org/10.1080/09205063.2020.1813062

732   Cialla-May, D., Krafft, C., Rösch, P., Deckert-Gaudig, T., Frosch, T., Jahn, I.J., Pahlow, S., Stiebing, C.,
733   Meyer-Zedler, T., Bocklitz, T., Schie, I., Deckert, V., Popp, J., 2022. Raman Spectroscopy and
734   Imaging in Bioanalytics. Anal. Chem. 94, 86–119. https://doi.org/10.1021/acs.analchem.1c03235

735   Coons, A.K., Busch, K., Lenz, M., Hentschel, U., Borchert, E., 2021. Biogeography rather than substrate
736   type determines bacterial colonization dynamics of marine plastics. PeerJ 9, e12135.
737   https://doi.org/10.7717/peerj.12135

738   Di Pippo, F., Venezia, C., Sighicelli, M., Pietrelli, L., Di Vito, S., Nuglio, S., Rossetti, S., 2020.

739   Microplastic-associated biofilms in lentic Italian ecosystems. Water Res. 187, 116429.
740   https://doi.org/https://doi.org/10.1016/j.watres.2020.116429

741   Feng, J., de la Fuente-Núñez, C., Trimble, M.J., Xu, J., Hancock, R.E.W., Lu, X., 2015. An in situ Raman
742   spectroscopy-based microfluidic "lab-on-a-chip" platform for non-destructive and continuous
743   characterization of Pseudomonas aeruginosa biofilms. Chem. Commun. 51, 8966–8969.
744   https://doi.org/10.1039/C5CC02744F

745   Fernandes, A.S., Nascimento, T.C. do, Jacob-Lopes, E., Rosso, V.V. De, Zepka, L.Q., 2018. Introductory
746   Chapter: Carotenoids - A Brief Overview on Its Structure, Biosynthesis, Synthesis, and
747   Applications, in: Zepka, L.Q., Jacob-Lopes, E., Rosso, V.V. De (Eds.), . IntechOpen, Rijeka, p. Ch.
748   1. https://doi.org/10.5772/intechopen.79542

749   Flemming, H., Wingender, J., 2010. The biofilm matrix. Nat. Rev. Microbiol. 8, 623–33.
750   https://doi.org/10.1038/nrmicro2415

751   Gkoutselis, G., Rohrbach, S., Harjes, J., Obst, M., Brachmann, A., Horn, M.A., Rambold, G., 2021.
752   Microplastics accumulate fungal pathogens in terrestrial ecosystems. Sci. Rep. 11, 1–13.
753   https://doi.org/10.1038/s41598-021-92405-7

754   Gomes, T., Bour, A., Coutris, C., Almeida, A.C., Bråte, I.L., Wolf, R., Bank, M.S., Lusher, A.L., 2022.
755   Ecotoxicological Impacts of Micro- and Nanoplastics in Terrestrial and Aquatic Environments BT
756   - Microplastic in the Environment: Pattern and Process, in: Bank, M.S. (Ed.), . Springer
757   International Publishing, Cham, pp. 199–260. https://doi.org/10.1007/978-3-030-78627-4_7

758   Harrison, J.P., Hoellein, T.J., Sapp, M., Tagg, A.S., Ju-Nam, Y., Ojeda, J.J., 2018. Microplastic-Associated
759   Biofilms: A Comparison of Freshwater and Marine Environments BT - Freshwater Microplastics :
760   Emerging Environmental Contaminants?, in: Wagner, M., Lambert, S. (Eds.), . Springer
761   International Publishing, Cham, pp. 181–201. https://doi.org/10.1007/978-3-319-61615-5_9

762   Hartmann, N.B., Hüffer, T., Thompson, R.C., Hassellöv, M., Verschoor, A., Daugaard, A.E., Rist, S.,
763   Karlsson, T., Brennholt, N., Cole, M., Herrling, M.P., Hess, M.C., Ivleva, N.P., Lusher, A.L.,
764   Wagner, M., 2019. Are We Speaking the Same Language? Recommendations for a Definition and
765   Categorization Framework for Plastic Debris. Environ. Sci. Technol. 53, 1039–1047.
766   https://doi.org/10.1021/acs.est.8b05297

767   Hossain, M.R., Jiang, M., Wei, Q.H., Leff, L.G., 2019. Microplastic surface properties affect bacterial
768   colonization in freshwater. J. Basic Microbiol. 59, 54–61. https://doi.org/10.1002/jobm.201800174

769   Hrubanova, K., Krzyzanek, V., Nebesarova, J., Ruzicka, F., Pilat, Z., Samek, O., 2018. Monitoring
770   Candida parapsilosis and Staphylococcus epidermidis Biofilms by a Combination of Scanning
771   Electron Microscopy and Raman Spectroscopy 1–19. https://doi.org/10.3390/s18124089

772   Huang, H., Liu, P., Shi, Y., Wu, X., Gao, S., 2022. Remarkable characteristics and distinct community of
773   biofilms on the photoaged polyethylene films in riverine microcosms. Environ. Pollut. 292, 118485.
774   https://doi.org/https://doi.org/10.1016/j.envpol.2021.118485

775   Imhof, H.K., Rusek, J., Thiel, M., Wolinska, J., Laforsch, C., 2017. Do microplastic particles affect
776   Daphnia magna at the morphological , life history and molecular level ? 1–20.
777   https://doi.org/10.5061/dryad.9d84j

778   Ivleva, N.P., Kubryk, P., Niessner, R., 2017. Raman microspectroscopy, surface-enhanced Raman
779   scattering microspectroscopy, and stable-isotope Raman microspectroscopy for biofilm
780   characterization. Anal. Bioanal. Chem. 409, 4353–4375. https://doi.org/10.1007/s00216-017-0303-
781   0

782   Ivleva, N.P., Wagner, M., Horn, H., Niessner, R., Haisch, C., 2008. In Situ Surface-Enhanced Raman
783   Scattering Analysis of Biofilm. Anal. Chem. 80, 8538–8544. https://doi.org/10.1021/ac801426m

784   Jehlička, J., Oren, A., 2013. Raman spectroscopy in halophile research. Front. Microbiol. 4, 1–7.
785   https://doi.org/10.3389/fmicb.2013.00380

786 Klein, S., Dimzon, I.K., Eubeler, J., Knepper, T.P., 2018. Analysis, Occurrence, and Degradation of
787   Microplastics in the Aqueous Environment BT - Freshwater Microplastics : Emerging
788   Environmental Contaminants?, in: Wagner, M., Lambert, S. (Eds.), . Springer International
789   Publishing, Cham, pp. 51–67. https://doi.org/10.1007/978-3-319-61615-5_3

790 Kot, A.M., Błażejak, S., Gientka, I., Kieliszek, M., Bryś, J., 2018. Torulene and torularhodin: "new" fungal
791   carotenoids for industry? Microb. Cell Fact. 17, 49. https://doi.org/10.1186/s12934-018-0893-z

792 Kumar B. N., V., Kampe, B., Rösch, P., Popp, J., 2015. Characterization of carotenoids in soil bacteria
793   and investigation of their photodegradation by UVA radiation via resonance Raman spectroscopy.
794   Analyst 140, 4584–4593. https://doi.org/10.1039/C5AN00438A

795 Kusić, D., Kampe, B., Ramoji, A., Neugebauer, U., Rösch, P., Popp, J., 2015. Raman spectroscopic
796   differentiation of planktonic bacteria and biofilms. Anal. Bioanal. Chem. 407, 6803–6813.
797   https://doi.org/10.1007/s00216-015-8851-7

798 Lawrence, J.R., Swerhone, G.D.W., Kuhlicke, U., Neu, T.R., 2016. In situ evidence for metabolic and
799   chemical microdomains in the structured polymer matrix of bacterial microcolonies. FEMS
800   Microbiol. Ecol. 92, fiw183. https://doi.org/10.1093/femsec/fiw183

801 Liao, C., Liang, X., Soupir, M.L., Jarboe, L.R., 2015. Cellular, particle and environmental parameters
802   influencing attachment in surface waters: a review. J. Appl. Microbiol. 119, 315–330.
803   https://doi.org/10.1111/jam.12860

804 Lobelle, D., Kooi, M., Koelmans, A.A., Laufkötter, C., Jongedijk, C.E., Kehl, C., van Sebille, E., 2021.
805   Global Modeled Sinking Characteristics of Biofouled Microplastic. J. Geophys. Res. Ocean. 126,
806   e2020JC017098. https://doi.org/https://doi.org/10.1029/2020JC017098

807 Lusher, A.L., Hollman, P.C.H., Mendoza-Hill, J., 2017. Microplastics in fisheries and aquaculture.

808 MacLeod, M., Arp, H.P.H., Tekman, M.B., Jahnke, A., 2021. The global threat from plastic pollution.
809   Science 373, 61–65. https://doi.org/10.1126/science.abg5433

810 Miao, L., Yu, Y., Adyel, T.M., Wang, C., Liu, Z., Liu, S., Huang, L., You, G., Meng, M., Qu, H., Hou, J.,
811   2021. Distinct microbial metabolic activities of biofilms colonizing microplastics in three freshwater
812   ecosystems. J. Hazard. Mater. 403, 123577.
813   https://doi.org/https://doi.org/10.1016/j.jhazmat.2020.123577

814 Möller, J.N., Löder, M.G.J., Laforsch, C., 2020. Finding Microplastics in Soils: A Review of Analytical
815   Methods. Environ. Sci. Technol. 54, 2078–2090. https://doi.org/10.1021/acs.est.9b04618

816 Munno, K., De Frond, H., O'Donnell, B., Rochman, C.M., 2020. Increasing the Accessibility for
817   Characterizing Microplastics: Introducing New Application-Based and Spectral Libraries of Plastic
818   Particles (SLoPP and SLoPP-E). Anal. Chem. 92, 2443–2451.
819   https://doi.org/10.1021/acs.analchem.9b03626

820 Nag, M., Lahiri, D., Banerjee, R., Chatterjee, A., Ghosh, A., Banerjee, P., Ray, R.R., 2021. Analysing
821   Microbial Biofilm Formation at a Molecular Level: Role of Fourier Transform Infrared and Raman
822   Spectroscopy BT - Analytical Methodologies for Biofilm Research, in: Nag, M., Lahiri, D. (Eds.), .
823   Springer US, New York, NY, pp. 69–93. https://doi.org/10.1007/978-1-0716-1378-8_3

824 Oberbeckmann, S., Loeder, M.G.J., Gerdts, G., Osborn, A.M., 2014. Spatial and seasonal variation in
825   diversity and structure of microbial biofilms on marine plastics in Northern European waters.
826   FEMS Microbiol. Ecol. 2, 478–492. https://doi.org/10.1111/1574-6941.12409

827 Paerl, H.W., 1975. Microbial attachment to particles in marine and freshwater ecosystems. Microb. Ecol.
828   2, 73–83. https://doi.org/10.1007/BF02010382

829 Pankin, D., Povolotckaia, A., Kalinichev, A., Povolotskiy, A., Borisov, E., Moskovskiy, M., Gulyaev, A.,
830   Lavrov, A., Izmailov, A., 2021. Complex Spectroscopic Study for Fusarium Genus Fungi Infection
831   Diagnostics of "Zalp" Cultivar Oat. Agronomy.

832   https://doi.org/10.3390/agronomy11122402

833   Parra-Rivero, O., Paes de Barros, M., Prado, M.D., Gil, J.-V., Hornero-Méndez, D., Zacarías, L., Rodrigo,
834   M.J., Limón, M.C., Avalos, J., 2020. Neurosporaxanthin Overproduction by Fusarium fujikuroi and
835   Evaluation of Its Antioxidant Properties. Antioxidants. https://doi.org/10.3390/antiox9060528

836   Raju, P., Santhanam, P., Pandian, S.S., Divya, M., Arunkrishnan, A., Devi, K.N., Ananth, S., Roopavathy,
837   J., Perumal, P., 2021. Impact of polystyrene microplastics on major marine primary (phytoplankton)
838   and secondary producers (copepod). Arch. Microbiol. 204, 84. https://doi.org/10.1007/s00203-
839   021-02697-6

840   Ramsperger, A.F.R.M., Stellwag, A.C., Caspari, A., Fery, A., Lueders, T., Kress, H., Löder, M.G.J.,
841   Laforsch, C., 2020. Structural diversity in early-stage biofilm formation on microplastics depends on
842   environmental medium and polymer properties. Water (Switzerland) 12, 1–21.
843   https://doi.org/10.3390/w12113216

844   Rhodes, C.J., 2018. Plastic pollution and potential solutions 101, 207–260.

845   Ritschar, S., Bangalore Narayana, V.K., Rabus, M., Laforsch, C., 2020. Uncovering the chemistry behind
846   inducible morphological defences in the crustacean Daphnia magna via micro-Raman spectroscopy.
847   Sci. Rep. 10, 22408. https://doi.org/10.1038/s41598-020-79755-4

848   Riveros, G., Urrutia, H., Araya, J., Zagal, E., Schoebitz, M., 2022. Microplastic pollution on the soil and
849   its consequences on the nitrogen cycle: a review. Environ. Sci. Pollut. Res. 29, 7997–8011.
850   https://doi.org/10.1007/s11356-021-17681-2

851   Rummel, C.D., Jahnke, A., Gorokhova, E., K?hnel, D., Schmitt-Jansen, M., 2017. The Impacts of Biofilm
852   Formation on the Fate and Potential Effects of Microplastic in the Aquatic Environment. Environ.
853   Sci. Technol. Lett. acs.estlett.7b00164. https://doi.org/10.1021/acs.estlett.7b00164

854   Rummel, C.D., Lechtenfeld, O.J., Kallies, R., Benke, A., Herzsprung, P., Rynek, R., Wagner, S., Potthoff,
855   A., Jahnke, A., Schmitt-Jansen, M., 2021. Conditioning Film and Early Biofilm Succession on Plastic
856   Surfaces. Environ. Sci. Technol. 55, 11006–11018. https://doi.org/10.1021/acs.est.0c07875

857   Schmid, B., Schindelin, J., Cardona, A., Longair, M., Heisenberg, M., 2010. A high-level 3D visualization
858   API for Java and ImageJ. BMC Bioinformatics 11, 274. https://doi.org/10.1186/1471-2105-11-274

859   Siboni, N., Lidor, M., Kramarsky-Winter, E., Kushmaro, A., 2007. Conditioning film and initial biofilm
860   formation on ceramics tiles in the marine environment. FEMS Microbiol. Lett. 274, 24–29.
861   https://doi.org/10.1111/j.1574-6968.2007.00809.x

862   Strungaru, S.-A., Jijie, R., Nicoara, M., Plavan, G., Faggio, C., 2019. Micro- (nano) plastics in freshwater
863   ecosystems: Abundance, toxicological impact and quantification methodology. TrAC Trends Anal.
864   Chem. 110, 116–128. https://doi.org/https://doi.org/10.1016/j.trac.2018.10.025

865   Takada, H., Koro, M., Kwan, C.S., 2022. Marine Plastic Pollution: Chemical Aspects and Possible
866   Solutions BT - Overcoming Environmental Risks to Achieve Sustainable Development Goals:
867   Lessons from the Japanese Experience, in: Nakajima, T., Nakamura, K., Nohara, K., Kondoh, A.
868   (Eds.), . Springer Singapore, Singapore, pp. 83–92. https://doi.org/10.1007/978-981-16-6249-2_10

869   Talari, A.C.S., Movasaghi, Z., Rehman, S., Rehman, I. ur, 2015. Raman Spectroscopy of Biological
870   Tissues. Appl. Spectrosc. Rev. 50, 46–111. https://doi.org/10.1080/05704928.2014.923902

871   Talbot, R., Chang, H., 2022. Microplastics in freshwater: A global review of factors affecting spatial and
872   temporal variations. Environ. Pollut. 292, 118393.
873   https://doi.org/https://doi.org/10.1016/j.envpol.2021.118393

874   Tao, Z., Wang, G., Xu, X., Yuan, Y., Wang, X., Li, Y., 2011. Monitoring and rapid quantification of total
875   carotenoids in Rhodotorula glutinis cells using laser tweezers Raman spectroscopy. FEMS
876   Microbiol. Lett. 314, 42–48. https://doi.org/10.1111/j.1574-6968.2010.02139.x

877   Tiwari, N., Bansal, M., Santhiya, D., Sharma, J.G., 2022. Insights into microbial diversity on plastisphere

878   by multi-omics. Arch. Microbiol. 204, 216. https://doi.org/10.1007/s00203-022-02806-z

879   Trotter, B., Wilde, M. V, Brehm, J., Dafni, E., Aliu, A., Arnold, G.J., Fröhlich, T., Laforsch, C., 2021.
880   Long-term exposure of Daphnia magna to polystyrene microplastic (PS-MP) leads to alterations of
881   the proteome, morphology and life-history. Sci. Total Environ. 795, 148822.
882   https://doi.org/https://doi.org/10.1016/j.scitotenv.2021.148822

883   Vaksmaa, A., Knittel, K., Asbun, A.A., Goudriaan, M., Ellrott, A., Witte, H.J., Vollmer, I., Meirer, F.,
884   Lott, C., Weber, M., Engelmann, J.C., Niemann, H., Kirstein, I.V., 2021. Microbial Communities on
885   Plastic Polymers in the Mediterranean Sea 12, 1–15. https://doi.org/10.3389/fmicb.2021.673553

886   Wagner, M., Ivleva, N.P., Haisch, C., Niessner, R., Horn, H., 2009. Combined use of confocal laser
887   scanning microscopy (CLSM) and Raman microscopy (RM): Investigations on EPS – Matrix. Water
888   Res. 43, 63–76. https://doi.org/https://doi.org/10.1016/j.watres.2008.10.034

889   Wang, J., Li, J., Liu, S., Li, H., Chen, X., Peng, C., Zhang, P., Liu, X., 2021. Distinct microplastic
890   distributions in soils of different land-use types: A case study of Chinese farmlands. Environ. Pollut.
891   269, 116199. https://doi.org/https://doi.org/10.1016/j.envpol.2020.116199

892   Webb, H.K., Crawford, R.J., Sawabe, T., Ivanova, E.P., 2009. Poly(ethylene terephthalate) polymer
893   surfaces as a substrate for bacterial attachment and biofilm formation. Microbes Environ. 24, 39–
894   42. https://doi.org/10.1264/jsme2.ME08538

895   Weig, A., Löder, M.G.J., Ramsperger, A.F.R.M., Laforsch, C., 2021. In situ Prokaryotic and Eukaryotic
896   Communities on Microplastic Particles in a Small Headwater Stream in Germany 12, 1–14.
897   https://doi.org/10.3389/fmicb.2021.660024

898   Withnall, R., Chowdhry, B.Z., Silver, J., Edwards, H.G.M., de Oliveira, L.F.C., 2003. Raman spectra of
899   carotenoids in natural products. Spectrochim. Acta Part A Mol. Biomol. Spectrosc. 59, 2207–2212.
900   https://doi.org/https://doi.org/10.1016/S1386-1425(03)00064-7

901   Wright, R.J., Langille, M.G.I., Walker, T.R., 2021. Food or just a free ride? A meta-analysis reveals the
902   global diversity of the Plastisphere. ISME J. 15, 789–806. https://doi.org/10.1038/s41396-020-
903   00814-9

904   Wright, S.L., Thompson, R.C., Galloway, T.S., 2013. The physical impacts of microplastics on marine
905   organisms: A review. Environ. Pollut. 178, 483–492. https://doi.org/10.1016/j.envpol.2013.02.031

906   Xie, H., Chen, J., Feng, L., He, L., Zhou, C., Hong, P., Sun, S., Zhao, H., Liang, Y., Ren, L., Zhang, Y.,
907   Li, C., 2021. Chemotaxis-selective colonization of mangrove rhizosphere microbes on nine different
908   microplastics. Sci. Total Environ. 752, 142223.
909   https://doi.org/https://doi.org/10.1016/j.scitotenv.2020.142223

910   Yabuzaki, J., 2017. Carotenoids Database: structures, chemical fingerprints and distribution among
911   organisms. Database 2017, bax004. https://doi.org/10.1093/database/bax004

912   Zettler, E.R., Mincer, T.J., Amaral-zettler, L. a, 2013. Life in the ' Plastisphere ': Microbial communities
913   on plastic marine debris. https://doi.org/10.1021/es401288x

914   Zhang, S.-J., Zeng, Y.-H., Zhu, J.-M., Cai, Z.-H., Zhou, J., 2022. The structure and assembly mechanisms
915   of plastisphere microbial community in natural marine environment. J. Hazard. Mater. 421, 126780.
916   https://doi.org/https://doi.org/10.1016/j.jhazmat.2021.126780

917   Zhou, Y., Kumar, M., Sarsaiya, S., Sirohi, R., Awasthi, S.K., Sindhu, R., Binod, P., Pandey, A., Bolan,
918   N.S., Zhang, Z., Singh, L., Kumar, S., Awasthi, M.K., 2022. Challenges and opportunities in
919   bioremediation of micro-nano plastics: A review. Sci. Total Environ. 802, 149823.
920   https://doi.org/https://doi.org/10.1016/j.scitotenv.2021.149823

921

922

1   Manuscript – Supplementary Information

2   **Title**

3   Spatio-chemical analysis of the plastisphere using Raman spectroscopy

4

5   **Authors**

6   Vinay Kumar Bangalore-Narayana[1], Anja FRM Ramsperger[1,2], Marvin Kiene[1], Julian Brehm[1], Martin GJ
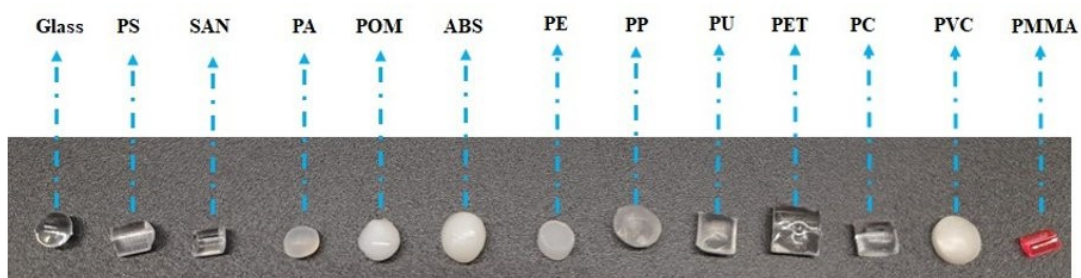
7   Löder[1] & Christian Laforsch[1,#]

8

9   **Affiliations**

10   [1] Animal Ecology I, University of Bayreuth, Bayreuth, Germany

11   [2] Biological Physics, University of Bayreuth, Bayreuth, Germany

12   [#] corresponding author

13

14 **Figure S1: Glass and *MPs pellets incubated in freshwater (FW) and seawater (SW)*;** Glass, Polystyrene (PS),
15 Styrene Acrylonitrile (SAN), Polyamide (PA), Polyoxymethylene (POM), Acrylonitrile Butadiene Styrene (ABS),
16 Polyethylene (PE), Polypropylene (PP), Polyurethane (PU), Polyethyleneterepthalate (PET), Polycarbonate (PC),
17 Polyvinylchloride (PVC) and Polymethylenemethacrylate (PMMA).

18

Figure S2: *Microcosm setup consisting of MPs incubated in freshwater (FW) and seawater (SW);* The front row represents the samples incubated in SW environment and the row behind facing the stainless steel casings represent the samples incubated in FW environment respectively.
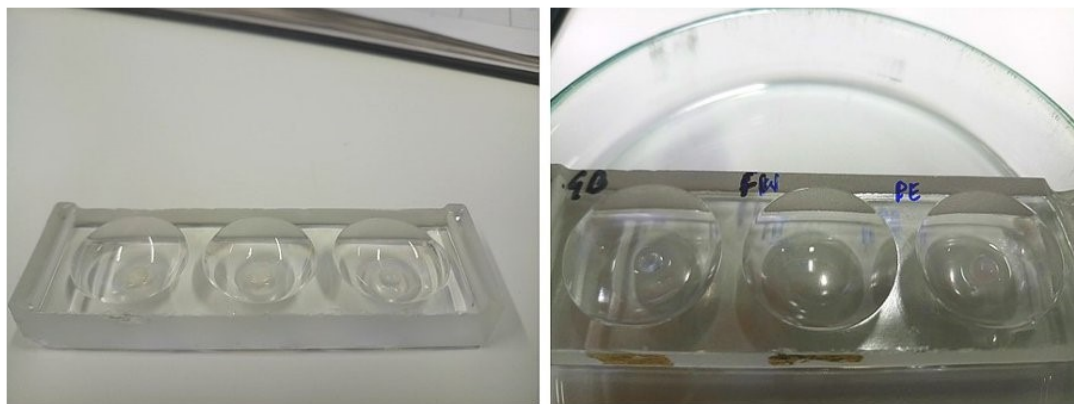
22

23 **Figure S3:** *Concavity slides used for micro-Raman spectroscopic measurements*; the two images presented
24 here visualize the glass pellet sample and PE MPs samples placed in a drop of tap water. This arrangement was used
25 for the Raman measurements.

26   Table S1: Sources of microplastics and glass pellets

Microplastics	Polymer type	Source
1.	Polyamide (PA)	Ultramid B27E MKNR. 96589
2.	Polyethylene (PE)	Lupolen 6031M natur, Art.Nr. 147678
3.	Polyethyleneterepthalate (PET)	Typ M Trevira
4.	Polycarbonate (PC)	Pro-Plast, PANLITE L 1250Y, glasklar, Art.nr. 143055
5.	Acrylonitrile Butadiene Styrene (ABS)	Pro-Plast, Novodur P2MC, natur, Art.nr. 165444
6.	Styrene Acrylonitrile (SAN)	Pro-Plast, Luran 368 R, glasklar, Artnr. 168175
7.	Polystyrene (PS)	Pro-Plast,BASF PS 158k, glasklar 00013, Art.nr.148786
8.	Polyvinylchloride (PVC)	TRO/LIT VB 537-HE
9.	Polyurethane (PU)	Pro-Plast, Desmopan 385E, natur, Art.nr. 165295
10.	Polyoxymethylene (POM)	Pro-Plast, Dettin 500, natur, NC010, Art.nr. 166654
11.	Polypropylene (PP)	Pro-Plast, PP-Home, Moplen HP 570 M, Art.nr. 148812
12.	Polymethylenemethacrylate (PMMA)	UV-Leuchtgranulat, Art.nr M 133344
13.	Glass pellets	Supelco. Merck KGaA

27

28 **Table S2:** *Assignments of the Raman molecular signatures corresponding to the plastisphere* (ν) denotes
29 stretching vibrational mode, (δ) denotes bending, rocking and wagging vibrational modes (τ) denotes twisting
30 vibrational mode (s) symmetric stretching (as) asymmetric stretching

Plastisphere Molecular Profiling	Plastisphere fingerprint molecules	Raman Band Positions/cm⁻¹	Functional Groups/Bond Vibration
1.	*Polysaccharides*	~560, 891, 1094, 1203, 1280-1288, 1355-1380	Glycosidic link δ(C-O-C), ν(C-C), glycosidic link δ(C-O-C), saccharide band, δ(C-H$_2$), δ(C-H)
2.	*Proteins*	~520, 531, 643, 665, 670, 677, 691, 696, 741, 746, 747, 833, 871, 876, 1004, 1203, 1540, 1564, 1586, 1661, 1668, 1670, 2924 and 2925 cm⁻¹	ν(S-S) in cysteine, τ(C-C) in tyrosine, ν(C-S) in cysteine, ring breathing of tryptophan, tyrosine, ν(C-C) of tryptophan and ν(C-C) of hydroxyproline, ν(C-C) tryptophan and tyrosine, ring breathing of phenylalanine, Amide III- due to ν(C-N) and δ(N-H), Amide II due to ν(C-N) and δ(N-H), Amide I due to ν(C=O), ν(C-H$_3$), ν(C-H$_2$) and ν(C-H)
3.	*Nucleic acids (DNA/RNA)*	~693, 713, 754, 908, 952, 961, 962, 980, 1094 and 1570 cm⁻¹	Ring breathing modes in the DNA bases (Guanine), (C-N) nucleotide band, DNA/RNA ring breathing modes, Ribose vibration (RNA), ν(PO$_4^-$), ν(PO$_2^-$) vibration of the DNA backbone, ring breathing modes in the DNA bases G, A
4.	*Lipids*	~592, 1302, 1320, 1325, 1334, 1339, 1420, 1426, 1437, 1444, 1452, 1724, 1728, 1775, 1787, 1793, 2835, 2853, 2866, 2958, 2966, 2971, 2995 and 3097 cm⁻¹	Phosphatidylinositol, δ(C-H$_2$), τ(C-H$_3$)/(C-H$_2$), δ(C-H$_3$), δ(C-H$_3$, C-H$_2$), ν(C=O), ν_{as}(C-H$_3$), ν_s(C-H$_3$), ν_{as}(C-H$_2$) ν_s(C-H$_2$), ν_s(C-H), ν(=C-H)
5.	*Carotenoids*	~1150-1160 cm⁻¹ and 1499-1528 cm⁻¹	ν(C-C) and ν(C=C)
6.	*Water*	~3200-3500 cm⁻¹	ν(O-H)
7.	*Cytochrome c*	~1123, 1129 and 1596 cm⁻¹	ν(C$_b$-CH$_3$), ν(C$_a$C$_m$), ν(C$_a$C$_m$H), ν(C$_a$C$_b$) of pyrrole half ring

31

32 **Table S:** *Assignments of the marker Raman bands corresponding to the polymer constituting the MPs;* (ν)
33 denotes stretching vibrational mode, (δ) denotes bending, rocking and wagging vibrational modes (τ) denotes twisting
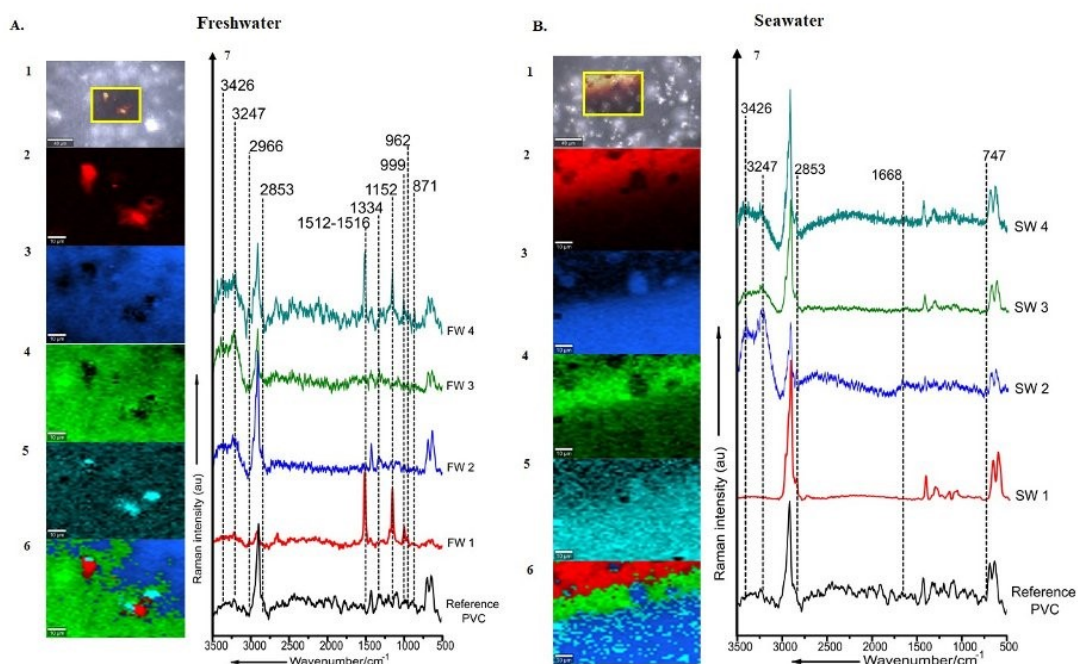34 vibrational mode (s) symmetric stretching (as) asymmetric stretching

| Pristine Polymer Profiles	Polymer type	Raman Band Positions/cm⁻¹	Functional Groups/Bond Vibration
1.	Polyamide (PA)	~1632, 3296 cm⁻¹	ν(C=N), ν(N-H)
2.	Polyethylene (PE)	~2842, 2877 cm⁻¹ sharp doublet profile	ν_s(C-H$_2$), ν_s(C-H), ν(=C-H)
3.	Polyethyleneterepthalate (PET)	~1608, 1719 cm⁻¹	ν(Ring breathing), ν(C=O)
4.	Polycarbonate (PC)	~884, 1109, 3073 cm⁻¹	ν(C-O-C), (C-H) ring, ν(C=O)
5.	Acrylonitrile Butadiene Styrene (ABS)	~1003, 1606, 1666, 2236 cm⁻¹	ν(Ring breathing), ν(Ring skeletal stretch) ν(C=C), ν(C≡N)
6.	Styrene Acrylonitrile (SAN)	~1003, 1606, 2236 cm⁻¹	ν(Ring breathing), ν(Ring skeletal stretch) ν(C≡N)
7.	Polystyrene (PS)	~1003, 1606 cm⁻¹	ν(Ring breathing), ν(Ring skeletal stretch)
8.	Polyvinylchloride (PVC)	~637, 694 cm⁻¹	ν(C-S) aliphatic
9.	Polyurethane (PU)	~1181, 1247, 1309 triplet, 1613 cm⁻¹	ν(C-O-C), ν(C-N), δ(C-H)
10.	Polyoxymethylene (POM)	~916 cm⁻¹	ν(C-O-C)/ δ(O-C-O)
11.	Polypropylene (PP)	~802, 834, 2834, 2879, 2954 cm⁻¹	δ(C-H), δ(C-H$_3$), ν_{as}(C-H$_2$), ν_s(C-H$_3$), ν_{as}(C-H$_3$)

35
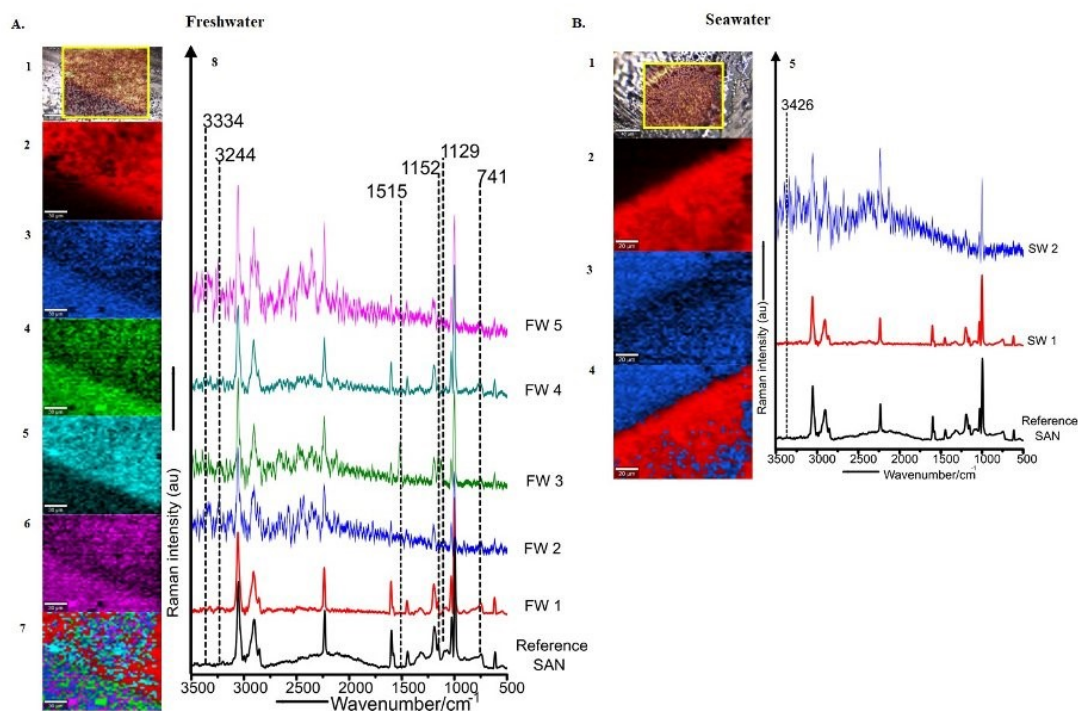
36

37 **Figure S4:** *Molecular profiles of the plastisphere on the surface of SAN MPs incubated in FW and SW as*
38 *revealed by micro-Raman imaging* (**A.**) FW incubation {1} Bright field microscopic image of the surface of the
39 SAN incubated for 30 days with the inset representing the region of interest selected for imaging {2-6} False coloured
40 Raman images indicating the spatial and differential intensity distribution of the respective demixed spectral
41 components {7} Combined image inclusive of all demixed spectral components {8} Mean spectrum of the respective
42 demixed spectral components compared with the pristine or reference SAN spectrum (Ref, FW 1-FW 5) (**B.**) SW
43 incubation {1} Bright field microscopic image of the surface of SAN incubated for 30 days with the inset representing
44 the region of interest selected for Raman imaging {2-3} False coloured Raman images indicating the spatial and
45 differential intensity distribution of the respective demixed spectral components {4} Combined image inclusive of all
46 demixed spectral components {5} Mean spectrum of the respective demixed spectral components compared with the
47 pristine SAN spectrum (Ref, SW 1-SW 2) The spectral components represent the respective mean spectrum calculated
48 from n=25,000 spectra constituting the Raman images analysed via TCA coupled with spectral demixing. The Raman
49 image has been acquired from the surface of a single SAN MPs sample (FW n=1 and SW n=1).

Figure S5: *Molecular profiles of the plastisphere on the surface of PVC MPs incubated in FW and SW as revealed by micro-Raman imaging* (**A.**) FW incubation {1} Bright field microscopic image of the surface of PVC incubated for 30 days with the inset representing the region of interest selected for imaging {2-5} False coloured Raman images indicating the spatial and differential intensity distribution of the respective demixed spectral components {6} Combined image inclusive of all demixed spectral components {7} Mean spectrum of the respective demixed spectral components compared with the pristine or reference PVC spectrum (Ref, FW 1-FW 5) (**B.**) SW incubation {1} Bright field microscopic image of the surface of PVC incubated for 30 days with the inset representing the region of interest selected for Raman imaging {2-5} False coloured Raman images indicating the spatial and differential intensity distribution of the respective demixed spectral components {6} Combined image inclusive of all demixed spectral components {5} Mean spectrum of the respective demixed spectral components compared with the pristine PVC spectrum (Ref, SW 1-SW 4) The spectral components represent the respective mean spectrum calculated from n=25,000 spectra constituting the Raman images analysed via TCA coupled with spectral demixing. The Raman image has been acquired from the surface of a single PVC MPs sample (FW n=1 and SW n=1).
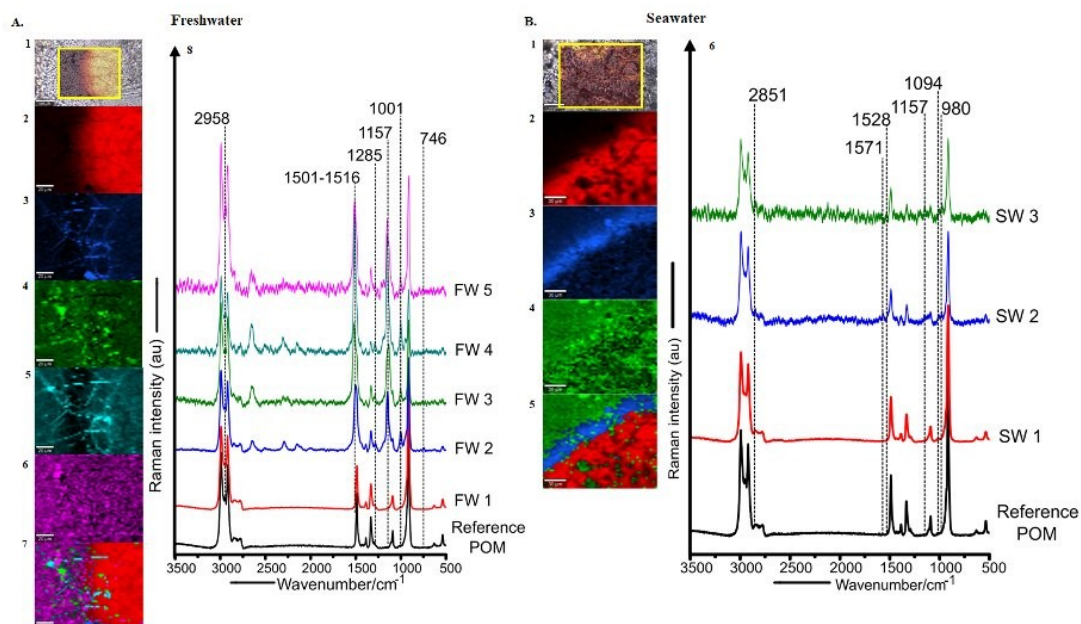
64
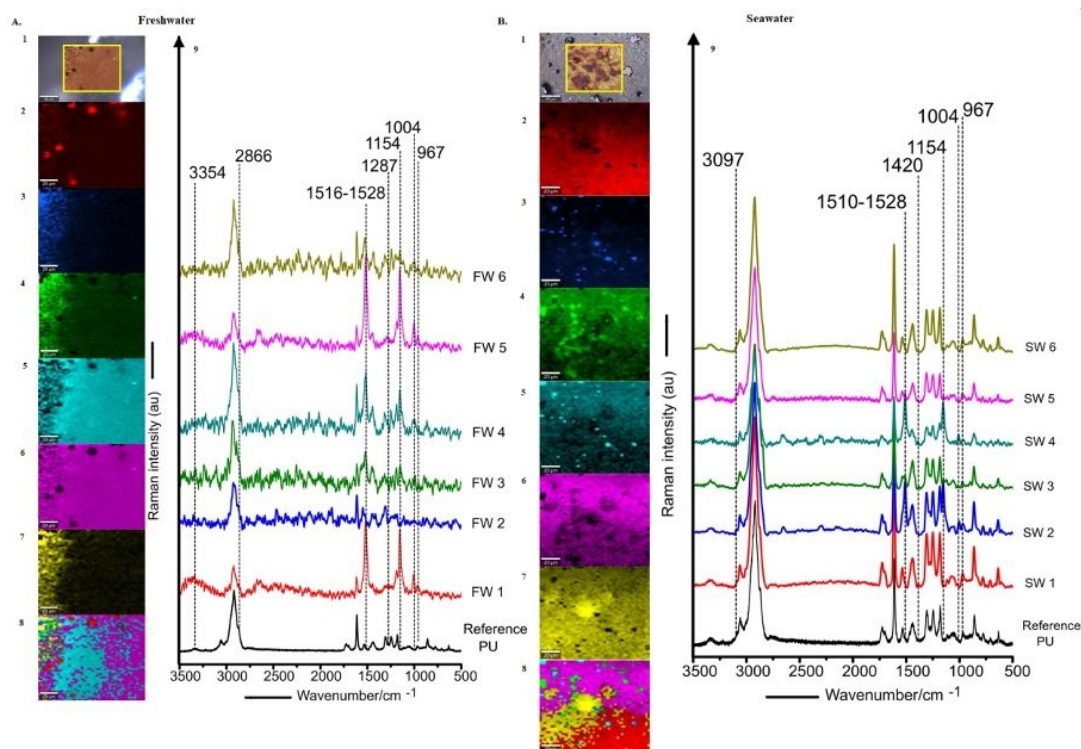
Figure S6: *Molecular profiles of the plastisphere on the surface of PU MPs incubated in FW and SW as revealed by micro-Raman imaging* (**A.**) FW incubation {1} Bright field microscopic image of the surface of the PU incubated for 30 days with the inset representing the region of interest selected for imaging {2-7} False coloured Raman images indicating the spatial and differential intensity distribution of the respective demixed spectral components {8} Combined image inclusive of all demixed spectral components {9} Mean spectrum of the respective demixed spectral components compared with the pristine or reference PU spectrum (Ref, FW 1-FW6) (**B.**) SW incubation {1} Bright field microscopic image of the surface of PU incubated for 30 days with the inset representing the region of interest selected for Raman imaging {2-7} False coloured Raman images indicating the spatial and differential intensity distribution of the respective demixed spectral components {8} Combined image inclusive of all demixed spectral components {9} Mean spectrum of the respective demixed spectral components compared with the pristine PU spectrum (Ref, SW 1-SW 6) The spectral components represent the respective mean spectrum calculated from n=25,000 spectra constituting the Raman images analysed via TCA coupled with spectral demixing. The Raman image has been acquired from the surface of a single PU MPs sample (FW n=1 and SW n=1).

78
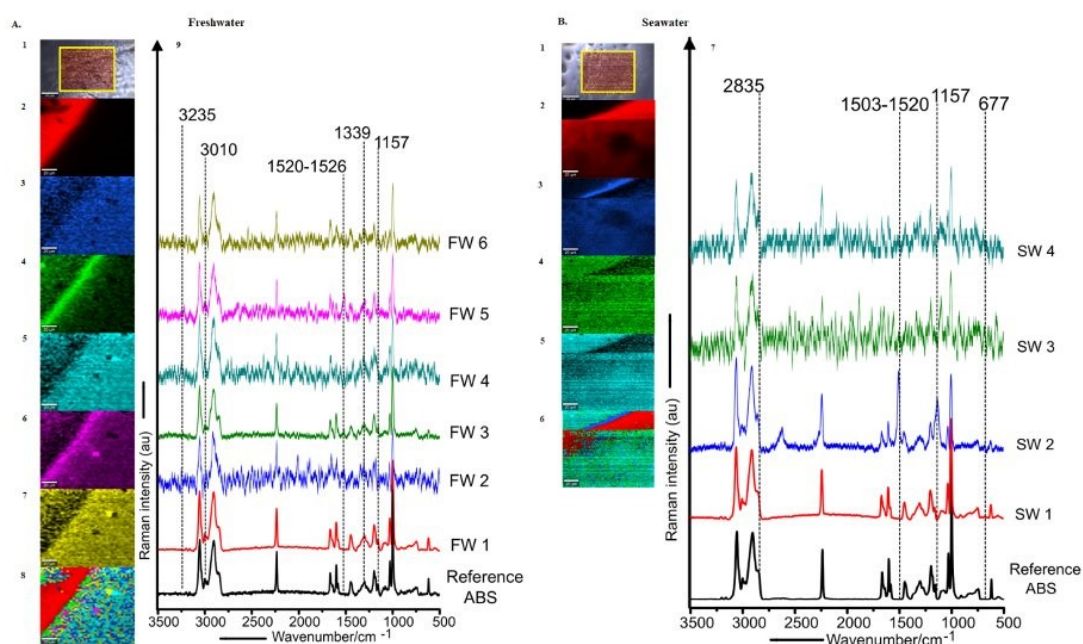
Figure S7: *Molecular profiles of the plastisphere on the surface of ABS MPs incubated in FW and SW as revealed by micro-Raman imaging* (**A.**) FW incubation {1} Bright field microscopic image of the surface of the ABS incubated for 30 days with the inset representing the region of interest selected for imaging {2-7} False coloured Raman images indicating the spatial and differential intensity distribution of the respective demixed spectral components {8} Combined image inclusive of all demixed spectral components {9} Mean spectrum of the respective demixed spectral components compared with the pristine or reference ABS spectrum (Ref, FW 1-FW6) (**B.**) SW incubation {1} Bright field microscopic image of the surface of ABS incubated for 30 days with the inset representing the region of interest selected for Raman imaging {2-5} False coloured Raman images indicating the spatial and differential intensity distribution of the respective demixed spectral components {6} Combined image inclusive of all demixed spectral components {7} Mean spectrum of the respective demixed spectral components compared with the pristine ABS spectrum (Ref, SW 1-SW 4) The spectral components represent the respective mean spectrum calculated from n=25,000 spectra constituting the Raman images analysed via TCA coupled with spectral demixing. The Raman image has been acquired from the surface of a single ABS MPs sample (FW n=1 and SW n=1).
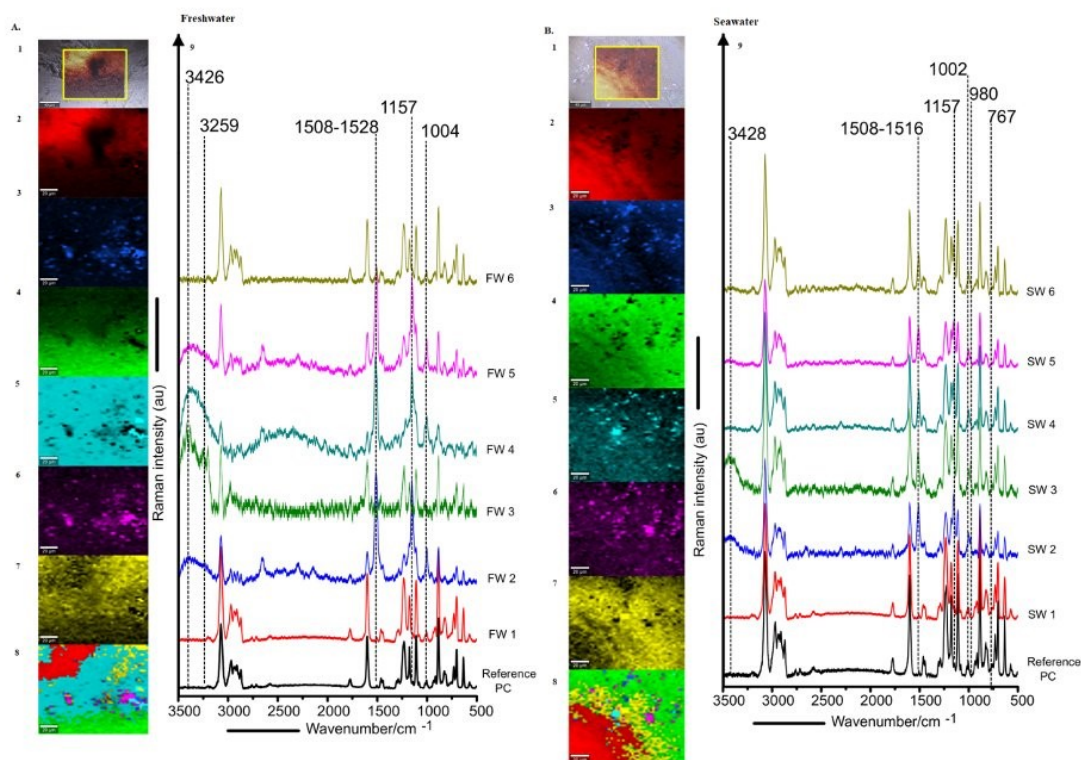
92

Figure S8: *Molecular profiles of the plastisphere on the surface of POM MPs incubated in FW and SW as revealed by micro-Raman imaging* (**A.**) FW incubation {1} Bright field microscopic image of the surface of the POM incubated for 30 days with the inset representing the region of interest selected for imaging {2-6} False coloured Raman images indicating the spatial and differential intensity distribution of the respective demixed spectral components {7} Combined image inclusive of all demixed spectral components {8} Mean spectrum of the respective demixed spectral components compared with the pristine or reference POM spectrum (Ref, FW 1-FW5) (**B.**) SW incubation {1} Bright field microscopic image of the surface of POM incubated for 30 days with the inset representing the region of interest selected for Raman imaging {2-4} False coloured Raman images indicating the spatial and differential intensity distribution of the respective demixed spectral components {5} Combined image inclusive of all demixed spectral components {6} Mean spectrum of the respective demixed spectral components compared with the pristine POM spectrum (Ref, SW 1-SW 3) The spectral components represent the respective mean spectrum calculated from n=25,000 spectra constituting the Raman images analysed via TCA coupled with spectral demixing. The Raman image has been acquired from the surface of a single POM MPs sample (FW n=1 and SW n=1).

Figure S9: *Molecular profiles of the plastisphere on the surface of PC MPs incubated in FW and SW as revealed by micro-Raman imaging* (**A.**) FW incubation {1} Bright field microscopic image of the surface of the PC incubated for 30 days with the inset representing the region of interest selected for imaging {2-7} False coloured Raman images indicating the spatial and differential intensity distribution of the respective demixed spectral components {8} Combined image inclusive of all demixed spectral components {9} Mean spectrum of the respective demixed spectral components compared with the pristine or reference PC spectrum (Ref, FW 1-FW6) (**B.**) SW incubation {1} Bright field microscopic image of the surface of PC incubated for 30 days with the inset representing the region of interest selected for Raman imaging {2-7} False coloured Raman images indicating the spatial and differential intensity distribution of the respective demixed spectral components {8} Combined image inclusive of all demixed spectral components {9} Mean spectrum of the respective demixed spectral components compared with the pristine POM spectrum (Ref, SW 1-SW 6) The spectral components represent the respective mean spectrum calculated from n=25,000 spectra constituting the Raman images analysed via TCA coupled with spectral demixing. The Raman image has been acquired from the surface of a single PC MPs sample (FW n=1 and SW n=1).

References

Aderem, A., & Underhill, D. M. (1999). Mechanisms of phagocytosis in macrophages. *Annual Review of Immunology*, *17*, 593–623. https://doi.org/10.1146/annurev.immunol.17.1.593

Albanese, A., Walkey, C. D., Olsen, J. B., Guo, H., Emili, A., & Chan, W. C. W. (2014). Secreted biomolecules alter the biological identity and cellular interactions of nanoparticles. *ACS Nano*, *8*(6), 5515–5526. https://doi.org/10.1021/nn4061012

Anbumani, S., & Kakkar, P. (2018). Ecotoxicological effects of microplastics on biota: a review. *Environmental Science and Pollution Research*, *25*(15), 14373–14396. https://doi.org/10.1007/s11356-018-1999-x

Andrady, A. L. (2011). Microplastics in the marine environment. *Marine Pollution Bulletin*, *62*(8), 1596–1605. https://doi.org/10.1016/j.marpolbul.2011.05.030

Artham, T., Sudhakar, M., Venkatesan, R., Madhavan Nair, C., Murty, K. V. G. K., & Doble, M. (2009). Biofouling and stability of synthetic polymers in sea water. *International Biodeterioration and Biodegradation*, *63*(7), 884–890. https://doi.org/10.1016/j.ibiod.2009.03.003

Arthur, C., Baker, J., & Bamford, H. (2009). Proceedings of the international research workshop on the occurrence, effects, and fate of microplastic marine debris. Sept 9-11, 2008. *NOAA Technical Memorandum NOS-OR&R-30*

Barboza, L. G. A., Lopes, C., Oliveira, P., Bessa, F., Otero, V., Henriques, B., Raimundo, J., Caetano, M., Vale, C., & Guilhermino, L. (2020). Microplastics in wild fish from north east atlantic ocean and its potential for causing neurotoxic effects, lipid oxidative damage, and human health risks associated with ingestion exposure. *Science of the Total Environment*, *717*, 134625. https://doi.org/10.1016/j.scitotenv.2019.134625

Barnes, D. K., Galgani, F., Thompson, R. C., & Barlaz, M. (2009). Accumulation and fragmentation of plastic debris in global environments. *Philosophical Transactions of the Royal Society of London. Series B, Biological Sciences*, *364*(1526), 1985–1998. https://doi.org/10.1098/rstb.2008.0205

Brachner, A., Fragouli, D., Duarte, I. F., Farias, P. M. A., Dembski, S., Ghosh, M., Barisic, I., Zdzieblo, D., Vanoirbeek, J., Schwabl, P., & Neuhaus, W. (2020). Assessment of human health risks posed by nano-and microplastics is currently not feasible. *International Journal of Environmental Research and Public Health*, *17*(23), 1–10. https://doi.org/10.3390/ijerph17238832

Brehm, J., Wilde, M. V., Reiche, L., Leitner, L. C., Petran, B., Meinhart, M., Wieland, S., Ritschar, S., Schott, M., Boos, J. P., Frei, S., Kress, H., Senker, J., Greiner, A., Fröhlich, T., & Laforsch, C. (2022). In-depth characterization revealed polymer type and chemical content specific effects of microplastic on Dreissena bugensis. *Journal of Hazardous Materials*, *437*(March). https://doi.org/10.1016/j.jhazmat.2022.129351

Browne, M. A., Dissanayake, A., Galloway, T. S., Lowe, D. M., & Thompson, R. C. (2008). Ingested microscopic plastic translocates to the circulatory system of the mussel, Mytilus edulis (L.). *Environmental Science and Technology*, *42*(13), 5026–5031. https://doi.org/10.1021/es800249a

Bulannga, R. B., & Schmidt, S. (2022). Uptake and accumulation of microplastic particles by two freshwater ciliates isolated from a local river in South Africa. *Environmental Research*, *204*(Pt B), 112123. https://doi.org/10.1016/j.envres.2021.112123

Canton, J. (2018). Macropinocytosis: New insights into its underappreciated role in innate immune cell surveillance. *Frontiers in Immunology*, *9*(OCT), 1–8. https://doi.org/10.3389/fimmu.2018.02286

Carpenter, E. J., & Smith, K. L. (1972). Plastics on the Sargasso sea surface. *Science*, *175*(4027), 1240–1241. https://doi.org/10.1126/science.175.4027.1240

Carr, K. E., Smyth, S. H., McCullough, M. T., Morris, J. F., & Moyes, S. M. (2012). Morphological aspects of interactions between microparticles and mammalian cells: Intestinal uptake and onward movement. *Progress in Histochemistry and Cytochemistry*, *46*(4), 185–252.

References

https://doi.org/10.1016/j.proghi.2011.11.001

Cooksey, K. E., & Wigglesworth-Cooksey, B. (1995). Adhesion of bacteria and diatoms to surfaces in the sea: A review. In *Aquatic Microbial Ecology* (Vol. 9, Issue 1, pp. 87–96). https://doi.org/10.3354/ame009087

CS3. (2020). Science to Enable Sustainable Plastics - A white paper from the 8th Chemical Sciences and Society Summit (CS3). *Royal Society of Chemistry*, *68*(2), 82. https://doi.org/10.1002/nadc.20204095424

Deng, Y., Zhang, Y., Lemos, B., & Ren, H. (2017). Tissue accumulation of microplastics in mice and biomarker responses suggest widespread health risks of exposure. *Scientific Reports*, *7*(April), 1–10. https://doi.org/10.1038/srep46687

Desforges, J.-P. W., Galbraith, M., & Ross, P. S. (2015). Ingestion of microplastics by zooplankton in the northeast pacific ocean. *Archives of Environmental Contamination and Toxicology*. https://doi.org/10.1007/s00244-015-0172-5

Devriese, L. I., van der Meulen, M. D., Maes, T., Bekaert, K., Paul-Pont, I., Frère, L., Robbens, J., & Vethaak, A. D. (2015). Microplastic contamination in brown shrimp (Crangon crangon, Linnaeus 1758) from coastal waters of the Southern North Sea and Channel area. *Marine Pollution Bulletin*, *98*(1–2), 179–187. https://doi.org/10.1016/j.marpolbul.2015.06.051

Doherty, G. J., & McMahon, H. T. (2009). Mechanisms of endocytosis. *Annual Review of Biochemistry*, *78*(1), 857–902. https://doi.org/10.1146/annurev.biochem.78.081307.110540

Donlan, R. M. (2002). Biofilms: microbial life on surfaces. *Emerging Infectious Diseases*, *8*(9), 881–890. https://doi.org/10.3201/eid0809.020063

Dris, R., Gasperi, J., Saad, M., Mirande, C., & Tassin, B. (2016). Synthetic fibers in atmospheric fallout: A source of microplastics in the environment? *Marine Pollution Bulletin*, 4–7. https://doi.org/10.1016/j.marpolbul.2016.01.006

Dris, R., Imhof, H., Sanchez, W., Gasperi, J., Galgani, F., Tassin, B., & Laforsch, C. (2015). Beyond the ocean : contamination of freshwater ecosystems with (micro-) plastic particles. *Environmental Chemistry*, *MARCH*, A-L. https://doi.org/10.1071/EN14172

PlasticsEurope. (2020). Plastics – the facts 2020. *PlasticEurope*, 1–64.

Fadare, O. O., Wan, B., Liu, K., Yang, Y., Zhao, L., & Guo, L. H. (2020). Eco-corona vs protein corona: effects of humic substances on corona formation and nanoplastic particle toxicity in Daphnia magna. *Environmental Science and Technology*, *54*(13), 8001–8009. https://doi.org/10.1021/acs.est.0c00615

Forest, V., Cottier, M., & Pourchez, J. (2015). Electrostatic interactions favor the binding of positive nanoparticles on cells: A reductive theory. *Nano Today*, *10*(6), 677–680. https://doi.org/10.1016/j.nantod.2015.07.002

Fournier, S. B., D'Errico, J. N., Adler, D. S., Kollontzi, S., Goedken, M. J., Fabris, L., Yurkow, E. J., & Stapleton, P. A. (2020). Nanopolystyrene translocation and fetal deposition after acute lung exposure during late-stage pregnancy. *Particle and Fibre Toxicology*, *17*(1), 1–11. https://doi.org/10.1186/s12989-020-00385-9

Frias, J. P. G. L., & Nash, R. (2019). Microplastics: finding a consensus on the definition. *Marine Pollution Bulletin*, *138*(November 2018), 145–147. https://doi.org/10.1016/j.marpolbul.2018.11.022

Fröhlich, E. (2012). The role of surface charge in cellular uptake and cytotoxicity of medical nanoparticles. *International Journal of Nanomedicine*, *7*(November 2012), 5577–5591. https://doi.org/10.2147/IJN.S36111

Galloway, T. S., Cole, M., & Lewis, C. (2017). Interactions of microplastic debris throughout the marine ecosystem. *Nature Ecology & Evolution*, *1*(5), 0116. https://doi.org/10.1038/s41559-017-0116

Gasperi, J., Mandin, C., & Tassin, B. (2015). First overview of microplastics in indoor and outdoor air. 15th EuCheMS International Conference on Chemistry and the Environment, Sep 2015, Leipzig,

References

Germany. ⟨hal-01195546⟩

Gasperi, J., Wright, S. L., Dris, R., Collard, F., Mandin, C., Guerrouache, M., Langlois, V., Kelly, F. J., & Tassin, B. (2018). Microplastics in air: are we breathing it in? *Current Opinion in Environmental Science and Health*, *1*(February), 1–5. https://doi.org/10.1016/j.coesh.2017.10.002

Gerritse, J., Leslie, H. A., Tender, C. A. De, Devriese, L. I., & Vethaak, A. D. (2020). Fragmentation of plastic objects in a laboratory seawater microcosm. *Scientific Reports*, 1–16. https://doi.org/10.1038/s41598-020-67927-1

GESAMP Joint Group of Experts on the Scientific Aspects of Marine Environmental Protection. (2016). Sources, fate and effects of microplastics in the marine environment: part 2 of a global assessment. *Reports and Studies GESAMP, No. 93, 96 P., 93*.

González-Fernández, D., & Hanke, G. (2017). Toward a harmonized approach for monitoring of riverine floating macro litter inputs to the marine environment. *Frontiers in Marine Science*, *4*(March), 1–7. https://doi.org/10.3389/fmars.2017.00086

Gregory, M. R. (2009). Environmental implications of plastic debris in marine settings-entanglement, ingestion, smothering, hangers-on, hitch-hiking and alien invasions. *Philosophical Transactions of the Royal Society of London. Series B, Biological Sciences*, *364*(1526), 2013–2025. https://doi.org/10.1098/rstb.2008.0265

Hodges, G. M., Carr, E. A., Hazzard, R. A., & Carr, K. E. (1995). Uptake and translocation of microparticles in small intestine - morphology and quantification of particle distribution. *Digestive Diseases and Sciences*, *40*(5), 967–975. https://doi.org/10.1007/BF02064184

Hodgson, D. J., Bréchon, A. L., & Thompson, R. C. (2018). Ingestion and fragmentation of plastic carrier bags by the amphipod Orchestia gammarellus: Effects of plastic type and fouling load. *Marine Pollution Bulletin*, *127*, 154–159. https://doi.org/10.1016/j.marpolbul.2017.11.057

Hossain, M. R., Jiang, M., Wei, Q. H., & Leff, L. G. (2019). Microplastic surface properties affect bacterial colonization in freshwater. *Journal of Basic Microbiology*, *59*(1), 54–61. https://doi.org/10.1002/jobm.201800174

Imhof, H. K., Ivleva, N. P., Schmid, J., Niessner, R., & Laforsch, C. (2013). Contamination of beach sediments of a subalpine lake with microplastic particles. *Current Biology*, *23*(19), R867–R868. https://doi.org/10.1016/j.cub.2013.09.001

Imhof, H. K., Sigl, R., Brauer, E., Feyl, S., Giesemann, P., Klink, S., Leupolz, K., Löder, M. G. J., Löschel, L. A., Missun, J., Muszynski, S., Ramsperger, A. F. R. M., Schrank, I., Speck, S., Steibl, S., Trotter, B., Winter, I., & Laforsch, C. (2017). Spatial and temporal variation of macro-, meso- and microplastic abundance on a remote coral island of the Maldives, Indian Ocean. *Marine Pollution Bulletin*, *116*(1–2), 340–347. https://doi.org/10.1016/j.marpolbul.2017.01.010

Jeong, C. B., Won, E. J., Kang, H. M., Lee, M. C., Hwang, D. S., Hwang, U. K., Zhou, B., Souissi, S., Lee, S. J., & Lee, J. S. (2016). Microplastic size-dependent toxicity, oxidative stress induction, and p-JNK and p-p38 activation in the monogonont rotifer (Brachionus koreanus). *Environmental Science and Technology*, *50*(16), 8849–8857. https://doi.org/10.1021/acs.est.6b01441

Kaevska, M., Videnska, P., Sedlar, K., & Slana, I. (2016). Seasonal changes in microbial community composition in river water studied using 454-pyrosequencing. *SpringerPlus*, *5*(1). https://doi.org/10.1186/s40064-016-2043-6

Kernchen, S., Löder, M. G. J., Fischer, F., Fischer, D., Moses, S. R., Georgi, C., Nölscher, A. C., Held, A., & Laforsch, C. (2021). Airborne microplastic concentrations and deposition across the Weser River catchment. *Science of the Total Environment*, 151812. https://doi.org/10.1016/j.scitotenv.2021.151812

Kerr, M. C., & Teasdale, R. D. (2009). Defining macropinocytosis. *Traffic*, *10*(4), 364–371. https://doi.org/10.1111/j.1600-0854.2009.00878.x

Khadka, P., Ro, J., Kim, H., Kim, I., Tae, J., Kim, H., Min, J., Yun, G., & Lee, J. (2014). Pharmaceutical particle technologies : An approach to improve drug solubility , dissolution and bioavailability. *Asian*

Journal of Pharmaceutical Sciences, *9*(6), 304–316. https://doi.org/10.1016/j.ajps.2014.05.005

Kirstein, I. V., Kirmizi, S., Wichels, A., Garin-Fernandez, A., Erler, R., Löder, M., & Gerdts, G. (2016a). Dangerous hitchhikers? Evidence for potentially pathogenic Vibrio spp. on microplastic particles. *Marine Environmental Research*, *120*, 1–8. https://doi.org/10.1016/j.marenvres.2016.07.004

Knight, L. J., Parker-Jurd, F. N. F., Al-Sid-Cheikh, M., & Thompson, R. C. (2020). Tyre wear particles: an abundant yet widely unreported microplastic? *Environmental Science and Pollution Research*, *27*(15), 18345–18354. https://doi.org/10.1007/s11356-020-08187-4

Kole, P. J., Löhr, A. J., Van Belleghem, F. G. A. J., & Ragas, A. M. J. (2017). Wear and tear of tyres: A stealthy source of microplastics in the environment. *International Journal of Environmental Research and Public Health*, *14*(10). https://doi.org/10.3390/ijerph14101265

Korn, E. D., & Weisman, R. A. (1967). Phagocytosis of latex beads by Acanthamoeba. II. Electron microscopic study of the initial events. *The Journal of Cell Biology*, *34*(1), 219–227. https://doi.org/10.1083/jcb.34.1.219

Lacerda, A. L. d. F., Rodrigues, L. dos S., van Sebille, E., Rodrigues, F. L., Ribeiro, L., Secchi, E. R., Kessler, F., & Proietti, M. C. (2019). Plastics in sea surface waters around the Antarctic Peninsula. *Scientific Reports*, *9*(1), 1–12. https://doi.org/10.1038/s41598-019-40311-4

Laist, D. (1997). Impacts of marine debris: entanglement of marine life in marine debris including a comprehensive list of species with entanglement and ingestion records. *In: Coe, J.M. & D.B. Rogers (Eds.): Marine Debris - Sources, Impacts and Solutions. Springer-Verlag, New York*, 99–139. https://doi.org/10.1007/978-1-4613-8486-1_10

Leeden, B. M. C. Van Der, & Frens, G. (2002). Surface properties of plastic materials in relation to their adhering performance. *Advanced Engineering Materials 5*, 280–289. https://doi.org/10.1002/1527-2648(20020503)4:5<280::AID-ADEM280>3.0.CO;2-Z

Liu, C., Li, J., Zhang, Y., Wang, L., Deng, J., Gao, Y., Yu, L., Zhang, J., & Sun, H. (2019). Widespread distribution of PET and PC microplastics in dust in urban China and their estimated human exposure. *Environment International*, *128*(January), 116–124. https://doi.org/10.1016/j.envint.2019.04.024

Liu, T., Zhang, L., Joo, D., & Sun, S. C. (2017). NF-$\varkappa$B signaling in inflammation. *Signal Transduction and Targeted Therapy*, *2*(April). https://doi.org/10.1038/sigtrans.2017.23

Liu, Z., Zhuan, Q., Zhang, L., Meng, L., Fu, X., & Hou, Y. (2022). Polystyrene microplastics induced female reproductive toxicity in mice. *Journal of Hazardous Materials*, *424*(PC), 127629. https://doi.org/10.1016/j.jhazmat.2021.127629

Lobelle, D., & Cunliffe, M. (2011). Early microbial biofilm formation on marine plastic debris. *Marine Pollution Bulletin*, *62*(1), 197–200. https://doi.org/10.1016/j.marpolbul.2010.10.013

Loeb, G., & Neihof, R. (1975). Marine conditioning films. *Advances in Chemistry*, *145*(4), 319–335. https://doi.org/10.1021/ba-1975-0145

Lorite, G. S., Rodrigues, C. M., de Souza, A. A., Kranz, C., Mizaikoff, B., & Cotta, M. A. (2011). The role of conditioning film formation and surface chemical changes on Xylella fastidiosa adhesion and biofilm evolution. *Journal of Colloid and Interface Science*, *359*(1), 289–295. https://doi.org/10.1016/j.jcis.2011.03.066

Lu, L., Wan, Z., Luo, T., Fu, Z., & Jin, Y. (2018). Polystyrene microplastics induce gut microbiota dysbiosis and hepatic lipid metabolism disorder in mice. *Science of the Total Environment*, *631–632*, 449–458. https://doi.org/10.1016/j.scitotenv.2018.03.051

Lu, Y., Zhang, Y., Deng, Y., Jiang, W., Zhao, Y., Geng, J., Ding, L., & Ren, H. (2016). Uptake and accumulation of polystyrene microplastics in zebrafish (Danio rerio) and toxic effects in liver. *Environmental Science & Technology*, *50*(7), 4054−4060. https://doi.org/10.1021/acs.est.6b00183

Lundqvist, M., Stigler, J., Cedervall, T., Berggård, T., Flanagan, M. B., Lynch, I., Elia, G., & Dawson, K. (2011). The evolution of the protein corona around nanoparticles: A test study. *ACS Nano*, *5*(9), 7503–7509. https://doi.org/10.1021/nn202458g

References

Lundqvist, M., Stigler, J., Elia, G., Lynch, I., Cedervall, T., & Dawson, K. A. (2008). Nanoparticle size and surface properties determine the protein corona with possible implications for biological impacts. *Proceedings of the National Academy of Sciences of the United States of America*, *105*(38), 14265–14270. https://doi.org/10.1073/pnas.0805135105

Luo, T., Wang, C., Pan, Z., Jin, C., Fu, Z., & Jin, Y. (2019). Maternal polystyrene microplastic exposure during gestation and lactation altered metabolic homeostasis in the dams and their F1 and F2 offspring. *Environmental Science and Technology*, *53*(18), 10978–10992. https://doi.org/10.1021/acs.est.9b03191

Mao, R., Lang, M., Yu, X., Wu, R., Yang, X., & Guo, X. (2020). Aging mechanism of microplastics with UV irradiation and its effects on the adsorption of heavy metals. *Journal of Hazardous Materials*, 122515. https://doi.org/10.1016/j.jhazmat.2020.122515

Meides, N., Mauel, A., Menzel, T., Altstädt, V., Ruckdäschel, H., Senker, J., & Strohriegl, P. (2022). Quantifying the fragmentation of polypropylene upon exposure to accelerated weathering. *Microplastics and Nanoplastics*, *2*(1). https://doi.org/10.1186/s43591-022-00042-2

Meides, N., Menzel, T., Poetzschner, B., Löder, M. G. J., Mansfeld, U., Strohriegl, P., Altstaedt, V., & Senker, J. (2021). Reconstructing the environmental degradation of polystyrene by accelerated weathering. *Environmental Science and Technology*, *55*(12), 7930–7938. https://doi.org/10.1021/acs.est.0c07718

Messinetti, S., Mercurio, S., Scarì, G., Pennati, A., & Pennati, R. (2019). Ingested microscopic plastics translocate from the gut cavity of juveniles of the ascidian Ciona intestinalis. *The European Zoological Journal*, *86*(1), 189–195. https://doi.org/10.1080/24750263.2019.1616837

Möller, J. N., Löder, M. G. J., & Laforsch, C. (2020). Finding microplastics in soils: a review of analytical methods. *Environmental Science and Technology*, *54*(4), 2078–2090. https://doi.org/10.1021/acs.est.9b04618

Monopoli, M. P., Åberg, C., Salvati, A., & Dawson, K. A. (2012). Biomolecular coronas provide the biological identity of nanosized materials. *Nature Nanotechnology*, *7*(12), 779–786. https://doi.org/10.1038/nnano.2012.207

Nasser, F., Constantinou, J., & Lynch, I. (2019a). Nanomaterials in the environment acquire an "eco-corona" impacting their toxicity to Daphnia magna—a call for updating toxicity testing policies. *Proteomics*, *1800412*, 1–15. https://doi.org/10.1002/pmic.201800412

Nasser, F., & Lynch, I. (2016). Secreted protein eco-corona mediates uptake and impacts of polystyrene nanoparticles on Daphnia magna. *Journal of Proteomics*, *137*, 45–51. https://doi.org/10.1016/j.jprot.2015.09.005

O'Connor, J. D., Mahon, A. M., Ramsperger, A. F. R. M., Trotter, B., Redondo-Hasselerharm, P. E., Koelmans, A. A., Lally, H. T., & Murphy, S. (2019). Microplastics in freshwater biota: a critical review of isolation, characterization, and assessment methods. *Global Challenges*, *1800118*, 1800118. https://doi.org/10.1002/gch2.201800118

O`Toole, G., Kaplan, H. B., & Kolter, R. (2000). Biofilm formation as microbial development. *Annu. Rev. Microbiol*, *54*, 49–79. https://doi.org/10.1146/annurev.micro.54.1.49

Oberbeckmann, S., Löder, M. G. J., & Labrenz, M. (2015). Marine microplastic-associated biofilms – a review. *Environmental Chemistry*, *12*(5), 551–562. https://doi.org/10.1071/EN15069

Oberbeckmann, S., Loeder, M. G. J., Gerdts, G., & Osborn, A. M. (2014). Spatial and seasonal variation in diversity and structure of microbial biofilms on marine plastics in Northern European waters. *FEMS Microbiology Ecology*, *2*(May), 478–492. https://doi.org/10.1111/1574-6941.12409

Oberbeckmann, S., Osborn, A. M., & Duhaime, M. B. (2016). Microbes on a bottle: Substrate, season and geography influence community composition of microbes colonizing marine plastic debris. *PLoS ONE*, *11*(8), 1–24. https://doi.org/10.1371/journal.pone.0159289

Piehl, S., Leibner, A., Löder, M. G. J., Dris, R., Bogner, C., & Laforsch, C. (2018). Identification and quantification of macro- and microplastics on an agricultural farmland. *Scientific Reports*, *8*(1), 1–9. https://doi.org/10.1038/s41598-018-36172-y

References

Piehl, S., Mitterwallner, V., Atwood, E. C., Bochow, M., & Laforsch, C. (2019). Abundance and distribution of large microplastics (1–5 mm) within beach sediments at the Po River Delta, northeast Italy. *Marine Pollution Bulletin*, *149*(May), 110515. https://doi.org/10.1016/j.marpolbul.2019.110515

Prietl, B., Meindl, C., Roblegg, E., Pieber, T. R., Lanzer, G., & Fröhlich, E. (2014). Nano-sized and micro-sized polystyrene particles affect phagocyte function. *Cell Biology and Toxicology*, *30*(1), 1–16. https://doi.org/10.1007/s10565-013-9265-y

Pulido-Reyes, G., Leganes, F., Fernández-Piñas, F., & Rosal, R. (2017a). Bio-nano interface and environment: a critical review. *Environmental Toxicology and Chemistry*, *36*(12), 3181–3193. https://doi.org/10.1002/etc.3924

Ramsperger, A. F. R. M., Narayana, V. K. B., Gross, W., Mohanraj, J., Thelakkat, M., Greiner, A., Schmalz, H., Kress, H., & Laforsch, C. (2020). Environmental exposure enhances the internalization of microplastic particles into cells. *Science Advances*, *6*(50), 1–10. https://doi.org/10.1126/sciadv.abd1211

Renner, L. D., & Weibel, D. B. (2011a). Physicochemical regulation of biofilm formation. *MRS Bulletin*, *36*(5), 347–355. https://doi.org/10.1557/mrs.2011.65

Robertson, G. L. (2016). Packaging and food and beverage shelf life. In *The Stability and Shelf Life of Food*. Elsevier Ltd. https://doi.org/10.1016/B978-0-08-100435-7.00003-4

Ross, P. S., Chastain, S., Vassilenko, E., Etemadifar, A., Zimmermann, S., Quesnel, S., Eert, J., Solomon, E., Patankar, S., Posacka, A. M., & Williams, B. (n.d.). Pervasive distribution of polyester fibres in the Arctic Ocean is driven by Atlantic inputs. *Nature Communications*, *2021*, 4–12. https://doi.org/10.1038/s41467-020-20347-1

Rozman, U., & Kalčíková, G. (2022). Seeking for a perfect (non-spherical) microplastic particle – The most comprehensive review on microplastic laboratory research. *Journal of Hazardous Materials*, *424*(October 2021), 127529. https://doi.org/10.1016/j.jhazmat.2021.127529

Rudolph, J., Völkl, M., Jérôme, V., Scheibel, T., & Freitag, R. (2021). Noxic effects of polystyrene microparticles on murine macrophages and epithelial cells. *Scientific Reports*, *11*(1), 1–17. https://doi.org/10.1038/s41598-021-95073-9

Rummel, C. D., Jahnke, A., Gorokhova, E., K?hnel, D., & Schmitt-Jansen, M. (2017). The impacts of biofilm formation on the fate and potential effects of microplastic in the aquatic environment. *Environmental Science & Technology Letters*, acs.estlett.7b00164. https://doi.org/10.1021/acs.estlett.7b00164

Semcesen, P. O., & Wells, M. G. (2021). Biofilm growth on buoyant microplastics leads to changes in settling rates: Implications for microplastic retention in the Great Lakes. *Marine Pollution Bulletin*, *170*(April), 112573. https://doi.org/10.1016/j.marpolbul.2021.112573

Sommer, F., Dietze, V., Baum, A., Sauer, J., Gilge, S., Maschowski, C., & Gieré, R. (2018). Tire abrasion as a major source of microplastics in the environment. *Aerosol and Air Quality Research*, *18*(8), 2014–2028. https://doi.org/10.4209/aaqr.2018.03.0099

Stanton, T., Johnson, M., Nathanail, P., MacNaughtan, W., & Gomes, R. L. (2019). Freshwater and airborne textile fibre populations are dominated by 'natural', not microplastic, fibres. *Science of the Total Environment*, *666*, 377–389. https://doi.org/10.1016/j.scitotenv.2019.02.278

Stock, V., Böhmert, L., Lisicki, E., Block, R., Cara-Carmona, J., Pack, L. K., Selb, R., Lichtenstein, D., Voss, L., Henderson, C. J., Zabinsky, E., Sieg, H., Braeuning, A., & Lampen, A. (2019). Uptake and effects of orally ingested polystyrene microplastic particles in vitro and in vivo. *Archives of Toxicology*. https://doi.org/10.1007/s00204-019-02478-7

Stock, V., Laurisch, C., Franke, J., Dönmez, M. H., Voss, L., Böhmert, L., Braeuning, A., & Sieg, H. (2021). Uptake and cellular effects of PE, PP, PET and PVC microplastic particles. *Toxicology in Vitro*, *70*(June 2020), 105021. https://doi.org/10.1016/j.tiv.2020.105021

Sutherland, I. W. (2001). The biofilm matrix - an immobilized but dynamic microbial environment. *Trends in Microbiology*, *9*(5), 222–227. https://doi.org/10.1016/S0966-842X(01)02012-1

References

Tenzer, S., Docter, D., Kuharev, J., Musyanovych, A., Fetz, V., Hecht, R., Schlenk, F., Fischer, D., Kiouptsi, K., Reinhardt, C., Landfester, K., Schild, H., Maskos, M., Knauer, S. K., & Stauber, R. H. (2013). Rapid formation of plasma protein corona critically affects nanoparticle pathophysiology. *Nature Nanotechnology*, *8*(10), 772–781. https://doi.org/10.1038/nnano.2013.181

Tenzer, S., Docter, D., Rosfa, S., Wlodarski, A., Rekik, A., Knauer, S. K., Bantz, C., Nawroth, T., Bier, C., Sirirattanapan, J., Mann, W., Treuel, L., Zellner, R., Maskos, M., & Stauber, R. H. (2011). Nanoparticle size is a critical physico-chemical determinant of the human blood plasma corona: a comprehensive quantitative proteomic analysis. *ACS Nano*, *5*(9), 7155–7167. https://doi.org/10.1021/nn201950e

Thompson, R. C., Ylva, O., P, M. R., Anthony, D., Rowland, S. J., WG, J. A., Daniel, M., & E, R. A. (2004). Lost at sea: where is all the plastic. *Science*, *304*(May), 838. https://doi.org/10.1126/science.1094559

Vandermeersch, G., Van Cauwenberghe, L., Janssen, C. R., Marques, A., Granby, K., Fait, G., Kotterman, M. J. J., Diogène, J., Bekaert, K., Robbens, J., & Devriese, L. (2015). A critical view on microplastic quantification in aquatic organisms. *Environmental Research*, *143*, 46–55. https://doi.org/10.1016/j.envres.2015.07.016

Verschoor, A., de Poorter, L., Dröge, R., Kuenen, J., & de Valk, E. (2016). Emission of microplastics and potential mitigation measures. *REPORT - RIVM Report 2016-0026*, 76. https://www.rivm.nl/dsresource?objectid=dad60794-a4a2-44f9-8416-624cfbc4861e&type=org&disposition=inline

Vianello, A., Jensen, R. L., Liu, L., & Vollertsen, J. (2019). Simulating human exposure to indoor airborne microplastics using a breathing thermal manikin. *Scientific Reports*, *9*(1), 1–11. https://doi.org/10.1038/s41598-019-45054-w

Visalli, G., Facciolà, A., Ciarello, M. P., De Marco, G., Maisano, M., & Di Pietro, A. (2021). Acute and sub-chronic effects of microplastics (3 and 10 µm) on the human intestinal cells ht-29. *International Journal of Environmental Research and Public Health*, *18*(11). https://doi.org/10.3390/ijerph18115833

von Moos, N., Burkhardt-Holm, P., & Koehler, A. (2012). Uptake and effects of microplastics on cells and tissue of the blue mussel Mytilus edulis L. after an experimental exposure. *Environmental Science & Technology*, *46*, 327–335. https://doi.org/10.1021/es302332w

Vroom, R. J. E., Koelmans, A. A., Besseling, E., & Halsband, C. (2017). Aging of microplastics promotes their ingestion by marine zooplankton. *Environmental Pollution*, *231*, 987–996. https://doi.org/10.1016/j.envpol.2017.08.088

Walkey, C. D., Olsen, J. B., Guo, H., Emili, A., & Chan, W. C. W. (2012). Nanoparticle size and surface chemistry determine serum protein adsorption and macrophage uptake. *Journal of the American Chemical Society*, *134*(4), 2139–2147. https://doi.org/10.1021/ja2084338

Wang, Y. L., Lee, Y. H., Hsu, Y. H., Chiu, I. J., Huang, C. C. Y., Huang, C. C., Chia, Z. C., Lee, C. P., Lin, Y. F., & Chiu, H. W. (2021). The kidney-related effects of polystyrene microplastics on human kidney proximal tubular epithelial cells hk-2 and male c57bl/6 mice. *Environmental Health Perspectives*, *129*(5), 1–18. https://doi.org/10.1289/EHP7612

Webb, H. K., Crawford, R. J., Sawabe, T., & Ivanova, E. P. (2009). Poly(ethylene terephthalate) polymer surfaces as a substrate for bacterial attachment and biofilm formation. *Microbes and Environments*, *24*(1), 39–42. https://doi.org/10.1264/jsme2.ME08538

Weisman, R. A., & Korn, E. D. (1967). Phagocytosis of Latex Beads by Acanthamoeba. I. Biochemical Properties. *Journal of Cell Biology 6*(2). https://doi.org/10.1083/jbc.34.1.219

White, A., & Lockyer, S. (2020). Removing plastic packaging from fresh produce – what's the impact? *Nutrition Bulletin*, *45*(1), 35–50. https://doi.org/10.1111/nbu.12420

Woodall, L. C., Sanchez-Vidal, A., Canals, M., Paterson, G. L. J., Coppock, R., Sleight, V., Calafat, A., Rogers, A. D., Narayanaswamy, B. E., & Thompson, R. C. (2014). The deep sea is a major sink for microplastic debris. *Royal Society Open Science*, *1*(4). https://doi.org/10.1098/rsos.140317

References

World Economic Forum. (2016). the New Plastics Economy- Rethinking the Future of Plastics. *January*, 1–120. http://www.ellenmacarthurfoundation.org/publications

Wright, R. J., Langille, M. G. I., & Walker, T. R. (2021). Food or just a free ride? A meta-analysis reveals the global diversity of the Plastisphere. *ISME Journal*, *15*(3), 789–806. https://doi.org/10.1038/s41396-020-00814-9

Wright, S. L., & Kelly, F. J. (2017). Plastic and human health: a micro issue? *Environmental Science and Technology*, *51*(12), 6634–6647. https://doi.org/10.1021/acs.est.7b00423

Wu, B., Wu, X., Liu, S., Wang, Z., & Chen, L. (2019). Size-dependent effects of polystyrene microplastics on cytotoxicity and efflux pump inhibition in human Caco-2 cells. *Chemosphere*, *221*, 333–341. https://doi.org/S0045653519300566

Zettler, E. R., Mincer, T. J., & Amaral-zettler, L. a. (2013). Life in the ' Plastisphere ': Microbial communities on plastic marine debris. *Environmental Science and Technology*. 47,13,7137-7146 https://doi.org/10.1021/es401288x

Zeytin, S., Wagner, G., Mackay-Roberts, N., Gerdts, G., Schuirmann, E., Klockmann, S., & Slater, M. (2020). Quantifying microplastic translocation from feed to the fillet in European sea bass Dicentrarchus labrax. *Marine Pollution Bulletin*, *156*(May), 111210. https://doi.org/10.1016/j.marpolbul.2020.111210

List of Publications

Publications in PEER-Reviewed Journals

2024

Wieland, S, **Ramsperger, A F R M**, Gross, W, Lehmann, M, Witzmann, T, Caspari, A, Obst, M, Gekle, S, Auernhammer, G K, Fery, A, Laforsch, C, Kress, H: Nominally identical microplastic models differ greatly in their particle-cell interactions, Nature Communications, 2024, Volume 15, 922, https://doi.org/10.1038/s41467-024-45281-4

2023

Ramsperger A F R M, Bergamaschi E, Panizzolo M, Fenoglio I, Barbero F, Peters R, Undas A, Purker S, Giese B, Lalyer C R, Tamargo A, Moreno-Arribas V M, Grossart HP, Kühnel D, Dietrich J, Paulsen F, Afanou A K, Zienolddiny-Narui S, Eriksen Hammer S, Kringlen Ervik T, Graff P, Brinchmann B C, Nordby KC, Wallin H, Nassi M, Benetti F, Zanella M, Brehm J, Kress H, Löder M G J, Laforsch C: Nano- and microplastics: a comprehensive review on their exposure routes, translocation, and fate in humans, NanoImpact, 2023, Volume 29, 100441, https://doi.org/10.1016/j.impact.2022.100441.

2022

Witzmann T, **Ramsperger A F R M**, Wieland S, Laforsch C, Kress H, Fery A, Auernhammer G K: Repulsive Interactions of Eco-corona-Covered Microplastic Particles Quantitatively Follow Modeling of Polymer Brushes, Langmuir. 2022 Jul 26;38(29):8748-8756. doi: 10.1021/acs.langmuir.1c03204.

Saha, S, Laforsch, C, **Ramsperger, A F R M**, Niebel, D: Mikroplastik und dermatologische Versorgung, Die Dermatologie, doi: 10.1007/s00105-022-05035-z

Wieland, S, Balmes, A, Bender, J, Kitzinger, J, Meyer, F, **Ramsperger, A F R M**, Roeder, F, Tengelmann, C, Wimmer, B H, Laforsch, C, Kress, H: From properties to toxicity: comparing microplastics to other airborne microparticles, Journal of Hazardous Materials, 3(1), 128151 (2022), doi: 10.1016/j.jhazmat.2021.128151

Ramsperger, A F R M, Jasinski, J, Völkl, M, Witzmann, T, Meinhart, M, Jérôme, V, Kretschmer, W P, Freitag, R, Senker, J, Fery, A, Kress, H, Scheibel, T, Laforsch, C: Supposedly identical microplastic particles substantially differ in their material properties influencing particle-cell interactions and cellular responses, Journal of Hazardous Materials, 5(3), 425,127961 (2022), doi: 10.1016/j.jhazmat.2021.127961

2021

Weig, A; Löder, MGJ; **Ramsperger, A F R M**; Laforsch, C: In situ Prokaryotic and Eukaryotic Communities on Microplastic Particles in a Small Headwater Stream in Germany, Frontiers in Microbiology, 29(11), (2021), doi: 10.3389/fmicb.2021.660024

2020

Ramsperger, A F R M; Bangalore Narayana, VK; Gross, Wolfgang; Mohanraj, John; Thelakkat, Mukkundan; Greiner, Andreas; Schmalz, Holger; Kress, Holger; Laforsch, C: Environmental exposure enhances the internalisation of microplastic particles into cells, Science Advances, 6(50) (2020), doi:10.1126/sciadv.abd1211

Ramsperger, A F R M; Stellwag, A; Caspari, Anja; Fery, Andreas; Kress, Holger; Löder, MGJ; Laforsch, C: Structural Diversity in Early-Stage Biofilm Formation on Microplastics Depends on Environmental Medium and Polymer Properties, Water, 12(11), 3216 (2020), doi:10.3390/w12113216

2019

Trotter, B; **Ramsperger, A F R M**; Raab, P; Haberstroh, J; Laforsch, C: Plastic waste interferes with chemical communication in aquatic ecosystems, Scientific Reports (2019), online: 10.04.2019, doi:10.1038/s41598-019-41677-1

O´Connor, J D; Mahon, A M; **Ramsperger, A F R M**; Trotter, B; Redondo-Hasselerharm, P E; Koelmans, A A; Lally, H T; Murphy, S: Microplastics in Freshwater Biota: A Critical Review of Isolation, Characterisation, and Assessment Methods, Global Challenges (2019), doi:10.1002/gch2.201800118

2017

Imhof, H K; Sigl, R; Brauer, E; Feyl, S; Giesemann, P; Klink, S; Leupolz, K; Löder, M G J; Löschel, L; Missun, J; Muszynski, S; **Ramsperger, A F R M**; Schrank, I; Speck, S; Steibl, S; Trotter, B; Winter, I; Laforsch, C: Spatial and temporal variation of macro-, meso- and microplastic abundance on a remote coral island of the Maldives, Indian Ocean, Marine Pollution Bulletin, 116(1-2), 340-347 (2017), online: 18.01.2017, doi:10.1016/j.marpolbul.2017.01.010

BOOK Chapter

2020

Laforsch, C, **Ramsperger, A F R M**, Mondellini, S, Galloway, T: Microplastics: A Novel Suite of Environmental Contaminants but Present for Decades. In: Franz-Xaver Reichl, Michael Schwenk (eds.): Regulatory Toxicology. - Berlin: Springer, 1-26 (2020), doi:10.1007/978-3-642-36206-4_138-1

NON-PEER-REVIEWED CONTRIBUTIONS

2023

Laforsch, C, **Ramsperger, A F R M**, Ritschar, S: Themenband Planetary Health: Mikroplastik und der Einfluss auf die menschliche Gesundheit. In: Klima- und Gesundheitsschutz: Planetary-Health-Lösungsansätze" – Viviane Scherenberg und Johanne Pundt (Hrsg.). 1. Auflage 2023, Bremen: APOLLON University Press, 388 Seiten – ISBN: 978-3-943001-84-6

2019

Moses, S R, Piehl, S, **Ramsperger, A F R M**, Löder, M G J, Laforsch, C: Plastik im aquatischen Ökosystem. Sammelband „Ressourcen im globalen Wandel". Mohr Siebeck Tübingen. ISBN 978-3-16-156276-1 / eISBN 978-3-16-156277-8. doi: 10.1628/978-3-16-156277-8

CONFERENCE CONTRIBUTIONS

2022   CUSP early stage researchers meeting. Oral presentation. Title of the presentation: Biofilm on Microplastics and the Role of an Eco-corona for Particle Cell Interactions

2022   Micro2022 conference. Oral presentation. Title of the presentation: How Surface Properties of Pristine and Environmentally exposed Microplastics determine Particle-Cell-Interactions

2021   SETAC. Oral presentation. Title of the presentation: Environmental Exposure Enhances the Internalization of Microplastics into Cells

2021   PhD symposium Molekulare Biowissenschaften. Oral presentation. Title of the presentation: Environmental Exposure Enhances the Internalization of Microplastics into Cells

2020   Micro2020 conference. Oral presentation. Title of the presentation: Environmental Exposure Enhances the Internalization of Microplastics into Cells

2019   Deutsche Physikalische Gesellschaft, Regensburg. Poster presentation. Title of the poster: Environmental Exposure Enhances the Internalisation of Microplastics into Cells

INVITED TALKS

2021   Young Macromolecular Webinar, Title of the talk: Environmental Exposure Enhances the Internalisation of Microplastics into Cells

Acknowledgements

There are countless people to whom I am deeply indebted, who have and will accompany me on my way to completing my PhD thesis and beyond. Each and every one of you has made an outstanding contribution to my doctoral work, be it as mental support or through scientific input. I thank the team of the animal ecology department and the biological physics department. I thank my financial support from the Elite Network of Bavaria, the DFG – SFB Mikroplastik 1357 and EU H2020 – PlasticsFatE. Since I cannot express another 100 pages of gratitude, I will mention only a few by name. I want to thank all those not mentioned by name who accompanied me on my way, my loved ones. Thank you!

Nevertheless, I would like to highlight some people who have accompanied and supported me particularly intensively concerning my PhD thesis.

Christian. Thank you! It was great fun to be able to write my dissertation with you. I learned an incredible amount, not only about scientific work but also about myself. I felt in good hands and listened to and understood at all times. I appreciate that you also support me with my ideas and give me the freedom for my professional and personal development! I am very happy that our joint path is not over with the completion of my doctoral thesis, and I vow to do better for the following Christmas parties ;)

Holger. Thank you! You also deserve my special thanks. When I started my work for my PhD thesis, I was very excited and a bit scared to do part of my work in physics. I was never bad in physics at school, but here we talk about another level! You welcomed me very well and made me feel like a full member of your research group as a biologist (ecologist ;)). My fear quickly subsided as you gladly took extra time to explain various facts again understandably. I have learned a lot and hope our ways will not separate soon!

Jul. Thank you! Thank you for being there. Of course, a PhD thesis brings not only positive vibes but also days of frustration, anger and sometimes overload. You were and are, and will always be, a support for me. Thank you for understanding my bitching when disturbed in my tunnel of thought. You have it already not easy with me, but otherwise, it would be boring, right?

Family. Thank you! Thank you all, Mom, Dad, Dennis, Verena, Anna, Sarah, Nils, Marie, Lisa-Annabell and Sophia, for your support! You made me what I am today and supported and encouraged me in every decision in my life. Without you, all that I am today would not have been possible. I thank you, especially for the emotional support I have always received from you. And mom, you were right when you said: "You will become a biologist one day" ;). Thank you!

I also thank my dog Skylla who was responsible for my inner peace of mind. You are my teacher in patience. I want to close my PhD thesis with my quote from the beginning thesis by John Muir, which I may experience every day anew with you: "I only went out for a walk and finally concluded to stay out till sundown, for going out, I found, was really going in".

(Eidesstattliche) Versicherung und Erklärung

(§ 9 Satz 2 Nr. 3 PromO BayNAT)

Hiermit versichere ich eidesstattlich, dass ich die Arbeit selbständig verfasst und keine anderen als die von mir angegebenen Quellen und Hilfsmittel benutzt habe (vgl. Art. 64 Abs 1 Satz 6 BayHSchG).

(§ 9 Satz 2 Nr. 3 PromO BayNAT)

Hiermit erkläre ich, dass ich die Dissertation nicht bereits zur Erlangung eines akademischen Grades eingereicht habe und dass ich nicht bereits diese oder eine gleichartige Doktorprüfung endgültig nicht bestanden habe.

(§ 9 Satz 2 Nr. 4 PromO BayNAT)

Hiermit erkläre ich, dass ich Hilfe von gewerblichen Promotionsberatern bzw. -vermittlern oder ähnlichen Dienstleistern weder bisher in Anspruch genommen habe noch künftig in Anspruch nehmen werde.

(§ 9 Satz 2 Nr. 7 PromO BayNAT)

Hiermit erkläre ich mein Einverständnis, dass die elektronische Fassung meiner Dissertation unter Wahrung meiner Urheberrechte und des Datenschutzes einer gesonderten Überprüfung unterzogen werden kann.

(§ 9 Satz 2 Nr. 8 PromO BayNAT)

Hiermit erkläre ich mein Einverständnis, dass bei Verdacht wissenschaftlichen Fehlverhaltens Ermittlungen durch universitätsinterne Organe der wissenschaftlichen Selbstkontrolle stattfinden können.

…………………………………………

Ort, Datum, Unterschrift